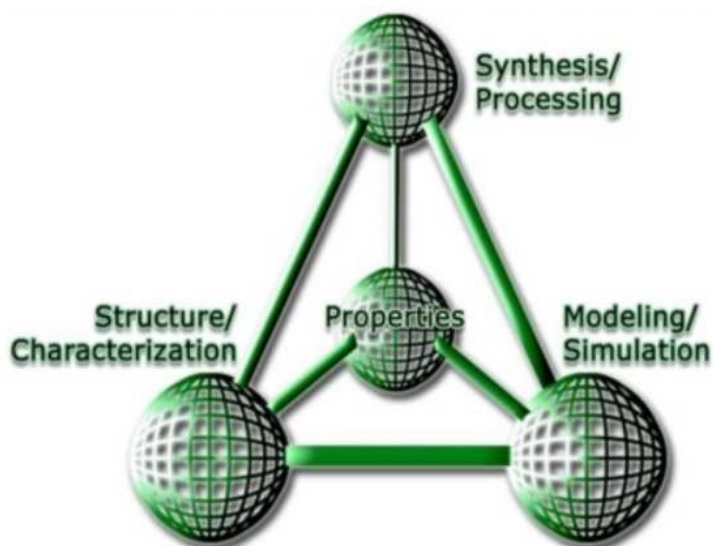


Novelties in Fibrous Material Science

**Volume-IV
2017**



Key authors and Editors

**Rajesh Mishra
Jiří Militký
Dana Křemenáková**

Název Novelties in Fibrous Material Science

Autor Doc. Rajesh Mishra, PhD, Prof. Ing. Jiří Militký, CSc. EURING,
Doc. Dr. Ing. Dana Křemenáková

Určeno pro specialisty v oboru materiálového inženýrství vláknenných systémů a širší
odbornou veřejnost

Vydavatel Technická univerzita v Liberci, Studentská 1402/2, Liberec

Schváleno Rektorátem TU v Liberci dne 19.12.2017, čj. RE 71/17

Vyšlo v prosinci 2017

Vydání 1.

Tiskárna Vysokoškolský podnik Liberec, spol. s r.o., Studentská 1402/2, Liberec

Č. publikace 55-071-17

Tato publikace neprošla redakční ani jazykovou úpravou.

Vydání odborné knihy schválila vědecká redakce TUL.

ISBN 978-80-7494-390-4



TECHNICKÁ UNIVERZITA V LIBERCI

Textilní fakulta

Katedra materiálového inženýrství

Doc. Rajesh Mishra, PhD
Prof. Ing. Jiří Militký, CSc. EURING
Doc. Dr. Ing. Dana Křemenáková

NOVELTIES IN FIBROUS MATERIAL SCIENCE

Liberec 2017

recenzent: Prof. B. K. BEHERA, PhD

© Technická univerzita v Liberci - 2017

ISBN 978-80-7494-390-4

Rajesh Mishra
Jiří Militký
Dana Křemenáková

*Technical University of Liberec, Faculty of Textile Engineering,
Studentská Street No 2, CZ-461 17 Liberec, Czech Republic*

Novelties in Fibrous Material Science



 TECHNICAL UNIVERSITY OF LIBEREC
Faculty of Textile Engineering

TUL FT Liberec 2017

Edited by: Rajesh Mishra, Jiří Militký and Dana Křemenáková,

Reviewed by: B K Behera

504 pp: printed and bound

Manufactured in the Czech Republic

ISBN 978-80-7494-390-4

CONTENTS

Chapter No.	Title	Pages
PART - I: Natural Fibers, Bio-Materials and Composites		
1	Basalt fibers and their composites Hafsa Jamshaid, Jiri Militký, Rajesh Mishra, Ludmila Koukolikova	02
2	A study of residual pesticides on conventional and organic cotton comparing biosensor and gas chromatography techniques Syed Zameer Ul Hassan*, Jiří Militký, Jan Krejčí, Rajesh Mishra, Muhammad Salman Naeem, Saima Javed, Ali Asghar, Muhammad Kashif, Jawad Naeem	62
3	Geotextiles and environmental protection textiles Jiří Militký, Rajesh Mishra, Mohanapriya Venkataraman and Vijay Baheti	81
4	Natural dyes usage in textile industry in Czech Republic and Turkey: comparative analysis Hana Křížová	145
5	Analyze the weavability problem during production of basalt hybrid fabrics Hafsa Jamshaid, Rajesh Mishra, Jiri Militky	167
6	Review on hybrid yarns, textile structures and techniques Mohanapriya Venkataraman, Xiaoman Xiong, Kasthuri Rajagopala Venkatesh, Rajesh Mishra and Jiri Militky	183
PART-II: Advanced Technical Fibrous Materials		
7	A novel method of developing activated carbon web from waste acrylic fibers for effective EMI shielding applications Muhammad Salman Naeem, Vijay Baheti, Jiri Militky, Veronika Tunakova, Syed Zameer Ul Hassan, Saima Javed, Qummer Zia Gilani, Hafiz Affan Abid, Jawad Naeem	224
8	Experimental study on compressibility of 3D spacer fabrics for cushioning applications Veerakumar Arumugam*, Rajesh Mishra, Jiri Militky, Dana Kremenakova, Jana Salacova, Mohanapriya Venkataraman, Miroslav Vaclavik	242
9	Development of cost effective cut resistant gloves by using virgin and recycled PPTA Haritham Khan, Hafsa Jamshaid, Rajesh Mishra, Jiri Militky, Rudolf Sramek	273
10	Development of electrical conductive films of polylactic acid reinforced with carbon particles derived from waste acrylic fibers Muhammad Salman Naeem, Vijay Baheti, Jiri Militky, Zafar Javed, Abher Rasheed, Saima Javed, M. Tahir Siddique	287

11	Equilibrium and kinetic studies of acid red adsorption on activated carbon web derived from acrylic fibrous waste	307
	Muhammad Salman Naeem, Vijay Baheti, Jiri Militky, Saima Javed, Qummer Zia Gilani, Syed Zameer Ul Hassan, Hafiz Affan, Zafar Javed, Zuhaib Ahmed	
12	Theoretical and experimental investigation on shear performance of 3D spacer fabrics	323
	Veerakumar Arumugam*, Rajesh Mishra, Maros Tunak, Jiri Militky, Dana Kremenakova, Mohanapriya Venkatraman, Blanka Tomkova, Miroslav Vaclavik	
13	Compressibility of sandwich composite structures for impact absorbance	352
	Kasthuri R Venkatesh, Jana Novotna, Rajesh Mishra and Jiri Militky	

PART - III: Miscellaneous Fibrous Materials

14	Investigation on performance of nanoporous fibrous composites	371
	Xiaoman Xiong, Tao Yang, Mohanapriya Venkataraman, Rajesh Mishra and Jiří Militký	
15	Multicriteria decision making in clothing textiles	394
	Srabani Misra, Jana Salacova, Bibhu Prasad Dash and Jiri Militky	
16	Aliphatic polyamide fibres	413
	Mohanapriya Venkataraman, Jiri Militký, Rajesh Mishra	
17	The mechanical, comfort & UV resistance properties on interlock derivatives	457
	Hafsa Jamshaid, Habib Awais, Rajesh Mishra	
18	Textile sector in Turkey	477
	Hamdi Ayyildiz, Hana Křížová	

PREFACE

The current book is the **FOURTH** in a series of manuscripts under “PROGRESS IN FIBROUS MATERIAL SCIENCE”. These books are collection of chapters dealing with state of the art technologies and the science of polymeric materials in specific.

Research in this area primarily focuses on efforts to design materials at a molecular level to achieve desirable properties and applications at a macroscopic level. With this broad focus, research ranges from fundamental scientific investigations of the interactions, properties and assembly of such molecular constituents to applied, engineering efforts that translate such fundamental information to futuristic technological advances.

Much of the research is highly interdisciplinary, involving collaborations with chemists, biochemists, materials scientists, mechanical engineers and biologists. Moreover, most of the researchers and graduate students are affiliated with Department of Material Engineering, Faculty of Textile Engineering, Technical University of Liberec, facilitating the use the world-class equipment and resources established in the laboratories.

The first part deals with “**Natural Fibers, Materials and Composites**”. During the last few decades there has been a renewed interest in the natural fiber as a substitute for glass, motivated by potential advantages of weight saving, lower raw material price, and 'thermal recycling' or the ecological advantages of using resources which are renewable. On the other hand natural fibers have their shortcomings, and these have to be solved in order to be competitive with glass. Natural fibers have lower durability and lower strength than glass fibers. However, recently developed fiber treatments have improved these properties considerably. To understand how fibers should be treated, a closer look into the fiber is required.

The second part is “**Advanced Technical Fibrous Materials**”. Clothing protects mankind from the extremes of nature. While providing protection, it is also imperative that textiles provide comfort too. In textiles, heat insulation is an important factor for estimating apparel comfort for the user. Devices that work according to principles of thermodynamic systems are largely used for measuring thermal properties of textile fabrics. This section of the book deals with many novel fibrous materials in high performance applications.

The third part titled “**Miscellaneous Functional Fibrous Materials**” is a combination of diversified fibrous materials used in a wide range of applications.

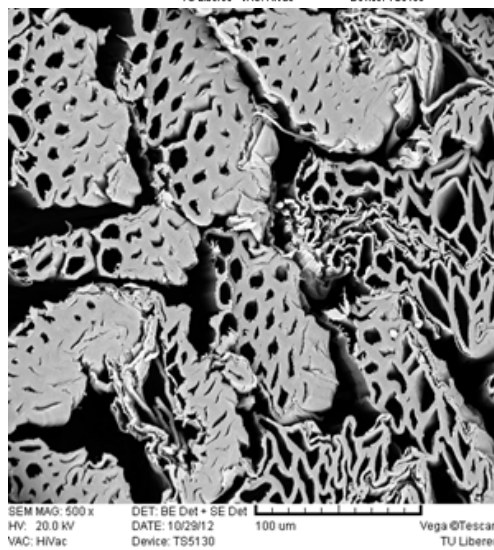
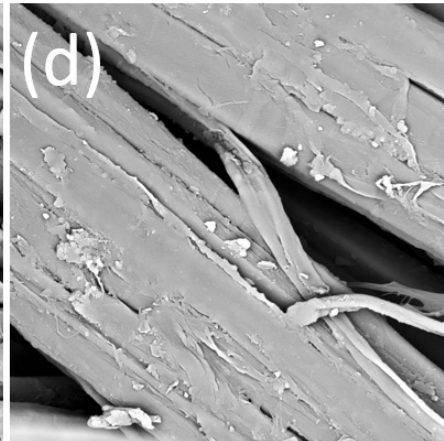
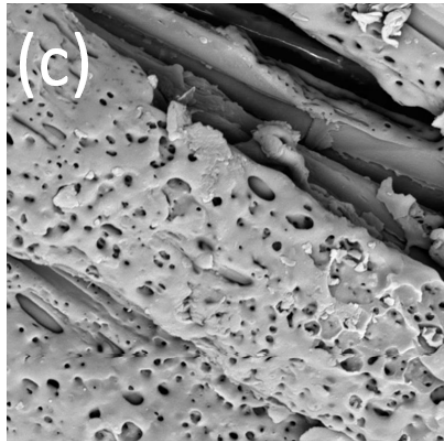
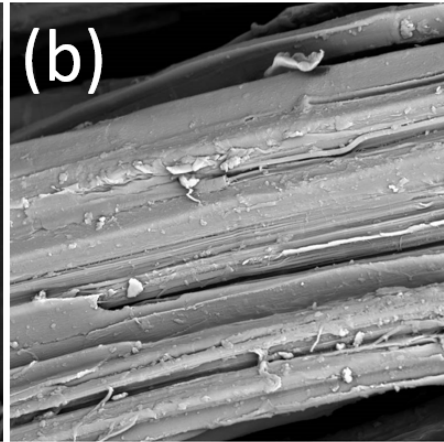
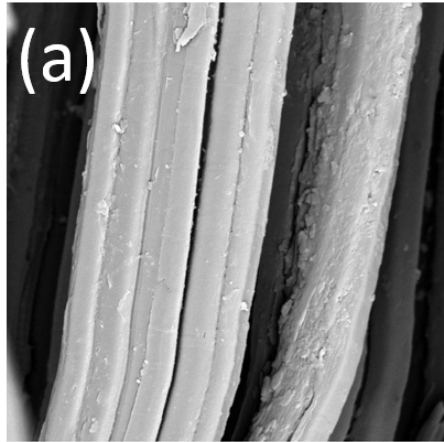
The editors and the authors have put their best efforts to enable the reader to have a broad understanding of these advanced fibrous materials aimed at futuristic areas of application.

Rajesh Mishra
Jiří Militký
Dana Křemenáková

FT, TUL, 2017.

PART - I

Natural Fibers, Materials and Composites



Basalt fibers and their composites

Hafsa Jamshaid, Jiri Militký, Rajesh Mishra, Ludmila Koukolikova*

Technical University of Liberec, Czech Republic

*VUTS, Textile Machinery Research Institute, Liberec, Czech Republic.

1. Introduction

Technical textiles are new horizon for achievements in textile industry and it has become talk of the town in the recent past. They have a variety of applications in several industries. Meeting the end product specification is a big challenge especially for industrial goods. Technical textiles are rapidly developing and growing at a high pace in the industry. Textiles are replacing traditional materials in various sectors of the international economy. The use of polymer composite materials in various field of technical textiles applications demands the development of products able to fulfill both technical and stricter environmental requirements [1]. Fiber reinforcements in composite material are generally used to improve the physico-mechanical properties and durability when exposure to extreme environment takes place. The most common fiber reinforcement in resin are glass and carbon fibers. Glass fibers have very good strength related properties and good interfacial adhesion to the matrix. For advanced applications like use in aero space and space technology, carbon fibers are usually preferred. The constraint for carbon fibers is, their production cost is higher than glass fiber and adhesion between the matrix and carbon fiber is often difficult to achieve [2]. The study of natural fibers has become increasingly important in recent years due to the growing awareness to protect ecological and environmental resources [3-4]. Despite the advantages of natural fibers over traditional ones (low cost, low density, acceptable specific strength properties, reduced tool wear and biodegradability), they suffer from several drawbacks, such as their hydrophilic nature (which affects the compatibility with hydrophobic polymeric matrix) and variability in mechanical properties. As a consequence, other reinforcement materials are currently studied. Such a potentially beneficial reinforcement could be basalt fiber [5-6]. Fibers from basaltic rocks are not new, but their suitability as reinforcement in polymer composites is a relatively new issue. Basalt fibers have good physical and chemical properties, excellent thermal, electrical and acoustic insulation properties as well as good adhesion to metals, epoxies and glues. Since its discovery by French Paul Dhé who was the first with the idea to extrude fiber from basalt and received U.S patent in 1923, basalt was a classified material of choice for military research and was extensively used in defense and aeronautical applications during World War II by the United States (US), Europe and the Soviet Union [7-9]. Basalt is an environment friendly natural material (see. Fig. 1). The basaltic rocks are used for extrusion of fibers (BFs) during industrial production. It is one type of high performance inorganic fibers which are made from natural basalt. Safe and abundant, basalt rock has long

been known for its thermal properties, strength and durability. BFs are environmental friendly as its recycling is much more efficient than glass fibers. Growing environmental awareness throughout the world has triggered a paradigm shift towards designing materials compatible with the environment. BF can be classified as a sustainable material because they are made of natural material and during its production no chemical additives or any solvents, pigments or other hazardous materials are added. When the BFs in resin are recycled the same material is obtained again as natural basalt powder as its melting point is quite high i.e. about 1400° C, this mean that composite containing basalt is incinerated, the only product left in an unmolten basalt that can be used again [12].



Fig. 1: Basalt stone [10-11].

BFs are 100% natural and inert. basalt products have no toxic reaction with air or water, are non-combustible and explosion proof. When in contact with other chemicals they produce no chemical reactions that may damage health or the environment. Even if asbestos and basalt fibres present similar composition, basalt seems to be safe, because of different morphology and surface properties which avoid any carcinogenic or toxicity effects, which are presented by asbestos instead [13-14]. In particular, Kogan et. al [13] made rats inhale air containing asbestos and basalt fibres for 6 months. In the case of asbestos fibres at a dose of 1.7 g/kg (referred to the body weight of the rat), one third of the animals died, while a dose of 2.7 g/kg killed all the rats. In the case of the basalt fibre, all the animals survived even when the dose reached the 10 g/kg concentration. Similar investigations were conducted by McConnell et. al [15] and they also concluded that basalt fibres pose no risk to human beings. It is know that the fibrous fragments with diameter of 1.5 μm or less and length (l) of 8 μm or greater should be handled and disposed of using the widely accepted procedures for asbestos. Fibres falling within the following three criteria are of concern [16]: fibres with diameters lower than 1.5 μm (some say <3.5 μm) remain airborne and are respirable; fibres with an l/d aspect ratio higher than 3 do not seem to cause the serious problems associated with asbestos; fibres durable in the lungs do not cause problems if they are decomposed in the lungs. Since most of nonpolymeric fibres have diameter significantly higher than 3.5 μm but break into long thin pieces, emission of particles, including fibres, occurs during handling. For simulation of these phenomena, the abrasion of basalt weaves was made by Militký et.

al [17]. The experimental results showed that, because the mean value of fibre fragment diameter is the same as diameter of fibres, no splitting of fibres during fracture occurs. The aspect ratio l/d of basalt fibre fragments is equal to 20.8, higher than the critical value. basalt fibers & fabrics are labeled as safe according to both the USA and the European occupational safety guidelines. Its particles or fibrous fragments due to abrasion are too thick to be inhaled and deposited in the lungs, but care in handling is recommended [18]. Basalt is a new type of fiber prepared by drawing a natural ore, melted at a high temperature, through a platinum-rhodium alloy [5]. It has numerous raw material sources. It is inexpensive [19], it has excellent properties such as corrosion resistance, minimal moisture absorption and the ability to withstand high temperatures, provide thermal insulation, and absorb sound [20-21]. It is also a high-strength material [22-24] that has been widely used in road construction [25], buildings and other applications that require reinforcement [26].

2. Chemistry and production of basalt fibers

BF is obtained from natural material which is dark colored, fine grained solidified volcanic rock. Basalt is a common term used for a variety of volcanic rocks. A hard, dense, inert rock found worldwide, basalt is an igneous rock i.e .it melts when heated, which is solidified volcanic lava. Basalt originates from volcanic magma and flood volcanoes, a very hot fluid or semi fluid material under the earth's crust, solidified in the open air. Basalt flows cover about 70% of the earth's surface. Basalt is chemically rich with oxides of magnesium, calcium, sodium, potassium, silicon, iron and alumina, in which silicon oxide (SiO_2) accounts for the main part, followed by Al_2O_3 , then Fe_2O_3 , FeO , CaO and MgO . For this reason, basalt rocks are classified according to the SiO_2 content as alkaline (up to 42% SiO_2), mildly acidic (43–46% SiO_2) and acidic basalts (over 46% SiO_2). Only acidic type basalts satisfy the conditions for fiber preparation. High silica contents are required to get glass network. The content of FeO and Fe_2O_3 plays a very important role in determining many physico–mechanical properties of BFs, such as density, color (from brown to dull green, depending on the FeO content), lower heat conduction and better temperature stability/heat resistance compared to E-glass fibers [23,26].

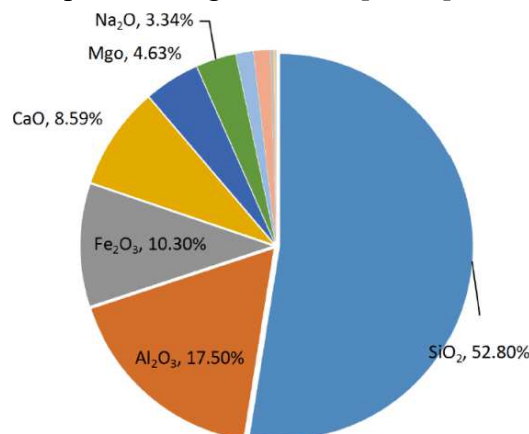


Fig. 2: Percentage distribution of chemical constituents in basalt [25]

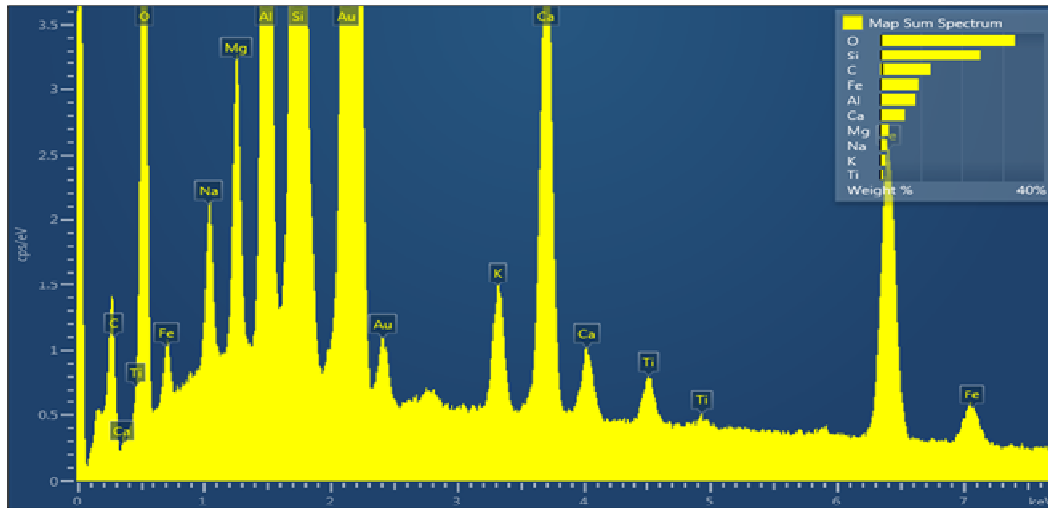


Fig. 3: Energy-dispersive X-ray analysis of basalt [27]

Table 1 shows the summary of elements detected in energy-dispersive X-ray (EDAX) analysis. Spectral analysis detected number of elements in basalt. Presence of silica (Si) (24.58 wt %) and oxygen (O) (32.98 wt %) was found to be dominant as compared to other elements.

Table 1: Elemental composition of basalt.

Element	Wt%
C	12.37
O	32.98
Na	1.64
Mg	2.16
Al	8.69
Si	24.58
K	1.34
Ca	6.03
Ti	0.81
Fe	9.40
Total:	100.00

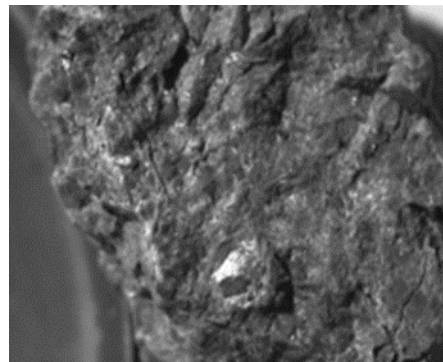
Figures 2 and 3 depict the overall percentage distribution of the chemical constituents in basalt. The chemical content may differ based on the geographical distribution. Basalt fibers are manufactured from finely powdered basalt, which is melted at around 1500–1700°C to yield a glassy molten liquid, which is then extruded in the form of thin threads. Its state is strongly influenced by the temperature rate of quenching process that leads to more or less complete crystallization. Quickly quenched melt gets solidified to glass like nearly amorphous solid. Slow cooling leads

to more or less complete crystallization, to an assembly of minerals. The chemical composition of basalt rocks influences the properties of resulting fibers probably due to different chemical components and processing conditions like drawing temperature [19, 28, 29]

Basalt rock-beds with a thickness of as high as 200 meter have been found in the East Asian countries. Russia has unlimited basalt reserves. There are large deposits of these rocks in the Ural, Kamchatka, Far East, Sakhalin, Kola Peninsula, Northwest Siberia, and the Transcaucasia. Basalt formations in the Ukraine are particularly well suited to fiber processing. Perhaps 80% of basalts are made up by two essential minerals; i. e. plagioclase and pyroxene shown in Figure 4.



Plagioclase



Pyroxenes

Fig. 4: Some basalt minerals [30-31]

The fibers are chemically composed of pyroxene, clinopyroxene, olivine, and plagioclase minerals [32]. Based on the above chemistry, if the basalt is rich in silica and poor with sodium it is categorized as tholeiitic basalt. If the basalt is rich in sodium and deficient in silica then it is categorized as alkaline basalt. Further, if the mineral is rich in alumina with a concentration over 17%, then the basalt is categorized as an intermediate between the tholeiitic and alkaline basalt. Magnesium-rich basalt is called boninite, which has extremely small concentrations of titanium and other trace metals [7]. In Figure 5, the network structure of basalt is shown[33].

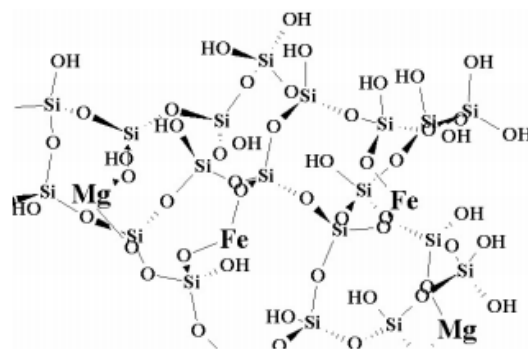


Fig. 5: Network structure of basalt

Interest to BF emerged in the middle of 20th century when rocket, nuclear and electronic sectors were in demand for materials with special properties like strength of alloyed steel while significantly lighter and heatproof. Properties of fiberglass, for which industrial production had been already adopted in 1940s, failed to meet requirements of special applications. Carbon fibers are the best in terms of strength, durability and temperature range of application, but they are the most expensive also. Basalt continuous fibers were considered to be a material that excels fiberglass in most of technical characteristics, and at the same time is comparable in terms of production cost and price. The next generation inorganic basalt fiber is expected to rival the general-purpose glass fiber [34]. Basic physical and mechanical properties of basalt fibers and a comparison with different other commercial fibers are depicted in Table 3, which shows that basalt has an excellent tensile strength and also a good modulus. When compared with other materials, one can infer that the majority of the materials of choice are costly, heavy, chemically unstable, or tough to handle and require longer curing preparations and methodologies to obtain good composites. In contrast, basalt is eco-friendly, nontoxic, lightweight and easily affordable, making it an ideal candidate for fabricating composites for several applications.

Table 2: Comparison of chemical compounds in glasses and basalt (in weight % = w%)

Compound	w% in E-glass	w% in S-glass	w% in C-glass	w% in Basalt
SiO ₂	52-56	64-66	64-68	51.6-57.5
Al ₂ O ₃	12-16	24-26	3-5	16.9-18.2
CaO	16-25	0-0.3	11-15	5.2-7.8
MgO	0-5	9-11	2-4	1.3-3.7
B ₂ O ₃	5-10	-----	4-6	-----
Na ₂ O	0.8	0-0.3	7-10	2.5-6.4
K ₂ O	0.2-0.8		7-10	0.8-4.5
Fe ₂ O ₃	Less than 0.3	Less than 0.3	-	4.0-9.5
FeO	-	-	-	2.14

Table 3: Physical and mechanical properties [26, 35, 36]

Properties	Basalt	E-glass	S2-glass	Aramid	Carbon
Density [kg/m ³]	2630-2800	2540-2570	2540	1450	1780-1950
Filament diameter [μm]	6-21	6-21	6-21	5-15	5-15
Tensile strength of single filament [MPa]	3000-4840	3100-3800	4020-4650	2900-3450	3500-6000
Initial modulus [GPa]	93-110	72.5-75.5	83-97/86	70-140	230-600
Elongation at break [%]	3.1-6	4.7	5.3	2.8-3.6	1.5-2.0
Sound absorption coefficient [-]	0.95-0.99	0.8-0.93			

Basalt applications are well known from roman age where this material was used in its natural form as a paving and building stone. The first basalt fiber samples were received in 1959-61 by the Ukraine scientific research institute in the former Soviet Union. The first continuous basalt fibres of satisfactory quality were produced with laboratory equipment in 1963. It was in 1963, when the first publication about BCF appeared in “The glass and ceramics” magazine. By 1985, the first industrial installation i. e furnace that adopted 200 nozzles drain board combination oven bushing process for BCF production was designed and commissioned in a factory near Kyiv Region (Ukraine) [38]. Today, basalt fiber research, production and most marketing efforts are principally based in some of countries once part of the Soviet Union (Georgia, Ukraine, the same Russia) and in China [7,19]. In 2000 the joint Ukraine-Japanese enterprise of BCF production was established. In addition to Japan, South Korea, China, Austria and USA are working on BCF technology. The EU and some other countries have basalt fiber research programs.

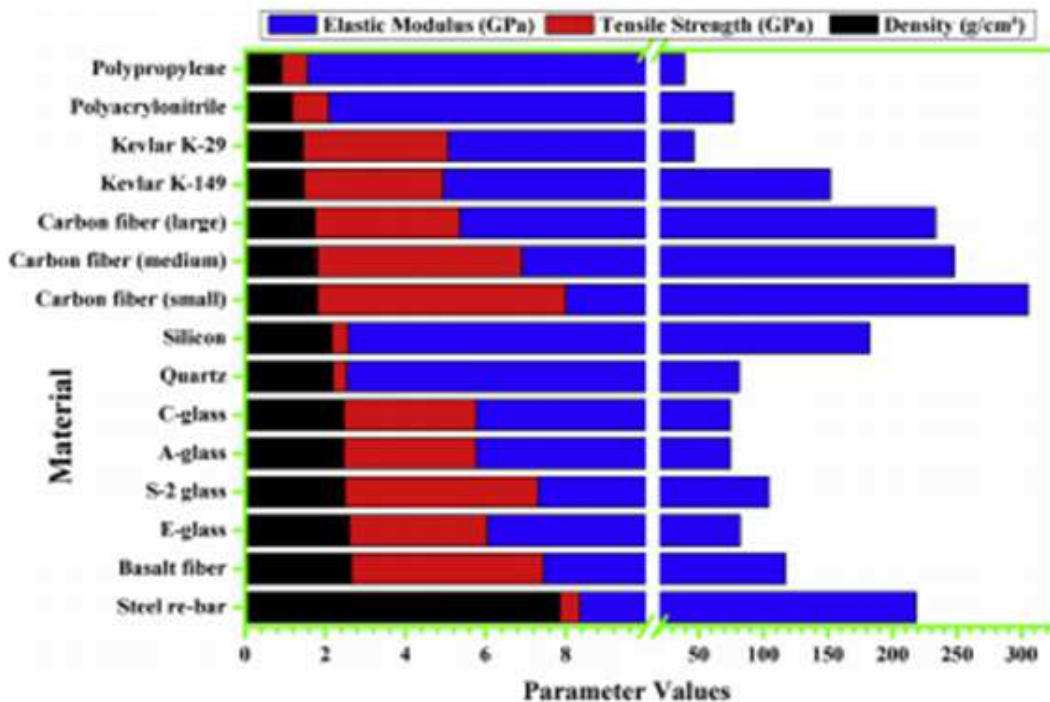


Fig. 6: Stacked bar chart depicting the comparative mechanical properties of different known materials [37].

Overall, the manufacturing process of this kind of fibre is similar to that of glass fibre, but with less energy consumed and no additives, which makes it cheaper than glass or carbon fibres. Basalt fibers are divided into two big groups: Discrete/Short fiber (mineral insulating wool, staple fiber) also known as basalt fiber (BF) and basalt continuous fiber (BCF). BCF production technology is young enough and being improved further. Short length basalt fibers can be produced directly from crushed basalt stones and the technology is very simple so the fibers are very cheap, but they have relatively poor and uneven mechanical properties.

BF can be manufactured by Centrifugal methods/melt blowing technology (centrifugal-blowing and centrifugal-multiroll)and BCF by spinneret method [39]. The technology is very simple and efficient so the fibers are very cheap, but they have relatively poor and uneven mechanical properties. An important application of basalt fibers is the substitution for asbestos, e.g. in car brake pads, due to its high temperature resistance. The basalt fibers used as insulating materials in the construction and automotive industries are produced by so-called blowing technology with centrifugal cylinders (e.g. Junkers method). It is used for manufacturing cheap fibers with 60–100 mm length and 6 – 10 μ m diameter. Basalt fibers are produced in one step, directly from crushed basalt stone. Continuous process is used for the production of basalt fiber just like glass. Quarried basalt rock is crushed, washed and loaded into a bin attached to feeders that transfer the material into melting baths in gas-heated furnaces. As basalt fiber is less complex so its processing is much easier than glass fiber. Glass is typically 50 percent silica and consists of boron oxide, aluminum and several other minerals materials that must be fed independently into a metering system before entering the furnace. Unlike glass, basalt fibers feature no secondary materials. The process requires a single feed line to carry crushed basalt rock into the melt furnace. The essence of the method is that the basalt rock melt 1450 -1500^oC coming from the gas-heated furnace is transmitted to a horizontal shaft fibre spinning machine that has three centrifugal heads and consists of one accelerating and two fibrillizing cylinders. The lava adhered to the heads flies off due to the centrifugal force and as a result of blowing 60-100 mm long fibers of 6-10 μ m diameter are formed from the viscous liquid [40-42] As the melt is blown off from the cylinders by air jets, fibres are formed in the air blast and solidify quickly in a glassy amorphous phase. The characteristics of Junkers technology cause the formation of the so-called fiber heads. The fiber heads are spherical objects with the diameter of 10 to 100 times the fiber diameter. While some of them break from the fibers, the others mostly the smaller ones – remain on the fiber end. This happened due to reason that molten basalt is cooled down gradually from very high temperature to get fiber and hence smaller or larger "heads" remain at their ends depending on fiber length and affect adversely to the strength and toughness of fiber[43].

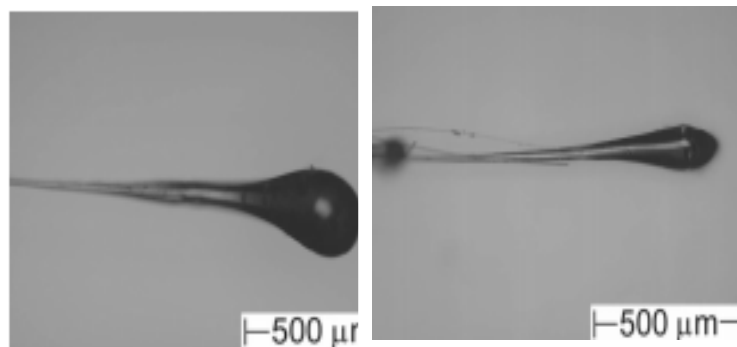


Fig. 7: Optical micrographs of fiber heads on short basalt fiber made by Junkers method [43].

Other technology used for production of fibers for insulating purposes is the centrifugal-multiroll system, comprising a number of high speed rotating wheels. The stream of basalt rock melt coming from the gas-heated furnace flows vertically down onto the surface of the first wheel, where it is thrown sideways by the wheel motion. Further strategically placed wheels continue the process until finally fibres, with a typical diameter of approximately 10 microns, are produced [44]. For more demanding applications continuous fibers, which can be processed by textile technologies, are prepared by spinneret technology from the melt spinning, similarly to traditional glass fiber production. Glass and basalt have different manufacturing processes despite the fact that both are inorganic. Glass fibers are produced from melted charge (composed of quartz sand, soda, limestone, fluxing agents, etc.) to obtain glass, needed to create the desired chemical and physical properties of the final product, from which fibers are obtained by blow with steam, air or at centrifugal.

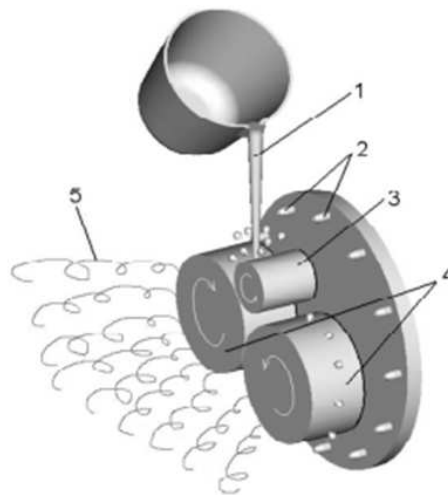


Fig. 8: Junkers type basalt production (1 – basalt lava, 2 – blowing valves, 3 – accelerating cylinder, 4 – fiberization cylinder, 5 – basalt fibers) [39-42]

Additional steps and ingredients will always increase production cost. No flux like boric oxide is added for processing. Basalt fiber is obtained, from melted of basalt rocks without any additives [45,46]. At present, there are several methods for fabrication of continuous basalt fiber that differ from each other in furnace and feeder designs, cooling and winding mechanisms, etc. At present time in the world there are two main variants of technologies and equipment for basalt continuous fiber production. There are big melting furnaces with long feeder (feeding installation and technological lines consisting from modular units. In principle manufacturing process of all producers includes following key operations: [47,48].

- Raw material preparation;
- Rocks melting;
- Melt homogenization and delivery to bushings;
- Melt drawing through bushing units;
- Drawing of elementary filaments, application of sizing agent and winding on bobbins.

Raw material preparation for basalt is much easier than glass fiber preparation. Raw material can be stored in open air without packing. Basalt rocks for BCF manufacture are prepared in peculiar way – crushing to fractions of 5 mm - 40 mm, separation of metal and magnetic impurities by method of magnetic separation, screening and washing out small inclusions (dust, etc.) then drying either at natural air circulation, or in a special dryer. Prepared raw material is periodically loaded into the hopper of the loader mounted above the smelting furnace. The manufacture of basalt fiber requires the melting of the quarried basalt rock at about 1450 °C. The molten rock is then extruded through small nozzles to produce continuous filaments of basalt fiber. These operations are quite simple, especially if we consider that primary fusion, homogenization and enrichment of basalt initial raw material was made by ancient volcanoes, i.e. by nature. Basalt fibers are produced from basalt rock using single component raw material by drawing and winding fibers from the melt. There are certain things about basalt that make it attractive and economically comparable with production of glass fibers, like S-2.

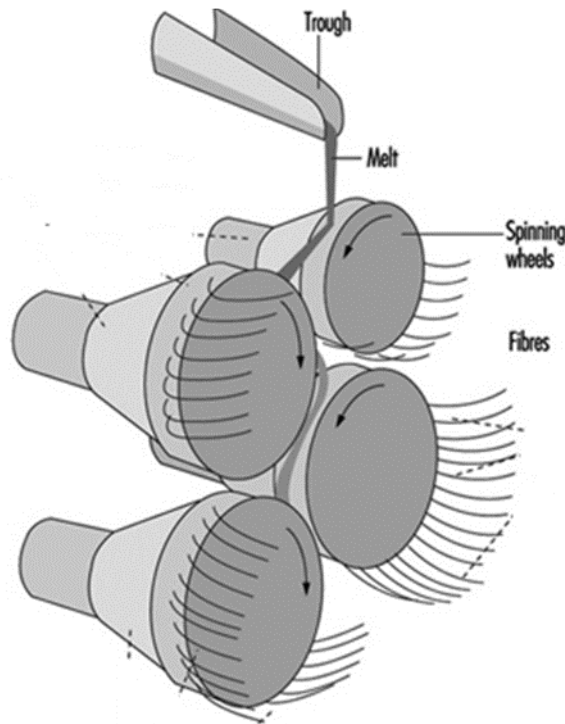


Fig. 9: Centrifugal-multiroll system[44]

The production of basalt fiber in commercial scale is not easy as for glass fiber. As basalt stone is of natural origin, basalt fiber manufacturers have less direct control over the purity and consistency of the raw basalt stone, as mineral level and chemical composition can differ from one location to another. Basalt and glass are both silicates, molten glass, when cooled, forms a non crystalline solid. Basalt, however, has a crystalline structure that varies based on the specific conditions during the lava flow at each geographical location. Moreover, the rate of cooling, when the original flow reached the earth's surface, also influenced the crystal structure [39,46, 49].

The main problem in manufacturing of basalt fibers are the gradual crystallisation of various structural parts like plagioclase, magnetite and pyroxene. This arises mainly because of difference in the crystallisation temperature (T_c) of the different components, which varies from $720^\circ - 1010^\circ \text{C}$ (magnetite $T_c - 720^\circ$, pyroxene $T_c - 830^\circ$ and plagioclase $T_c - 1010^\circ \text{C}$) melt. Crushed basalt enters the furnace, the material is liquefied at a temperature of 1450°C (glass melting point varies between 1400°C and 1600°C). Opaque/dark color of basalt absorbs rather than transmits infrared radiation unlike molten glass which is more or less transparent to Infra red radiation, which allows heating from the top (gas burners) while obtaining a sufficiently homogeneous temperature in case of basalt is challenging. Heating molten basalt from the top results in a non-homogeneous temperature in the melt with a negative temperature gradient of about 80°C per inch from the bath's surface down. Use of overhead gas burners in conventional glass furnaces is more difficult for uniformly heat the entire basalt mix. This can be overcome to some extent by holding the melting basalt in the reservoir for extended periods of time - up to several hours - to ensure a homogenous temperature [25].

Basalt producers have employed several strategies to promote uniform heating, including the immersion of electrodes in the bath with high currents running between them. The Joule effect ensures the needed additional heating of the melt. Finally, a two-stage heating scheme is employed, featuring separate zones equipped with independently controlled heating systems. Only the temperature control system in the furnace outlet zone, which feeds the extrusion bushings, requires great precision, so a less sophisticated control system may be used in the initial heating zone [40, 49].

The next stage is the filament stretching and winding, with automatic speed control, to get the filament down to its precise diameter.

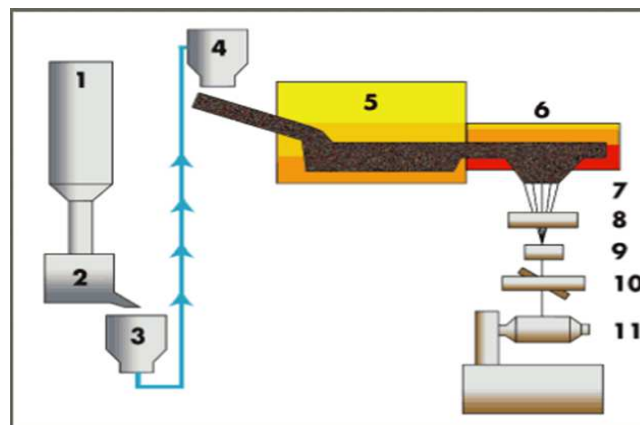


Fig. 10: Basalt fiber spinning [43]. 1) Crushed stone Silos (raw material supply) ,2) weighing, dosing and mixing station, 3) Transporting system, 4) batch charging station, 5) Initial melt zone, 6) Secondary controlled heat zone (forehearth), 7) Bushings (BCF formation), 8) Sizing applicator, 9) Strand formation, 10) Traversing, 11) Winding.

Basalt stone is molten in two steps: in the initial furnace it is fused, then conveyed to the secondary heating zone feeding the extrusion bushings, equipped with a

precise temperature control system. A single-component basalt material is fed into a gas-fired furnace. The basalt broken stone is heated to about 1,450°C (2,650° F) and melted in a rhenium-platinum pot, lead to a spinneret made from the same material and spun gravitationally through holes in the spinneret bottom at 1350–1420 °C. The filament bundle is taken up downwards at about 2000–5000 m/min, prepared at 1.0 to 1.2 meters below the spinneret, then spooled. From the furnace, the molten material flows into a fore-hearth where the temperature of the molten material is more precisely controlled and distributed to each strand-making position. The molten material is gravity-fed from the fore-hearth at each forming position into a platinum alloy “bushing”. Electricity is passed through the bushing to provide a final stage of resistance heating and precise adjustment of the viscosity of the molten mixture. Each bushing has hundreds of micro-orifice each make a filament that is gathered into a single strand of continuous-filament basalt fiber. The no. of orifice (holes) and its diameter of the spinnerets are determined by the end use of the fibre. The fiber dimensions are generally in the range of 10–20 µm. The combination of micro-hole size and viscosity of the melt determine the diameter of the resulting filaments. Silane based sizing liquid is applied on them to impart strand lubricity, integrity and resin compatibility. These Filaments strands are collected together and forwarded take up device for winding. Recently, Kim et. al [50] proposed melt-spinning method based on dielectric heating in order to produce fibres on laboratory scale. The continuous strand of multiple filaments can then be twisted into a yarn, plied into a multi strand roving or cut into chopped fiber. The BCF can be converted into woven or nonwoven textiles or used to reinforce composite structures with techniques similar to those used with continuous filament fiberglass.

3. Influence of acids and alkalis on mechanical behavior of basalt fibers

Basalt fibers have high chemical resistance / durability and superior corrosion resistance as reported in the literature. Basalt fibers belong to the first hydrolytic class, and on acid and alkali steam resistance is far superior to glass fiber [49-54]. Basalts are more stable in strong alkalies than glass, but stability in strong acids is slightly lower. However, other authors showed better resistance of the basalt fibres in acid environment rather than in alkali one [52]. Therefore pipes made of basalt fibers may be used in the chemical production for transporting hot acids, in the construction of sewerage systems, transportation of aggressive liquids etc. For the first time, the chemical durability of basalt fibre was studied by Ramachandran et. al as early as 1981 [56]. The authors stated that this fibre has excellent resistance to alkaline attack, but it has poor resistance to acids. Van de velde et.al [57] investigated mechanical properties (rovings after immersion in 0.4N KOH (in saturated Ca(OH)₂, pH = 13.2, simulation of concrete conditions) were carried out. These results confirm basalt's better resistance to alkali, compared to E-glass. Nasir et. al [58] later showed that the better mechanical behaviour of the basalt fibres than glass ones after corrosion treatments. They investigated crack formation and corrosion of basalt fiber in sulfuric acid. Using microscopy and elemental mapping tools, they attempted to examine and explain the cause of corrosion in terms of leaching of calcium and ferric

ions from the surface of the basalt fiber. The appearance of spiral and axial cracks throughout the surface of the fiber is attributed to longer exposure times. Even if the corrosion mechanism is similar, the degradation in E-glass fibres is more severe and it is concluded that basalt fibres would be a suitable replacement in corrosive environments. Wei et. al [52-53] studied the effects of surface chemical corrosion on basalt and glass fibers in both acidic (HCl) and alkaline (NaOH) media. They also examined post-treated fibers in terms of their strength maintenance ratio and mass loss ratio. They observed that basalt fibers were extremely resistant to acid attack rather than alkaline attack, whereas for glass fiber, alkali and acid resistance was similar [59]. They concluded that amongst these solutions, alkaline conditions were the most corrosive for basalt.

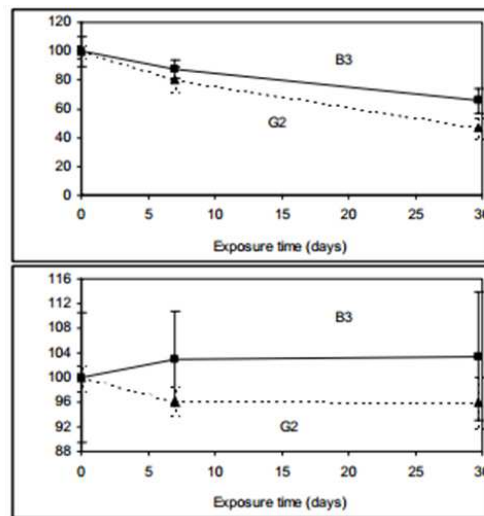


Fig. 11: Relative tensile strength of basalt and glass fiber[57]

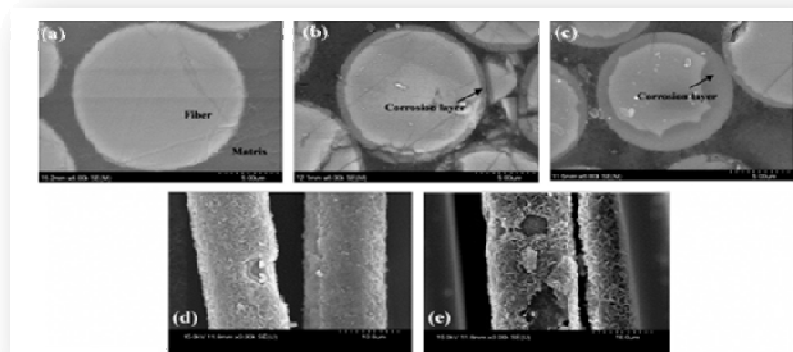


Fig. 12: Cross sectional SEM images of basalt fiber before and after acidic (HCl) treatment, (a) original basalt fiber, (b) 1 h post acidic treatment, (c) 3 h after acid treatment. Alkali (NaOH) treated SEM images of (d) glass fiber and (e) basalt fiber surface. [53].

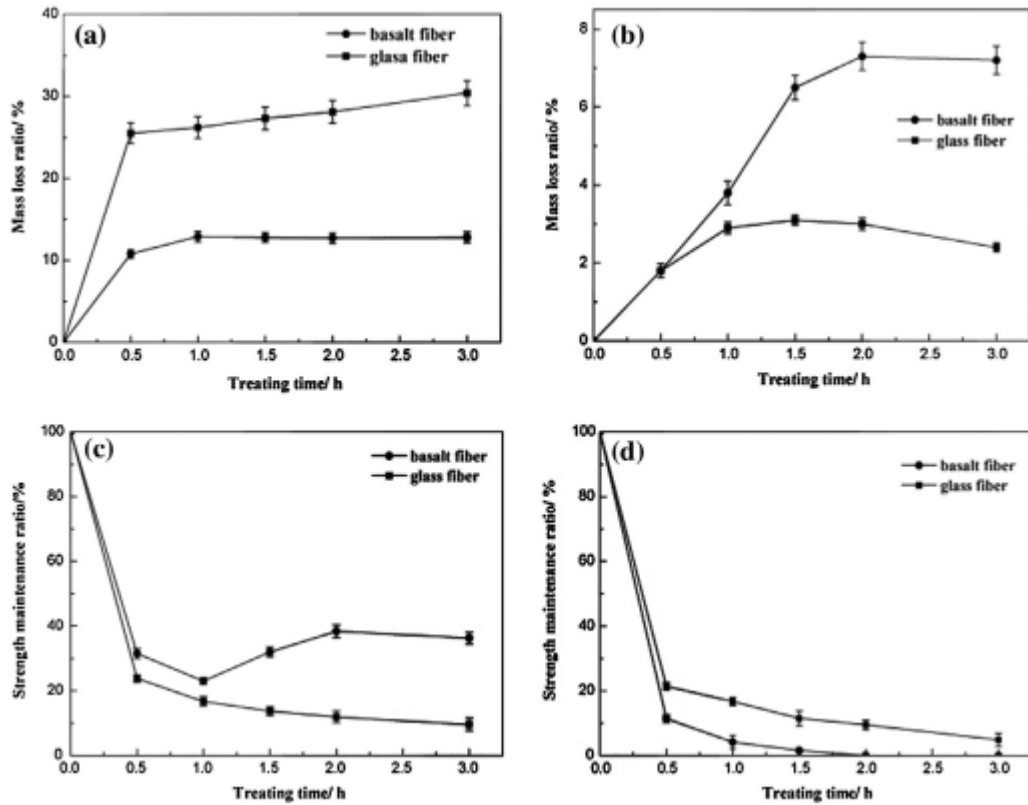


Fig. 13: Depicting activity of acid and alkali on the basalt fibers and glass fibers, respectively. (a) Relation between mass loss ratio and treating time of fibers during acid treatment. (b) Relation between mass loss ratio and treating time of fibers during alkali treatment. (c) Relation between strength maintenance ratio and treating time of fibers during acid treatment. (d) Relation between strength maintenance ratio and treating time of fibers during alkali treatment [53].

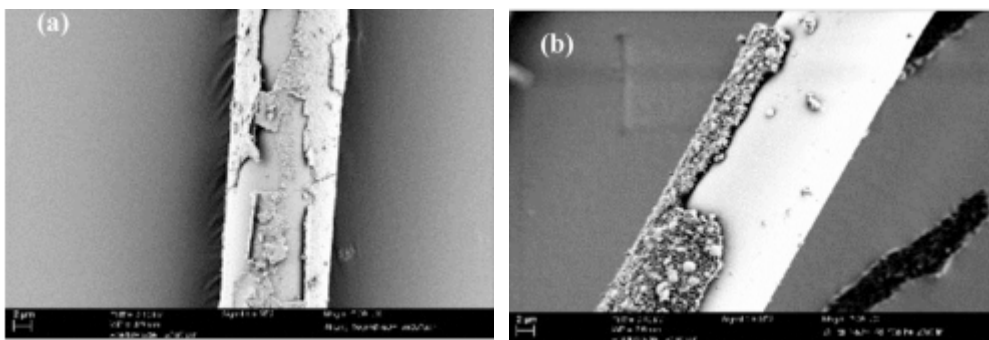
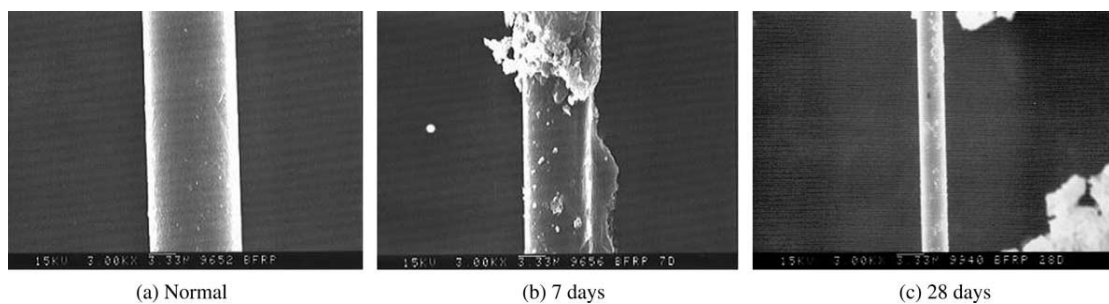


Fig. 14: SEM image revealing the formation of corrosion layer on the surface of (a) glass fiber-AR grade stored at 60 C in 5% NaOH for 7 days and (b) basalt fiber stored at 40 C in 5% NaOH for 7 days [55].

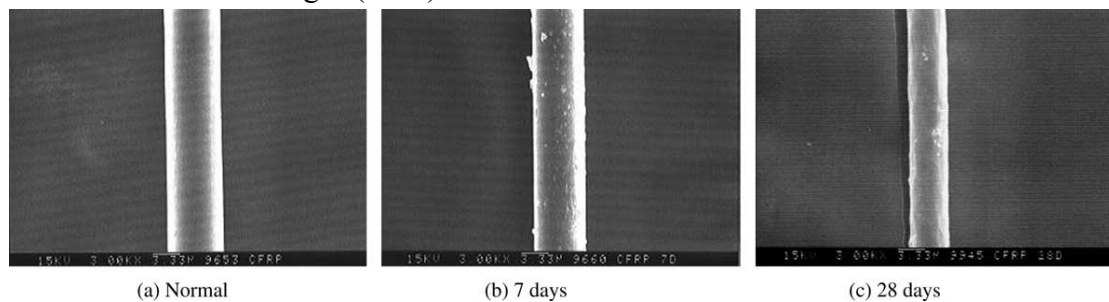
Scheffler et. al [55] Investigated the ageing of glass and basalt fibres with different chemical compositions in NaOH and cement. They observed that calcium ions play an important role in the inhibition of corrosion activity. Also, they observed that during aging in a NaOH solution, the outer surface of the fibers corroded i.e the formation of a brittle layer surrounding the axial length of the fibers extensively when

compared to the fibers exposed to the cement solution for a very long ime. Under such conditions, local attack was revealed on the fibers. This brittle layer often is peeled off, resulting in a decrease in the diameter of the fiber and degradation of its mechanical properties. In particular, in NaOH solution the failure stress steadily decreases, being interrupted by phases of increasing stresses. In contrast, the filaments in cement solution do not reveal decreasing failure stresses over a vast interval of temperature and time.

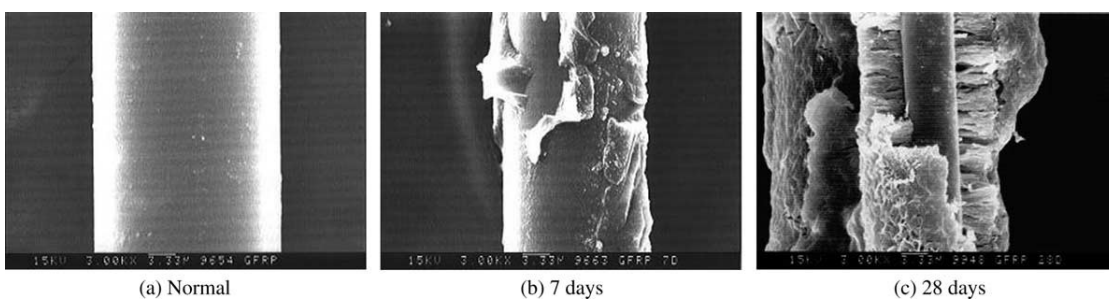
Sim J et.al [19] in order to investigate the alkali resistance of the basalt fiber, glass fiber and carbon fiber immersed in a 1 M NaOH solution for 7, 14, 21. and 28 days.They observed that the basalt and the glass fibers lost their volumes and strength significantly under alkali condition as compared to carbon fiber at 28 days of immersion.



SEM images (3KX) of basalt fibers under NaOH solution



SEM images (3KX) of Carbon fibers under NaOH solution

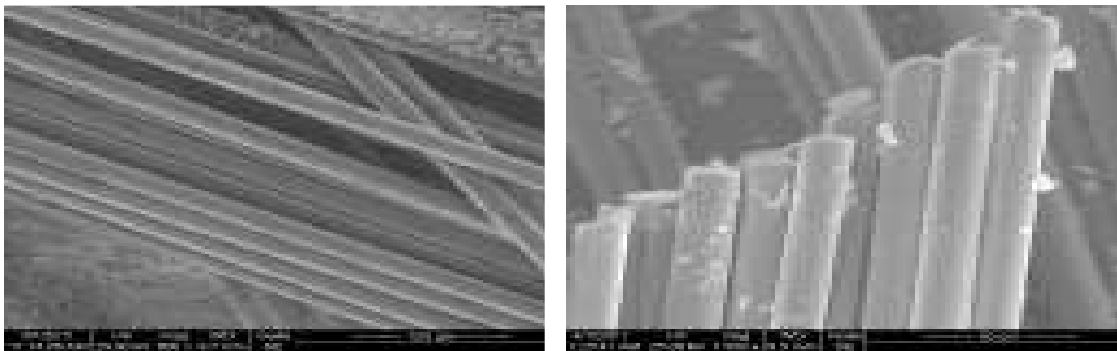


SEM images (3KX) of Glass fibers under NaOH solution

Fig. 15: Comparison of damage under alkaline conditions [19].

Rybin et. al [59] showed that the zirconia coating slows down the corrosion of basalt fibre in alkali solution, with higher extent by applying dense zirconia coating than the porous coating on fibre surface. Moreover, the uncoated and coated basalt fibres were used as reinforcements in cement matrix showing that the surface of the coated fibre

is affected by the alkaline medium of the cement matrix to a smaller extent than the surface of as-received basalt fibre. Basalts are slightly less stable in strong acids as compared to their behavior against alkalis which is very stable when exposed to strong alkali; rather it can with stand alkaline medium as strong as pH of 13-14. They can retain up to 92% of their properties in 2 (n) NaOH and up to 75% of their properties in 2 (n) HCl acid and results in weight loss of only 2.75 % and 2.2% respectively as shown in figure 15. At short-term exposure in strong mineral acid solutions, no fiber strength was observed while a long-term (more than 100 h) impact of hydrochloric acid solutions can cause strength reductions of 15%-20% [18]. This reduction proceeds more slowly for basalt roving with smaller filament diameter than for glass roving. When basalt is boiled with water, alkali or acid, its weight loss is significantly low that is why it is common in use in concrete reinforcement materials in the form of bars [18,19, and 52].



Basalt fiber under 2N HCl at 20 °C after 32 days

Glass fiber under 2N HCl at 20 °C after 32 days

Fig. 16: SEM images of basalt and glass fiber [18]

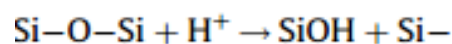
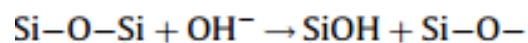
Table 4: Comparative chemical resistance properties

Properties	Basalt	E-Glass
% Weight loss in 3 hours boiling in water	0.2	-
%Weight loss in 3 hours boiling in saturated cement solution(pH=12.9)	0.35	4.5
%Weight loss in 3 hours boiling in 2N HCL	2-7	38.5
%Weight loss in 3 hours boiling in H ₂ SO ₄	6	22
%Weight loss in 3 hours boiling in NaOH	6	-

Militký et.al [60] explained the mechanism of degradation of basalt fiber during chemical action. They investigated that during the degradation process the chemical solution attacks the surface and subsurface layers. Direct investigation of fibers diameter after long-term degradation has shown that the predominant mechanism is opening of crazes and degradation in the volume of fibers. Step by step removal of surface layers was negligible. Therefore the reason of degradation is the reaction of chemical solution with some cations (in the case of acids) or anions (in the case of alkalis) from basalt fiber body. The mechanisms involved in acid or alkaline attacks on the fibers are totally different. The strength of both of these attacks is directly proportional to time and temperature. Further, the chemical makeup of the fibers determines the resistance to wetting by water.

In case of acid attack, it is very interesting that degradation is due to opening and creation of long crazes in the fiber axis mainly. After long-term exposure the crazes in direction perpendicular to fiber axis are appeared. Result is great loss of durability and disintegration of fibers in long degradation times. The degradation is accompanied by the great loss of mechanical properties especially tensile strength. The increasing of pH acid solution after degradation is in accordance with assumption of reaction of HCl with cations and destroying the glass like network. The chloride salts replace the intermediate oxides as MnO₂, Fe₂O₃ and Al₂O₃. These salts are typically well soluble in water and these phenomena supported the basalt degradation due to action of acid.

During an alkali attack, the chemical resistance depends purely upon the mixture of various oxides. The acid resistance increases with increasing silica content, whereas the alkali resistance increases due to the presence of a high concentration of alkaline earth elements and alumina. On the surface of the fiber, reaction products developed and fell apart as the immersion period increased, consequently, decreasing a sound part or volume of the fibers. Those reaction products were assumed to be from the reaction between SiO₂ in the fibers and alkali solution. The hydroxyl ion of the alkali breaks the Si-O-Si linkage [53]. In acid and alkali solution, the Si-O-Si network is destroyed by OH⁻ and H⁺. The reactions are explained by the following equation:



Thus, an increase in the treatment concentration of fibers strengthens the surface OH peak intensity. Whereas, metal oxide peaks are weakened in FTIR analysis as examined by researchers [23,59,61]. The presence of intermediate oxides like MnO₂, Fe₂O₃ and Al₂O₃ always improve the alkaline durability. An attack over a long period of time dissolves the Si₂O skeleton structure, which results in loss of mass and also, the surface of the fiber eventually becomes rough. Further, this deteriorates the fiber elasticity and makes it brittle. Thus, the fiber surface progressively forms a loosely bound layer of reaction products, which thickens over the time and does not prevent further alkali attack. This corrosive activity of an alkali over the fibers results in loss of rigidity.

4. Influence of temperature on mechanical behavior of basalt fibers

Recent research showed that basalt fibers have a good thermal/heat resistance and humid absorption. ,moisture absorption of basalt fiber for 24 hour is less than 0.02% while for glass it is 1.7%. Moisture regain of basalt fibers is 1% [39]. Producing industrial glass fiber especially in the neutral composition can absorb significant amounts of moisture in the humid air. This affects their physical and technical properties and durability and eventually leads to destruction of fibers. Basalt fibers absorbency is low and is not changing over time hygroscopicity (0.2-0.3%), due to its chemical composition. Basalt fibers have excellent heat and flame resistance, nonflammable, no dripping behavior and no or very low smoke development (combustion of sizing). Hao et. al [62] investigated the thermal stability of basalt and glass fiber .In the initial stage, where the temperature range is below 200 °C,with the increase of temperature the mass remains nearly constant. However, the mass loss occurs in the temperature range of 200–350 °C. In this stage, the mass loss is very fast and significant. It is clearly observed that the fibers resemble in the thermal behavior, but basalt fiber has better thermal stability than glass fiber.Also its mass loss is less than glass fiber 1.76% for glass fiber and 0.74 for basalt fiber.

Table 5: Comparative Thermal properties [26, 39]

Properties	Basalt	E-glass	S2 -glass	Aramid	Carbon
Temperature withstand [°C]	-260 +600	-50....+450	50....+300	+205	-50....+700
Max application temperature [°C]	Approx. 700-720	Approx. 380	Approx. 500	Approx. 250	Approx. 400
Melting temperature [°C]	1450	1120	1550	NA	NA
Thermal conductivity at 25+/-5 [W/m K]	0.031-0.038	0.034-0.04		0.04	
Thermal expansion coefficient [ppm/°C]	8.0	5.4			

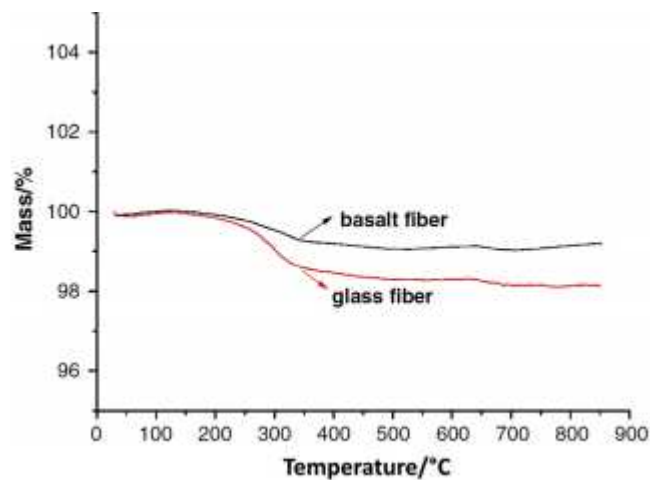


Fig. 17: TGA curves for glass and basalt fibres [62]

Basalt fibers provide thermal stability characteristics in the long run. They are resistant to the influence of high temperature for a short time period up to 750 °C whereas during longer work the working temperature is in the range from 260 °C to 700 °C; single impact of temperatures – up to 1000 °C. After exposure under 400 °C Basalt fiber loses their initial strength only 20-25% without loss of insulation properties, while strength of E glass under same conditions drop more than 40-45% [12,63,64]. Militky et. al [17] studied the tensile properties of basalt fiber by tempering it at different temperatures of 50, 100, 200, and 300 °C. They found that, due to the thermal effect, there were some morphological and structural changes observed within the fibers including a change in tensile properties. They concluded that the fibers showed strong tensile properties when the fibers were treated below 300 °C for a period of 1, 15 and 60 min. At high temperature structural changes are observed. Gilewicz P et. al [63] studied the influence of the fatigue bending of textile packages consisting of aluminised basalt woven fabrics, textile inserts and linings on their structural and thermal insulation properties. Milman SB et.al [64] also investigated the basalt fibre cardboard at compressive load at 77–293 K, for their application as load-bearing insulation for flat-wall cryogenic Dewars with flexible shells. Sim et.al [19] investigate the thermal stability of basalt, glass and carbon fibers, the fiber samples were heated in a high-temperature oven for 2h at 100, 200, 400, 600 and 1200 °C. 1200 °C temperature is good simulation of fire event. Up to 200 °C, the variation in strength was neither significant nor clear in tendency. Over 200 °C, however, a decrease in strength became distinctive as the heating temperature increased. The reduction was more significant in the carbon and the glass fibers but the basalt fibers retained about 90% of the normal temperature strength up to 600 °C. At 1200°C, the carbon fibers looked completely molten losing volumetric stability and the glass fibers partially. The basalt fibers still maintained its shape and seemed to have not lost the mechanical integrity. Li [65] confirmed this conclusion.

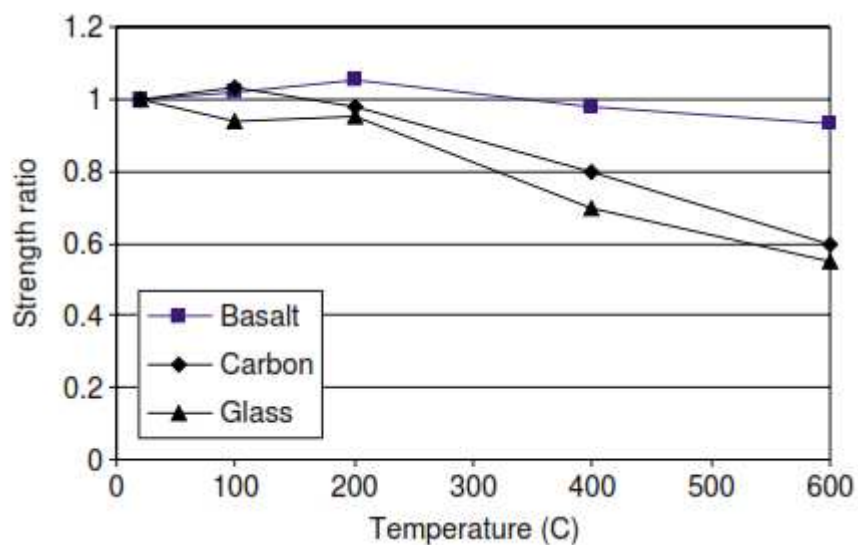


Fig. 18: Strength variation with respect to heat exposure[19]

This high thermal stability, i.e. heat resistance, is based on the material characteristics of natural basalt rocks, which nucleates at high-temperature. Desirable physical and mechanical properties of fibrous materials are attributed to the homogeneous and fine distribution of crystalline phases. This desired microstructure can be obtained by adding a nucleating agent such as TiO_2 , ZrO_2 or P_2O_5 . The basalt rocks, however, do not require but produces a natural nucleating agent (nucleates at high temperature) such as Fe_3O_4 during the melting process, hence giving advantages over the other fibers, where nucleating agents are necessary to obtain similar microstructure [66]. Van de velde et. al [57] investigated mechanical properties with respect to temperature. After thermal treatment (2h) on basalt and glass it is concluded that basalt can retain its properties over a greater temperature range than glass. At temperatures over 400-500°C it becomes weaker than glass, but it does retain integrity and still provides protection against heat.

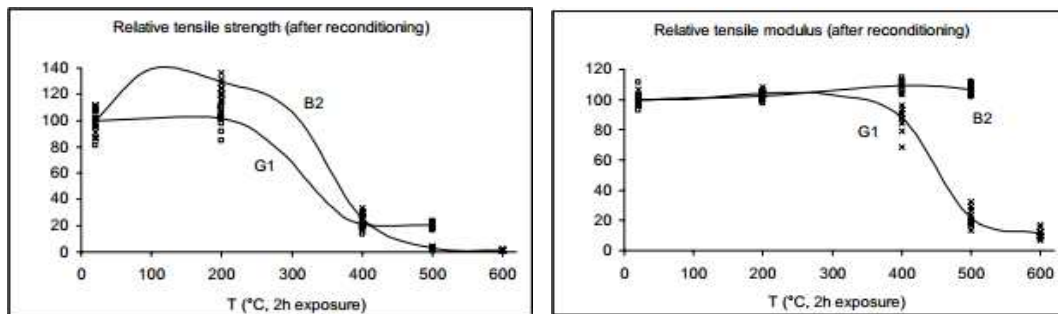


Fig. 19: Relative tensile properties after thermal treatment.[57]

Knot'ko et. al [67] studied the heating of basalt glass up to a temperature higher than 600°C is accompanied by competitive processes of oxidation of Fe^{2+} with the evolution of spinel phases ($(\text{Mg}, \text{Fe})_3\text{O}_4$) and the crystallization of a glass matrix (including formation of a mixture of crystalline silicates and aluminosilicates). Excellent resistance to acids and other aggressive chemicals in combination with thermal properties make basalt fibers suitable in applications, where other materials fail and does not work any more.

5. Tensile strength and failure of basalt filament fibers

High modulus, good strength, elastic behaviour and excellent impact properties make basalt fiber, a good alternative to the traditional ones and in particular, continuous basalt fibres are competitive with glass fibres. Similar Density to E-Glass by much more higher performance. Regarding the mechanical properties are basalt fibers positioned between E-Glass fibers and S-Glass fibers. Militky et.al[33] investigated the mechanical properties of commercial basalt filament roving from company Kaneniy Vek (abbreviation KV) and basalt filament roving company Basaltex (abbreviation BAS). There exist significant differences between ultimate mechanical characteristics of basalt fibers from both sources. The strength distribution of basalt filaments was modeled by the two parameter Weibull type model.

Table 6: Geometrical and mechanical parameters of basalt

Material	KV	BAS
Fiber diameter [μm]	12.96	13.74
Roving fineness [tex]	320	330
Fiber fineness [tex]	0.336	0.377
Number of fibers in roving	952	975
Mean fiber strength [GPa]	3.58	2.79
Standard deviation of fiber strength [GPa]	1.06	0.45
Coefficient of variation of fiber strength [-]	29.61	16.29
Mean bundle strength experiment. [GPa]	1.35	0.92
Standard deviation of fiber strength experiment [GPa]	0.13	0.06
Mean bundle strength predicted [GPa]	2.13	1.97
Standard deviation of fiber strength predicted [GPa]	2.81	0.98
Fiber strength utilization factor [-]	0.377	0.330
Weibull scale parameter A	0.056	0.000732
Weibull shape parameter C	3.77	7.32

Militky et. al [25] studied the tensile properties of basalt fiber (coated with PET) and commercial glass fiber sewing threads i.e Tygaflor. They investigated that fracture occurs due to nonhomogeneities such as surface flaws, structure defects and impurities in the fiber bulk (probably near small crystallites of minerals). These heterogeneities make the measured mechanical properties remarkably lower than their maximum theoretical values and can be described by a three-parameter Weibull distribution.

Table 7: Properties of glass and basalt sewing threads

Property	Tygaflor	Basalt/PET
Fineness [tex]	284+ ₋₂	283.3+ _{-1.6}
Thread diameter [mm]	0.56+ _{-0.02}	0.72+ _{-0.05}
Strength at break [N/tex]	0.32	0.34
Strngth at break in loops [%]	49.81	33.35
Elongation at break [%]	1.87+ _{-0.16}	2.3+ _{-0.2}
Abrasion resistance [cycles]	1214+ ₋₁₇₈	180+ _{-49.8}
Number of breaks in sewing test	8	0

Deak et. al [68] investigated the mechanical properties of glass fiber ,short basalt fiber and three Continuouse basalt fibers from different manufacturer .They concluded that all tested fibres have a rigid behaviour, without plastic deformation. The tensile modulus and strength of continuous basalt fibres and glass fibre are quite similar, while short basalt fibres are considerably less stiff. The joint SiO_2 and Al_2O_3 content (denominated as ceramic-like materials) of basalt fibers showed correlation with tensile properties of fibers, especially if basalt fibers were considered without glass fibers. It was concluded that continuous basalt fibers were competitive with glass fibers and short basalt fibers were weaker in terms of quality and mechanical properties [69].

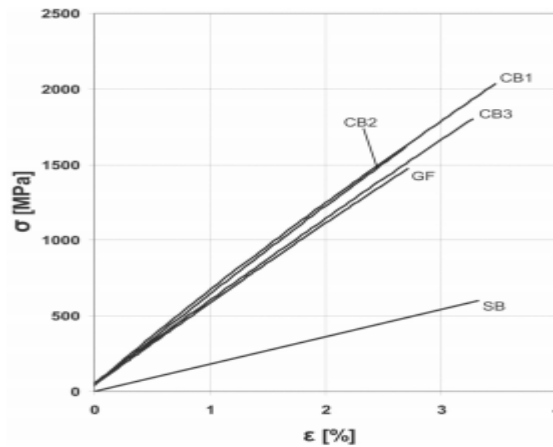


Fig. 20: Typical tensile diagrams of basalt and glass fibre tensile tests [68]

6. Textile processing of basalt filament fibers and their mixtures

Basalt application in composites is widespread. Accordingly, the exploration of the superficial modification technology do well not only to the understanding of this new material, but also to the widely market application requirement. Another feature of the basalt fibres is their good compatibility with the matrix materials even if there are some research focused on the surface treatment of these fibres in order to modify their surface morphology and improve their wettability with the matrix materia[70-73]. The mechanical strength of basalt fibers is thought to be closely related to the presence of surface heterogeneities such as surface flaws, structure defects and impurities [16]. Surface heterogeneities are expected to act as stress-concentrators facilitating the fracture development, and enhance water adsorption. so fiber surafce modification technology is very useful for composite manufacturing. he IFSS in fibre-reinforced composites can be improved by introduction of chemical functionality by oxidation or plasma treatment of the fibre surface and/or by the use of commercial coupling agents for compatibility of fibre and matrix. The fiber surface modification can be improved by introduction of chemical functionality i.e oxidation or plasma treatment (glow discharge method)of the fibre surface or by the use of commercial coupling agents for compatibility of fibre and matrix or by the coating modification technology. Matko et. al [74] in their study improved the adhesion in basalt and Polypropylen by commercial and non-commercial maleic anhydride derivatives. From the results , authors conclude that ,due to the interface modification with the additives in low concentration the mechanical properties improved.

T. Cziga [75] in his study the fibers were treated with the reaction mixture of maleic acid anhydride and sunflower oil to achieve a sufficient interfacial adhesion between fiber and PP matrix. The hybrid effect in these composites was examined as a function of fiber content and fiber combination. The strength properties of hybrid composites improved owing to surface treatment and this was proven by mechanical tests and microscopic analysis, as well. Basalt fibers were surface modified by organic/inorganic nano-hybrid sizing was studied by Bin Wei et. al [76].

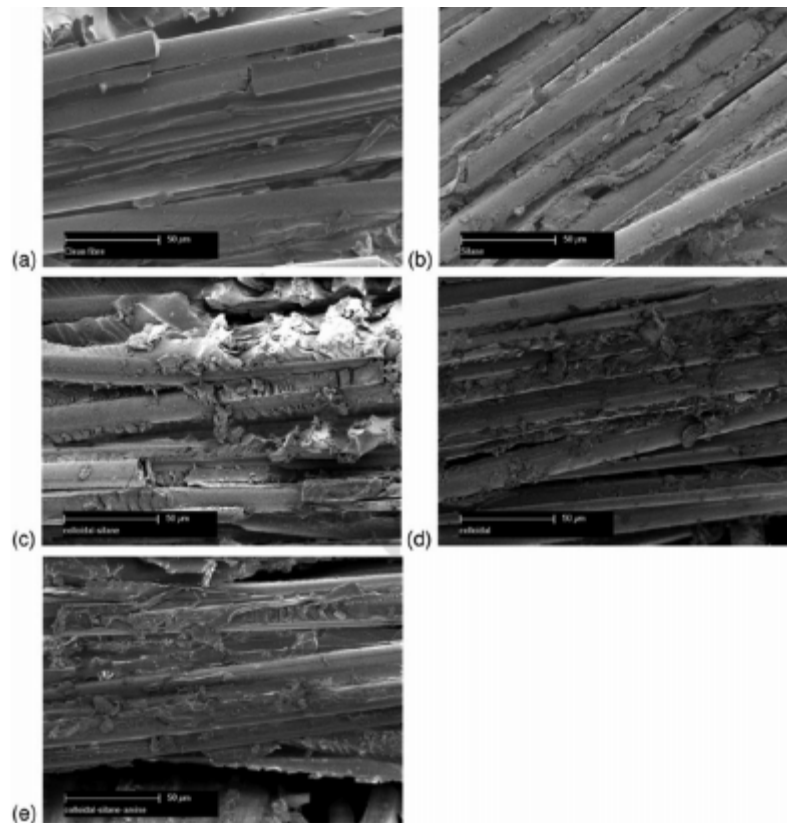


Fig. 21: SEM micrographs of the multi-ply basalt compression laminates after failure for the (a) clean fibre, (b) the silane modified fibre, (c) the colloidal/silica modified fibre, (d) the colloidal/silica/silane modified fibre, and (e) the colloidal/silica/amine-modified fibre [76].

In their work, epoxy/SiO₂ was synthesized by sol–gel method and macromolecule of epoxy resin was grafted onto nano-sized SiO₂ particles successfully. When the basalt fibers were modified by hybrid sizing with an optimum concentration, the surface morphology of the fiber was rough, the tensile strength was increased by 15 %, and the impact strength of its composites was improved by 10%. Varley et. al [77] compared different modification methods to better understand the influence of matrix-fibre interaction on the mechanical properties of epoxy-basalt composites. In particular, they employed two basic strategies: i.e. the first was to apply colloidal silica to increase the surface roughness of the fibre, whereas the second to chemically attach an epoxy silane to the fibre surface using sol gel methods. In addition to this, a hybrid approach which combined these two strategies was used and, finally, this hybrid functionalized surface of the fibre was further modified through the addition of triethylenetetramine. Plasma treatment is a more eco-friendly approach than the usual wet processing technique where the wetting solutions used, are either acidic, alkaline or silane-based. Using this approach, the surface modification of basalt fiber can be achieved with improved mechanical results [78]. Kurniawan et. al [79] investigated the effects of atmospheric pressure glow discharge plasma polymerization on silane treated basalt fiber to assess the mechanical and thermal properties of the basalt fiber/polylactic acid composite by irradiating basalt fibers from 0.5 to 6 min at

intervals. The results obtained showed that the composite properties (strength and modulus) were 45% and 18% higher, respectively, than the untreated ones. This study showed that plasma exposure time on basalt fibres affects mechanical properties of the composites. The optimized time for such improvement was found to be 4.5 min. They also found that when the irradiation time is below 1.5 min, it leads to a decline in the properties of the composite. This decrease in the properties can be attributed to the breakage of the silane bonds instead of the formation of the polymeric bonds. The SEM micrograph of the cross section of optimally plasma polymerized basalt fibres/PLA composite, Figure 22 reveals gaps between matrix and plasma polymerized basalt fibres. Moreover, it was shown that the regions where basalt fibres adhere with PLA matrix are likely the sites of silane and plasma polymer acrylic acid stacks occurred.

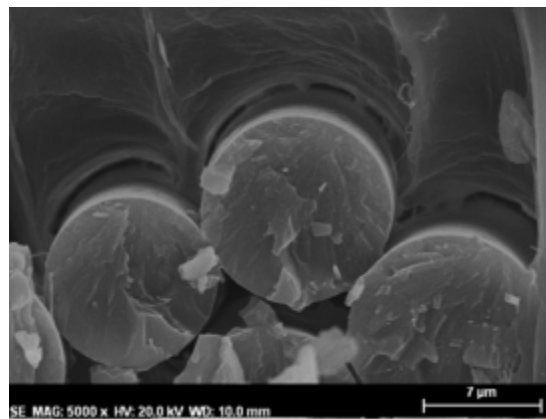
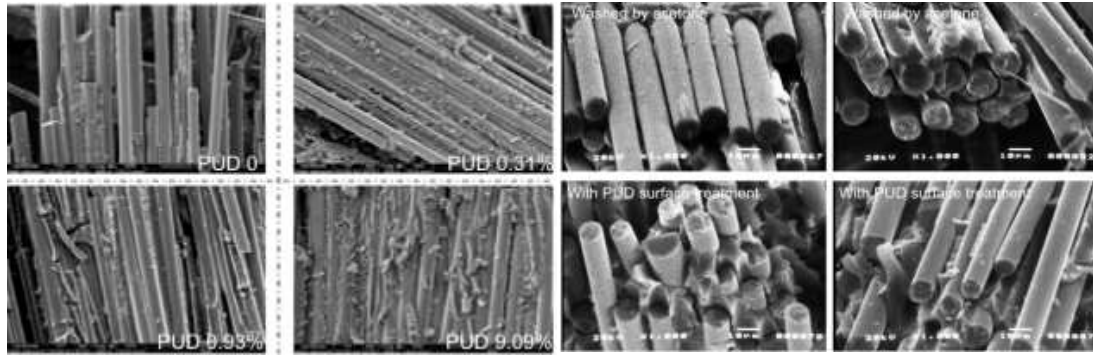


Fig. 22: Cross section of optimally plasma polymerized BF/PLA composite[79]

Kim et. al [78] studied the effects of surface treatment of a basalt fibre by low-temperature atmospheric oxygen plasma on the interlaminar fracture behaviour of basalt/epoxy woven composites. The experimental results showed that the wettability of the basalt fibre was remarkably increased, accompanied by physical etching and by the formation of chemical functional groups containing oxygen and nitrogen on the fibre surface. The interlaminar fracture toughness of basalt/epoxy woven composites was improved by oxygen plasma treatment and SEM micrographs of the fractured surface showed that epoxy resin adhered well around the basalt fibres of the oxygen plasma treated specimen compared to that of the untreated specimen. Ting et.al [80] used polyurethane dispersion (PUD) for surface modification and conclude that it increased tensile strengths. Comparison and analysis have been carried out in order to discuss the different influence by PUD surface treatment between normal and bulked yarn basalt fabric composites and the change of mechanical property by changing the PUD treatment's pick-up ratio and improved mechanical and thermal properties compared with virgins which shows that PUD surface treatment has a great influence for materials' mechanical properties of normal basalt fabric.



(a) Normal basalt woven composite

(b) Bulked basalt woven composite

Fig. 23: SEM images[80]

Seong et. al [81] investigated the acid H_2SO_4 and alkali KOH chemical treatments led to significant changes in the surface characteristics of the fibers. They make the surface rough which lead to microetched formations on the surface of basalt fibers that result in improved interfacial adhesion between the fibers and epoxy resin . The chemically treated fibers improved the mechanical interfacial properties between fiber and epoxy , interlaminar shear strength (ILSS) and fracture toughness (KIC) of the composites. As shows Atomic Force Microscopy (AFM) images of the chemically treated fiber, In the initial state, the non-treated fibers have slight surface flaws. In state A, Si–O–Si network is attacked by OH and H^+ ions. Then the fiber surfaces are assumed to include defects in the few areas. The fiber surfaces have a uniform structure because of OH and H^+ ions attack in suitable concentration solution (state B). In high concentration, the fiber surfaces are peeled by corrosion (state C). Surface treatment of the fibers effects roughness of the fiber surfaces. Thus, it influences the mechanical properties of the composites.

7. Composites based on basalt Fibers

The idea of using basalt fibres as reinforcement of composite materials first emerged in the former Soviet Union in an aerospace research program [70, 81] .In recent decades, an increasing research interest in the use of basalt fibers due to their enhanced mechanical properties has taken the polymer industry by storm. Basalt fibers have been studied extensively as reinforcement for polymer composites and are mainly focused on the **thermoset polymers** as epoxy, polyester and vinyl ester resins to manufacture composite structures useful in several applications[82-84]. Overall, epoxy resins are more expensive, but show better mechanical properties and higher resistance to moisture absorption, to corrosive liquids and to environmental agents, if compared with the vinyl ester resins. Another positive aspect of the epoxy resins is their low shrinkage during the curing process: i.e. the vinyl ester resins shrink up to 12% in volume whereas the epoxy resins shrink less than 5%. Due to the absence of styrene, the epoxy resins have significantly less toxic emissions than the vinyl ester

ones during the curing process, making possible their use also with “open-mold” manufacturing technologies (e.g. hand lay up or vacuum bagging).

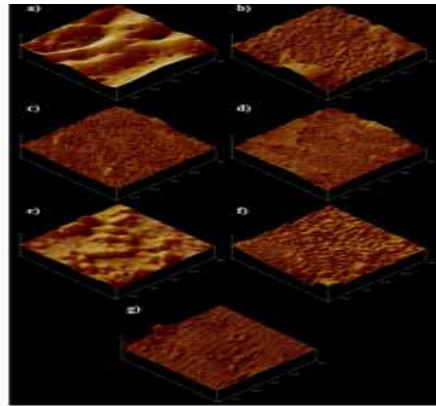


Fig. 24: AFM images of treated basalt fibers: (a) non-treated, (b) 0.5 M H₂SO₄, (c) 1M H₂SO₄, (d) 3 M H₂SO₄, (e) 0.5 M KOH, (f) 1 M KOH, and (g) 3 M KOH.

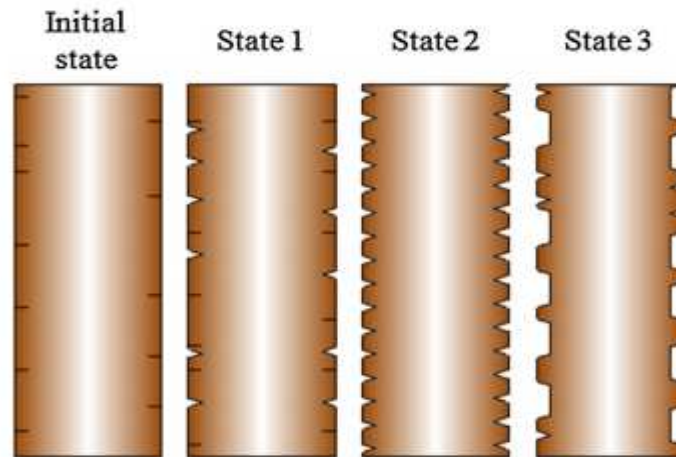


Fig. 25: Scheme of the treated process in H₂SO₄ and KOH solution.

Lopresto et. al [85] compared the E-glass and basalt plain weave epoxy laminates, mechanical properties with the aim of using basalt composites in fields like the automotive, railway, shipbuilding and aerospace as well as in the chemical industry, where glass composites are already largely applied. These composites were manufactured by vacuum bag method. The experimental results showed a high performance of the basalt material in terms of young modulus, compressive and bending strength, impact force and energy. Furthermore, the short-beam strength tests confirmed a quite good interfacial adhesion between basalt fibres and epoxy matrix, not worse than the one between E-glass and epoxy matrix. Dorigato and Pegoretti [86] compared the fatigue and tensile properties of woven, epoxy based basalt, E-glass and carbon fibres with the same areal density by vacuum bagging technique. From the experimental result it is inferred that the basalt fibres laminates present higher elastic moduli and strength values than those with glass fibres, while tensile strength values near to that of carbon fibres based laminates. The investigation of the fatigue

behaviour indicated higher performances of the laminates reinforced with basalt fabrics with respect to the corresponding glass fibre composites, with an improved capability of sustaining progressive damaging and slightly higher damping properties. Author suggested that as far as the fatigue behavior is concerned, basalt composites may therefore represent a valid substitute of glass composites in structural composites. Chairman et. al [87] with the aim to determine basalt composites' acceptability in tribological applications, the two-body abrasive wear behaviour of basalt and glass fabric-reinforced epoxy composites was investigated. Both composites were prepared by hand layup technique using basalt and E-glass plain weave fabrics. The experimental results showed that the basalt reinforced epoxy composite had higher tensile, compressive and interlaminar shear strength than glass composite. Moreover, the good bonding between basalt fibres and epoxy resin, determined by inter-laminar shear strength. Shokrieh and Memar [88] investigated the stress corrosion behaviour of basalt/epoxy composites, manufactured by filament winding method, under bending loading when submerged in 5% sulphuric acid corrosive medium. In particular, they applied three states of stress, equal to 30%, 50% and 70% of the ultimate strength of composites showing that the strength of composites degrades by time and, when loading is more than 50% of the ultimate strength, the degradation is accelerated. Moreover, degradations of bending strength, bending modulus and fracture energy were modelled by exponential functions. Liu et. al [89,90] investigated the tolerance of basalt-fibre-reinforced epoxy composites towards salt water immersion, moisture absorption, temperature and moisture cycling. To this aim, the authors used two twill fabrics (i.e. basalt and glass) with the same weave pattern and yarn ratio in both warp and weft directions and two polymers (i.e. epoxy resin and vinyl ester) as matrix, thus manufacturing four composites. As regard the seawater resistance, the vinyl ester resins show comparable behaviour than the epoxy ones. Tensile and short beam tests were carried out showing that, after a 240 days' ageing in salt water or water, a slight but significant decrease in Young's modulus and tensile strength of basalt composites was found. The ageing results indicated that both the interfacial region in basalt composites can be more vulnerable to damage than that in glass composites and the interfacial region of basalt reinforced composites requires modification prior to use in long-term applications involving exposure to water. The degradation in seawater of epoxy composites reinforced with basalt and glass plain weave fabrics was investigated by Wei B et. al [51]. They fabricated the samples by using the hot-pressing process and compared monitoring both the mass gain ratio and the strength maintenance ratio. In particular, the samples were immersed in an artificial seawater. In general, they showed that the anti-seawater corrosion property of the basalt fibre reinforced composites was almost the same as that of the glass fibre reinforced ones. He et. al [91] investigated the impact damage modes and the postimpact mechanical properties of S-2 glass, aramid and basalt fibres based epoxy composites. The experimental results showed that, under low velocity impact, glass reinforced beam have a mutational damage evolution whereas damage is similar in basalt and glass beams at the initial stage. At the high impact energy, basalt laminate exhibited a progressive damage with the fibres on the back face tension fractured

layer by layer and aramid beam also displays a progressive evolution. The reduction in residual flexural modulus is slightly larger than that in strength, especially for aramid reinforced beam. The comparison of damage features caused by impacts on glass and basalt fibre reinforced laminates has been reported in the paper of Sfarra et. al [92]. The analysis of hysteresis cycles obtained from falling weight impact tests has been assisted by nondestructive techniques, in particular interferometric and thermographic techniques, which all gave a distinctive contribution to the study. The authors showed that the increased directionality of impact damage observed in basalt fibre reinforced composites, slightly superior to glass fibre reinforced ones, may represent a limitation on the predictability of their behaviour. The experimental results suggest that the production of glass/basalt fibre hybrids in different configurations, though presenting an increased manufacturing complexity, would nonetheless present additional advantages in allowing a better predictability of impact damage patterns.

The chemical durability and mechanical properties of a basalt fiber and its reinforced epoxy resin matrix composites are investigated by Wang et. al [21]. Mass loss and strength change was studied after the basalt fiber was boiled in distilled water, sodium hydroxide and hydrochloric acid, respectively. The study shows that the alkali resistance of the basalt fiber is better than acid resistance. The flexural properties and surface morphologies of the composites were investigated after being immersed in 8 kinds of chemical mediums (i.e. 30% vitriol, 5% hydrochloric acid, 5% nitric acid, 10% sodium hydroxide, saturated sodium carbonate solution, 10% ammonia, acetone and distilled water) for 15, 30 and 90 days. Due to the difference of basalt fiber resistance in two kinds of mediums, the composites corrosion behaviors differ greatly in acid and alkaline reactions. In acid mediums, the flexural strength and flexural modulus change in the same way. In alkaline mediums, the flexural modulus keeps close to the original value while the flexural strength declines gradually.

De la Rosa Garcia et. al [93] proved the good behaviour of epoxy based composites reinforced with basalt unidirectional fibre as bending reinforcement of pine timber beams. Kim [94-95] studied the possibility of utilizing basalt chopped fibre in order to prepare thermally stable composites using a bicomponent resin system based on epoxy and benzoxazine monomer or two different curing systems for bisphenol F type epoxy resin (i.e. an epoxy-amine curing system and an epoxy-anhydride curing system). Espana et. al [96] studied the influence of different silane coupling agents on the mechanical properties of composite laminates made from a commercial epoxy resin (biobased) having 55% of its molecular structure originating from plants and basalt woven fabrics. There is also some scientific literature available regarding modifications of epoxy resin systems to improve the mechanical properties of composites. Khosravi et. al [97] analyzed the effects of multi-walled carbon nanotubes at various contents with respect to the matrix (0–0.5 wt% at a step of 0.1 wt%) on the mechanical responses of unidirectional basalt fiber/epoxy composites. On the mechanical characterizations of unidirectional basalt fiber/epoxy laminated composites with 3-glycidoxypropyltrimethoxysilane functionalized multi-walled carbon nanotubes—enhanced matrix properties. Chen et. al [98] analyzed the influence of functionalized multiwalled carbon nanotubes (MWCNTs) on the properties of

cross-ply epoxy laminates reinforced with basalt fibres and functionalized multiwalled carbon nanotubes. The dispersion of the MWCNTs in the epoxy was improved by surface modification, resulting in improved composite mechanical properties as well. They showed that the reinforcement effects of multi-walled carbon nanotubes on the composite elastic modulus exceeded micromechanics based semi-empirical predictions and were independent of surface functionalization. This work demonstrated the feasibility of in situ alignment and dispersion of functionalized nanotubes in multi-scale epoxy based laminates reinforced with basalt fibres.

Kim et. al [99-100] investigated the effect of carbon nanotube (CNT) modification with the silane and acid treatments on the flexural and fracture behaviours of epoxy/basalt composites. To this aim, flexural and mode I fracture tests were performed using acid-treated and silane-treated carbon nanotube/epoxy/basalt composites, respectively. The results showed that the flexural properties and fracture toughness of silane-treated carbon nanotube/epoxy/basalt composites are higher than those of acid-treated carbon nanotube/ epoxy/basalt composites. SEM examination revealed that the improvement in the flexural and fracture properties of silane treated carbon nanotube/epoxy/basalt composites occurred due to enhanced dispersion and interfacial interaction between the silane-modified carbon nanotubes and the epoxy resin used as matrix. Kim et. al [101] showed also that the addition of the acid-treated carbon nanotubes improves the wear properties of basalt/epoxy woven composites, due to the homogeneous load transfer between basalt fibres and epoxy matrix mixed with 1% in weight of carbon nanotubes. Kim et. al [102-103] also also studied the effect of moisture absorption on fracture toughness of seawater-absorbed carbon nanotube/epoxy/basalt composites for its application in concrete bridges and marine application. Lee et. al [104] studied the effect of carbon nanotube (CNT) modification on the tensile and thermal properties of CNT/basalt/epoxy composites. They showed that the better tensile and thermal properties of silanized carbon nanotube/woven basalt/epoxy composites in comparison with those of unmodified and acid modified carbon nanotube based composites. The enhancement of the mechanical and thermal properties of silanized CNT/basalt/epoxy composites is attributed to improved dispersibility and strong interfacial interaction between the silane functionalized CNTs and the epoxy in the basalt fabric/epoxy composites.

Bashar et. al [105] studied the effect of nano-reinforcements on mode-I interlaminar fracture toughness of quasi-uniaxial basalt fibre-reinforced epoxy laminates, manufactured by filament winding method followed by vacuum bag to consolidate the part and bleed out excess resin. In particular, a 50 mm thin ethylene tetrafluoroethylene film insert was placed at the mid-plane of each laminate investigated, as a crack initiator. An organically modified sodium-montmorillonite nanoclay and an acrylic based tri-block-copolymer were chosen for this study from among the many different nano-reinforcements available. The authors showed that the fracture energy of the bulk epoxy nanocomposites significantly increased with acrylic triblock-copolymer addition but remained unchanged with incorporation of nanoclay. Moreover, delamination fracture toughness was not influenced by the presence of nanoparticles in the matrix. The decrease fibre volume fraction, on the other hand,

significantly improved interlaminar fracture energy since the rigid fibres in these composites constrict the stress field ahead of the crack. Hence, increasing resin content enhanced composite delamination energy by increasing the capacity for matrix deformation. Ary Subargia et. al [106] studied the effect of different tourmaline micro/nano particle loading, with and without a surfactant to better disperse the tourmaline particles, on the mechanical properties of epoxy composite laminate reinforced with basalt fibres. The experimental results showed that significant improvement in both tensile and flexural strength and modulus was achieved when tourmaline particles were incorporated in the basalt/epoxy composite.

Viny ester resins

Vinyl ester resin have been widely used as matrix for basalt fibre reinforced composites due to their good properties. Carmisciano et. al [107] carried out a preliminary comparative study on basalt and E-glass woven fabric reinforced epoxy based vinyl ester resin. The laminates were manufactured by resin transfer moulding method. Basalt fiber composites showed higher flexural modulus and apparent interlaminar shear strength in comparison with E-glass ones but also a lower flexural strength and similar electrical properties. The compression behaviours of plain woven basalt/vinyl ester resin composites under high strain rates have been investigated experimentally and by use of finite element analyses by Zhang et. al [108]. From the results of the finite element, the authors concluded that the plain woven fabric structure and the rate dependent behaviours of the matrix are the key factors which affect the strain rate sensitivity of the compressive properties.

De Rosa et. al [109] studied two woven fabric laminates, one based on basalt fibres, the other on E-glass fibres, as a reinforcement for vinylester matrix, were compared in terms of their post-impact performance. The matrix used was a Bisphenol-A epoxy based vinyl ester resin. The laminates were manufactured by resin transfer moulding method. First the non-impacted specimens were subjected to interlaminar shear stress and flexural tests, then mechanical tests were repeated on laminates impacted using a falling weight tower at three impact energies (i.e. 7.5, 15 and 22.5 J). Tests were also monitored using acoustic emission analysis of signal distribution with load and with distance from the impact point. The experimental results showed similar both damage tolerance to impact and also their post-impact residual properties after impact did not differ much, with a slight superiority for basalt fibre reinforced laminates. Moreover, the authors stated that the principal difference is represented by the presence of a more extended delamination area on E-glass fibre reinforced laminates than on basalt fibre reinforced ones.

In order to use basalt reinforced composites for **structural applications**, some authors have compared the use as matrices of epoxy resins and vinyl ester ones. In particular, Czigany et. al [110] investigated mechanical and failure behaviour of basalt fibre mat reinforced composites with vinyl ester/epoxy hybrid resins as a function of resin hybridization and treatment of basalt fibre surface. The experimental results showed that the toughness of the brittle vinyl ester was effectively improved by hybridizing with a suitable epoxy resin. The authors stated that the hybrid resin

systems in the studied range possess an interpenetrating network structure, which may be very advantageous in fibre-reinforced composites. In particular, it was established that for the ratio of 1 to 1 vinyl ester/ epoxy hybrid resin-based composites both strength and toughness could be enhanced at the same time when using surface treated basalt fibres. Moreover, the authors proved that the shape and size of the damage zone in the composites, detected by location of the acoustic emission activity, are independent both of the type of treatment of basalt fibre surface and of the resin composition. Colombo et. al [8] studied the static and fatigue properties of basalt fibre composites, using as matrix vinyl ester and epoxy resins. In particular, the technique used for composites manufacturing is the vacuum infusion process and both the panels showed fibre volume ratio equal to 50%. Different kinds of mechanical tests are performed. The epoxy composites evidenced higher mechanical properties with respect to vinyl ester and the failure mode is more compact, since fibres do not tend to explode.

Polyester resins

Polyester resin can also be used for reinforcement due to its advantages like cost effective, easiness in processability, lower density. Although major research work is concentrated on epoxy and vinyl ester Nevertheless, few informations are available in the literature on the use of basalt fibres as a reinforcement of polyester resins. However, it is worth nothing that the first published paper of the study on the basalt fibre as a possible polymer reinforcing material was focused on the effect of the use of silane coupling agents on the mechanical properties of polyester based composites [111]. Manikandan et. al [112] studied the effect of fibre surface modifications on the mechanical properties of unsaturated polyester reinforced with basalt and glass fabrics. The objective of this investigation was to study the effect of surface modifications (NaOH & H₂SO₄) on mechanical properties, including tensile, shear and impact strengths. The results showed that the performance of basalt fibre reinforced composites with unsaturated polyester is superior to the glass fibre reinforced composite. Moreover, the acid-treated basalt fibre reinforced composite shows higher tensile strength values than other combinations, the glass fibre composite is much more affected by the alkali treatment than the basalt fibre reinforced composites. The acid-treated basalt fibre reinforced composite had greater impact strength. Amuthakkannan et.al [113] investigated the effect of fibre length and fibre content of basalt fibre in polyester resin on mechanical properties of the fabricated composites. Specimens were subjected to tensile strength, flexural strength and impact strength test and the failure of the composite was examined with the help of scanning electron microscopy. Gideon et. al [114] investigated the responses of basalt unsaturated polyester laminates under static three-point bending loading and low-velocity. Three kinds of laminates (i.e. unidirectional, cross-ply and woven laminates) were fabricated. On the basis of the experimental data, the authors concluded that unidirectional laminate was superior to the woven and cross-ply in static loading while cross-ply and woven laminates was superior in dynamic loading, respectively. It was also observed that the failure of unidirectional laminates was

along the fibre direction while, for cross-ply and woven, the damage was localized around the impacted locations. Gideon et. al [115] also studied the damage behaviours of plain woven basalt-unsaturated polyester laminates under low-velocity impact from experimental at varying the impact energy and finite-element approach. The finite-element method results were in good accord with the experimental results regarding peak force, maximum absorbed energy and damage area. The mechanical properties (i.e. tensile, flexural and impact properties) and the thermal stability of basalt fibre reinforced poly(butylene succinate) PBS composites were studied by Zhang et. al [116]. To this aim, composites with fibre contents up to 15% in volume have been fabricated by injection moulding method. The good thermal stability of basalt fibres allows to apply an additional heat treatment (i.e. partial pyrolysis in nitrogen at high temperatures) to a polymer matrix composite, which yields a ceramic matrix composite with enhanced resistance to oxidation. In another reaserch Li, Y. et. al [117] investigated poly(butylene succinate) composites were prepared by melt blending method using twin-screw extruder followed by injection molding. Mechanical properties and thermal stability of composites with various basalt contents were investigated by different techniques. The tensile and impact properties of the composites were improved markedly with the addition of basalt fiber. Crystallization and melting behavior of PBS in its composites kept almost unchanged, indicating that the nucleation effect of basalt fiber was minimal and, meanwhile, it played a role in hindrance of chain motion. TG analysis showed that the thermal stability of PBS/BF composites was enhanced by the addition of BF. Mishra et. al [118] investigated the containing TiO₂ nanoparticles, polysiloxane resin, and basalt fabric. The loading effect of TiO₂ nanoparticles on the thermal and mechanical properties of basalt fabric reinforced polysiloxane composite materials has been investigated. Composite samples were prepared, each using two layers of basalt fabric with TiO₂ nanoparticles loading from 0.5, 1, 1.5, 2, 2.5, and 3% by weight. Tensile results show that 1.5 wt.% loading of TiO₂ nanoparticles in the nanocomposites resulted in highest improvement in tensile modulus compared to the neat system. DMA studies also revealed that 1.5 wt.% doped system exhibits highest storage modulus as compared to the neat and other loading percentages. DSC and TGA studies show that T_g and HDT of the composite increases with the increase in wt.% of nanofillers in the composite. Cerný et. al used polysiloxane resins as matrix pre-cursors in several works [119-123]. Their study focused on the exposure of the basalt fibres to 1000 C temperature but this is inappropriate since the amorphous fibre showed a pronounced creep and the formation of crystalline phases which causes the brittleness of the fibres, in the temperature range of 600-700 C. Mechanical properties of the basalt fibres Basaltex and Kamenny Vek were studied [119]. In another study [120] they studied the heat resistant of composites reinforced with continuous basalt fibres made by incomplete pyrolysis of a polysiloxane matrix, also analyzing the effect of the fibre lubrication. In other studies [121-123], they studied the heat resistant of composites reinforced with continuous basalt fibres made by incomplete pyrolysis of a polysiloxane matrix, also analyzing the effect of the fibre lubrication to unidirectionally reinforced basalt fibre composites. The composite pyrolysed at 650 °C revealed the best room temperature

properties. Its exploitation in a common environment up to 550 °C is possible but some reduction of strength and fracture toughness must be taken in consideration which takes place already after its short-time exposition in hot air. Moreover, the pyrolysis temperature was more determining for matrix-governed elastic properties (i.e. shear modulus) than for those dominated by the fibres (i.e. Young's modulus). It was also shown that a relatively short exposition to hot air (i.e. 4 h at 750 °C) both deteriorated the flexural strength of the composites studied in this work and changed the failure mode to brittle fracture.

Furan resins

Furan resins are another class of thermoset resins recently used as matrix for basalt reinforced composites. Differently from phenolic resins, which are synthesized from highly toxic and hazardous compounds as phenol and formaldehyde, furan resins are based on furfuryl alcohol, which is less toxic component. Besides, the eco formulations can reduce up to 50% of CO combustion. The impact behaviour of basalt fibre reinforced furan composites manufactured by microwave technology was studied by Lopez De Vergara et. al [124]. Results showed that the microwave cured composites presents higher values for interlaminar shear strength, delamination threshold force, maximum load and penetration threshold than the conventionally cured ones.

Thermoplastic polymer resins

The scientific literature also reports the basalt thermoplastic-based composites i.e polypropylene and polyethylene. Botev et. al [22] studied first time , a series of commercial-grade polypropylenes filled with different contents of short basalt fibres, using as coupling agent a poly(propylene-gmaleic anhydride), to determine the suitability of untreated short basalt fibres as a reinforcing agent for polypropylenes. Results showed that the composites with no coupling agent showed deterioration of stress and strain at yield with increasing of the fibre content whereas the impact strength was fourfold higher than that of unfilled polypropylene. On the other hand, it was observed that the tensile properties of the obtained materials and their impact strengths increased significantly with increasing of the amount of the coupling agent in the blend. After this first work, several authors focused their attention on the study of mechanical properties of polypropylene filled with basalt fibres. In another research ,Szabo and Czigany [125] investigated the static properties of polypropylene composites reinforced with different short mineral fibres (i.e. basalt and ceramic) and with different reinforcing contents. Commercial and non-commercial (i.e. reactive surfactants prepared in laboratory) maleic anhydride derivatives as coupling agents, to improve the adhesion between basalt short fibres and polypropylene matrix is studied by Matko et. al [126]. The experimental results showed that both the commercial and they prepared non-commercial interfacial additives are effective at low concentration. Eslami Farsani et. al [128] presented a comparative study on the tensile properties of clay reinforced polypropylene nanocomposites and chopped basalt fiber reinforced. PP matrix are filled with 1, 3 and 5 wt.% of nanoclays. The ultimate

tensile strength, yield strength, Young's modulus and toughness are measured at various temperature conditions. The thermal conditions are included the room temperature (RT), low temperature (LT) and high temperature (HT). They showed that the addition of nanoclay improves the yield strength and Young's modulus whereas it reduces the ultimate tensile strength of polypropylene based composites. Bashtannik et. al [129] investigated the effect of temperature, adhesion time, and surface treatment of basalt fibres on the mechanical properties of composites based on a high-density polyethylene and a copolymer of 1,3,5-trioxane with 1,3-dioxolan reinforced with basalt fibres. The experimental results showed that the surface modification of basalt fibres in acidic and alkaline media intensifies the adhesion of thermoplastics to them. In particular, it was revealed that the treatment in the acidic medium is more efficient and considerably improves the mechanical properties of composites. Akinci [130] showed that the basalt fibres affect structural integrity and mechanical properties of composites. With increasing the amount of the basalt addition to the LDPE results in a decrease in elongation at break values influences the structural integrity and the quasi static mechanical properties of low density polyethylene based composites. In particular, the elongation at break of the composites decreases by increasing the basalt fibres amount. Moreover, it was revealed that the crystallization increases by increasing the basalt content and the basalt weight percent increases the hardness. Low-density polyethylene based composites reinforced with basalt filler were evaluated also in term of friction and wear performance under dry sliding conditions by the same researcher [130] the results showed that the wear rates for neat matrix and basalt filled composites increase with increasing loads and sliding speeds. Moreover, the wear rates of the basalt filled composites were significantly affected from the basalt content.

Polytetrafluoroethylene-based (PTFE) composites were also studied by some researchers as matrix for basalt fibre composites. For instance, Wang et. al [131] investigated the tribological behaviours of two **PTFE** composites reinforced with carbon fibers and basalt fibers sliding against stainless steel under water lubrication and compared with those of pure PTFE. The experimental results showed that carbon fibres were well bonded with polytetrafluoroethylene matrix differently from the basalt fibres which were poorly bonded with the matrix. Due to the great accelerating effect of poor fibre/ matrix interfacial adhesion on water absorption, polytetrafluoroethylene reinforced with basalt fibres with the highest crystallinity unexpectedly showed the highest water absorption, resulting in serious matrix plasticization and degradation of fibre/matrix interfacial adhesion. As a result, as the reinforcement failure of basalt fibres occurred, BF/PTFE exhibited the highest wear rate. Zhang et. al [132] investigated the tribological properties of polyimide composites reinforced by short basalt fibres also filled with solid lubricants as MoS₂ and graphite. The results revealed that the low incorporation of BFs could improve the tribological behavior of the PI composites remarkably. The friction coefficient and wear rate decreased with increases in the sliding speed and load respectively. In another research the authors [133] also showed that MoS₂ and graphite as fillers

significantly improved the wear resistance of the basalt fibres reinforced polyimide composites. Deak et. al [134] studied the effect of surface treatment with coupling agents on the dynamic mechanical properties of polyamide-6 reinforced with basalt fibres showing that the interfacial adhesion between basalt fibres and polyamide can be largely improved by the application of silane coupling agents in the entire temperature range evaluated. The presence of coupling agents on the surface of basalt fibers was proven by Fourier transform infrared spectroscopy. The best results were obtained by 3-glycidoxypyltrimethoxysilane coupling agent.

In another work [135], Deak et. al compared **Polyamide 6** reinforced with long and short basalt fibres. The results showed that long fibre reinforced thermoplastic composites are particularly advantageous in the respects of dynamic mechanical properties and injection moulding shrinkage. In particular, the fibre orientation in long basalt fibre reinforced fundamentally differs from short basalt fibre reinforced ones, resulting in more isotropic moulding shrinkage in case of long basalt fibre reinforced composites. Moreover, the main advantage of the used long fibre thermoplastic technology was that the special long fibre reinforced pellet can be processed by most conventional injection moulding machines. Meszaros et. al [136] studied the effect of nanotube content on the mechanical properties of polyamide-6 reinforced with basalt fibers. The experimental results showed that the combination of macroscopic and nanosized reinforcements improves the mechanical properties significantly, and synergetic effects can also be observed. In another work [137], Meszaros et. al studied the mechanical properties of basalt fibre and montmorillonite co-reinforced polyamide 6 matrix hybrid nanocomposites. In particular, the hybrid nanocomposites showed high tensile and flexural properties, and a synergistic effect of the co-reinforcement has been demonstrated. Moreover, it was observed that the presence of short basalt fibres can enhance the dispersion of the nanoparticles in the matrix.

The molten viscosity of polyamide-6 currently used in industry was very high, which makes it difficult to impregnate thermoplastic resin into fibre bundles. To overcome this problem, anionic reactive processing was used as an alternative way to obtain polyamide-6. In particular, initial low viscosity raw reactants (i.e. Monomer (ϵ -caprolactam) β Activator β Initiator) were injected through the reinforcement, being it a low energy consumption process. The result was a high molecular weight linear polymer (anionic(A) PA-6). Hoto et. al [138] analyzed the use of APA-6 as matrix material of basalt fibres studying the dependency between **injection flow rate** and void content, which affects final mechanicals properties of the composites. The influence of basalt fibre on morphology, mechanical properties, **contact angle**, melting and crystallization behaviours of polyamide 1012 was studied by Song et. al [139]. The experimental results showed that the interface properties between basalt fibre and polyamide 1012 were improved effectively by silane coupling agent thus increasing the tensile and flexural strength of the composites. Although basalt fibre does not change polyamide 1012 crystal structure, it alters the melting temperature and degree of crystallinity of polyamide 1012. In addition, by virtue of the changes in crystallization temperature, the nucleation ability of polyamide 1012 in composites is confirmed to be enhanced. Moreover, the strong interaction between epoxy groups of

silane coupling agent and amide groups of polyamide 1012 elevates the hydrophobic properties of composites. Song et. al [140] studied the morphology, melting and crystallization, structure, mechanical properties of poly(vinylidene fluoride)/Poly(methyl methacrylate) blends by adding basalt fibre. The tensile and flexural strengths increased by increasing the basalt fibres content up to 20% in weight. The melting temperature was not influenced by the presence of the basalt fibres, but the degree of crystallinity of composites increased as basalt fibres content increase up to 20% in weight. Moreover, the heat resistance, evaluated by Vicat softening temperature (VST), is improved due to basalt fibres.

Sándor S et.al [141] investigated the static and dynamic mechanical properties of composites with short basalt fibre (BF) reinforced with polypropylene/polyamide (PP/PA) blends were prepared by homogenization of the components in a twin-screw extruder followed by injection molding. Composites with different PA (0, 10, 20, 30, 40, and 50 wt%) and basalt fibre (0, 10, and 20 wt%) contents were used. From the results it has been realized that the composite structure is very sensitive to the ratio of PA12 content. In case of small PA content (10–20 wt%), PA and basalt fibre have been experienced to form a kind of random network structure inside the PP matrix. This way could be improving the mechanical properties of the composite despite the relatively short fibre length. These results have been supported by acoustic emission (AE) tests and scanning electron (SEM) micrographs.

Biodegradable polymer resins

Thermoplastics matrix composites are being developed as advanced composites for wide range of primary and secondary structure components as well as for non-structural materials. It is possible to combine environmentally friendly constituents for making green composites. To accomplish this target, use of bioplastics as the matrix is one of the available options. Polylactid acid (PLA), with its plant origin and biodegradable nature, has ecofriendly image and fair physical properties to be the bio-based thermoplastic matrix of choice. It has good mechanical and thermal properties, easy processing feature, low shrinkage and harmless biodegradable. As basalt is natural material and sustainable material. For these reasons, basalt fibre reinforced biodegradable polymer composites are expected to provide environmentally friendly yet economically justifiable structural and functional materials. Although a lot of research studies reported the mechanical behaviour of various vegetable fibres/PLA composites in detail, there are few articles regarding PLA based composites reinforced with basalt fibres.

Chen et. al [142] used basalt for the first time as reinforcement of PLA matrix to fabricate composite materials for **hard tissue repair**. In particular, the authors produced basalt composites and pure PLA by the methods of solution blending and freeze drying. The results showed that basalt fibres can be uniformly dispersed in the PLA matrix and significantly improve the mechanical properties and hydrophilicity of the PLA matrix. Moreover, the authors stated that the presence of basalt fibres may retard the polymer degradation rate and neutralize the acid degradation from PLA. Osteoblasts were cultured in vitro to evaluate the cytocompatibility of the composite

and the results suggested that the presence of basalt fibres does not noticeably affect osteoblastic behaviour and the designed composites are osteoblast compatible. Kurniawan et. al [79] studied the effects of atmospheric pressure glow discharge plasma polymerization on basalt fibres on the properties of basalt plain woven fabric/polylactic acid composites. Characterization was conducted on the plasma polymerized fibers by identifying the molecular bonds and surface morphology. Properties (mechanical and thermal) and water absorption behavior of the fabricated composites were tested. In particular, optimum plasma polymerization on basalt fibres was for 4.5 min of plasma exposure time where the composite's strength and modulus were 45% and 18% higher, respectively, compared to those of untreated one.

The tensile, flexural and impact properties of PLA composites reinforced with basalt and glass fibres were compared by Liu et. al [143]. To this aim, composites with fibre weight content up to 40% were prepared by means of a twin screw extruder. The results showed that basalt fibre/PLA composites had significant reinforcing and toughening effect in comparison with glass fibre/PLA composites. The impact strength of basalt fibre/PLA composites achieved the maximum value with the content of basalt fibre equal to 20%.

Tabi et. al [144] focused their attention on PLA composites reinforced with chopped basalt fiber silane treated and untreated basalt fibres. Composites with fibre weight content up to 40% were prepared using extrusion and injection moulding methods. Mechanical tests ,dynamic mechanical analysis, differential scanning calorimetry, heat deflection temperature analysis, dimensional stability test, melt flow index analysis and scanning electron microscopic observations were carried out. On the basis of experimental data, it was shown that silane treated chopped basalt fibres are much more effective in reinforcing PLA than untreated fibres.

Tabi et. al [145] compared the properties of long fibre reinforced composites to chopped basalt fibre reinforced PLA composites produced by using the conventional dry mixing, extrusion and injection moulding methods. In particular, tensile, three-point bending and Charpy impact tests, dynamic mechanical analysis, differential scanning calorimetry, heat deflection temperature analysis and scanning electron microscopic observations were carried out. They showed that the mechanical properties of the long basalt fibre reinforced PLA was found to be superior to short basalt fibre reinforced PLA. Moreover, fibre length analysis revealed that the remaining average fibre length highly increased, while electron microscopy demonstrated that there is very strong adhesion between the phases. Finally, it was found that the long basalt fibres also have nucleating ability, however, not as efficient as short basalt fibres. Wheat gluten and starch resin are other biodegradable polymers that have been considered in the last years as matrix for basalt-reinforced polymers. Fatimat et.al. [146] used Low viscosity thermoset bio-based resin which was synthesised from lactic acid, allyl alcohol and pentaerythritol. The resin was impregnated into cellulosic fibre reinforcement from flax and basalt and then compression moulded at elevated temperature to produce thermoset composites. The mechanical properties and thermal properties of composites were characterised .The results showed a decrease in mechanical properties with increase in fibre load after 40.

wt.% for the neat flax composite due to insufficient fibre wetting and an increase in mechanical properties with increase fibre load up to 60. wt.% for the flax/basalt composite. The results of the ageing test showed that the mechanical properties of the composites deteriorate with ageing; however, the flax/basalt composite had better mechanical properties after ageing than the flax composite before ageing. Aruljeyakumar et. al [147] analysed the Chitosan (CS) particles used as filler in PLA/BF composites to fabricate Hybrid polymer Composite Material. Twin Screw Extrusion and Injection Moulding techniques were employed to fabricate specimens.. A significant improvement in thermal properties of the Hybrid Composites was observed as the weight percentage of BF and Chiton increased. Thermo gravimetric Analysis (TGA) reveals that the degradation rate of the composites increased with temperature. From Dynamic Mechanical Analysis (DMA) it is inferred that with increase in temperature the storage modulus reduced whereas the loss factor $\tan\delta$ increased when the weight fraction of BF and CS decreased.

In particular, Ye et. al [148] examined the biodegradation behaviour of wheat gluten/basalt composites by putting specimens into soil of prescribed moisture content. Wittek e Tanimoto [149] studied the effect of silane coupling agents and of the adding of fire retardants on the mechanical and the thermal properties of starch resin reinforced with basalt plain fabrics.

8. Hybrid composites

The study of hybrid composites has been growing attention for structural applications due to their better properties than their individual material constituents . In hybrid composites two or more types of fibres are simultaneously used as reinforcement in a common matrix. The advantage of one type of fiber could complement with what is lacking in the other..Due to the good properties of basalt fibres began to be used as a new reinforcing material for hybrid and composite laminates.

Czigany [75] analyzed the mechanical properties of polypropylene reinforced with basalt, hemp, glass and carbon fibre and their basalt hybrid composites. In particular, it was revealed that basalt fibre hybridization resulted in only a slight increase in the mechanical properties in case of hemp fibre composites, while in case of carbon fibre and primarily glass fibre composites, a significant improvement was experienced. Chikhradze et. al [150] investigated the use of hybrid epoxy composites reinforced by carbon, basalt and E-glass fibres for the manufacturing of **wind turbines**. A study on the influence of the substitution of carbon fibres by basalt ones was performed showing that at 20% and 40% substitution of carbon fibre for basalt gives approximately the same deterioration of the strength- and elasticity characteristics so that it is acceptable as solution in view of economical optimization. Cao et. al [151] analyzed the tensile properties of hybrid carbon/basalt and carbon/glass reinforced polymers. Tensile tests were performed at different temperatures to verify the thermal behaviour of the composites. Similar reductions of the tensile strength of carbon/glass and carbon/basalt composites compared to the all carbon composites were found. Ary Subagia et. al [152] investigated the effect of different stacking sequences of carbon and basalt woven fabrics on the flexural properties of hybrid composite laminates,

manufactured by vacuum assisted resin transfer moulding method. All the stacking sequences showed a positive hybridization effect and the flexural properties of hybrid composites were strongly dependent on the sequence of fibre reinforcement. In particular, the interply hybrid composite with carbon fibre at the compressive side exhibited higher flexural strength and modulus than when basalt fabric was placed at the compressive side. Zhang et. al [153] developed hybrid epoxy composites with alternate stacking sequences of plain basalt and carbon fabrics to improve the toughness properties of conventional carbon reinforced composites. The toughness properties of each laminate were studied by an open hole compression test and the results showed that hybrid composites display higher open hole compression strength than that of plain carbon fibre composites. Fiore et. al [154] studied the use of basalt fibres in substitution of glass one for naval application. To this aim, hybrid composites were manufactured by means of ply substitution techniques and tested by three point bending and tensile tests. It was shown how the substitution of the most external lamina improves both the flexural and tensile properties in comparison with glass fibres mat fabric reinforced composite. Moreover, this solution was then applied to a naval bulkhead demonstrating that, considering costs, environment impact, and mechanical performances, this kind of material could substitute the traditional glass fiber composites in naval application. Later Amuthakkannan et.al [155] also studied the mechanical properties of basalt fiber and Glass fiber reinforced hybrid composites developed by using compression moulding techniques. Woven basalt fibers and Glass fibers were used for fabricating the hybrid composites, polyester resin as matrix with different fiber stacking sequences. The result shows that the reinforcement of woven Basalt and Glass fibers hybrid composites significantly influencing on the mechanical properties of the composites and it found that the intermediate properties between basalt glass fibers reinforced composites.

Amuthakkannan et. al [156] also investigated the mechanical properties of polyester composites by the introduction of basalt fibers in jute fiber. basalt/jute fiber-reinforced hybrid polymer composites were fabricated with a varying fiber percentage by using compression molding techniques. Incorporation of basalt fiber into the composites was at approximately 10%, 20%, up to 90%, and the jute fiber percentage was reduced from 90%, 80%, to 10% correspondingly. It has been observed that the addition of jute fiber to the basalt fiber polyester composites enhanced the mechanical properties. Water absorption of hybrid composites was also analyzed and was found to be proportional to fiber percentage.

Petrucci et. al [157] compared the mechanical properties of different hybrid composite laminates, based on basalt fibre composites as the inner core, and using also glass, flax and hemp fibre laminates to produce symmetrical configurations. In particular, all the composite, having fibre volume contents in the range of 21-23%, were manufactured by vacuum infusion method. The mechanical performance of all the hybrid laminates appears superior to pure hemp and flax fibre reinforced laminates and inferior to basalt fibre laminates. Among the hybrids, the best properties are offered by those obtained by adding glass and flax to basalt fibre reinforced.

The mechanical properties (i.e. tensile, flexural and impact strengths) of phenol formaldehyde based composites reinforced with hemp fibres, basalt fibres and hemp/basalt fibres were investigated as a function of fibre loading by Ozturk [158]. The experimental result showed that the tensile strength of basalt reinforced composites increases by incorporation of basalt fibre up to 32% in volume and increases beyond this value whereas the flexural strength decreased linearly with fibre loading. However, the maximum impact strength was obtained for 48% basalt fibre content. Moreover, the addition of basalt fibres decreased the tensile strength of the hemp composites and the mechanical properties of hemp composites are higher than that of basalt composites for the same fibre loading. Wu et. al [159] compared the fatigue behaviour of composites subjected to a hybridization process using different materials. In particular, six different types of epoxy polymers reinforced with unidirectional fibres were used for this study: i.e. four traditional (reinforced with carbon, polyparaphenylene benzobisoxazole, glass, and basalt fibres) and two hybrid ones (carbon/glass and carbon/ basalt). The experimental results showed that the carbon/basalt hybrid composites significantly improve the fatigue resistance in comparison to the homogeneous basalt composite, whereas the resistance of the carbon/glass hybrid composites does not provide such effects.

Dorigato et. al [160] compared the basalt and E-glass fabrics combined with carbon fiber fabrics in order to prepare epoxy-based interlaminar hybrid composites and to investigate the properties. The flexural modulus of the composites depended on their composition according to a rule of mixture, while an important synergistic effect was detected for the ultimate flexural properties. Moreover, the Charpy impact tests evidence a strength increase with increasing of basalt and glass fibres content. In particular, the hybridization with basalt fibres promotes an increase of the adsorbed impact energy due to an enhancement of the fracture propagation component.

Wang et. al [161] studied the effect of fiber arrangement in 3D woven hybrid composites on their low velocity impact properties, aramid (Kevlar129), basalt fibers, and epoxy resin were used. To this aim, aramid and basalt fibres were used to fabricate two epoxy structures: i.e. the first one, namely interply hybrid composite, in which different yarn types were placed in different layers and the second one, namely intraply hybrid composite, in which each layer was composed of two types of alternately arranged yarns. Results reveal that the interply hybrid composite showed higher ductile indices (8–220%), lower peak load (5–45%), and higher specific energy absorption (9–67%) in both warp and weft directions than that of the intraply hybrid composite due to a layer-by-layer fracture mode for the interply hybrid composite.

The superiority of basalt fibres in hybrid composite over glass fibres for post impact behaviour is also demonstrated by De Rosa et. al [162]. In a similar way, Sarasini et. al [163] studied the low-velocity impact behaviour of hybrid laminates reinforced with woven aramid and basalt fabrics and manufactured by resin transfer moulding. Results indicate that hybrid laminates with intercalated configuration (alternating sequence of basalt and aramid fabrics) have better impact energy absorption capability and enhanced damage tolerance with respect to the all-aramid laminates, while basalt and hybrid laminates with sandwich-like configuration (seven basalt

fabric layers at the centre of the laminate as core and three aramid fabric layers for each side of the composite as skins) present the most favourable flexural behavior. Sarasini et. al also studied the behaviour of glass-basalt [164] carbon-basalt [165] hybrid composites, manufactured by resin transfer moulding technique, under low impact velocity. The experimental results showed that hybrid laminates with an intercalated configuration (i.e. alternating sequence of basalt and glass, carbon fabrics) exhibit higher impact energy absorption capacity and enhanced damage tolerance capability than the traditional laminates. Conversely, the most favourable flexural behaviour was shown by hybrid laminates with symmetrical sandwich-like configuration (with glass or carbon fabrics at the centre of the laminate as core in glass or carbon-basalt structures, basalt fabrics as core in basalt/ aramid structures, respectively). Manoharan et. al [166] analyzed compressive strength, hardness and thermomechanical properties of phenolic composite with fiber i.e aramid and basalt fiber reinforcement. Hardness of phenolic composites was found to increase with increase in basalt fiber loading from 72.2 to 85.2. The DMA results clearly reveal that sample with high basalt fiber loading has got highest storage modulus and loss modulus values. Fiber incorporation decreases the damping properties of composite by acting as barrier to molecular chain movement. Najafi et. al [167] studied the impact and flexural properties of woven basalt fiber/phenolic woven carbon fiber/phenolic and woven basalt/woven carbon hybrid phenolic composites are investigated. The hybridization effect of woven basalt and woven carbon fibers on the impact energy absorption and flexural properties is investigated. Results reveal that the impact properties of the composites are strongly improved when the basalt fiber increased. Impact energy absorption of composite showed a regular trend of increase with increasing weight ratio of basalt fiber in hybrid fiber composite. The experimental evidence shows that the hybrid composites based on combinations of stiff carbon fibers and tough basalt fibers have good flexural properties and therefore, they can be used as promising materials in a number of engineering sectors such as the protective structures.

Eslami-Farsani et. al [168] investigated the effects of thermal cycles on impact resistance of carbon/basalt hybrid phenolic composites, compared to those of all basalt and all carbon composites. In particular, all the investigated composites were manufactured by hand lay-up method, using plain woven carbon fabrics (and twill woven basalt fabrics as reinforcement). The experimental results showed that the mean Charpy impact energy of the basalt/phenolic composites is higher than that of the hybrid composites and all carbon composites, at all thermal cycles. Moreover, the Charpy impact energy of carbon/phenolic composites and hybrid composites was not significantly affected by thermal cycles. On the contrary, the impact resistance of basalt/phenolic composites showed a sharp decline with increasing thermal cycling, and reaches a plateau after a certain cycles. Jamshaid et. al [169] also investigated the thermal and mechanical behavior of woven basalt/PP and basalt/Jute fiber hybrid and nonhybrid woven fabrics and their composite laminates with epoxy. Mechanical properties and thermal properties are studied. The results reveal that the hybridization of basalt with polypropylene and jute in different weaves leads to significant

improvement in the static and dynamic mechanical properties of composites. Structure of weave, fiber type and resin properties have strong influence on mechanical properties of composites of basalt hybrid fabrics. In an other study Jamshaid et. al [170] also studied the green composites produced by bio epoxy resin composites based on B/B and B/J fabrics. The mechanical properties of the composites are studied. From the results it is found that pure basalt fiber combination maintains higher values in all mechanical tests. Thermo-gravimetric (TG/DTG) composites showed that thermal degradation temperatures of composites shifted to higher temperature regions compared to jute fabrics. However, it should be noted that hybridization with basalt fiber gave noticeable mechanical and thermal performances, while being the cheapest and most environmentally friendly way to perform.

With the aim of combine the good mechanical properties of basalt fibre with the excellent impact resistant of **nylon** fibre, the low velocity impact behaviour of homogenous and hybrid composite laminates reinforced by basalt/nylon intra-ply fabrics was experimentally investigated by Dehkordi et. al [171-172]. In the work [171] five different types of woven fabrics with different volume percentages of nylon (0%, 25%, 33.3%, 50% and 100%) were used as reinforcement of epoxy resin. The effect of nylon/basalt fibre content on maximum force, maximum deflection, residual deflection, total absorbed energy, elastic energy, size and type of damage were studied at several low velocity impact nominal energy levels (i.e. 16, 30 and 40 J). The experimental results showed that the impact performance of these intraply hybrid laminates is significantly affected by the nylon/basalt fibre content. In an other paper [172], the authors performed low velocity impact and compression after impact tests at different nominal impact energy levels (16, 30 and 40 J) on hybrid composite laminates reinforced by basalt-nylon intraply fabrics. Five different types of fabric were produced with a rapier loom: i.e. a homogeneous basalt fabric, a homogeneous nylon fabric and three hybrid basalt/nylon fabrics with different volume percentages of nylon (i.e. 25%, 33.3% and 50%). For hybrid fabrics, the percentage of nylon or basalt was equal in the warp and weft directions. The results showed that at low impact energy, hybridization and variation in basalt/nylon fibre content can not improve the impact performance of composite plates. Results reveal that the impact performance becomes more and more dependent on the content of nylon and basalt with increasing impact energy.

9. Hybrid sandwich structures

In the recent years, basalt fibres have been also used in **hybrid sandwich structures**. In particular, Lopresto et. al [173] carried out physics and mechanical tests on innovative sandwiches for civil applications. In this study core a polyurethane matrix filled with short basalt fibres was used. The experimental results showed that better behaviours are found in terms of compression strength and elastic modulus, compression energy absorption capability, impact force and energy in comparison with sandwiches made without any reinforcement in the polyurethane core. From physics tests, a good behaviour as insulator of the innovative sandwiches is noted together with an increase in performances at the increasing of the reinforcement.

Torres et. al [174] investigated the green composite sandwich structures with basalt Fiber and bio epoxy resin. This material system was combined with cork as core material for the fabrication of fibre composite sandwich structures. Mechanical properties of both skin and core materials were assessed through flexural and tensile tests. Permeability measurements of the basalt fabrics were carried out in order to perform numerical simulations of liquid composite moulding (LCM) processes on the PAMRTM software. Finally, the load-bearing capacity of the board was studied by means of FEM simulations, and the presented design proved to be acceptable for service. Hoto et. al [175] studied the flexural behaviour and the water absorption of asymmetrical sandwich composites manufactured by means of vacuum assisted hand lay-up process. In particular, the authors used a commercially available cork board as core and basalt fibre unidirectional fabric, as reinforcement for one of the skins. The other skin was made of flax unidirectional fabric. A bio-based epoxy resin was also used as matrix for each skin. Moreover, for some specimens the core material was altered allowing resin infiltration between the granules. The experimental results showed that the presence of different fibre skins greatly influences the failure mechanism and significant enhancement of the energy-absorbing capability are found when specimens are loaded in the proper conditions. It was found that the water absorption of the specimens is significantly reduced by the infiltration of resin between the granules of the core. Colomina et. al [176] studied green composite sandwich with biobased epoxy resin. Hybrid basalt-flax fabrics have been used as reinforcements for composites and the influence of the stacking sequence has been evaluated in order to optimize the appropriate laminate structure for the sandwich bases. Core cork materials with different thickness have been used to evaluate performance of sandwich structures thus leading to high renewable content composite sandwich structures. Results show that position of basalt fabrics plays a key role in flexural fracture of sandwich structures due to differences in stiffness between flax and basalt fibers.

10. Metallic matrices

Basalt fibres have been widely used as reinforcement both of thermoset and of thermoplastic polymers in the last decades. Due to their ceramic nature and to their less price than other ceramic fibres, basalt fibres represent a good candidate as reinforcing components also in metallic matrices. Nevertheless, the applicability of basalt fibre as a reinforcing material for metallic matrix composites (MMCs) has been marginally investigated. Casting and powder metallurgy methods are the main techniques for the manufacturing of metal matrix composites under different pressure and thermal conditions. For this reason, the prospect of using basalt fibre as reinforcement of metal matrices significantly depends on the stability of fibres to the effect of processing conditions.

Khalili et. al [177] has investigated the mechanical behaviour of basalt fiber-reinforced(BFRE) and basalt fiber metal laminate (BFML) composed of steel, aluminum composites under tensile and bending loads. To study the effect of fillers in epoxy, the micro glass powder (MGP) was only added into the epoxy resin in

BFRE composites at various volume fractions. It was found that the MGP had no significant effect on tensile strength, but it raised the stiffness and decreased the failure strain of BFRE. On the other hand, bending strength increased by adding MGP. BFML showed superiority in energy absorption via tensile strength. This FML had flexibility much higher than that of BFRE. Adding MGP or metal layer to basalt-reinforced composites improved the mechanical properties in tensile and bending loads. Selective bending specimens of BFRE are studied by SEM to show the positive role of MGP in raising the bending strength and further analysis of the nature of fracture surfaces. High fragmentation of matrix was obvious.

Fiore et. al [178] analyzed the possibility to join aluminium alloy 6086 and epoxy composites reinforced with basalt fibres by means of three joining techniques: i.e. mechanical by self piercing riveting, adhesive by co-curing technique and mixed in which the traditional joining techniques were combined. Two manufacturing technologies (i.e. hand lay-up and vacuum bagging) were used both to produce composite substrates and to realize co-curing adhesion between the substrates to be joined. The experimental results have shown that adhesive joints, realized by vacuum bagging method, show higher average failure load and lower standard deviation than those realized by hand lay-up. By comparing mixed joints, different results are obtained: i.e. the hand lay-up joints show both higher average failure load and standard deviation than those realized by vacuum bagging. Farsani et. al [179] studied the effect of adding micro glass powder into basalt fiber reinforced epoxy composites on the Charpy impact behavior is investigated by both flatwise and edgewise specimens. Also, the effect of adding micro glass powder at two temperatures is examined on the Charpy impact behavior in order to obtain a more detailed knowledge of the role of micro glass powder in polymer composites. Moreover, the effect of adding metal layers to basalt fiber reinforced epoxy composites with various combinations of metals is also investigated. Akhlaghi et. al [180] investigated the dependence of the strength from the temperature and exposure time. Results reveal that a severe loss of the strength was observed for long holding time and high temperature: i.e. the exposure time have not exceed 15 min. Despite this, the high stability of basalt was confirmed by the micro-morphological analysis that indicated that the fibres maintained their own shape. Furthermore, a high dependence of the porosity and void contents was observed. The different behavior at high temperature between ceramic fibres and metallic matrix in terms of plastic deformation and flowing, even if a good grade of adhesion is demonstrate by micrograph analysis, leads to a higher percentage of defect as higher is the fibres volume fraction. Sabet et. al [181] studied the feasibility of basalt/metal matrix composite through the study of the thermal behaviour of the fibres. In order to find the best range of the controlling parameter, the effect of high temperature and exposure time on the strength was studied. Vannan and Vizhian [182] show as squeeze infiltration could be a good solution to manufacture short basalt fibres-Al alloy matrix composites. In particular, the experimental observations showed that a homogeneous dispersion can be obtained and an analytical model can provide a tool to predict the elastic properties of this kind of material. Furthermore, it was shown how, increasing

the volume fibres fraction, the ductility decrease. Karthigeyan et. al [183] performed a deposition of copper coating on short basalt fibres to improve the interface between the metal matrix and reinforcement. The electroless process used to deposit the copper coating onto the basalt fibre relies on a sequence of sensitization time, activation time and metallization time. Aim of this work was to optimize the above parameters to know the amount of coating thickness. The authors stated that it is possible to obtain a uniform and continuous coating of copper. In particular, the maximum thickness is obtained at 15 min of sensitization time, 15 min of activation time, 3 min of metallization time, 45 C bath temperature and pH 13.

11. Concrete composites

Fibre reinforced concrete is a most widely used solution for improving tensile and flexural strength of concrete. Various types of fibres such as steel, polypropylene, glass and polyester are generally used in concrete. Fibre reinforced concrete is a cement-based composite material that has been developed in recent years. It is used in construction for its excellent flexural-tensile strength, resistance to splitting, impact resistance and excellent permeability, and frost resistance. It is an effective way to increase toughness, shock resistance and resistance to plastic shrinkage cracking of the mortar. Basalt fibre for cement and concrete is not expensive, it is a competitive alternative product of polypropylene and polyacrylonitrile fibres. It is easy to disperse when mixed with cement concrete and mortar.

Basalt fibre, made of crude lava (containing basalt), possesses excellent physical and mechanical properties, and thus, has been used as reinforcing material for concrete recently. Basalt fibres have also been used studied as reinforcement for concrete materials. In particular, Li and Su [184-185] showed that the addition of basalt fibre can significantly improve deformation and energy absorption capacities of geopolymeric concrete while there is no notable improvement in dynamic compressive strength. Jiang et. al [186] showed that adding basalt fibres reduces markedly dry shrinkage of cement mortar, especially at early ages. Moreover, the basalt fibres reinforced mortars have greater compressive and flexural strengths at early hydration period but have little less strength at the age of 28- days than mortar without fibres. In another research. Zhang et. al [187] experimental results showed that bending resistances of short – chopped basalt fiber concrete is increased .Dias and Thaumaturgo [188] analyzed the influence of the volume fraction of short basalt fibre on the fracture toughness of geopolymeric cement concretes. According to the experimental results, geopolymeric concretes show better fracture properties and were so less sensitive to the presence of cracks than conventional Portland cement. In particular, the basalt fibres were found to be more efficient in strengthening geopolymeric concretes than Portland cements. On the other hand, they were found to be more efficient in toughening geopolymeric concretes than Portland cements only for the highest fibre concentrations. Kabay [189] evaluated the effect of basalt fibre on physical and mechanical properties of concretes To this aim, ten mixtures were prepared by incorporating different amounts and sizes of basalt fibres. The mechanical characterization showed that improvements of flexural strength, fracture

energy and abrasion resistance can be obtained by using basalt fibre even at low contents. While inclusion of basal fibre in concrete resulted in a decrease of the compressive strength. Similarly, the effects of the volume fraction and length of basalt fibres on the mechanical properties of concretes were analyzed also by Jiang et. al [190]. To this aim, three types of fibre were used (i.e. Polypropylene fibre and basalt fibres with length equal to 12 mm and 22 mm, respectively). This work showed that the basalt fibres significantly improve tensile strength, flexural strength and toughness index of the composites, whereas the compressive strength shows no obvious increase. Furthermore, it was found that the fibre length also influences the mechanical properties. Moreover, basalt fibres have been lately considered instead of carbon fibres as technical textiles acting as reinforcement in cement-based mortars (i.e. textile-reinforced mortars) by Larrinaga et.al [191-192]. Borhan [193] studied mechanical and thermal properties of concretes manufactured using recycled waste mixed colour glass as a partial replacement (i.e. 20%, 40%, and 60% by weight) for the natural fine aggregate and chopped basalt fibres (i.e. 0%, 0.1%, 0.3%, and 0.5% by total volume of the mix) as reinforcement. Basalt fibres lead to an enhancement in concrete compressive strength for all the mixes investigated. As regard the thermal properties, a significant reduction in heat transfer for all temperature levels was found using high percentages of waste glass and basalt fibres. The strengthening of reinforced concrete structures has emerged as a necessity due to different causes that affect a building during the life span. Besides using basalt fiber as reinforcement of concrete based matrices, it finds its application in polymer based composites as a strengthening material for structural concrete applications. Sim et. al [19] demonstrated this by experimental tests for durability, mechanical properties, and flexural strengthening, author concludes that when moderate structural strengthening but high resistance for fire is simultaneously sought, e.g. for building structures, basalt fibres can be a good alternative to glass or carbon fibres in reinforced polymer (FRP) strengthening systems. Chen et. al [194] conducted an experimental investigation on the strengthening of two-way RC slabs using different type of composite materials. In their study they analysed strengthening with carbon (CFRP), glass (GFRP) and basalt (BFRP) composites. For strengthening design, the authors have chosen a crossshape scheme, based on engineering practice, to simulate the steel reinforcement in the slab. The experimental results showed that there is almost no strengthening effect for a reinforced concrete slab when the cross-shape strengthening scheme was used, except in the case of using carbon fibre reinforced polymer as a strengthening material. Moreover, there was found a slight improvement when using two layers of basalt fibre reinforced polymer. Thus it is important to choose appropriate FRP material system in order to achieve good strengthening effect. Campione et. al [195] compared the behaviour in compression of concrete cylinders externally wrapped with basalt and carbon fibres. In particular, the main variables investigated were the number and type of plies (i.e. full or partial wrapping), the type of loading (i.e. monotonic and cyclic actions) and the type of fibre (i.e. basalt and carbon). The experimental results showed the possibility of reducing the brittleness of unconfined concrete, resulting

significantly increased both the post-peak resistance and the axial strain of confined concrete corresponding to BFRP failure.

Gore Ketan et. al [196], studied the mechanical performance of basalt fibre reinforced concrete of grade M40 and the effect of different proportion of basalt fibre in the mix and to find optimum range of basalt fibre content in the mix. Portland cement, Fine and course aggregates, super plasticizer and basalt fibres were used to prepare the concrete samples. The compressive strength, split tensile strength, flexural strength of the material were tested and analysed results reveal that there is a decrease in the strength values after the addition of basalt fibre at 7 and 14 days, but various other research works have suggested that the strength increase substantially at 28 days. In another research Ramakrishnan et. al [197], investigated the use of basalt fibre bars for reinforcing concrete members. Test results indicated that specimens reinforced with BFRP bars with short bond lengths exhibited gradual slip prior to failure. Specimens with long bond lengths exhibited sudden failures due to rupture of the BFRP bars. Patnaik [198] studied the flexural strength of 13 concrete beams reinforced with BFRP bars and compared the measured failure loads to those predicted by ACI 440.1R-06 guidelines. The study concluded that prediction of moment capacities by ACI 440.1R-06 agrees well with the measured values. Ovitigala [199] investigated the behavior of lightweight and normal weight concrete beams reinforced with BFRP bars. In addition, the study reported higher deflections for BFRP-reinforced concrete beams in comparison to steel-reinforced concrete beams with the same flexural capacity. Fathima [200], investigated and compared the compressive, flexural and splitting tensile strength of basalt fibre reinforced concrete with plain M30 grade concrete. In this study, the effect of inclusion of basalt fibres on the compressive, flexural and splitting tensile strength of fibre reinforced concrete. The experimental test results demonstrated a considerable increases in compression, flexural and splitting of specimen at 3, 7 and 28 days with addition of basalt fibres. Nayan Rathod et. al [201], investigated concrete cubes and concrete beams with basalt fibres and without basalt fibres are to show the difference in compressive strength and flexural strength and indicates the tremendous potential of BFRC as an alternative construction material. The chemical tests were also carried on the basalt fibre to check their strength and stability with effect on their physical properties. Results showed that increase in strength is observed when basalt fiber are introduced. Another application of basalt fibres as reinforcement of concrete structures regards also bars made of thermoset polymer used in the concrete structures instead of traditional steel reinforcement was conducted by Urbanski et. al [202]. In another investigation, Zhu et. al [203] investigated the fire resistance of reinforced concrete beams strengthened with near surfacemounted bars, which were composed of basalt fibre and three different resin matrices: i.e. a heat-resistant vinyl ester resin, a common vinyl ester resin and a heat-resistant epoxy resin. Pearson et. al [204] compared the long-term behaviours of prestressed **basalt fibre reinforced** polymer bars and steel ones. To this aim, three basalt reinforced polymer samples, two steel high yield reinforcing bars, and one high tensile steel cable sample were tested carrying out creep tests at room temperature and setting tension equal to 16 kN. The

experimental results showed that prestress losses are seen to be equal or less with basalt reinforced bars and steel in comparison to steel cable. Banibayat and Patnaik [205] have produced basalt fiber reinforced polymer (BFRP) bars for potential use as internal reinforcement of concrete, by means of a new type of automated wet lay-up process. The objective of this study was to determine the variability of mechanical properties of BFRP bars in order to verify the usefulness of the new process. Statistical analysis techniques were applied to investigate the variation and distribution of the data set obtained from tensile tests of BFRP bars. This study revealed that the basalt reinforced bars manufactured by using the new automated wet-layup process shows variation in mechanical properties similar to that of fibre reinforced bars manufactured by other methods. However, it was shown that this process has economic benefit compared to the traditional pultrusion method due to its simplicity and cost effectiveness resulting from less stringent production controls. Due to their strong tensile properties and corrosion resistance, basalt fibre reinforced polymer bars are also deemed as a substitute material of steel bar to enhance the durability of reinforced **concrete bridges** [206]. Recently, some researches were focused on the feasibility of the use of basalt fibre also in **hot mix asphalt concrete** [207-208]. Gao et. al [209-211] studied the water stability and the performances at low and high temperatures of asphalt concretes reinforced with basalt fibres, showing the beneficial effect of basalt fibre on the evaluated performances.

12. Conclusion

From the literature review it is understood that basalt fiber will be a potential replacement for glass fibers and other synthetic fibers. It is cost effective and eco-friendly material. Basalt fiber reinforced polymer having wide range of applications due to their great mechanical property and thermal stability. The basalt fiber is now being a popular choice for the material scientist for the replacement of steel and carbon fiber due to its high rigidity and low elongation or extension at break. Its supreme tenacity value makes it as a useful reinforcement material in the present and also for the future era to come. Basalt fibres can be considered environmentally friendly and non-hazardous materials. Basalt, being an ecologically pure substance, has a wide spectrum of applications. It is not a new material, but its applications are surely innovative in many industrial and economic fields, from building and construction to energy efficiency, from automotive to aeronautic, thanks to its good mechanical, chemical and thermal performances. Its applications are numerous. Basalt-based geo-composites are extensively used in making radiation-proof protective caps for nuclear waste disposal sites. Another example is basalt geo-mesh. Basalt casting can be a good solution for the equipment facing high wear and tear in the using basalt lined casted pipes. Basalt has already replaced asbestos as a heat insulator due to its low thermal conductivity. Apart from these examples, basaltic tapes/fabrics have also been in use for insulating high tension wires during power transmission and for protection against fire hazards. In the automobile industry, basalt fibers are employed in the fabrication of car brakes. Hence, basalt fibre has gained increasing attention as a reinforcing material especially compared to traditional glass

fibres. The production process, even if it is very similar to the glass fibres one, does not require additives and a lower amount of energy is needed with benefits in terms of environmental impact, economics and plants' maintenance. The base cost of basalt fibres depend on the quality and the chemical composition of the raw material and this leads to have several kind of fibres with different thermal, chemical and mechanical properties. Basalt fibres within polymer (i.e. thermoplastic, thermoset and biodegradable), metallic and concrete matrices exhibit promising properties. Due to this, these fibres have the potential to be the next generation materials for structural application for infrastructure, automotive industry and consumer application.

ACKNOWLEDGEMENT

The authors gratefully acknowledge the support by project No. L1213 of program NPU from MSMT Czech Republic.

13. References

1. RL Shishoo ,Technical textiles-Technological and market developments and trends, Indian Journal of Fibre and Textile Research 22, 213-221 ,1997.
2. Pramod Chaphalkar, Ajit D. Kelkar ,Classical laminate theory model for twill weave fabric composites, Composites Part A Applied Science and Manufacturing , 32(9),1281-1289,2001.
3. John MJ, Thomas S., Biofibres and biocomposites, Carbohydr Polym,71,343–364, 2008.
4. John MJ, Anandjiwala RD. Recent developments in chemical modification and characterization of natural fiber-reinforced composites. Polym Compos ,29,187–207,2008
5. Czigany T.; Vad, J.; Poloskei, K. Basalt fiber as a reinforcement of polymer composites. Period. Polytech. Mech. Eng. 49(1), 3–14,2005
6. Czigány T. Trends in fiber reinforcements – the future belongs to basalt fiber. Express Polym Lett 1,59,2007.
7. Ross A. Basalt fibers: Alternative to glass. Compos Technol ,12,44–48,2006.
8. Colombo C, Vergani L, Burman M., Static and fatigue characterization of new basalt fibre reinforced composites. Compos Struct ,94(3),1165–1174,2012.
9. Pavlovski D, Mislavsky B, Antonov A. CNG cylinder manufacturers test basalt fibre. Reinf Plast ,51(4):36–7,2007.
10. <http://en.wikipedia.org/wiki/Basalt>
11. <http://scienceforkids.kidipede.com/geology/rocks/igneous/basalt.htm>
12. Kamenny, V. (2015). Advanced basalt fiber, Basfiber. Retrieved from <http://www.basfiber.com>
13. FM Kogan, OV Nikitina, Solubility of chrysotile asbestos and basalt fibres in relation to their fibrogenic and carcinogenic action. Environ Health Perspect 102,205-6.1994.
14. Quagliarini E, Monni F, Lenci S, Bondioli F. Tensile characterization of basalt fibre rods and ropes: a first contribution. Constr Build Mater 34, 372-380,2012.
15. McConnell EE, Kamstrup O, Musselman R, Hesterberg TW, Chevalier J, Miller WC ,Chronic inhalation study of size-separated rock and slag wool insulation fibres in Fischer 344/N rats. Inhal Toxicol ,6:571-614,1194.
16. Weddell JK., Continuous ceramic fibres. J Text Inst 4,333-359,1990.

17. Jiri Militky, Kovačić V, Rubnerova J. Influence of thermal treatment on tensile failure of basalt. *Eng Fract Mech* 69 ,1025-33,2002.
18. Piero De Fazio “Basalt fiber: from earth an ancient material for innovative and modern application”. Retrieved on July 2104 from <http://www.enea.it>
19. Sim, J., Park, C., & Moon, D. Y., Characteristics of basalt fiber as a strengthening material for concrete structures. *Composites Part B– Engineering*, 36, 504–512,2005.
20. Matkó, S., Keszei, S., Csontos, I., Anna, P., Marosi, G., Zsuga, M. Borda, J. & Nagy, G. Fire retarded insulating sheets from recycled materials. *Macromolecular Symposia*, 233,217–224, 2006.
21. Wang, M. C., Zhang, Z. G., & Li, Y. B. , Chemical durability and mechanical properties of alkali-proof basalt fiber and its reinforced epoxy composites. *Journal of Reinforced Plastics and Composites*, 27, 393–40.,2008.
22. Botev, M., Betchev, H., Bikiaris, D., & Panayiotou, C. ,Mechanical properties and viscoelastic behavior of basalt fiber-reinforced polypropylene. *Journal of Applied Polymer Science*, 74, 523–531, 1999.
23. Dalinkevich, A. A., Gumargalieva, K. Z., Marakhovsky, S. S., & Soukhanov, A. V. , Modern basalt fibrous materials and basalt fiber-based polymeric composites. *Journal of Natural Fibers*, 6, 248–271, 2009.
24. Liu, Q., Shaw, M. T., Parnas, R. S., & McDonnell, A. M., Investigation of basalt fiber composite mechanical properties for applications in transportation. *Polymer Composites*, 27, 478–48.2006.
25. Militky, J., & Kovacic, V.,Ultimate mechanical properties of basalt filaments. *Textile Research Journal*, 66,225–229,1996.
26. Chantladze, T. (2015). Industrial assimilation of the effective type of fiber with multicomponent charge. Retrieved from <http://www.tctv.ne.jp>
27. Hafsa Jamshaid & Rajesh Mishra ,A green material from rock: basalt fiber – a review, *The Journal of The Textile Institute*, 107(7), 923-937,2016.
28. Subramanian, R.V., Tang, T. J. Y. and Austin, H. F., Reinforcement of Polymers by Basalt Fibers. *SAMPE Quarterly*, 1977: p. 1-10.
29. Artemenko, S.E., Polymer composite materials made from carbon, basalt, and glass fibers. Structure and properties. *Fiber Chemistry*, 35(3), 226-229,2003.
30. <https://en.wikipedia.org/wiki/Plagioclase>
31. <https://en.wikipedia.org/wiki/Pyroxene>
32. Palmieri, A., Matthys, S., Tierens, M., & Pikakoutas, K. ,Basalt fibers for reinforcing and strengthening concrete. In *Proceedings of the 9th International Symposium of the Fiber-Reinforced Polymer Reinforcement for Reinforced Concrete Structures (FRPRCS-9)*, Adelaide, Australia, 13–15 July, 2009.
33. Jiri Militký and Vladimír Kovačič ,Mechanical properties of basalt fibres ,Selected topics of textile and material science ISBN 978-80-261-0062-1
34. Kim, Y.; Yang, D.; Yoon, S.; Lee, B. W.; Park, S.; Kim, D.;Bae, C. W.; Moon, K. ,A Study on the Mechanical Properties Comparison for the Composites Application of basalt Fibers with GFRP, *Adv. Sci.Lett.* 4(4-5), 1633-1637,,2011
35. Toropina, L.V. et. al “New cloth from basalt fibres”. *Fibre Chemistry*, 27, 67-68, 1995.
36. Landucci, G. et. al “Design and testing of innovative materials for passive fire protection”. *Fire Safety Journal*, 44, 1103-1109, 2009.

37. Vivek Dhand , Garima Mittal , Kyong Yop Rhee , Soo-Jin Park , David Hui, A short review on basalt fiber reinforced polymer composites Composites: Part B, 73 , 166–180,2015.
38. Morova N. Investigation of usability of basalt fibres in hot mix asphalt concrete. Constr Build Mater ,47,175-80,2013.
39. Edited by R Fangueiro, Fibrous and Composite Materials for Civil Engineering Applications, page 21, Wood head publishing Ltd. 2011
40. Saravanan, D., Spinning the rocks – basalt fibers. Journal of the Institute of Engineers (India): Textile Engineering Division, 86, 39–45,2006.
41. Nolf, J. M. ,Basalt fibers – Fire blocking textiles. Technical Usage Textile, 49, 38–42,2003.
42. Czighny T; Polymer composites , Part IV, 309-328, Chapter 17, Discontinuous basalt Fiber-Reinforced Hybrid Composites., 2005 .
43. Vas, L. M., Pölöskei, K., Felh s, D., Deák, T., and Czigány, T., Theoretical and Experimental Study of the Effect of Fiber Heads on the Mechanical Properties of Non-continuous basalt Fiber Reinforced Composites, *Express Polym. Lett.* 1, 109–121 ,2007.
44. Kunalsingha: A short review on basalt fiber .International Journal of Textile Science 1(4), 19-28,2012.
45. Bender, J., Hadley, J. G., Hellerstein, J. P., & Hohman, C. M. (2011). Glass, pottery and related materials. In J. M. Stellman (editor-in-chief), *Encyclopedia of occupational health and safety* (pp. 225–263). Geneva: International labor organization.
46. Gajanan Deshmukh; Basalt - The Technical Fibre; Man-made Textiles in India,258-261,2007.
47. Basaltex, The thread of stone', <http://www.basaltex.com>
48. Inorganic fiber technology, <http://www.usbasalt.com/about-us/inorganic-fiber-technology>
49. Basalt fiber & composite materials technology development, <http://basaltm.com/en/tehnologii/basalt-continuous-fiber-bcf-production-techniques.htm>
50. Kim JS, Lim JH, Huh Y. Melt-spinning basalt fibres based on dielectric heating and steady-state process characteristics. *Fibres Polym* ,14,1148-56,2013.
51. Wei B, Cao HL, Song SH.. Degradation of basalt fibre and glass fibre/epoxy resin composites in seawater. *Corros Sci* 53(1),426–31,2011
52. Wei B, Cao H, Song S., Environmental resistance and mechanical performance of basalt and glass fibers. *Mater Sci Eng A* ,527(18–19),4708–15,2010.
53. Wei B, Cao H, Song S., Tensile behavior contrast of basalt and glass fibers after chemical treatment. *Mater Des* ,31(9),4244–50,2010.
54. Huang G., Tensile behaviors of quartz Aramid and glass filaments after NaOH treatment. *Mater Des* 29(10),1893–6,2008.
55. Scheffler C, Förster T, Mäder E, Heinrich G, Hempel S, Mechtcherine V. Aging of alkali-resistant glass and basalt fibers in alkaline solutions: evaluation of the failure stress by Weibull distribution function. *J Non Cryst Solids* ,355(52–54),2588–95,2209.
56. Ramachandran BE, Velpari V, Balasubramanian N. Chemical durability studies on basalt fibres. *J Mater Sci* 16,3393-7,1981.
57. Van de Velde, K., Kiekens, P., Van Langenhove, L., Cater, S., 2002. Basalt fibers as reinforcement for composites, Editorial, *International Composites News*.

58. Nasir V, Karimipour H, Taheri-Behrooz F, Shokrieh MM. Corrosion behaviour and crack formation mechanism of basalt fibre in sulphuric acid. *Corros Sci* 64,1-7,2012.
59. Rybin VA, Utkin AV, Baklanova NI. Alkali resistance, microstructural and mechanical performance of zirconia-coated basalt fibres. *Cem Concr Res* ,53:1-8,2013.
60. J. Militký, V. Kovačič, Chemical degradation of basalt fibers ,*Textile industry technology* № 3c (317) 55-59,2009.
61. S. J. Park, M. K. Seo, T. J. Ma, and D. R. Lee, Effect of chemical treatment of Kevlar fibers on mechanical interfacial properties of composites, *J. Colloid Interface Sci.*, 252, 249-255 ,2002.
62. Hao L C & Yu W ,Evaluation of thermal protective performance of basalt fibre nonwoven fabrics. *J Therm Anal Calorim* ,100,551-5,2010.
63. Gilewicz P, Dominiak J, Cichočka A, Frydrych I. Change in Structural and Thermal Properties of Textile Fabric Packages Containing basalt Fibres after Fatigue Bending Loading. *Fibres & Textiles in Eastern Europe* 21, 5(101) 80-84,2013.
64. Milman SB, Velikanova MG and Kotov LE.,Development and study of load bearing heat insulation., *Cryogenics* 36, 127–130,1996.
65. Li, X., Study on Thermal Resistance of basalt Filament Yarn. *Advanced Materials Research*, 146, 666-669,2011.
66. Yilmaz S, Ozkan OT, Gunay V. Crystallization kinetics of basaltglass, *Ceram Int.*, 1996;22:477–81.
67. A. V. Knot'koa, b, A. V. Garshevb, I. V. Davydovab, V. I. Putlyaevb, V. K. Ivanova, and Yu. D. Tret'yakova, Chemical Processes during the Heat Treatment of basalt Fibers ISSN 0033-1732, *Protection of Metals*, 2007, Vol. 43, No. 7, pp. 694–700. © Pleiades Publishing, Inc., 2007.
68. Deak T, Czigany T. Chemical composition and mechanical properties of basalt and glass fibre a comparison, *Text Res J* 79(7),645-51,2009.
69. Jung, T., and Subramanian, R. V., Strengthening of basalt Fiber by Alumina Addition, *Scr. Metall. Mater.* 28, 527–532,1993.
70. Wei B, Song S, Cao H. Strengthening of basalt fibres with nano-SiO₂ epoxy composite coating, *Mater Des.*32,4180-6,2011.
71. Wei B, Cao H, Song S. Surface modification and characterization of basaltfibres with hybrid sizings.*Compos Part A* 42,22-9,2011.
72. Wang GJ, Liu YW, Guo YJ, Zhang ZH, Xu MX, Yang ZX. Surface modificationand characterizations of basalt fibres with non-thermal plasma. *Surf CoatTechnol* 201,6565-8,2007.
73. Xie K, Liu H, Hu W, Sun H, Yang S, Yang T. Surface treatment of choppedbasalt fibres and mechanical properties of wood-based composite, *AdvMater Res* .627,796-9,2013.
74. Matko, S., Anna, P., Marosi, G., Szep, A., Keszei, S., Czigany, T. and Posloskei, K., Use of reactive surfactants in basalt fiber reinforced polypropylene composites, *Macromol. Symp.*, 202, 255–26,2003.
75. T. Czigany, Special manufacturing and characteristics of basalt fiber reinforced hybrid polypropylene composites: Mechanical properties and acoustic emission study' *Composites Science and Technology* 66 , 3210–3220,2006.
76. Bin Wei , Hailin Cao , Shenhua Song , Surface modification and characterization of basalt fibers with hybrid sizings *Composites: Part A* 42 , 22–29,2011.

77. Varley RJ, Tian W, Leong KH, Leong AY, Fredo F, Quaresimin M. The effect of surface treatments on the mechanical properties of basalt-reinforced epoxy composites. *Polym Compos* 34:320-9,2013.
78. Kim MT, Kim MH, Rhee KY, Park SJ. Study on an oxygen plasma treatment of a basalt fiber and its effect on the interlaminar fracture property of basalt/ epoxy woven composites. *Compos Part B – Eng* 42(3),499–504,2011.
79. Kurniawan D, Kim BS, Lee HY, Lim JY. Atmospheric pressure glow discharge plasma polymerization for surface treatment on sized basalt fiber/polylactic acid composites. *Compos Part B – Eng* ,43(3),10104,2012.
80. Ting yang , Zhenjin cui ,Jiahui yang , Yuqiu yang , Hiroyuki hamada ,Polyurethane surface treatment on two kinds of basalt fiber composite and mechanical properties comparison Conference: ASME 2013 International Mechanical Engineering Congress and Exposition
81. Seong-Ock Lee , Kyong Yop Rhee , Soo-Jin Park , Influence of chemical surface treatment of basalt fibers on interlaminar shear strength and fracture toughness of epoxy-based composites , *Journal of Industrial and Engineering Chemistry* 32 , 153–156,2015.
82. Kukureka, S.N., Hooke, C.J., Rao, M., Liao, P., Chen, Y.K.: The effect of fiber reinforcement on the friction and wear of polyamide 66 under dry rolling-sliding contact, *Tribol. Int.* 32, 107–116 ,1999.
83. Bashtannik, P. I.; Ovcharenko, V. G.; Boot, Y. A. Effect of combined extrusion ... basalt-plastics based on polypropylene, . *Mech. Compos. Mater.* 33, 299, 1997.
84. T. Czigány, "Basalt Fiber Reinforced Hybrid Polymer Composites", *Materials Science Forum*, 473-474, 59-66, 2005.
85. Lopresto V, Leone C, De Iorio I. Mechanical characterization of basalt fibre reinforced plastic. *Compos B Eng* ,42,717-23,2011.
86. Dorigato A, Pegoretti A. Fatigue resistance of basalt fibres-reinforced laminates. *J Compos Mater* 46,1773-85,2012.
87. Chairman CA, Kumaresh Babu SP. Mechanical and abrasive wear behavior of glass and basalt fabric-reinforced epoxy composites. *J Appl Polym Sci.* 130, 120-30,2013.
88. Shokrieh MM, Memar M. Stress corrosion cracking of basalt/epoxy composites under bending loading. *Appl Compos Mater* ,17,121-35,2010.
89. Liu, Q. et. al Investigation of basalt fiber composite mechanical properties for applications in transportation”. *Polymer Composites*, vol. 27, pp. 478-483, 2006.
90. Liu Q, Shaw MT, Parnas RS, McDonnel AM. Investigation of basalt fibre composite aging behaviour for applications in transportation. *Polym Compos*27,475-83,2006.
91. He C, Li Y, Zhang Z, Sun Z. Impact damage modes and residual flexural properties of composites beam. *J Reinf Plast Compos* ,27,1163-75,2008.
92. Sfarra S, Ibarra-Castanedo C, Santulli C, Paoletti A, Paoletti D, Sarasini F, et. al Falling weight impacted glass and basalt fibre woven composites inspected using non-destructive techniques. *Compos Part B* 45,601-8,2013.
93. De La Rosa García P, Escamilla AC, Nieves Gonzalez García M. Bending reinforcement of timber beams with composite carbon fibre and basalt fibre materials. *Compos Part B* ,55,528-36,2013.
94. Kim H. Thermal characteristics of basalt fibre reinforced epoxy-benzoxazine composites. *Fibres Polym* ,13,762-8,2012.
95. Kim H., Enhancement of thermal and physical properties of epoxy composite reinforced with basalt fibre. *Fibres Polym* ,14,1311-6, 2013.

96. Espana JM, Samper MD, Fages E, Sánchez-Núñez L, Balart R., Investigation of the effect of different silane coupling agents on mechanical performance of basalt fibre composite laminates with bio-based epoxy matrices. *Polym Compos* ,34,376-81,2013.
97. Khosravi H., Eslami-Farsani R. ,On the mechanical characterizations of unidirectional basalt fiber/epoxy laminated composites with 3-glycidoxypropyltrimethoxysilane functionalized multi-walled carbon nanotubes-enhanced matrix - *Journal of Reinforced Plastics and Composites*, 2015
98. Chen W, Shen HB, Auad ML, Huang CZ, Nutt S. Basalt fibre epoxy laminates with functionalized multi-walled carbon nanotubes. *Compos Part A* 40,1082-9,2009.
99. Kim MT, Rhee KY, Park SJ, Hui D. Effects of silane-modified carbon nanotubes on flexural and fracture behaviors of carbon nanotube-modified epoxy/basalt composites. *Compos B Eng* 43,2298-302,2012.
100. Kim MT, Rhee KY, Lee BH, Kim CJ. Effect of carbon nanotube addition on the wear behavior of basalt/epoxy woven composites. *J Nanosci Nanotechnol* 13,5631-5,2013.
101. Kim MT, Rhee KY. Flexural behavior of carbon nanotube-modified epoxy/basalt composites. *Carbon Lett* 12(3),177-9,2011.
102. Kim MT, Rhee KY, Kim HJ, Jung DH. Effect of moisture absorption on the flexural properties of basalt/CNT/epoxy composites. *Carbon Lett* 13(3),187-9,2012.
103. Kim MT, Rhee KY, Kim HJ, Jung DH. A study on the fracture toughness of seawater-absorbed carbon nanotube/epoxy/basalt composites. *Carbon Lett* 14(3),190-2,2013.
104. Lee JH, Rhee KY, Park SJ. The tensile and thermal properties of modified CNT reinforced basalt/epoxy composites. *Mat Sci Eng A Struct.* 527(26),6838-43,2010.
105. Bashar MT, Sundararaj U, Mertiny P. Mode-I interlaminar fracture behaviour of nanoparticle modified epoxy/basalt fibre-reinforced laminates. *Polym Test* 32,402-12,2013.
106. Ary Subagia IDG, Tijing LD, Kim Y, Kim CS, Vista IVFP, Shon HK. Mechanical performance of multiscale basalt fibre epoxy laminates containing tourmaline micro/nano particles. *Compos Part B* 58,611-7,2014.
107. Carmisciano S, De Rosa IM, Sarasini F, Tamburrano A, Valente M. Basalt woven fibre reinforced vinyl ester composites: flexural and electrical properties. *Mater Des* 32,337-42,2011.
108. Zhang F, Wu L, Wan Y, Gideon RK, Gu B, Sun B. Numerical modeling of the mechanical response of basalt plain woven composites under high strain rate compression. *J Reinf Plast Compos.* 33,1087-104,2014.
109. De Rosa IM, Marra F, Pulci G, Santulli C, Sarasini F, Tirillo J, et al. Post-impact mechanical characterisation of glass and basalt woven fabric laminates. *Appl Compos Mater* .,19,475-90,2012.
110. Czigany T, Poloskei K, Karger-Kocsis J. Fracture and failure behavior of basalt fibre mat-reinforced vinyl ester/epoxy hybrid resins as a function of resin composition and fibre surface treatment. *J Mater Sci* ,40, 5609-18,2005.
111. Subramanian RV, Austin HF. Silane coupling agents in basalt-reinforced polyester composites. *Int J Adhes Adhes* .1:50-4,1980.

112. Manikandan V, Winowlin Jappes JT, Suresh Kumar SM, Suresh Kumar, Amuthakkannan P. Investigation of the effect of surface modifications on the mechanical properties of basalt fibre reinforced polymer composites. *Compos B Eng* ,43,812-8,2012.
113. Amuthakkannan P., Manikandan V. Winowlin Jappes J.T , Uthayakumar M., Effect of fibre length and fibre content on mechanical properties of short basalt fibre reinforced polymer matrix composites ,*Materials Physics and Mechanics* 16,107-117,2013.
114. Gideon RK, Hu H, Wambua P, Gu B. Characterizations of basalt unsaturated polyester laminates under static three-point bending and low-velocity impact loadings. *Polym Compos.*35,203-13,2014.
115. Gideon RK, Zhang F, Wu L, Sun B, Gu B. Damage behaviors of woven basalt unsaturated polyester laminates under low-velocity impact. *J Compos Mater* 53, 706-718,2014.
116. Zhang Y, Yu C, Chu PK, Lv F, Zhang C, Ji J, et. al Mechanical and thermal properties of basalt fibre reinforced poly(butylene succinate) composites. *Mater Chem Phys.*133,845-9,2012.
117. Li, Y., Sang, L., Wei, Z. Chen Ding, Ying Chang, Guangyi Chen, Wanxi Zhang, Jicai Liang, Mechanical properties and crystallization behavior of poly(butylene succinate) composites reinforced with basalt fiber, *J Therm Anal Calorim* 122(1) 261-270, 2015.
118. Rajesh Mishra, Richa Tiwari , Miroslava Marsalkova , B.K. Behera & Jiri Militky, Effect of TiO₂ nanoparticles on basalt/polysiloxane composites: mechanical and thermal characterization, *The Journal of The Textile Institute*, 103(12), 1361-1368,2012.
119. Cerný M, Glogar P, Goliša V, Hruška J, Jakeš P, Sucharda Z, et. al Comparison of mechanical properties and structural changes of continuous basalt and glass fibres at elevated temperatures. *Ceram Silik* ,51(2),82-88,2007.
120. Cerný M, Glogar P, Sucharda Z. Mechanical properties of basalt fibre reinforced composites prepared by partial pyrolysis of a polymer precursor. *J Compos Mater.*43,1109-20,2009.
121. Cerný M, Glogar P, Sucharda Z, Chlup Z, Kotek J. Partially pyrolyzed composites with basalt fibres e mechanical properties at laboratory and elevated temperatures. *Compos Part A Appl S* .40,1650-9,2009.
122. Cerný M, Halasová M, Schwaigstillová J, Chlup Z, Sucharda Z, Glogara P, et. al Mechanical properties of partially pyrolysed composites with plain weave basalt fibre reinforcement. *Ceram Int.*40,7507-21,2014.
123. Cerný M , Sucharda Z and Glogar P ,Mechanical behavior of polysiloxane matrix – based composite reinforced with basalt fibres at elevated temperatures *Acta Geodyn. Geomater.*, 5(4) (152), 399–406, 2008
124. De Vergara UL, Sarrionandia M, Gondra K, Aurrekoetxea J. Impact behaviour of basalt fibre reinforced furan composites cured under microwave and thermal conditions. *Compos Part B* ,66,156-161,2014.
125. Szabo JS, Czigany T. Static fracture and failure behavior of aligned discontinuous mineral fibre reinforced polypropylene composites. *Polym Test.*,22,711-9,2003.
126. Matko Sz, Anna P, Marosi Gy, Szep A, Czigany T, Pölöskei K. Use of reactive ϵ surfactants in basalt fibre reinforced polypropylene composites. *Macromol Symp* 202,255-67,2003.
127. Eslami-Farsani R, Reza Khalili SM, Hedayatnasab Z, Soleimani N. Influence of

- thermal conditions on the tensile properties of basalt fibre reinforced polypropylene-clay nanocomposites. *Mater Des* .53,540-9,2014.
128. Bashtannik PI, Kabak AI, Yakovchuk YuYu. The effect of adhesion interaction on the mechanical properties of thermoplastic basalt plastics. *Mech Compos Mater* 2003;39:85-8.
 129. Akinci A. Mechanical and morphological properties of basalt filled polymer matrix composites. *J Mater Sci Eng*.35,29-32,2009.
 130. Akinci A, Yilmaz S, Sen U. Wear behavior of basalt filled low density polyethylene composites. *Appl Compos Mater*.19,499-51,2012.
 131. Wang J, Chen B, Liu N, Han G, Yan F. Combined effects of fibre/matrix interface and water absorption on the tribological behaviors of waterlubricated polytetrafluoroethylenebased composites reinforced with carbon and basalt fibres. *Compos Part A* ,59,85-92,2014.
 132. Zhang X, Pei X, Wang Q. Friction and wear properties of polyimide matrix composites reinforced with short basalt fibres. *J Appl Polym Sci*.111,2980-85,2009
 133. Zhang X, Pei X, Wang Q. Friction and wear properties of basalt fibre reinforced/solid lubricants filled polyimide composites under different sliding conditions. *J Appl Polym Sci*.,114,1746-52,2009.
 134. Deak T, Cziganany T, Tamas P, Nemeth C. Enhancement of interfacial properties of basalt fibre reinforced nylon 6 matrix composites with silane coupling agents. *eXPRESS Polym Lett* .4,590-8,2010.
 135. Deak T, Cziganany T, Marsalkova M, Militký J. Manufacturing and testing of long basalt fibre reinforced thermoplastic matrix composites. *Polym Eng Sci* .50,2448-56,2010.
 136. Meszaros L, Gali IM, Cziganany T, Czvikovszky T. Effect of nanotube content on mechanical properties of basalt fibre reinforced polyamide 6. *Plast Rubber Compos Process Appl* .,40,28993,2011.
 137. Meszaros L, Deak T, Balogh G, Czvikovszky T, Cziganany T. Preparation and mechanical properties of injection moulded polyamide 6 matrix hybridnanocompositi. *Compos Sci Technol*.75,22-7,2013.
 138. Hoto R, Andres J, Cabillic B, Gascón Ll, García JA. Optimization of mechanical properties of basalt woven/APA-6 composite parts by means of velocitycontrol. In: *Proceedings of ICCM 18, ICC Jeju, Korea*; . p. 21-6, August 2011
 139. Song J, Liu J, Zhang H, Chen L, Zhong Y, Yang W. Basalt fibre-reinforced PA1012 composites: morphology, mechanical properties, crystallization behaviours, structure and water contact angle. *J Compos Mater* ,49,415-24,2015.
 140. Song J, Liu J, Zhang H, Yang W, Chen L, Zhong Y, et. al PVDF/PMMA/basalt fibre composites: morphology, melting and crystallization, structure, mechanical properties, and heat resistance. *J Appl Polym Sci*.,131,404- 94,2014.
 141. Sándor S " Zabó, Zoltán Kocsis and Tibor Czigány , Mechanical properties of basalt fibre reinforced PP/pa blends jeno ,*Periodica polytechnica ser. mech. eng.* 48(2),119–132 ,2004.
 142. Chen X, Li Y, Gu N. A novel basalt fibre-reinforced polylactic acid compositefor hard tissue repair. *Biomed Mater*.5,044104-8 ,2010.
 143. Liu T, Yu F, Yu X, Zhao X, Lu A, Wang J. Basalt fibre reinforced and elastomer toughened polylactide composites: mechanical properties, rheology, crystallization, and morphology. *JAppl Polym Sci* .125,1292-301,2012.
 144. Tabi T, Tamas P, Kovacs JG. Chopped basalt fibres: a new perspective in

- reinforcing poly(lactic acid) to produce injection moulded engineering composites from renewable and natural resources. *eXPRESS Polym Lett* 7,107-19,2013.
145. Tabi T, Egerhazi AZ, Tamas P, Czigan T, Kovacs JG. Investigation of injection moulded poly(lactic acid) reinforced with long basalt fibres. *Compos Part A* 64:99-106,2014.
 146. Fatimat O. Bakare, Sunil Kumar Ramamoorthy, Dan Åkesson, Mikael Skrifvars Thermomechanical properties of bio-based composites made from a lactic acid thermoset resin and flax and flax/basalt fibre reinforcements, *Composites Part A Applied Science and Manufacturing* ,83 ,176-184,2016
 147. Aruljeyakumar.A ,Srinivasan.V., Thermal Characteristics of Chitosan Filled PLA/basalt Fiber Hybrid Composites Volume 1 Issue No:1,2016 16-22
 148. Ye P, Reitz L, Horan C, Parnas R. Manufacture and biodegradation of wheat gluten/basalt composite material. *J Polym Environ* .14,1-7,2006.
 149. Wittek T, Tanimoto T. Mechanical properties and fire retardancy of bidirectional reinforced composite based on biodegradable starch resin and basalt fibres. *eXPRESS Polym Lett* .2,810-22,2008.
 150. Chikhradze NM, Marquis FD, Japaridze LA, Abashidze GS, Okujava LM. Polymer based composite and hybrid materials for wind power generation. *Mater Sci Forum* ,654-6,2612-5,2010.
 151. Cao SH, Wu ZS, Wang X. Tensile properties of CFRP and hybrid FRP composites at elevated temperatures. *J Compos Mater*.43,315-30,2009.
 152. Ary Subagia IDG, Kim Y, Tijing LD, Kim CS, Shon HK. Effect of stacking sequence on the flexural properties of hybrid composites reinforced with carbon and basalt fibres. *Compos B Eng*.58,251-8,2014.
 153. Zhang CH, Zhang JB, Qu MC, Zhang JN. Toughness properties of basalt/carbon fibre hybrid composites. *Adv Mater Res*.150-151,732-5,2011.
 154. V. Fiore, A. Valenza, and G. DiBella, A. Glass–basalt/epoxy hybrid composites for marine applications. *Mater. Des.* 32, 2091-99 ,2011.
 155. Amuthakkannan P., Manikandan V. Winowlin Jappes J.T , Uthayakumar M,Uthayakumar Mechanical Properties of basalt and Glass Fiber Reinforced Polymer Hybrid Composites Journal of Advanced Microscopy Research 9(1) 1-6 ,2014.
 156. Amuthakkannan P., Manikandan V. Winowlin Jappes J.T , Uthayakumar M, Uthayakumar Hybridization effect on mechanical properties of short basalt/jute fiber-Reinforced polyester composites Science and Engineering of Composite Materials 20(4) ,343-350, 2013.
 157. Petrucci R, Santulli C, Puglia D, Sarasini F, Torre L, Kenny JM. Mechanical characterisation of hybrid composite laminates based on basalt fibres in combination with flax, hemp and glass fibres manufactured by vacuum infusion. *Mat Des*.49,728-35,2013.
 158. Ozturk S. The effect of fibre content on the mechanical properties of hemp and basalt fibre reinforced phenol formaldehyde composites. *J Mater Sci* .40,4585-92,2005.
 159. Wu ZS, Wang X, Iwashita K, Sasaki T, Hamaguchi Y. Tensile fatigue behaviour of FRP and hybrid FRP sheets. *Compos Part B* .41,396-402,2010.
 160. Dorigato A, Pegoretti A. Flexural and impact behaviour of carbon/basalt fibres hybrid laminates. *J Compos Mater* .48,1121-30,2014.

161. Wang X, Hu B, Feng Y, Liang F, Mo J, Xiong J, et. al Low velocity impact properties of 3D woven basalt/aramid hybrid composites. *Compos Sci Technol* .68,444-450,2008.
162. De Rosa IM, Marra F, Pulci G, Santulli C, Sarasini F, Tirillo J, et. al Post-impact mechanical characterisation of E-glass/basalt woven fabric interply hybrid laminates. *eXPRESS Polym Lett* .5,449-59,2011.
163. Sarasini F, Tirillo J, Valente M, Ferrante L, Cioffi S, Iannace S, et. al Hybrid composites based on aramid and basalt woven fabrics: Impact damage modes and residual flexural properties. *Mat Des*. 49,290-302,2013.
164. Sarasini F, Tirillo J, Valente M, Valente T, Cioffi S, Iannace S, et. al Effect of basalt fibre hybridization on the impact behavior under low impact velocity of glass/basalt woven fabric/epoxy resin composites. *Compos Part A* 47,109-23,2013.
165. Sarasini F, Tirillo J, Ferrante L, Valente M, Valente T, Lampani L, et. al Drop-weight impact behaviour of woven hybrid basaltcarbon/epoxy composites. *Compos Part B* 59,204-20,2014.
166. Sembian Manoharan, Bhimappa Suresha, Govindarajulu Ramadoss, and Basavaraj Bharath ,Effect of Short Fiber Reinforcement on Mechanical Properties of Hybrid Phenolic Composites *Journal of Materials*,2014.
167. M Najafi, SMR Khalili, R Eslami-Farsani Hybridization effect of basalt and carbon fibers on impact and flexural properties of phenolic compositesR. *Iran Polym J* ,23(10),767-773,2014.
168. Eslami-Farsani R, Reza Khalili SM, Najafi M. Effect of thermal cycling on hardness and impact properties of polymer composites reinforced by basalt and carbon fibres. *J Therm Stress* 36,684- 698,2013.
169. Hafsa Jamshaid, Rajesh Mishra,, Thermomechanical characteristics of basalt hybrid and nonhybrid woven fabric–reinforced epoxy composites *Polymer composites*, 37(10) 2982-2994, 2016
170. Hafsa Jamshaid, Rajesh Mishra, Jiri Militky, Miroslava Pechociakova, and Muhammad Tayyab Noman,,Mechanical, Thermal and Interfacial Properties of Green Composites from basalt and Hybrid Woven Fabrics *Fibers and Polymers* (in press)
171. Dehkordi MT, Nosraty H, Shokrieh MM, Minak G, Ghelli D. Low velocity impact properties of intra-ply hybrid composites based on basalt and nylon woven fabrics. *Mat Des* ,31,3835-44,2010.
172. Dehkordi MT, Nosraty H, Shokrieh MM, Minak G, Ghelli D. The influence of hybridization on impact damage behaviour and residual compression strength of intraply basalt/nylon hybrid composites. *Mater Des.*,43283-90,2013.
173. Lopresto V, Leone C, Caprino G, De Iorio I. Innovative sandwiches for civil applications. *Procedia Eng*.10,2058-67,2011.
174. Torres JP, Hoto R, Andres J, García JA. Manufacture of green-composite sandwich structures with basalt fibre and bioepoxy resin. *Adv Mater Sci Eng* 2013.
175. Hoto R, Furundarena G, Torres JP, Munoz E, Andres J, Garcia JA. Flexural behavior and water absorption of asymmetrical sandwich composites from natural fibres and cork agglomerate core. *Mater Lett*.127,48 52,2014.
176. S. Colomina, T. Boronat, O. Fenollar, L. Sánchez-Nacher, R. Balart, High Renewable Content Sandwich Structures Based on Flaxbasalt Hybrids and Biobased Epoxy Polymers ,*AIP Conference Proceedings* 1593, 467 ,2014.

177. S. M. R. Khalili, V. Daghigh, and R. E. Farsani, Mechanical behavior of basalt fiber-reinforced and basalt fiber metal laminate composites under tensile and bending loads, *J. Reinf. Plast. Compos.*30(8), 647–659, 2011.
178. Fiore V, Alagna F, Di Bella G, Valenza A. On the mechanical behavior of BFRP to aluminum AA6086 mixed joints. *Compos Part B* 48,79-87,2013.
179. RE Farsani, SMR Khalili, V Daghigh -Charpy impact response of basalt fiber reinforced epoxy and basalt fiber metal laminate composites: Experimental study *International Journal of Damage Mechanics*, 2014
180. Akhlaghi F, Eslami-Farsani R, Sabet SMM. Synthesis and characteristics of continuous basalt fibre reinforced aluminum matrix composites. *J Compos Mater.* 47, 3379-88,2013.
181. Sabet SMM, Akhlaghi F, Eslami-Farsani R. Production and optimization of aluminum-basalt composites by hand lay-out technique. In: *Proceedings of the World Congress on Engineering*, vol. III; July 2012. London, UK.
182. Vannan E, Vizhian P. Prediction of the elastic properties of short basalt fibre reinforced al alloy metal matrix composites. *J Miner Mater Charact Eng* 2,61-9,2014.
183. Karthigeyan R, Ezhil Vannan S, Ranganath G, Paul Vizhian S, Annamalai K. Effect of coating parameters on coating morphology of basalt short fibre for reinforcement preparation of al/basalt metal matrix composites. *Int J Electrochem Sci* 2013;8:10138-48
184. Li W, Xu J. Mechanical properties of basalt fibre reinforced geopolymeric concrete under impact loading. *Mat Sci Eng A Struct.*505, 178-86,2009.
185. Li W, Xu J. Impact characterization of basalt fibre reinforced geopolymeric concrete using a 100-mm-diameter split Hopkinson pressure bar. *Mat Sci Eng A Struct* 513-514,145-53,2009.
186. Jiang CH, McCarthy TJ, Chen D, Dong QQ. Influence of basalt fibre on performance of cement mortar. *Key Eng Mater.*426-427,93-6,2010.
187. J. Z. Zhang, H. T. Liu, Y. D. Zhu, Z. Q. Fu, J. Zhao, Bending Resistance of Short-Chopped basalt Fiber Hydraulic Concrete and RC Element, *Advanced Materials Research*, 261-263, 407-410, 2011
188. Dias DP, Thaumaturgo C. Fracture toughness of geopolymeric concretes reinforced with basalt fibres. *Cem Concr Compos.*27, 49-54,2005.
189. Kabay N. Abrasion resistance and fracture energy of concretes with basalt fibre. *Constr Build Mater* .50,95-101,2014.
190. Jiang C, Fan K, Wu F, Chen D. Experimental study on the mechanical properties and microstructure of chopped basalt fibre reinforced concrete. *Mats Des* .58,187-93,2014.
191. Larrinaga P, Chastre C, San-Jose JT, Garmendia L. Non-linear analytical model of composites based on basalt textile reinforced mortar under uniaxial tension. *Compos Part B* 55,518-27,2013.
192. Larrinaga P, Chastre C, Biscaia HC, San-Jose JT. Experimental and numerical modeling of basalt textile reinforced mortar behavior under uniaxial tensile stress. *Mater Des.*55,66-74,2014.
193. Borhan TM. Properties of glass concrete reinforced with short basalt fibre. *Mater Des.*42,265-71,2012.
194. Chen ZF, Wan LL, Lee S, Ng M, Tang JM, Liu M, et. al Evaluation of CFRP, GFRP and BFRP material systems for the strengthening of RC slabs. *J Reinf Plast Compos.* 27, 1233-43,2008.

195. Campione G, La Mendola L, Monaco A, Valenza A, Fiore V. Behavior in compression of concrete cylinders externally wrapped with basalt fibers. *Compos Part B* 69,576-86,2015.
196. Gore Ketan R, Suhasini M.Kulkarni, The Performance Of basalt Fibre In High Strength Concrete, *Journal of Information, Knowledge and Research In Civil Engineering*, 2(2)117,2013.
197. Ramakrishnan, V., Tolmare, Neeraj S., Brik, Vladimir B, Performance Evaluation of 3-D basalt Fibre Reinforced Concrete & basalt Rod Reinforced Concrete. Final Report for Highway IDEA Project 45, Transportation Research Board, 1998; 79.
198. Patnaik, A., Adhikari, S., Bani-Bayat, P., and Robinson, P. Flexural Performance of Concrete Beams Reinforced with basalt FRP Bars. 3rd fib. International Congress, Washington D.C. May 2010: 3821-3833.
199. Ovitigala, T., Issa, M.A. Flexural Behavior of Concrete Beams Reinforced with basalt Fibre Reinforcement Polymer (BFRP) Bars. 11th International Symposium on Fibre Reinforced Polymer for Reinforced Concrete Structures, Guimarães, Portugal. June 2013: 249-260.
200. Fathima Irine I .A, Strength Aspects of basalt Fibre Reinforced Concrete, *International Journal of Innovative Research in Advanced Engineering* 1(8), 2349-2163,2014.
201. Nayan Rathod et. al, basalt Fibre Reinforced Concrete, *International Journal of Science and Research* 2013; 2319-7064
202. Urbanski M, Lapko A, Garbacz A. Investigation on concrete beams reinforced with basalt rebars as an effective alternative of conventional R/C structures. *Procedia Eng* .57,1183-91,2013.
203. Zhu H, Wua G, Zhang L, Zhang J, Hui D. Experimental study on the fire resistance of RC beams strengthened with near-surface-mounted high-Tg BFRP bars. *Compos Part B* 60,680-7,2014.
204. Pearson M, Donchev T, Salazar J. Long-term behaviour of prestressed basalt fibre reinforced polymer bars. *Procedia Eng* 54,261-9,2013.
205. Banibayat P, Patnaik A. Variability of mechanical properties of basalt fibre reinforced polymer bars manufactured by wet-layup method. *Mat Des* .56,898-906,2014.
206. Zhang S, Shan W. Prospect analysis of the application of BFRP bar to bridges. *Key Eng Mater.*,574,21-9, 2014.
207. Chen Y, Li Z. Study of road property of basalt fibre asphalt concrete. *Appl Mech Mater* .328,22-5,2012.
208. Wenxiao F, Shifu Z, Liging L. Laboratory study of Marshall of basalt fibre modified asphalt mixture. *Appl Mech Mater* .256-259,1851-7,2013.
209. Gao CM, Zhang Q, Zhang HZ. Research on basalt fibre asphalt concrete's water stability. *Appl Mech Mater*.505-506,117-20, 2014.
210. Gao CM, Han S, Chen S, Li H. Research on basalt fibre asphalt concrete's low temperature performance. *Appl Mech Mater*.505-506,35-8,2014.
211. Gao CM, Han S, Zhu KX, Wang ZY. Research on basalt fibre asphalt concrete's high temperature performance. *Appl Mech Mater*.505-506,39-42, 2014.

A study of residual pesticides on conventional and organic cotton comparing biosensor and gas chromatography techniques

Syed Zameer Ul Hassan^{1*}, Jiří Militký², Jan Krejčí³, Rajesh Mishra², Muhammad Salman Naeem², Saima Javed⁴, Ali Asghar¹, Muhammad Kashif¹, Jawad Naeem²

^{1*} *Balochistan University of Information Technology, Engineering and Management Sciences, Quetta, Balochistan, Pakistan*

² *Faculty of Textile Engineering, Dept. of Material Engineering, Studentská 2, Technical University of Liberec 461 17 Czech Republic*

³ *BVT Technologies, a.s., Hudcova 78c, Brno 61200, Czech Republic*

⁴ *Department of Microbiology and molecular genetics, University of The Punjab, Lahore*

1. INTRODUCTION

Cotton alone accounts for 38% of the world textile utilization [1]. Cotton production is complicated concerning environment and pest attack and is responsible for approximately 16% of the world's pesticide consumption [2]. Well over 500 active substances have already been authorized to date and an estimated about 2.5 million tons of pesticides have been applied on this crop. There's a tremendous danger with regard to people to become subjected through these types of pesticides via direct or indirect means. The exposure may be during utilizing the pesticides or through the food sources, or being in close contact to areas treated with pesticides [3]. That is the reason the endeavors have been made to develop cotton without utilizing any fertilizers or pesticides on it. Organic cotton is developed ashore that has been dealt with and given adequate time (no less than three years) for the evacuation of all the harmful buildups of synthetic fertilizers and pesticides utilized before on it [4]. Pesticides are toxic compounds that may cause adverse effects on the human and the environment. Benzoylureas, carbamates, organophosphorus compounds, organochlorine, pyrethroids, sulfonylureas and triazines are the most important groups. There is currently overpowering proof that these chemicals do represent a potential danger to people so the checking the deciding result of human presentation as deposit levels is vital to minimize the risk. For the recognition of pesticides, a lot of analytical procedures have been established over the past few years. The most commonly used techniques are gas chromatography (gc), gas chromatography coupled to mass spectrometry (gc-ms), high-performance liquid chromatography (HPLC) and fluorescence Immunoassay. Nevertheless, these techniques, which are lavish, tedious and require exceedingly prepared work force, are accessible just in advanced labs [5]. Biosensors in view of the restraint of Acetyl cholinesterase (AChE) have been broadly utilized for the identification of Organophosphorus (OP) mixes [6]. Electro investigative sensors and biosensors offer an energizing and achievable chance to

perform natural, nourishment, biomedical, and industrial investigation far from an intense research facility because of their favorable circumstances, for example, their quick reaction, minimal effort of manufacture, probability of scaling down, high selectivity and specificity, and simple to incorporate in programmed gadgets [7]. Electrochemical biosensors for investigation of these pesticides depend on the hindrance of AChE and the restraint degree is proportionate to the pesticide intensity [8]. The capability of Inhibition of AChE by any xenobiotic compound can be considered as an instrument for appraisal of poisonous quality of pesticides, for example, organophosphates and carbamates [9].

For multi residue analysis, Gas Chromatography has been the overwhelming instrument for more than 30 years. It has been comprehensively utilized for the discovery of pesticide buildups showing high constancy and low polarity [10]. Numerous multi residue techniques have been concentrated on for the determination of Organophosphorus, Organochlorine and Organonitrogen pesticides utilizing gas chromatography for partition of individual mixes, trailed by recognition with specific and sensitive sensors (AED, NPD, ECD, FPD or MS). Multi residue investigation and trace-level identification of an extensive variety of pesticides through mass spectrometry has been considered because of its affectability [11]. GC combined with mass spectrometry (GC-MS) has been utilized for the confirmation of identity of pesticide residues [12]. In GC/MS/MS, there are two continuous phases of mass discontinuity where guardian particles dividing into girl particles are scrutinized. This technique has revealed more discriminating and affectability of the determination contrasted with single-stage MS, because of disposal of isobaric obstructions and decrease of the chemical noise. A standout amongst the most unique patterns in pesticide residue analysis is to utilize both of these methods at the last influential step and is considered as a down to earth approach to resolve troubles in target analyte determination on account of troublesome matrices having extreme measures of possibly meddling elements [13]. Positively, tandem mass spectrometry provides much higher level of sureness in analyte determination comparative to single stage mass spectrometry procedure, in light of the fact that isobaric obstructions are kept away from and various-element spectra can be determined. The affirmation of target analytes can be accomplished with more elevated amount of confidence. Amongst the diverse mass analysers, triple quadrupole mass spectrometers have as of late been suggested for the discovery of pesticide remainders in crops [14]. The aim of this study is to examine the risk evaluation taking into account procedures with a specific end goal to choose if the risk is low and satisfactory in scientific terms. The distinguishing proof of pesticide remainders has been accomplished using both the modes of agriculture. The claim to fame of this strategy is that every one of the samples alongside the control points can be analyzed in one run, The aggregate time used for one complete test was around 50 ~ 55 minutes. The target of this investigation is to compute the execution of biosensor and comparing these outcomes with those achieved utilizing the most sophisticated equipment i.e. GC-MS/MS.

2 Experimental Methods

2.1 Materials

The descriptions of the materials used for this study are as follows:

2.1.1 Sample Collection

The samples of three different varieties of cotton namely, Egyptian cotton Giza 86, Pakistani cotton MNH 93 and Indian Cotton were collected. Both varieties have classical conventional cotton and organic cotton. For understanding, we abbreviate the samples as follows:

Egyptian Giza Conventional Cotton	GC
Egyptian Giza Organic Cotton	GO
Pakistani Conventional Cotton	PC
Pakistani Organic Cotton	PO
Indian Conventional Cotton	IC
Indian Organic Cotton	IO

Another three cotton samples were taken after the first harvest from BahawalPur (Pakistan). The detail of these samples is as follows:

BT - 114	SH - 1	Z - 33
----------	--------	--------

The analyses were made within three months of their collection from the field.

2.1.2 Chemicals and Reagents

Table 1: Description of the solvents used

Solvents	Formula	Density (g/mL)	BP (°C)	E_T [a]	$\mu \cdot 10^{30}/\text{cm}$ [b]	E_T^N [c]	Water solub. (g/100g)	Polar ?	[d]
Methanol	CH ₃ OH	0.791	64.5	32.66	5.9	0.762	Miscible	Y	Green
Acetonitrile	CH ₃ CN	0.786	81.6	35.94	13.0	0.460	Miscible	Y	Orange
Acetone	CH ₃ O CH ₃	0.786	56.1	20.56	9.0	0.355	Miscible	Y	Green
Dichloromethane	CH ₂ Cl ₂	1.326	39.6	8.93	3.8	0.309	1.32	N	Red
Toluene	C ₆ H ₅ CH ₃	0.867	110.6	2.38	1.0	0.099	0.05	N	Orange
Hexane	CH ₃ (CH ₂) ₄ CH ₃	0.659	68.7	1.88	0.0	0.009	0.014	N	Red

[a] E_T , Relative permittivity (“dielectric constant”) of the pure liquid at 250C

[b] Dipole moment in Coulombmetre (Cm), measured in benzene, tetrachloromethane, 1,4-dioxane, or n-hexane at 20-300C. 1 Debye = 3.336.10⁻³⁰ Cm.

[c] E_T^N = derived from the transition energy at 250C of the long-wavelength visible absorption of a standard pyridinium N -phenolate betaine dye

[d] The Pfizer “traffic light” solvent preference system [15]

All the chemicals and reagents utilized were obtained commercially. Acetylcholinesterase (electric eel) (EC 3.1.1.7, 827 IU/mg), Acetylthiocholine chloride (A5626), Neostigmine methyl sulphate (N2126), MOPSO Sodium Salt (M8767) and Phosphate Buffer were purchased from Sigma Aldrich. Following HPLC grade solvents for residual analysis have been purchased from Verkon. Selection has been made on the basis of different characteristics of each solvent (Table 1).

2.1.3 Pesticide Standards

Different Pesticide standards were purchased commercially and their purity certified by the supplier to be greater than 99%. Pesticide Mix 155 and Pesticide Mix 17 were purchased from Dr. Ehrenstorfer GmbH, Germany. Pesticide Mix 3 & 14 and Pesticide Mix 18 were purchased from AccuStandard, USA. Pesticide Mix 155 which is abbreviated as KF contains 18 different pesticides mostly of which are the organophosphorous (OP) and carbamates. Pesticide Mix 18 abbreviated as KZ contains 16 different pesticides, mostly of which are organochlorine (OC) pesticides. The compounds of Pesticide Mix 3 & 14 abbreviated as KT contains 20 different pesticides mostly of which are pyrethroids. Whereas Pesticide Mix 17 which is abbreviated as KS contain 20 pesticides which are all OC compounds.

2.2 Sample Preparation

The advancement of a well suited specimen planning technique including extraction, improvement, and cleanup steps gets to be required to acquire a final extricate focused on target analytes. It is always indispensable to complete some pre handling to get a homogeneous and delegate subsample [4]. Following techniques have been implemented for the sample preparation.

2.2.1 Cryogenic Homogenization

CryoMill was utilized for the homogenization with 1 cm ball. All samples of cotton were orchestrated around within a pre-chilled Teflon plant as pallets which contained a concentric Teflon ring and Teflon puck in liquid nitrogen encompassing. Every specimen was processed with two cycles. Every cycle comprises of precisely two minutes for granulating with an interim of 15 seconds for cooling. After the processing the subsequent powder was sampled. This powder had been transferred to a clean Teflon bag and sealed were held overnight in liquid nitrogen vapor. Figure 1 shows the different steps for the cryogenic homogenization.

2.2.2 Ultrasound Assisted Extraction

Ultra sound extraction technique was utilized for the extraction from all of the cotton samples. An aggregate of 0.5 gm homogenized specimen was exchanged to the flask along with 10 ml of the solvent utilized. The flask was set in the extraction apparatus Sonorex at a controlled temperature of 60 OC (Fig 2). Samples were extracted for 30 minutes. The extracts were then filtered and stored for further investigation.

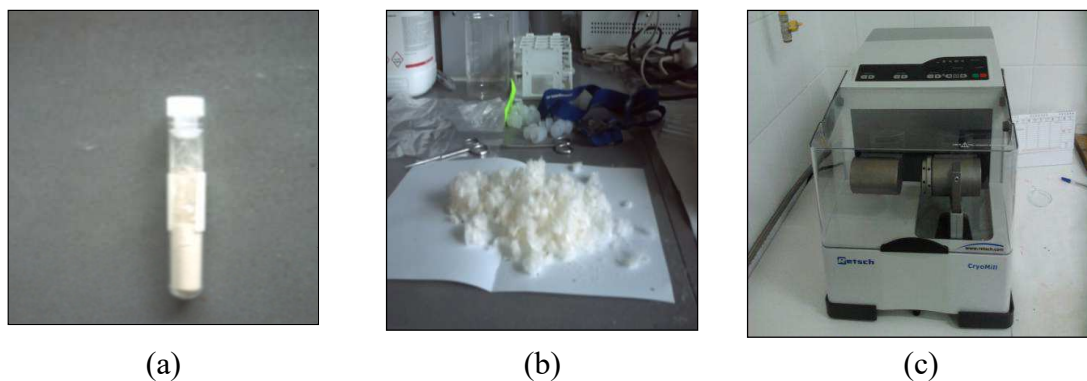


Fig. 1: (a) Raw cotton (b) CryoMill (c) Homogenized sample



Fig. 2: Ultra sonic Extraction and Cotton samples

2.3 Techniques Utilized

Following two different techniques have been employed for the detection of residual pesticides on cotton samples.

2.3.1 Biosensor based detection

Mini Thermostat (MT-1) was utilized for observing the pattern of AChE restraint with the avail of sensors furnished with immo immobilized AchE enzymatic membrane. AC1.W2.RS/AchE sensors were utilized for the analysis of AChE restraint, provided by Bvt Technologies (Fig 3). All quantifications were performed at a potential of 350 mV.



Fig. 3: Minithermostat (Left) & AC1.W2.RS/AChE Sensors (Right)

To follow the George L. Ellman's methodology, following two equipments were utilized (Fig 4). Multi function syringe pump TECHNIC I Linear Pump was used which is responsible for a continuous flow of buffer and also carry the injected analytes on to the surface of biosensor.



Fig. 4: Technic I linear pump & Low pressure dose valve

The flow rate (mL/min) can be adjusted according to the needs. Low pressure dose valve v-7 from Pharmacia Biotech was used for the injection of analytes. The maximum capacity of injection per analyte was 25 μ L.

The electrochemical measurements were performed at a controlled room temperature ($22 \pm 1^\circ\text{C}$). Mopso & phosphate buffer solutions were used. Acetylthiocholine chloride (ATCh) and Neostigmine methyl sulfate were used as enzyme substrate and enzyme inhibitor, respectively.

2.3.2 Biosensor Preparation

AC1.W2.RS/AChE Sensors were used for the monitoring of AChE inhibition, provided by Bvt Technologies (Fig 5). This is a thick film sensor, printed on a base made from Alumina Ceramic (Al_2O_3 -96%). This type of electrode has as a working surface 100 % platinum, as a reference 60/40 % Ag/AgCl and as auxiliary a 100 % platinum.



Fig. 5: AC1.W2.RS Sensors from BVT Technologies

The connection of the sensor occurs through silver conducting paths which are able to minimize the potential difference between the working electrode and the potential actually applied on the system. They have a mass of 0.4 g, a width of 7.26 mm, length of 25.4 mm, and a thickness of 0.63 mm. On the surface of the working electrode is an enzymatic membrane containing 1 IU (Unit) of AChE enzyme, which is immobilized. The diameter of the immobilized bioactive membrane is 2 mm and the mean applied activity is 1 unit/mm². AC1.W2.R1 sensors without immobilization of AChE were used for the enzymatic inhibition optimization.

2.3.2 Gas Chromatography coupled to Triple Quadrupole Mass Spectrometry

The Thermo Scientific TRACE 1310 Gas Chromatograph coupled with triple quadrupole mass spectrometry is utilized (Fig 6). TSQ 8000 mass detector is capable to screen full scan data & MRM analysis simultaneously. Affirmation of pesticide and quantitation was performed by utilizing Timed-SRM methodology. The limit of detection (LOD), the limit of quantitation (LOQ) and accuracy have been worked out in light of the rules for investigative estimations.



Fig. 6: TRACE 1310 Gas Chromatograph

TSQ 8000 mass detector has the ability to analyze full scan data at the same time of targeted MRM analysis. In addition to simplified method start up, another advantage of using the analyzer is that it utilizes Timed-SRM methodology, which enables accurate pesticide identification and quantitation, even for very dense pesticide methodologies. The usability and scanning efficiency of Timed-SRM are complemented by the fast-scanning capability of the TSQ 8000 instrument, making the analysis of hundreds of pesticides, with a total of over one thousand transitions.

By evaluating the retention times of target compounds, we are able to update the pesticides in the Pesticide Compound Database (CDB) with the known retention times. The software is capable of creating both the Trace Finder EFS processing method and the TSQ 8000 system Timed-SRM acquisition list, with acquisition windows centred on the retention times of the target peaks and allowing for acquisition window overlap, so that acquisition windows for all nearby eluting compounds are not forced to start and stop at the same time [16].

3 Results and discussions

3.1 Method development utilizing Biosensors

A rapid, sensitive and low cost method based on AChE-inhibition utilizing biosensor was developed. The working solutions of pesticide standard Mix 155 (KF) was prepared by taking 5 standard concentration levels (0, 1, 10, 100, 1000 ng/mL) along with the standard inhibitor and investigated all together of expanding concentration. The dilutions were prepared in methanol. The enzyme activity has been analyzed following the method adopted by George L. Ellman, in which the determination of acetylcholinesterase operation was measured by taking after the expansion of yellow shading created from thiocholine by a photometric strategy [17]. Optimization of different variables involved in the process like enzyme and substrate concentrations, time of incubation, buffers and their pH has been executed. The level of restraint was ascertained as a relative rot of the biosensor reaction.

$$I \% = 100 \times \frac{I_0 - I_i}{I_0}$$

Where I is the level of restraint of AChE; I_0 and I_i are the current values quantified preceding and after the chemical biosensor is treated with an inhibitor. There must be a certain positive correlation between current and the concentration of pesticides in principle [18].

The scheme of the final testing is described in Table 2.

Table 2: Scheme of final testing

Addition of Substances	Volume (μL)
0.1M Phosphate Buffer	100
ATCh (0.08 mM)	100
Calibration Std	100
Stirring	
AChE (0.5 IU/ μL)	2
Stirring	
After 60 minutes	
Neostigmine	10
Final Stirring	

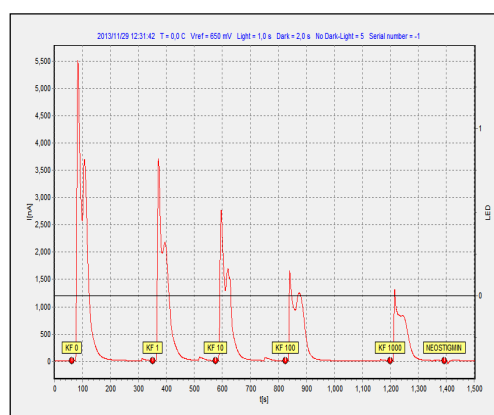


Fig. 7: Amperometric response of calibration samples with optimized concentrations

The results of the above mentioned procedure are shown in Figure 7. A good correlation between AChE activity and the calibration points was observed. Five repetitions (A, B, C, D, E) for the same test have been performed and the resultant graphs are shown in Figure 8, where as Figure 9 shows the overall average inhibition % with relevant concentration levels.

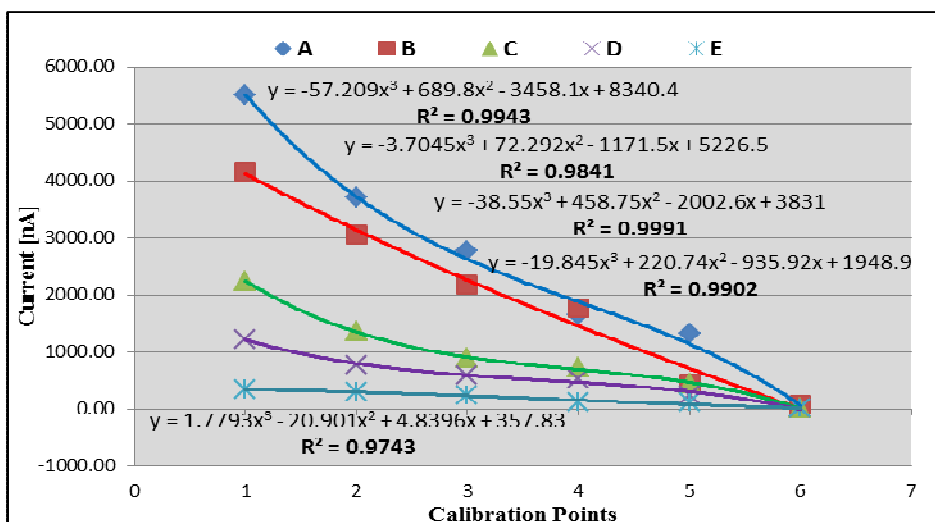


Fig. 8: Amperometric response of different calibration samples; $n=5$

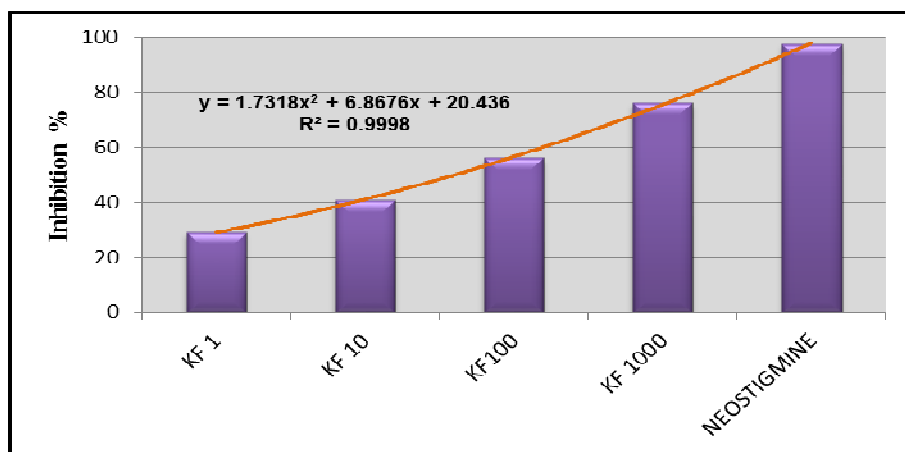


Fig. 9: Average AChE-inhibition caused by different concentrations; $n=5$

The equation of the best fit line is as follows:

$$y = 1.7318x^2 + 6.8676x + 20.436$$

The value of predicted squared coefficient of correlation (R^2) is found to be 0.9998, which is excellent and shows a strong relationship between our variables i.e. Concentration and Inhibition %. The method is utilized for real cotton samples extracted with different solvents (methanol, hexane, toluene, acetone & acetonitrile) after necessary sample pretreatments. The speciality of this method is that all the samples along with the control points can be tested in one run, The total time utilized for one complete test was approximately 50 ~ 55 minutes. The extracts of cotton samples were replaced by calibration points. After the complete procedure these final samples were introduced to the biosensor and the response is monitored. Figure 10 shows the activity of whole the experiment with solvent methanol and the graph which was plotted against the AUC and corresponding analytes.

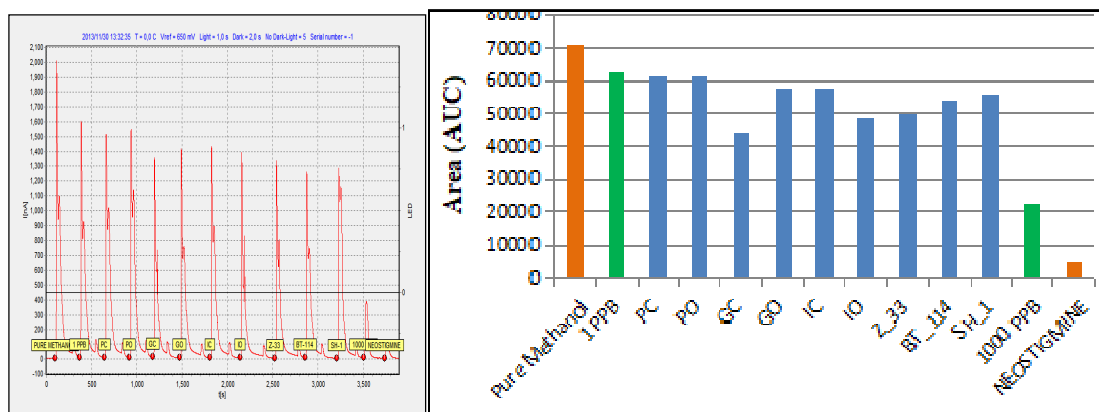


Fig. 10: Amperometric response & AUC of all cotton samples extracted with methanol

We are able to compare our extracts with the help of minimum and maximum concentration's area. It is quite visible that almost all our samples have the area with in the range of 1 ppb to 1000 ppb but none of the samples exceed 1000 ppb limit. The inhibition % was calculated based on the area under the corresponding curves for each analyte and represented in Figure 11. It shows that all of our samples show the inhibition % (on average of < 40) but with some variations. PC and PO samples show almost same inhibition closer enough to 1ppb. There is a significant difference between GC and GO. GC show more inhibition than GO and the opposite trend is seen in the case of IC and IO. IO is responsible for more inhibition than IC.

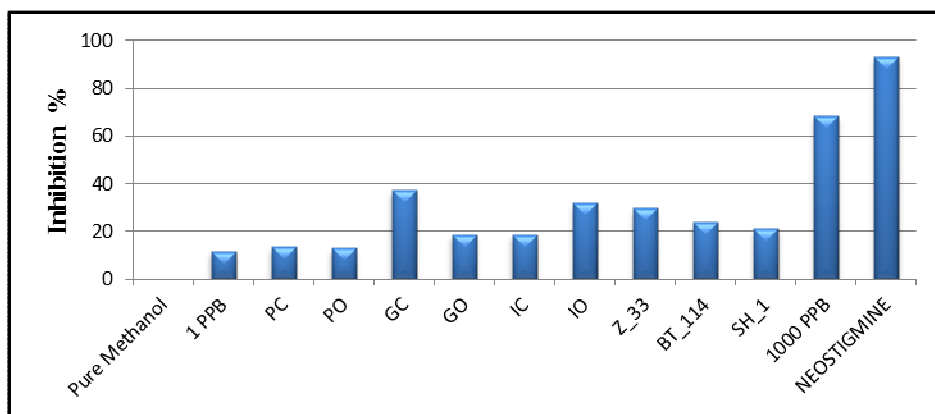


Fig. 11: AChE-Inhibition caused by all cotton samples extracted with methanol

Same procedure was implemented to test the extracts with other solvents like hexane and toluene. With acetone and acetonitrile we experience a very poor response of detector which is not measurable. A summary of all the cotton samples with different solvents has been shown in Figure 12.

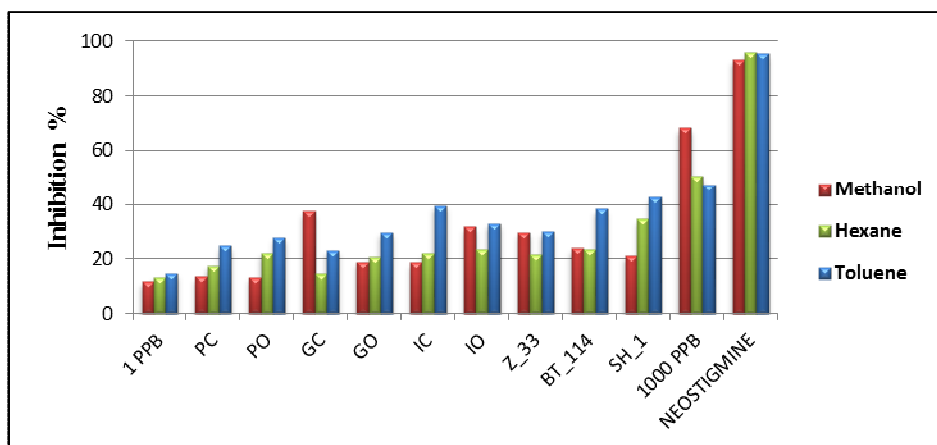


Fig.12: Summary of AChE-Inhibition caused by cotton samples with all solvents

Also the difference of inhibition between classical and organic cotton samples is also not substantial. We can conclude that there may be possibility of the presence of AChE inhibitors in almost all our samples without any discrimination.

3.2 Method development utilizing GC-MS/MS

A multiresidue strategy for examination of 76 pesticides with various physicochemical properties was produced. The technique includes a quick and little scale extraction methodology of real cotton samples collected from different regions (Egypt, Pakistan & India) with five different solvents (Methanol, Acetonitrile, Acetone, Toluene, Hexane) from polar to non-polar region, using Ultra Sound assisted Extraction (USE). Cryogenic Homogenization was being implemented for sample Pre-treatment. After final extraction and filtration the extracts were concentrated. The technology of Gas chromatography with Tandem mass spectrometry (GC-MS/MS) was utilized for the analysis of pesticide remainders. 57 out of 76 pesticides were detected successfully by the method developed. Nineteen (19) pesticides could not be determined by GC-MS/MS using EI ionization, frequently on account of conflict with phase transition of the in place molecules in the GC injector. All the essential parameters which are necessary for the method validation have been taken into account in the light of the document SANCO/12495/2011 for 'Method Validation and Quality Control Procedures for Pesticide Residues Analysis in Food and Feed'[19] which is the latest version of Commission Directive 96/46/EC. Moreover the document from Codex Alimentarius document 'Guidelines on Good Laboratory Practice in Pesticide Residue Analysis' has been also considered [20]. The stock solution of individual pesticide standards of $10\mu\text{g mL}^{-1}$ were prepared by dissolving the appropriate amounts of the analytical standards in the relevant solvent. Working standard solutions were prepared by taking 10 standard concentration levels (1, 2, 5, 10, 20, 50, 100, 200, 500 and 1000 ng/mL) for each standard pesticide mix (KF, KS ,KT & KZ), separately. The dilutions of the pesticide standards were made with the same solvent which they originally contain.

3.2.1. Evaluation of Retention time

The working solution of $1\mu\text{g mL}^{-1}$ of all the pesticide standard mixes (KF, KZ, KT, KS) was tested in EI-MS full scan mode for the typical mass range (35 to 500 amu). One of the resultant chromatograms has been shown in Figure 13 for KZ. Evaluation of retention time is accomplished by comparing the probability of the presence of related ions evaluated by the related chromatograms and electron impact mass spectra of the analyte from the two built in database of libraries i.e. NIST and Mainlib.

Each peak of the chromatogram is analysed for each compound of the standard mix by comparing the mass to charge ratios of precursor and product ions with that of the two built in libraries. The criteria of acceptance have been set for probability of the presence of the analyte $> 85\%$ in both the libraries. Figure 14 (LHS) shows the mass to charge ratio for Primiphos-methyl attained from this above mentioned chromatogram. This mass spectrum is compared with the above mentioned databases. Figure 14 (RHS) shows the resultant mass spectrum obtained from NIST database.

The probability of presence of Primiphos-methyl in NIST is 97 % where as in Mainlib it was 97.03 %. These values are acceptable so the retention time evaluated for Primiphos methyl was 17.28 same as retention time of the corresponding peak in the main chromatogram. All the compounds of KZ and other all mixes were analyzed for the retention time in the same way.

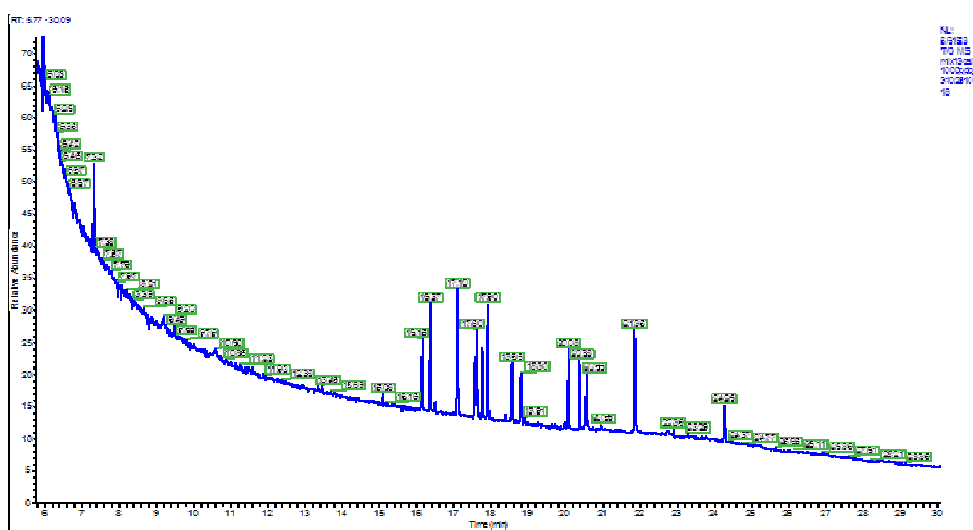


Fig.13: Gas Chromatogram for Pesticide Mix KZ

Calibration curves were built by plotting concentration of each pesticide versus GC reaction. For all samples tested within a concentration range of 1–1000 ng/mL, the GC reaction was quadratic with excellent regression coefficient ($r^2 > 0.99$) as can be seen for KF in Table 3, with the exception of primicarb (0.9591), Primiphos-methyl (0.8893), triadimefon (0.8992), procymidone (0.9298) & tetrachlorvinphos (0.9846).

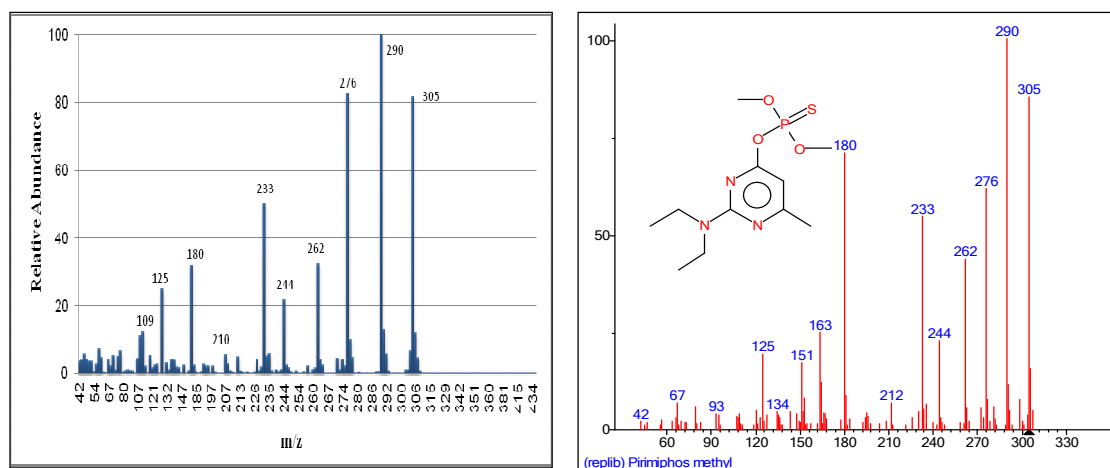


Fig. 14. Mass to charge ratio for Primiphos-methyl (LHS) & EI spectra for Primiphos-methyl from NIST database (RHS)

The summary of all the compounds of KF has been shown in Table 3.

Table 3: Retention time and precursor masses for KF

KF_MIX 155								
Analyte	Retention Time (min)	Precursor Mass	Product Mass	Collision Energy	a	B	r ²	Conc. range (mg/mL)
Thiometon	15.23	247	89	40	0.46	64.99	0.9998	0 - 50
Simazine	15.48	201	173	5	-15.01	3289.78	0.9966	0 - 100
Terbumeton	15.68	226	170	16	0.41	5.43	0.9962	0 - 50
Terbutylazine	15.82	230	174	14	-0.72	119.16	0.991	0 - 100
Pirimicarb	16.48	238	166	10	-18.36	7523.22	0.9591	0 - 20
Terbutryn	17.21	242	186	25	0.76	63.47	0.9975	0 - 50
Pirimiphos-methyl	17.28	305	180	8	-41.70	2166.69	0.8893	0 - 20
Triadimefon	17.64	208	111	20	-28.54	2580.47	0.8992	0 - 20
Procyridone	18.38	283	96	10	-51.52	5367.01	0.9298	0 - 20
Vamidotion	18.59	145	87	10	0.54	-52.93	0.9997	0 - 500
Tetrachlorvinphos	18.65	329	109	38	0.30	109.22	0.9846	0 - 100
Profenofos	18.98	339	269	15	0.31	186.64	0.995	0 - 500
Triazophos	19.97	257	162	10	1.62	346.61	0.9978	0 - 500
Pyrazophos	22.06	374	222	35	0.0002	0.03	0.9955	0 - 1000

3.2.2 Accuracy and precision of developed method

The accuracy, precision and recovery of the created procedure were determined at the minimum concentration level i.e. 1 ng/mL for all mixes except KT for which it has been measured at 2 ng/mL. Each concentration contained ten replicates, although five replicates are recommended by [19]. Precision was figured out by utilizing the

relative standard deviation (R.S.D.). The following equation was used to ascertain Accuracy [21].

$$\text{Accuracy} = \frac{\text{mean measured concentration}}{\text{nominal concentration}} \times 100$$

According to the guidance document SANCO/12495/2011 of European Commission [19], the mean recovery should be in the range of 70–120% where as repeatability which is estimated by the relative standard deviation (RSD) of recoveries, should be $\leq 20\%$ per commodity. According to Codex Guidelines, the acceptable range of recoveries should be in between 60-120 % with a RSD value of 30 % [20]. High precision, good accuracy, and better repeatability for all analytes of the standard pesticide mixes were accomplished. The range of recoveries for all analytes have been varied between 81- 120 % where RSD values lied between 0.93 - 14.16 %. The precision and accuracy results for all these analyses are within the acceptable range as prescribed by [19 & 20].

3.2.3 Determination of LOD and LOQ

The limit of detection is the least concentration of the analyte that can confidently be recognized with an assigned level of certainty.

Table 4: Precision, accuracy, LOD and LOQ description for KF

Analyte	Nominal Conc. (ng/mL)	Concen. measured (ng/mL)	Precision (R.S.D.)	Accuracy (%)	LOD ng/mL	LOQ ng/mL	R ²
Thiometon	1	1.02 ± 0.15	14.16	102	9.26	30.87	0.9996
Simazine	1	0.87 ± 0.03	3.52	87	1.14	3.79	0.9987
Terbumeton	1	0.89 ± 0.12	13.57	89	5.72	19.06	0.9997
Terbuthylazine	1	0.99 ± 0.01	1.04	99	0.24	0.81	0.9998
Pirimicarb	1	0.98 ± 0.05	5.32	98	0.50	1.67	0.9610
Terbutryn	1	1.14 ± 0.10	8.88	114	9.84	32.79	0.9388
Pirimiphosmethyl	1	0.99 ± 0.02	2.27	99	0.54	1.80	0.9992
Triadimefon	1	0.97 ± 0.05	5.46	97	0.30	1.00	0.9918
Procymidone	1	1.01 ± 0.02	1.82	101	0.17	0.56	0.9543
Vamidotion	1	0.90 ± 0.05	5.12	90	1.54	5.13	0.9784
Tetrachlorvinphos	1	0.98 ± 0.02	2.4	98	0.24	0.80	0.9019
Profenofos	1	0.96 ± 0.02	1.98	96	0.31	1.04	0.9998
Triazophos	1	0.99 ± 0.02	1.87	99	0.45	1.50	0.9733
Pyrazophos	1	1.05 ± 0.02	1.77	105	0.55	1.83	0.9998

A linear calibration graph between GC responses versus initial 5 concentration levels was constructed for which the slope has been calculated. The limit of quantitation is the most minimal concentration of analyte that can be resolved with an adequate level

of uncertainty. A value of $10s$ is mostly used (where s is the standard deviation of the values from replicate measurements of the lowest concentration level) [22]. For all analytes tested within a concentration range of 0-10 ng/mL, the GC response was linear with excellent regression coefficients ($r^2 > 0.99$) with a few exceptions. The Precision, accuracy, limit of detection (LOD), limit of quantification (LOQ) and regression coefficient for KF has been shown in Table 4. The LODs for KF are in the range of 0.17 - 9.84 ng/mL, whereas the LOQs for KF are in the range of 0.56 – 32.79 ng/mL.

3.2.4 Method Application

Comparing so as to distinguish proof of target analytes is refined the retention time and electron impact mass spectra of the analytes to that of a standard analyzed under the same conditions. The quantitative interpretation of a gas chromatogram is based on peak area. The procedure for quantitation by the peak area depends upon the measurement of the area of the peak of the compound from the extract solution to be analyzed and compared with the area of the peak measured for the compound from a standard (External or Internal), and from this comparison the amount of compound in the sample solution is calculated [23]. So as to evaluate the relevance of the created approach, cotton samples extracted with different solvents were analyzed following the above mentioned methodology. With external standards, the area of mass chromatogram is calibrated with 10 standard concentration levels for each pesticide standard mixes (KF, KS, KT, KZ). Cotton samples extracted with different solvents (methanol, hexane, toluene, acetone & acetonitrile) were injected for analysis. The maximum residue limit (MRL) for cottonseed were also mentioned which are recommended by EU Pesticide Database [24] and Codex Alimentarius Commission database [25], as MRL values for cotton fibers have still not been established. PCB 209 was used as an internal standard. An amount of 0.4 $\mu\text{g/mL}$ was added homogeneously in all the cotton sample extracts along with method blanks and all calibration samples prior to the analysis. The overall residual pesticides obtained by this method from KF are summarized in Table 5. Terbutylazine, Profenofos, Terbutryn, Tetrachlorvinphos & Triazophos from KF were found present in the cotton samples. In case of Triazophos, 7 samples out of ten exceed MRL. The worth mentioning point is that PC (Pakistani classical) cotton samples contain more amount of residual pesticides than PO samples. In case of using ISTD, the residues of all insecticides in KF remained below MRL in all samples with the exception of Z33_M having residue more than MRL.

Table 5: Description of residual pesticides detected with ESTD & ISTD from KF

	Analyte	ESTD		ISTD			Analyte	ESTD		ISTD	
		Area	Amount in samples (mg/Kg)	Area Ratio	Amount in samples (mg/Kg)			Area	Amount in samples (mg/Kg)	Area Ratio	Amount in samples (mg/Kg)
Triazophos (0.2)	BT114_A	39724	0.331	0.1869	0.057	Profenofos (3)	GC_ACN	4263	0.088	0.0176	0.017
	BT114_H	38423	0.322	0.1810	0.055		GC_H	3331	0.069	0.0140	0.014
	PC_A	36686	0.311	0.2466	0.074		GO_ACN	19768	0.368	0.0800	0.078
	PC_H	43163	0.353	0.2513	0.076		GO_H	20850	0.386	0.0885	0.086
	PC_T	38818	0.325	0.2863	0.086		GO_M	17930	0.338	0.0897	0.087
	PO_ACN	2424	0.027	0.0099	0.003*		IC_A	192	0.004*	< LOD	
	PO_M	1732	0.020	0.0071	0.002*		IC_ACN	240	0.005	0.0028	0.003*
	SH1_M	9299	0.096	0.0531	0.016		IC_H	285	0.006	0.0018	0.002*
	Z33_ACN	73150	0.524	0.4253	0.126		IC_M	248	0.005	0.0018	0.002*
	Z33_M	104084	0.673	0.7506	0.217		IO_H	361	0.008	0.0016	0.002*
Terbuthylazine (0.1)	GC_ACN	173	0.006	0.0014	0.004	IO_M	509	0.011	< LOD		
	GC_H	129	0.004	0.0004	0.001*	SH1_ACN	1322	0.028	0.0071	0.007	
	GO_A	201	0.007	< LOD		SH1_H	1231	0.026	0.0062	0.006	
	GO_T	125	0.004	0.0009	0.003*	SH1_M	1196	0.025	0.0052	0.005	
	IC_H	313	0.011	< LOD		Z33_T	3084	0.064	0.0123	0.012	
	PC_A	276	0.009	0.0015	0.004	SH1_M	1102	0.039	0.039	< LOD	
	PC_ACN	266	0.009	< LOD		Z33_T	1811	0.068	0.068		
	PO_ACN	501	0.017	0.0012	0.004	Z33_M	1674	0.062	0.062		

* Values >LOD but < LOQ.

Analytes that exceed MRL are in **bold** type.

4. Conclusion

A rapid, sensitive and low cost method based on AChE-inhibition utilizing biosensor has been developed for the identification of residual pesticides. It can be seen throughout the testing that the enzyme inhibition is a complicated mechanism. All the variables involved in AChE inhibition activity have been studied and optimized such as enzyme & substrate concentrations, buffer, pH and incubation time. Each of these variables has a significant role in this mechanism. Suitable calibration curves were obtained by preparing 5 standard concentration levels of Mix 155 along with Neostigmine as standard inhibitor and analysed in order of increasing concentration. The values of RSD of inhibition % for 5 repetitions are found to be in a range of 1.51 – 34.45. The detection limit is found to be below 1 ppb. The method is utilized for real cotton samples extracted with different solvents (methanol, hexane, toluene). We are able not only to estimate the inhibition % of each individual sample but also we can compare this inhibition with the standard control points. A multiresidue strategy for examination of 76 pesticides with various physicochemical properties has been developed for quantitative determination. The technology of Gas chromatography with Tandem mass spectrometry (GC-MS/MS) was utilized for the analysis of pesticide remainders. 57 out of 76 pesticides were detected successfully by the method developed. Confirmation of pesticide and quantitation was performed in selected-reaction monitoring mode (SRM). The range of recoveries for all analytes have been varied between 81- 120 % where RSD values lied between 0.93 - 14.16 %. The precision and accuracy results for all of these analyses have been found within the acceptable range as prescribed by [19 & 20]. The method has the capability to determine pesticide remainders in real cotton samples. The GC-MS/MS technique portrayed in this work gives a solid system to the discovery of pesticide remainders on cotton. The procedure was proven to be effective, fast, sensitive and applicable to a wide range of pesticides. All validation criteria mentioned by European Commission document SANCO/12495/2011 for ‘Method Validation and Quality Control Procedures for Pesticide Residues Analysis in Food and Feed’ [19] were fulfilled. The results of both the techniques utilized have been compared and we are able to say that biosensor approach is effective and may be used for preliminary investigation prior to go through the sophisticated and advanced technique i. e. GC/MS/MS.

Acknowledgement

This work was supported under the student grant scheme (SGS-21198) by Technical University of Liberec, Czech Republic. The authors would also be thankful for ORIC, BUIITEMS for their support.

References

- [1]. MYERS, D., ORGANIC COTTON: A more sustainable approach, In: STOLTON, and MYERS (Eds.), *Org. Cott.*, Intermediate Technology Publications Limited, London, UK, 1999: pp. 1–7.
- [2]. GROSE, L., Sustainable Cotton Production, In: Blackburn (Ed.), *Sustain. Text. LIFE CYCLE Environ. IMPACT*, Woodhead Publishing Limited, Cambridge, UK,

2009: pp. 33–62.

[3]. Tadeo, J.L., Sánchez-Brunete, C., and González, and L., Pesticides: Classification and Properties, In: Tadeo (Ed.), *Anal. Pestic. Food Environ. Samples*, Boca Raton, 2008: pp. 1–34.

[4]. HEARLE, J.W.S., Physical structure and properties of cotton, In: Gordon, and Hsieh (Eds.), *Cott. Sci. Technol.*, Woodhead Publishing Limited, Cambridge, 2007: pp. 35–67.

[5]. Mulchandani, P., Mulchandani, A., Kaneva, I., and Chen, W., Biosensor for direct determination of organophosphate nerve agents. 1. Potentiometric enzyme electrode, *Biosensors & Bioelectronics*. 14 1999 pp. 77–85.

[6]. Randhir Prakash. Deo, Determination of organophosphate pesticides at a carbon nanotube/organophosphorus hydrolase electrochemical biosensor, *Analytica Chimica Acta*. 530 2005 pp. 185–189.

[7]. Buerk. Donald G, *Biosensors: Theory and Applications*, 1st ed., Technomic Publishing Company, Lancaster, 1995.

[8]. Krstic D, Colovic M, Bavcon Kralj M, Franko M, Krinulovic K, Trebse P, V. V, Inhibition of AChE by malathion and some structurally similar compounds, *Journal of Enzyme Inhibition and Medicinal Chemistry*. 23 2008 pp. 562–573.

[9]. Hannam, M.L., Characterisation of esterases as potential biomarkers of pesticide exposure in the lugworm *Arenicola marina* (Annelida: Polychaeta), *Environmental Pollution*. 152 2008 pp. 275–281.

[10]. Fi, F.U.A., Hajjo, R.M., and Battah, A.H., Medicinal Plants, Pesticide Residues, and Analysis, In: Nollet, and Rathore (Eds.), *Handb. Pestic. Methods Pestic. Residues Anal.*, CRC Press, Boca Raton, 2010.

[11]. Štajnbaher, D., and Zupančič-Kralj, L., Multiresidue method for determination of 90 pesticides in fresh fruits and vegetables using solid-phase extraction and gas chromatography-mass spectrometry, *Journal of Chromatography A*. 1015 2003 pp. 185–198.

[12]. Gelsomino, A., Petrovi, B., Tiburtini, S., Ermenegildo Magnani, and Felici, M., Multiresidue analysis of pesticides in fruits and vegetables by gel permeation chromatography followed by gas chromatography with electron-capture and mass spectrometric detection, *Journal of Chromatography A*. 782 1997 pp. 105–122.

[13]. Walorczyk, S., Development of a multi-residue method for the determination of pesticides in cereals and dry animal feed using gas chromatography-tandem quadrupole mass spectrometry II. Improvement and extension to new analytes., *Journal of Chromatography. A*. 1208 2008 pp. 202–14.

[14]. Walorczyk, S., Development of a multi-residue screening method for the determination of pesticides in cereals and dry animal feed using gas chromatography-triple quadrupole tandem mass spectrometry., *Journal of Chromatography. A*. 1165 2007 pp. 200–12.

[15]. Kerton, F.M., *Alternative Solvents for Green Chemistry*, The Royal Society of Chemistry, Cambridge, UK, 2009

[16]. Thermo Scientific. [Online] [Cited: 24 06 2013.] <http://www.thermoscientific.com/en/product/tsq-8000-triple-quadrupole-gc-ms-ms.ht>

[ml](#).

- [17]. ELLMAN, G.L., COURTNEY, K.D., VALENTINO ANDRES, J., and FEATHERSTONE, R.M., A NEW AND RAPID COLORIMETRIC OF ACETYLCHOLINESTERASE DETERMINATION, *Biochemical Pharmacology*. 7 1961 pp. 88–95.
- [18]. Somerset, V., Baker, P., and Iwuoha, E., Mercaptobenzothiazole-on-Gold Organic Phase Biosensors for Organophosphate and Carbamate Pesticide Determination, In: Somerset (Ed.), *Intell. Biosens.*, InTech, Croatia, 2010: pp. 185–204.
- [19]. European Commission, METHOD VALIDATION AND QUALITY CONTROL PROCEDURES FOR PESTICIDE RESIDUES ANALYSIS IN FOOD AND FEED, SANCO/12495/2011, 2012.
- [20]. GUIDELINES ON GOOD LABORATORY PRACTICE IN PESTICIDE RESIDUE ANALYSIS CAC/GL 40-1993, Codex Alimentarius Commission, 1993.
- [21]. Zhang, B., Pan, X., Venne, L., Dunnum, S., McMurry, S.T., Cobb, G.P., et al., Development of a method for the determination of 9 currently used cotton pesticides by gas chromatography with electron capture detection., *Talanta*. 75 2008 pp. 1055–60.
- [22]. Ellison, S.L.R., Barwick, V.J., and Farrant, T.J.D., *Practical Statistics for the Analytical Scientist*, 2nd ed., The Royal Society of Chemistry, Cambridge, UK, 2009.
- [23]. Thier, H.-P., and Zeumer, H., *Manual of Pesticide Residue Analysis Volume I*, VCH Verlagsgesellschaft mbH, Weinheim, Germany, 1987.
- [24]. EU Pesticide Database. [Online] [Cited: 20 08 2013.] http://ec.europa.eu/sanco_pesticides/public/?event=substance.selection.
- [25]. Pesticide Residues in Food and Feed. [Online] [Cited: 22 08 2013.] <http://www.codexalimentarius.net/pestres/data/pesticides/index.html?lang=en>.

Geotextiles and environmental protection textiles

Jiří Militký, Rajesh Mishra, Mohanapriya Venkataraman and Vijay Baheti
Department of Materials Engineering, Faculty of Textile Engineering, Technical
University of Liberec, Czech Republic

Abstract:

Textile uses are increasing every day as the growing world needs more intakes of textiles for its betterment. As the detailed study of textiles is done, more and more fields are diversified as per usage of textile materials as the alternative rather better alternative of previously used materials. As the advancements of technology are taking place, technical textiles is coming as a major branch of textiles with an aim to provide the solutions of problems for materials lacking in certain properties, materials not available for specific purposes. Geotextiles are the branch of technical textiles which is implemented in various regions for specific uses. Geo textiles is mainly constituting of the materials which are used for the enhancement of soil either by removing moisture, by providing better bondage or by effective drainage of waste water. To make concept of geo textiles further clear, its importance is more clearly realized where heavy budget wastages were made in maintenance of roads, dams, sanitations etc when geotextiles was not used. In this paper, we have studied some aspect of geo textiles in detail. We studied the raw material and production techniques in details.

Keywords: Geotextiles, sustainability, woven, nonwoven, natural fiber

1. Introduction

Textile uses are no longer restricted to apparel and upholstery. Textiles were used in roadway construction in the days of the Pharaohs to stabilize roadways and their edges. These early textiles made up of natural fibers, fabrics or vegetation mixed with soil was used to improve the road quality, particularly when roads were made on unstable soil [1]. Geotextiles are the fast growing advancement of this era. Geotextiles have proven to be among the most versatile and cost-effective ground modification materials. Their use has expanded rapidly into nearly all areas of civil, geotechnical, environmental, coastal, and hydraulic engineering. They form the major component in the areas of geosynthetics, the others being geogrids, geofoams etc. Geotextiles are permeable fabrics, which are used to filter, reinforce, and separate, when work in association with soil. The term geotextile refers to “Geo” that is Earth and “Textile” means Fabric. According to the definition of ASTM, the geotextile is defined as follows.

"A permeable geosynthetic comprised solely of textiles. Geotextiles are used with foundation, soil, rock, earth, or any other geotechnical engineering-related material as an integral part of human-made project, structure, or system." Or simply, "permeable textile materials used in contact with soil, rock, earth or any other geotechnical related material that is an integral part of a civil engineering project, structure or system." Examples of the using natural fiber for reinforcement can be traced back 3000 years ago, when Babylonians constructed Ziggurat in Dur-Kurigatz (present Agar-Quf) and the Great Wall of China, completed circa 200 BC, used tamarisk branches with mixture of clay. The earliest materials which were used as geotextiles are based on natural fiber. The use of synthetic fiber based geotextiles in 20th century made a revolutionary change. One of the earliest documented cases was a water front structure built in Florida in 1958. Then, the first nonwoven (needle punched) geotextile was developed in 1968 by the Rhone-Poulenc company in France and was used in dam construction in France during 1970 [2].

Talking about the serious work in this direction as per reference of geotextiles, in 1977 Rankilor produced the first 'design' manual about geotextile. It was the first manual for a commercial use of geotextile [3]. In 1980s a significant book was published by Koerner and Welsh, which was about the work conducted up till then in USA at advanced level [3]. This was the time when engineers started doing serious work on geotextiles in their own respective countries. In 1978 International Geotextile Society was established for development of geotextile design and its utilization. The society provided a platform for publications, providing exposure of developments to all interested engineers. Once textile was recognized as a good material for reinforcement, engineers started developing new type of textiles and composites to solve more difficult problems. In 1984-85, researchers developed the design and use of warp knitted fabrics for civil engineering [4]. During the last 20 years, the use of geotextile increased across the world and advanced developments were made in design for their better performance. The kind of development and increasing usage of geotextiles in the fields of expertise, is expected to gain more share in the developments in the coming future.

2. Geotextiles

Different types of textile structures are available for a broad range of geotechnical applications. For such applications, an understanding of the dynamic interaction between the textile structure and the geotechnical environment is very important. Two and three dimensional fabric structure, method to weave, multiaxial warp knit structures and braided structures are used as examples and their potential as multifunctional structural geotextiles is also explored. A novel method of joining geotextiles by robotic one-side stitching technology is also examined. Implication of emerging nanofiber technologies for the next generation of geotextiles may help further our understanding [5]. The main processes used for technical textiles are weaving, nonwoven, braiding, knitting, tufting etc. Traditional as well as contemporary fabric structures are increasingly gaining acceptance in industries such as defense and civilian areas as transportation, automobile, energy and marine

industries, due to their attractive specific performances and low cost in use for the technical textiles [6, 7]. Biaxial, triaxial and more sophisticated multiaxial 3D fabric structures are used as structural elements in these areas [8].



Fig. 1: Geotextiles in use

Geotextiles is a sub-set of industrial textiles or technical textiles. Industrial textiles can be categorized according to the form and the manner textile structures into three categories (see tab. 1)

Table 1: Categories of industrial textiles [9].

Composite Industrial Textiles	Textiles prepared by coating, impregnating, laminating or other processes not normally undertaken within the textile industry. Examples of products in this category include reinforced rubber; reinforced plastics, metal, ceramics and carbon matrices; abrasive fabrics; asphalt impregnates; etc.
Processing Industrial Textiles	Textile structures used as a component in a manufacturing process. Examples include filtration fabrics such as paper making felts; polishing fabrics; laundry machine aprons etc.
Direct Use Industrial Textiles	Textile structures that are manufactured or incorporated directly into the finished products such as awnings, tarpaulins, marine equipment, outdoor furniture, sporting goods, canvas bags, shoe linings etc.

Geotextiles fall into the first and the third categories. For many years, industrial textiles were known as ‘mechanical fabrics’ as described by Haven in his 1932 treatise focusing on tire fabrics, balloon fabrics and wing fabrics using woven cotton cord as the primary material [10]. Many industrial textiles have traditionally been produced by members of the Canvas Product Association (CPA) in the US. The diversification of fiber materials and expansion of applications from awning to geotechnical and other industrial applications, as well as the trend in market globalization in the 1970s, led to the reorganization of the CPA to the Industrial Fiber

Association International (IFAI), which has played an important role in promoting geotextiles. This transition was highlighted by the introduction of the Journal of Industrial Fabrics in 1982 [11]. Industrial fiber manufacturers such as Owens Corning Fiberglas, DuPont, Celanese, Allied, Union Carbide and Dow Corning played an important role in developing the enabling materials and processing technology that supported the growth of the industrial textiles market.

According to SANS ISO 10318:2013, *geosynthetics* are products with several components made from raw material derived from synthetic or natural origins. Components may be in the form of a sheet, a strip or three-dimensional structure employed in contact with soil and/or other materials for geotechnical and civil engineering applications. The major members of geosynthetic family are geomats, geonets, geogrids, geocells, geostrips, geoliners, geospacers, geomembranes, geotapes, geotextiles, geocomposites etc. (see fig. 2).

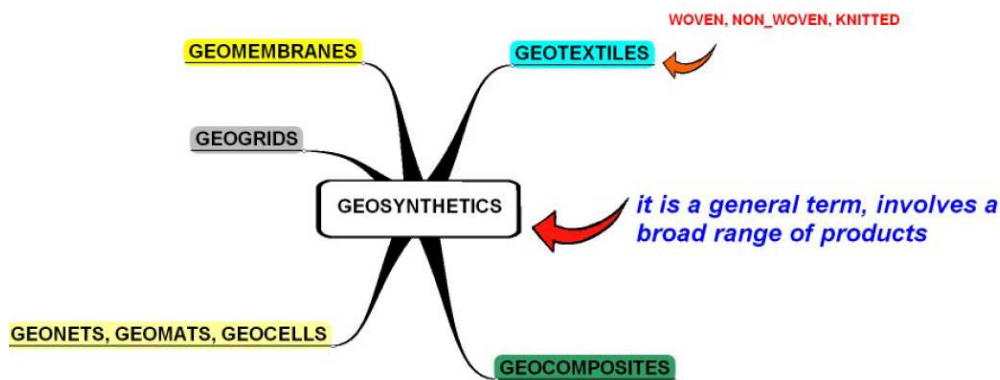


Fig. 2: Geosynthetics family [135].

Main functions of geotextiles are separation, filtration, drainage and reinforcements.

Separation: Separation is defined as, “The introduction of a flexible porous textile placed between dissimilar materials so that the integrity and the functioning of both the materials can remain intact or be improved” [12, 13]. It actually acts as a separator between fine soil and crushed stone. The geotextile prevents mixing of the two materials.

Filtration: Filtration is defined as “the equilibrium geotextile-to-soil system that allows for adequate liquid flow with limited soil loss across the plane of the geotextile over a service lifetime compatible with the application under consideration. Filtration applications are highway under drain systems, retaining wall drainage, landfill leachate collection systems, as silt fences and curtains, and as flexible forms for bags and tubes.

Drainage: A geotextiles acts as a drain when it acts as a conduit for the movement of liquids or gases in the plane of the geotextile. Geotextile materials which have good filtration and permittivity characteristics can be used for this purpose.

Reinforcements: A geotextile can be used as reinforcement material when the stability of the road is not good. To reinforce embankments and retaining structures, a

woven geotextile is recommended because it can provide high strength at small strains.

Although there are numerous textile structures suitable for geotechnical applications, a textile structure is not a geotextile until the interaction of the fabric with soil or the geotechnical environment is considered as a total system [13]. Observing the lack of understanding at the time on the importance of soil/fabric interaction, it was pointed out that almost every geotextile application is multifunctional, involving separation, reinforcement and drainage; and that fabric forming deals with water and its proper dissipation [14, 15]. This feature underscores the necessity of determining a given fabrics' hydraulic properties; more specifically, its flow rate, permeability or permittivity (permeability divided by thickness). Toward this end, many organizations have recommended test methods and specifications for the laboratory determination of these fabric properties. Note should be made, however, that these procedures are generally for the fabric alone, e.g., ASTM's "Standard Method for Testing the Water Permeability of Geotextiles – Permittivity Method" as proposed by Subcommittee D13.61 on Geotextiles. While of interest in comparing one fabric to another, these tests have no indication of the hydraulic behavior of the combined soil/fabric system. Researchers went on to explain that, as soon as soil is placed adjacent to the fabric, it is seen that the soils' hydraulic properties dominate the initial behavior of the system [13, 16, 17]. Only after a period of time does the fabric begin to play a role and, ideally, not at all in the long-term, e.g. when a properly designed configuration exists. In this latter instance, the flow passing through the soil/fabric system becomes constant and an equilibrium situation exists thereafter. To verify and quantify these long-term hydraulic behaviors, a simple test for various soil/fabric systems was established. This system consists of water at a constant head, flowed downward through the soil, then through the fabric and out of the system where it is collected and a flow rate is calculated [2]. Design of geotextiles is described in many publications [141-145]. The porosity of geotextiles is here one of most important parameter.

3. Performance Characteristics

Fabric performance characteristics are a result of the interaction between fiber (material properties), yarn and fabric geometry, and finishing treatment. Textile structures in fabric form (produced by yarn-to-fabric such as woven and knitted fabrics or fiber-to-fabric processes such as nonwoven fabrics) can be characterized in terms of geometric and performance properties. Performance maps provide an overview of the range of behavior of various fabrics as a function of four geometric parameters and four performance parameters [18].

The geometric parameters include:

a. Porosity: the amount of open space in a unit volume of the fabric. As the fiber diameter and yarn diameter increases, the structure tends to be porous. The porosity of a fabric is inversely proportional to the areal coverage or cover factor of a fabric. A

porous fabric tends to be lighter and more permeable. The permeability k of nonwoven geotextiles is nonlinear function of their porosity P , $k \approx P^3 / (1-P)^2$ [141].

Woven and knitted structures are generally worse in comparison with nonwovens because some pores are larger which leads to the unwanted increase of air permeability. Nonwoven structures can be tailor-made by simple modification of fabrication process. Especially perpendicularly laid structures of ROTIS type can be prepared in huge variation of porosities due to changing density of “waves”.

b. Surface Texture: The surface geometry of a fabric is characterized by the smoothness of the surface, which in turn is governed by fiber and yarn diameter. Modular fiber or yarn length is the geometric repeating units of the fabric.

c. Voluminosity: A reflection of the bulkiness of a fabric for a given areal density (mass per unit area). A fabric tends to be more voluminous if the fiber/yarn diameter is larger and the freedom of fiber mobility in the geometric repeating unit is high. Voluminosity is directly related to fiber thickness in that a voluminous fabric tends to be thick.

d. Thickness of the fabric: Similar to voluminosity, fabric thickness is related to fiber and yarn diameter. The larger the fiber and yarn diameter, the thicker and bulkier the fabric [19].

Porosity of textile structures can be investigated based on the geometrical arrangement of fibers in the textile structure. Various approaches are based on the available information.

For evaluation of fiber porosity P_f [-] it is simple to use experimentally evaluated fiber density ρ_f [kg/m³] (by weighting of fibers of known diameter and length) and density of corresponding polymer (fiber mass density) ρ .

$$P_f = 1 - \rho_f / \rho \quad (1)$$

Fiber porosity is usually relatively low (for natural fibers about 0.05- 0.2 and for synthetic fiber around 0.01-0.02).

Yarn porosity P_y [-] (usually around 0.5) is closely connected with packing density μ as ratio between fiber volume V_f and whole yarn volume V_y ,

$$P_y = 1 - \mu = 1 - V_f / V_y = 1 - 4T / \pi D^2 \rho \quad (2)$$

The product of the effective cross-section area of yarn S , (sum of fiber areas in yarn cross-section) and fiber mass density ρ [kg/m³] is in fact the yarn fineness T [tex]. Real yarn diameter D derived from equation (2) has the form

$$D = \sqrt{4T/\pi\mu\rho} \quad (3)$$

From eq. (3) it is evident, that yarn diameter is a function of yarn fineness, packing density and fiber mass density. On the base of yarn internal mechanics the following relation between yarn fineness T , twist Z and packing density μ was derived by Neckář [136].

$$\frac{\left(\frac{\mu}{\mu_m}\right)^{5/2}}{\left[1 - \left(\frac{\mu}{\mu_m}\right)^3\right]^3} = \frac{M\sqrt{\pi}}{2\mu_m^{5/2}\sqrt{\rho}} \left(ZT^{1/4}\right)^2 \quad (4)$$

This relationship is based on the following assumptions: the fiber arrangement in the yarn is following a helix model, fibers are compressed due to yarn twist, compression is caused by the outer fibrous layers and thickness of layer is constant.

In eqn. (4) μ_m is the limit packing density, k_p is material and fiber orientation parameter and M the material and technology parameter. A suitable value of parameter M for ring and rotor cotton yarns was evaluated by [136] and for compact yarns was evaluated by [137], see tab. 1.

Table 1: Suitable value of parameter M [m] for cotton yarns

Combed ring	Carded ring	Rotor	Combed compact	Carded compact
0.0064	0.0042	0.0027	0.0100	0.0066

Basic construction parameters of woven fabric are sett (texture) of weft D_C [1/m], sett of warp D_M [1/m], fineness of weft yarn T_C [tex] and fineness of warp yarn T_M [tex]. For the idealized circular yarn with the same packing density is simple to compute yarn diameters d_C and d_M from relations

$$d_C = \frac{2\sqrt{T_C}}{10^6 \pi \rho_C} \quad \text{and} \quad d_M = \frac{2\sqrt{T_M}}{10^6 \pi \rho_M} \quad (5)$$

Here ρ_C and ρ_M are unknown densities of weft and warp yarns. For the moderate level of twist it has been empirically found that $\rho_C / \rho_f \approx \rho_{eM} / \rho_f \approx 0.53$ and this correction should be used in eqn (5).

Classical Pierce definition of the cover factor CF is based on the idealized projection of fabric into a plane (fig. 3).

The CF [-] is defined as the area of yarn in the solid unit cell rectangle and has the form

$$CF = D_C d_C + D_M d_M - D_C d_C D_M d_M \quad (6)$$

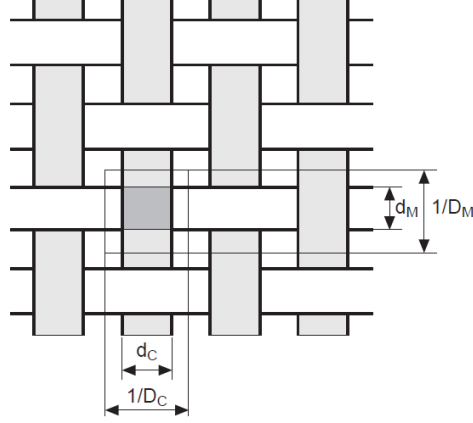


Fig. 3: Definition of cover factor

From a pure geometrical point of view can be surface porosity P_S [-] evaluated from the cover factor CF of fabric.

$$P_S = 1 - CF \quad (7)$$

The volume P_V [-] porosity of fabric is defined as [137]

$$P_V = 1 - \frac{\text{volume covered by yarns in unit cell}}{\text{whole accesible volume of unit cell}} \quad (8)$$

The determination of volume porosity based on the idealized fabric structure is described in [137]. Final eqn. has the form

$$P_V = 1 - \frac{1.9 \cdot 10^{-6}}{\rho_F H} (D_C T_C + D_M T_M) \quad (9)$$

where H [m] is fabric thickness. There are close connections between P_V and P_S [137]. For all kind of fabrics (woven, knitted, nonwoven) it is possible to calculate total density porosity P [-] from relation

$$P = 1 - \frac{W}{H \rho_F} \quad (10)$$

where W [kg m^{-2}] (usually [g m^{-2}]) is the planar mass – gsm.

The fabric density ρ_F is defined as function of the planar mass and thickness

$$\rho_T = \frac{W}{H} = \rho_F v_F + \rho_a (1 - v_F) = \rho_a + v_F (\rho_F - \rho_a) \quad (11)$$

where v_F is volume portion of fibrous phase ρ_F is fiber density and ρ_a is air density. The air density at 21°C, 65 % relative humidity and elevation above sea level 300 m is 1.15 kg/m³. This is very low in comparison with fibers density (from 900 till 1600 kg/m³) an the eqn. (11) can be simplified

$$\rho_T = \frac{W}{H} \approx \rho_F v_F \quad \text{and} \quad v_F \approx \frac{\rho_T}{\rho_F} = \frac{W}{\rho_F H} \quad (12)$$

The dependence of polyester fibers ($\rho_F = 1360$ kg/m³) volume portion on polyester fabric planar mass for various small fabric thickness is shown in fig. 4.

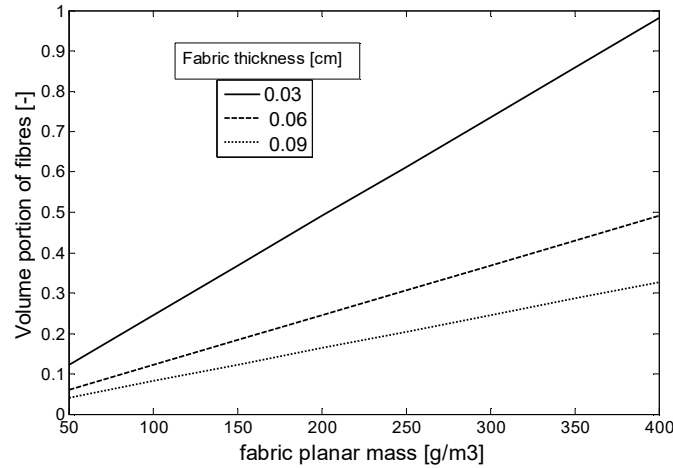


Fig. 4: Dependence of fabric planar mass on volume portion of fibers for various small fabric thicknesses

Dependence of polyester fibers volume portion on fabric thickness for various planar mass is shown in fig 5. It is visible that the volume portion of fibrous phase for heavy fabrics and small thickness is nearly 15 %. This corresponds to the total porosity 85%. Low planar mass and high thickness leads to the portion of fibers below 5 % i.e. porosity is over 95%. Special formulae for modeling of nonwovens pore size distribution are summarized in the books [139, 141].

4. Fibers for geotextiles

Fiber is generic name for long (length $l = 10^{-2}$ to 10^{-1} m) and thin (diameter $d = 10^{-6}$ to 10^{-4} m) rod like formations prepared from polymeric or non-polymeric substances. Typical length to diameter ratio – aspect ratio l/d is about 10^3 . Polymeric fibers have typical fibrous structure characterized by the hierarchy of bundles of long thin element (molecular chains, micro-fibrils, macro-fibrils) oriented preferably in the fiber axis direction and having more or less ordered three-dimensional arrangements. (semicrystalline state).

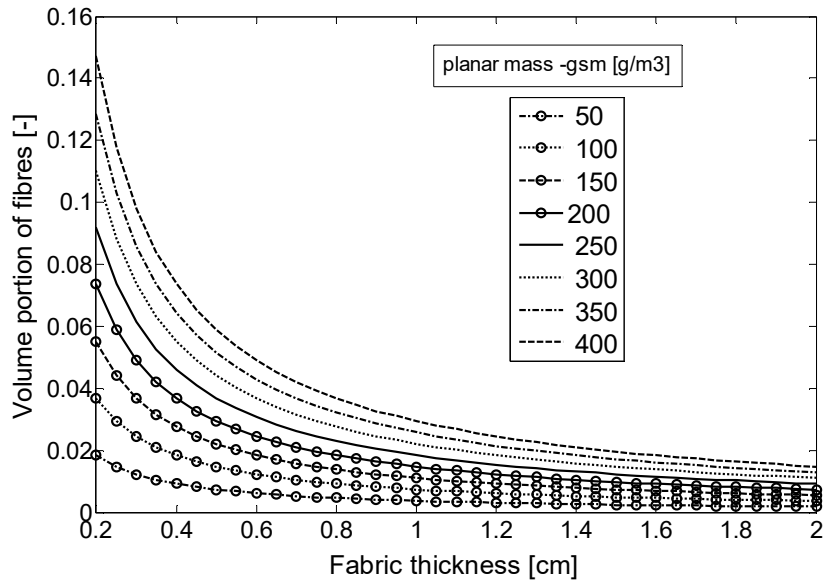


Fig. 5: Dependence of fabric thickness on volume portion of fibers for various planar mass

Due to this special structural arrangements fibers have strong anisotropy of physical and mechanical properties and extraordinary good mechanical/physical properties in fibrous axis direction in comparison with plastics of the same chemical composition. For example typical modulus of crystalline phase in the longitudinal (fiber axis) direction $E_{CL} = 150$ GPa, modulus of crystalline phase in the transversal (perpendicular to fiber axis) direction is $E_{CT} = 4$ GPa and modulus of amorphous phase is $E_A = 0.6$ GPa (on the level of plastics). Typical feature of fibers is cooperative character of deformation where deformation process acts on the group of molecular chains (elements) together. Textile fibers have special organoleptic properties (luster, hand), technological properties (length, strength, crimp, surface roughness etc.) and utility properties (sorption, ability to stabilize form, abrasion resistance etc.). Majority of these properties are changed due to aging, weathering or environmental degradation, which is important especially when these processes are long term and intensive as in the case of geotextiles. Here soil itself is responsible for combined chemical, physical and microbial degradation (see section 5). The textile fibers can be divided according to their preparation and source of raw polymers to the three groups:

- Natural fibers** (prepared by nature from natural polymers),
- Chemical fibers** (prepared artificially from natural polymers),
- Synthetic fibers** (prepared artificially from synthetic polymers),
- Non-polymeric fibers** (prepared from non-polymeric materials)

The fibrous structure is originated due to larger or smaller orientation of *polymeric chains* along fiber axis. Orientation in natural fibers is caused by biological requirements during their growth. The molecular alignment is an inherent characteristic of fiber (it is often significantly different in different morphological

parts of natural fibers) and is commonly stable. Within the groups of cellulosic fibers, ramie and jute both have extremely high degree of fibrils orientation, whereas that of cotton is much lower. In cotton the chains are helically oriented. The orientation of man-made fibers is started during spinning stage. After spinning fiber are progressively elongated in the fiber axis direction during *fiber drawing*. Polymeric chains are oriented and partial crystallization occurs. Result is drawn fiber. Drawing ratio, i.e. ratio between length of drawn and undrawn fiber, is usually = 3 – 5 (standard fibers) or in special cases until 10. Spinning ability can be characterized by natural draw ratio λ_p , which is dependent on temperature and rate of deformation.

1. Stiff polymers (polystyrene, aramids) have $\lambda_p = 1.5 - 2.5$ (as for viscose),
2. Semicrystalline polymers with lower stiffness (PA, PES) have $\lambda_p = 3 - 5$,
3. High crystalline, flexible polymers (PP, PE) have $\lambda_p = 5 - 10$
4. For gel spinning of PE is $\lambda_p = 50$ and more.

Polymeric chains in undrawn fibers are randomly oriented, i.e. the 33 % only lie in the fiber axis direction. Polymeric chains in drawn fiber are mainly oriented to the fiber axis (around 80–90 % of chains are oriented to fiber axis direction). Drawing is therefore responsible for increasing of fiber strength, decreasing of the deformation at break and originating the fibrous (fibrillar) structure.

For geotextiles the cheaper fibers are commonly used. The durability and degradation in soil aspects are usually not the main issues.

4.1 Natural fibers

The commercially important natural fibers for geotextiles are based on cellulose (vegetable fibers) extracted from different part of plants. Typical vegetable fibers are:

Seed fibers (fibers cover seeds) – cotton;

Fruit fibers (nuts are covered by fibers) - kapok, coir;

Bast fibers (fiber bundles lie between the outer bark and the woody core of the stem) - flax, hemp, jute, ramie, kenaf, nettle, sugar cane, bamboo;

Leaf fibers (fiber bundles are located in the leaf's tissue) - sisal, abaca, (Manila hemp), agave, ananas, aloe, cabuya.

Major part of these fibers is cellulose, one of the most abundant materials in nature. It is a renewable and biodegradable material, available widely and at low cost, with a low-energy consumption profile and good mechanical properties such as high modulus. Another advantage of cellulose is creation of long fibrous cells, which can be aligned and oriented easily [102, 105]. Cellulose is polyalcohol having one primary and two secondary –OH groups. In backbone are ether bonds (glycoside link) –C – O – C–. Contracted notation is cel – OH or cel – (OH)₃. The –OH groups are the sites for creation of hydrogen bonds and some chemical reactions as esterification. Cellulose chains are connected by various systems of hydrogen bonds, which have a significant influence on properties (see fig. 6).

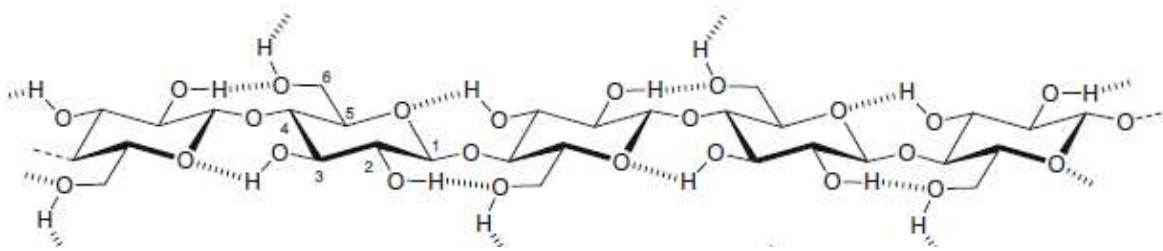


Fig. 6: Cellulosic chain with hydrogen bonds [100]

These bonds are responsible for the limited solubility of cellulose in most solvents, the swelling in water and reactivity of the hydroxyl groups, and the morphological features (crystallinity). Cellulose also contains hydrophobic areas (around the C atoms) that have partial influence on the overall solubility. Intermolecular hydrogen bonds are responsible for the strong interaction between cellulose chains. These bonds are produced between adjacent cellulose macromolecules located along the (002) plane in the crystal lattice of cellulose I (native cellulose), mainly between the oxygen atom in C3 and the -OH at C6 [100]. Together, the hydrogen bonding, weak C–H–O bonds, and hydrophobic interactions are responsible for the assembly of cellulose in layers [100]. Density of α -cellulose is about 1560 kg m^{-3} . Well aligned bundles of cellulose chains are creating crystalline nanofibrils [102]. The main building element of vegetable fibers is the cellulose microfibrils aligned mainly along the fiber axis, which ensure maximum tensile and flexural strengths, in addition to improved rigidity (high initial modulus) [103].

The main components of vegetable fibers are cellulose (α -cellulose), hemicellulose, lignin, pectin and waxes. These fibers can be considered to be composites of cellulose fibrils held together by a lignin and hemicellulose matrix. The amorphous matrix phase in a cell wall is very complex and consists of hemicellulose, lignin, and in some cases pectin [101]. Schematic structure of these constituents are shown in fig. 7.

Typical content of these constituents in typical fibers used commonly for geotextiles is shown in tab. 2.

Table 2: Typical composition of selected vegetable fibers

Fiber type	Cellulose [wt. %]	Hemi cellulose [wt. %]	Lignin [wt. %]	Pectin [wt. %]
bamboo	26-43	15-26	21-31	-
flax	60-81	14-19	2-3	0.9
hemp	70-92	18-22	3-5	0.9
sisal	43-78	10-13	4-12	0.8-2
jute	51-84	12-20	5-13	0.2

Lignin is a complex thermoplastic hydrocarbon based three- dimensional copolymer with both aliphatic and aromatic constituents shown in fig. 8. Hydroxyl, methoxyl and carbonyl groups have been identified. Density of lignin is about 1260 kg m^{-3} and initial modulus is 5.9 GPa [106].

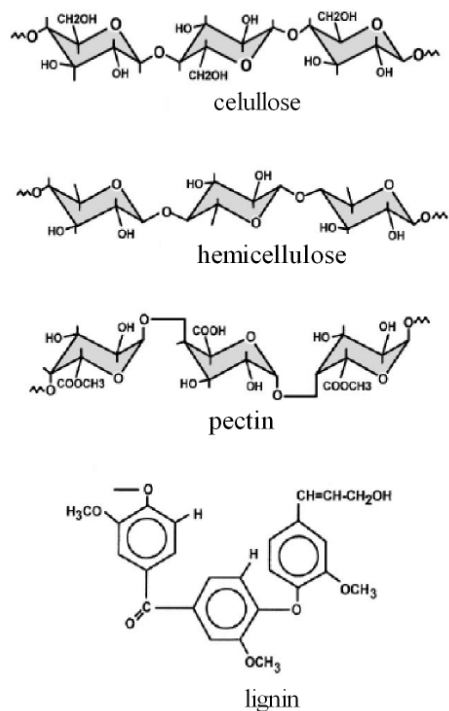


Fig. 7: Schematic structure of vegetable fibers constituents

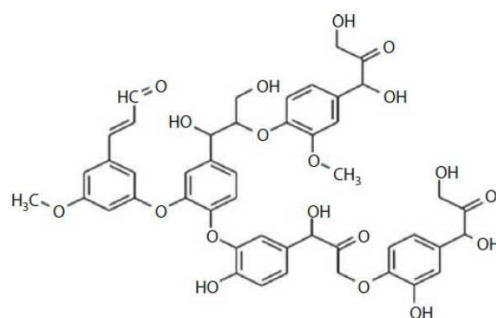


Fig. 8: Structure of lignin

Lignin is fully insoluble in most solvents and cannot be broken down to monomeric units. Lignin is totally amorphous and hydrophobic in nature. Glass transition temperature of around 90°C and a melting point around 170°C . It is the compound that gives rigidity to the plants. One of the basic unit of lignin is 3-(4-hydroxyphenyl) prop-2-methoxy and eneol group in the ortho position of the phenol ring (fig. 9).

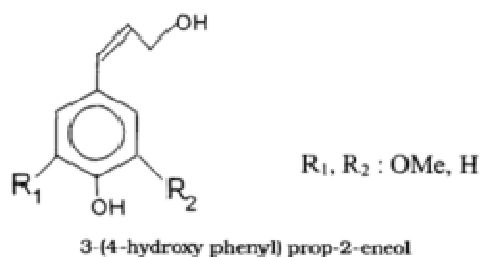


Fig. 9: Basic unit of lignin

Lignin can be used also as a replacement for phenol in the preparation of phenol-formaldehyde resins. It is not hydrolyzed by acids, but soluble in hot alkali, readily oxidized, and easily condensable with phenol. Lignin can be removed from fibers by chlorination forming a complex chloro-lignin, which is soluble, like hemicellulose in dilute alkalis. In some vegetable fibers degradation or removal of lignin accompanied by evolving of very short ultimate fibers in form of “dust” (e.g. in the case of jute).

Lignin is a macromolecular framework difficult to degrade even by microorganisms. Only lignolytic microorganisms can do it. It is beneficial especially for geotextiles because durability in soil is longer.

Pectin (see fig. 7) consisting of polysaccharides characteristic by high content of glucuronic acid and the corresponding methyl ester, and partially also the acetyl ester. Component D-galacturonic acid is combined with D-galactose and L-arabinose. They give plants flexibility.

Pectin can be removed readily in alkalis and it is sensitive to microbial attack and enzymes (pectinases). Soil degradation is easy.

Hemicelluloses (see fig. 7) are characterized by irregularities in the chains. They consist mainly of low molecular chains composed of hexoses, pentoses and parts of uronic acids. Single chains contain D-xylose portion as well. Branched portions consist of both D-xylose component as well as components of glucuronic acid and the corresponding methyl ester. Density of hemicelluloses is about 1450 kg m^{-3} and initial modulus is 8.4 GPa [106]

Hemicelluloses differ from cellulose in three aspects.

1. they contain several different sugar units whereas cellulose contains only 1,4- β -D-glucopyranose units.
2. they exhibit a considerable degree of chain branching containing pendant side groups giving rise to its non crystalline nature, whereas cellulose is a linear polymer.
3. the degree of polymerization (DP) of hemicellulose is around 50–200 [105]. This is 10–100. times lower than native cellulose.

Hemicelluloses are very hydrophilic, soluble in alkali and easily hydrolyzed in acids.

Waxes make up the last part of fibers and they consist of different types of alcohols.

The cotton fibers only are in fact single cell and rests of fibers are multi-cell connected by natural glues (pectin and lignin). Majority of natural fibers can be then considered as naturally occurring composites of cellulose micro fibrils in a matrix of intertwined hemicellulose and lignin or pectin [101]. Hemicellulose and lignin matrix is called lignin-carbohydrate complex (LCC) and cellulose glued by pectin mainly is called pecto-cellulose complex (PCC). Density of LCC is about 1340 kg m^{-3} and initial modulus is 6.93 GPa [106]

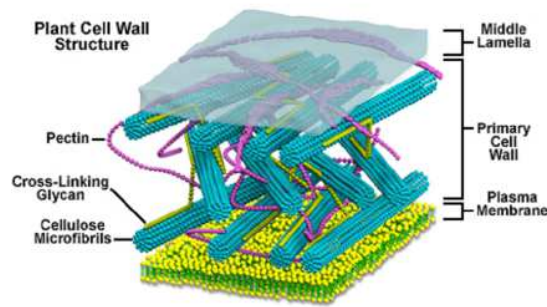


Fig. 10: Schematic arrangement of primary wall [105].

The average electrostatic energies between cellulose microfibril faces and hemicellulose, LCC and lignin are 38 mJ/m^2 , 57 mJ/m^2 and 58 mJ/m^2 , respectively, and the average van der Waals energies between cellulose microfibril faces hemicellulose, LCC and lignin are 44 mJ/m^2 , 76 mJ/m^2 and 95 mJ/m^2 , respectively. Lignin van der Waals energy is therefore around 116% higher than that of hemicellulose whereas the electrostatic energy are higher just by about 50%. The superiority of lignin adhesion energies to cellulose comes from the relatively higher van der Waals energies [106]. Many plant cells have a primary cell wall, which accommodates the cell as it grows, and a secondary cell wall they develop inside the primary wall after the cell has stopped growing. The main chemical components of the primary plant cell wall are cellulose in the form of organized microfibrils (see fig. 10). The cell wall contains two groups of branched polysaccharides, the pectins and cross-linking glycans (derivatives of polysaccharides [107]). Cellulose microfibrils cross-linked by glycans increase the tensile strength of the cellulose, and network of pectins provides the cell wall with the ability to resist compression. In addition to these networks, a small amount of protein can be found in all plant primary cell walls [105]. In the secondary cell wall additional substances, especially lignin, are often found. Lignin also makes plant cell walls less vulnerable to attack by fungi or bacteria. Bast fiber (e.g. flax, jute and hemp) bundles are located in the outer layer of the stem. Their cross sections consist of 10–40 elementary fibers glued together with pectin and/or lignin. The length of the elementary fibers varies between 5 and 55 mm and the thickness is about $20 \text{ }\mu\text{m}$. Bast fibers have a thicker cell wall and a smaller lumen. Common features of bast and other vegetable fibers are:

- a) Technical fibers are multi cell, consisting of a series of elementary (ultimate) fibers bonded by pectins or lignin.
- b) The fibers have a similar chemical composition: cellulose 65 to 85%; waxes, 2-4%; pectins, hemicelluloses from 2 to 10%; lignin from 1 to 20%; humidity 10%.
- c) The fibers have a similar microscopic appearance
- d) The fibers have similar properties: They are strong enough (wet strength is higher); have low deformation at break; are resistant to both freshwater and saltwater.

The plants, technical fibers bundles and surface structure of fibers for selected vegetable fibers are shown in fig. 11.

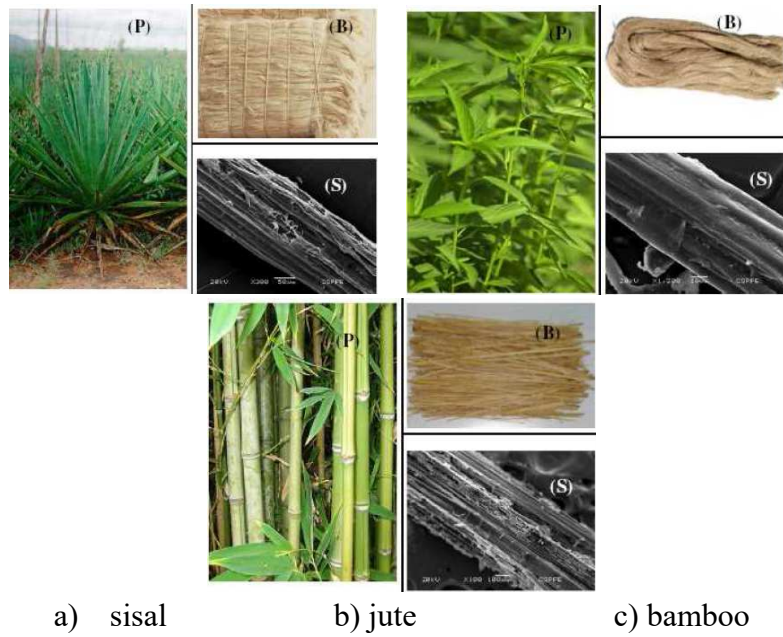


Fig. 11: Plant (P); a bundle (B) and SEM surface (S) for the sisal (a), jute (b) and bamboo (c) fibers [109]

The selected vegetable fiber crystallinity and an average polymerization degree of cellulose of different origin are given in the tab. 3.

Table 3: Crystallinity and cellulose polymerization degree of selected vegetable fibers

fiber	hemp	sisal	jute	flax	bamboo
crystallinity [%]	88	71	72	91	70-75
Polymerization degree of cellulose	1170	4500	1123	2801	891

Lowest polymerization degree is in case of bamboo fiber. Polymerization degree is directly connected with strength and resistance to external influences.

Selected physical parameters of some vegetable fibers are given in tab. 4. Low fiber density compared with the density of the cellulose 1560 kg/m^3 indicates their porosity and partially presence of lignin.

Table 4: Selected physical parameters of some vegetable fibers

fiber	density $[\text{kg/m}^3]$	moisture regain at 65 % RH [%]	porosity [%]
flax	1540	12	10
jute	1500	13.8	14-15
hemp	1480	12	11
sisal	1200-1450	14	17
bamboo	850-1100	6-8	high

It is evident that the highest porosity and content of lignin is in bamboo fiber. The density of fiber without pores ρ composed from weight fraction w_C of α -cellulose (density ρ_C), weight fraction w_H of hemicelluloses (density ρ_H), weight fraction w_L of lignin (density ρ_L) and weight fraction w_P of pectin (density ρ_P) is in fact weighted harmonic mean i.e.

$$\frac{1}{\rho} = \frac{w_C}{\rho_C} + \frac{w_H}{\rho_H} + \frac{w_L}{\rho_L} + \frac{w_P}{\rho_P} \quad (13)$$

If the density of fiber with pores is equal to ρ_f , it is simple to calculate the fiber porosity P_f (neglecting the air density around 1 kg m^{-3}) from eqn. (1)

In majority of vegetable fibers technical fibers are composed from many ultimate (elementary) fibers. Especially the bast fibers, where ultimate fibers are glued by pectin mainly, are relatively strong (wet strength is higher) with low deformation at break and better degradation resistance to the normal water and seawater.

Ultimate (elementary) vegetable fibers form long elongated cells, sealed at the ends, have typically lumen i.e. central channel. It can be seen that only for flax and hemp are ultimate fibers sufficiently long and soft for textile processing. For other fibers, it is necessary for textile processing (spinning) to use technical fibers (bundles of ultimate fibers glued by pectin or lignin). Lignin (particularly in bamboo and jute) causes an increased stiffness of technical fibers, which limits their use for textile purposes but can be beneficial for some geotextiles.

The most abundantly used multicellular cellulose fiber is flax (3 to 6 cells constitute a fiber cross-section). Each fiber consists of cells cemented together by wax and pectin and hemicelluloses (see fig. 12).

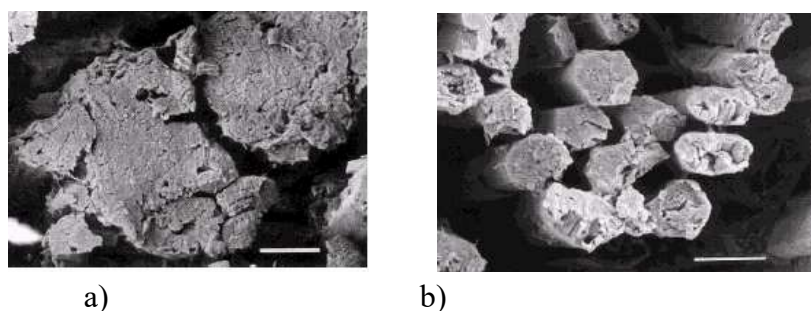


Fig. 12: Bundle of ultimate flax fibers a) glued by pectin, b) after removal of pectin

Dimensions of elementary (ultimate) bast fibers are given in tab. 5. It is visible that these dimensions are for some bast fibers too small for spinning. The elementary flax fibers dimensions are comparable with cotton and therefore can be used for direct spinning. Process of preparation of elementary flax fibers is called cottonization.

It is visible that the flax fibers have the best tensile properties. Their application in geotextiles is often limited due to relatively quick degradation in soils

Table 5: Ultimate fiber dimensions of some vegetable fibers

fiber	Average length [mm]	Range of lengths [mm]	Average width [μm]	Range of widths [μm]
flax	33	9-70	19	5-38
jute	2	1-5	20	10-25
hemp	25	5-55	25	10-51
sisal	3	1-8	20	8-41
bamboo	2.7	1.5-4.4	14	7-27

The geometrical characteristics of selected technical vegetable fibers are shown in tab. 6.

Table 6: Geometrical characteristics of selected technical vegetable fibers

fiber	length [mm]	diameter [mm]	fineness [tex]
flax	200-1400	0.04-0.62	0.18 - 2
jute	1500-3600	0.03-0.14	1.4 - 3
hemp	1000-3000	0.16	0.34 - 2.2
sisal	600-1000	0.1-0.46	2 - 40
bamboo	60-80	0.5-0.6	3.5

Mechanical properties of selected vegetable fibers are summarized in tab. 7.

Table 7: Mechanical properties of selected vegetable fibers [108]

fiber	Strength [MPa]	deformation at break [%]	Modulus [GPa]
flax	345-2000	1.6 - 3	27.5-85
jute	393-773	1.7	10-30
hemp	368-800	1.6	17-70
sisal	350-700	2 - 7	9-22
bamboo	140-230	2.8 - 4	11-17

Most common fibers in geotextiles are jute, flax, coconut matting, and straw. Every fiber is used with reference to its specific properties. Jute is easily degradable when it absorbs moisture so this is mostly used on sea shores to give wind shield to small trees till they are mature. By the time trees grow larger, jute shielding it gets degraded and the cover of jute is removed automatically to give way to the growing tree. In general, natural fibers are used in geotextiles for short term application only (see. section 5).

4.2 Synthetic fibers

Geotextiles are commonly made from polypropylene, polyester, polyethylene, polyamide (nylon), polyvinylidene chloride. Polypropylene (PP) is the mostly used fiber because its water sorption is approximately equal to zero and degradation in soil is very slow. For creation of PP fibers the isotactic polypropylene only is suitable. The space helix of polymer chains is here due to presence of voluminous side – CH₃ group. Helix unit is composed from three monomer units (gauche). Glass transition temperature is $T_g = -10$ to 0°C , density is 900 kg m^{-3} and melting temperature is $T_m = 165^\circ\text{C}$. The moisture content is only 0.05 %. Preparation of isotactic PP was firstly described in 1954 (*Natta*). Principle is coordination stereospecific polymerization of propylene with special catalyst TiCl_3 , $\text{Al}(\text{C}_2\text{H}_5)_3$ (Ziegler – Natta catalyst). Polymerization at 100°C and pressure 3 MPa leads to highly crystalline isotactic PP. Molecular mass of polymer before spinning $M_n = 100\,000$ to $600\,000$ and molecular mass of fiber is $50\,000$ to $250\,000$. Industrial production of PP fiber Meraklon IT (Montecatini) started in 1960. Standard process of PP fibers preparation consists from these steps:

- melt spinning in inert atmosphere (PP melt is sensitive to O₂),
- cooling in the long cooling tube (due to low temperature conductivity of POP).
- Undrawn fiber contains about 70% of crystalline phase,
- cold drawing (with neck) to draw ratio 3 – 5

Crystallinity degree of drawn fibers is about 70-80 %. In dependence on the drawing temperature the micro voids are appeared. Drawn fiber is characterized by high orientation of crystalline phase $f_c = 0.98$ but very low orientation of amorphous phase $f_a = 0.2 - 0.4$. Structural features are micro voids (20%), tie chains (3 %), crystalline phase (70%), and amorphous phase (7 %).

Setting (stabilization) at 130°C in free-state (shrinkage till 40%) leads to the improvement of recovery properties. The properties of polypropylene fibers differ substantially from common synthetic fibers. They are hydrophobic and practically do not have any group capable to water bonding. PP fibers show excellent chemical resistance. Low glass transition temperature and melting point are for geotextiles not important. For not chemically degraded PP fibers is bacterial resistance excellent. PP fibers show brittleness, low mechanical performance and low impact because of its high crystallinity.

Sewing thread for geotextiles is made from Kevlar or any of the above polymers. The physical properties of these materials can be varied by changing condition of drawing and heat setting by or by the use of additives. Yarns may be composed of very long fibers (filaments) or relatively short pieces cut from filaments i.e. staple fiber.

4.3 Non-polymeric fibers

Some geotextiles are made from fiberglass or basalt mainly or these materials are used in preparation of hybrid structures in combination with natural fibers (see. section 5).

Mineral fibers from basalt are not new, but their suitability as reinforcement in composites or in hybrid woven structures is a relatively new issue. Basalt fibers have good physical and chemical properties, as well as good adhesion to metals, epoxies and glues. Basalts also exhibit excellent thermal, electrical and acoustic insulation properties. Due to all these favorable properties, basalt fiber can be used in several applications in technical textiles. Basalt fiber density is 2733 kgm^{-3} and softening temperature is about 960°C . The diameter of standard fibers is around $9\text{-}12 \mu\text{m}$. Glass transition temperature from thermomechanical curves is $T_g = 596^\circ\text{C}$. Axial thermal expansion under T_g is $a_1 = 4.9 \cdot 10^{-6} \text{ deg}^{-1}$ and above T_g is $a_2 = 19.1 \cdot 10^{-6} \text{ deg}^{-1}$. The shear modulus of basalt fibers is about 21.76 GPa . The modulus of elasticity in the axial compression is 112 GPa [110]. From the cross-section of broken fibers (see Fig. 13) the brittle fracture caused by structure heterogeneities is evident. Basalt has excellent stability in soil and it is not attacked by microorganisms.

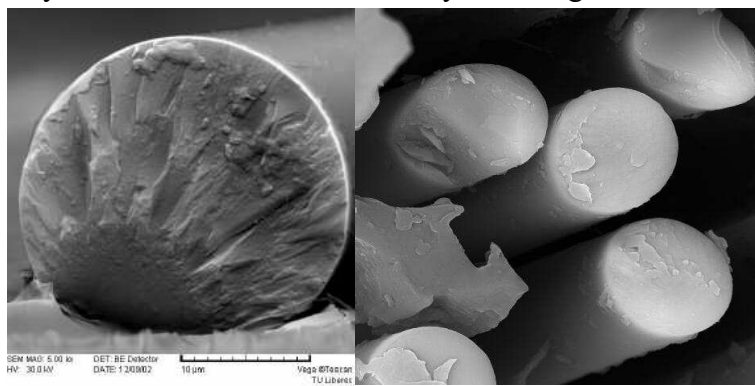


Fig. 13: Cross section of broken basalt fiber

Basic physical and mechanical properties of basalt fibers and a comparison with different other commercial fibers are depicted in tab. 3, which shows that basalt has an excellent tensile strength and also a good modulus. Regarding to the mechanical properties are basalt fibers positioned between E-glass fibers and S-glass fibers. Deak et al. [111] investigated the mechanical properties of glass fiber, short basalt fiber and continuous basalt fiber from different manufacturer. They concluded that all tested fibers have a rigid behavior, without plastic deformation. The tensile modulus and strength of continuous basalt fibers and glass fibers are quite similar, while short basalt fibers are considerably less stiff. The joint SiO_2 and Al_2O_3 content (denominated as ceramic-like materials) of basalt fibers showed correlation with tensile properties of fibers. It was concluded that continuous basalt fibers were competitive with glass fibers and short basalt fibers were weaker in terms of mechanical properties. Physical and tensile properties of basalt, glass and carbon fibers are summarized in tab. 8.

It is known that the fibrous fragments with diameter of $1.5 \mu\text{m}$ or less and length of $8 \mu\text{m}$ or greater should be handled and disposed of using the widely accepted procedures for asbestos. The experimental data of basalt particles dimensions created by the abrasion of basalt weaves showed that, because the mean value of fiber fragment diameter is the same as diameter of fibers, no splitting during fracture occurs [112]. Basalt fibers and fabrics are labeled as safe according to both the USA and the European occupational safety guidelines. Its particles or fibrous fragments due to




abrasion are too thick to be inhaled and deposited in the lungs, but care in handling is recommended.

Table 8: Physical and tensile properties of basalt, glass and carbon fibers.

Properties	Basalt	E-glass	S2 - glass	Carbon
density [kg/m ³]	2630-2800	2540-2570	2540	1780-1950
filament diameter [μm]	6-21	6-21	6-21	5-15
single filament tensile strength [MPa]	3000-4840	3100-3800	4020-4650	3500-6000
initial modulus [GPa]	93-110	72.5-75.5	83-97/86	230-600
elongation at break [%]	3.1 - 6	4.7	5.3	1.5-2.0

Basalt filaments can be used as one component of hybrid fabrics containing natural fibers for creation of geotextiles with enhanced resistance in soil burial conditions. Influence of fiber type on selected properties of hybrid plain woven fabrics with basalt filaments in the warp and basalt or jute yarns in the weft are shown in tab. 9. All fabrics were made on the CCI sample loom under the same technological conditions with the same density for all fabrics. The sett was 12 threads/cm in warp and 8 threads/cm in weft [133].

Table 9: Influence of weft and warp composition on mechanical properties of plain fabrics

Material	basalt/basalt	basalt/jute	jute/jute
Fabric Composition			
Tensile modulus [MPa] warp	3912.9	926	369.95
Tensile modulus [MPa] weft	3839.7	466.1	77.41
Shear rigidity [MPa]	0.05	0.372	0.095
Strength [MPa] weft	1154.9	192.9	153.7
Strength warp [MPa]	1403.5	535.1	101.9

The presence of basalt yarns is enhancing tensile mechanical properties of fabric and this fabric portion will be not degraded in soil.

5. Geotextiles and soil

Geotextiles are during their whole service time buried in soils. Majority of soils have *solid phase* include inorganic solids and organic solids, *liquid phase* include dilute aqueous solution of inorganic and organic compounds and *gas phase* as a mixture of

some major (e.g., nitrogen, oxygen) and trace (e.g., carbon dioxide, methane, nitrous oxide) gases (see fig. 14) [113].

Under optimal conditions for growth of upland plants, the solid components (inorganic and organic) constitute about 50% of the total volume, while liquid and gases comprise 25% each. Particles constitute the soil are called *sand* (2 – 0.02 mm), *silt* (0.02 – 0.002 mm) and *clay* (<0.002 mm). Sand grains comprise mostly quartz but also contain fragments of feldspar and mica, and traces of heavy minerals. There is practically not cohesion between sand particles. Silt is an intermediate size fraction, and also constitutes the skeleton of the soil. Mineralogical composition of silt is similar to that of sand, but silt has higher surface area.

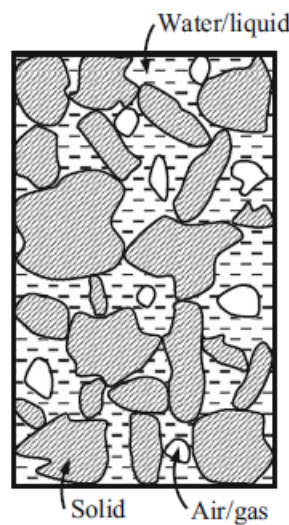


Fig. 14: Basic phase of soils [117].

Clay is the fine fraction, and constitutes the reactive fraction of the soil. Because of its very fine size, the clay fraction is colloidal, highly reactive, has large surface area, and high charge density. The clay particles are plate-like or needle-like. The clay particles comprise a group of clay minerals, called aluminosilicates. These are secondary clay minerals, and also contain fine particles of iron oxide (Fe_2O_3), aluminum oxide (Al_2O_3), calcium carbonate (CaCO_3), and other salts. Because of its larger surface area, the clay fraction has the most influence on many soil properties [113]. Immediately after rain or irrigation, the entire pore space or the voids in between the particles are completely filled with water, and the soil is saturated. In dry state the pores are filled by air or gases. Under optimal conditions for foundation for buildings and roads or runways, the pore space is minimized by compaction or compression. The solid components are here 80–90% of the total soil volume. Some industrial functions may require *anaerobic conditions*. Due to transformation of organic matter by the methanogenesis the emissions of methane (CH_4) to the atmosphere occurs. Mechanism of degradation under anaerobic conditions is shown in fig. 15.

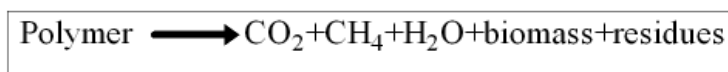


Fig. 15: Degradation under anaerobic conditions

In *aerobic conditions* the oxidation and mineralization of organic matter may cause release of carbon dioxide (CO₂) to the atmosphere [114]. Mechanism of degradation under aerobic conditions is shown in. fig. 16.

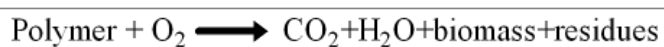


Fig. 16: Degradation under aerobic conditions

Particle size of soil could affect process of decomposition. Decomposition can be decreased in soil formed by coarse-textured due to diffusion of gasses through the soil matrix. On the other hand, fine-textured (clay) soil have lower rate of gas diffusion than the coarse-textured soil, therefore, oxygen-CO₂ exchange might not be sufficient to produce aerobic microbes and these conditions cause domination of anaerobes which are less efficient decomposers [115]. Soil liquid phase properties are one of main factors influencing behavior of geotextiles in soil. Soil liquid phase may be explained by the diversity of water forms in soil and the characteristics of water. Basic water forms in soil are chemically hard bonded, crystallizational water, physically bonded (hygroscopic), slightly bonded (at interface between water and solid particles), capillary, gravitational etc. [116]. Capillary water also called free or pore moisture, is a major part of the soil liquid phase. It is the readily available to interact with geotextiles. Capillary water composition and properties are not constant. The soil liquid phase is heterogeneous as a result of non-equilibrium processes of mass transport from soil particles, diffusion transport in liquid phase, possible emissions of substances by plants or micro-organisms and leaching of substances from geotextiles as well. The soil solution contains the following ions mainly: HCO₃⁻, Cl⁻, SO₄²⁻, Ca²⁺, Mg²⁺. Most of soils are slightly acidic (pH = 5 - 6.5), for podzolic virgin soil it was found pH around 3 and for some soils is pH slightly over 7 [116]. Acid soils are degradation prone for buried cellulose based textiles. Alkali soil have opposite effect i.e. degradation is slightly slower. Under the majority of soil conditions, textile materials based on the natural polymers do not survive long-term burial. Natural fibers are readily degraded by the action of soil-resident microorganisms often in combination of degradation promoted by components of soil water or gases presented in soil. Degradation occurs over a comparatively short period of time unless the burial conditions inhibit biodegradation. Soil burial biodegradability depends on polymer type and structure. Polymers of lower molecular weight, lower crystallinity or orientation, and higher hydrophilicity have shown greater biodegradability [119]. Biodegradation can occur by two different mechanisms; namely *hydro-biodegradation* and *oxo-biodegradation* [122]. The *hydro-biodegradation* is much more important in the case of hydrolysable natural polymers such as cellulose. The *oxo-biodegradation* predominates in the case of other natural polymers such as rubber and lignin. Lignin normally requires the presence of enzymes that initiate peroxidation [119]. The synthetic hydrocarbon polymers (e.g. polyethylene, polypropylene) do not hydrolyze under normal environmental conditions but it was found that, after transition metal catalyzed thermal peroxidation,

they biodegrade readily in the presence of a variety of thermophilic microorganisms [123]. Fig. 17 shows the microscopic photographs of cellulose based fabric specimens after the soil burial test [118]. Linen fabric developed more fungi than other samples and exhibited the most serious shape deformation caused by fiber damage. The thickness of yarns is not significantly changed in comparison with cotton and viscose materials. Cotton and viscose samples also formed quite a few fungi and their shape was changed and damaged as burial time developed. Acetate showed the least amount of fungi formed and the least shape deformation as time passed because of its highest hydrophobicity and slowest rate of degradation. These results are valid for fabrics after textile pretreatment which can partly attack the pectins in flax fibers. Desiccation, freezing, and the presence of metal ions such as chromium or copper will considerably retard microbial action. Waterlogged soils with anoxic or low oxygen concentrations will exclude aerobic fungi, although anaerobic bacteria may still flourish. Under these conditions, soil pH is a major factor in the differential preservation of textiles. In acid conditions, protein fibers (wool, and silk) are partially protected, but cellulosic materials (cotton, vegetable fibers) degrade more rapidly. Under anaerobic alkaline conditions, cellulosic-based materials are more protected.

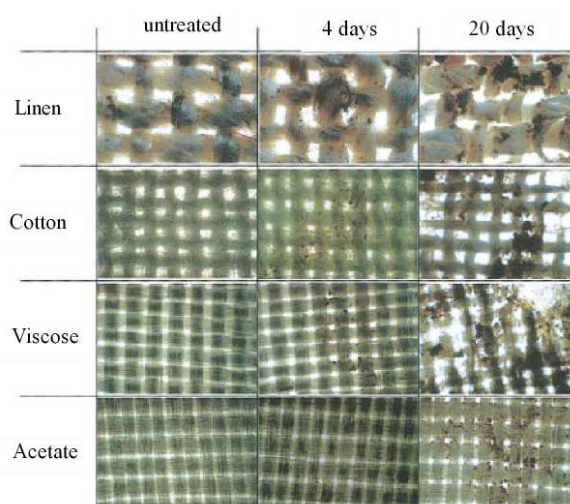


Fig. 17: Biodegradation of cellulose based textiles during soil burial test (CO-cotton, LI-linen, CV-viscose and AC-cellulose acetate)) [118].

Cellulose is readily attacked by the cellulolytic enzymes of microorganisms. The enzymatic cleavage of cellulose is catalyzed by cellulases, which in fungi consists of at least three enzymes. Some fungi can only degrade modified cellulose, which has already been subject to chain scission by other microorganisms or acid hydrolysis. In well-aerated soils, cellulose is degraded by fungi, myxobacteria, and eubacteria, while under anaerobic conditions it is bacteria of the genus *Clostridia* that predominate. The appearance and morphology changes of some cellulose type fabric biodegradation by soil burial for different time were presented in work [120] (see figs. 17 till 19). The cotton fabric (planar mass = 182 g m⁻²) was partially degraded after one week and totally degraded after 3 weeks only (see fig. 18).

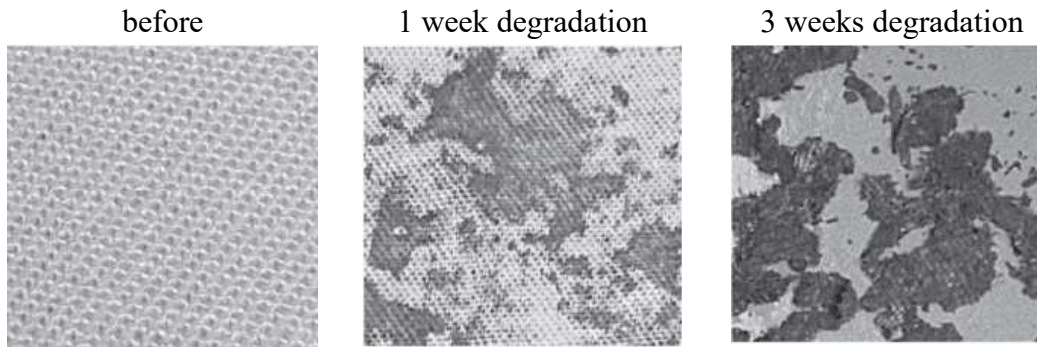


Fig. 18: Cotton samples [120].

The jute fabric (planar mass = 263 g m^{-2}) was slightly degraded after two weeks and totally degraded after 4 weeks (see fig. 19). Jute fabric is heavier and has more compact structure. Presence of lignin is hindering of degradation. The linen fabric (planar mass = 211 g m^{-2}) was partly destroyed after one week and totally degraded after 2 weeks only (see fig. 20). In fact the pectin parts in flax fibers in linen fabric are partially damaged during chemical pretreatment. Synthetic polymers are generally resistant to biodegradation. The only important exceptions are polymers with aliphatic esters in the main chain and polyurethanes based on polyester diols [121]. It was found that polyolefin polymers (polyethylene, polypropylene) are not supporting growth of microorganisms. Oligomers present originally in these polymers augmented by those produced by e.g. photooxidation support growth if separated from the polymer matrix [121].

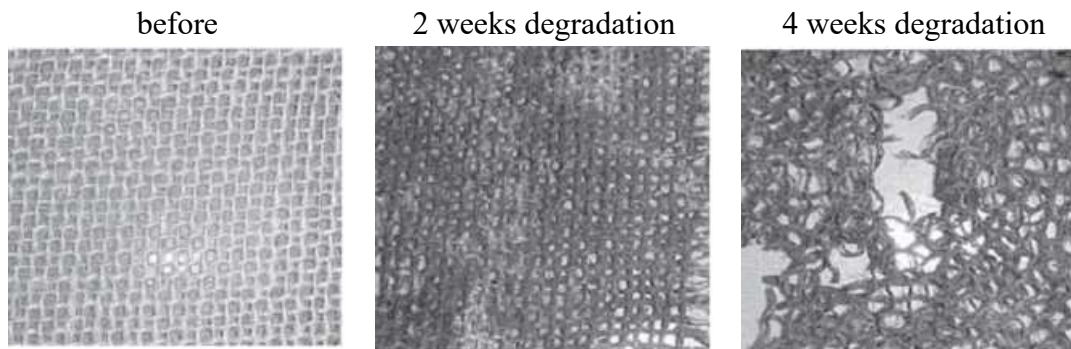


Fig. 19: Jute samples [120].

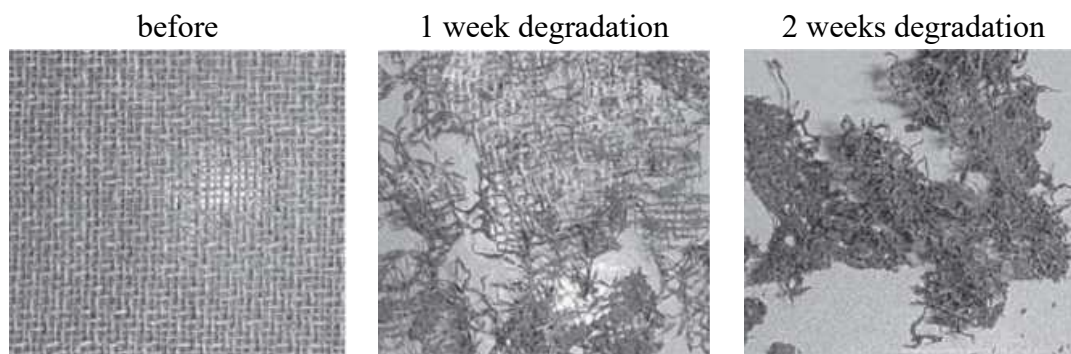


Fig. 20: Linen samples [120].

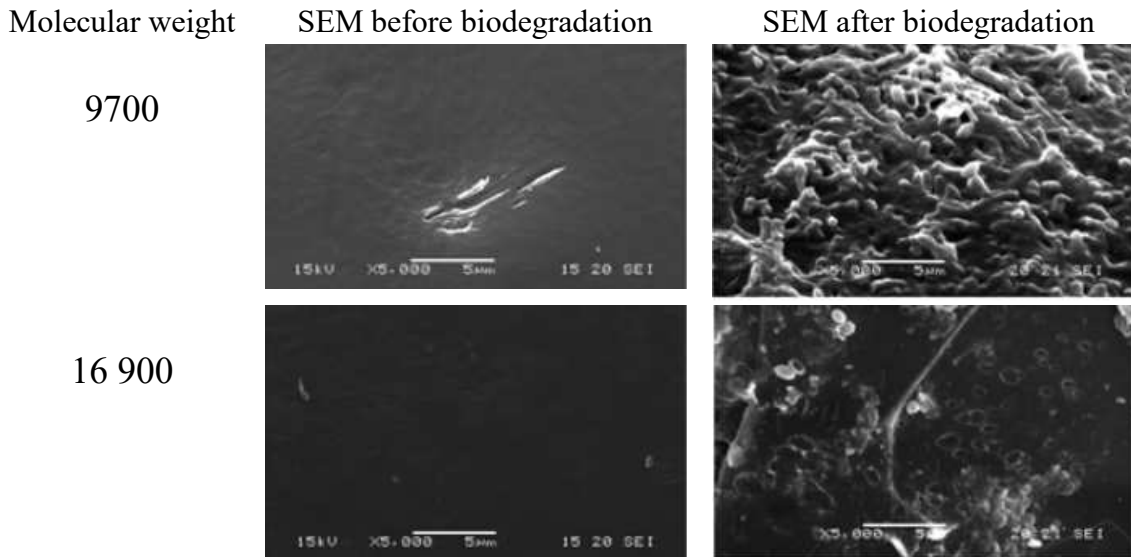


Fig. 21: SEM images of the LMWPE sheets before and after 80 days of composting (5 000 magnification) [124].

Pretreatment such as weathering, UV irradiation and thermal treatment was employed to raise the hydrophilicity of polyolefin polymers by introducing carbonyl groups – C = O to the backbone chains which enables their microbial metabolization [123, 124]. A few microbes capable of degradation of the pretreated polyolefin polymers have so far been isolated. The isolation of a strain capable of the polyethylene degradation from a crude oil contaminated soil at room temperature is described by Yoon, Jeon and Kim [124]. Morphology of low molecular weight polyethylene (LMWPE) after the biodegradation in the sterilized compost inoculated with the isolated bacterium *Pseudomonas* sp. E4 for 80 days at 37°C is shown in fig. 21 [124]. It is visible that the smooth surface of the LMWPE sheets were eroded as a result of the biodegradation. A lot of the bacterial cells adhering to the surface of the LMWPE sheets can be seen. The degree of the surface erosion is more pronounced for LMWPE with lower Mw. The degradability/biodegradability of polypropylene films (PP) for packing applications after 11 months burial in the São Giacomo landfill in Caxias do Sul wea (Brazil) were investigated by Longo et al. [125]. Comparing the buried PP film to a sample of virgin PP, two peaks of degrading activity appeared at the TG curve as well as structure modification typified by occurrence of new absorption bands at FTIR, which can be due to changes in crystallinity. Thermal analysis carried out on the buried PP showed decreases in the percentage of crystallinity due to chain scission. The SEM revealed the start of degradation/biodegradation processes of the polymeric film in the landfill typified by microorganism colonies on the polymer surface, chromatic alteration and formation of cracks [125]. The stability of geotextiles are generally dependent on their nature and type of soil or microorganisms presented. For geotextiles from natural fibers it is relatively simple to partially enhance durability in soil burial conditions by increase of their surface hydrophobicity [126, 128] or use of antimicrobial treatment [127]. Recent possibilities of the different natural fiber treatments used to reduce the moisture absorption and fiber degradation is reviewed

by Azan et al. [128]. Wide range of different pretreatments are available, such as acetylation, silanization, benzylation, fluorocarbon or isocyanate treatment, methacrylate treatment etc. Very efficient is plasma mediated surface modification, pre-activation and grafting. Cold plasma of high-frequency can be produced by microwave energy, whereas alternating current of a lower frequency discharge at atmospheric pressure produces corona plasma. Plasma effects on the fiber surfaces can be tuned by distance of samples to plasma source, treatment time, intensity of plasma treatment, and by type of gas mainly [129]. For surface hydrophobization the fluorocarbons atmosphere CF_4 and C_2F_6 , SF_6 is commonly used. In the case of the plasma treatment of fibers the particular surface modification does not affect bulk substrate properties since the depth of surface penetration, which approximately is a function of plasma power and treatment time, is typically <100 nm (0.1 μ m). In atmospheric plasma is mean free path of plasma particles is nearly 0.1 μ m and in for thicker geotextiles will then plasma radicals not contacting majority of fibers.

6. Manufacturing Techniques

Of the large family of textile structures, the woven fabrics and nonwoven fabrics have found extensive applications as geotextiles because of their broad availability and low cost. Two traditional but less widely known technologies (braiding and warp knitting) are introduced herein. These technologies have been rediscovered recently and found many applications in geo technical applications. Taking advantage of its multidirectional reinforcement capability, multiaxial warp knits (MWK) have been adopted extensively for large area coverage/reinforcement applications.

There is a large family of textile structures available for geotextiles. Fig. 22 illustrates examples of these structures. In the past two decades, aside from traditional woven fabrics, a diversification into various forms including knits and specialty nonwovens has occurred. A particular class of textile structures that has been rediscovered and undergone extensive development for advanced geo-composites and many other industrial applications is the 3-D textile structure [18].

6.1 2D Woven Fabric

2D woven fabric is the most popular material in geo-composite industry, with nearly 70% of production. Typically, 2D woven fabric have two yarn sets as warp (0°) and filling(90°) interlaced to each other to form the surface. Using traditional weaving, plain, twill and satin weaves are produced (fig. 23). 2D woven fabric in rigid form suffers from its poor impact resistance because of crimp, low delamination strength because of the lack of binder fibers (Z-fibers) to the thickness direction and low in-plane shear properties because no off-axis fiber orientation other than material principal direction [20]. Although through-the-thickness reinforcement eliminates the delamination weakness, it reduces the in-plane properties [18, 19]. On the other hand, uni-weave structure with structure one yarn set as warp (0°) and multiple warp yarns locked by the stitching yarns was developed [20].

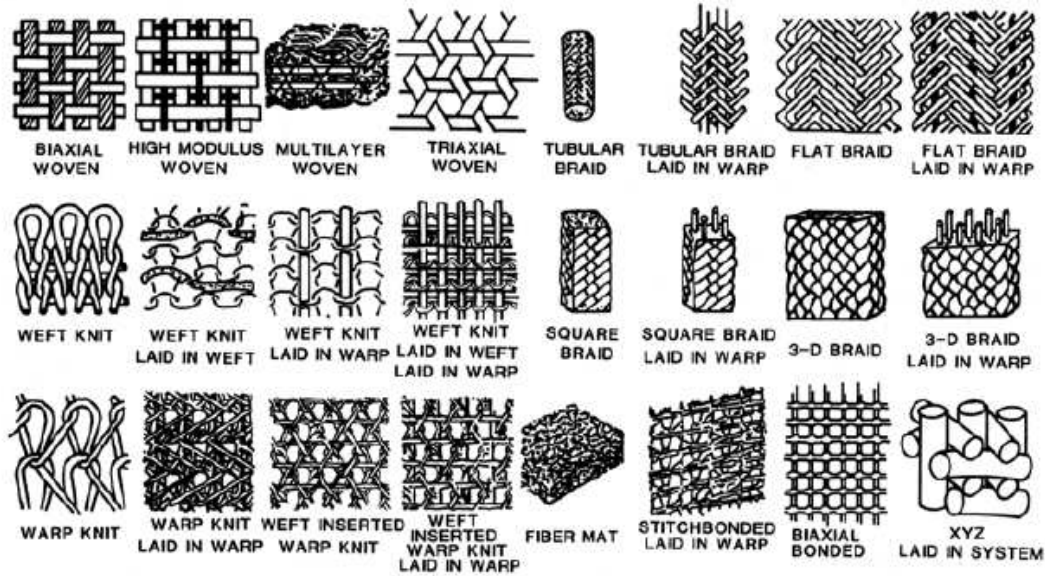


Fig. 22: Textile structures for geo applications [2].

Selected methods available to manufacture these geo-based technical textiles are described here. Bi-axial non-crimp fabric was developed to replace the unidirectional cross-ply lamina structure [21]. Fabric has basically two sets of fibers as filling and warp and locking fibers. Warp positioned to 0° direction and filling by down on the warp layer to the cross-direction (90°) and two sets of fibers are locked by two sets of stitching yarns' one is directed to 0° and the other is directed to 90° . Traditional weaving loom was modified to produce such fabrics. Additional warp beam and filling insertions are mounted on the loom. Also, it is demonstrated that 3D shell shapes with high modulus fibers can be knitted by weft knitting machine with a fabric control sinker device as shown in Figure 24.

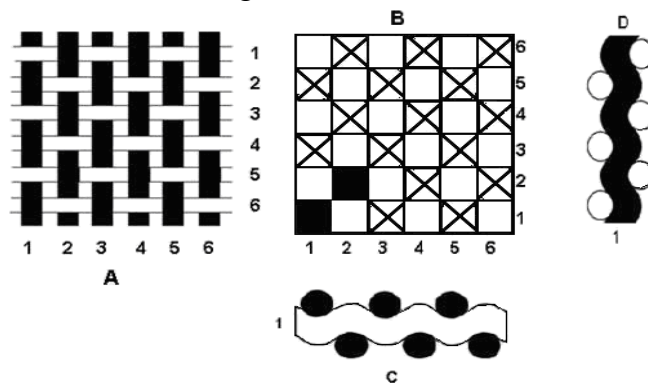


Fig. 23: 2D woven fabric (A) interlacement, (B) scheme, (C) longitudinal cross-section and (D) transverse cross-section.

Influence of weave type on selected properties of hybrid woven fabrics with basalt filaments in the warp and jute yarns in the weft are shown in tab. 10. All fabrics were made on the CCI sample loom under the same technological conditions with the same density for all fabrics.

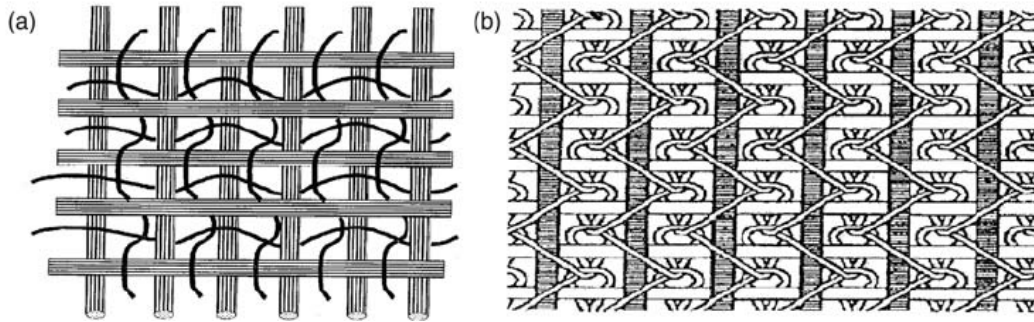





Fig. 24: Biaxial non-interlaced (a) woven fabrics and (b) knitted fabric [21].

The sett was 12 threads/cm in warp and 8 threads/cm in weft [133]. The number of pores was deduced from the number of interlacing points given by warp and weft yarn density, i.e. as the product of measured warp and weft densities. Pore volume and shape of these fabrics woven with identical yarn diameter and yarn spacing will vary depending on the manner of interlacing of the threads. The pore walls are not flat and their cross section changes with the fabric thickness with respect to the type of pores, type of yarns and their characteristics.

Table 10: Influence of weave on selected properties of basalt/jute woven fabrics [133].

Weave	Plain	Matt	1/3 Twill
type			
Cover factor [%]	79.3	78.6	74.9
Thickness [mm]	1.77	1.82	1.80
Areal mass [g m ⁻²]	658	678	698
No of pores [100cm ²]	88.3	97.6	106.9
Open area [%]	20.7	21.4	25.1
Tensile modulus [MPa] warp	926	838.48	478.44
Tensile modulus [MPa] weft	256.5	467.75	466.1
Shear rigidity [MPa]	0.37	0.32	0.25
Strength [MPa] weft	192.9	290.43	170.75
Strength [MPa] warp	535.1	247.2	469

It is visible that the plain weave corresponds to most compact structure and the best mechanical properties. Plain weave has relatively lower porosity parameters, i.e. fewer numbers of pores and lower portion of open area as compared to matt and twill weaves. Both matt and twill weaves have higher thickness due to longer float lengths of yarn and lower area, thus more fluids can be entrapped in the structure. In fact plain weave is composed from regularly interlaced weft and warp yarns with highest density (see fig. 25).

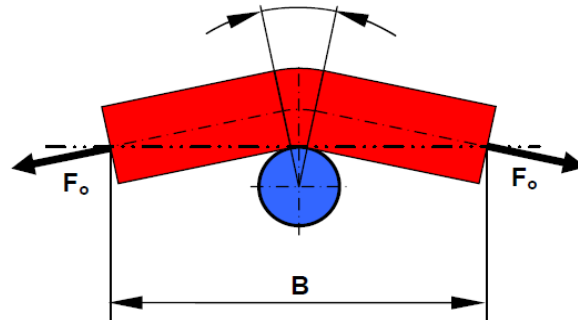


Fig. 25: Structure of plain weave binding point

Leno fabrics comprise a warp and weft thread system just the same as normal plain fabrics. The warp system is split into straight and looping warp threads. Straight warp threads are always under the weft threads and represent the lower shed during weaving. Looping warp threads are always above the filling threads and represent the upper shed during weaving. The number of crossings threads within a binding point is higher and the wrapping angle of thread crossings is larger (see fig. 26).

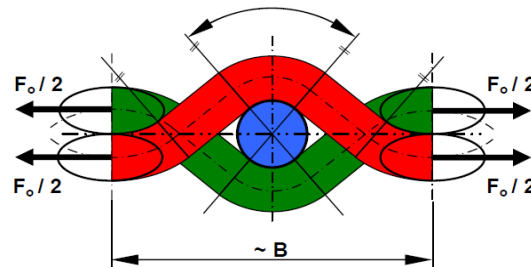


Fig. 26: Structure of leno weave binding point [131].

Binding point for plain weave is planar but for Leno is spatially arranged. Warp threads are crossing in the plane having some angle γ , from plane „weft – warp“. The cross sections for Leno threads are elliptical. The length l_M is then solution of four biquadratic equations [132]. Slip force in the fabric element F_P is generally defined as force in thread which leads to the disrupt balance in the binding point. For plain weave the F_P depends on the thread axial force F_0 , friction coefficient f and wrap angle θ_p , according to the relation

$$F_p = F_0 \exp(f \theta_p) \quad (14)$$

For leno fabrics is F_L (in the warp direction) defined as

$$F_L = F_0 \exp(f(\theta_L + \sigma_L)) \quad (15)$$

where θ_L is wrap angle of weft-warp and σ_L is wrap angle warp-warp. For the Pierce model and symmetric angles $\theta_L = \sigma_L$ is valid

$$F_L = F_0 \exp(2f\theta_L) \quad (16)$$

The ratio between slip forces is then [131].

$$F_L / F_p = \exp[f(2\theta_L - \theta_p)] \quad (17)$$

The ratio between slip forces as function of yarn spacing for $f = 0.5$ is shown on the fig. 27.

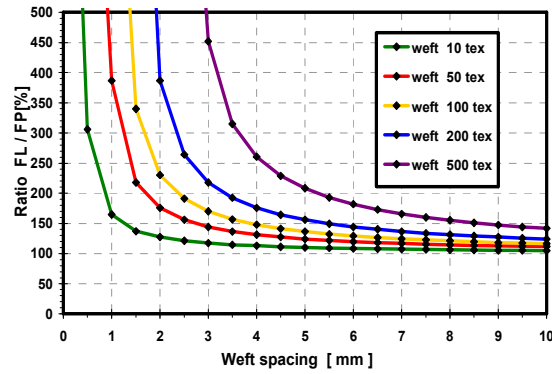


Fig. 27: Slip forces ratio for various weft spacing [131].

6.2 Triaxial Fabrics

Triaxial weave has basically three sets of yarns as \pm bias (\pm warp) and filling [22]. They interlaced to each other at about 60° angle to form fabric as shown in fig. 28.

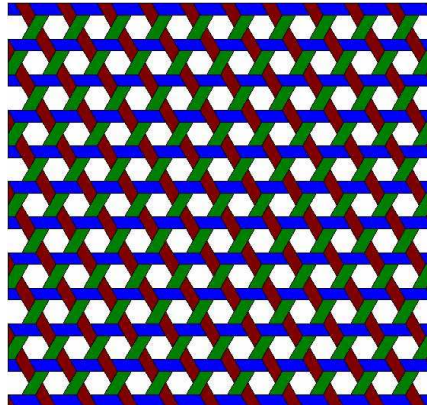


Fig. 28: Triaxial woven fabrics.

The interlacement is similar to traditional fabric which meant one set of yarns is above and another one below and this repeats through the length and width of the fabric. Normally, the fabric has large open areas between the interlacements. While

dense fabrics can be produced, it may not be woven in a very dense structure compared to the traditional fabrics. This process has mainly open reed. Triaxial fabrics have two variants: (1) Loose-weave and (2) Tight weave. The open-weave triaxial fabric has certain stability and shear stiffness to $\pm 45^\circ$ direction compared to the biaxial fabrics and has more isotropy [22].

6.3 3D Woven Fabrics

3D orthogonal woven performs have three yarn sets: warp, filling, and z-yarns [23]. These sets of yarns are all interlaced to form the structure wherein warp yarns were longitudinal and the others were orthogonal. Filling yarns are inserted between the war players and double picks were formed. The z-yarns are used for binding the other yarn sets to provide the structural integrity. The unit cell of the structure is given in fig. 29. A state-of-the-art weaving loom can be modified to produce 3D orthogonal woven fabric [23-27].

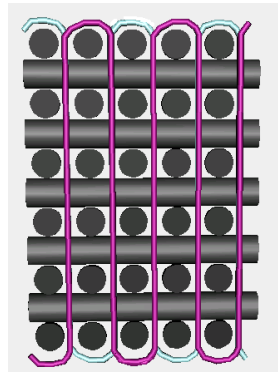


Fig. 29: 3D orthogonal woven fabric.

3D angle interlock fabrics can be fabricated by 3D weaving loom [28]. They are considered as layer-to-layer and through-the-thickness fabrics as shown in fig. 30. Layer to-layer fabric has four sets of yarns as filling, \pm bias and stuffer yarns (warp). \pm Bias yarns oriented at thickness direction and interlaced with several filling yarns. Bias yarns make zigzag movement at the thickness direction of the structure and changed course in the structure to the machine direction.

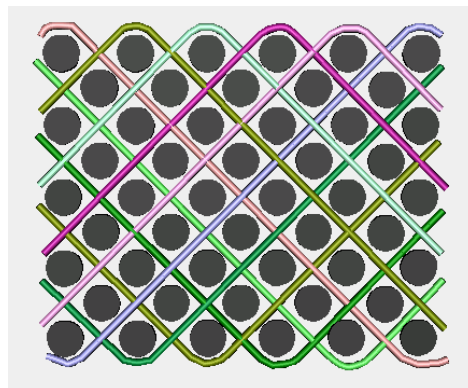


Fig. 30: 3D angle interlock fabrics.

6.4 Nonwovens

Nonwoven geotextile is produced by bonding or interlocking fibers, or both, through mechanical, thermal, or chemical means. It has captured more than 75% market in a very short span of time. It is extensively used for drainage, filtration and stabilization. Constructed from a felt-like fabric, geotextiles are light in weight and act as filter and reinforcements. These fabrics are typically classified into light weight, medium weight or heavy weight details of which are given in tab. 11 [29].

Table 11: Types of nonwoven geotextiles [29].

Type	Weights (kg)/m ²	Applications
Light Weight	0.088 to 0.119	High Drainage Areas, Landscaping, Asphalt Overlay
Medium Weight	0.170 to 0.227	Drain Filtration, Erosion Control, Aggregate Separation
Heavy Weight	0.283 to 0.455	Aggregate Separation, High Filtration Areas

Nonwoven geotextile is generally manufactured by placing and orienting the filaments or fibers onto a conveyor belt, which are subsequently bonded by needle punching or by melt bonding.

6.4.1 Standard nonwovens

Mostly two methods are used for its manufacturing in geotextile i.e. Heat bonded non woven and Needle punched non woven. Heat bonded nonwoven textiles are made from continuous filament fine fibers that are laid randomly onto a moving belt and passed between heated rollers. These fabrics can have different melting points so get there coherence and strength from the partial melting of fibers between the hot rollers or resins can be used on fiber matt for bonding. Needle punched non-woven fabrics are made from blended webs of continuous or staple filaments that are passed through banks of multiple needles. The fabric derives mechanical coherence from the entangling of fibers caused by the needles. Recent advances of nonwoven for technical textiles including geotextiles are described in the book [140].

6.4.2 Thick nonwovens

Thickness of nonwoven structures is made by stratification of “semi-products”- fibres, carded webs, 2D nonwovens. Directions of this stratification can be different, predominate directions are horizontal (fig. 31 a) and vertical (fig. 31 b). Direction of stratification determinates an orientation of structural elements in the structure of product and significantly influences the choice of fixation principle. 3D products with horizontal orientation of structural elements, for example, cannot be fixed on the surfaces of product only. Decomposition of the product in this case is evident.

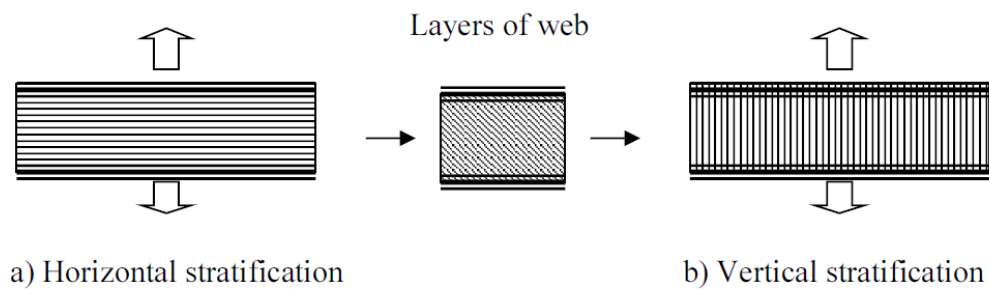


Fig. 31: Basic types of stratification

6.4.2.1 Mechanical fixation of surfaces of nonwoven structures

The industrial application of a web “wave” as the basic “construction” element of a 3D nonwoven fabric inspired to look for a mechanical method of fixation of these web (or nonwovens) waves in products, to look for such a method that would not significantly change the fixed structure (as it happens e.g. in case of needle-punching) [30]. For the 3D textiles manufactured through vertical folding of a web into “waves”, the main characteristic fact is, that the folded formation (fibres, nonwoven) goes “through” the product from its one side to the other one (fig. 32). The basic relations between the product parameters and technology parameters are known and were derived [30]. Today, there are two following generally known methods of mechanical surface fixation of nonwoven structures that can be applied onto 3D structures. Splicing by means of fibre bundles which is executed on the MULTIKNIT machine supplied at the market.

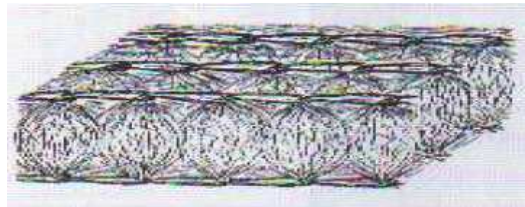


Fig. 32: Multiknit structure

Method developed at the TUL is based on twisting of fibre ends protruding from the web wave peaks into so-called quasi-yarns [31]. The machine for implementation of this method includes no parts performing oscillatory motion. The appearance and properties of the products of course conform to the different fixation principles. A big advantage of this method is, in contrast to the first method, it makes possible to add and to bond reinforcing nets to the surface of fixed structures. The basic idea of this method is to splice the waves of web into a cohesive whole just on their peaks [32]. In case of such method we can a priori suppose that it will be less energy demanding than e.g. the „heat fixation“ and that neither the structure nor the shape of the product will not be significantly changed. In course of this time it has been also verified. To its purposeful development we come only now, in connection with the development of „corrugated“ 3D textile fabrics [33] and with the effort to find their applications in “quick” technologies like spun-bond, spun-lace.

6.4.2.2 Principle of quasi-yarn formation

Both classic and quasi-yarns belong to fibre formations that are made by fibre twisting. In contradiction to classic yarns, quasi-yarns are formed by twisting of ends or, as the case may be, of loose segments of fibres situated on surface of a structure - fleece or of other sort of a textile product. A model of a quasi-yarn structure can be illustrated e.g. according to the fig. 33.

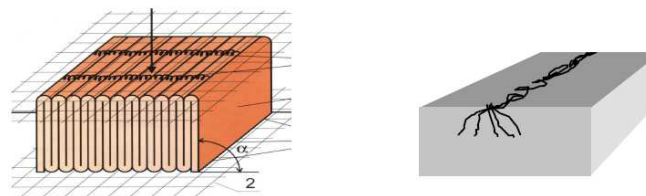


Fig. 33: Characteristics of quasi-yarns

It can be compared to a “centipede”. Its body represented by twisted fibers lies on the structure surface, its legs reach to the depth of the structure. As to principle of rise of quasi-yarn, it is found that if a rotating cylinder- or cone-shaped body moves on the web surface by its base or by its surface line (Fig. 34), it leaves behind a “track” in form of twisted fibers. The shape of this “track” is similar to the classical yarn and therefore it is called “quasi-yarn”. Quasi-yarns can be laid out on the web surface for example parallel, theoretically though in optional spacing.



Fig. 34: Principle of quasi-yarn creation

By suitable mutual layout of the rotating body and the textile fabric surface, e.g. according to fig. 35, it is possible to bond textile fabrics together by “surface-broad” lamination. By repeated lamination it is possible to produce textile fabrics of requested thickness (e.g. 10 to 200 mm).

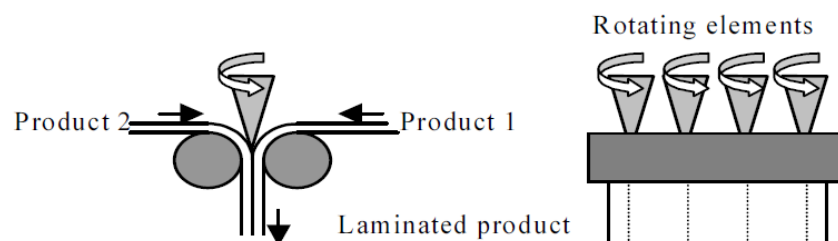


Fig. 35: Principle of lamination

6.4.2.3 ROTIS principle of nonwoven structures production

The main characteristics of “conventional” nonwoven products are their constant parameters (constant height and density); “non-conventional” products are characteristic by locally different parameters of products. One possibility how to create 3D product based on conventional 2D nowoven web is shown in fig 36.

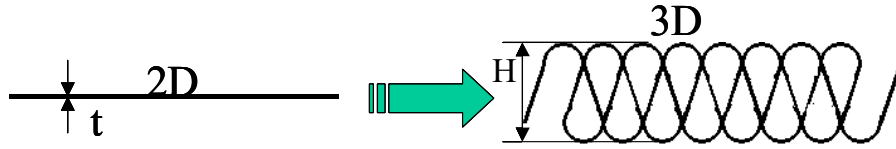


Fig. 36: Creation of 3D product

For forming of 3D textile structures with prescribed thickness in the range 4 till 10 mm based on conventional planar web with thickness 0,2 till 2 mm the ROTIS device was invented and designed. Principle is preparation of perpendicularly laid structures by deformation between toothed gears. Combination of ROTIS principle with quasi yarns formation is shown in fig. 37.

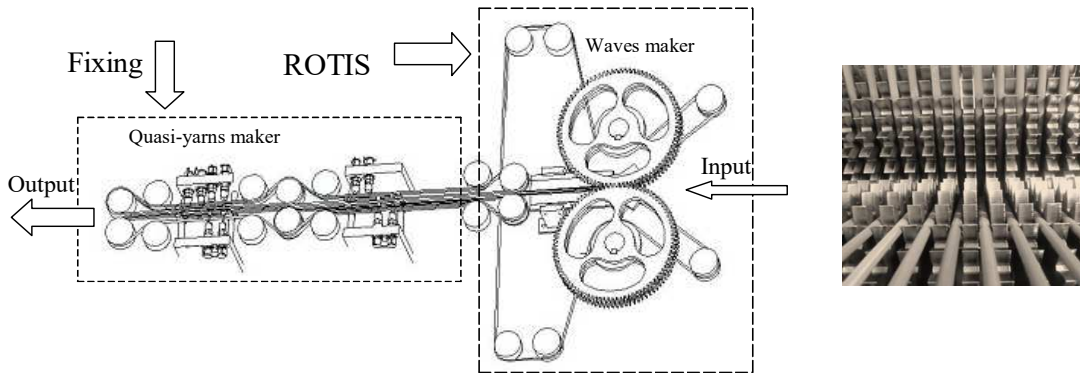


Fig. 37: Combination of ROTIS and quasi yarns

Rotis type 3D structures can be prepared in huge variation of porosities due to changing density of “waves”. Provided that a “wave” made of semi-article (web, nonwoven) is the basic “building unit” of the product, one can easily deduce the basic relations between the parameters of technology and the geometric dimensions of the product [34]. The product thickness H [m] is expressed as

$$H = \frac{A v_1}{2v_3}, \quad (18)$$

where v_1 [m/s] is web input rate, v_3 [m/s] is rate of the working roller 3 and A [m] is tooth pitch of the working roller 3. The wave number of ROTIS structure [number of waves per 1 m] w_n is equal to

$$w_n = \sqrt{\frac{t^2 - 1}{4H^2}} \quad (19)$$

and required thickening of starting web t is equal to

$$t = \sqrt{4H^2 w_n^2 + 1} \quad (20)$$

The output rate of the conveyor 2 v_2 [m/s] and rate v_3 are interrelated with product characteristics by

$$v_2 = \frac{v_1}{t} \quad \text{and} \quad v_3 = \frac{w_n A v_1}{t} \quad (21)$$

The wave number of ROTIS structure is dependent on rates by relation

$$w_n = \frac{z n_3}{v_2} = \frac{v_3}{A v_2} \quad (22)$$

where n_3 [1/s] is revolutions of the working roller 3 and z is teeth count of the working roller. Using of these relations between the product parameters H , w_n and technological parameters v_1 , v_2 , v_3 , it is possible to project and produce nonwoven products of the required macro geometrical structures. Using for example the assumption that v_1 , v_2 , and v_3 velocities are constant, machine produces conventional (plane) product (fig. 38). Using for example the assumption that, v_1 is constant and v_2 , v_3 velocities are changing, the ROTIS machine produces various non-conventional products.

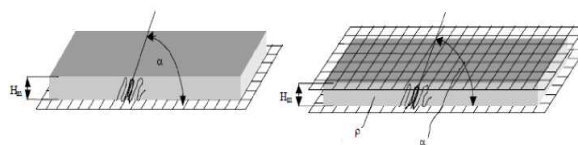


Fig. 38: Conventional 2D structure with quasi yarns

Laminated products

By means of mutual laminating of these mentioned types of textiles it is possible to obtain other types of non-conventional products, like “hollow” products or products of structured surface, for instance according to the scheme in fig. 39 [35].

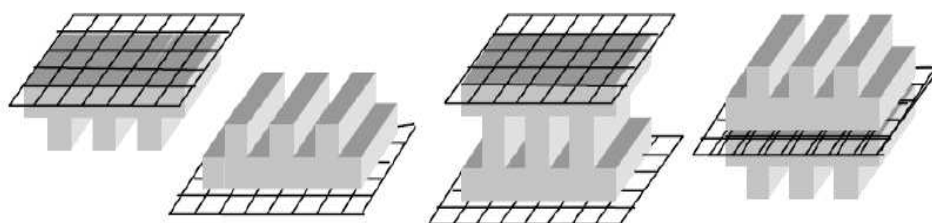


Fig. 39: Product created by lamination

Three layer ROTIS nonwovens: outer layers- spun bond with nanofibrous net, inner layer -FIBERTEX type Fiberback 80 CB is shown in fig. 40. Before creating of final product were these layers joined by needle punching.

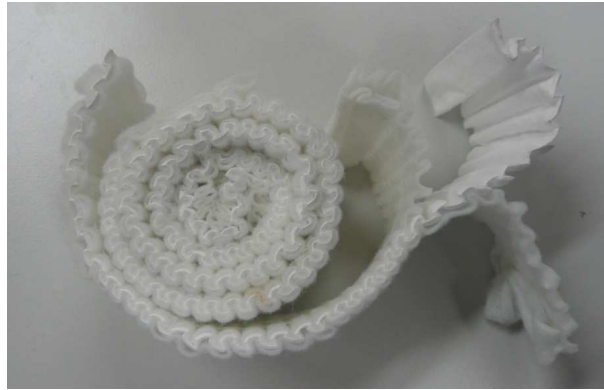


Fig. 40: Three layer ROTIS structure with nanofibrous net

Some other examples of 3D structures prepared by ROTIS technology are shown in fig. 41.

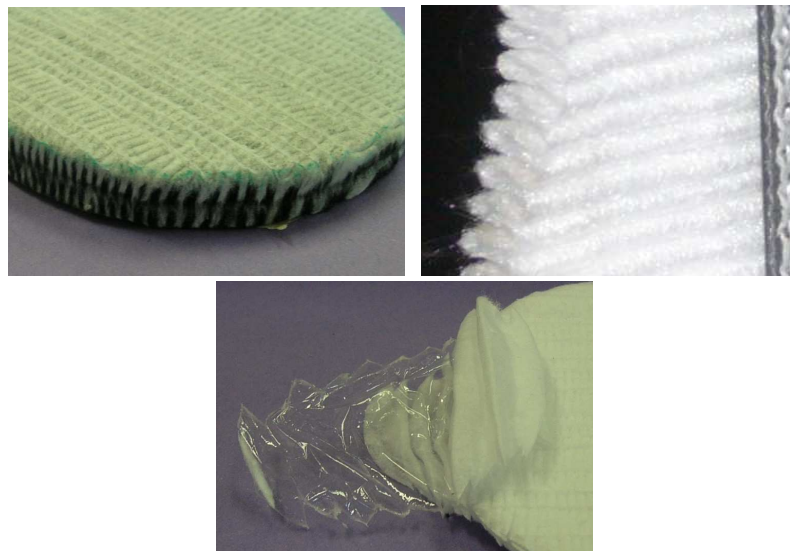


Fig. 41: Some 3D structure prepared by ROTIS technology

6.5 Geocomposites

Composites, which are combinations of different materials leading to a new material, are often used in civil engineering. The reason is that the optimal plain material with regard to structural and economical performance does not often exist. Thus, it is necessary to combine the advantageous properties of single materials for instance load-bearing capacity, durability, weight and costs to eliminate mutually their drawbacks. Portland cement is the most widely used construction materials for decades due to its excellent thermal performance, mechanical properties and durability. However, there is a growing debate in environmental circle on the

tremendous energy consumption and emission of carbon dioxide during its production. With the mounting pressure to reduce energy consumption and pollution in all industrial processes in global manufacturing, the pursuit of alternative cement materials with less energy consumption and pollution have become important objective of many recent research studies. The production of cement is increasing about 3% annually. The cement industry is the second largest producer of the greenhouse gas. Among the greenhouse gases, CO₂ contributes about 65% of global warming. Additionally, cement production and resulting emissions are expected to increase by 100% from the current level by 2020. Beside the emission of CO₂, cement industry launches SO₃ and NO_x which can cause the greenhouse effect and acid rain. This is particularly serious in the current context of climate change caused by CO₂ emissions worldwide, causing a rise in sea level and the occurrence of natural disasters and being responsible for future meltdown in the world economy. In the light of these problems, the scientific community has undertaken to seek new processes, technologies and materials to provide the construction industry with alternative binders. Incorporation of supplementary cement materials in cement-based composites is of primary importance today, most of which focus on fly ash and silica fume or micro-SiO₂. Also, supplementary cement materials are attractive due to improvements in the rheology, durability and strength of the concrete. In addition to the environmental benefits, supplementary cement materials can enhance the microstructure based on the filling effect and/or the pozzolanic reaction. Geopolymer is a new environment friendly inorganic binder. It has attracted spotlight over the past decade with its comparable performance with Portland cement and is regarded as a most promising alternative to Portland cement. Geopolymers can be produced by alkaline solution activating alumina-silicate source material, such as meta-kaolin, fly ash and slag. Due to easy, energy efficient, eco-friendly processing and excellent mechanical properties, geopolymers are fast emerging materials of choice for a range of construction and building materials, fire resistance ceramics, composites, matrix for immobilization of toxic wastes, precursor for monolithic and many others. Fly ash is comprised of fine spherical particles, mostly amorphous, in addition to unburnt carbon, crystalline mullite, quartz and hematite. Fly ash is the residue of power plants generated during combustion of coal. They consist mostly of SiO₂, Al₂O₃ and Fe₂O₃. Use of fly ash as a fine aggregate improved the mechanical properties and a reduction in water absorption, with good compatibility between sand and ash. Fly ash improves the workability of fresh mortar and the resulting concrete shows excellent surface finish. The small size of spherical fly ash particles also contributes to a better packing of the aggregate materials, which reduces porosity and hinders the penetration of aggressive agents, thus considerably improving the chemical resistance. Alkali activators have been used to activate the alumina-silica materials; thus the activated material could change vitreous structures into compact cementations skeletons. The limiting factor which has hindered the development of fly ash based geopolymers is its low reactivity. The reactivity of fly ash largely depends on its amorphous content which undergoes faster dissolution in alkali solution, whereas the crystalline fraction takes a longer time. Most of the research effort on improving the reactivity is directed

towards addition of calcium bearing substance such as Ca(OH)_2 , limestone and blast furnace slag. However, the modification of precursor chemistry often leads to additional reaction paths which are not desirable. Concrete is the most frequently used construction material all over the world. However, its major drawback is the brittleness and susceptibility to crack formation and growth that reduces its performance and durability. Conventional concrete has poor resistance in tension, limited ductility, low impact and abrasion resistance and little resistance to cracking. Traditional building structures with steel skeleton reinforced concrete are very heavy weight structures with steel vulnerable to corrosion. Most of these concrete structures tend to undergo large deformations in the event of a strong earthquake. The novel textile reinforced concrete solution is an alternative way to reinforce concrete other than traditional steel bar. The main purpose of fiber reinforcement is to increase its structural integrity and improve flexural behavior and hence exhibit superiors in terms of the durability factor. The textile structure reinforced concrete also reduces concrete thickness and therefore reduces cement consumption leading to a sustainable novel building solution.

Basalt is a common term used for a variety of volcanic rocks, which are gray, dark in color, formed from the molten lava after solidification. Common minerals in basalt include olivine, pyroxene, and plagioclase. Basalt as an igneous mineral ore can be grinded into particular form or can be melted and formed into 3D products, continuous fibers and staple fibers. Basalt fibers have been used to make e.g. papermaking fabrics, zirconia coated for alkali resistance, used for internally reinforcing cement in concrete, to reinforce thermosetting resins, particularly epoxy resins and polyester resins. It has been found that basalt particles, when combined with a resin binder and a reinforcing material, such as fiberglass, provide unexpected strength, fire-resistance, radiation impermeability, and projectile shielding for ballistic armor/shields, fire-resistant building panels, construction blocks and protective coatings on substrates. The main problems of basalt based materials (mainly fibers) preparation are due to gradual crystallization of some structural parts (plagioclase, magnetite, and pyroxene) and due to non-homogeneity of melt.

Basalt fibers have very good hardness and thermal properties, and thus can have various application as construction materials like pipes, bars, fittings etc. Basalt based composite pipes can transport corrosive liquids and gases. The same equipment as for fiber glass pipes can be used for this. These pipes are reported to be several times stronger than glass-fiber pipes. Due to basalt's low thermal conductivity, deposition of salts and paraffin inside the pipes is also reduced. Other, structural basalt composite components (such as pipes and rods) are made from unidirectional basalt reinforcement. In combination with its high specific strength (9.6 times higher than steel), high resistance to aggressive media, and high electrical insulating properties, this results in specialty products such as insulators for high voltage power lines. As is well known, steel material tends to corrode if not protected adequately. There are many ways to limit the oxidation, using stainless steel or more expensive solution than simple steel - or bars obtained from glass fiber pultrusion. However this last solution is limited because of the lower resistance of the glass fiber in the alkaline

environment associated with concrete. Using pultruded bars made with basalt fibers may be a right solution for this problem, given that basalt fibers are more resistant than glass fibers in the alkaline environment and, moreover they cannot corrode. Therefore, pultruded bars made with basalt fibers should insure good durability to the reinforced concrete, because they do not react in alkaline environments and with corrosive elements. Sudaglass (Houston, Texas) produces several products from basalt fiber, including concrete reinforcement rods. Pultruded from unidirectional basalt fiber, the rods are reportedly 89 percent lighter than steel reinforcement rods, have the same coefficient of thermal expansion as concrete and are less susceptible to degradation in an alkaline environment. The company claims that 1 ton of basalt rods can provide reinforcement equal to 4 tons of steel rods. Basalt fibers can also be used in machine building because of their good frictional, heat and chemical resistance. It can be also used for making products for sports activity like hockey sticks, tennis rackets, skis, snowboards, arrows etc. Mervin manufacturing is one of the companies who are dealing in basalt based composites for snowboard. The board was on exhibit first time in the Basaltex booth at the 2005 JEC Composites.

The structural materials most often used in civil engineering are concrete and steel. Concrete is quite cheap and has relatively large compressive load-bearing capacity, but the tensile load-bearing capacity is very low. Thus, plain concrete is not applicable if significant tensile loading cannot be ruled out in advance, as it is the case in arch structures or short columns where predominantly compressive loading comes into picture. In contrast, steel has relatively high tensile load-bearing capacity but it is quite expensive. A big advantage of embedding steel bars in concrete is due to the alkalinity of concrete, which automatically protects the steel from corrosion resulting from oxidation over long time periods. This protection is also referred to as passivation. Nevertheless, the alkalinity of concrete reduces successively due to chemical reactions with carbon dioxide. This process, also known as carbonation of the concrete, initiates at the surfaces and moves towards the inner parts of the concrete where it enables steel corrosion due to the lost passivation.

Conventional steel in combination with reinforcement of concrete is most common for construction despite some of the historical disadvantages of vulnerability to corrosion attack and durability. Various remedial methods have been applied to overcome the shortcomings of this building material, such as increasing the concrete cover, which, however, leads to an increased self-weight of the structure. In recent past, an attempt to improve sustainability of reinforced concrete came in the shape of development of Textile Reinforced Concrete (TRC), which is by providing non-corrosive textile materials as reinforcement with fine grained concrete matrix. It has evolved as a perfect alternative with excellent properties of thin and light weight structures along with corrosion resistance. Textile composites have certain other advantages too like high strength-to-weight ratio, ease of handling, drape-ability, speed of installation, and visual impact, reversibility etc. For the improvement of tensile and flexural strength of concrete material, textile reinforced concrete is used worldwide; it also adds structural integrity to the concrete beam. Textiles are used in concrete to control cracking due to plastic shrinkage and drying shrinkage. They also

reduce the permeability of concrete and thus reduce bleeding of water. The concept of using fibers to improve the characteristics of construction materials is very old. Their use as reinforcement started since ancient times. Historically, horse hair was used in mortar and straw in mud bricks. Asbestos fibers were used in concrete in 1900. In the 1950s, fiber-reinforced concrete gained the interest due to evolution of the concept of composite materials. As soon as the health risks associated with asbestos were found, an urge to find a replacement for building materials was raised and generated. By the 1960s, materials for reinforcement of concrete were Glass, Steel and Synthetic fibers such as Polypropylene. Extensive research work is carried out to find out new fiber-reinforced concretes. Varieties of fibers are used to increase toughness and prevent cracking of cement. Sustainable, energy efficient and eco-friendly construction material is sought around the world. Sustainable, green construction material, natural fiber based reinforcement in a cement matrix is a feasible approach. A cement is a binder, whereas concrete is the composite material resulting from the mixing and hardening of cement with water (or an alkaline solution in the case of geo polymer cement), and stone aggregates. Ordinary cement often called as Portland cement is a heterogeneous fine grained material but it has serious environmental concerns. Geo polymer cement (GPC) can be used in applications to fully or partially replace OPC with environmental and technical benefits, including an 80-90% reduction in CO₂ emissions and improved resistance to fire and aggressive chemicals [36-41].

The composites behavior between textile reinforcement and concrete matrix determines important properties of the textile reinforced concrete, such as durability and load bearing capacity/structural performance. Despite the fact that TRC based research has revealed many promising attributes, it has yet to reach its recognition due to a lack of available design tools, standards and long-term behavior. Although TRC has been extensively researched, the formalization of experimental methods and design standards is still in progress.

Textile reinforced concrete is a three-phase material consisting of textile reinforcement, concrete matrix and an interface. The force transferred from the brittle concrete matrix to the reinforcement is governed by the quality of the bond between the reinforcement and matrix. The safe introduction and transfer of the forces is required for the functionality of composite constructions. In fiber based composite materials, such as TRC, bond behavior between the yarn or roving and the cementitious matrix is a principal factor influencing the global structural behavior [42]. Yarns or rovings consist of multitudes of filaments which creates a complex heterogeneous structure. Pull-out tests is a common method applied to study the bond or pull-out behavior of reinforcement embedded in a matrix.

A concrete structure should be designed, constructed and maintained to ensure durability over a required service life. The durability of a structure is important so that it can fulfil a safe functionality, while reducing costs, energy, extraction and production of new materials, maintenance, rehabilitation, replacement and deconstruction. To incorporate durability into design, the long-term performance of the applied building materials should be known or should be projectable using

experiments. Durability is a broad term which consists of deteriorating processes such as chemical attack, fire resistance and many more effects. The durability performance pertaining to chemical attack on fibers should be investigated. The durability performance is most accurately measured in real-time though due to time constraints, accelerated aging are typically applied to predict the long-term performance of materials. In some research works, the effect of accelerated ageing on the tensile properties of textile reinforcement materials was investigated. The durability of TRC was characterized according to the influence of accelerated ageing based on alkali resistance on the structural performance of textile reinforcement. The hydration of cement is the reaction between the solid compounds and the liquid phase. Hydration of cement is a complex sequence of interactions occurring between water and chemical phases of the cement (viz., tricalcium silicate ($3\text{CaO}\cdot\text{SiO}_2$), dicalcium silicate ($2\text{CaO}\cdot\text{SiO}$), tricalcium aluminate ($3\text{CaO}\cdot\text{Al}_2\text{O}_3$) and tetra calcium aluminoferrite ($\text{Ca}_2(\text{Al,Fe})_2\text{O}_5$) [43]. Calcium hydroxide and calcium silicate hydrate are produced predominantly as hydrated cement products [44-49]. However, the cement hydration reaction equilibrium as well as nucleation and growth of the hydrated cement product may be disturbed by the presence of foreign substances like textile.

The degradation of fiber due to the alkaline pore solution in the cement matrix seriously decreases the durability and may cause premature failure of the concrete composite. Calcium hydroxide is the primary cause of alkaline environment in cement. In this case, the high concentration of alkali is the main cause of fibers damage. Particularly, weight loss and reduction in mechanical properties could appear. In the technical literature different studies are present, but the reported results appear somewhat contrasting. In the last decade, the research and development of all hybrid FRP (Fiber Reinforced Plastic) structures in civil engineering has progressed substantially in several countries [50]. The first all hybrid FRP bridge was constructed in Okinawa, Japan prefecture in 2001 (Ueda, 2005). This bridge is a two span continuous girder pedestrian bridge as shown in fig. 42 which is located in the road-park of Ikei-Tairagawa road. All the structural elements have been made with Hybrid Fiber Reinforcement Plastics (GFRP & CFRP). The all HFRP solution was chosen for this bridge due to its heavily corrosive environment where the bridge is surrounded by the ocean.



Fig. 42: Pedestrian Bridge in Okinawa, Japan made of Hybrid Composite [51].

The effect of basalt fiber (see fig. 43) on physical and mechanical properties of concretes was also evaluated. The mechanical characterization showed that

improvements of flexural strength, fracture energy and abrasion resistance can be obtained by using basalt fiber even at low contents.



Fig. 43: Basalt fiber reinforced geopolymeric concrete

The basalt fibers significantly improved tensile strength; flexural strength and toughness index of the composites, whereas the compressive strength shows no obvious increase. The addition of basalt fibers shown significant improvement in deformation and energy absorption capacities of geopolymeric concrete while no notable improvement in dynamic compressive strength. According to the experimental results, geopolymeric concretes with basalt fibers showed better fracture properties and were so less sensitive to the presence of cracks than conventional Portland cement. In particular, the basalt fibers were found to be more efficient in strengthening geopolymeric concretes than Portland cements. On the other hand, they were found to be more efficient in toughening geo-polymeric concretes than Portland cements (see fig. 44) only for the highest fiber concentrations (i.e. $V_f = 1\%$). The addition of basalt fibers reduced markedly the dry shrinkage of cement mortar, especially at early ages. Moreover, the basalt fibers reinforced mortars have greater compressive and flexural strengths at early hydration period but have little less strength at the age of 28- days than mortar without fibers. As regard the thermal properties, a significant reduction in heat transfer for all temperature levels was found using high percentages of waste glass and basalt fibers. Besides its use as reinforcement of concrete based matrices, basalt fibers were also used in polymer based composites as a strengthening material for structural concrete members. Through various experimental tests for durability, mechanical properties, and flexural strengthening, previous studies demonstrated that, when moderate structural strengthening but high resistance for fire is simultaneously sought, e.g. for building structures, basalt fibers can be a good alternative to glass or carbon fibers in reinforced polymer (FRP) strengthening systems.

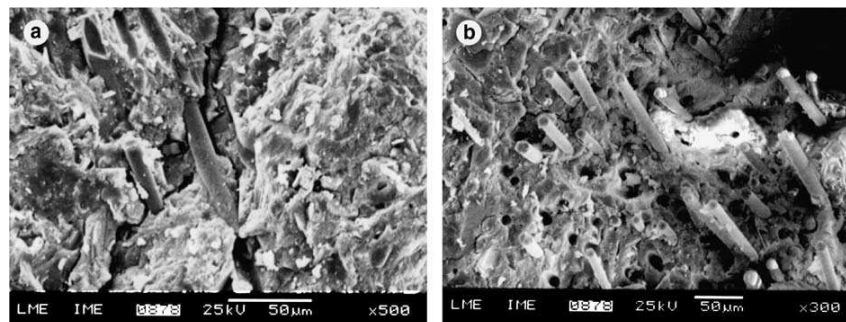


Fig. 44: Toughening mechanisms with $V_f 1\%$: (a) bridging action and (b) pullout of the fibres.

Due to their strong tensile properties and corrosion resistance, basalt fiber reinforced polymer bars are also deemed as a substitute material of steel bar to enhance the durability of reinforced concrete bridges. Recently, some researches were focused on the feasibility of the use of basalt fiber also in hot mix asphalt concrete. In particular, it was observed that the use of basalt fiber additions in hot-mix asphalt concrete had a positive impact for stability. Nevertheless, it may be considered by adding them only to binder course in order to avoid the negative effects due to basalt fibers that can be damage for vehicle tires. Although additional costs may be required to add basalt fibers to the asphalt mixtures, when its overall long-term contributions are taken into account, it is still considered that basalt fiber asphalt concrete can be utilized in the binder course. Basalt fibers are useful in transporting and storage of radioactive nuclear materials since they do not absorb any kind of nuclear radiation. Basalt-based geo-composites are extensively used in making radiation-proof protective caps for nuclear waste disposal sites. These caps provide protection for several centuries to protect public health and the environment against leaching or release of nuclear underground wastes. Nuclear landfill sites are often situated in arid, sub-humid zones, which have zero or limited underground water; the area is often devoid of any life forms, is leak-proof and should also be a maintenance-free zone. These dumping pits are often deep and made of several layers of sand, gravel, coarse materials and basalt rock armor. Another example is basalt geo-mesh, which possesses remarkable properties like chemical inertness, very high thermal sustainability against molten asphalt/tar and is lighter than other known metallic meshes. Therefore, glass and metals used for pavement reinforcement are thus substituted by basalt geo-meshes. Since basalt is environmentally friendly, it is appropriate for use in soil and embankment stabilization. Furthermore, basalt fiber-based geo-polymeric concretes show enhanced mechanical properties over conventional cement.

7. Nanotechnology

Briefly, nanofiber technology is the synthesis, processing, manufacturing and application of fibers in the nanoscale. By definition, nanofibers are fibers with diameter equal to or less than 100 nm. Due to product requirements and manufacturing capability limitations, some industries tend to consider any fibers of submicron diameter to be “nanofibers”. When looking to future generations of geotextiles, an examination of the role of nanotechnology in the functional enhancement of geotextiles is in order. By reducing fiber diameter down to the nanoscale, an increase in specific surface area to the level of 1000 m²/g is possible. This reduction in dimension and increase in surface area greatly affects the chemical/biological reactivity and electroactivity of polymeric fibers. Because of the extreme fineness of the fibers there is an overall impact on the geometric and thus the performance properties of the fabric. There is an explosive growth in worldwide research efforts recognizing the potential nano-effect that will be created when fibers are reduced to nanoscale [52].

7.1 Nanomaterials used in textiles

The most common type of nano-enhanced fiber to be explored is a simple composite of a conventional, natural or synthetic fiber with nanoparticles which improve the performance or add novel properties to the fabric.

7.1.1 Nanoparticles

The recent couple of decades indeed have seen significant spurs in the developments and innovations of the nano technology in many industries and manufacturing sectors, including fibres and textiles. This is because of the fact that at or near its molecular level or dimension material exhibits considerable improvements in some of its classical physical, mechanical, chemical, biological, light spectrum, electronic energy, and the like properties. And when the material at its nano dimensions, even in small quantity, say 2 to 5 % by weight of the bulk material, is integrated with a compatible bulk matter/substrate then there is considerable enhancement in desirable attributes of the ultimate end-product. For example, nano particles of certain materials, when somehow impregnated into or embedded in cotton fibre, yarn or fabric, can significantly improve the latter's durability, softness, stain resistance, dye-ability, thermal resistance/stability, wrinkle resistance, dimensional stability, abrasion resistance, fluid absorbency or repulsion, antimicrobial/biocide effects, UV protection or the like. Using a variety of synthesis methods, it is possible to produce nanostructured materials in the various forms like thin films, tubes or whiskers, powders. In case of films, only one dimension is in nano size, for whiskers two dimensions are in nano size while for powder, all the three dimensions are in nano size. This means the interfacial effects of nanotechnology will be more with the nanoparticles as they have more surface area to volume ratio, so the more realisation of benefits of nanotechnology from nano-powder. However, it is difficult to keep them separated during application as they tend to formation of agglomerations due to significant degree of overlap. Some typical nanoparticles are given in the Table 3 below.

Basalt particles

The basalt fibrous wastes can be utilized for preparation of basalt particles. Basalt is a common term used for a variety of volcanic rocks, which are gray, dark in color, formed from the molten lava after solidification. Common minerals in basalt include olivine, pyroxene, and plagioclase. The basalt particle filled polymer or concrete composites have reported to provide improved impact strength, thermal stability, fire-resistance, radiation impermeability, etc. These particles could be useful in applications of Body armor and ballistic barriers, Heat protecting barriers, Thermal insulation layers, Flame resistant finishing of textiles.

Fly ash

Fly ash (FA) is a waste by-product, generated abundantly by combustion of coal in thermal power stations. It is mixture of oxides, rich in silicon (SiO_2), iron (Fe_2O_3), and aluminum (Al_2O_3) [54]. Fly ash consists of fine, powdery particles predominantly spherical in shape, either solid or hollow, and mostly glassy (amorphous) in nature [54].

Table 12: Properties of typical nanoparticles used in textiles [53].

Nanomaterial	Properties
Carbon black nanoparticles or nanofibers	Abrasion resistance
	Higher tensile strength
	Good chemical resistance
	Electrical conducting
Carbon nanotubes	Exceptionally strong (100x tensile strength of steel)
	Lightweight
	Electrically conducting
	Thermally conducting
Metal oxide nanoparticles	Photocatalytic
	Electrically conductive
	UV Protection
	Antimicrobial
Metal nanoparticles	Antimicrobial
	Solar cells
	Aesthetic properties
Clay nanoparticles	Electrical resistance
	Chemical resistance
	Fire retardant
	UV shielding
Basalt particles	Fire retardant
	Thermal resistance
	Mechanical strength
Fly ash particles	Fire retardant
	Thermal resistance
	High toughness
Nanocellulose	Stiffness
	Mechanical strength
	Moisture absorbency

Fly ash particles are empty spheres (cenospheres) filled with smaller amorphous particles and crystals (plerospheres). The cenosphere fraction constitutes as much as 1% of the total mass and gets easily airborne. Fly-ash generally has a silt loam texture with 65–90% of the particles having a diameter of less than 0.010 mm. The carbonaceous material in the fly ash is composed of angular particles. Ash from bituminous coal is usually finer as compared with that of lignite one. The particle size distribution of most bituminous coal fly ash is generally similar to that of silt (less than a 0.075 mm or No. 200 sieve). Although sub-bituminous coal fly ash is also silt-sized, it is generally slightly coarser than bituminous coal fly ash. Fly ash has low bulk density (1.01–1.43 g cm⁻³), hydraulic conductivity and specific gravity (1.6–3.1 g cm³).

The SEM images of unmilled and milled fly ash particles in Fig. 45 (a) and (b) show that the milling destroyed a large proportion of the spherical morphology of as received fly ash and subsequently resulted into nano fly ash with more active surfaces.

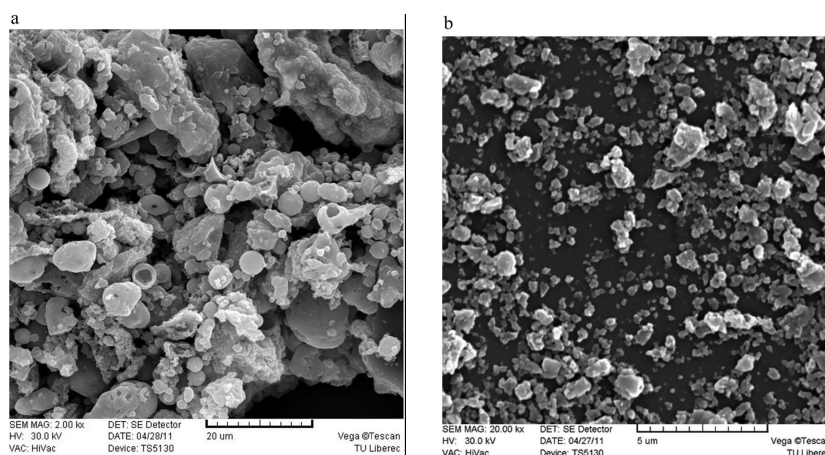


Fig. 45: (a) SEM image of unmilled fly ash. (b) SEM image of 5 h wet milled fly ash.

The composition, surface chemistry and reactivity of fly ash are of fundamental importance for development of its various applications. On the basis of silica, alumina and iron oxide content, ASTM C-618 categorizes coal combustion fly ash into two classes: Class F (low lime) and Class C (high lime) [55]. The following section described few examples of value added concepts for fly ash waste utilization.

Building and construction materials. The considerable amount of research was carried out on development of fly ash based building and construction materials to reduce the ordinary Portland cement consumption [56]. Geopolymers are inorganic polymers synthesized via chemical reaction between highly alkaline solution and the Si–Al minerals present in the fly ash. Portland cement is a major contributor to green-house gases as compared to geopolymers which in general emit less green-house gases due to their lower calcium carbonate based raw materials and production temperature [57]. In previous studies, F type fly ash based geopolymers exhibited better mechanical properties under severe environmental conditions than those of ordinary Portland cement. The use of fly ash resulted in significant enhancement of the basic characteristics of concrete both in its fresh and hardened states. The advantages of fly ash based concrete are

- Improved long-term strength, performance and durability
- Reduced heat of hydration
- Reduced water requirement for equal workability
- Minimized risk of alkali silica reaction

Sorbent for volatile organic compounds. The physicochemical properties of fly ash particles, such as its bulk density, particle size, porosity, water holding capacity, and surface area, make it suitable for use as a sorbent [58]. The incorporation of adsorbent fly ash particles into electro spun polyurethane fibers was studied for adsorption efficiency of volatile organic compounds. It was observed that the adsorption capacity of polyurethane fibers increased with the amount of fly ash particles. This result was

attributed to the decreased fiber diameter of composite fibers (i.e. increased surface area) and the presence of hollow fly ash on fiber surfaces.

Thermal barrier coatings. Fly ash coatings exhibited high thermal stability, low thermal expansion, high creep resistance in oxidative and corrosive environments, high resistance to crack propagation and high thermal shock resistance [59]. The lower thermal conductivity was related to the hollow nature of cenospheres. The fly ash-coated diesel engine components resulted into decrease in surface cracking as compared to zirconia. Therefore, further applications such as, gas burners, molten metal filters, kitchen stoves and many others could be expected from fly ash due to its resistance to micro cracking under thermal expansion.

Fillers in composites. Due to developments in structural applications of polymeric materials in aerospace, marine, automobile, construction, etc., the improvement of their damping properties is necessary. The previous studies have suggested promising results after incorporation of inorganic nanoparticles into polymers [60-64]. The inorganic nanoparticles are attractive fillers because of their light weight, high strength, corrosion resistance, and elevated temperature applicability. The benefits of filling inorganic particles are realized for variety of structural products like sport equipment, insulation, automobile bodies, marine craft bodies, and fire and heat protection devices [65]. The addition of sand, chalk dusts, etc into epoxy matrix was found to improve its mechanical, electrical or rheological properties. The incorporation of fly ash is interesting because of its low density, low cost, strong filling ability, and smooth spherical surface.

Nanocellulose

The cellulose nanostructures have attracted attention in recent years due to their reduced weight, relatively good stiffness and strength, low cost and ease of disposal [66]. The crystalline segments in cellulose have greater axial elastic modulus than the synthetic fiber Kevlar, and their mechanical properties are within the same range as those of other reinforcement materials such as carbon fibers, steel wires and carbon nanotubes. The nanostructures of cellulose are considered as bundles of molecules, elongated and stabilized through hydrogen bonding. The remarkable improvements in mechanical properties of cellulose nanostructures, in range of 130-170 GPa, are considered due to this parallel arrangement of molecular chains which are present without folding [67]. Previous work on composites made from cellulose nanostructures showed improved strength and stiffness with a little sacrifice of toughness, reduced gas/water vapor permeability, lower coefficient of thermal expansion, and increased heat deflection temperature [68]. These properties showed promise in replacement of conventional petroleum based composites by new, high performance, and lightweight green nanocomposite materials. Currently, the isolation, characterization, and search for new applications of cellulose nanostructures are generating much activity. Such isolated cellulosic materials with one dimension in the nanometer range are referred as nanocellulose. Novel methods for their production range from top-down methods involving enzymatic, chemical, physical methodologies to the bottom-up production from glucose by bacteria [69]. Depending on the source and extraction method, the size and shape of the nanocellulose

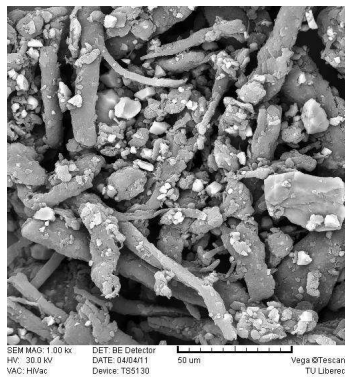
structures are different. On the basis of their dimensions, functions, and preparation methods, nanocelluloses are classified in two main subcategories as nano-fibrillated cellulose (NFC) and nano-crystalline cellulose (NCC). The NFC is composed of more or less individualized cellulose nano-fibrils, presenting lateral dimensions in the order of 10 to 100 nm, and length generally in the micrometer scale, and consisting of alternating crystalline and amorphous domains [70]. The nano-fibrils have a high aspect ratio and exhibit gel-like characteristics in water, with pseudo plastic and thixotropic properties. The NFC is obtained by a simple mechanical shearing disintegration process. The process for isolating NFC consists of the disintegration of cellulose fibers along their long axis. Different mechanical treatments have been reported to prepare NFC. They mainly consist of steam explosion, high-pressure homogenization and grinding [71].

The NCC also known as whiskers, consist of rod like cellulose crystals with widths and lengths of 100 nm and several micrometers, respectively [72]. Although similar in size to NFC, they have very limited flexibility, as they do not contain amorphous regions but instead exhibit elongated crystalline rod like shapes. Cellulose nanocrystals are generated by the liberation of crystalline regions of the semi crystalline cellulosic fibers by hydrolysis with mineral acids. This chemical process starts with the removal of polysaccharides bound at the fibril surface and is followed by the cleavage and destruction of more readily accessible amorphous regions to liberate rod like crystalline cellulose sections. The hydronium ions penetrate the cellulosic material in the amorphous domains, promoting the hydrolytic cleavage of the glycosidic bonds and releasing individual crystallites. The structure, properties, and phase-separation behavior of cellulose-nanocrystal suspensions are strongly dependent on the type of mineral acid used and its concentration, hydrolysis temperature and time [73]. Different strong acids have been reported to successfully degrade cellulose fibers, but hydrochloric and sulfuric acids are extensively used. The other processes allowing the release of crystalline domains from cellulosic fibers have also been reported, including enzymatic hydrolysis treatment, TEMPO oxidation, hydrolysis with gaseous acid, and treatment with ionic liquids [74].

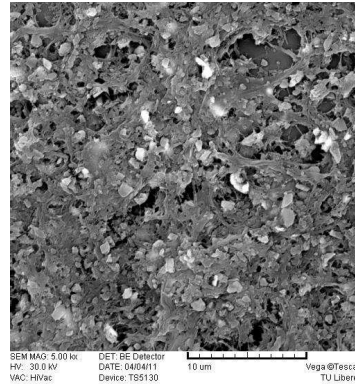
In addition to combining nanoparticles with conventional textiles to enhance their properties, textiles made entirely out of nanoscale fibers can now be manufactured. The jute based submicron particles obtained by 1 hour dry milling (mean diameter 480 nm) and by 1 hour wet milling (mean diameter 85 nm) are shown in fig. 46 [134].

6.1.2 Nanofibres

Using these nanofibers, researchers have been able to progress much in developing fabrics with unique and valuable properties [75]. The nanofibrous layers can be prepared by continuous deposition on selected substrates by electrospinning in industrial scale. They can therefore to add functionality on the surface of textile structures. In fact the same technology can be used for creation of porous membranes based on electrospaying principle (deposition of droplets) or electronetting principle (see. Fig. 47).

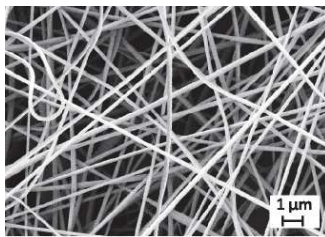


a) Dry milling

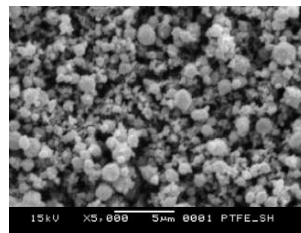


b) wet milling

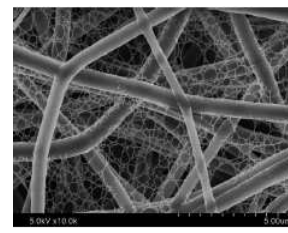
Fig. 46: Jute based cellulose particles after 1 hour milling [134].



Elspun nanofiber membrane



Electrospayed PTFE



Electronetting effect

Fig. 47: Porous layers prepared in electrostatic field

Some of the applications of nano-fibrous products and products are shown in tab. 13.

Electrospinning

Electrospinning is a well-established technique used for manufacturing polymer fibers. The apparatus consists of a syringe with a capillary needle. A high voltage across the needle creates a charged jet of material, which spins out into fibers to be collected on a charged plate. Although the technique is well understood, production is very slow, and the quality of the fibers is not very high. Novel applications for nanofibers have renewed interest in this technique, as they can make it commercially viable.

Electrospinning, an electrostatic fiber fabrication technique, is versatile and applicable in diverse fields. The nanoscale fibers are generated by the application of strong electric field on polymer solution, dispersion or melt [76]. The assembly of fibers produced by this process, offer various advantages like high surface area to volume ratio, changeable porosity and the ability to change composition to get desired function. Over the years, more than 200 polymers have been electrospun for various applications and the number is still increasing with time [77]. Electrospinning is superior in production and construction of ordered or more complex nanofibrous assemblies (see fig. 48). The random orientation of fibrous mats fabricated by the conventional electrospinning may limit the potential applications, especially in the fields of electronics, photonics, photovoltaics and tissue engineering which need fast charge transfer or regular structures. To solve this problem, a variety of strategies

have been proposed, such as pair electrodes collection, rotating drum or disk collection, auxiliary electric or magnetic electrospinning, double spinning, near-field electrospinning, direct-writing electrospinning, etc. Some approaches such as rotating drum collection have been used in the commercial electrospinning setup. The ability to consistently fabricate highly aligned fibers in large quantity over a large area is still a challenge [79].

Electrospraying utilizes electrical forces for liquid atomization [80]. Droplets obtained by this method are highly charged. The advantage of electrospraying is that the droplets can be extremely small (tens nanometers), and the charge and size of the droplets can be controlled to some extent by electrical means. Motion of the charged droplets can be controlled by electric field. The deposition efficiency of the charged spray on an object is usually higher than that for uncharged droplets. The nanostructured film morphologies can be categorized into two main groups: dense and porous. The dense layer can be amorphous, crystalline (of different structures) or amorphous with incorporated particles (intrusions). The porous layer can be reticular, grainy, or fractal like. These structures are schematically shown in fig. 49. The nanostructured film morphology depends, in general, on the temperature, the solvent used for spraying, voltage, physical properties of liquid phase (emulsion, dispersion, solution, density and surface tension), distance of collector from source, doping agents and the time of solvent evaporation. Post annealing and post treatment e.g. by plasma or microwaves can also modify the final morphology [81].

Table 13: Applications of nanofibers and products [75].

Applications	Products
Air and water filtration Controlled drug delivery Tissue reconstruction Barrier materials Anti-microbial fabric	<i>Sports fabrics with improved mechanical properties, and odour-reducing antibacterial properties</i> <i>Medical textiles such as antimicrobial wound dressings, clothing and bedding</i> <i>PPE (personal protective equipment) with improved chemical or heat resistance</i> <i>Military textiles, such as flexible body armor, radio shielding and camouflage</i> <i>Wearable electronics, which could range from conducting fabrics to connect devices together to full portable computers made from nanofibers and flexible circuit boards [75].</i>

Electrospinning/netting or **electronetting** is a one-step strategy for fabricating nanofiber/net nanostructured film comprising common electro spun nanofibers and two-dimensional (2D) soap bubble-like structured nano-nets [82]. Nano-nets, assembled from net-like structured nanowires with an ultrafine diameter (5–40 nm), exhibit several amazing characteristics, such as an extremely large specific surface area, high porosity and superior mechanical performance. The nano-net formation is connected with fast phase separation of the charged droplets [83].

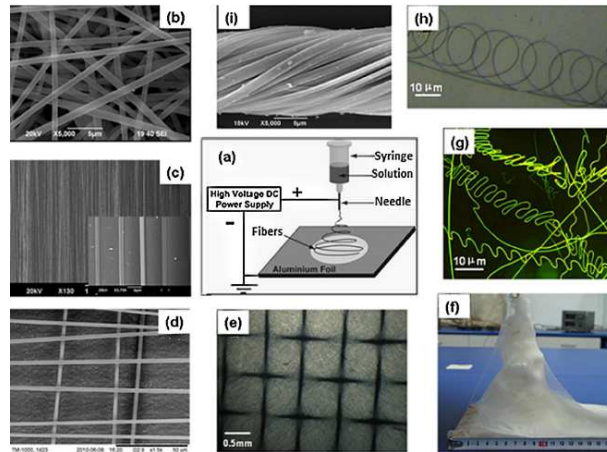


Fig. 48: (a) Schematic diagram of electrospinning method, (b) electrospun polymer nanofiber mesh without orientation, (c) parallel and (d) crossed fiber array, (e) patterned fiber web, (f) 3D fibrous stack, (g) wavy and (h) helical fibers, and (i) twisted fiber yarns [78].

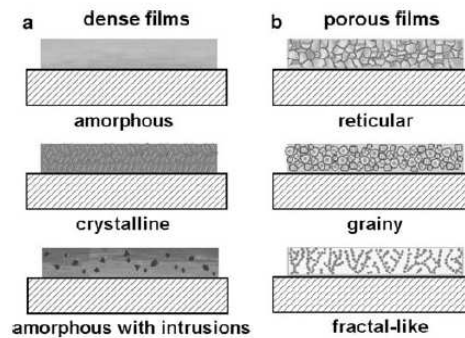


Fig. 49: Typical morphologies obtained by electrospaying [82].

Split spinning

Split spinning involves splitting a filament into multiple smaller filaments. This technique is more suited to large scale manufacturing, but it is difficult to produce filaments smaller than a few micrometers in diameter. Research is ongoing to push the capabilities of split spinning into the nanoscale range.

Self-Assembly

This is a biomimetic, "bottom-up" nanofabrication technique, which relies on the tendency of materials to assemble into nanoscale structures. This kind of process is difficult to control, and is limited to a specific set of materials, but could produce some fascinating materials with unique properties, as well as enhancing our understanding of nanoscale interactions [84].

6.2 Nano-Enhanced Finishing Treatments

Traditionally, textiles are imbued with application specific properties at the finishing stage, where chemical or physical treatment of the fibers can change their appearance and improve their resistance to water, chemicals and general wear. Nanotechnology offers multivarious options for these types of process. Wet finishing, such as dyeing,

produces large amounts of contaminated waste water. Dry finishing processes like lamination and coating often consume large amounts of energy, and are limited by the amount of material that can be applied to a fabric without adversely affecting its properties.

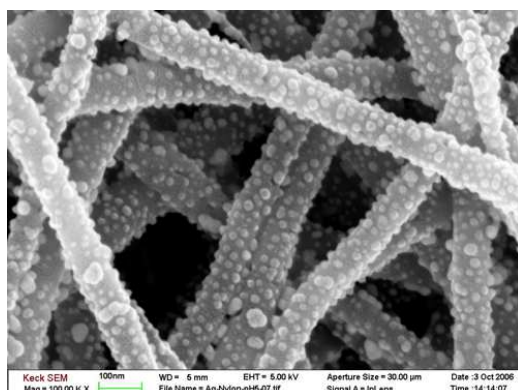


Fig. 50: Electrospun nylon nanofibers, coated with antibacterial silver nanoparticles, make an effective sterilizing air filter. Image credit: Cornell Centre for Materials Research.

Nanoformulations for dyes could greatly reduce the amount of coloring agent needed, reducing the amount of waste produced. Nanocoatings are capable of modifying fabric properties much more drastically whilst remaining flexible and transparent, opening up many applications for treated textiles which have been difficult to achieve previously [85]. The rapid growth of nanofiber technology in recent years can be attributed to the rediscovery of electrostatic spinning (or electrospinning) technology originally developed in the 1930s [86]. This technique has been used to produce high-performance filters [87], wearable electronics and scaffolds for tissue engineering [88] that utilize the high surface area unique to these fibers. A schematic drawing of the electrospinning process is shown in Figure 51 (a), where a high electric field is generated in a polymer fluid contained in a glass syringe with a capillary tip and a metallic collection screen. When the voltage reaches a critical value, the electric field overcomes the surface tension of the deformed drop of the suspended polymer solution formed on the tip of the syringe and a jet of ultra-fine fibers is produced. The electrically-charged jet undergoes a series of electrically-induced bending instabilities during its passage to the collection screen that results in the hyper-stretching of the jet. This stretching process is accompanied by the rapid evaporation of the solvent molecules, which reduces the diameter of the jet in a cone-shaped radius. The dry fibers are accumulated on the surface of the collection screen, resulting in a non-woven mesh of nanometer to micron-diameter fibers. The process can be adjusted to control fiber diameter by varying the electric field strength and polymer solution concentration, while the duration of electrospinning controls the thickness of the fiber deposition. Nanofibers in linear yarn or planar nonwoven mat form can be produced by proper control of the electrodes.

The enormous specific surface area of these nanofibrous assemblies may make them excellent candidates for gas collection layers in landfill cover systems. By controlling the porosity and proper selection of the polymer system, barrier membranes may be

produced having selective permeable characteristics similar to that used in chemical and biological protective barriers [89].

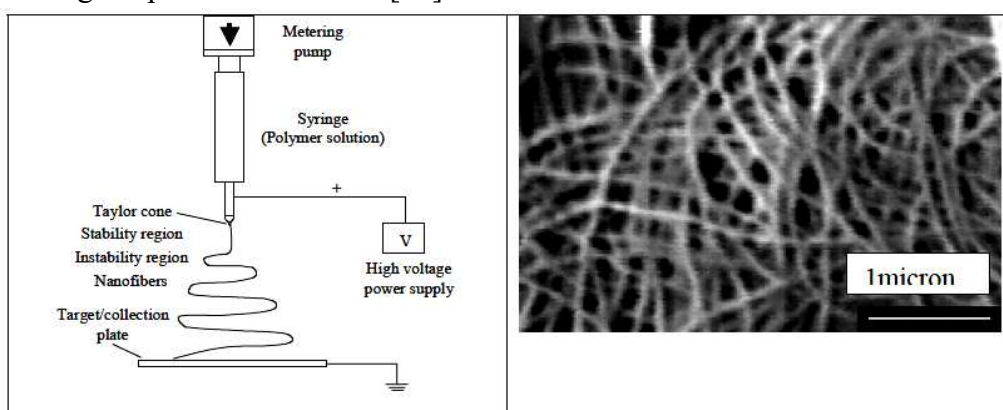


Fig. 51: (a) Schematic Drawing of the Electrospinning Process (b) Electrospun nanofiber membrane.

8. Sustainability and ecological aspects

Sustainability has been defined by Brundtland as, [90]: “development that meets the needs of the present without compromising the ability of future generations to meet their own needs”. This section deals with key parameters of sustainability with special focus on Carbon dioxide (CO_2) emissions. It provides scenarios where geotextiles can improve the sustainability credentials of an engineered solution.

Global need for sustainable development

Climate change challenges the very existence of our life on earth. There exists overwhelming scientific evidence that links increasing greenhouse gases (GHG) and CO_2 emissions with the changing climate [91]. Once CO_2 emission was established as a clear and present danger, United Nations Environment Program (UNEP) and World Meteorological Organization (WMO) formed the Intergovernmental Panel on Climate Change (IPCC) in 1988. The major goal of this consortium was to develop a scientific view on climate change and its potential impacts [92]. In 1992, an international treaty called the United Nations Framework Convention on Climate Change (UNFCCC) was formed [93]. The participating countries acknowledged the limited success in reducing emissions. Hence, legally binding emissions targets in the form of the Kyoto Protocol was established [94]. This protocol eventually came into effect in 2005.

Carbon foot printing

Carbon footprint can be defined as the total CO_2 emissions produced by an organization, activity, project, product, event or person. Carbon foot printing is the method utilized to measure such emissions and the level of impact they have on the environment. Embodied carbon and embodied energy are measures used to calculate carbon footprint. Embodied carbon (EC) of a material is the amount of CO_2 emissions released in the extraction, manufacture and transport of the material, and it is used interchangeably with the term embodied energy (EE) depending on the type of analysis undertaken. EE of a material is measured using appropriate energy meters and then converted to EC values using appropriate conversion factors for different

energy mixes (e.g. coal, nuclear or renewable) used in the manufacturing process [95]. The unit descriptor for EC obtained from EE is t CO₂e/t.

8.3 Geotextiles and Sustainable Development

With increasing adoption of geotextiles, it was imperative to study the environmental impact of its usage. Various studies have carried out in this regard and the case study by Raja et al is prominent [96]. In this study, embodied carbon data for two geotextile product ranges produced by two different manufacturers was calculated. The manufacturer producing needle-punched product and the other one producing thermal bonded geotextiles had used different manufacturing process. This study provided data for a range of products with varying masses. This allowed the overall energy consumption per kg of product produced to be calculated. The small difference in EC values (tab. 14) may be attributed to different manufacturing processes and fuel sources. In this research, the mean value for non-woven geotextiles was 2.35 tCO₂e/t. While broad conclusions as to thermally bonded material being more sustainable than a needle punched material cannot be implied, these results can be used to build a database of EC footprint of Geotextiles. Such a database will increase the accessibility, transparency, repeatability and rigor of sustainability assessment.

Environmental impacts of Geotextiles

The environment impact of Geotextiles, throughout their lifecycle, can be assessed using a technique called Life cycle analysis (LCA) [97]. During LCA, clearly defined boundary conditions in material production, manufacture and deployment are considered. The stages and system boundaries are given in fig. 52.

Table 14: Embodied Carbon values for geotextiles [96].

Geotextile Type	Polymer embodied carbon (tCO ₂ e/t)	Conversion of Granules to fibers (tCO ₂ e/t)	Manufacturing Carbon emissions (tCO ₂ e/t)	Total Embodied Carbon (tCO ₂ e/t)
Non-woven Needle punched	1.983	0.241	0.053	2.28
Non-woven Thermally Bonded/Needle Punched			0.189	2.42

A research by Waste and Resources Action Program (WRAP) [98] highlighted lower transportation emissions as a key advantage of geotextiles due to their comparatively low weight and volume compared to carrying soil or aggregate to site. Plastics are typically high EC materials [99], however, when used correctly and efficiently, a geotextile based solution can have significantly lower EC than alternative solutions. With increasing research on sustainability of Geotextiles, there are encouraging indicators that use of geotextiles can bring both cost and EC savings.

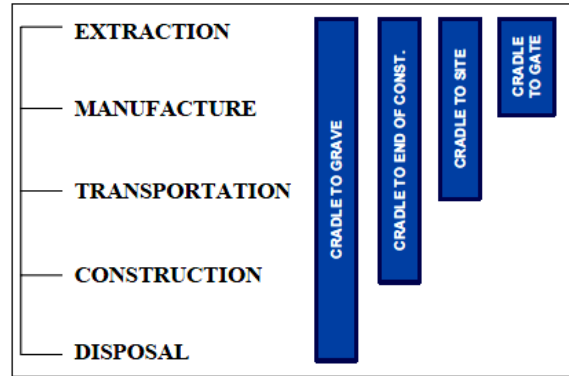


Fig. 52: Stages and system boundaries of LCA [97].

Conduct of rigorous LCA requires clear definition of boundaries which fit for purpose of intended comparison. Most commonly used LCA conditions are given in tab. 15.

Table 15: Common LCA conditions [97]

Boundary Conditions	Description
Cradle-gate	Includes all emissions in the extraction and manufacture of a product, including all transport related emissions associated with interim stages of manufacture (such as moving of polymer fibers and granules);
Cradle-site	Includes transportation of material to the site. This must include the cumulative emissions from all transportation types (e.g. road, rail, ship);
Cradle to end of construction	Includes all of the emissions associated with the manufacturing process. For geotextiles this may include items such as the preparation of the subgrade by rollers, excavators used to lift rolls of material, excavation and filling. Items such as provision of cabins and welfare facilities should also be considered as these have an associated embodied carbon for the construction phase.
Cradle-grave	Includes demolition and disposal emissions associated with the end of life of a structure.

9. Conclusion

Different types of geotextiles have been developed and applied. In general they are made from some natural (jute mainly) and synthetic fibers such as polypropylene (PP), polyester (PET), and polyethylene (PE), in either woven or nonwoven forms. A woven geotextile could be manufactured from monofilament, multifilament, and slit-film or fibrillated fibers. A nonwoven geotextile could be fabricated from either continuous filaments or staple fibers. Woven geotextiles have pore sizes within a relatively narrow range than nonwovens because of the limitations in the manufacturing process, including the number of warp and weft yarns used and types of weave. 3D corrugated ROTIS structures provide higher potential for several

applications. A large portion of the research work has been concentrated on testing and experimental characterization of structure and/or hydraulic behavior, including pore size and pore size distributions, permeability, and the soil transport process in geotextiles. Some of the frequently adopted approaches have been standardized, mainly by ASTM. Theoretical work is obviously less available than experimental studies. A comprehensive research in this area is needed to meet requirements of future.

References

1. Horrocks A. R, Ananad S. *Handbook of Technical Textiles*, 2nd ed. 2015.
2. Ko F. K.: *From Textile to Geotextiles*, Seminar in Honor of Professor Robert Koerner September 13 2004.
3. Hearle J.W.S.: *Textile for composites*, Textile Horizons, **11**, 11-15. (1994)
4. Mouritz A.P., et al.: *Review of applications for advanced three dimensional fiber textile composites*, Composites **A30**, 1445-1461 (1999).
5. Beyer S., et al.: *Advanced composite materials for current and future propulsion and industrial applications*, Advances in Science and Technology, **50**, 178-171 (2006)
6. Yamamoto T, Hirokawa T.: *Advanced joint of 3D composite materials for space structure*, 35th international SAMPE symposium, Anaheim, USA, 1990, pp. 1069–1077.
7. Donnet J.B., Bansal R. C.: *Carbon Fibers*, Marcel Dekker Inc., New York, 1990
8. Bilisik K.: *Dimensional Stability of Multiaxis 3D Woven Carbon Preform*, Journal of the Textile Institute, **101**(5), 380–388 (2010)
9. Atkinson K.R., Skourtis C., Hutton S. R.: *Properties and applications of dry-spun carbon nanotube yarns*, Advances in Science and Technology **60**, 11-20 (2008)
10. Kaswell E.R.: *Handbook of Industrial Textile*, New York, West Point Pepperell, 1963.
11. Haven G.B.: *Mechanical Fabrics*, New York, John Wiley & Sons, 1932, pp. 206-13.
12. Chou T.W.: *Microstructural Design of Fiber Composites*, Cambridge University Press 1992
13. Koerner R.M., Ko F.K.: *Laboratory Studies of Long Term Drainage Capability of Geotextiles*, Proceedings, Part I. Second International Congress on Geotextiles, Las Vegas, August 1982.
14. Koerner R.M. et al.: *Construction and Geotechnical Engineering Using Synthetic Fabrics*, John Wiley and Sons, New York, 1980.
15. Rankilor P.R.: *Membranes in Ground Engineering*, John Wiley and Sons, New York, 1981
16. Dierickx, W.: *The influence of Filter Materials and their Use as Wrapping Around Agricultural Drains*, C.R. Coll. Int. Sols Textiles, Paris, 1977, Vol.2,pp.225-229.
17. Hoffman G.L.,Malasheskie G.: *Laboratory Evaluation of Materials and Design Characteristics of PennDOT Underdrain System*, Transportation Res. Rec. 675, Natl. Acad. Sci., Washington, DC, 1978, pp.32-43.
18. Dow M.B., Dexter H. B., *Development of stitched, braided and woven composite structures in the ACT Program and at Langley Research Center (1985 to 1997)*. NASA/TP-97-206234. (1997).

19. Kamiya R., et al.: *Some recent advances in the fabrication and design of three dimensional textile preforms: A review*, Composite Science and Technology **60**, 33-47. (2000).
20. Cox B.N., Flanagan G.: *Handbook of analytical methods for textile composites*, NASA Contractor Report 4750. (1997).
21. Bhatnagar A., Parrish, E. S.: *Bidirectional and multiaxial fabric and fabric composites*, US Patent 7073538. (2006).
22. Dow N.F.: *Triaxial fabric*, US Patent 3446251 (1969).
23. Goldstein A.D.: *Textile material*, US Patent 2244835. (1939).
24. Kazumara M.: *Tetraxial fabric and weaving methods*, European Patent 0263392. (1988).
25. Mamiliano D.: *Tetraxial fabric and weaving machine for its manufacture*, US Patent 5351722. (1994).
26. Lida S., et al.: *Multiaxial fabric with triaxial and quartaxial portions*, US Patent 5472020. (1995).
27. Deemey S.: *The new generation of carpet weaving machines combines flexibility and productivity*, Technical notes, Van de Wiele Incorporations 2002.
28. Mohamed M.H., Bilisik A. K.: *Multilayered 3D Fabric and Method for Producing*, US Patent 5465760. (1995).
29. King R.W.: *Three dimensional fabric material*, US Patent 4038440. (1977).
30. Hanuš J., Jirsák O.: *Twist May Produce Nonwovens*, In: Textile Technology Forum '95. Charlotte, N.C. USA, 1995.
31. Krčma R., Hanuš J., Sanetník F.: Pat. EP 0 648 877 A1 (CZ 192 693). *Befestigungsverfahren für voluminöse Fasergebilde und Anlage zur Realisierung dieses Verfahrens*. Europäische Patentanmeldung. 19.04.95.
32. Hanuš J., Militký J., Aneja A. P.: *Local Compression of Corrugated Nonwoven Structures*, In: Ninth International Conference on Composites Engineering, San Diego, July 1-6, USA, 2002
33. Hanuš J., Militký J.: *Quasi-Yarn Applications in Nonwoven Production*, In: HPTEx Coimbatore. July 7 -9, India, 2004
34. Gibson P. W., Schreuder-Gibson H. L.: *Influence of Hydration State on Permeation Testing and Vapor Transport Properties of Protective Clothing Layers*, Journal of Engineered Fibers and Fabrics **4**, 11-20 (2009)
35. Bock N. et al.: *Electrospraying of polymers with therapeutic molecules: State of the art*, Progress in Polymer Science **37**, 1510 – 1551 (2012)
36. Havelka A., Kůs Z.: *The transport phenomena of semi-permeable membranes for sport clothing*, Int. Journal of Clothing Sci. and Tech., **23**, 119-130 (2011)
37. Lukáš D., et al.: *Physical principles of electrospinning (Electrospinning as a nano-scale technology of the twenty first century)*, Textile Progress **41**, 59-140 (2009)
38. Komárek M., Martinová L.: *Design and evaluation of melt-electrospinning electrodes*. Proc. 2nd Int. Conf Nanocon, Olomouc, October 2010
39. Yalcinkaya F., et al.: *Preparation of Antibacterial Nanofibre/Nanoparticle Covered Composite Yarns*, Journal of Nanomaterials, article ID 7565972, 7 pp. (2016)
40. Mishra R., Militký J., et al.: *The production, characterization and applications of nanoparticles in the textile industry*, Textile Progress **46**, 133-226 (2015)
41. Fukuta K., et al.: *Three dimensional fabric, and method and loom construction for the production thereof*, US Patent 3834424. (1974).

42. Crawford J.A.: *Recent developments in multidirectional weaving*, NASA Publication No. 2420, pp. 259-269 (1985).
43. Khokar N., *3D-Weaving: Theory and Practice*, Journal of the Textile Institute, **92**(2): 193-207 (2001).
44. Evans R.G.: *Air jet machine and diagonal Z loop fabric pattern for three dimensional fabrics*, US Patent 5924459. (1999).
45. Yasui Y., et al.: *Three dimensional fabric and method for making the same*, US Patent 5091246. (1992).
46. Edgson R.T.: *Fibre preforms for structural composite components*, US Patent 5783279. (1998).
47. Homma K.N., A.: *Reinforcing woven fabric and preformed material, fiber reinforced composite material and beam using it*, US Patent 5100713. (1992).
48. Abildskow D.: *Three dimensional woven fabric connector*, US Patent 5533693. (1996).
49. Jonas P.J.: *Method for fastening aircraft frame elements to sandwich skin panels covering same using woven fiber connectors*, US Patent 4671470. (1987).
50. Ruzand J.M.G.: *Multiaxial three-dimensional fabric and process for its manufacture*, International Patent WO 94/20658. (1994).
51. Mood G.I.: *Multiaxial yarn structure and weaving method*, US Patent No 5540260. (1996).
52. Bryn L., et al.: *Three-dimensional woven forms with integral bias fibers and bias weaving loom*, US Patent 6742547. (2004).
53. Nayfeh S.A., et al.: *Bias Weaving Machine*, US Patent No. 7077167. (2006).
54. Kimbara M. et al.: *Three dimensional multi-axis fabric composite materials and methods and apparatuses for making the same*, US Patent 5076330. (1991).
55. Anahara M., Yasui Y.: *Three dimensional fabric and method for producing the same*, US Patent 5137058. (1992).
56. Uchida H., et al.: *Three dimensional weaving machine*, US Patent 6003563. (1999).
57. Bilisik K.: *Multiaxis Three Dimensional (3D) Circular Woven Preforms-Radial Crossing Weaving and Radial In-Out Weaving: Preliminary investigation of and feasibility of weaving and methods*, Journal of the Textile Institute., **101**(11): 967-987 (2010)
58. Wilkens C.: *Warp knitted ware with reinforcing thread*, US Patent 4518640. (1985).
59. Naumann R., Wilkens C.: *Warp knitting machine*, US Patent 4703631. (1987).
60. Hutson H.K.: *Biased multilayer structural fabric composites stitched in a vertical direction*, US Patent 4550045. (1985).
61. Wunner R.: *Apparatus for laying transverse weft threads for a warp knitting machine*, US Patent 4872323. (1989).
62. Ko F.K., et al.: *Electrostatically Generated Nanofibers for Wearable Electronics*, in ed. Tao X.M Wearable Electronics,. Woodhead, 2004.
63. Ko F.K., et al.: *Handbook of Industrial Braiding*, Drexel University, 1989.
64. Somboosong W.: *Development of Ductile Hybrid Fiber Reinforced Polymer (DHFRRP) Reinforcement for Concrete Structures*, PhD Thesis, Drexel University 1977
65. Lam H.L.: *Composite Manufacturing with the Braidtrusion Process*, MS Thesis, Drexel University 2001

66. Hampton F.P.: *Cyclic Behavior, Development, and Characteristics of a Ductile Hybrid Fiber Reinforced Polymer (DHFRRP) Reinforced Concrete Members*, PhD Thesis, Drexel University 2004
67. Hampton F.P., et al.: *Low-Cycle Fatigue Strength Of A Ductile Hybrid Fiber Reinforced Polymer Bar For Earthquake Resistant Concrete Structures*, Proceedings, ICCM 14, San Diego, CA., Paper ID: 1295, July 14-18, 2004.
68. <http://www.azonano.com/article.aspx?ArticleID=3058>.
69. Ko F.K.: *Nanofiber Technology: Bridging the Gap between Nano and Macro World*, in NATO ASI on Nanoengineered Nanofibrous Materials, 2003, Anatalia, Turkey,
70. Formhals A.: US Patent # 1,975,504, 1934.
71. Doshi J. D., Reneker H.: *J. Electrospinning process and applications of electrospun fibers*, *Electrost.*, **35**, 151-160 1995
72. Gibson P.W., et al.: *Transport properties of porous membranes based on electrospun nanofibers*, *AIChE J.*, **45**, 190-195 (1999)
73. Ko F.K., et al.: *The Dynamics of cellfiber architecture interaction*, in: Proceedings, Annual Meeting, Biomaterials Research Society, San Diego, April 1998.
74. Ko F.K., et al.: *Electrospinning of Improved CB Protective Fibrous Materials* , Proceedings, Techtexil Atlanta, March 30-31, 2004
75. Bhardwaj N., Kundu S. C.: *Electrospinning: A fascinating fiber fabrication technique*, *Biotechnology Advances* **28**, 325–347 (2010)
76. Jaworek A.: *Electrospray droplet sources for thin film deposition*, *J. Mater. Sci.* **42**, 266–297 (2007)
77. Gibson P.W., et al. : *Electrospun fiber mats: transport properties*, *AIChE J.* **45**,190–195 (1999)
78. Gibson P.W., et al.: *Transport properties of porous membranes based on electrospun nanofibers*, *Colloids Surf. A Physicochem. Eng. Asp.*;**187**, 469–481 (2001)
79. Ramakrishna S., et al.: *Electrospun nanofibers: solving global issues*. *Mater. Today* **9**, 40–50 (2006)
80. Sun B., et al.: *Advances in three-dimensional nanofibrous macrostructures via electrospinning*, *Progress in Polymer Science* **39**, 862–890 (2014)
81. Hu J., et al.: *One-step Electro-spinning/netting Technique for Controllably Preparing Polyurethane Nano-fiber/net*, *Macromol. Rapid Commun.*, **32**, 1729–1734 (2011)
82. Ding B., et al.: *Formation of novel 2D polymer nanowebs via electrospinning*, *Nanotechnology*, **17**, 3685-3691 (2006)
83. Zhang C., et al.: *Electrospun Microfibrous Membranes Based on PIM-1/POSS with High Oil Wettability for Separation of Oil–Water Mixtures and Cleanup of Oil Soluble Contaminants*, *Ind. Eng. Chem. Res.*, **54**, 8772–8781 (2015)
84. Park H. B., et al.: *Polymers with Cavities Tuned for Fast Selective Transport of Small Molecules and Ions*, *Science* **318**, 254-258 (2007)
85. Geise G. M., et al.: *Water Purification by Membranes: The Role of Polymer Science*, *J. Polym. Sci. Part B: Polym. Phys* **48**, 1685- 1718 (2010)
86. Gugliuzza A., Ed.: *Smart Membranes and Sensors, Synthesis, Characterization, andApplications*, Scrivener Publishing, Danvers 2014
87. Obendorf S. K.,*Improving Personal Protection Through Novel Materials*, *AATCC Review*, July/August, 44-50 (2010)

88. Krokida M. K., Maroulis Z. B.: *Effect of drying method on shrinkage and porosity* *Drying Technol.* **15**, 2441–2458 (1997)
89. Datta A. K.: *Porous media approaches to studying simultaneous heat and mass transfer in food processes. I. Problem formulations.* *J. Food Eng.* **80**, 80–95(2007)
90. Brundtland G., *Our common future: The World Commission on Environment and Development*, Oxford University Press, Oxford, UK. 1987.
91. EPA., *Causes of Climate Change*, United States Environmental Protection Agency, See <http://www.epa.gov/climatechange/science/causes.html> [accessed on 06/02/2017].
92. IPCC I.-g.P., *on Climate Change Organization*, (2014) see <http://www.ipcc.ch/organization/organization.shtml> (accessed 05/02/2017).
93. United Nations: *United Nations Framework Convention on Climate Change*, S, Treaty Doc No. 102-38, 1771 U.N.T.S. 107.
94. European Union: *The EU Emissions Trading System*, (EU ETS).
95. TSO (The Stationary Office), *Climate Change Act 2008*: Elizabeth II, Chapter 27, 2008, London, TSO.
96. DEFRA: *Guidelines to Defra's GHG conversion factors for company reporting*, Department for Environment, Food and Rural Affairs, London, UK.
97. Raja J., et al.: *Sustainable Construction Solutions Using Geosynthetics: Obtaining Reliable Embodied Carbon Values*. Geosynthetics International (Accepted for publication). (2015).
98. EcoInvent Centre, EcoInvent data v2.2. Ecoinvent reports No. 1-25, Swiss Centre for Life Cycle Inventories, Duebendorf, Switzerland.
99. Menzies G.F., et al.: *Life-cycle assessment and embodied energy: A review*. *Proceedings of the ICE-Construction Materials*, **160**, 135-143. (2007).
100. Tashiro K., Kobayashi M.: *Theoretical evaluation of three-dimensional elastic constants of native and regenerated celluloses: role of hydrogen bonds*, *Polymer* **32**,1516–1526 (1991)
101. Muralisrinivasan N. S.: *Polymer Blends and Composites Chemistry and Technology*, John Wiley & Sons, Hoboken 2017
102. Hamad W. Y. : *Cellulose Nanocrystals*, John Wiley & Sons, Chichester 2017
103. Kalia S. Avérous L. Eds.: *Biodegradable and Biobased Polymers for Environmental and Biomedical Applications*, Scrivener Publishing, Beverly 2016
104. Rojas J. O. Ed.: *Cellulose Chemistry and Properties: Fibers, Nanocelluloses and Advanced Materials*, Springer Cham 2016
105. <http://micro.magnet.fsu.edu/cells/plants/cellwall.html>
106. Youssefian S., Rahbar N.,: *Molecular Origin of Strength and Stiffness in Bamboo Fibrils*, www.nature.com/ Scientific Reports, 1-12, June 2015
107. Yu, X., et al.: *Detailed Glycan Structural Characterization by Electronic Excitation Dissociation*, *Anal. Chem.* **85**, 10017-10021 (2013)
108. Céline A. et al.: *The hygroscopic behavior of plant fibers*, *Frontiers in chemistry* **1**, 1-12 (2014)
109. Monteiro S.N., et. al.: *Selection of high strength natural fibers*, *Revista Matéria*, **15**, 488 – 505 (2011)
110. Militký J., Kovačič V., Křemenáková D.: *Basalt Filaments – Properties and Applications*, chap 22 in Holeček M. et al. eds: *Some thermodynamic, structural and behavioral aspects of solids accentuating amorphous materials*, Publishing house of West Bohemian University in Pilsen 2009

111. Deak T., Czigany T.: *Chemical composition and mechanical properties of basalt and glass fibre a comparison*, Text. Res. J. **79**(7), 645-651 (2009).
112. Militký J., Kovacic V., Rubnerova J.: *Influence of thermal treatment on tensile failure of basalt*, Eng. Fract. Mech. **69**,1025-1033 (2002).
113. Lal R., Shukla M.K.: *Principles of soil physics*, Marcel Dekker, New York 2004
114. Shukla M.K.: *Soil physics an introduction*, CRC Press, Boca Raton 2014
115. Tumer A. R., et al.: *Effects of different types of soil on decomposition: An experimental study*, Legal Medicine **15**, 149–156 (2013)
116. Snakin V.V., et al.: *Soil Liquid Phase Composition*, Elsevier, Amsterdam 2001
117. Shukla S.K: *Fundamentals of Fibre-Reinforced Soil Engineering*, Springer Nature, Singapore 2017
118. Park Ch. H., et al. : *Biodegradability of Cellulose Fabrics*, Journal of Applied Polymer Science, **94**, 248–253 (2004)
119. *on of Natural Textile Materials in Soil*, Tekstilec, **57**, 118–132 (2014)
120. Cornell J. H. et al.: *Biodegradability of Photooxidized Polyalkylenes*, Journal of Applied Polymer Science, Vol. 29, 2581-2597 (1984)
121. Scott G.: *Polymers and the environment*, Royal Society of Chemistry, Cambridge 1999
122. Sykers G., Skinner F. A. eds: *Microbial aspects of pollution*, Academic Press, London 1971
123. Yoon M.G., et al.: *Biodegradation of Polyethylene by a Soil Bacterium and AlkB Cloned Recombinant Cell.*, J Bioremed. Biodegrad., **3**,145-153 (2012)
124. Longo C., et al.: *Degradation Study of Polypropylene (PP) and Bioriented Polypropylene (BOPP) in the Environment*, Materials Research, **14**(4), 442-448 (2011)
125. Goldthwait Ch. F.,et al.: *Chemical Substitution in Fibrous Cotton and Resistance of Substituted Cotton to Microbiological Deterioration*, Tex. Res. J., **21**, 831-840 (1951)
126. Lazic' V., et al.: *Negative influence of Ag and TiO2 nanoparticles on biodegradation of cotton fabrics*, Cellulose, **22**,1365–1378 (2015)
127. Azam A., et al.: *Hydrophobic treatment of natural fibers and their composites -A review*, Journal of Industrial Textiles, 1-31, First Published June 14, 2016
128. Kan Ch. W.: *A Novel Green Treatment for Textiles-Plasma Treatment as a Sustainable Technology*, CRC Press, Boca Raton 2015
129. Jamshaid H., Mishra R., Militký J.: *Thermal and mechanical characterization of novel basalt woven hybrid structures*, J. Text. Inst. **107**, (4), 462–471 (2016)
130. Militký J., et al.: *Prediction of glass leno fabrics porosity and strength*, Proc 19th Annual International Conference on Composites and Nano Engineering ICCE, Shanghai July 24-30, 2011
131. Dvořák, J., Karel, P.: *Webmaschine mit litzenlosen System*, Meliand Textilberichte, **No. 3**, 118-119 (2007)
132. Jamshaid H., et al.: *Investigation of electrical properties of basalt and its hybrid structures*, Text. Res. J., **87**(6) 715–725 (2017)
133. Baheti V., Militký J.: *Nanoindentation Measurements of Jute/Poly Lactic Acid Composites*, chap in book Fangueiro R., Rana S. eds: *Natural Fibres: Advances in Science and Technology Towards Industrial Applications*, Springer Nature, Dordrecht 2016

134. Anandjiwala R. D.: *The Role of Geotextiles in Geosynthetic Applications*, GhIGS GeoAfrica Conference Accra, Ghana 18 – 20 November 2013
135. Neckář, B.: *Yarn. Creation, structure and properties*. SNTL Praha 1990 (in Czech).
136. Křemenáková D.: *Modeling of cotton yarn geometry and strength*, Report of Research Center Textile, Faculty of Textile Engineering, TU Liberec, 2004 (in Czech).
137. Militký J., et al.: *Air Permeability and Light Transmission of Weaves*, International Journal of Clothing Science and Technology, **11** (2/3), 116-124 (1999)
138. Berlin A. A., et al.: *Engineering Textiles Research Methodologies, Concepts, and Modern Applications*, chap 1, Apple Academic Press, Inc. Oakville, Canada 2016
139. Kellie G., ed.: *Advances in Technical Nonwovens*, Elsevier Ltd. , Amsterdam 2016
140. Koerner R. M., ed.: *Geotextiles from Design to Applications*, Elsevier Ltd., Amsterdam 2016
141. Provis J. L., van Deventer J. S. J., eds.: *Geopolymers Structure, processing, properties and industrial applications*, CRC Press, Boca Raton 2009
142. Koerner R.M.: *Designing with Geosynthetics*, Prentice Hall, New Jersey, 5th ed. 2005
143. Giroud J.P.: *Development of criteria for geotextile and granular filter*, In: Proceedings of the 9th International Conference on Geosynthetics, Guarujá, Brazil. 2010. p. 4564.
144. Eddleston M.: *In search of the perfect geotextile/geocomposite filter for retro-fitting old embankment dams*, in book Hewlett E., ed.: Improvements in reservoir construction, operation and maintenance, Thomas Telford, London 2006

Natural dyes usage in textile industry in Czech Republic and Turkey: comparative analysis.

Hana Křížová

*Faculty of Textile Engineering, Dept. of Material Engineering,
Technical University of Liberec, Czech Republic*

1. INTRODUCTION

Parts of plants (leaves, flowers, fruits, roots, bark) as well as animal products (molluscs, insects) and some minerals have been used as natural sources of colour for thousands of years. Colour has always been a magical element depending on the presence of light for a man's mind. Therefore, before the man began to cover his body with skin and textile, he began to decorate his body with natural dyes. What was the purpose of this colouration, and how much it played the role of magic, religion, mysticism or simple vanity, or the desire to please, can only be guessed based on the studies of today's indigenous native peoples. With the development of clothing, this natural desire in beauty of man has grown, and so man has soon begun to use these dyes on the skin and fabric to which he has dressed. Modern age and industrial revolution have brought many discoveries, including synthetic dyes, which create a reliable and easy repetition of colouring results. The first discoveries and syntheses of synthetic dyes date to the middle of the 19th century. The rapid development of dyeing chemistry and dyeing technology dates from 1856 to 1900. With the industrial and technical revolution of the 19th century, more expensive and rare natural dyes worldwide have been replaced by artificial dyes. Nowadays, most fabrics and fibres in the world are dyed with synthetic dyes. In contrast to natural dyes, they have many advantages - besides a huge range of shades, colour brilliance, repeatability and much lower price thanks to their industrial production, they are also "tailor-made" for textile fibres. This means that they are much more bound to them, and this is reflected in their wet and dry fastnesses. In 1836, the Russian chemist N. N. Zinin produced aniline by the reduction of nitrobenzene. This was a prerequisite to produce one large group of dyes - aniline dyes. In 1856 W. H. Perkin prepared the first aniline dye, purple. Followed by the synthesis of methylviolet (1861), methylene blue (1876), malachite green (1877) and others. The discovery of diazotisation (Griess, 1858) and azo coupling (Kekulé, Hidegh, 1870) was an assumption for the production of another significant group of colourants - azo dyes. Highly stable azo dyes were prepared by diazotization of aniline and coupling with phenols.

After the discovery of synthetic alizarin in the 19th century, collapse occurred in the cultivation and production of madder. The fact that the research of synthetic dyestuffs was significant is proved, for example, by the fact that in 1905 the German chemist Adolf von Baeyer received the Nobel Prize for the preparation of synthetic indigo and other discoveries in organic chemistry. The boom of synthetic dyes has hit

the entire industrial world, and natural dyes have begun to be the past in the industrial world.

Despite the many advantages of synthetic dyes, however, natural dyes have been maintained in many countries of the world as the main source of fabric dyeing or at least as a good competitor of industrial synthetic dyes. What is the reason that some countries, such as the Czech Republic, have turned away from natural sources of dyes in their textile industry, and others such as Turkey, on the contrary, successfully develop and prosper this thousand-year tradition? What are the prospects for the future and how can a return to natural colouring be encouraged where this tradition is forgotten? We will try to answer these questions in the following chapters dealing with the use of natural dyes in the textile industry in the Czech Republic and Turkey, which are two countries with a significantly different approach to this topic.

2. NATURAL DYES IN CZECH TEXTILE INDUSTRY

2.1 From the past to today

In the Czech Republic the natural dyes were used for textile dyeing exclusively until the middle of the 18th century. Textile dyers specialized there: so-called black-dyers dyed black and brown, the beauty-dyers dyed textiles for yellow, red and green, and since the blue colour was always exceptional in natural sources and very desirable on textile, the blue-dyers and blue-printers have been specializing in blue colour since the Middle Age. [1] The blue-printers first dyed using so-called reserve printing and various plants. The most used was the European woad (*Isatis tinctoria*), later replaced by Indian indigo. It is proved that many dye plants have been growing in the Czech Republic since the 13th century (woad, saffron). However, since the second half of the 19th century the synthetic dyes were increasingly applied, which in turn gradually pushed out the use of the natural ones. Fields of dyeing plants that throughout the Middle Ages and even into the 17th and 18th centuries belonged to the normal rural hometowns (fields of woad, madder or reseda) [1,2,3] have been disposed of and the chemical industry began to produce their synthetic substitutes instead. At the beginning of the 21st century, only a fraction of the fabric was dyed with natural dyes. There is no specialized company in the Czech Republic to deal directly with the use of natural dyes, so there are no cultivating dye plants there. But, for example, courses for dyeing with natural dyes are organized, and recently several books have been published on this topic. Today even the oldest living people in this country have never experienced the common use of natural resources for textile dyeing. There is no one in this society who could orally pass its colouring experience. It's not just a technical matter (recipes and equipment). This can be restored and deduced from historical written records, it is also possible to learn and inspire in countries that are currently dyeing textiles with natural dyes (such as India or Turkey). Finally, even at Czech universities or botanical institutes there are sporadically people who study, restore or improve traditional dyeing recipes from a scientific point of view [2, 4] or at least from a layman's view of enthusiastic promoters of traditional hand crafts. [5, 6] However, personal communication, experience, personal impressions, and a sense of connection with the folk dyeing tradition that no longer has anyone else in this

country, are important. This value and an important part of the cultural heritage are, it seems, irretrievably lost. Nevertheless, there are minor exceptions, such as colour fragments of the original mosaic... Still active manufactory of blueprints in Olešnice na Moravě (eastern part of the Czech Republic), where this hand-made technique of dyeing by indigo with use of kaolin and arabic rubber as reserve is provided by the 10th generation of family business. It is a real national rarity. The manufactory was founded in 1849 and originally, they used the natural indigo. Still today the wooden historical printing forms are used there (**Fig.1**), the oldest comes from 1819. Fine filigree floral landscape motifs decorate mainly textile products homewares (**Fig.2**, **Fig.3**).



Fig. 1: Wooden printing form (Czech Museum of Textile Printing in Česká Lípa)



Fig. 2: Blueprint from Olešnice manufactory (Moravia)



Fig. 3: Blueprint from Strážnice manufactory (Moravia)

Another Moravian family manufactory in Strážnice has been operating in Moravia since 1906. Today, these two manufactories use exclusively the synthetic indigo but this hand-made production in the Czech Republic is a great rarity reminding of the colouring history of the Moravian people. Despite the market that is overwhelmed by industrial textile production, these hand-made blueprints are of great interest because they symbolize the tradition and landscape colour. [7]

2.2 Natural dye sources in Czech Republic

Each culture uses primarily natural resources on its territory, so the plants used for textile dyeing on the Czech territory include not only traditional dye plants (largely those with the Latin adjective “*tinctoria*”, **Tab.1**), but also a number of other plants that have a certain colouring potential, but are not considered to be the correct dyeing material (Annexe 1), such as nettles, horsetail, marigold, rose, chamomile, shepherd's purse, etc. The textiles, however, were mostly dyed to shades of green, brown and gray, although the use of mordans intensified these shades. Many of the dye plants that were cultivated on the territory of the Czech lands are not the original species. They mostly came from warmer areas (for example, the Mediterranean) and got into the wild, so they can occasionally be found in the nature. Madder is a typical example.

Table 1: “Thru” dye plants occurring on the Czech territory

Latin name	Common name	Provided colours	Native or Introduced (N/I)
<i>Rubia tinctorum</i>	madder	red	I
<i>Reseda luteola</i>	weld	yellow	I
<i>Carthamus tinctorius</i>	safflower	yellow, red	I
<i>Polygonum tinctorium</i>	Chinese (Japanese) indigo	blue	I
<i>Asperula tinctoria</i>	dyer's woodruff	red	N
<i>Isatis tinctoria</i>	woad	blue	N
<i>Genista tinctoria</i>	dyer's broom	yellow	N
<i>Anthemis tinctorial</i> (<i>Cota tinctoria</i>)	golden marguerite	yellow, buff, orange	N

Common **madder** (*Rubia tinctorum* L., **Fig.4**) produces anthraquinone pigments in its roots, one of them is alizarin (1,2 dihydroxy anthraquinone) which has been used for dyeing textiles since 2000 B.C. It comes from the Mediterranean area but in the past, it was cultivated in the Czech lands and in several places, it came to the wild. Similarly, in the neighboring Slovakia where it was collected, for example, by the famous Dutch botanist Carolus Clusius (1526-1609) [8].

Weld (*Reseda luteola*) also comes from the Mediterranean region. Nowadays it can be found in nature in the southern regions of the Czech Republic.

Safflower (*Carthamus tinctorius*) is an old dye plant that can not be said with certainty when it has actually spread to Central Europe. The ancient Egyptians used it

for dyeing. Again, it is not the original species, but has come to Europe probably from Kazakh steppes.

The other non-native species, indigodary plant *Polygonum tinctorium*, called Chinese or Japanese indigo, comes from East Asia.

Dyer's woodruff (*Asperula tinctoria*) is, on the contrary, one of the original Central European dye plants, like **golden marguerite** (*Anthemis tinctoria*) and **dyer's broom** (*Genista tinctoria*).

3. NATURAL DYES IN TURKEY TEXTILE INDUSTRY

3.1 From the past to today

Natural dyeing has been carried out as an ancestral art at high level for hundreds of years in Turkey. The colour range of the plants used in dyeing is quite large and mordants used in dyeing also widen the colour range further. Traditional Turkish rugs and carpets are famous all over the world. Since these art products have long been dyed with natural dyes, carpets are an important reason why natural dyeing in Turkey is so preferred. Natural dyeing has been maintained at a high level since the time of the Ottoman Empire and even from this area, as well as some dye plants, this knowledge spread to other countries. However, in the 19th and 20th centuries, thanks to lower prices, synthetic dyes eventually penetrated the Turkish market, where it began, as in other parts of the world, to push out the natural ones. The quality of the first (especially aniline) dyes was not too high, so their use led to the loss of bright hues and early fading. Turkish rugs and carpets were mostly woven from sheep wool, which can be dyed (in addition to completely unsuitable aniline dyes) with acidic and metallic complex dyes. Metallic complex dyes have very good fastness, but they are mostly dyes with somewhat faded tones, typical of the shades of brown, dark green, gray. Such colours, of course, could not compete with the bright shades of some good natural dyes. No wonder this trend tended to hurt the traditional craft industry. Fortunately, Turkey understood in time that hand-made production of naturally dyed carpets is a good business for the country. It is understandable that customers who are looking for original traditional Turkish rugs also prefer traditional methods of their production and dyeing and do not want to buy synthetic substitutes. The use of natural dyes has begun to increase by encouraging government with various scientific projects [9], such as the DOBAG project. [10] DOBAG is the Turkish acronym for Natural Dye Research and Development Project that was launched in Turkey with German assistance in cooperation with Marmara University, Istanbul in 1981. This project represents a big success in reviving the lost art of producing naturally dyed carpets. The certification system has even been developed within this project where the University of Marmara is ensuring the quality of each natural dyed carpet having the DOBAG tag. [11] It is well known that authentically and from the quality point of view fibers dyed by natural dyes are more valuable and that buyers pay higher prices.

3.2 Natural dye sources in Turkey

Republic of Turkey lies at the nexus of Europe, the Middle East, Central Asia and Africa. Turkey is surrounded by three seas. Turkey's land area is covered by three

biogeographic regions with significant levels of biodiversity (Caucasus, Irano-Anatolian, and Mediterranean). Since today, 123 plants were identified as sources of natural dyes in the Turkish regions where carpet and rug weaving are still common. About a quarter of them are cultivated, the rest is mostly native to Turkey. The amount of shades that come out of 10 basic colours is supported by the use of about two dozens of mordants having natural (for example, cupula of oak, juice of unripe grape, vinegar, seville orange juice, ox urine, rock algae, lime, wood ash, mud with animal urine) or chemical origin (especially metal salts as potassium aluminium, copper or iron sulphate, tin chloride, and also potassium bitartrate, potassium dichromate, etc.). [12] Probably the most famous Turkish natural dye is alizarine obtained from madder (*Rubia tinctorum*). In conjunction with alum, it provides the brilliant red colour known worldwide as "Turkish Red". Today in Turkey, traditional known dye-producing plants are still cultivated, besides the madder mentioned above, it is henna (*Lawsonia inermis*), common whet (*Triticum sativum*), morus, curcuma, safflower and eucalyptus and another lesser known dye plants (Annexe 2).

4. COMPARATIVE ANALYSIS

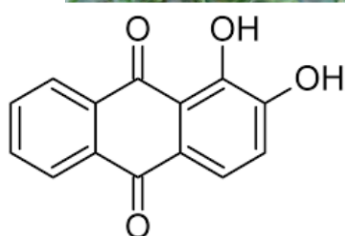
4.1 Comparison of the number of plant species

The Czech flora currently contains about 3557 species, 194 other subspecies and 609 known hybrids. There are 1454 non-native species, of which 350 are among the archeophytes (introduced from the beginning of the Neolithic to the Middle Ages) and 1104 are neophytes (introduced in modern times, after 1492). In the context of global warming, but also due to the globalization and facilitated migration of plant species, their numbers have steadily grown over the last 200 years. Less than 68 % of non-native species are classified as casual, 28 % are naturalized, or domesticated, and only 4 % are invasive. [13] If we deduce from the total number of plant species occurring on the territory of the Czech Republic non-native species, approximately 2350 to 2550 indigenous species and subspecies of higher plants can be found here. [14] [15]. It is difficult to determine what percentage of these were used in the past for natural dyeing because detailed mapping of plants used as natural dye sources in Czech lands (Bohemia and Moravia) was not carried out. Currently available overviews of Czech Dyeing Literature cite only the most well-known plant species that can be used for dyeing, which is about 50 [5] or possibly listed as 135 [6]. As regards the colour shades that can be created by plants occurring in Czech nature and in combination with various mordants, (although their use is highly controversial and mostly non-ecological [16]), shades of green, yellow and brown colours significantly predominate. The blue colour is rare: the source of true blue colour (not purple, as provided mainly by plants and fruits containing anthocyanins) in local conditions is represented only by the woad (*Isatis tinctoria*) and by the imported Chinese indigo (*Polygonum tinctorium*). *Polygonum* was imported into England in 1776 to replace *Isatis*, but its yields were not as good as expected in European conditions [5]. If we look for a red colour, its best source here represents the non-original madder. From the native species, the roots of dyer's woodruff (*Asperula tinctorial*, **Fig.5**) or the various species of bedstraw (*Galium* genus, **Fig.6**), which grow in the Czech Republic

in 26 species, can be used as substitutes for madder. *Asperula* and *Galium* contain ruberythric acid in the roots (alizarin 2-O- β -primveroside) which is the primveroside of rubiadin and can be split into red alizarin [17]), however, the yield of alizarin from these subtle plants is much lower compared to the madder and the resulting shade is even using different mordants rather pink than red. Asia Minor is the meeting point of the Euro-Siberian, Mediterranean and Irano-Turanian floras. With over 9000 plant species, Turkey is one of the richest countries of Europe and the Middle East, of which about a third [18, 19] (elsewhere is a fifth [20]) are endemic species. The number of plant species in Turkey is therefore more than double compared to the Czech Republic. In both countries, according to the literature, a similarly low percentage of plants (1-2 %) is used for dyeing. However, the comparison lags a bit when we aware that many Czech plants are mostly of a lesser quality colour sources, although some often-shady shades can be obtained by use of mordants. On the other hand, Turkish plant sources of dyestuffs documented in workshops and crafts are in fact predominantly the top dyeing sources selected and proven by long-term practice. So, the fact that only a tiny fraction (about 1.4 %) of such many plant species is used in Turkey for dyeing, (123 plants identified by [12]) is not surprising.

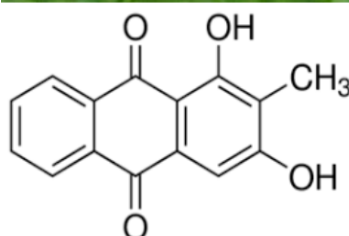
The graph in **Fig.7** shows the frequency of colours that can be made from local available plants and common mordants on textiles in the Czech Republic and Turkey. Their comparison comes from 2 available sources [12, 5] that contain the most accessible and comprehensive list of local dye plants. If we look at the spectrum of colours that can be obtained from Turkish plants, the yellow, green and brown shades predominate here, similarly to Czech plants. [12] However, the three basic colours (red, yellow and blue) are also present in this spectrum in sufficient quantity and quality (yellow from 84, red from 7 and blue from 3 plant species: *Isatis tinctoria*, *Euphorbia tinctoria* and *Rheum ribes* L.). According to the principle of the subtraction mixing of colour pigments, many other shades can be easily created. The subtractive colour model explains the blending of a limited set of dyes or pigments to create a wider range of colours. Each of them is the result of partially or completely subtracting (absorbing) some wavelengths of light. The colour that a surface displays depends on which parts of the visible spectrum are not absorbed and therefore remain visible.

However, in the colour triangle for subtractive colour synthesis (**Fig.8**), it depends very much on the saturation of all three basic pigments at the vertices of the triangle. If all three are the same saturation, they ideally meet in the middle of the triangle in the black colour. This triangle of "strong" primary colours (yellow, red, blue) can be formed for example by safflor, madder and indigo. From these strong, high-quality colours, a rich and bright palette of other shades can be created by blending. In the original Central European nature, however, such strong colours are not, as has been described above. There we can find sources for strong pink rather than red, strong violet rather than blue, and relatively strongly are represented brown and orange. In fact, the Central European nature has its palette closer to subtractive mixing in the triangle of secondary colours (orange, purple, green), the mixing of which creates rather "dirty" and cloudy shades, such as brown, gray, impure green, etc.



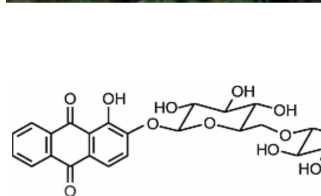
alizarin

Fig. 4: Madder
(*Rubia tinctorum*)



rubiadin

Fig. 5: Dyer's woodruff
(*Asperula tinctoria*)



ruberythric acid

Fig. 6: Lady's bedstraw
(*Galium verum*)

Sources of red colour

4.2 Comparison of the yield of some natural dyes

Some small farms in the Czech Republic are attempting an additional activity to promote traditional crafts, including dyeing of textiles (batikking, printing) using natural dyes. However, they use dyes imported from abroad (indigo, annato, turmeric, henna), a relatively high quality and proven dyestuff obtained mainly from tropical or subtropical plants, which provide good and deep hues for textile dyeing and which plants occur at such high concentrations that their production is worthwhile. For example, tropical **indigo** derived from *Indigofera tinctoria* (**Fig.9**) contains approximately $42 \pm 11\%$ of the total indican within the cells [22], while the European woad (*Isatis tinctorial*, **Fig.10**) has an incredibly low yield of indigo, only 2-5 % of indican (!) (indigo precursor). [23, 24] This means in practice that about one ton of leaves need to be processed to obtain 2 kg of indigo dye. Fortunately, woad is such a tough and vigorous plant that its cultivation is not difficult. One acre of soil produces about 10,000 tons of this plant per year at a double harvest. [25]

Even though woad leaves have a nasty taste, it is also necessary to protect them from omnivorous slugs. They have been imported into Central Europe from Spain and are doing so well here that in some places they pose a serious problem and cause great agricultural losses. Although, due to the increasing pollution of the environment by pesticides, the number of butterflies decreases overall in Czech nature, however, cabbage white butterfly (*Pieris brassicae*), which specializes in cruciferous plants, is

still very widespread due to the cultivation of monocultures. *Isatis* is a cruciferous plant and in the Central European climate it is necessary to protect it from the caterpillars of this otherwise cute white butterfly. However, this plant grows so lushly and quickly that it has been included among the so-called energy plants providing fast biomass usable for combustion. [26] Due to its lush growth, *Isatis* has become difficult weeds in parts of the world, where they are not destroyed by the pest (for example, in the USA).

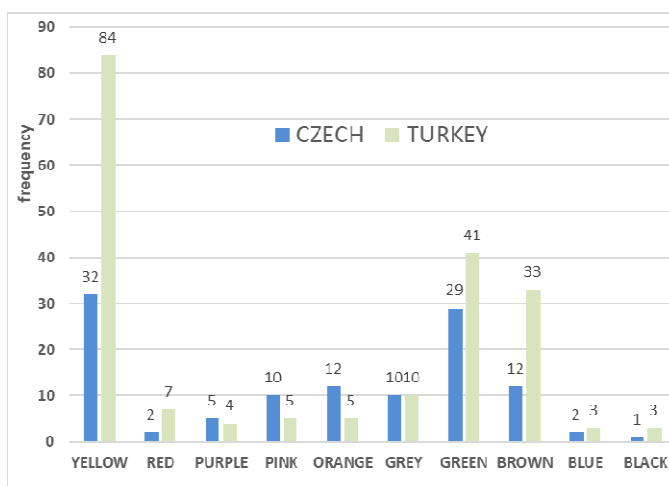


Fig. 7: The colours obtained from dye plants and their distributions: Czech and Turkey, according to [12,5]

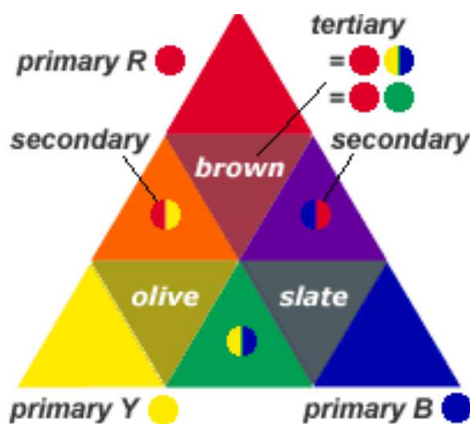
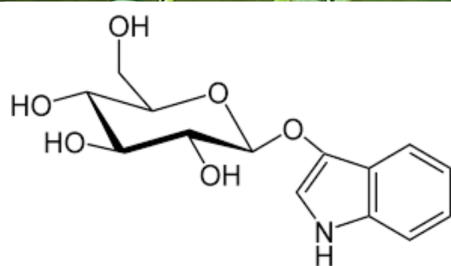
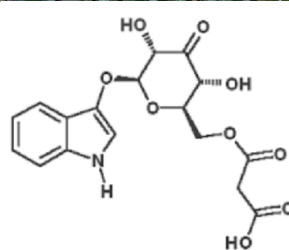


Fig. 8: Triangle of primary and secondary colour synthesis [21]

Mediterranean weld (*Reseda luteola*, **Fig.11**) and European dyer's broom (*Genista tinctoria*, **Fig.12**), both contain the yellow luteolin. However, when comparing the content of these substances and the pigment yield of both plants, luteolin is contained in a lower amount in *Genista tinctoria*. Using HPLC, luteolin in the *Genista tinctoria* plant from the Romanian area was detected in an amount corresponding to the concentration 47.7 ± 4.8 mg/1 kg of dried plant [27]. In the Mediterranean *Reseda luteola* was similarly extracted and HPLC-quantified 8.6 ± 0.2 g of luteolin/1 kg of dried weld material [28].



indican



isatan A

Fig. 9: True indigo (*Indigofera tinctoria*)

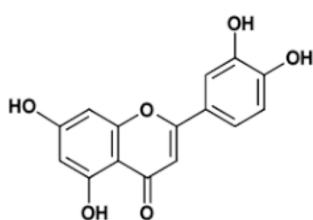
Fig. 10: Woad (*Isatis tinctoria*)

Sources of blue colour

We can also compare some plant sources of red colour, for example Central European dyer's woodruff (*Asperula tinctoria*) and Mediterranean madder (*Rubia tinctorum* L.). Both are plants from the family *Rubiaceae* and both contain high quality red anthraquinone dyes. Dyer's woodruff is a native of northern and Central Europe from France to Russia. Thermophilic madder comes from Asia Minor to Central Asia. Some 36 anthraquinones have been detected in *R. tinctorum* by various scientists [24, 29], such as alizarin, purpurin, xanthopurpurin, rubiadin, munjistin, lucidin, pseudo-purpurin, etc. Alizarin (CI Natural Red 8) is the most significant and the most famous anthraquinone contained in madder's roots. Dyer's woodruff contains mainly its methylated variant rubiadin (CI Natural Red 13) [30].

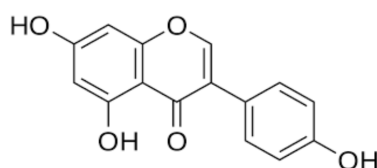
Madder may contain more than 900 mg of alizarin per plant, depending on the age of the plant, cultivar, and growth conditions [31]. Depending on the extraction agent used, alizarin was obtained from madder roots in amount of $0.18 \text{ g} \pm 0.03$ (ether, acetone), $1.06 \text{ g} \pm 0.08$ (water) until $1.5 \text{ g} \pm 0.2/\text{kg}$ of dry plant matter. [32] Concerning the content of dyes, madder is much more productive than its European relative [33]. Perhaps only Central European walnuts can compete with their (sub)tropical counterparts due to their high content of hydroxy-naftoquinones. Red-orange, brown-red or brown-orange hydroxy-naphthoquinone dye is contained in tropical henna and the chemically very similar compound is contained in leaves and hulls of walnuts. **Henna** is a dye present in the leaves of the tropical henna plant (*Lawsonia inermis*). This dye is called lawsone (**Fig.13**) and its chemical structure is similar to walnuts juglone (**Fig.14**) growing in the north temperate zone. The content

of lawsone in *L. inermis* leaves by TLC-densitometry was found to be 0.76 ± 0.05 g/100 g of dried crude drug [34]. The content of juglone in walnut hulls (there is the highest content) according to the cultivar, was in quantity from 0.45 to 1.6 g/100 g of dried hulls. [35]



luteolin

Fig. 11: Weld (*Reseda luteola*)



genistein

Fig. 12: Dyer's broom (*Genista tinctoria*)

Sources of yellow colour

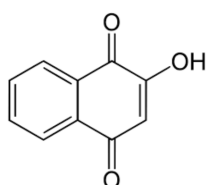


Fig. 13: Lawsone from henna

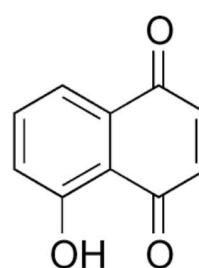


Fig. 14: Juglone from walnut

The large variability in the amount of juglone contained in leaves of walnuts appears even in other studies. It is obvious that the content of the juglone is very dependent not only on the cultivar, but also on the vegetation conditions, which are changing during the year in the moderate zone of Central Europe. For example, [36] reports the content of juglone in walnut leaves in a content of 71 mg in May, with a maximum of

approximately 900 mg in the middle of July and then drop back to 528 mg/100 g of dried leaves in August.

4.3 Comparison of historical and economic development

The Serfdom Patent from Emperor Jopseph II in 1781 was a breakthrough in the development of society in the Czech lands, then part of the Austro-Hungarian Empire. The Serfdom Patent to abolish the rural population's dependence on nobility and to enable the migration of the population that has begun to move to cities and to offer its labor force in the emerging industry. The textile industry was the first to develop massively there. The first textile factories were created in the Czech lands since the 90s of 17th century. The local natural conditions allow the production of flax and sheep breeding so that the main textile raw material were flax fibres and sheep wool at the beginning of textile production. They were used from the production of fine and coarse woven linen canvas and wool broadcloth. Since the end of the 18th century, many manufactories and factories have been created to produce a fine cotton printed fabric (**Fig.15**), the so-called cattun-factories.



Fig. 15: Old printed floral motif (Czech Museum of Textile Printing in Česká Lípa)



Fig. 16: Traditional hand-made production of Turkish carpets and rugs

Since the Industrial Revolution in the first half of the 19th century, the Czech Republic has been primarily an industrialized country. Since the 19th century, there have been textile companies and other traditional Czech industrial fields were rapidly developing: glass, ceramics, machinery, food (breweries, sugar factories), chemical industry, paper industry, and energy and transport infrastructure. These traditional Czech industrial branches form the basis of a strong Czech economy until today, except for the textile industry, which has suffered a significant decline in the past 25 years. At the moment, the Czech Republic is the 16th most developed economy in the European Union, the lowest unemployment rate and the lowest poverty rate in the

whole of Europe. Czech exports focus mainly on the automotive industry and the so-called high-tech industries [37], such as the pharmaceutical industry, medical technology, optical instruments, production of nanofibres, etc. For example, between 1999 and 2007, the Czech Republic underwent significant structural changes in exports. the share of technology-intensive commodities (such as office machines, telecommunication equipment) has increased significantly, while the share of labor-intensive products (textiles and clothing products) has declined significantly [38]. Above all, due to globalization and economic liberalization in developing countries, there is an influx of cheap textile goods from Southeast Asia, which the Czech textile industry was unable to compete with. The same problem is faced, for example, by the traditional Czech glass industry. Most traditional Czech textile companies ceased to exist. Although paradoxically, in the last decades, the population's interest in sheep farming is increasing. The problem, however, is that the sheep's wool is not even processed there or purchased at all, and this raw material is practically unused. Today, only rare companies in the Czech Republic are engaged in textile dyeing. The textile industry is competitive, for example, in the area of technical textiles, due a relatively strong collaboration with applied research. In the apparel industry, a stronger position is held by few companies focused on the sale of high fashion and stylish collections, where they are able to reach relatively high profit margins. [38]. Turkey has always traditionally been a heavily agricultural-oriented country. Throughout the 20th century, Turkey has transformed from an agricultural economy into an industry based one. Currently, Turkey has the 17th most powerful world economy. [39] Even in the 1970s, agricultural production accounted for more than a third of GDP. In the 1990s, 48.7% of the working-age population was engaged in agriculture, still in the year 2000 it was 41.5%, but on the current trend it is projected to be only 28.2% in 2025. [40] The outflow of workers from agriculture to the sphere of industry and services is the most significant among women. In 1993 the total amount of arable land was about 27.6 million hectares (35 % of the land of Turkey). [18] Turkey is not only food self-sufficient, but exports part of agricultural production (2.7 % of the total volume of exported goods in 2016). In 2016 Turkey exported cars, machinery and equipment to the world (22.6 % of exports), iron, steel, and products made from them (7.8 % of exports), metals and other mineral resources (8.5 % of exports). Clothing and woven carpets (**Fig.16**) accounted for 6.2% of the total volume of Turkey's exports. [39]

5. CONCLUSION

In this comparative study focused to comparison of plant natural resources use for textile dyeing in the Czech Republic and Turkey, we tried to find a response to a research question as to the likely causes of both countries' differing approaches to natural dyes. Both countries have been dependent on natural dyes for many centuries. In both countries, in the context of the development of industry and chemistry, cheaper and more readily applicable synthetic textile dyes have been launched since the second half of the 19th century. The industrially oriented Czech Republic has readily accepted the emergence of synthetic dyes and the development of chemistry in

the 19th and 20th centuries. The initial period of synthetic dyes is also associated with the rapid development of the textile industry in the Czech lands. The so-called cattun-factories where the fine cotton or linen fabric was printed, were developed. It is not easy to dye cellulose fibres (cotton, flax) and you practically do not find plants in Czech nature that would do it well. In the Czech lands, *Gossypium* (cotton) can not be grown, the silkworms do not grow very well there; the suitable conditions for the breeding of large herds of sheep are more in agricultural Moravia. So, the Czech Republic was, from the outset, dependent on imports of these primary fibre raw materials. From this point of view, synthetic dyes represented a huge positive potential for the development of the Czech textile industry.

Turkey, in particular as a rural and agricultural country, has focused on the use of internal biological resources, including cotton, wool and silk production, which are also basic raw materials for the production of world-famous Turkish carpets and rugs. Traditional Turkish handicraft is also its successful export item. While the textile industry in Turkey is booming due to the return to old practices, the Czech Republic is now struggling with an uncontrolled flow of cheap textiles from Southeast Asia, leading to the practical extinction of the Czech clothing and textile industry. The only area where the Czech Republic strives to build on its once strong textile production is the specialized production of technical textiles, non-woven textiles and nanofibres. Traditional production of Turkish carpets was a neural point in the use of synthetic dyes: worse durability and unsatisfactory shades reduced the quality of these products, resulting in a decline in interest in this article. Fortunately, Turkey has become aware of its mistakes and, with the support of experts from all over the world and the support of the Turkish government, has achieved the renewal of traditional practices, including the use of the highest quality and proven plant colour sources. The quality of natural dye sources is one of the other likely reasons for such a different approach for both countries. Most of the high-quality dye plants come from the subtropical zone in which Turkey is located. In a warmer and wetter climate, of course, a larger number of plant species succeeds than in the colder Central European temperate zone. Greater biodiversity of natural resources also implies the presence of a greater number of high-quality dye plants and similar to that of the dyeing substances contained in them. Comparison of indigo content in the European *Isatis* and thermophilic *Indigofera* is a very good example of how different growth and climatic conditions can affect the content of active substances in plants. Colour pallets resulting from the blending of primary and secondary colours in the colour subtractive triangles representing the symbolic natural resources of Turkey and the Czech Republic indicate the issue with which the Central European culture must face in the event of a return to natural dyeing. Native plant sources offer, with the use of problematic mordants, mostly low-yields, dull and faint shades. The few truly quality natural colour sources such as safflor, indigo, madder, annatto, curcuma or cochineal are non-originating and imported resources. Some of them can not be grown under normal temperate conditions. Their role would necessarily have to play the import of good dyes and pigments from countries that are their successful producers. Today, large number of chemicals is used in the production of textiles. The usage of chemicals starts from the

cultivation of natural fibres where different pesticides are used, as well as production of man-made fibres consist of many chemical and mechanical processes. The basic source of raw materials for the production of synthetic dyes are petroleum and coal tar obtained from coke, ammonia and dry distillation of charcoal. By contrast, natural dyes are obtained from renewable sources. From this point of view, the toxic pollution of the environment, especially of the waste water, when dyed with artificial dyes appears to be significantly higher than in the case of natural dyes. Environmental considerations are now becoming vital factors during the selection of consumer goods including textiles all over the world. Due to increased awareness of the polluting nature of textiles effluents, social pressure is increasing on textile processing. The public is becoming increasingly aware of the health and environmental problems associated with the use of artificial dyes, which are consumed around a million tons a year worldwide. Interest in natural dyes has been increasing recently in countries like the Czech Republic, which have used almost exclusively synthetic dyes for textile dyeing for more than a century. Obviously, the growing demand for naturally dyed fabrics will in the future require at least a partial return to this production. Due to the broken tradition and the relatively small market compared to Turkey (the population in the Czech Republic is about 10 million, Turkey has more than 80 million inhabitants) it is not possible to expect that natural dyes will fundamentally affect the main trends of the textile industry and the economy in Czech Republic. However, a balanced approach should be applied to offer customers the choice and alternative products dyed with high-quality, although partly imported dyes. This opens the opportunity for closer cooperation of Czech Republic with countries such as Turkey, India or Thailand, who can share their knowledge and experience with natural colouring, and from which the interested Czech people can learn a lot about traditional crafts. Turkey, which has always represented not only a geographical but also a cultural bridge between Europe and Asia, is the first choice for this partnership.

Annexe 1: An overview of some Central European dye herbs and shrubs – English and Latin names, parts of plants applicable to dyeing and colours obtained using alum as mordant.

European privet (*Ligustrum vulgare*)

fruits (pink), bark (yellow), leaves (green)



Buckthorn (*Rhamnus cathartica*)
fruits (green)

Saint John's wort (*Hypericum perforatum*)

inflorescence, whole plant (beige)



Alkanet (*Anchusa officinalis*)
roots (pink-brown)



Field gromwell (*Lithospermum arvense*)
roots (red)



Tansy (*Tanacetum vulgare*)
inflorescence (yellow-orange)



Annexe 2: An overview of some Mediterranean dye herbs and shrubs – English and Latin names, parts of plants applicable to dyeing and colours obtained using different mordants

Turpentine tree (*Pistacia terebinthus*)
leaves (yellow, grey, green)



Myrtle (*Myrtus communis*)
leaves (yellow)



Tobacco (*Nicotiana tabacum*)
leaves (green, brown)

(*Daphne gnidioides*)
above ground (yellow, green)



Cotton (*Gossypium hirsutum*)
leaves (yellow)



Cypress (*Cupressus sempervirens*)
cone (pink, brown)



Annexe 3: Some recipes for wool dyeing with plants

Plant	Mordanting	Dyeing	Resulting colour	Source
St. John's wort (<i>Hypericum perforatum</i>)	40 g of alum and 12 g of tartar/2 litres of water, bring to boil and then remove the wool and rinse in cold water	200 flowers/1 litre of water, cook, filter, insert the wool for 20 minutes	green	[5]
		see previous procedure, but keep the wool in the bath for more than 12 hours	yellow	
	without mordanting	see previous procedure, but keep the wool in the bath for 1-2 hours	red-brown	

Plant	Mordanting	Dyeing	Resulting colour	Source
Dandelion (<i>Taraxacum officinale</i>)	0.5 – 2 g of tin chloride/1 litre of water, bring to boil, leave an hour in the cooling bath, remove and rinse in cold water, squeeze	200 g of flowers/1 litre of water, dyeing bath ratio 1:100 (1 g of wool, 100 ml of dyeing bath), 15 minutes of boiling, left the wool in the bath for 24 hours, then remove and wash	brilliant yellow	[4]
Marigold (<i>Calendula officinalis</i>)	20% alum, bath ratio 1:40, bring to boil, leave an hour in the cooling bath, remove and rinse in cold water, squeeze	pH of dye bath adjusted to 5 with formic acid, 10 kg of flowers of marigold/1 litre of water, dyeing at 85 °C for 1 hour	yellow-green	[41]
	the same procedure, then place in 5% ammonia solution for 10 minutes at room temperature, remove and rinse in cold water, squeeze		red-brown	
Eggplant (<i>Solanum melongena</i>)	15% alum, bath ratio 1:50, 1 hour of boiling with wool, remove and rinse in cold water, squeeze	eggplant skin powder poured into water (0.1 w/w) for 24 hours, then pH of dye bath adjusted to 5 with acetic acid, dyeing at 85 °C for 1 hour, bath ratio 1:50	ochre	[42]
	15% tin chloride, other steps as above		orange-brown	
	15% ferric sulphate, other steps as above		brown	
Mint (<i>Mentha spicata</i> L.)	iron (II) sulphate 2-10%, approximately one hour at 90 °C	dyeing at 90 °C for approximately one hour	grey to black	[43]
Thyme (<i>Thymus vulgaris</i>)				
Lichen (different species, for exemple genus <i>Cladonia</i> , <i>Pseudevernia</i> , <i>Hypogymnia</i> , <i>Xanthoparmelia</i>)	15-30% alum, approximately one hour at 80 °C	1. place the wool, lichen and 3% ammonia solution into the jar, close well, ferment in the dark and cool for 10 weeks 2. place the wool, lichen and water into the jar, close well, cook every day for 20 minutes, repeat for 7 days, then remove, wash and dry in the shade	dirty yellow to red-brown	[44]

Plant	Mordanting	Dyeing	Resulting colour	Source
Madder (<i>Rubia tinctorum</i>)	2.5 g of alum, 0.4 litre of water, 10 g of wool, heat to 90 °C for 1 hour and then let it cool, then squeeze and dry or directly put in dye bath	20 g of powdered roots from madder/1 litre of water, macerate for 12 hours, filter, add 20 g of premordanted wool, dyeing at 80 °C for two hours, then remove, wash and dry in the shade	dark red	[45]
Woad (<i>Isatis tinctoria</i>)		1. preparation of dyeing bath: 5-15 g finely chopped leaves of <i>Isatis</i> / 1 litre of of boiling water, cover, and let leach at 70-90 °C for 10 minutes max., filter, immediately cool this extract to about 40 °C, then alkalize using NaOH to pH 10-12 (2 g of NaOH/litre) until the blue grains of indigo appear in the bath 2. vatting (reduction of indigo): 5 g of sodium dithionite/1 litre of dyeing extract with indigo grains, 20 minutes, 45 °C 3. dyeing of wool: add wool (liquor ratio 1:50), dye for 30 minutes at max. 55-60 °C, let cool for 30 minutes 4. oxidation of indigo: wash in cold water, the green colour turns to blue during the washing or in the air	blue	[46]
Pomegranate (<i>Punica granatum</i>)	15% alum bath, boil at simmering point (90-92 °C) for 30 minutes, rinse the mordanted wool with water	1. preparation of dyeing bath: powdered raw material (30 %) soak in water for 12 hours, boil at simmering point (90 °C) for 0.5-1 hour, filter	yellow-green	[47]
	5% copper sulphate mordanting bath, procedure as above	2. dyeing: add mordanted wool and dye at 90 °C for 0.5-1 hour, then wash and dry	olive green	
	4% ferrous sulphate mordanting bath, procedure as above		green-brown	

References

- [1] JANOTKA, M., LINHART, K.: Zapomenutá řemesla: Vyprávění o lidech a věcech. Praha: Nakladatelství Svoboda, 1984. 192 p.
- [2] KONVALINA, P., Barviva: nepotravinářské využití v průmyslové výrobě. Jihočeská univerzita v Českých Budějovicích, 2006.
- [3] UHŘÍČKOVÁ, A., MALÍKOVÁ, Z.: Kouzlo zapomenutého. Brno: Rezekvítek, 2001. 57 p.
- [4] KRÍŽOVÁ, H., WIENER, J.: Dyeing of woollen fabric pre-treated with tin chloride using yellow blossoms. *International Education and Research Journal*, 2.9., 2016.
- [5] BIDLOVÁ, V.: Barvení pomocí rostlin. Grada Publishing, spol. sro, 2005.
- [6] TICHÝ, L., TICHÁ, I.: Barvy z rostlin. Brno: Rezekvítek, 1998.
- [7] <http://www.ireceptar.cz/rucni-prace/modrotisk-starobyla-technika-barveni-latek/>
- [8] LUMNITZER, S.: Flora Posoniensis exhibens plantas circa Posonium sponte crescentes secundum systema sexuale Linneanum. Crusius, 1791, p. 62.
- [9] CUKUL, D.: The Ottoman Clothing Heritage: The Contribution of Turkish Designers and the Natural Dye Research & Development Laboratory (DATU). *International Journal of the Arts in Society*, 2012, 6.3.
- [10] SCHMIDTKUNZ, R.: Using Lost Knowledge to Found Cooperatives. In: *Knowledge Loves Company*. Palgrave Macmillan UK, 2009. p. 215-238.
- [11] SAXENA, S., RAJA, A. S. M.: Natural dyes: sources, chemistry, application and sustainability issues. In: *Roadmap to sustainable textiles and clothing*. Springer Singapore, 2014. p. 37-80.
- [12] DOĞAN, Y., et al.: Plants used as natural dye sources in Turkey. *Economic Botany*, 2003, 57.4: 442-453.
- [13] PYŠEK, P. et al.: 2012: Plant invasions in the Czech Republic: current state, introduction dynamics, invasive species and invaded habitats. *Preslia* 84: 576-630.
- [14] DANIHELKA, J., et al.: Checklist of vascular plants of the Czech Republic. *Preslia*, 2012, 84.3: 647-811.
- [15] HOSKOVEC, L.: Veškeré druhy rostlin České republiky, 2008. Online: <http://botany.cz/cs/kvetena-ceske-republiky/>
- [16] KRÍŽOVÁ, H.: Natural dyes: their past, present, future and sustainability. *Recent Developments in Fibrous Material Science*, Křemenáková, D.(ed.), Militký, J.(ed.), Mishra, R.(ed.), Ops Kanina, 2015, 59-71.
- [17] STEGLICH, W.; FUGMANN, B.; FUGMANN, S. L.: *Römpp Encyclopedia of Natural Products*, edn. 2001.
- [18] TAN, A.: Turkey; Country report to the FAO international technical conference on plant genetic resource. Leipzig, Germany, 1996, 46.
- [19] KORFALI, D. K., USTUBICI, A., DE CLERCK, H.: Turkey country and research areas report. 2010.
- [20] DAVIS, P. H., et al.: *Flora of Turkey*. Edinburgh University Press, 1965.
- [21] <http://www.handprint.com>
- [22] WU, E., KOMOLPIS, K., WANG, H. Y.: Chemical extraction of indigo from *Indigofera tinctoria* while attaining biological integrity. *Biotechnology techniques*, 1999, 13.8: 567-569.
- [23] KRÍŽOVÁ, H.: Verification of the possibility of dyeing with extract of woad. Bachelor thesis, FT TUL, 2009.
- [24] SCHWEPPE, H.: *Handbuch der Naturfarbstoffe. Vorkommen. Verwendung. Nachweis*. Ecomed Verlagsgesellschaft, 1993.
- [25] <http://www.woad.org.uk/index.html>

- [26] PETŘÍKOVÁ, V.: Produkce energetických rostlin v pánevních oblastech, VÚRV, Praha, 1996.
- [27] TERO-VESCAN, A., et al.: Determination of some isoflavonoids and flavonoids from *Genista tinctoria* L. by HPLC-UV. *Farmacia*, 2009, 57.1: 120-127.
- [28] CERRATO, A., DE SANTIS, D., MORESI, M.: Production of luteolin extracts from *Reseda luteola* and assessment of their dyeing properties. *Journal of the Science of Food and Agriculture*, 2002, 82.10: 1189-1199.
- [29] DERKSEN, Goverdina CH, et al.: High-performance liquid chromatographic method for the analysis of anthraquinone glycosides and aglycones in madder root (*Rubia tinctorum* L.). *Journal of Chromatography A*, 1998, 816.2: 277-281.
- [30] BECHTOLD, T., MUSSAK, R. (ed.). *Handbook of natural colorants*. John Wiley & Sons, 2009.
- [31] ANGELINI, L. G., et al.: *Rubia tinctorum* a source of natural dyes: agronomic evaluation, quantitative analysis of alizarin and industrial assays. *Industrial crops and products*, 1997, 6.3: 303-311.
- [32] DE SANTIS, D.; MORESI, M.: Production of alizarin extracts from *Rubia tinctorum* and assessment of their dyeing properties. *Industrial Crops and Products*, 2007, 26.2: 151-162.
- [33] BAILEY, L. H., BAILEY, E. Z.: *Hortus Third* i–xiv, 1–1290. 1976.
- [34] CHAROENSUP, R., et al.: Pharmacognostic specifications and lawsone content of *Lawsonia inermis* leaves. *Pharmacognosy research*, 2017, 9.1: 60.
- [35] LEE, K.-C.: Nature and occurrence of juglone in *Juglans nigra* L. 1967.
- [36] SOLAR, A., et al.: Seasonal variations of selected flavonoids, phenolic acids and quinones in annual shoots of common walnut (*Juglans regia* L.). *Plant Science*, 2006, 170.3: 453-461.
- [37] ROJÍČEK, M.: *Strukturální analýza české ekonomiky*. Pracovní sešity CES VŠEM, 2006.
- [38] ROJÍČEK, M., et al.: Konkurenceschopnost obchodu ČR v procesu globalizace [Competitiveness of the Trade of the Czech Republic in the Process of Globalisation]. *Politická ekonomie*, 2010, 2010.2: 147-165.
- [39] Souhrnná teritoriální informace Turecko, 2017. Online: [http://publiccontent.sinpro.cz/PublicFiles/2017/06/06/Nahled%20STI%20\(PDF\)%20Turecko%20-%20Souhrnna%20teritorialni%20informace%20-%202017.140845516](http://publiccontent.sinpro.cz/PublicFiles/2017/06/06/Nahled%20STI%20(PDF)%20Turecko%20-%20Souhrnna%20teritorialni%20informace%20-%202017.140845516).
- [40] AKKOK, F., WATTS, A. G.: *Country report on Turkey*. Public Policies and Career Development, 2003.
- [41] MONTAZER, M.; PARVINZADEH, M.: Dyeing of wool with marigold and its properties. *Fibers and Polymers*, 2007, 8.2: 181-185.
- [42] PARVINZADEH, M.; KIUMARSI, A.: Using eggplant skin as a source of fruit waste colorant for dyeing wool fibers. *Progress in Color, Colorants and Coatings*, 2008, 1: 37-43.
- [43] TUTAK, M., GÜLCAN, A. C. A. R., AKMAN, O.: Natural Dyeing of Wool Fiber Using Mint (*Mentha Spicata* L.) and Thyme (*Thymus Vulgaris* L.). 2014 (Volume: 21), 2014, 93.
- [44] HAZIN, Ş. E. N., et al.: Natural dyeing works on some lichens species distributed in Ayvacık (Çanakkale) and İvrindi (Balıkesir/Turkey). 2008.
- [45] DE SANTIS, D., MORESI, M.: Production of alizarin extracts from *Rubia tinctorum* and assessment of their dyeing properties. *Industrial Crops and Products*, 2007, 26.2: 151-162.

[46] KŘÍŽOVÁ, H.: Verification of the possibility of dyeing with extract of woad. Bachelor thesis, Faculty of Textile Engineering. Technical University of Liberec, Czech Rep. (2009)

[47] KHAN, M. A., et al.: Extraction of natural dyes from myrobalan, gallnut and pomegranate, and their application on wool. *Colourage*, 2005, 52.12: 53-60.

Analysis of the weavability problem during production of basalt hybrid fabrics

Hafsa Jamshaid, Rajesh Mishra, Jiri Militky

Department of material Engineering ,Technical university of Liberec, Czeck Republic

Department of Knitting,National Textile University, Faisalabad, Pakistan

1. Introduction:

Woven structure is defined by orthogonal interlacement of at least two sets of yarns called warp and weft. The yarns which run horizontally or lengthwise are termed the warp, and the vertical yarns are referred to as the weft. The pattern in which the warp and weft yarns are interlaced is termed the weave.

The style of interlocking of the yarns determines the surface smoothness and formability of a fabric. The most common weave forms are plain, matt, twill and satin. Plain weaves have each warp yarn passing alternately under and over each weft yarn, in matt weave two or more yarns are passing alternately under and over groups of two or more weft, while twill weaves have two or more warp yarns alternately woven over and under two or more weft yarns in a regular repeated manner. Satin weaves are twill weaves modified to produce fewer intersections of warp and weft. The harness number indicates the number of yarns crossed and passed over or under, before the yarn repeats the pattern. Woven fabrics can also be classified depending upon the tightness and looseness of the interlacing yarns. In a closed-packing weave, the fabric is woven tightly, providing almost no gap between adjacent yarns, while in the case of open packing weaves, there are gaps between adjacent yarns, resulting in a loose weave. Woven fabrics are anisotropic, flexible, and with distinct viscoelastic properties. Hence, their mechanical characteristics depend upon complicated combinations of fiber bundles, yarn spacing's, stacking sequences, yarn sizes, fiber orientations, fiber architecture, and fiber volume fractions. Due to interlacing of fiber bundles, woven fabrics offer extra-high resistance to damage growth and exceptionally high values of the strain at failure in tension, compression, and impact loadings [1-4]. They also possess good dimensional stability in the warp and weft directions, which results in a higher out-of-plane strength.

Composites are need of present time. Our modern day technologies require materials bearing unusual combination of properties which cannot be present in conventional materials such as metal, ceramics and polymeric materials. It is especially evident with materials in use for construction applications. Composites are emerging as realistic alternatives to the metal alloys in many applications like construction, automobiles, marine, aerospace applications, sports goods, etc. Composites used UD (uni-directional/dimensional), woven, knitted prepreg etc.

To mitigate the handling and forming difficulties associated with UD (uni-directional/dimensional) prepreg, reinforcing fibers are bunched together into warp and weft yarns or tows which are woven into a fabric. Woven fabric composites

particularly offer better dimensional stability when they are exposed to a large range of temperatures. Woven fabric is one of the most widely used materials in structural applications [40]. Woven structures formulate an important part of technical textiles and their applications. Weave structure helps in providing better and balanced properties in plane of fabric area where as interlacement of yarns provide out of plane strength which results in take up of secondary load due to load path eccentricities, load buckling, tolerance and better impact resistance in comparison with unidirectional laminated composites [5-8]. Considering that the woven fabric reinforced composite materials are not entirely homogeneous, large resin rich areas are formed by the interlacing of undulating warp and fill yarns. In the high performance fiber-polymer matrix system, the difference of damping is much larger than that of the stiffness. Large resin rich areas act as the built-in damper elements. Their distribution, depending on the architectures of the weave, determines the damping of the composite structure.

The fiber/textile is an important constituent in Fiber/textile Reinforced composites. FRCs find applications in construction industries, decking, window and door frames, sports equipment such as bicycle frames, baseball bats, exercise equipment and so on. They are also suited for many automotive applications. The textile composites are composed of two materials i.e., a textile skeleton for reinforcement (called perform) and a binding adhesive (called matrix) material to keep the skeleton integrated into a specific shape. The output and the scope of application for reinforced fibers within polymeric composites have been gradually expanding all over the world. In comparison with conventional materials, fiber composites boast a number of advantages: corrosion resistance, chemical inertness, low factor of heat conductivity, high specific mechanical properties, small specific weight, high operating temperature, long wearing life, low cost of design installation. Fiber/textile reinforcements in composite material are generally used to improve the mechanical properties.

Materials selection has always involved a number of compromises for the engineering designer. Of course, the material's properties are extremely important, since the performance of the structure or component to be designed relies in the properties of the material used in its construction. However, properties come at a cost, and the engineer must balance cost factors in making a materials selection. The fiber generally occupies 30% - 70% of the matrix volume in the composites. The fibers can be chopped, woven, stitched, and braided. The most common fiber reinforcement in resin is glass fiber. There are other types of fibers for reinforcement such as carbon fiber, other plastic fibers.

Depending on the source, fibers are largely divided into two categories: natural and synthetic. A lot of work has been done by many researchers on composites containing natural and synthetic fibers. But both these fibers have advantages and drawbacks. As Fiber-reinforced polymer composites are widely applied in modern industry and many researches have been carried out to develop environmental fiber materials for the last decade. As a result, basalt fiber has taken notice of researchers as a new reinforcing fiber material [9-15]. Basalt fiber is extruded from melted basalt rock that consists mainly of Si and Al oxides. The tensile strength of single basalt fiber can be as high as

carbon and also it has excellent thermal and chemical stability. Since its manufacturing process is simpler compared to that of glass fiber, basalt consumes less energy, and reduces environmental waste such as carbon dioxide through the manufacturing process

At present a lot of research is conducted on its use for various technical applications [15-1]. As Basalt is new type of fiber so there is limited information available regarding its weave ability. The purpose of this work is to study compatibility of basalt with other fibers in terms of weavability. The fibers in consideration are both thermoset and thermoplastic i.e Polyester (PET), Polypropylene(PP) and Jute(J) . Three types of weave structures were selected for the study i.e. plain, twill and matt weave. The structures produced were both hybrid and non-hybrid. During the sample production in weaving, behavior of each group was studied. For each combination of fibers monitoring, time study, breakages, efficiency and final settings were observed and noted. A special arrangement, during running of any combination of fibers was noted separately for future reference. Every weave and combination of fibers was allocated with separate time and special attention was given till the completion of each sample. All the record was maintained along with the working efficiency to keep up to date working of respective combinations. Later on thread spacing and crimp are estimated by using geometrical model.

2. Material and Methods:

The polyester and jute yarns used in our study were available commercially. Polypropylene yarn was taken from company Synthetic (Pakistan). The basalt yarn was used as received from company Kamenny Vek (KV) (Russia). Materials used are Basalt, Polypropylene, polyester and Jute yarn.

The weaving trials were first undertaken on CCI sample loom before weavability on commercial Picanol rapier loom so as to identify the efficiency of using basalt with other thermoplastic and thermoset yarns. Total of 27 samples are produced. approx. 12 threads/cm in warp and 8 threads/cm in weft are maintained in all fabric constructions. The results of weavability efficiency was analyzed with the help of MINITAB[®] statistical software package (MINITAB, State College, PA; <http://www.minitab.com/en-US/default.aspx>). The results were evaluated statistically according to two-way variance analysis (ANOVA), and the factors were the 'fibre type' and 'weave pattern'. The mean values were compared with each other according to the Student-Newman-Keuls (SNK) Test by using a statistical package program separately for every test. $P < 0.05$ was regarded as statistically significant. The Minitab statistical package was used to execute the statistical analysis. All test results were statistically assessed at significance level, p -value, $0.05 \leq p\text{-value} \leq 0.01$. If the p -value is smaller than or equals 0.05, the effect of weave structure and fiber type are considered to be significant. Number of yarns per unit distance, was measured according to ASTM D 3775-03.15. Measurements were taken at five randomly selected areas. All the fabric samples were tested for their ends and picks per centimeter value using pick counting glass. Fabric cover % was calculated using the following expression;

$$\text{Fabric cover \%} = [d_1 n_1 + d_2 n_2 - d_1 d_2 n_1 n_2] \times 100 \quad (1)$$

Where, d_1 and d_2 are the warp and weft yarn diameter (cm), respectively, and n_1 and n_2 are ends per centimeter and picks per centimeter values, respectively. Estimation of thread spacing and crimp by using geometrical models. The relationship between thread spacing in warp and weft direction is estimated by using geometrical models for plain, twill and matt weave. The weave factors as shown in table 2 are considered. It is a number that accounts for the number of interlacements of warp and weft in a given repeat [6].

Table 1: Fabric structure developed

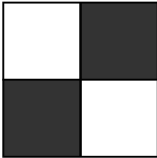

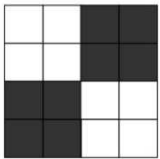
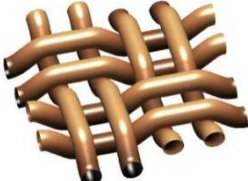
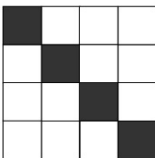
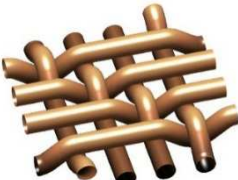
Sr #	Textile weave	Complete repeat	Schematic diagram
1.	Plain weave (PW)		
2.	2/2 Matt weave (MW)		
3.	1/3 Twill weave (TW)		

Table 2: Weave factors for various weaves

Weave	No. of warps/ repeat	No. of warp interlacements	No. of wefts/ repeat	No. of weft interlacements	Warp weave factor	Weft weave factor
1/1 Plain	2	2	2	2	1	1
1/3 Twill	4	2	4	2	2	2
2/2 Matt	4	2	4	2	2	2

A simplified algorithm is used to solve fabric geometrical model equations and relationships between useful fabric parameters such as thread spacing and crimp. Such relationships help in guiding the direction for moderating fabric parameters. Soft computing was used to provide a platform to manoeuvre crimp in warp and weft over a wide range with only three fabric parameters; yarn tex, modular length of warp and modular length of weft yarn. Soft computing has enabled solutions by interaction of crimp interchange and crimp balance equations. This exercise offers several solutions for fabric engineering by varying the above three parameters.

3. Results & Discussions:

3.1 Production of hybrid and non-hybrid fabrics

Basalt is a relatively new material for the weaving industry. There is no established setting available to run such a yarn. In the case with some of the other materials like cotton, polyester or blends of both for instance runs extensively across the industry. The advantage of extensively used fibers are that, there is always a reference of settings available from where one can start the initial running and then fine tuning can be done, which was not the case with basalt. Basalt is a relatively stronger yarn as compared to others used in this work, and thus it was difficult to handle weft insertion. Once initial settings for basalt were optimized, it was successful in running compared to all the other yarns. The details are shown in Table 3.


Table 3: Weavability efficiency of all hybrid and non-hybrid combinations

Sl. No.	Weave	Machine speed (rpm)	Warp breakage per hour)	Weft breakage per hour	Running time (h)	Efficiency (%)
1.	B/B1/1 plain	300	17	18	3	68
2.	B/B 2/2 matt	300	15	16	3	70
3.	B/B1/3 twill	300	14	15	3	73
4.	B/PP1/1 plain	300	17	19	3	66
5.	B/PP 2/2 matt	300	15	17	3	69.5
6.	B/PP 1/3 twill	300	15	16	3	70
7.	B/PET 1/1 plain	275	16	20	3	64
8.	B/PET 2/2 matt	275	15	17	3	69
9.	B/PET 1/3 twill	275	15	17	3	69
10.	B/Jute 1/1 plain	275	17	25	3	56
11.	B/Jute 2/2 matt	275	16	23	3	58
12.	B/Jute 1/3 twill	275	16	22	3	61
13.	PP/PP 1/1 plain	300	18	20	3	62
14.	PP/PP 2/2 matt	300	16	18	3	69
15.	PP/PP 1/3 twill	300	15	16	3	71
16.	PP/B 1/1 plain	300	18	19	3	65
17.	PP/B 2/2 matt	300	16	17	3	69
18.	PP/B 1/3 twill	300	15	15	3	71
19.	PET/PET 1/1 plain	250	3	18	20	60
20.	PET/PET 2/2 matt	250	3	17	17	67
21.	PET/PET 1/3 twill	250	3	16	17	67
22.	PET/B 1/1 plain	250	3	18	19	65
23.	PET/B 2/2 matt	250	3	16	17	69
24.	PET/B 1/3 twill	250	3	15	15	71
25.	Jute/Jute 1/1 plain	150	3	26	32	38
26.	Jute/Jute 2/2 matt	150	3	24	30	40
27.	Jute/Jute 1/3 twill	150	3	25	30	40

3.11 Weavability of basalt warp with basalt weft

The first sample produced was in the basalt non--hybrid type, where basalt was used in both warp and weft. Plain weave was the weave selected for the sample. The back rest setting did not affect basalt yarn with the running on machine, rather it helped in making clear warp shed line. The shed height and shed angle were adjusted so that it forms a clear shed and does not create any kind of problem in weft insertion. The sample running took some time before the final settings were made. It caused some wastage of yarn too but ultimately the setting was finalized, it was a smooth and clear running till the completion of one sample. 2/2 matt weave is a weave that requires less tightness of bottom shed line as compared to plain weave. Rest of all the settings was same except the change in back rest height. This was done in order to make the bottom shed line just a little less tight compared to plain weave. As plain weave was the first weave in the line, the tension and other settings were known and they were kept same for the matt weave. The third combination of basalt warp and weft, was made with 1/3 twill weave. The initial problem with this weave was, most of the yarns were in the bottom shed at the time of weft insertion which was creating a problem with frequent end breakages. The tension was reduced as a first step but yarn shed was becoming slack with the decrease in tension to the level where breakage stopped. The aim for running of a yarn with successful results is to have minimum possible alterations with the change of weave, so that a standard result can be achieved. In this case lower back rest position helped in making the bottom shed line slightly slack which helped in finally controlling the warp breakages. The loom parameters are mentioned in Table 4 for different weave combinations.

Table 4: Machine settings for basalt/basalt

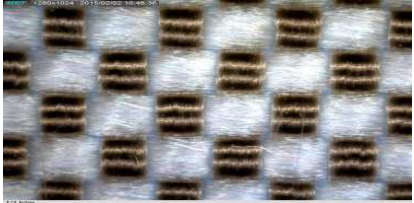
		1/1 plain	2/2 matt	1/3 twill
		Back rest position (mm)	7	6
Machine Speed (RPM)		300	300	300
Warp tension (kN)		4	3.5	3
Frame height (mm)	1	100	100	100
	2	102	101	101
	3	104	102	102
	4	106	103	103
Shed angle (degrees)		30	28	28

3.12 Weavability of basalt warp with polypropylene weft

To start with the running of PP yarns, the machine settings were the same as basalt/basalt plain weave. The back rest was raised, in order to make the bottom shed tighter rather than increasing tension. This was successful with no warp or weft breakage at all. It was open to the maximum angle for clear weft insertion. With 2/2

matt weave, same settings were kept as for plain weave. The only problem was the necessity of slightly loose bottom shed line as compared to plain weave. The back rest position was lowered by 1cm which resulted in lower tension on bottom shed line. This low tensioned bottom shed line helps in performing better for matt weave, because in this case two sets of yarns move at the same time in opposite directions. 1/3 twill has majority (75%) of threads in the bottom shed when the weft insertion takes place; it is therefore the requirement for the shed to be less tight in the bottom line. The sample was run with same settings as matt weave but it resulted in frequent warp breakages in the process, a lower tension resulted in the entanglement of warp yarns as was the case experienced with basalt/basalt combination. Thus the tension was maintained at the same level as the other two combinations of basalt/polypropylene and the position of back rest was lowered by 2cm as compared to matt weave. It resulted in a smooth running of the whole sample and no further issue was found during the running. One problem that was associated with all three above mentioned weaves was the cutting of weft yarn before the new pick insertion. Polypropylene is a slippery yarn and normal cutter does not cut it properly. The cutter angle was changed in order to solve the problem. An early cutting was started so that longer time was available to cut the yarn also use of special cutters helped in smooth and proper cutting of yarn without much of the problems. The machine settings for plain, matt and twill weaves with basalt warp and polypropylene weft are given in Table 5.

Table 5: Machine settings for basalt/PP


		1/1 plain	2/2 matt	1/3 twill
		Back rest position (mm)	7	6
Machine Speed (RPM)		300	300	300
Warp tension (kN)		4	3.5	3
Frame height (mm)	1	100	100	100
	2	102	101	101
	3	104	102	102
	4	106	103	103
Shed angle (degrees)		30	28	28

3.13 Weavability of basalt warp with polyester weft

The difference in running of polyester to that of polypropylene is due to less compact structure of PET yarn as compared to that of PP and this would mean a low tensioned shed line. To start with the running, the warp tension was reduced by moving the back rest down, in order to have minimum contact surface of yarn. The shed angle was increased to give more space for insertion of a bulkier PET yarn. This was successful

with no filling breakages. The problem associated was cutting of this yarn which was very difficult to handle even with the special cutter. Therefore, two cutters were used at the same time to cut the yarn. No weft breakage took place with this. With 2/2 matt weave, similar settings were kept as for plain weave, the only problem that occurred was the cutting of polyester yarn. The shed was kept open enough and tension was less so there was less chance of pick to entangle with the warp shed. The same cutter combination that was used with plain weave was a successful one. 1/3 twill has majority of threads in the bottom shed when the weft insertion takes place; it is therefore the requirement for the shed to be low tensioned in the bottom shed. The machine settings for the plain weave were such that shed was wide open to have space for the polyester weft insertion with ease, no difference in setting was done in this case, which resulted in a smooth running of the whole sample and no further issue was caused during the running. The machine settings for plain, matt and twill weaves with basalt warp and polyester weft are given in Table 6.

Table 6: Machine settings for basalt/polyester


		1/1 plain	2/2 matt	1/3 twill
Back rest position (mm)		6	6	6
Machine Speed (RPM)		275	275	275
Warp tension (kN)		3.5	3.5	3.5
Frame height (mm)	1	98	98	98
	2	100	100	100
	3	102	102	102
	4	104	104	104
Shed angle (degrees)		30	30	30

3.14 Weavability of basalt warp with jute weft

This was the most challenging task for weft insertion. For plain weave; the original settings for basalt warp did not work with jute weft yarn. There were so many protruding fibers with jute that forced to change the settings for clear shed. With increased tension to the shed, jute fibers were flying in the shed. Therefore minimum possible tension was applied to the warp sheet, and then the back rest was raised and adjusted in order to make a tight and straight shed as much as possible. Weft yarn from jute was still creating problems to be inserted into the sheds and was probably the toughest due to hairiness in yarn. The settings for 2/2 matt and 1/3 twill did not change much. Jute is easier to cut, there was no issue with the cutter, but the machine settings were the ones which were done with most dense qualities in industry where it was necessary to avoid the entanglement of warp sheet as well as entanglement of

weft yarn with the warp sheet. The trick for weaving jute is, to make a small shed which is open enough in order to avoid contact with weft yarn. This could be achieved due to superior property of basalt warp in contrast to running jute warp with jute weft.


Table 7: Machine settings for basalt/jute

		1/1 plain	2/2 matt	1/3 twill
		Back rest position (mm)	6	6
Machine Speed (RPM)	275	275	275	
Warp tension (kN)	2.5	2.5	2.5	
Frame height (mm)	1	104	104	104
	2	101	101	101
	3	103	103	103
	4	100	100	100
Shed angle (degrees)	32	32	32	

3.15 Weavability of polypropylene warp with basalt weft

Plain weave was selected for the first sample with same settings as basalt warp. The PP warp was able to sustain the tension quite well due to its strength and even a moderate tension helped in formation of clear warp shed line. The consideration was that, no untwisting of yarn takes place during weft insertion. The settings for 2/2 matt and 1/3 twill weaves were also similar as basalt warp. The settings are mentioned in Table 8.


Table 8: Machine settings for polypropylene/basalt

		1/1 plain	2/2 matt	1/3 twill
		Back rest position (mm)	7	6
Machine Speed (RPM)	300	300	300	
Warp tension (kN)	4	3.5	3	
Frame height (mm)	1	100	100	100
	2	102	101	101
	3	104	102	102
	4	106	103	103
Shed angle (degrees)	30	28	28	

3.16 Weavability of polyester warp with basalt weft

As polyester was a bulkier yarn, a higher shed angle was necessary. The angle of shed formation was increased for a smooth weft insertion reducing chance of contact of weft yarn with the warp line. Normal combination of cutters for this sample was suitable. For 2/2 matt weave the shed was a little tighter for running of this bulkier yarn effectively. The sample was completed without much of the problem once the minor adjustments were done. For 1/3 twill similar tension level was maintained. The settings are given in Table 9.

Table 9: Machine settings for polyester/basalt

		1/1 plain	2/2 matt	1/3 twill
		Back rest position (mm)	6	5
Machine Speed (RPM)		250	250	250
Warp tension (kN)		3	3	3
Frame height (mm)	1	100	100	100
	2	105	105	105
	3	98	98	98
	4	103	103	103
Shed angle (degrees)		30	30	30

3.17 Weaving of non-basalt fabrics

3.171 Propylene/polypropylene

Polypropylene is a synthetic filament yarn and it is sufficiently strong. It was an interesting proposition to use polypropylene as it needs some effort to start with. Once it is done with all the settings, it gives almost no warp breakages over a longer period of time. The important considerations were:

- This raw material is used on commercial scale in the industry, it is not required to be sized due to its strength but vegetable oil is applied to the yarn which helps in enabling the protruding fibers to settle down in case it is needed. During the production of this sample, it was desired to start it as early as beam is ready because of its tendency to stick with each other due to static charges.
- It is a strong yarn so at some points it was difficult to handle when it comes to weft insertion.
- During the start of a sample, there was a problem with shed settings which was observed in general.

Once initial settings of polypropylene were made, it was successful in running without creating much of the problems. The settings are given in Table 10.

3.172 Polyester/polyester

Polyester is also a synthetic filament yarn. This raw material is used on commercial level in the industry; it is not required to be sized due to its strength. There is a problem of static charges with polyester, when a sample was stored overnight; leading to huge pill formation due to protruding fibers attracting each other. The settings were similar as PP yarn weaving. Details of settings are given in Table 11.

Table 10: Machine settings for PP/PP



		1/1	2/2	1/3
		plain	matt	twill
Back rest position (mm)		6	5	5
Machine Speed (RPM)		300	300	300
Warp tension (kN)		4	3.5	3
Frame height (mm)	1	100	100	100
	2	102	101	101
	3	104	102	102
	4	106	103	103
Shed angle (degrees)		30	28	28

Table 11: Machine settings for PET/PET

		1/1	2/2	1/3
		plain	matt	twill
Back rest position (mm)		5	5	5
Machine Speed (RPM)		250	250	250
Warp tension (kN)		3	3	3
Frame height (mm)	1	100	100	100
	2	100	100	100
	3	95	95	95
	4	95	95	95
Shed angle (degrees)		30	30	30

3.13 Jute/Jute


Jute is the most difficult yarn to weave among all the fibers under investigation. The options that can be tried before running of jute in warp can be either application of size liquor or wax. Jute yarn strand has a real abrasive nature, most of the fibers are

protruding from the yarn surface and they are very hard to control. The features of jute which cause it to be most difficult to handle are, stiffness of yarn, abrasive nature of yarn, tendency of strand of fibers to open when put under tension and minimum residual elongation when used for weaving which makes it most difficult when the tension is applied on yarn.

- It was not possible to apply size liquor to the cone of jute as the liquor is normally applied to yarn in the form of warp sheet.
- The second option for jute running in warp was application of wax, which stays on the strand of yarn on slow speeds but with higher speed the wax just drops off from the strand of yarn.
- Another way for the running of jute was to maintain higher humidity level; however, yarns started to stick together. Another problem associated with the moisture is, jute absorbs moisture so rapidly that it starts losing its strength.
- Jute yarns were run on a moderate speed. The problems associated with change of tension and nature of shed were sticking of yarns together in the shed line, which was causing pill formation and cuts in the surface of the fabric which were never desired.

For the matt weave, a special drawing in of sample was done and machine started working smoothly. For 1/3 twill weave, skip draft was used with a lowered position of back rest. By moving dropper box to the front, an open and tight shed was formed. Details of settings are given in Table 12.

Table 12: Machine settings for jute/jute

		1/1 plain	2/2 matt	1/3 twill
		Back rest position (mm)	5	5
Machine Speed (RPM)		150	150	150
Warp tension (kN)		2	2	2
Frame height (mm)	1	95	92	94
	2	95	96	94
	3	90	90	88
	4	90	88	88
Shed angle (degrees)		30	30	30

3.2 Statistical analysis of weaving Efficiency

The output of analysis of variance (ANOVA) is given in Table 4.11. The ANOVA results show that there is significant difference (p value of less than 0.05 at α level = 0.05) in weave and yarn material.

Table 13: Analysis of variance output for Efficiency

Source	DF	Adj SS	Adj MS	F-value	P-Value
Regression	9	2412.72	268.080	128.58	0.00
Float	1	133.39	133.389	63.98	0.000
Materials	8	2279.33	284.917	136.65	0.000
Error	17	35.44	2.085		
Total	26	2448.17			

S
R-sq
R-sq(pred)
1.44394
96.36%

R-sq
98.55%

R-sq(adj)
97.79%

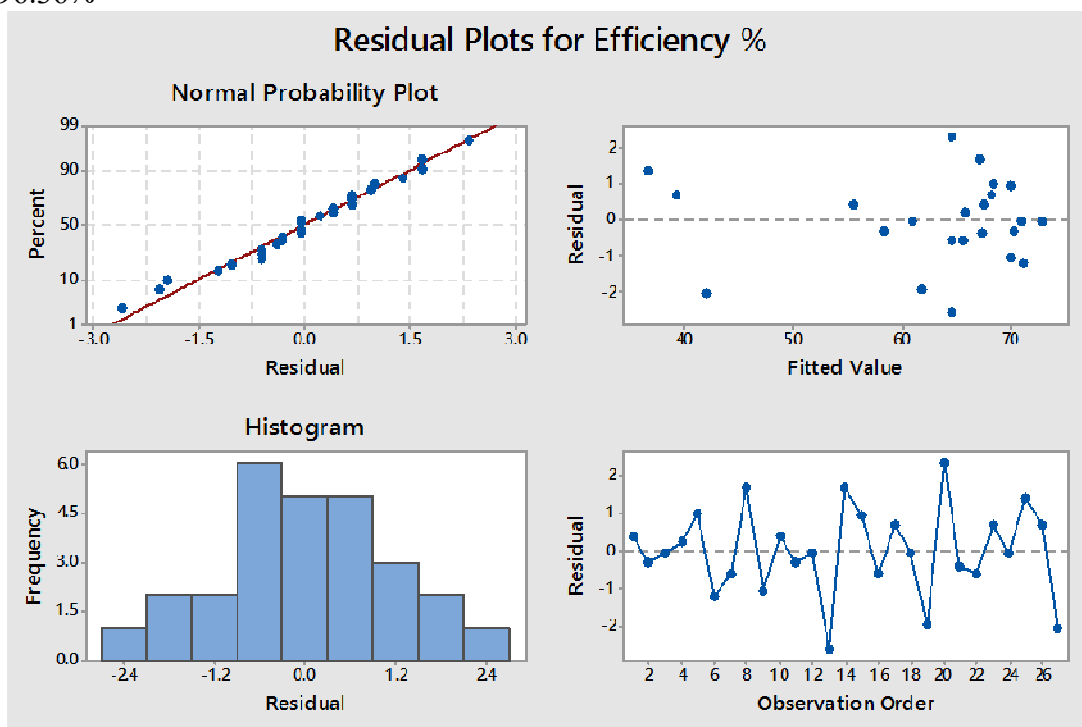
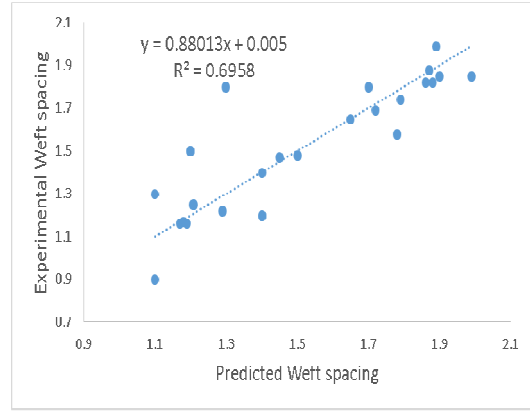
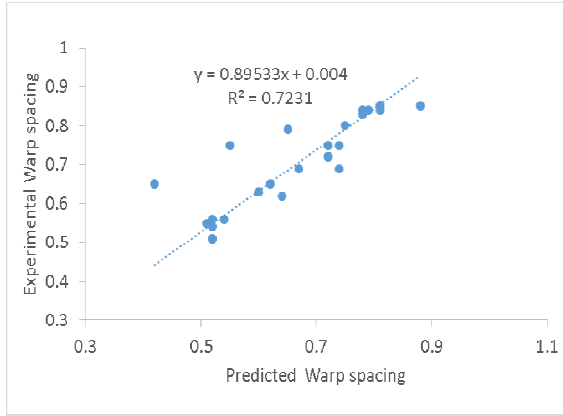


Fig. 1. Residual Plots for Efficiency %

For the Efficiency data, the histogram does not follow a normal curve. Evaluate the normal probability plot to assess whether the residuals are normal. For the Efficiency data, the residuals appear to follow a straight line. No evidence of nonnormality, skewness, outliers, or unidentified variables exists. For the Efficiency data, the residuals appear to be randomly scattered around zero. No evidence of nonconstant variance, missing terms, outliers, or influential point's exists. For the Efficiency data, the residuals appear to be randomly scattered about zero. No evidence exists that the error terms are correlated with one another.

3.3 Estimation of thread spacing and crimp based on geometrical model

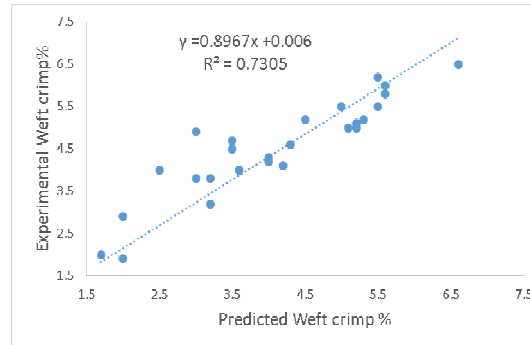
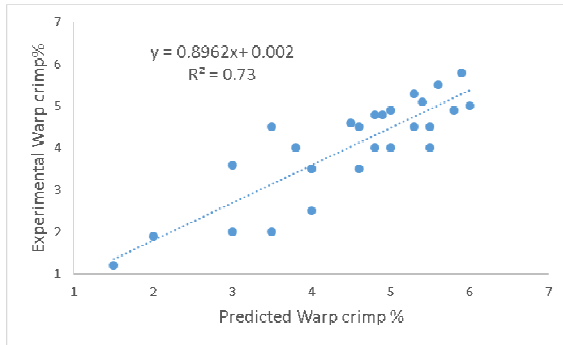
The warp and weft thread spacings as well as crimps were estimated using geometrical models as stated in methodology section. The experimentally measured values are correlated with estimations. Results are shown in Figure 2.



Equation $y = a + b \cdot x$	Value	t-test Significance "Yes" or "No"	Adj. R-Square	F-test Significance "Yes" or "No"	Equation $y = a + b \cdot x$	Value	t-test Significance "Yes" or "No"	Adj. R-Square	F-test Significance "Yes" or "No"
Intercept	0.004	Yes	0.72	Yes	Intercept	0.005	Yes	0.69	Yes
Slope	0.89	Yes			Slope	0.88	Yes		

Warp thread spacing estimated and measured

Weft thread spacing estimated and measured



Equation $y = a + b \cdot x$	Value	t-test Significance "Yes" or "No"	Adj. R-Square	F-test Significance "Yes" or "No"	Equation $y = a + b \cdot x$	Value	t-test Significance "Yes" or "No"	Adj. R-Square	F-test Significance "Yes" or "No"
Intercept	0.002	Yes	0.73	Yes	Intercept	0.006	Yes	0.73	Yes
Slope	0.89	Yes			Slope	0.89	Yes		

Warp crimp estimated and measured

Weft crimp estimated and measured

Fig. 2. Correlation of physical parameters from geometrical model with experimental results

4. Conclusion:

In this research work, new kind of yarns were run on the weaving machine and set of parameters for efficient weavability was developed. Parameters for weaving of basalt hybrid fabrics were optimized. During the sample production in weaving, behavior of

each group was studied. With certain fibers there were too many problems in terms of weaving efficiency and end breakages. Fibers like polyester and polypropylene caused greater problems during weaving due to static charges associated with synthetics. The problems associated with breakages were more in starting of samples as different settings were required for different combination of fibers and variable weaves within the same combination of fibers. During the running of polyester, certain special treatments like special cutter adjustment and different settings which vary from the recommended ones were observed. A special cutter was developed for polypropylene as it is slippery in nature and normal cutter was unable to cut the yarn. Statistical analysis also showed effect of yarn and weave on efficiency. Further research can be conducted for; Industrial large scale weaving operations may be carried out to optimize and further improve weavability of basalt based hybrid fabrics. Suitable surface finish may improve weaving efficiency

References:

1. Sathishkumar, T.P. et al. "Hybrid fiber reinforced polymer composites – a review". *Journal of Reinforced Plastics and Composites*, vol. 33(5), pp. 454–471, 2014.
2. Chou, T.W. and Ko, F.K. *Textile Structural Composites*. Composite Materials Series, Amsterdam: Elsevier Science Publishers B.V., 1993.
3. Laroche, et al. "Forming of woven fabric composites.". *Journal of Material Composites*, vol. 28, pp. 1825-1839, 1994.
4. Mohammed, U. et al. "Experimental studies and analysis of draping of woven fabrics". *Composites Part A: Applied Science and Manufacturing*, vol. 31, pp. 1409-1420, 2000.
5. Mishra, R. "Meso-scale finite element modeling of triaxial woven fabrics for composite inplane reinforcement properties". *Textile Research Journal*, vol. 83, pp. 1836-1845, 2013.
6. Woven fabric edited by Edited by Han-Yong Jeon, chapter 1. B. K. Behera, Jiri Militky, Rajesh Mishra and Dana Kremenakova, *Modeling of Woven Fabrics Geometry and Properties*, 2012.
7. Behera, B.K. and Mishra R. "3-Dimensional weaving". *Indian Journal of Fibre and Textile Research*, vol. 33, pp. 274-287, 2008.
8. R. A. Naik, "Failure analysis of woven and braided fabric-reinforced composites," *J. Compos. Mater.*, vol. 29, pp. 2334-2363, 1995.
9. Rabinovich, F.N et al. "Stability of basalt fiber in a medium of hydrating cement". *Journal of Glass and Ceramics*, vol. 58, pp. 11-12, 2001.
10. Medvedyev and Tsybulya, Y.L. "The outlook for the use of basalt continuous fiber for composite reinforcement". International Sample technical conference. Covina, CA: SAMPE, 2004, pp. 275-279.
11. Wang, M.C. et al. "Chemical Durability and Mechanical Properties of Alkali-proof Basalt fibre and its Reinforced Epoxy Composites". *Journal of Reinforced Plastics and Composites*, vol. 27, pp. 393-407, 2008.
12. Matko, S. et al. "Fire retarded insulating sheets from recycled materials". *Macromolecular Symposia*, vol. 233, pp. 217-224, 2006.
13. Militky, J. et al. "Influence of thermal treatment on tensile failure of basalt fibre". *Engineering Fracture Mechanics*, vol. 69, pp. 1025-1033, 2002.

14. Dalinkevich, A.A. et al. "Modern basalt fibrous materials and basalt fibre-based polymeric composites". *Journal of Natural Fibers*, vol. 6, pp. 248-271, 2009.
15. Botev, M. et al. "Mechanical properties and viscoelastic behavior of basalt fibre-reinforced polypropylene". *Journal of Applied Polymer Science*, vol. 74, pp. 523-531, 1999.
16. Liu, Q. et al. "Investigation of basalt fibre composite mechanical properties for applications in transportation". *Polymer Composites*, vol. 27, pp. 41-48, 2006.
17. Jamshaid, H. and Mishra, R. "A green material from Rock: A basalt fiber". *Journal of the Textile Institute*, vol.107,pp.923-937,2015.
18. Wittek, T. and Tanimoto, T. "Mechanical properties and fire retardancy of bidirectional reinforced composite based on biodegradable starch resin and basalt fibers". *EXPRESS Polymer Letters*, vol. 2, No.11, pp. 810-822, 2008.

Chapter 6

Review on hybrid yarns, textile structures and techniques

Mohanapriya Venkataraman, Xiaoman Xiong, Kasthuri Rajagopala Venkatesh,
Rajesh Mishra and Jiri Militky

*Faculty of Textile Engineering, Dept. of Material Engineering, Studentská 2,
Technical University of Liberec 461 17 Czech Republic,*

Abstract

The demand of lightweight solutions is continuously increasing in many industries like transportation, offshore industries and the sports world. Composite materials can be an ideal solution for those industries. Due to fiber orientation and content can be adapted specifically to the load cases, resulting in weight reduction. In addition, fiber reinforced thermoplastic composites can be reprocessed, recycled and repaired when failure occurs through polymer chain pull out. Various polymers can be used as matrix system for composite applications. Selection of composites is due to their cost-effectiveness, chemical and/or mechanical properties. Various processes that can produce fiber reinforced thermoplastic parts are hand lay-up with autoclave molding, fusion bonding, press molding, diaphragm forming, liquid composite molding, roll forming, automated tape placement, filament winding and automated tape winding[1].

1.1 Fiber Forms

Many types of reinforcement fibers are currently available. The fibers that have been used include glass, aramid, carbon (graphite) and boron (Ref. 1-2). Reinforcements like ceramic fibers, metallic fibers, and whiskers have also been used in specific applications. Glass fibers are produced by mixing various ingredients in specific proportions, melting the mixture in a furnace, and drawing molten glass in the form of filaments. The proportions of various ingredients depend on the product form desired. E glass fibers are used in electrical applications and S glass fibers are used in strength critical situations. S glass fibers are sometimes woven in composite materials to increase toughness and impact resistance. Carbon or graphite fibers are produced by pyrolytic degradation of an organic precursor material. The commonly used precursor materials include polyacrylonitrile (PAN), rayon and pitch. The fibers produced from PAN precursor are high strength and low modulus, whereas pitch fibers are high modulus and low strength. Carbon fibers contain 92 to 99 percent carbon and graphite fibers contain 99 percent carbon. Aramid fibers are aromatic polyamide fibers made from a polymer solution that is pressure extruded into a chemical bath by a procedure standard for synthetic textiles fibers. Commercially available fibers are Kevlar 29, Kevlar 49 and Nomex. Boron fibers are obtained by depositing elemental boron over a tungsten substrate, using chemical vapor plating. Boron fibers are larger in size as compared to glass, carbon and aramid fibers. The reinforcement fibers are generally available in the form of a tow, or in a band as shown in Figure 1. A woven form of the

reinforcements is also used in certain cases, depending on the application of the composite.

1.2 Hybrid Yarns

Hybrid yarns consisting of reinforcing and matrix fibers are one kind of basic material (semi-finished product) with which continuous fiber reinforced thermoplastic composites can be constructed [2, 3]. Composite properties are influenced mainly by the arrangement of the reinforcing fibers and the homogeneity of the fiber distribution in the composite, as well as by impregnation of the glass fibers with the polymer matrix. Hybrid yarns are usually manufactured into thermoplastic composites by hand lay-up [4], filament winding [5, 6] or—as done recently—by the pultrusion process [7].

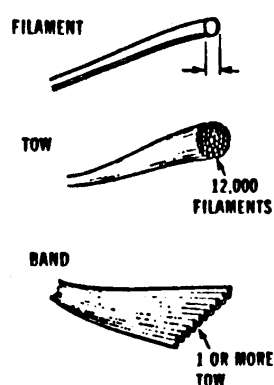


Fig. 1: Fiber Forms

The hybrid yarns were manufactured on the basis of glass and polyamide fibers, the properties of which are summarized in Table 1. The fineness of the fibers is given in Tex ($\text{tex}^{\frac{1}{4}} \text{g}/1000 \text{ m}$). From these filaments, hybrid yarns have been produced by different technologies, resulting in different structures of the semi-finished product:


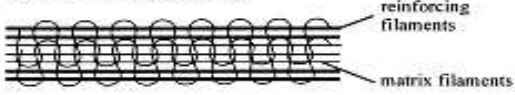


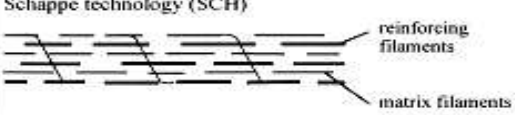
- Parallel arrangement of glass and polyamide fibers (side by-side, SBS);
- Parallel arrangement of matrix fibers surrounded by parallel glass fibers in the core, sheathed by matrix fibers in the skin ('Kemafil' technology, KEM);
- Commingled glass and polyamide fibers made by air texturing (commingled yarn, COM);
- Parallel arrangement of glass fibers in the core and spun matrix fibers in the skin (friction spinning, FS); and
- Mixture of glass and matrix fibers, both discontinuous, surrounded by a continuous matrix filament (Schappe technology, SCH).

The air-texturing process for the production of commingled yarn is demonstrated in Figure 2. The reinforcing glass fibers and the polyamide matrix fibers are subjected to pressurized air while moving through the texturing device. The air turbulence causes mixing of glass and polyamide fibers, resulting in the commingled yarn.

1.3 Kemafil Technology

The ‘Kemafil’ technology is a turning thread technique. By means of mechanical interlacing of yarns into a knitted structure, linear textiles are produced (laces, strings, cords and ropes). Kemafil machines are circular knitting machines operating with loopers that are arranged around a guide tube and give a tubular knitted structure which can cover any type of core yarn. SBS yarns are made much more simply by parallel winding of reinforcing and matrix fibers and give a tubular knitted structure which can cover any type of core yarn. SBS yarns are made much more simply by parallel winding of reinforcing and matrix fibers. The SCH and COM composites show the best degree of mixing of reinforcing and matrix fibers. However, this is a merely qualitative description of the yarns’ microstructure which influences more profound quantities that determine the consolidation quality of the composite.

Table 1: Hybrid yarn structures and corresponding production technology [8].

Technology	Geometry of fibre arrangement
Parallel winding of reinforcing and thermoplastic matrix filaments (side-by-side, SBS) 	parallel arrangement of reinforcing and matrix filaments
Kemafil technology (KEM) 	parallel arrangement of matrix fibres surrounded by parallel reinforcing fibres in the core, sheathed by matrix fibres in the skin
Air texturing (COM) 	reinforcing and matrix fibres are commingled; the arrangement of reinforcing fibres is out of yarn axis
Friction spinning (FS) 	parallel arrangement of reinforcing fibres in the core and spun fibres in the skin
Schappe technology (SCH) 	mixture of discontinuous reinforcing and matrix fibres surrounded by continuous matrix filaments

Impregnation of the reinforcing fibers with matrix material is determined mainly by the average flow distance of the polymer, a parameter that is also difficult to express quantitatively but one depending on the degree of mixing. The yarns may be ranked according to increasing flow distance as follows: SCH, COM, KEM, SBS and FS. Consequently one can expect that the impregnation quality of the glass fibers with polyamide matrix for the yarn structures investigated will be the highest for SCH composites and decrease towards FS composites. Another parameter is the possibility

of fiber flow, i.e. the fibers themselves can move together with the matrix. In compression moulding of a flat plate, this movement is negligible for continuous yarns, which can be considered to be fixed. The Schappe yarn consists of discontinuous fibers and thus such movements are possible. If all of these parameters are compared, the Schappe and COM yarns come out best, being comparable, followed by SBS then KEM, and the worst material is the FS. This is reflected by a comparison of the micrographs of Figure 3[8].

Table 2: Basic materials for manufacturing hybrid yarns [8].

	SBS	KEM	COM	FS	SCH
<i>Glass</i>					
Filament diameter (μm)	10	10	10	9	10
Fineness of filament yarn (tex)	40	40	40	135	-
<i>Polyamide 6</i>					
Fibre fineness (dtex)	-	-	-	13	-
Fineness of filament yarn (tex)	40	40	40	-	-
<i>Hybrid yarn</i>					
Glass:polyamide (mass%)	60:40	66:34	66:34	67:33	72:28
Fineness (tex)	200	1440	720	200	588
Producer	IPF	IPF	IPF	ITA ^a	Schappe ^b

^aInstitut für Textiltechnik der RWTH Aachen

^bprospectus Schappe Techniques

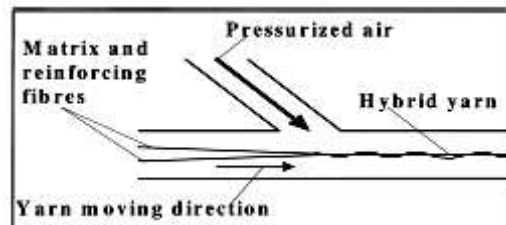


Fig. 2: Principle of air texturing to produce commingled yarn (COM) [8].

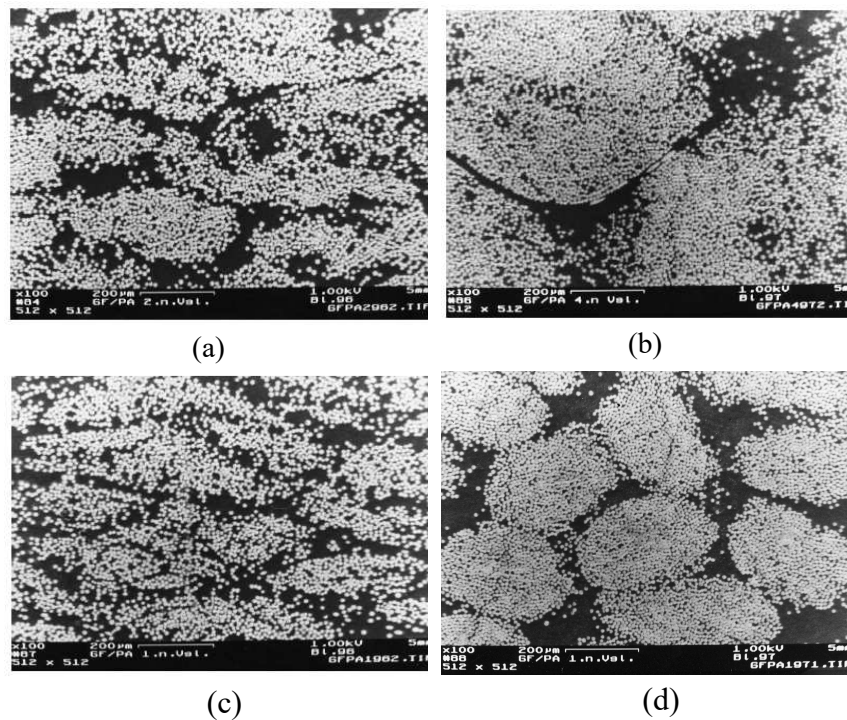


Fig. 3: Micrograph of a polished area of (a) SBS composite (b) KEM composite (c) COM composite and (d) FS composite [8].

1.4 Compression Moulding

Composites consisting of 15 unidirectional laminate were manufactured by compression moulding. Hybrid yarns were wound with a filament winding device on a plate core and then consolidated under 3 MPa pressure at a temperature of 245°C into plates. These plates were cut into the different sample geometries necessary for the delamination and tension tests. Although efforts were taken to achieve composites with the same glass fiber volume fraction by using the same mass ratio between glass and polyamide fibers for each yarn, the resulting composites showed a variation in the glass fiber volume fraction. These fiber volume fractions were determined by the matrix burn-off method for some parts of the specimens [8].

High performance composites in Textiles

Composites consisting of fillers in the form of inorganic/organic fiber or powder as well as metallic powders of relatively high strength and modulus embedded in or bonded to a matrix with distinct interface between them. Most usual fillers are fibers. Both fillers and matrix retain their physical and chemical identities, and they produce a combination of properties that cannot be achieved with either of the constituents acting alone. In the recent years, the use of textile structures made from high performance fibers is finding increasing importance in composites applications. In textile process, there is direct control over fiber placements and ease of handling of fibers. Besides economical advantages, textile preform technologies also provide homogenous distribution of matrix and reinforcing fiber. Thus, textile preforms are considered to be the structural backbone of composite structures¹. This technology is of particular importance in the context of improving certain properties of composites like inter-laminar shear and damage tolerance apart from reducing the cost of manufacturing. Textile industry has the necessary technology to weave high performance multifilament fibers, such as glass, aramid and carbon, which provide high tensile strength, modulus, and resistance to chemicals and heat to various types of preforms. Depending upon textile preforming method, the range of fiber orientation and fiber volume fraction of preform vary, subsequently affecting the matrix infiltration and consolidation. As a route to mass production of textile composites, the production speed, material handling and material design flexibility are major factors responsible for the selection of textile reinforcement production. This opens a new field of technical applications with a new type of semi-finished material produced by textile industry. The basic element of reinforcement is the single fiber or filament. In the case of short fiber composites, the continuous filaments are cut into specific length and then mixed with the resin using a suitable process. For example, in the case of injection molding, the short fibers are mixed with polymers and then the mixture is injection molded. The short fibers are also used as chopped strand mats. The mat is used primarily in hand lay-up, continuous lamination and some closed molding applications. Figure 4 shows the schematic diagrams of the chopped strand and continuous strand mat. Swirling of continuous strands of fibers onto a moving belt forms continuous strand mat. The mat is finished with a chemical binder that holds the fiber in place. Continuous strand mat is primarily used in compression molding,

resin transfer molding and pultrusion applications as well as to fabricate preforms and stampable thermoplastics.

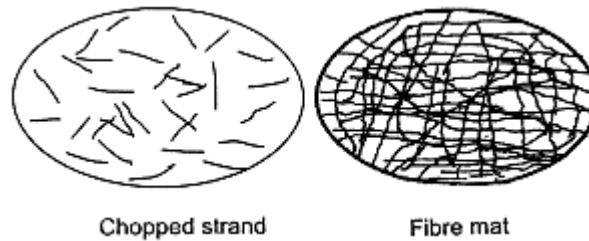


Fig. 4: Forms of reinforcement [9].

Another form of reinforcement is known as roving. A roving refers to a collection of untwisted strands or yarns. The glass strands are wound together to form a roving package suitable for internal or external unwinding. The roving is tailor made to suit specific applications with polyester, epoxy and vinyl ester resin systems. It can also be used for compounding with various thermoplastics and to produce a wide variety of reinforcing materials, including mats, woven fabrics, braids, knitted fabrics and hybrid fabrics. Prepregs are another class of reinforcement in which the fibers and resin are already mixed together. Advantages of prepregs include faster curing, improved distribution of resin throughout the part, cleaner manufacturing facilities, more precise fiber alignment and placement, ability to use higher fiber contents and, therefore, less resin overall, and ability to lay-up the material into some shapes that would be difficult with wet systems. Flexible prepregs, like powder-impregnated tows, commingled yarns and core spun yarns are used for textile preforming operations. The present paper reviews the developments made in the field of textile preforms along with their advantages and disadvantages. A filament is a single segment of reinforcement. Tow count is the number of filaments in the carbon fiber bundle which can vary such as 3K, 6K, 12K, 24K, and 50K tow fibers. Smaller tow count carbon fibers are generally of higher strength and modulus compared to standard modulus 50K tow carbon fibers commonly used for less demanding non-aerospace applications. Standard modulus carbon fibers are generally of 12K-50K tow size range and constitute 80-90% of the total carbon fiber market today. A filament can be used in continuous fiber processes such as filament winding and pultrusion. Filaments may also be woven or stitched into fabrics. Preforms are three-dimensional fabric forms designed to conform to a specific shape to meet specific mechanical and structural requirements. A pre-impregnated composite, or pre-preg, is where fibers, often in the form of a weave or fabric, are held together with a matrix resin. The matrix is partially cured to allow easy handling but must be cold stored to prevent complete curing. Bulk Molding Compounds (BMC) are primarily the crosslinking thermoset materials which are widely used in low-end composite applications today. Sheet Molding Compounds (SMC) are thin sheets of fibers pre-compounded with a thermoset resin and are primarily used in compression molding processes.

1.4.1 Semi-Finished Products

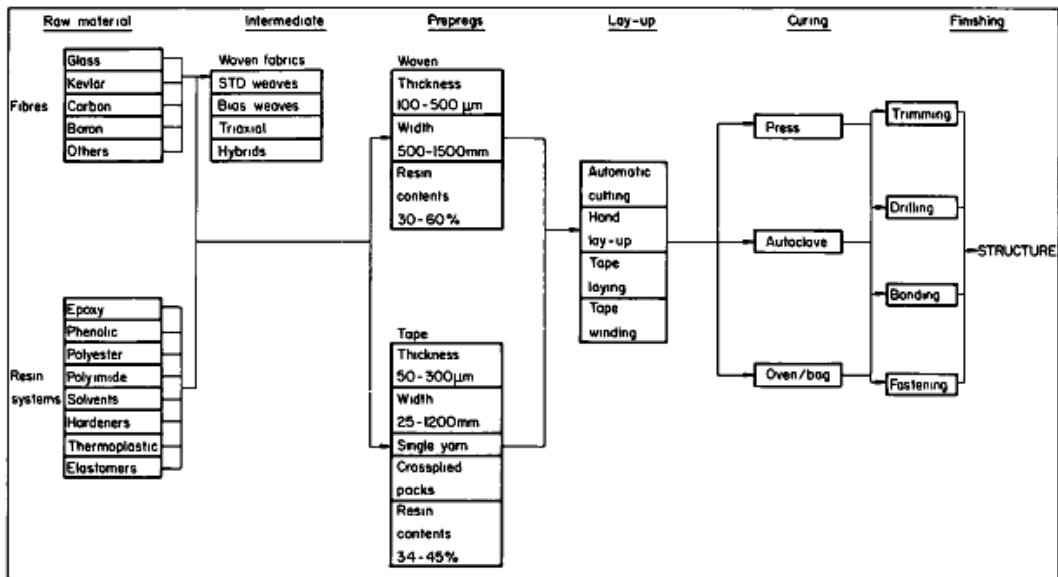


Fig. 5: Flow chart showing key stages in the fabrication of composite structures from raw materials

Textile Preforms For Composites

1.5 Woven Preforms

Developments in the field of preforming have led to the production of preforms with fibers orientated in different directions with weaving, knitting and braiding individually or in combinations. Table 3 provides a comparative account of different preforming techniques with respect to yarn direction and fabric formation principles. While 2D woven textile structures are usually formed into shape by molding or stitching, 3D textile preforms are more suitable for the creation of net-shaped thicker structures. Very good drapability and complex shape formation with no gap and reduced manufacturing cost are the main features of woven fabrics. The plain woven fabric is symmetrical with good stability and reasonable porosity. However, it is the most difficult of the weaves to drape, and the high level of fiber crimp imparts relatively low mechanical properties as compared to the other weave styles. With thick fibers, this weave style gives excessive crimp and, therefore, it tends not to be used for very heavy fabrics. In twill fabrics, the warp yarns alternately weave over and under two or more weft yarns in a regular repeated manner. Superior drape is observed in the twill weave over the plain weave with only a small reduction in stability. With reduced crimp, the twill fabric also has a smoother surface and slightly better mechanical properties. Satin weaves are fundamentally twill weaves modified to produce fewer inter-sections of warp and weft. Therefore, the low crimp gives good mechanical properties. Satin weaves allow fibers to be woven in the closest proximity and are capable of producing tight and compact preforms [10].

Basket weave is fundamentally the same as plain weave except that two or more warp fibers alternately interlace with two or more weft fibers. Basket weave is flatter due to less crimp. Although the basket weave is stronger than a plain weave, it shows poor

stability than plain woven fabrics. Basket weave can be used to develop heavy weight fabrics from thick fibers to avoid excessive crimping. Leno weave improves the stability in open fabrics which have a low yarn count. Leno woven fabrics are normally used in conjunction with other weave styles, because if used alone, their openness does not produce an effective composite component. Triaxial weaves show high levels of isotropy and dimensional stability even at low fiber volume fraction [10, 11]. The characteristics of some woven preforms are compared in Table 4.

Table 3: A comparison among different fabric formation techniques [9].

Parameter	Direction of yarn introduction	Fabric formation principle
Weaving	Two (0°/90°) (warp and weft)	Interlacing (By selective insertion of 90° yarns into 0° yarn system)
Knitting	One ((0° or 90°) (warp or weft)	Interlooping (By drawing loops of yarns over previous loops)
Braiding	One (machine direction)	Intertwining (Position displacement)
Nonwoven	Three or more (orthogonal)	Mutual fiber placement

Table 4: A comparative properties of some woven preforms [9].

Property	Woven preform					
	Plain	Twil	Satin	Basket	Leno	Mock-leno
Higher stability	4	3	2	2	1	3
Good drape	2	4	5	3	5	2
Low porosity	3	4	5	2	1	3
Smoothness	2	3	5	2	1	2
Balance	4	4	2	4	2	4
Low crimp	2	3	5	2	5	2

Rating scale: (5) Excellent (4) Very good (3) Good (2) Poor (1) Very poor

Weaving is extensively used in the composite industry, as it produces the vast majority of single layer, broadcloth fabric which can be used as reinforcement. The poor impact performance reduces in-plane shear properties, and the poor de-lamination resistance of such structures has led to the use of stitching techniques. In addition to weave crimp, stitching is often considered as a factor which reduces the mechanical efficiency of reinforcing fibers [12]. With some modifications, the standard industry machines can be used to manufacture flat, multi-layer fabrics of wide variety of structures which have highly improved impact performance. Multi-axial 3D weaving apparatus has also been reported. Bias yarns sandwiched between weft yarns and the resulting assemblies bound together by warp yarns have

produced unique structures. However, the main disadvantage of these multi-layer fabrics is that the standard looms cannot produce fabric that contains in-plane yarns at angles other than 0° and 90° [13]. This results in structures having very low shear and torsion properties, thereby making them unsuitable in many aircraft structures where materials with anisotropic properties are required. To overcome this problem, a great deal of effort has been made for the development of looms that can produce fabric with $\pm 45^\circ$ fibers [14]. Several weaving techniques have been reported to produce multi-axial multi-layer 3D preforms. These include lappet weaving, tri-axial weaving and pile weaving [12, 14, 15]. Lappet weaving is a special technique in which extra warp threads are introduced traditionally to develop isolated design motifs on open weave background. A standard weaving machine can be modified to incorporate lappet system to develop integrally woven multi-axial multi-layer preform structures for composites. The extra warp yarns (bias yarns) can be made to run at any angle between warp and weft directions. To get the through-the-thickness reinforcements, the extra warp yarns can be interlaced with weft yarns at any position within a multi-layer structure with the two extremes corresponding to weft yarns at the same and opposite fabric surfaces. However, the location of extra warp yarn which is limited to the outer surface of preform and the control of lappet bar movement in the reverse direction are the main limitations to develop multi-layer preforms on lappet weaving machines. Triaxial multi-layer fabric structures for composite reinforcements can be developed by inclusion of axial warp yarns as a third warp set in the basic triaxial process. However, the modification of triaxial weaving machine to incorporate such yarns would be a major engineering task. A patent [16] also describes the use of a jacquard shedding mechanism to manufacture multi-layer woven textile preforms. Greenwood et al. [17] described a method to develop stress oriented T-shaped woven preforms for composites. To develop T cross-sections, two sets of parallel threads at right angles to each other and at 45° angle to warp are required. To achieve correct orientation of threads, two sets of weft threads have been used to form this angle separately. This can be done by joining of two layers either along one side or side-by-side. The typical examples of 3D woven fabrics are simple interlock, orthogonal and complex shaped structures. Different multi-layer 3D woven structures and multi-axial pile fabrics are shown in Figure 6. Using the multi-warp weaving method, various fiber structures can be developed including solid orthogonal panel, variable thickness solid panels and core or truss like structures. Orthogonal cross-lapped fabrics can be formed by the placement of yarns at right angle to each other, typically in either rectangular or cylindrical space. There is no interlacing or other form of entanglement to hold the structure. Yarn is alternately laid between the edges in alternating orthogonal direction to create thick structure [9].

1.6 Knitted Preforms

Flat knit and shape knit products show the ability of the knitting process to manufacture complex shaped components. Jet engine vanes, T-shaped connectors, medical prosthesis, car wheel wells and aerospace fairings have all been successfully manufactured. The structure of yarn in the preform is highly curved and the

interlooping of yarn permits a very elastic and flexible structure. This is an advantage where components of complex shape without crimp are required and better formability and drapability of preforms are critical. Because of good drapability, a high degree of deformation can be possible. The yarn structure of the knit also tends to improve the impact performance of the composites; however, the structural performance of knitted composites is generally low. Hong et al. [18] described the various methods to develop 3D shaped knitted preforms, including tubular, spherical and box forms, by using SES 122FF flat knitting machines. 3D shapes can be developed by using a variety of structural combinations, such as different loop lengths and alteration in the number of knitting needles and courses. Wilde and Zigmann [19] compared woven fabric, outstretched glass/polyester (GF/PET) knit and 73% pre-stretched GF/PET knit. GF/PET co-knitted fabrics have been developed by simultaneous knitting of glass and polyester yarns. They also developed a weft knitted preform from GF/PET commingled yarns and observed that the stiffness of knitted fabric is more isotropic than that of woven fabrics. Further, they commented that the size of loops in knitted fabrics would determine the strength and stiffness of composites.

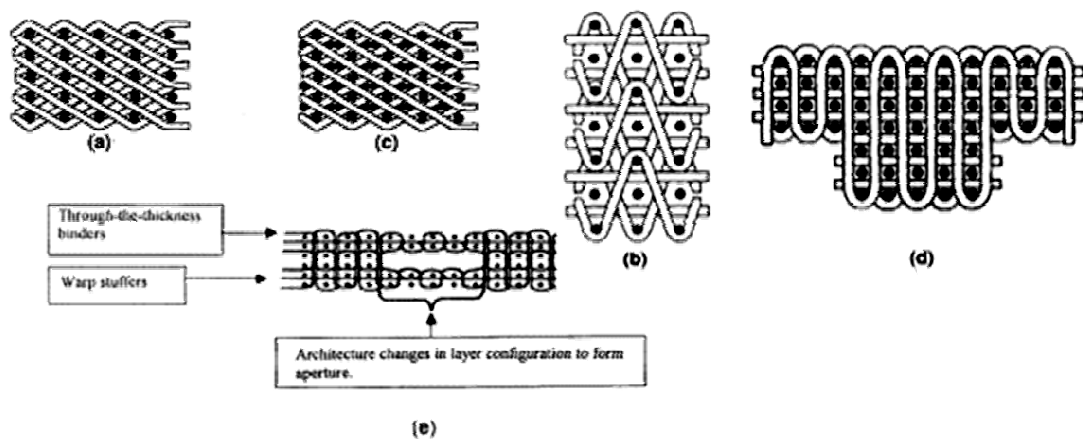


Fig. 6: Multi-layer 3D weave and its variants (a) multi-layer 3D weave, (b) change of angle, (c) angle interlock, (d) variable thickness solid panel, and (e) near net shaped preform[9].

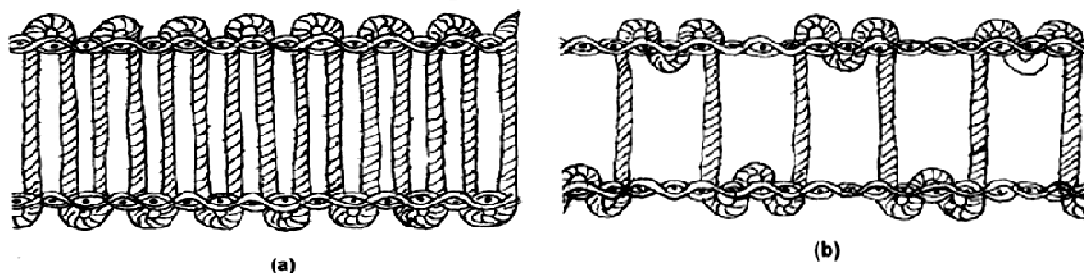


Fig. 7: Pile interlacing patterns (a) V interlacing, and (b) W interlacing [9].

The properties of flat knitted fabrics are different from those of other textile preforms. This area of knitting does overcome the problem of poor mechanical performance and it is the subject of intense interest within the aerospace industry. Woven and multi-axial fabrics are stiffer than conventional knitted fabrics and therefore more suitable for high performance applications where high tenacity and lower strains are

required. With insertion of weft inlay threads, the stiffness of these fabrics can be increased.

Table 5: Comparison among different multi-axial weaving techniques [9].

Bias fiber placement	Uniformity of bias fiber layers	Through-the-thickness reinforcement	Multiple layers
Rapier	No	Yes	Yes
Lappet	Yes	No	No
Screw shaft	No	Yes	Yes
Split reed	Yes	Yes	Yes
Guide Block	Yes	Yes	Yes
Bobbin (polar)	Yes	Yes	Yes

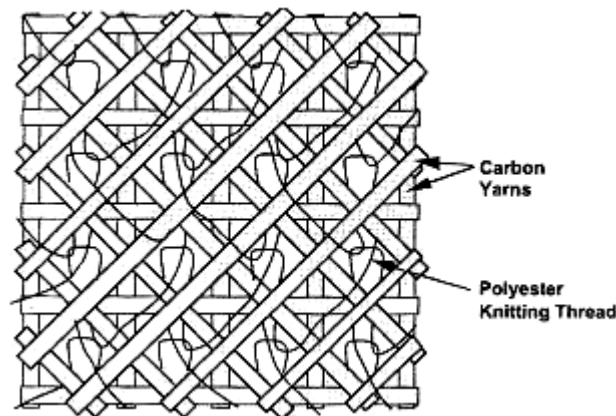


Fig. 8: Multi-axial warp knit (MWK) structure [9].

By using warp knitting techniques in conjunction with fiber placement concepts, multi-layer fabrics can be produced containing straight and relatively uncrimped fibers stacked in the required orientations. Karl Mayer Textil maschinen fabrik GmbH and LIBA Maschienen fabrik GmbH developed this technology. Figure 8 shows multi warp knitted (MWK) structure. MWK structure is produced on special raschel machine and the structure consists of two diagonal weft yarns, followed by a warp yarn and a horizontal weft yarn. The layers are held together by pillar stitches from both sides. The diagonal weft insertions ensure parallel placement of yarns at constant distance. Weft insertion makes it possible to arrange the least part of the fiber in stretched form. The diagonal angle of weft can be varied in the range of $\pm 30^\circ$ - 60° by suitably altering the course density. By using LIBA technique, multi-axial fabrics can be produced on a special tricot machine using 5-7 weft inlaid yarn layers and a warp inlaid yarn layer. At each weft station, the yarn can be laid horizontally in the range $\pm 30^\circ$ - 60° and therefore easy interchangeability of layer positions is possible. LIBA technique gives Quadra-axial structures, where yarns are arranged at 0° , $+45^\circ$, -45° and 90° . Malimo technique is another method to develop multi-axial stitch bonded knitted structures by stitching of several layers of yarns together at various angles or piles of skewed fabric on modified stitch bonding machine. This will improve mechanical properties and structural consistency [9]. In knitted multi-axial structures, materials for inlays are normally high modulus or high temperature

resistant polymer filaments such as polyester, nylon and PEEK, whereas glass, aramid or carbon threads can be used as reinforcing fiber materials. The use of these fabrics can lead to cost savings in the manufacture of composite components and the uncrimped nature of the yarn can also produce improved mechanical performance when compared to traditional woven fabrics. These fabrics have excellent dimensional stability and outstanding in-plane shear resistance in all directions. The warp inlay multi-axial structures show higher elastic modulus compared to woven fabrics. Tear strength of warp inlay multi-axial structure is found to be higher than that of woven fabrics. This may be due to the shifting of yarn layers under force and bunch together to resist tearing.

1.7 Braided Preforms

Two-dimensional braided structures are intertwined fibrous structures capable of having 0° and fiber orientation. Thickness is built by over braiding on previously braided layers, similar to ply layup process. Braiding can take place vertically or horizontally but the majority of composite braids is horizontal. The braiding process is capable of forming quite intricate preforms and has been successfully used with glass, aramid, carbon, ceramic and metal fibers. The braiding process can be varied during operation to produce changes in the cross-sectional shape as well as tapers, bends and bifurcations. Due to the high level of conformability and damage resistance capability of braided structures, the composites industry has used the braided composites in various applications ranging from rocket launchers to automotive parts to aircraft structures. By simply changing the relative position of carriers on track ring, different interlacing patterns can be produced. The pattern can be designed as 1/1 or diamond braid; however, the 2/2, 3/3 2/1 and 3/1 are the interlacing patterns of common use. Among all these patterns, 2/2 braid is the most popular and is referred as regular, standard, plain or flat braid. The braid has the tightest structure when each yarn is in contact with all neighboring yarns. However, due to bulky fiber structure and crimp, it is very difficult to form tightest structure. The braided structure enables the composite to endure shearing and impact better than woven preforms. Braids are continuously woven on the bias and have at least one axial yarn that is not crimped in the braiding process. This arrangement of yarns allows highly efficient load distribution throughout the braid. Either flat or tubular configurations are available as braids. Flat braids are used primarily for selective reinforcement, such as strengthening specific areas in pultruded parts. Tubular braid can be pultruded over a mandrel to produce hollow cross-sections in a variety of parts such as windsurfer masts, lamp and utility poles. Braiding was the first textile process used to manufacture a 3D fiber preform for a composite. 3D braiding is an extension of 2D braiding in which the fabric, constructed by intertwining or orthogonal interlacing of yarns to form an integrated structure through position displacement, provides through-the-thickness reinforcement and ready acceptability to the fabrication of wide range of complex shapes. 3D braids show comparatively high level of fiber content and at the same time less than 1% voids by interlocking continuous layers of braid. There are basically two types of braiding machines, one is

rectangular and other is circular, to produce I or T beams and thick wall tubular structures respectively. Furthermore, multiply preforms can be developed by interlacing adjacent layers on 3D braider. The key geometric parameters of 3D braids are fiber orientation, total fiber volume fraction, void and axial fiber percentage of total fibers. The speed ratio between braiding and take up as well as the linear density ratio of braider and axial yarn are the simple process parameters to adjust or control the microstructure of 3D braids. Although 2D braided preforms offer numerous applications, the major limitation of 3D braiding is that the maximum preform size is determined by the braiding machine size and most available machines are only able to braid preforms with small dimensions only. Larger and more expensive machines will be needed to produce preforms suitable for a wider range of structural uses. Furthermore, many 3D braiding machines are still in a research and development stage and thus only a few machines are presently able to commercially manufacture preforms. 3D braiding machines are also slow and have short production runs. As a result, 3D braids cannot compete with 2D braids and laminates on a cost saving basis [9].

1.8 Stitched Preforms

Stitching of textile preforms is considered as one of the important techniques to develop complex textile preforms. The process of stitching can be used in two ways: Firstly, the stitching can be used simply as a way of assembling the single or multi-layered textile preforms together and holding them into the required shape during consolidation process. The second use of stitching is to improve the impact performance of composite structures by the addition of through-the-thickness reinforcement.

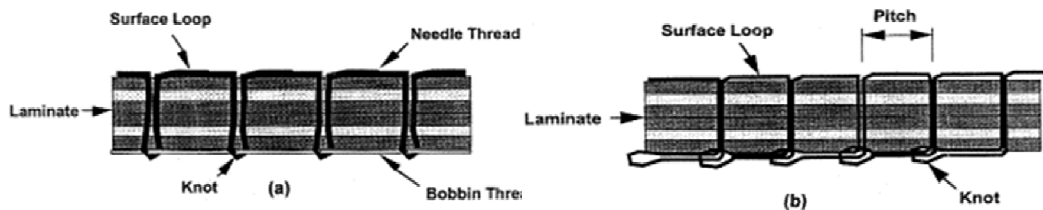


Fig. 9: Different types of stitches for through the thickness reinforcements (a) lock stitch, and (b) chain stitch [9].

Stitching involves sewing high performance yarn (e.g. glass, carbon or Kevlar), through an uncured prepreg laminate or dry fabric plies using an industrial sewing machine. Stitching has also been performed using polyester thread, though Kevlar is the most popular yarn because of its high strength and flexibility. A variety of sewing machines can be used to stitch composites, although they can usually be classified as single-needle or multi-needle machines. Figure 9 shows different types of stitches through-the-thickness of reinforcements. Stitching equipment currently used in the textile industry is capable of manufacturing preforms from aerospace-grade materials and a significant amount of research effort has been devoted to the performance of these stitched composites. Special attention is provided particularly in manufacture of

complex shaped structures using stitching. Commonly available 2D fabrics are used as the main reinforcement in the structure. This provides large amount of flexibility in engineering textile structures to get the desired composite properties. For making near net shape preform and joining textile reinforcement materials, stitching is very important tool. It makes preform material ready to use and easy to handle. However, the stitching of preform creates faults in the plane of material which affects the structural properties of composites and some of the reinforcement fabric related properties. This damage adversely affects the mechanical properties of composites. Weimer et al.[20]studied the various parameters that affect the stitching process and observed that, in addition to the type of textile preforms and stacking sequence, the other parameters such as stitch direction, properties and appearance of thread material and stitching process strongly affect in-plane fiber distortion and compaction during stitching and impregnation process. Improved damage tolerance under impact and better post-impact mechanical properties have been major reasons for the burgeoning amount of research into stitched composites.

1.9 Nonwoven Preforms

Nonwoven structures are fiber-to-fabric assemblies produced by chemical, thermal or mechanical means or a combination of them. The thickness of sheet may vary from 25 μm to several centimeters and weight from 10 g/cm^2 to 100 g/cm^2 . Nonwovens have density less than usually demanded in structural composites. As nonwovens become more readily available with the range of properties, the market for composites is also expected to increase. Composites made from nonwoven glass with epoxy resins reduce exfoliation between layers at high temperature. Nonwoven-based composites are finding increased application in automotive, marine and other applications.

Two very popular types of composites used in medical applications are SMS (Spun bond, Melt blown and Spun bond) and MSM (Melt blown, Spun bond and Melt blown) which in actual sense are laminate structures. A method to develop composite material by coating nonwoven fabrics made of carbon fiber or a blend of carbon fiber and other organic fiber with a filler-containing liquid has been described in a patent [21]. This low-priced pitch-based carbon fiber nonwoven can be used cost effectively in composites as friction materials, packaging and gasket applications. Composites developed from a nonwoven mat consisting of acrylic continuous filaments and impregnated with an inorganic matrix offer a wide range of applications in the fields of construction, aerospace, filtration, industrial, marine, medical protection, sports and transportation.

1.10 Characterization of Textile Preforms

The essential properties of textile preforms for composites include high flexibility, formability, stability and high axial rigidity. Table 6 shows some of the important properties of textile preforms. Consideration of geometrical properties in designing textile preforms will help to predict the resistance of preforms to mechanical deformation such as initial extension, bending and shear in terms of resistance to deformation of individual fibers. It will also provide the information regarding

maximum achievable packing of a fabric. Textile preforms are subjected to a wide range of complex deformations during manufacturing of composites. This includes intra-ply shear, inter-ply shear (if two or more plies are used), viscous friction between tool and material, inter-tow slip and applied pressure during consolidation. Some other serious problems are also observed during composite formation, such as wrinkling (buckling of fibers), and variations in fiber volume fraction due to spreading or bunching of fibers. The behavior of textile preforms extended at any angle involves the consideration of shear behavior of fabrics. Tensile forces along the fiber axis may lead to fiber straightening and compressive force can cause buckling. Chen and Chou [22] studied the mechanical properties of multilayer and angle interlock woven structures and observed that the mechanical properties of 3D woven structures heavily depend on the fabric structure. Straight yarns in orthogonal weaves provide high tensile strength and stiffness and this is directly proportional to the number of layers of orthogonal weave. However, the breaking elongation of orthogonal woven structure is independent of weave and number of layers, as breaking elongation primarily depends upon the type of yarn used. Further, they stated that the shear rigidity and shear hysteresis depend on binding weaves. Shear rigidity and hysteresis increase with the increase in number of layers. They also observed that the tighter binding weaves and more layers of orthogonal structure would produce higher bending stiffness and bending hysteresis and vice versa. Finally, it is concluded that the straight yarns in orthogonal weaves provide high tensile strength and stiffness and this is directly proportional to the number of layers of orthogonal weave. However, the breaking elongation of orthogonal woven structure is independent of weave and number of layers. Many researchers used kinematic (pin-joint) approach to study deformation behavior of textile fabrics. The acute angle between warp and weft can be used as a measure of deformation caused due to shearing. Before any deformation, this angle for woven fabric is 90° . However, the angle decreases continuously with the increase in deformation until it reaches to critical shearing angle (called as locking angle) just before buckling of fibers. The traditional kinematic model cannot represent the later stages of deformation and locking angle. This model can be used only for single layer and critical experiments are necessary to determine locking angle. To overcome these problems, Prodromou and Chen³⁴ modified the fabric geometrical parameters, such as tow width and tow spacing, and fiber properties like friction and buckling resistance which determine locking angle. Their study shows that besides geometric modifications in fabric parameters, the factors independent of fabric construction parameters, such as high friction coefficients, inter-ply shear interactions and reduction in global stiffness, may affect wrinkling behavior. Draping is particularly important in processes like Liquid Composites Molding (LCM) and thermoforming of prepregs. Drape with other preform properties such as wrinkling are also clearly related to bending properties of textile preforms. Formation of complex shaped composites involves bending of preforms in more than one direction and, therefore, the preforms are subjected to form double curvature, which leads shear deformation of preforms. Measurement of fabric buckling is relatively a good method to observe bending rigidity and frictional resistance to

bending of fabric. The traditional approach to drape modeling for fabric reinforcements uses a geometric mapping which is based on fabric shear. Long et al. [23] developed a geometrical model which describes shear force and shear strain energy as the function of fabric shear angle. They used warp knitted and woven preforms for the study. They found that the fiber structure has a significant effect on deformation characteristics of fabric. They also developed a mechanical model to determine shearing behavior of woven and warp knitted preforms based on inter-tow friction. The obtained shear properties can be used for draping simulation.

Table 6: Properties of some textile preforms [9].

Textile preform	Advantage	Limitation
Low crimp uniweave	High in-plane properties; good tailorability; highly automated preform fabrication process	Low transverse and out-of-plane properties; poor fabric stability; labor intensive ply lay-up
2-D Woven	Good in-plane properties; good drapability; highly automated preform fabrication process; integrally woven shapes possible; suited for large area coverage and extensive data base	Limited tailorability for off-axis properties ; low out-of-plane properties
3-D Woven	Moderate in-plane and out-of-plane properties; automated preform fabrication process and limited woven shapes are possible	Limited tailorability for off-axis properties and poor drapability
2-D Braid	Good balance in off-axis properties; automated preform fabrication process; well suited for complex curved shapes; good drapability	Size limitation due to machine availability and low out-of-plane properties
3-D Braid	Good balance in in-plane and out-of-plane properties; well suited for complex shapes	Slow preform fabrication process; size limitation due to machine availability
Multi-axial warp knit	Good tailorability for balanced in-plane properties; highly automated preform fabrication process; multi-layer high throughput; material suited for large area coverage	Low out-of-plane properties
Stitched fabrics	Good in-plane properties; highly automated process; provides excellent damage tolerance and out-of-plane strength and excellent assembly aid	Small reduction in in-plane properties; poor accessibility to complex curved shapes

The drape simulation indicates the feasibility of draped form and gives undeformed fabric pattern as well as other important information such as distribution of yarn orientation, fiber volume fraction and thickness of the fabric stack. Wang et al. [24] predicted the draping behavior of preforms by bias extension and simple shear test methods which are based on pin-jointed model. They also studied the effects of

aspect ratio and boundary conditions on permeability. They observed considerable differences in preform permeability when different test methods, aspect ratios and boundaries were used. Page and Wang [25] also studied yarn slippage in textile preforms by comparing carbon and glass fabrics and observed higher yarn slippage in carbon fabrics, whereas no such slippage of yarns was observed in glass fabric. The observed yarn slippage was found to be affected by the non-uniformity of deformation, boundary conditions and differences in fabric materials.

Although the various technologies are available for manufacturing composites, only liquid composite molding has the capability of manufacturing polymer composites with large size and complex shapes at low cost. In LCM, a fiber preform, which consists of several layers of dry continuous strand mat, woven roving or cloth, is placed into the mold cavity. The mold is then closed and resin is injected into the cavity to impregnate the preform. Therefore, the permeability of preforms is of prime importance in LCM. Fiber preform permeability is usually dependent on the fiber content, preform structure, binder, arrangement angle of fiber plies, etc. Therefore, the permeability of a given preform is a function of the fiber content only. There are two techniques (parallel flow and radial) for permeability measurements of fiber mats or preform. Han et al.³⁸ used pressure transducers to measure the permeability of an individual layer in a multi-layered preform. Stoven et al. [26] determined the transfer permeability of planer textile reinforcements such as non-crimped stitched fabric by ultrasound transmission technique. They observed that the sound velocity inside the stack of fibers changes when it gets impregnated and the dry regions of the fiber stack depend on the dimensions of dry regions along the path of acoustic waves.

In the preparation of composites with various LCM techniques, the compaction of textile preforms during tool closure is another important parameter. The yarn bundles in preform get flattened during compaction and, therefore, reduce pores and gaps among fibers and yarns. This results in elastic deformation, inter-layer packing and nesting. As the compressive force increases, the elastic deformation of fabric extends further and the thickness of preform reduces while fiber volume fraction increases. When the force reaches to a certain value, the fabric cannot be further compressed. Chen and Chou[22] developed a 3D compaction model to study the compressive behavior of multi-layer woven preforms in terms of nesting and elastic deformation, which can be used to predict permeability of preform. They found that the compressive force and reduction in preform thickness have empirical relationship and suggested that some further studies are required to understand nonlinear pressure-preform thickness relationship exhibited at the initial stages of experiments.

1.1 Laminated Structures

Composite materials consist of a combination of materials that are mixed together to achieve specific structural properties. The individual materials do not dissolve or merge completely in the composite, but they act together as one. Normally, the components can be physically identified as they interface with one another. The properties of the composite material are superior to the properties of the individual materials from which it is constructed.

An advanced composite material is made of a fibrous material embedded in a resin matrix, generally laminated with fibers oriented in alternating directions to give the material strength and stiffness. Fibrous materials are not new; wood is the most common fibrous structural material known to man [27]. Applications of composites on aircraft include:

- Fairings
- Flight control surfaces
- Landing gear doors
- Leading and trailing edge panels on the wing and stabilizer
- Interior components
- Floor beams and floor boards
- Vertical and horizontal stabilizer primary structure on large aircraft
- Primary wing and fuselage structure on new generation large aircraft
- Turbine engine fan blades
- Propellers

1.10.1 Major Components of a Laminate

An isotropic material has uniform properties in all directions. The measured properties of an isotropic material are independent of the axis of testing. Metals such as aluminum and titanium are examples of isotropic materials. A fiber is the primary load carrying element of the composite material. The composite material is only strong and stiff in the direction of the fibers. Unidirectional composites have predominant mechanical properties in one direction and are said to be anisotropic, having mechanical and/or physical properties that vary with direction relative to natural reference axes inherent in the material. Components made from fiber reinforced composites can be designed so that the fiber orientation produces optimum mechanical properties, but they can only approach the true isotropic nature of metals, such as aluminum and titanium. A matrix supports the fibers and bonds them together in the composite material. The matrix transfers any applied loads to the fibers, keeps the fibers in their position and chosen orientation, gives the composite environmental resistance, and determines the maximum service temperature of a composite [27].

1.10.2 Strength Characteristics

Structural properties, such as stiffness, dimensional stability, and strength of a composite laminate, depend on the stacking sequence of the plies. The stacking sequence describes the distribution of ply orientations through the laminate thickness. As the number of plies with chosen orientations increases, more stacking sequences are possible. For example, a symmetric eight-ply laminate with four different ply orientations has 24 different stacking sequences [27].

1.10.3 Fiber Orientation

The strength and stiffness of a composite buildup depends on the orientation sequence of the plies. The practical range of strength and stiffness of carbon fiber extends from values as low as those provided by fiberglass to as high as those provided by titanium.

This range of values is determined by the orientation of the plies to the applied load. Proper selection of ply orientation in advanced composite materials is necessary to provide a structurally efficient design. The part might require 0° plies to react to axial loads, $\pm 45^\circ$ plies to react to shear loads, and 90° plies to react to side loads. Because the strength design requirements are a function of the applied load direction, ply orientation and ply sequence have to be correct. It is critical during a repair to replace each damaged ply with a ply of the same material and ply orientation. The fibers in a unidirectional material run in one direction and the strength and stiffness is only in the direction of the fiber. Pre-impregnated (prepreg) tape is an example of a unidirectional ply orientation. The fibers in a bidirectional material run in two directions, typically 90° apart. A plain weave fabric is an example of a bidirectional ply orientation. These ply orientations have strength in both directions but not necessarily the same strength. The plies of a quasi-isotropic layup are stacked in a 0° , -45° , 45° , and 90° sequence or in a 0° , -60° , and 60° sequence. These types of ply orientation simulate the properties of an isotropic material. Many aerospace composite structures are made of quasi-isotropic materials.

1.10.4 Warp Clock

Warp indicates the longitudinal fibers of a fabric. The warp is the high strength direction due to the straightness of the fibers. A warp clock is used to describe direction of fibers on a diagram, spec sheet, or manufacturer's sheets. If the warp clock is not available on the fabric, the orientation is defaulted to zero as the fabric comes off the roll. Therefore, 90° to zero is the width of the fabric across. [Figure 12]

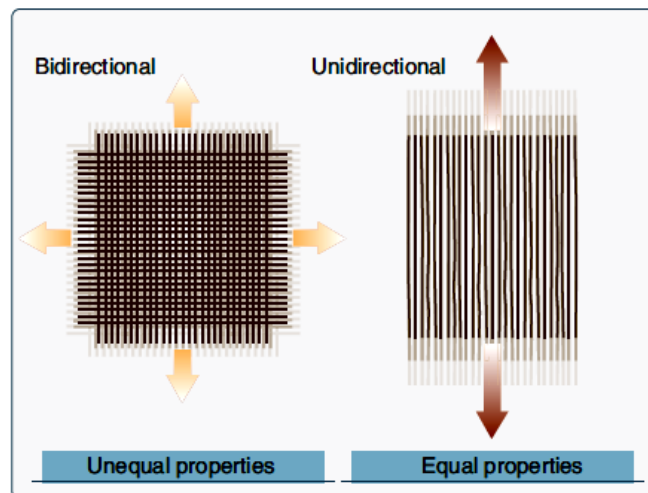


Fig. 10: Bidirectional and unidirectional material properties [27].

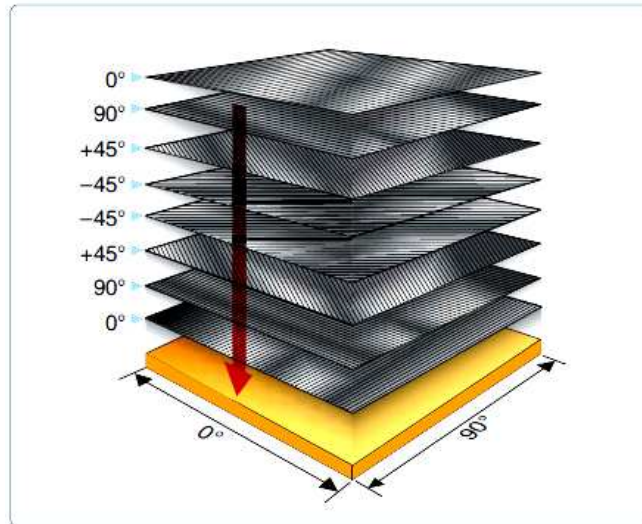


Fig. 11: Quasi-isotropic material lay-up [27].

1.11 Fiber Forms

All product forms generally begin with spooled unidirectional raw fibers packaged as continuous strands. An individual fiber is called a filament. The word strand is also used to identify an individual glass fiber. Bundles of filaments are identified as tows, yarns, or rovings. Fiberglass yarns are twisted, while Kevlar® yarns are not. Tows and rovings do not have any twist. Most fibers are available as dry fiber that needs to be impregnated (impreg) with a resin before use or prepreg materials where the resin is already applied to the fiber [27].

1.11.1 Roving

A roving is a single grouping of filament or fiber ends, such as 20-end or 60-end glass rovings. All filaments are in the same direction and they are not twisted. Carbon rovings are usually identified as 3K, 6K, or 12K rovings, K meaning 1,000 filaments. Most applications for roving products utilize mandrels for filament winding and then resin cure to final configuration.

1.11.2 Unidirectional (Tape)

Unidirectional prepreg tapes have been the standard within the aerospace industry for many years, and the fiber is typically impregnated with thermosetting resins. The most common method of manufacture is to draw collimated raw (dry) strands into the impregnation machine where hot melted resins are combined with the strands using heat and pressure. Tape products have high strength in the fiber direction and virtually no strength across the fibers. The fibers are held in place by the resin. Tapes have a higher strength than woven fabrics.

1.11.3 Bidirectional (Fabric)

Most fabric constructions offer more flexibility for layup of complex shapes than straight unidirectional tapes offer. Fabrics offer the option for resin impregnation either by solution or the hot melt process. Generally, fabrics used for structural applications use like fibers or strands of the same weight or yield in both the warp

(longitudinal) and fill (transverse) directions. For aerospace structures, tightly woven fabrics are usually the choice to save weight, minimizing resin void size, and maintaining fiber orientation during the fabrication process.

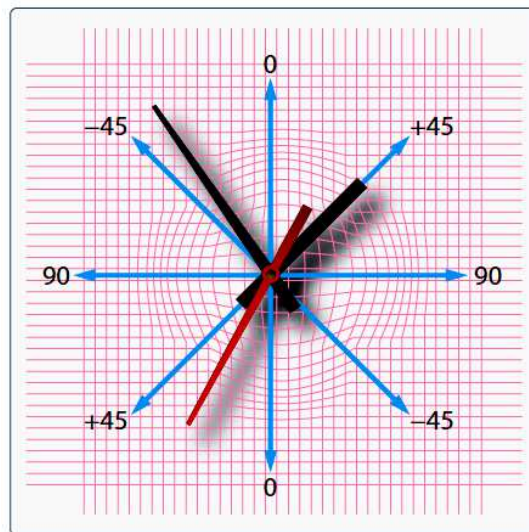


Fig. 12: A warp clock [27].

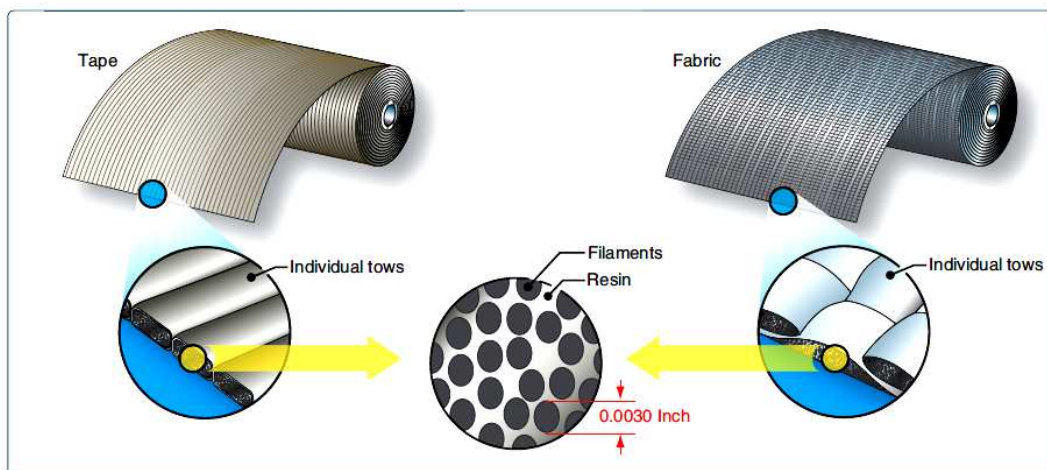


Fig. 13: Tape and fabric products [27].

Woven structural fabrics are usually constructed with reinforcement tows, strands, or yarns interlocking upon themselves with over/under placement during the weaving process. The more common fabric styles are plain or satin weaves. The plain weave construction results from each fiber alternating over and then under each intersecting strand (tow, bundle, or yarn). With the common satin weaves, such as 5 harness or 8 harness, the fiber bundles traverse both in warp and fill directions changing over/under position less frequently. These satin weaves have less crimp and are easier to distort than a plain weave. With plain weave fabrics and most 5 or 8 harness woven fabrics, the fiber strand count is equal in both warp and fill directions. Example: 3K plain weave often has an additional designation, such as 12 x 12, meaning there are twelve tows per inch in each direction. This count designation can be varied to

increase or decrease fabric weight or to accommodate different fibers of varying weight [27].

1.11.4 Nonwoven (Knitted or Stitched)

Knitted or stitched fabrics can offer many of the mechanical advantages of unidirectional tapes. Fiber placement can be straight or unidirectional without the over/under turns of woven fabrics. The fibers are held in place by stitching with fine yarns or threads after preselected orientations of one or more layers of dry plies. These types of fabrics offer a wide range of multi-ply orientations. Although there may be some added weight penalties or loss of some ultimate reinforcement fiber properties, some gain of interlaminar shear and toughness properties may be realized. Some common stitching yarns are polyester, aramid, or thermoplastics.

1.12 Types of Fiber

1.12.1 Fiberglass

Fiberglass is often used for secondary structure on aircraft, such as fairings, radomes, and wing tips. Fiberglass is also used for helicopter rotor blades. There are several types of fiberglass used in the aviation industry. Electrical glass, or E-glass, is identified as such for electrical applications. It has high resistance to current flow. E-glass is made from borosilicate glass. S-glass and S2-glass identify structural fiberglass that have a higher strength than E-glass. S-glass is produced from magnesia-alumina-silicate. Advantages of fiberglass are lower cost than other composite materials, chemical or galvanic corrosion resistance, and electrical properties (fiberglass does not conduct electricity). Fiberglass has a white color and is available as a dry fiber fabric or prepreg material. Kevlar® is DuPont's name for aramid fibers. Aramid fibers are light weight, strong, and tough. Two types of Aramid fiber are used in the aviation industry. Kevlar® 49 has a high stiffness and Kevlar® 29 has a low stiffness. An advantage of aramid fibers is their high resistance to impact damage, so they are often used in areas prone to impact damage. The main disadvantage of aramid fibers is their general weakness in compression and hygroscopy. Service reports have indicated that some parts made from Kevlar® absorb up to 8 percent of their weight in water. Therefore, parts made from aramid fibers need to be protected from the environment. Another disadvantage is that Kevlar® is difficult to drill and cut. The fibers fuzz easily and special scissors are needed to cut the material. Kevlar® is often used for military ballistic and body armor applications. It has a natural yellow color and is available as dry fabric and prepreg material. Bundles of aramid fibers are not sized by the number of fibers like carbon or fiberglass but by the weight.

1.12.2 Carbon/Graphite

One of the first distinctions to be made among fibers is the difference between carbon and graphite fibers, although the terms are frequently used interchangeably. Carbon and graphite fibers are based on graphene (hexagonal) layer networks present in carbon. If the graphene layers, or planes, are stacked with three dimensional order, the

material is defined as graphite. Usually extended time and temperature processing is required to form this order, making graphite fibers more expensive. Bonding between planes is weak. Disorder frequently occurs such that only two-dimensional ordering within the layers is present. This material is defined as carbon. Carbon fibers are very stiff and strong, 3 to 10 times stiffer than glass fibers. Carbon fiber is used for structural aircraft applications, such as floor beams, stabilizers, flight controls, and primary fuselage and wing structure. Advantages include its high strength and corrosion resistance. Disadvantages include lower conductivity than aluminum; therefore, a lightning protection mesh or coating is necessary for aircraft parts that are prone to lightning strikes. Another disadvantage of carbon fiber is its high cost. Carbon fiber is gray or black in color and is available as dry fabric and prepreg material. Carbon fibers have a high potential for causing galvanic corrosion when used with metallic fasteners and structures.

1.12.3 Kevlar®

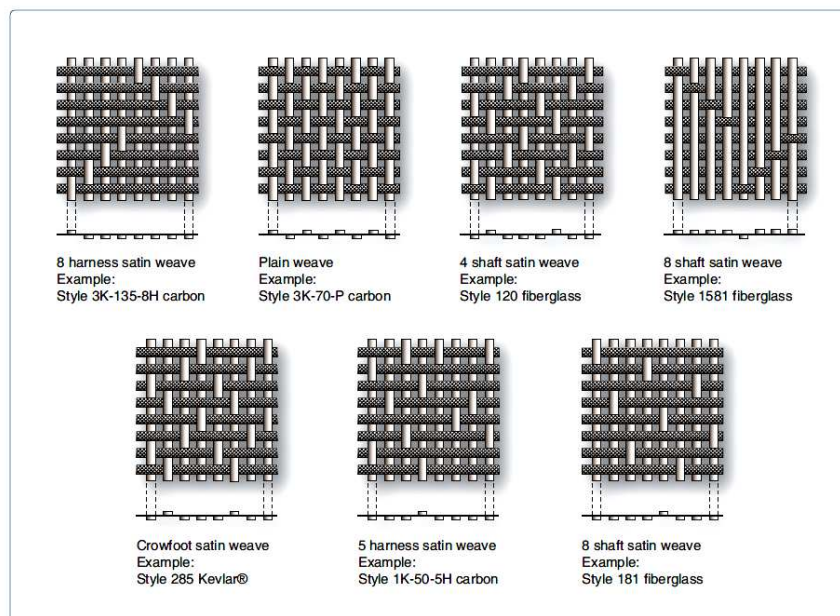


Fig. 14: Typical fabric weave styles [27].

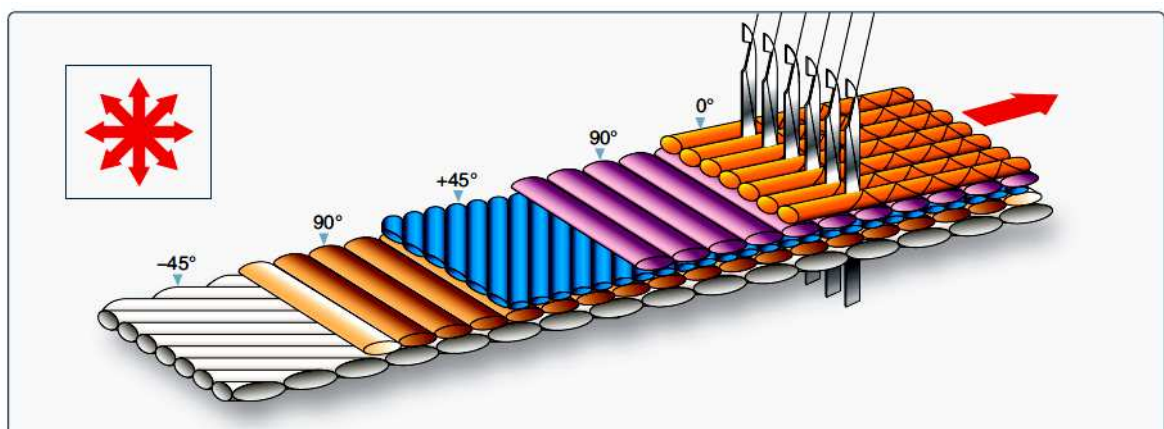


Fig. 15: Nonwoven material (stitched) [27].

1.12.4 Boron

Boron fibers are very stiff and have a high tensile and compressive strength. The fibers have a relatively large diameter and do not flex well; therefore, they are available only as a prepreg tape product. An epoxy matrix is often used with the boron fiber. Boron fibers are used to repair cracked aluminum aircraft skins, because the thermal expansion of boron is close to aluminum and there is no galvanic corrosion potential. The boron fiber is difficult to use if the parent material surface has a contoured shape. The boron fibers are very expensive and can be hazardous for personnel. Boron fibers are used primarily in military aviation applications.



Fig. 16: Fiberglass (left), Kevlar (middle), and carbon fiber material (right) [27].

1.12.5 Ceramic Fibers

Ceramic fibers are used for high-temperature applications, such as turbine blades in a gas turbine engine. The ceramic fibers can be used to temperatures up to 2,200 °F.

1.13 Matrix Materials

1.13.1 Thermosetting Resins

Resin is a generic term used to designate the polymer. The resin, its chemical composition, and physical properties fundamentally affect the processing, fabrication, and ultimate properties of a composite material. Thermosetting resins are the most diverse and widely used of all man-made materials. They are easily poured or formed into any shape, are compatible with most other materials, and cure readily (by heat or catalyst) into an insoluble solid. Thermosetting resins are also excellent adhesives and bonding agents.

1.13.2 Polyester Resins

Polyester resins are relatively inexpensive, fast processing resins used generally for low cost applications. Low smoke producing polyester resins are used for interior parts of the aircraft. Fiber-reinforced polyesters can be processed by many methods. Common processing methods include matched metal molding, wet layup, press

(vacuum bag) molding, injection molding, filament winding, pultrusion, and autoclaving.

1.13.3 Vinyl Ester Resin

The appearance, handling properties, and curing characteristics of vinyl ester resins are the same as those of conventional polyester resins. However, the corrosion resistance and mechanical properties of vinyl ester composites are much improved over standard polyester resin composites.

1.13.4 Phenolic Resin

Phenol-formaldehyde resins were first produced commercially in the early 1900s for use in the commercial market. Ureaformaldehyde and melamine-formaldehyde appeared in the 1920–1930s as a less expensive alternative for lower temperature use. Phenolic resins are used for interior components because of their low smoke and flammability characteristics.

1.13.5 Epoxy

Epoxyes are polymerizable thermosetting resins and are available in a variety of viscosities from liquid to solid. There are many different types of epoxy, and the technician should use the maintenance manual to select the correct type for a specific repair. Epoxyes are used widely in resins for prepreg materials and structural adhesives. The advantages of epoxyes are high strength and modulus, low levels of volatiles, excellent adhesion, low shrinkage, good chemical resistance, and ease of processing. Their major disadvantages are brittleness and the reduction of properties in the presence of moisture. The processing or curing of epoxyes is slower than polyester resins. Processing techniques include autoclave molding, filament winding, press molding, vacuum bag molding, resin transfer molding, and pultrusion. Curing temperatures vary from room temperature to approximately 350 °F (180 °C). The most common cure temperatures range between 250° and 350 °F (120–180 °C).

1.13.6 Polyimides

Polyimide resins excel in high-temperature environments where their thermal resistance, oxidative stability, low coefficient of thermal expansion, and solvent resistance benefit the design. Their primary uses are circuit boards and hot engine and airframe structures. A polyimide may be either a thermoset resin or a thermoplastic. Polyimides require high cure temperatures, usually in excess of 550 °F (290 °C).

Consequently, normal epoxy composite bagging materials are not usable, and steel tooling becomes a necessity. Polyimide bagging and release films, such as Kapton® are used. It is extremely important that Upilex® replace the lower cost nylon bagging and polytetrafluoroethylene (PTFE) release films common to epoxy composite processing. Fiberglass fabrics must be used for bleeder and breather materials instead of polyester mat materials due to the low melting point of polyester.

1.13.7 Polybenzimidazoles (PBI)

Polybenzimidazole resin is extremely high temperature resistant and is used for high temperature materials. These resins are available as adhesive and fiber.

1.13.8 Bismaleimides (BMI)

Bismaleimide resins have a higher temperature capability and higher toughness than epoxy resins, and they provide excellent performance at ambient and elevated temperatures. The processing of bismaleimide resins is similar to that for epoxy resins. BMIs are used for aero engines and high temperature components. BMIs are suitable for standard autoclave processing, injection molding, resin transfer molding, and sheet molded compound (SMC) among others.

1.14 Thermoplastic Resins

Thermoplastic materials can be softened repeatedly by an increase of temperature and hardened by a decrease in temperature. Processing speed is the primary advantage of thermoplastic materials. Chemical curing of the material does not take place during processing, and the material can be shaped by molding or extrusion when it is soft.

1.14.1 Semicrystalline Thermoplastics

Semicrystalline thermoplastics possess properties of inherent flame resistance, superior toughness, good mechanical properties at elevated temperatures and after impact, and low moisture absorption. They are used in secondary and primary aircraft structures. Combined with reinforcing fibers, they are available in injection molding compounds, compression-moldable random sheets, unidirectional tapes, prepregs fabricated from tow (towpreg), and woven prepregs. Fibers impregnated in semicrystalline thermoplastics include carbon, nickel-coated carbon, aramid, glass, quartz, and others.

1.14.2 Amorphous Thermoplastics

Amorphous thermoplastics are available in several physical forms, including films, filaments, and powders. Combined with reinforcing fibers, they are also available in injection molding compounds, compressive moldable random sheets, unidirectional tapes, woven prepregs, etc. The fibers used are primarily carbon, aramid, and glass. The specific advantages of amorphous thermoplastics depend upon the polymer. Typically, the resins are noted for their processing ease and speed, high temperature capability, good mechanical properties, excellent toughness and impact strength, and chemical stability. The stability results in unlimited shelf life, eliminating the cold storage requirements of thermoset prepregs.

1.14.3 Polyether Ether Ketone (PEEK)

Polyether ether ketone, better known as PEEK, is a high temperature thermoplastic. This aromatic ketone material offers outstanding thermal and combustion characteristics and resistance to a wide range of solvents and proprietary fluids. PEEK can also be reinforced with glass and carbon.

1.15 Curing Stages of Resins

Thermosetting resins use a chemical reaction to cure. There are three curing stages, which are called A, B, and C.

- A stage: The components of the resin (base material and hardener) have been mixed but the chemical reaction has not started. The resin is in the A stage during a wet layup procedure.
- B stage: The components of the resin have been mixed and the chemical reaction has started. The material has thickened and is tacky. The resins of prepreg materials are in the B stage. To prevent further curing the resin is placed in a freezer at 0 °F. In the frozen state, the resin of the prepreg material stays in the B stage. The curing starts when the material is removed from the freezer and warmed again.
- C stage: The resin is fully cured. Some resins cure at room temperature and others need an elevated temperature cure cycle to fully cure.

1.15.1 Pre-Impregnated Products (Prepregs)

Prepreg material consists of a combination of a matrix and fiber reinforcement. It is available in unidirectional form (one direction of reinforcement) and fabric form (several directions of reinforcement). All five of the major families of matrix resins can be used to impregnate various fiber forms. The resin is then no longer in a low-viscosity stage, but has been advanced to a B stage level of cure for better handling characteristics. The following products are available in prepreg form: unidirectional tapes, woven fabrics, continuous strand rovings, and chopped mat. Prepreg materials must be stored in a freezer at a temperature below 0 °F to retard the curing process. Prepreg materials are cured with an elevated temperature. Many prepreg materials used in aerospace are impregnated with an epoxy resin and they are cured at either 250 °F or 350 °F. Prepreg materials are cured with an autoclave, oven, or heat blanket. They are typically purchased and stored on a roll in a sealed plastic bag to avoid moisture contamination.

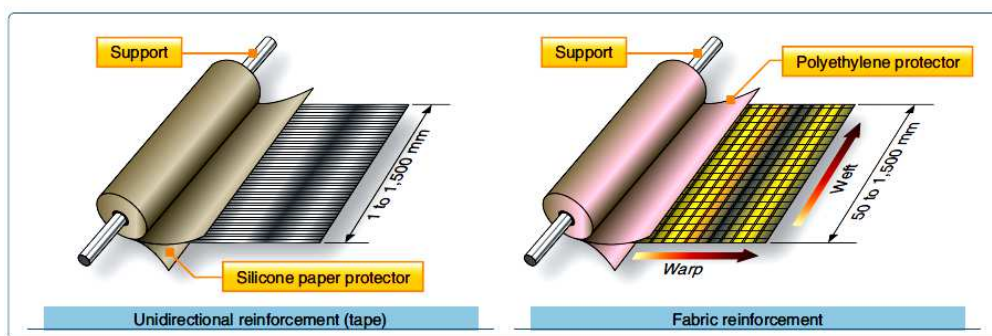


Fig. 17: Tape and fabric prepreg materials [27].

1.15.2 Dry Fiber Material

Dry fiber materials, such as carbon, glass, and Kevlar®, are used for many aircraft repair procedures. The dry fabric is impregnated with a resin just before the repair work starts. This process is often called wet layup. The main advantage of using the wet layup process is that the fiber and resin can be stored for a long time at room temperature. The composite can be cured at room temperature or an elevated

temperature cure can be used to speed up the curing process and increase the strength. The disadvantage is that the process is messy and reinforcement properties are less than prepreg material properties.

1.15.3 Thixotropic Agents

Thixotropic agents are gel-like at rest but become fluid when agitated. These materials have high static shear strength and low dynamic shear strength at the same time to lose viscosity under stress.

1.16 Adhesives

1.16.1 Film Adhesives

Structural adhesives for aerospace applications are generally supplied as thin films supported on a release paper and stored under refrigerated conditions ($-18\text{ }^{\circ}\text{C}$, or $0\text{ }^{\circ}\text{F}$). Film adhesives are available using high temperature aromatic amine or catalytic curing agents with a wide range of flexibilizing and toughening agents. Rubber-toughened epoxy film adhesives are widely used in aircraft industry. The upper temperature limit of $121\text{--}177\text{ }^{\circ}\text{C}$ ($250\text{--}350\text{ }^{\circ}\text{F}$) is usually dictated by the degree of toughening required and by the overall choice of resins and curing agents. In general, toughening of a resin results in a lower usable service temperature. Film materials are frequently supported by fibers that serve to improve handling of the films prior to cure, control adhesive flow during bonding, and assist in bond line thickness control. Fibers can be incorporated as short-fiber mats with random orientation or as woven cloth. Commonly encountered fibers are polyesters, polyamides (nylon), and glass. Adhesives containing woven cloth may have slightly degraded environmental properties because of wicking of water by the fiber. Random mat scrim cloth is not as efficient for controlling film thickness as woven cloth because the unrestricted fibers move during bonding. Spunbonded nonwoven scrims do not move and are, therefore, widely used.

1.16.2 Paste Adhesives

Paste adhesives are used as an alternative to film adhesive. These are often used to secondary bond repair patches to damaged parts and also used in places where film adhesive is difficult to apply. Paste adhesives for structural bonding are made mostly from epoxy. One part and two part systems are available. The advantages of paste adhesives are that they can be stored at room temperature and have a long shelf life. The disadvantage is that the bond line thickness is hard to control, which affects the strength of the bond. A scrim cloth can be used to maintain adhesive in the bondline when bonding patches with paste adhesive.

1.16.3 Foaming Adhesives

Most foaming adhesives are 0.025-inch to 0.10-inch thick sheets of B staged epoxy. Foam adhesives cure at $250\text{ }^{\circ}\text{F}$ or $350\text{ }^{\circ}\text{F}$. During the cure cycle, the foaming adhesives expand. Foaming adhesives need to be stored in the freezer just like prepregs, and they have only a limited storage life. Foaming adhesives are used to

splice pieces of honeycomb together in a sandwich construction and to bond repair plugs to the existing core during a prepreg repair. [27].

1.17 Composite fabrication method

Composite fabrication method in general can be divided into two main processes, namely open and closed moulding. For open mould technique, the top layer of the laminates and matrix are exposed to the atmosphere, resulting in uncontrolled surface condition [8]. Since the tooling fabrication process is relatively simple and low cost, rapid product development cycle is possible to be implemented using this method. The fabrication techniques are summarized in Table 7. The selection of fabrication method depends on several factors such as material, resin system, part complexity and application. Table 8 shows suitability of fabrication method with respect to the production amount.

Table 7: Fabrication method for open and closed mould [1].

Open Mould	Closed Mould
Hand Lay-Up	Vacuum Infusion Processing
Spray-up	Pultrusion
Filament Winding	Resin Transfer Moulding (RTM)
	Compression moulding
	Vacuum Bag Moulding

Table 8: Fabrication method according to volume production [1].

Low Volume	Medium Volume	High Volume
Hand Lay-Up	Filament Winding	Compression Moulding
Vacuum Bagging	Resin Transfer Moulding	Pultrusion
Spray Up	Centrifugal Casting	Continuous Lamination
Vacuum Infusion Processing	Wet Lay Up Compression Moulding	Reinforced Reaction Injection Molding (RRIM)

1.18 Sample fabrication process

The fabrication of a cylinder is described below in order to explain the basics of the automated tape winding process. The manufacturing process is divided in four stages: the preparation, the start, the process and the post-process. The preparation of the setup begins with the mounting of the spool on the spool holder. Then the tape is pulled manually up to the second tow guide (Figure 18). The winding machine is turned on. The motion axes of the winding machine are set. The winding program is loaded. The preheating channel and the nip heating are warmed up. The start procedure consists to feed the tape (at least up to the nip), to fix the incoming tape on the mandrel, to start the winding program and to apply the compaction force with the compaction roller. During the process, the spool supplies the composite material. The latter is warmed up in the preheating channel and by the nip heating. The incoming tape is compacted with the compaction roller at the nip. It is laid on different paths to fill free volumes. When the laying direction needs to be changed abruptly, the process can be stopped and restarted. The laid material composes the substrate, and its

quantity increases as the process is going on. The basic principle of the process is to bond (weld) on-line the incoming tape to the substrate (see sections 2.3.2, 2.3.3 and 2.3.4). The compaction force at the nip enforces the contact between the incoming tape and the substrate. The composite material must be warmed up in order to allow the bonding process. The process is terminated, when the desired quantity of composite material is laid on the planned locations. At this time, the winding program stops automatically. Then the incoming tape is cut and the compaction force is removed. Note that the substrate forms now the cylinder. Generally the cylinder and the mandrel constitute a single part at the end of the process. Therefore, a post-processing stage is necessary. The demolding is the action of separating the mandrel and the cylinder.

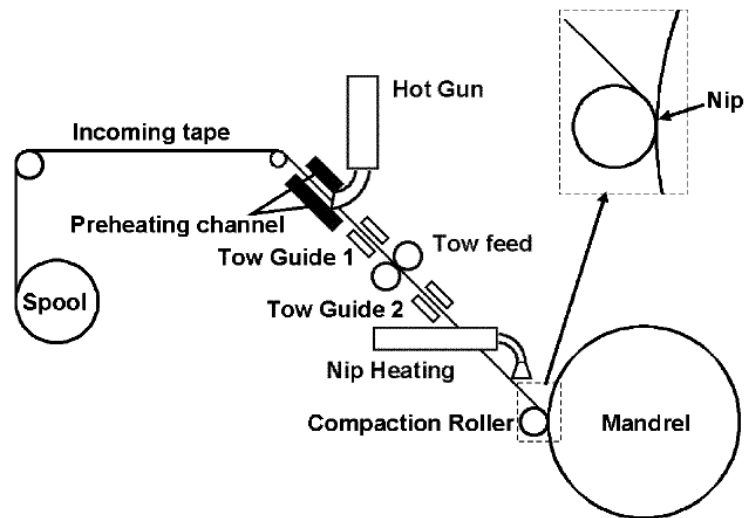


Fig. 18: Sketch of an automated tape winding setup at the ETH [1].

1.18.1 The incoming tape

The tapes are composed of fiber material and thermoplastic matrix: e.g. carbon fiber and poly-ether-ether-ketone or glass fiber and polypropylene. The advantages of tapes are that the fibers are pre-impregnated and the matrix pre-consolidated. This means that the fibers and the thermoplastic matrix are bounded, and that the void content is low. This enables to concentrate the research effort on the placement of the tape and the bonding between the substrate and the incoming tape. The latter is described in sections 2.3.2, 2.3.3 and 2.3.4. The disadvantage of the tapes is that they are expensive. The utilization of more usual preforms (bundles and yarns) permits therefore to reduce the material costs. On the other hand, the fibers need to be impregnated and the thermoplastic matrix consolidated in the bundles and yarns with matrix powder and fibers. The impregnation is the process that describes the evolution of the binding between the fibers and the matrix. The consolidation process depicts the reduction of the void content until the voids vanish. The impregnation and the consolidation stages must be performed on-line prior to the nip in the automated tape winding and the automated tape placement processes. They necessitates large compaction pressure and large energy inputs to heat the perform material closed to or above the melting temperature of the thermoplastic matrix. The elevated temperature

of the matrix is required to facilitate the deformations of the thermoplastic matrix and of the composite material.

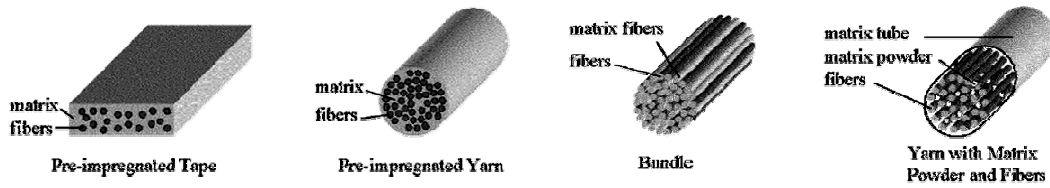


Fig. 19: Different types of preforms [1].

1.18.2 The nip point, line or curve

The nip is the location where the incoming tape comes into contact with the support or the substrate. In two-dimensional analysis, it is a point. In three dimensional analysis, the shape of the support (substrate) determines its form. It can be a line or a curve [1].

1.19 Filament winding

Filament winding is mainly used for fabricating open (cylinders) or closed end structures (pressure vessel or tanks) due to high stiffness-to-weight ratios. In a filament winding procedure, the fiber tows are wetted in a resin bath before being wound onto a mandrel in different orientations. The winding process is controlled by fiber feeding mechanism and rate of rotation of the mandrel. The schematic diagram of typical filament winding process. One of the well-known products of filament winding process is composite overwrapped pressure vessels (COPVs), which are vital to spacecraft propulsion, attitude control systems and life support applications. The COPV design requires integration between the analysis of the liner and the fiber overwrap. Ductile materials are usually used as the liners, such as soft aluminum, with only minimal load-sharing capabilities. The fiber is generally applied as ribbon of multiple tows wetted in resin bath. In previous research conducted by Madhavi et al. on design and analysis of filament wound COPV with integrated-end domes, material characterization of FRP of carbon T300/Epoxy for various configurations are determined using filament winding technique. It is found out that having alternate hoop and helical layers with hoop layers as the top and bottom most layers, gave the burst value of 12.4 MPa in the cylindrical zone [28].

Table 9: Characteristics of filament winding process [28].

Resins	Fibres	Advantages	Disadvantages
Matrix epoxy, polyester, polyvinyl ester, phenolic resin	Glass fibre, carbon fibre, aramid fibre, natural plant fibres (the fibres are used straight from a creel and not woven or stitched into a fabric form.)	1. Economic way of laying material down 2. Resin usage can be controlled 3. Minimum fibre cost 4. Good structural properties of laminates	1. Limited to convex shaped components 2. Difficult to lay fibre exactly along the length of component 3. High mandrel cost for large components

1.20 Automated Fiber Placement

Automated tow placement and tape placement are subsets of this method with the differences being in the starting materials and the material laydown rates feasible. The

fiber placement process automatically places multiple individual pre-preg tows onto a mandrel at high speed, using a numerically controlled, articulating robotic placement head to dispense, clamp, cut and restart as many as 32 tows simultaneously. Minimum cut length (the shortest tow length a machine can lay down) is the essential ply-shape determinant. The fiber placement heads can be attached to a 5-axis gantry, retrofitted to a filament winder or delivered as a turnkey custom system. Machines are available with dual mandrel stations to increase productivity. Advantages of fiber placement include processing speed, reduced material scrap and labor costs, parts consolidation and improved part-to-part uniformity. Often, the process is used to produce large thermoset parts with complex shapes. Automated tape laying (ATL) is an even speedier automated process in which pre-preg tape, rather than single tows, is laid down continuously to form parts. It is often used for parts with highly complex contours or angles. Tape layup is versatile, allowing breaks in the process and easy direction changes, and it can be adapted for both thermoset and thermoplastic materials. The head includes a spool or spools of tape, a winder, winder guides, a compaction shoe, a position sensor and a tape cutter or slit. In either case, the head may be located on the end of a multi-axis articulating robot that moves around the tool or mandrel to which material is being applied, or the head may be located on a gantry suspended above the tool. Alternatively, the tool or mandrel can be moved or rotated to provide the head access to different sections of the tool. Tape or fiber is applied to a tool in courses, which consist of one row of material of any length at any angle. Multiple courses are usually applied together over an area or pattern and are defined and controlled by machine-control software that is programmed with numerical input derived from part design and analysis. Capital expenditures for computer-driven, automated equipment can be significant [29].

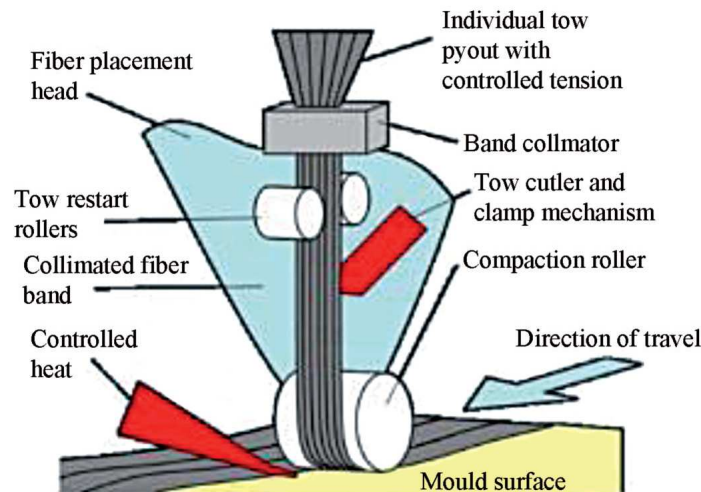


Fig. 20: Automatic Fiber Placement head laying pre-preg tape onto the mould [29]

Although ATL generally is faster than AFP and can place more material over longer distances, AFP is better suited to shorter courses and can place material more effectively over contoured surfaces. The latest equipment trend enables both AFP and ATL, switching between the two, in a matter of minutes, by swapping out dockable heads. Another development area is the pursuit of out of autoclave (OOA) in-situ

consolidation of high-performance thermoplastic ATL/ATP parts using laser heating and strategically placed mechanical rollers for consolidation. Both methods suffer, however, from the high capital cost of the equipment and facilities required. The payoffs with these methods for automobile applications are in large scale integrated, complex part fabrication where the lower assembly costs due to the reduced part count and reduced tooling fixture requirements can offset the capital costs [29].

1.20.1 Fiber arrangement

Samples were made from two configurations, first a UD arrangement by winding the co-mingled tows around a metal frame, and second from braided cloth made from the co-mingled fiber tows. The Herzog braiding machine at Technical University Munich (RF-128-100) uses a 128 bobbin set-up which can produce a tubular cloth with braiding angles between 30 and 60°. The 22% carbon fiber tows were 2mm in diameter and could be successfully braided at an angle of +45°. Various tubular diameters were braided, the most successful (in terms of good coverage of the mandrel) was 60mm. Once braided, the tubular cloth was cut to provide layers of cloth for hot compaction trials. The style of braiding was biaxial. The 13% carbon fiber tow was of a smaller diameter (~1mm) and so the maximum diameter that could be braided, without gaps, was slightly lower at 50mm. Figure 20 shows a picture of the braided cloth from the 22% carbon fiber tows and Figure 3b from the 13% carbon fiber tows. In both cases the bottom axis of the picture is 100mm long.



Fig. 21: Examples of braided cloth. Left hand side from 22% carbon fiber co-mingled tows, right hand side from 13% carbon fiber co-mingled tows.

The bottom axis of both images is equal to 100mm.

Future Composite Manufacturing Technology

A major new breakthrough in composites manufacturing technology is not likely to occur in the foreseeable future. Most likely, there will be a series of improvements to existing manufacturing technologies, and manufacturing concepts already generated will be proven. For composites to become competitive with metals, cost reduction has to occur in three areas: nonrecurring costs, recurring costs, and direct operating costs (DOC) (e.g., durability, maintainability, reliability, and repairability). IPD will continue to infiltrate all the disciplines for improved efficiency in design and manufacturing. It is expected that DOC will become a much bigger issue as many aircraft with composite components enter revenue service. There will be doubts as to

whether composites will ever become cost-effective for commercial use; however, these doubts can be assuaged by the facts. The reduction in manufacturing cost realized by improved technology will lose its value if it is offset by an increase in nonrecurring costs and DOC. Thus, life cycle cost analyses should be conducted along with the traditional trade-off studies of weight vs. strength and stiffness vs cost. Some of the manufacturing technology developments expected to occur in the foreseeable future is described below.

1.21 Stitched/RTM

Small to medium size stitched/RTM parts have been fabricated with some success; however, the fabrication of complete wing skins and box by this method is a long way off (Note: this method is not cost-effective for small to medium size thin parts; to take full advantage of this method, the parts must be thick and large). For this technology to be incorporated into wing design, an appropriate automatic stitching machine has to be developed. This machine must have the capacity to handle various skin thicknesses, ranging from less than 1/4" to more than 1", and with many different shape and thickness stiffeners attached to it. Concurrently, a new cost-effective resin system specifically for RTM application must be developed. Along with stitched/RTM manufacturing technology, other issues (e.g., repair method, certification, and joints) must be addressed and resolved.

1.22 Filament Winding

This is a mature manufacturing technique which has been in existence for a long time. Improvements in automation, speed, variable thickness, pad-up insertion, consistent quality, flexibility in fiber orientation, control of resin and void content, and shapes other than cylinders will be seen before more versatility appears in application. A combination of robotic and traditional filament winding (with seven to 10-axis) system is already available in crude form. If this system is perfected, it will be able to wind complex non-axisymmetric shapes, such as T and elbow shapes. One of the most critical requirements for a successful implementation of this method is controlling the tension of the deploying filament during the winding processes. This critical problem may be quickly solved with the aid of powerful computers.

1.23 Pultrusion

This method has the potential for cost reduction, but current technology is limited to constant cross sections and is restricted in fiber orientation. Pultrusion is not as popular as metal extrusions. Metal extrusions are attached to other structural members, such as skins and webs, by hundreds and thousands of fasteners and rivets. This method of assembly is not acceptable for composites, where the strong trend is to eliminate fasteners. Consequently, for pultrusion to become an acceptable and popular composites manufacturing technology, it must be possible to pultrude complex multi-element cross sections, such as J-stiffened panels and constant airfoil sections. It is expected that a new technique for making tapered sections with variable thickness and even variable shapes will be available within this decade; significant

progress has already been made toward that end in the last few years. Another new development is curved pultrusion. Preforming and braided pultrusion are variations of pultrusion for special applications. New developments can be expected in these areas.

1.24 Continuous Sandwich Panel

This method is already used in production. However, it is limited to making flat constant sandwich panels. Future improvements will increase speed of fabrication and quality. Floor panels, galleys, and partitions are the major uses of flat sandwich panels. Therefore, there is no need for a technology which produces a continuous sandwich panel of complex shapes and variable thickness.

1.25 3-D Weaving

The advantages of 3-D weaving are widely known, but the cost has been prohibitively high. A few automated and semi-automated systems have been created or are under development to reduce cost. Although 3-D weaving is still in its infancy, it has the potential to replace expensive titanium fittings, hinges, engine blades, etc. In addition to reduced costs of weaving, improvements in curing will be seen.

1.26 Mechatronics

Aircraft components in general and composite parts in particular have been known as hand-made custom products as opposed to automotive and electronic products. Full automation is probably not cost-effective for aircraft applications because of relatively low production rates. However, a semi-automated method using mechatronics may be a viable option for aircraft manufacturing. Currently, mechatronics is not a fully developed manufacturing technology, but its development should be followed with keen interest.

1.27 Automatic Tape Layup Machine

Significant progress has been observed in ATL technology. Both speed and accuracy have increased tremendously when compared to early ATL. Advancements in computer technology (hardware and software) have influenced ATL. Along with improvements in speed and accuracy, the capability in size of layup area has also increased. Although a new breakthrough is not expected to occur in ATL technology, improvements will be incremental but continuous.

1.28 Automatic Ply Cutting Machine

This technology has made significant progress in recent years. Three different methods of cutting are used for an APC machine: mechanical, laser, and water. Each has its own advantages and disadvantages. No new breakthroughs are expected in APC technology.

1.29 Tow Placement

Tow placement is relatively new and has received considerable attention in recent years. It combines the advantages of ATL and filament winding. Tow placement can

fabricate complex-shaped structures without limitations on fiber angles. It has the potential to reduce production costs significantly. Under the Air Force MANTECH and NASA ACT programs, this technology has proven its worth; however, its use at high production rates still remains to be seen. Future developments include optimized control systems, head position feedback, and in-process inspection for fast, accurate and high quality parts production.

1.30 Co-Curing Technology

The advantages of co-curing technology are numerous, but complex tooling, high risk, and the difficulty of adapting it to high production rates inhibit widespread usage. Continuous improvements in prepreg materials, tooling concepts, quick turnaround, and quality consistency may result in the elimination of those hurdles.

1.31 Forming, Stamping, Injection Molding, Rolling

These manufacturing methods have great potential for high volume production applications, especially when combined with the use of thermoplastics. Application is limited to small to medium size parts. Sporting goods and industrial products will benefit from this group of technologies.

1.32 Repair Technology

Repair technology is gaining more attention. Operators of aircraft are discovering that composites are showing a better service record than are metals, mainly due to their better fatigue and corrosion resistance properties. But at the same time composites are more prone to impact damages, which increase the importance of repair. As new generations of aircraft with tremendous amounts of composites enter flight service, both commercial and military operators will demand improved repair technology. Both the cost of repairs and the down-time resulting from the complexity and special facility and equipment requirements are putting severe demands on repair technology. Current repair technology is not satisfactory, and improvements are necessary.

1.33 Material Technology

Several years ago, the most popular topic in material technology was the "tough resin" system, followed by "thermoplastics." Today's popular materials are "stitched preforms," "tow placement," and "woven textile." Contrary to the original belief that thermoplastics greatly reduce manufacturing cost and time, the observation is now being made that thermoplastic parts cost more and are difficult to produce. In fact, some of the material suppliers are considering discontinuing thermoplastic production. It is still early to predict whether stitched preforms, tow placement, and textile will replace prepregs by the end of this decade. The next three years will be crucial for these so-called new advanced material systems to become dominant. It all depends upon how well these new materials can be adapted to a production mode where cost, quality and manufacturability play important roles. Operating temperatures of the High Speed Civil Transport will be 250°F to 450°F, depending upon the location of the structure within the aircraft. Epoxy systems alone cannot handle this temperature

range. The race for a new material system has already begun, and it is still too early to predict what will happen in an intensely competitive market. Candidate materials are polyimides, bismaleimides, metal matrix, ceramic matrix, etc [1].

Among the several manufacturing processes investigated in the past in the composite laboratory, the automated tape winding with on-line bonding is very promising. In comparison with the other techniques, it has a large potential in terms of economical attractiveness and implementation of tailored design solutions in the finished parts. Due to its high level of automation, the labor work is extremely reduced, the precision of the fiber orientation is high, and the reproducibility and the security during the process are enhanced. The automated tape winding process is very promising, but also very challenging. As tape bonding takes place during tape lay-up, the available process window is small. Since transient conditions exist during the automated tape winding process, the small process window is changing. When the process parameters are not adapted to the variations of the process conditions, the laminate respectively part quality will be affected. In order to fabricate lightweight products, the laminate quality must be maximized. For the automated tape winding process, the intralaminar quality is mainly dependent on the quality of the incoming tape. Therefore the main sensible properties depending on the process are the interlaminar bond properties. This signifies that the interlaminar bond properties must be optimized for the entire laminate with appropriate transient process conditions. The range of application of a process technique is related to the complexity of the parts that can be produced. During the placement of tapes on complex paths and/or geometries, the form of the nip varies rapidly. In order to bond correctly the tape to the substrate, the compaction system(s) must press the tape on its entire width for all the nip geometries [1]. The use of carbon fiber-reinforced composites has been growing exponentially in the past few decades. They offer excellent mechanical properties in combination with a low density, making them an ideal solution for many lightweight applications. However, they often suffer from a lack of toughness. In contrast with carbon fiber composites, self-reinforced (or all-polymer) composites have an excellent toughness, but a relatively low stiffness and strength. They consist of an oriented polymer fiber or tape in a matrix made from the same polymer. The present invention aims to break through the typical stiffness-toughness dilemma by hybridizing carbon fibers with self-reinforced polypropylene (SRPP) to design a material that has some optimum combination of stiffness and toughness [31].

Increasing global awareness on the environmental sustainability has led to numerous developments on renewable materials such as natural fibers in the fabrication of composite parts. Hybrid composites, which is a combination of two or more materials in a common matrix, has been implemented since natural fiber composites do not have adequate strength to substitute conventional synthetic fiber]. By having hybrid composites, the advantages of one type of fiber could complement what is lacking in the other, resulting in a balance in performance and cost through proper material design [3]. The mechanical properties of natural fiber reinforced composite (NFRC) such as stiffness, strength and moisture resistant behavior are also significantly improved by incorporation of stronger and more corrosion-resistant synthetic fiber

such as glass or carbon fiber. A study by M. Ramesh et al. [4] indicated that hybridization of glass fiber into sisal/jute reinforced epoxy composites showed good tensile strength of 68.55MPa. Another study by M. Thweet al. [5] depicted that incorporation of glass fiber up to 20% by mass with bamboo fiber increased tensile and flexural modulus by 12.5% and 10%, respectively. Sanjay [6] investigated flammability behavior and degradation of PP/banana and glass fiber-based hybrid composites and found out that hybridization with glass improved flame retardant characteristic. T. Subash et al. [7] discussed about bast fibers reinforced hybrid composites for aircraft indoor structures applications. These materials provide the benefits in the making of the body panels such as in seat cushions, cabin linings, parcel shelves and many more. The natural fibers such as jute, kenaf, bagasse, bamboo, coir, sisal proved that these materials have a greater strength in aerospace and automotive industry. These composites show lower density as compared to metal composites and have a higher potential to make lightweight sustainable finished parts that can reduce tremendous amount of energy consumption in the industry. There are various fabrication methods applicable for producing bio-sourced composites for usage in aerospace and automotive applications.

Hybridization of SRPP with carbon fibers resulted in a novel class of hybrid composites with a unique combination of stiffness, strength, ultimate failure strain and impact resistance. The key to the invention is to develop suitable strategies to maintain the toughness of the SRPP at the point when the carbon fibers fail. A key parameter in achieving this, is the bonding between both components. For strong bonding, the energy released by carbon fiber failure can create damage in the SRPP fraction, causing a decrease in the ultimate failure strain and hence toughness. For weak bonding, the hybrid composite can immediately delaminate over its entire length. The key is therefore to find the optimal level of bonding, thereby controlling the damage development while providing good stiffness and strength. A second key parameter is related to the distribution of the fibers in the hybrid composites. The carbon fibers should be distributed in the hybrid composites instead of grouped together in thick layers. Three strategies are proposed: thin layers (layer level), coveaving (intralayer level) and co-mingling (fiber level). The final parameter is the fiber volume fraction of the carbon fibers. At high fractions, the energy released by the carbon fibers can damage the SRPP. At an optimal fraction however, the ductility and impact resistance of SRPP can be maintained, while still achieving a substantial increase in stiffness and strength over a pure SRPP.

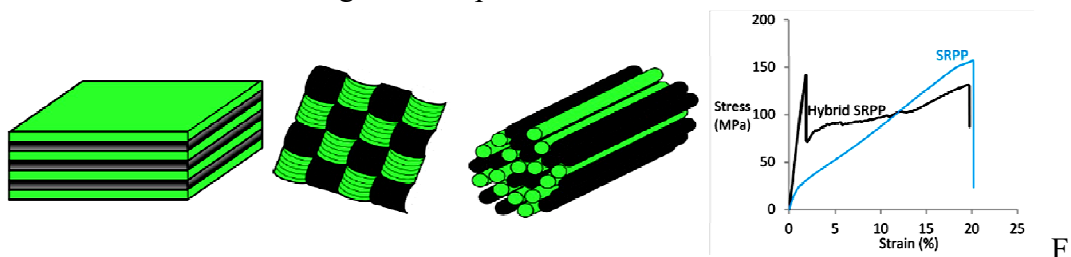


Fig. 22: Stress – Strain curve of SRPP [31]

The developed hybrid SRCs possess a unique combination of stiffness, strength and toughness. Since hybrid SRCs can be thermoformed, their products can be manufactured in high volumes. This material therefore has a strong potential to be used in the automotive industry [31].

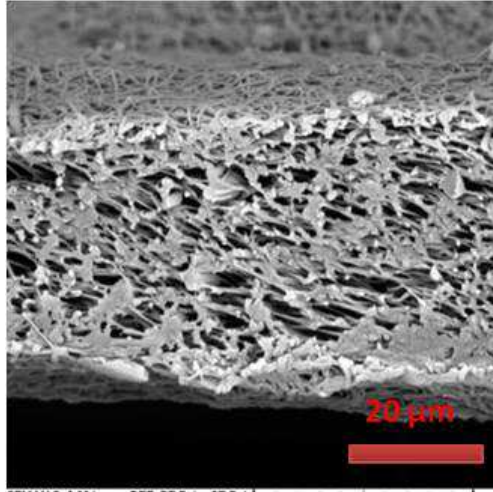
References

1. Yves Marcel Pierre Toso.: *Effective automated tape winding process with on-line bonding under transient thermal conditions*, Zurich, 2003, Swiss Federal Institute Of Technology, IMES, Center of Structure Technologies.
2. Fujita, A., Maekawa, Z., Hamada, H. Matsuda, M., Matsuo, T.: *Mechanical Behavior and Fracture Mechanism of Thermoplastic composites with Commingled Yarn*, Journal of Reinforced Plastics and Composites, Vol. 12, 1993, pp. 156-172.
3. Mader, E., Bunzel, U. and Mally, A., *Technische Textilien*, 1995, **38**, 205-208. and M.G. 3. Bader, in *Handbook of Composites*, vol. 4, ed. A. Kelly and S.T. Mileiko. Elsevier, New York, 1983.
4. Bader, M.G., in *Handbook of Composites*, vol. 4, ed. A. Kelly and S.T. Mileiko. Elsevier, New York, 1983.
5. Hauptert, F., Friedrich, K.: *Thermoplastic Filament Winding Using Powder Impregnated Yarns*, Advanced Composite Letters, Vol.2, pp.14-17, 1993.
6. Lauke, B., Friedrich, K.: *Evaluation of Processing Parameters of Thermoplastic Composites Fabricated by Filament Winding*, Composite Manufacturing, Vol.4, No.2, pp. 93–101, 1993.
7. Michaeli, W., Jürss, D.: *Thermoplastic pull-braiding: Pultrusion of profiles with braided fibre lay-up and thermoplastic matrix system (PP)*, Composites Part A, Vol. 27A, No.1, pp. 3-7, 1996.
8. B, Lauke., Bunzel, U., Schneider, K.: *Effect of hybrid yarn structure on the delamination behavior of thermoplastic composites*, Composites Part A, Vol. 29A, No.11, pp. 1397–1409, 1998.
9. Vinayak., O., Alagirusamya, R.: *Textile preforms for advanced composites*, Department of Textile Technology, Indian Institute of Technology, New Delhi 110 016, India. Received 25 July 2003; Revised received and accepted 10 October 2003.
10. Sondhelm, WS.: in *Handbook of Technical Textiles*, (edited by Anand SC), Woodhead Publications, Cambridge, pp. 62–94, 2000.
11. Punj, SK., Mukhopadhyay, A., Patnayak, A.: *Textile Asia*, 2002, 33(6), 33–36.
12. Mourtiz, AP., Banister, MK., Falzon, PJ., Leong KH.: *Review of applications for advanced three-dimensional fibre textile composite*, Composites Part A: Applied Science and Manufacturing, Vol.30, No.12, pp.1445-1461, 1999.
13. Mouritz, AP., Bains, C., Herszberg, I.: *Mode I interlaminar fracture toughness properties of advanced textile fibreglass composites*, Composites Part A: Applied Science and Manufacturing, Vol. 30, No. 7, pp. 859– 870, 1999.
14. Kmaiya R, C.B.A., Popper, P., Chou, TW.: *Some recent advances in the fabrication and design of three-dimensional textile preforms: a review*, Composites Science and Technology, Vol. 60, No. 1, pp. 33-47, 2000.
15. Ko, F.K.,Kutz, J.: *Multiaxial Warp Knit for Advanced Composites*, In: Proceedings of the Fourth Annual Conference on Advanced Composites , ASM International, pp. 367-370, 1988.

16. Mood, GI., Mahoubian-Jones, MGB.: International Patent WO 9 214 876, 3 (Bonas Machine Co. Ltd), 3 September 1992.
17. Greenwood, K., Zhao, L., Porat, I.: *Stress-orientated woven preforms for composites*, Journal of the Textile Institute, Vol. 84, No. 2, 255–266, 1993.
18. Hong, H., Filho, AA., Fanguerio, R., Araujo, MD.: *The development of 3D shaped knitted fabrics for technical purposes on a flat knitting machine*, Indian Journal of Fiber and Textile Research, Vol. 19, pp. 189-194, 1994.
19. Wilde, D., Zigmann, G.: Asian Textile Journal, pp. 95–90, 1997.
20. Weimer, C., *Preform-engineering: Applied sewing technologies to incorporate part and process functions into dry textile reinforcements*, Composites Science and Technology, Vol. 63, No. 14, pp. 2089–2098, 2003.
21. Sugino, M., Inoue, Y.: US Patent, 4 983 451 (To Kabushiki Kaisha Kobe Seiko Sho), January 1991.
22. Chen, B., Chou, TW.: *Compaction of woven fabric preforms: nesting and multilayer deformation*, Composites Science and Technology, Vol. 60, No. 12–13, pp. 2223–2231, 2000.
23. Long, AC., Rudd, CD., Blagdon, M., Smith, P.: *Characterizing the processing and performance of aligned reinforcements during preform manufacture*, Composites A, Vol.27, No.4, pp. 247–253, 1996.
24. Wang, J., Page, JR., Paton, R.: *Experimental investigation of the draping properties of reinforcement fabrics*, Composites Science and Technology, Vol.58, No.2, pp.229–237, 1998.
25. Page, J., Wang, J.: *Prediction of shear force and an analysis of yarn slippage for a plain-weave carbon fabric in a bias extension state*, Composites Science and Technology, Vol.6, No.7, pp.977–986, 2000.
26. Stöven, T., Weyrauch, F., Mitschang, P., Neitzel, M.: *Continuous monitoring of three-dimensional resin flow through a fibre preform*, Composites: Part A, Vol.34, No.6, pp.475–480, 2003.
27. https://www.faa.gov/regulations_policies/handbooks_manuals/aircraft/amt_airframe_handbook/media/ama_Ch07.pdf.
28. Zin, MH., Razzi, MF., Othman, S., Liew, K., Abdan, K., Mazlan, N.: *A review on the fabrication method of bio-sourced hybrid composites for aerospace and automotive applications*, IOP Conf. Series: Materials Science and Engineering, Vol.152, No.1, 2016.
29. Konrad, K.: *Automated Fiber Placement Systems Overview*, Transactions of the Institute of Aviation, Vol.245, No.4, pp. 52-59, 2016.
30. <https://lrd.kuleuven.be/doc/composite-materials-top>.

PART- II

Advanced Technical Fibrous Materials



SEM MAG: 5.00 kx DET: BE Det + SE Det
HV: 20.0 kV DATE: 05/27/15 20 µm Vega ©Tescan
VAC: HVac Device: TS5130 TU Liberec



A novel method of developing activated carbon web from waste acrylic fibers for effective EMI shielding applications

Muhammad Salman Naeem, Vijay Baheti, Jiri Militky, Veronika Tunakova, Syed Zameer Ul Hassan, Saima Javed, Qummer Zia Gilani, Hafiz Affan Abid, Jawad Naeem

*Faculty of Textile Engineering, Dept. of Material Engineering, Studentská 2,
Technical University of Liberec 461 17 Czech Republic*

1. INTRODUCTION

Nowadays electrically conductive textiles are gaining interest because of numerous applications in different fields like military and medical fields, as sensors and actuators and for electromagnetic shielding applications etc. Electrically conducting fabrics are obtained by different methods like metallization, electroless deposition, chemical coating, deposition of thin layers of conducting fillers like carbon black particles or carbon nanotubes or through the insertion of metallic yarns [1]. The synthetic fibers that are used in textiles are insulating materials having resistivity around $10^{15} \Omega / \text{cm}^2$. This resistivity is much higher than the desired resistivity for electromagnetic shielding and anti-electrostatic applications. For example the resistivity for shielding materials should be lower than $10^2 \Omega / \text{cm}^2$ and for anti-electrostatic materials it should be in the range of 10^9 - $10^{13} \Omega / \text{cm}^2$ [2]. In recent years, research on electromagnetic interference (EMI) shielding materials has attracted significant attention due to increase in electromagnetic population from widespread applications of computer and telecommunication technologies [3, 4]. Electromagnetic interference is a process in which electromagnetic energy from one device or circuit is transmitted to other device through conducted paths or radiations or both. The electromagnetic environment comprises on both conducted and radiated energy. Hence, electromagnetic compatibility has two possible aspects, susceptibility and emission. Susceptibility is the ability of a circuit or device to respond to unwanted electromagnetic energy also called noise. The immunity is opposite of susceptibility. The immunity level of a device or circuit is electromagnetic environment where device can work satisfactorily with well-defined level of safety. The difficulty in finding susceptibility or immunity levels is crucial what describes performance degradation. Emission pertains to interference hence causing potential of device or product. The objective in controlling emission is to reduce emitted electromagnetic energy in order to make working of other instruments smoothly [5]. By controlling emission of one product may reduce or eliminate interference problem for other products. Hence, it is desired to reduce emission so that electromagnetically compatible environment be established. The graphical presentation of EMI shielding

can be seen from figure 1. In modern applications of EMI shielding, along with technical protection of equipment, the protection of human beings operating the specific electrical equipment is also required. Hence, instead of using metallic sheets it is more appropriate to use different types of textile materials having additional benefit of flexibility and light weight.

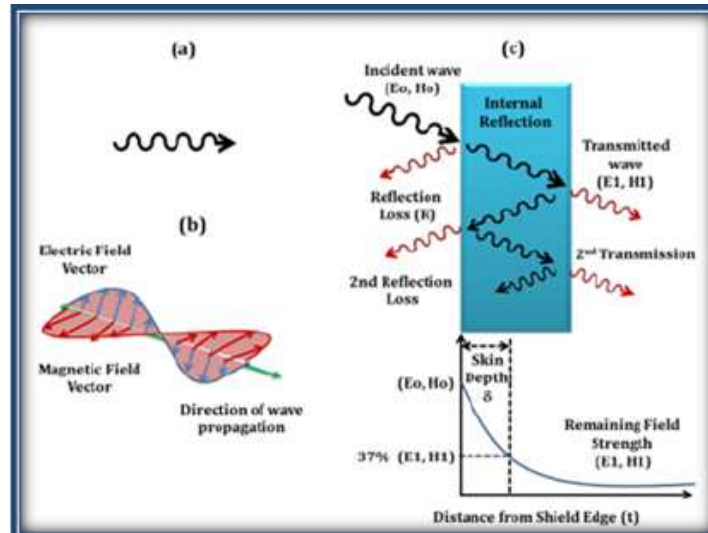


Fig. 1: EMI shielding mechanism, (a) EM wave representation, (b) shows the electric and magnetic field vector are perpendicular to the direction of wave propagation (c) Splitting of electromagnetic wave on passing through a shield [6]

The EMI shielding efficiency of materials is governed by reflection, absorption and multiple internal reflections of incident electromagnetic radiations [7, 8]. Reflection is commonly used shielding mechanism by high electrically conductive materials such as metals and their nanoparticles. However, high density, lack of flexibility, easy corrosion, costly processing and weak microwave absorption are main drawbacks of metals [9]. Recently, the carbon nanostructures and graphene are reported as promising alternatives to metal-based shielding materials [10]. The specific requirements for textile having electromagnetic shielding standards are given in table 1.

Table 1: Requirements for electromagnetic shielding textiles [11]

Type	Shielding Effectiveness (dB)	Classification
Class I (Professional use)	SE > 60 dB	Excellent
	60 dB ≥ SE > 50 dB	Very good
	50 dB ≥ SE > 40 dB	Good
	40 dB ≥ SE > 30 dB	Moderate
	30 dB ≥ SE > 20 dB	Fair
Class II (General use)	SE > 30 dB	Excellent
	30 dB ≥ SE > 20 dB	Very good
	20 dB ≥ SE > 10 dB	Good
	10 dB ≥ SE > 7 dB	Moderate
	7 dB ≥ SE > 5 dB	Fair

The shielding effectiveness of a material is equal to sum of reflection loss (R) plus sum of absorption loss (A) and plus a correction factor (B) to calculate multiple reflections in thin shields.

$$S = A + R + B \text{ [dB]} \quad (1)$$

Absorption loss, reflection loss and correction factors are all expressed in decibels. If the adsorption loss is greater than 9 dB then correction factor (B) can be neglected. General equations for adsorption and reflection loss are given as under.

$$A = 3.34t \sqrt{f \mu_r \sigma_r} \quad (2)$$

$$R = C + 10 \log \left(\frac{\sigma_r}{\mu_r} \right) \left(\frac{1}{f^{n_r m}} \right) \quad (3)$$

Here, 't' refers to the thickness of material in inches, 'f' is frequency in hertz, ' μ_r ' and ' σ_r ' are relative permeability and conductivity of the shield material respectively. In reflection loss equation, 'r' refers to distance from source to shield and C, n and m are constants to be used for calculating reflection loss. For eco-friendly advancements in EMI shielding effectiveness, the development of new light weight shielding materials having strong absorption and weak secondary reflection is necessary [12, 13]. This can be achieved by porous morphology, large specific surface area and higher electrical conductivity of shielding materials [14]. For instance, carbon-based shielding foams are considered predominant in effective shielding mechanism due to their light weight and the synergetic effect of electrical conductivity and multiple reflections. As a result, many lightweight polymer foams with graphene, CNTs, or carbon nano-fibers were produced [14-16]. Nevertheless, the addition of high concentration of electrically conductive nano fillers was found to cause undesirable effects on the foam ability of the polymers for formation of porous structure [17]. Therefore, the numbers of studies in recent years focused on the development of lightweight EMI shielding materials using various new approaches. Yan et al. proposed a combination of high-pressure compression molding plus salt-leaching method to fabricate porous graphene/polystyrene composites [18]. In addition, the chemical vapor deposition and self-assembly of highly aligned graphene sheets into 3D graphene porous structures was found to be efficient in improving the EMI shielding properties [19]. The development of carbon aerogels was attempted by some researchers to get maximum electromagnetic shielding due to their ultra-low density, ultra-high specific surface area, and large open pores [20].

Although number of research studies focused on development of porous carbon based EMI shielding materials, the construction of lightweight structures with excellent EMI shielding properties by simple and affordable method is still a big challenge. This work presented the simple and novel method for preparation of porous and electrically conductive activated carbon nonwoven web from acrylic fibrous wastes. The prepared activated carbon is advantageous over carbon made from other materials because of low cost, high density, better purity, and virtually dust-free nature of acrylic fibers [21]. The activated carbon web was prepared by sequential action of carding, needle punching and physical activation of acrylic fibrous wastes in presence of air. The

carbonization was performed under the layer of charcoal at 800 °C, 1000 °C and 1200 °C with the heating rate of 300 °C h⁻¹ and without any holding time. Further, electrical conductivity, EDX, X-ray diffraction, SEM, X-ray tomography and BET analysis was carried out to study the effect of carbonization temperature on physical and morphological properties of activated carbon web. At the end, the electromagnetic shielding ability of the produced three webs was investigated with respect to change in carbonization temperature and thickness of material using two different measurement approaches (i.e. waveguide method and coaxial transmission line method). In this way, the present study served to utilize large quantity of acrylic fibrous wastes for development of effective electromagnetic shielding materials.

Experimental methods

2.1. Materials

The acrylic fibrous waste was obtained from Grund Industries, Czech Republic in form of short lengths generated during mechanical processing of bath mats. The acrylic fibers are anionic copolymers containing 85-89% of acrylonitrile. Table 2 shows the physical properties of acrylic fibrous wastes.

Table 2: Physical properties of acrylic short fiber wastes.

Physical properties	
Fineness (Denier)	13
Tenacity (GPD)	2.7
Elongation (%)	45
Shrinkage (%)	2.5

Preparation of activated carbon nonwoven web

The fibers were further opened on laboratory roller card (Laboratory Roller Card, Befama, Poland) and converted into compact structure of non-woven web by using needle punching machine (Hansa, Germany). The speed of feeding the carded web to needle punching machine was fixed at the rate of 0.4 m/sec. The frequency of strokes was maintained at 200 strokes per minute with 5 mm depth of needle penetration. This produced the web having thickness of 11.6 mm and density 2.78 g/cm³.

The acrylic fibrous web was then cut into 30 cm (length) and 30 cm (width) for subsequent high temperature treatment using high temperature furnace (Elektrické Pece Svoboda, Czech Republic) for carbonization in two stages. The acrylic non-woven web was initially stabilized with 35 °C hr⁻¹ up to 250 °C to minimize the shrinkage during carbonization. During stabilization, predetermined tension was applied to avoid shrinkage. Later, the stabilized web was carbonized to 800 °C, 1000 °C and 1200 °C with different heating rate (150, 300 and 450 °C hr⁻¹) and no holding time under the layer of charcoal. The novel part of this study is single stage carbonization and physical activation in presence of air. The schematic of synthesis of activated carbon web from acrylic short fiber waste is shown in Fig. 2.

2.3 Characterization of activated carbon web

The physical properties of acrylic fibrous and activated carbon nonwoven web were determined in terms of shrinkage, flexibility and dusting tendency. The shrinkage

measurement was performed as per ASTM D 2259 standard available for testing textile fibers. The shrinkage was evaluated from change in length of acrylic fiber web before and after carbonization. The flexibility or stiffness was evaluated from bending length by employing the principle of cantilever bending of the web under its own weight as per ASTM D 1388 standard. The dusting tendency was evaluated from amount of generated dust particles after rubbing the surface of web on Taber wear and abrasion tester as per ASTM D 3884 standard. The rotary rubbing action was performed for 30 cycles under controlled conditions of pressure and abrasive action.

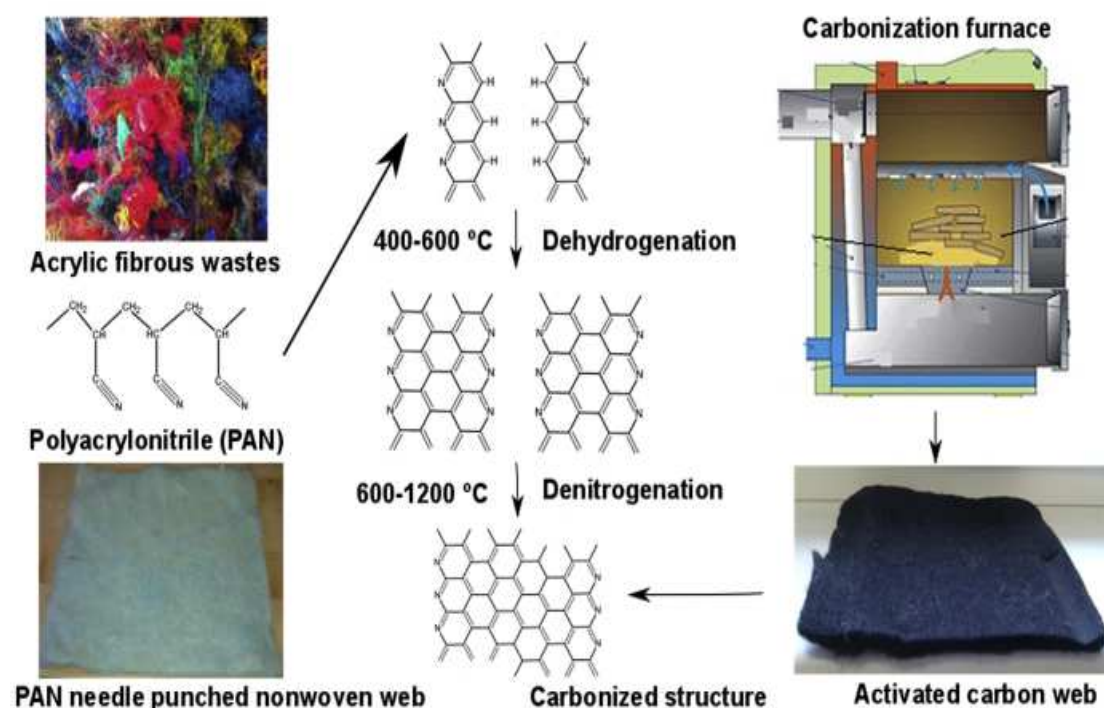


Fig. 2: Schematic of preparation of activated carbon from acrylic fibrous wastes

2.3.1. Energy dispersive x-ray (EDX) analysis

It was performed on Oxford Instruments, LZ 5 EDX detector, UK to know the change in relative proportion of different elements with respect to change in carbonization temperature.

2.3.2. X-ray diffraction (XRD) analysis

It was carried out on a PANalytical X₀ Pert PRO MPD diffraction system. The development of crystalline and amorphous regions in prepared activated carbon web was investigated with respect to change in carbonization temperature.

2.3.3. SEM analysis

The field emission scanning electron microscope Sigma, Zeiss, Germany was employed to investigate the morphology of acrylic fibrous web and prepared activated carbon web of 800 °C, 1000 °C and 1200 °C carbonization temperature. This helped to understand the development of porosity characteristics of activated carbon web with change in carbonization temperature. The micrographs were taken at 2 kV accelerated voltage and 1000 magnification. As prepared activated carbon web was electrically

conductive, so it was not metalized before test. However, the acrylic fibrous nonwoven web was metalized by sputter coating.

2.3.4. X-ray micro-computed tomography

In order to observe the three dimensional view of prepared activated carbon, the X-ray micro computerized tomography was performed on SKYSCAN 1272 of BRUKER. The micro graph of 1200 °C activated carbon web was compared with acrylic fibrous web at a pixel resolution of 1.60 mm. The scanned images of 5 mm length sample size were reconstructed using NRecon into three dimensional object, which was further analyzed for structural properties using CTan. A suitable thresholding was applied to remove the back ground noise. DE speckling function was operated to remove noise and to fill small holes within the fibers structure. Shrink-wrap technique was used to limit the region of interest boundaries as per the fiber spread contours. The CTvox and Data Viewer tools were utilized for visualization and measurement of image database.

2.3.5. BET surface area

The specific surface area of 1200 °C activated carbon web was measured from N₂ adsorption/desorption isotherms at 77.35 K using Autosorb iQ, Quantachrome Instruments, USA. The adsorption/desorption isotherm measurements were collected in the relative pressure range P/P_0 from 0.02 to 1, where P_0 is saturated pressure of nitrogen gas at 77.35 K temperature (i.e. 1 Atm). The samples were pre-treated in an oven at 45 °C in dry-room for at least 5 h and then out gassed overnight at 300 °C prior to the adsorption analysis. Both adsorption and desorption isotherms were obtained and the specific surface area was determined.

2.3.6. Electrical conductivity

Hewlett Packard 4339 B high resistance meter was used to measure the volume electrical resistivity of activated carbon web samples according to ASTM D257-14 at temperature 22 °C and relative humidity 40%. The specific voltage potential of 100 ± 5 V using direct current was applied across opposite ends of activated carbon web and resultant current flowing across the sample was measured after 15 ± 1 s.

2.4. Electromagnetic shielding effectiveness of activated carbon web

The electromagnetic shielding effectiveness of prepared activated carbon web was determined from two different measurement principles (i.e. waveguide method and coaxial transmission line method).

2.4.1. Waveguide method

The waveguide method examined the electromagnetic shielding ability at 2.45 GHz. This device consisted of a rectangular hollow waveguide having electrically conductive walls. A receiving antenna was placed inside of this waveguide, while a sample was placed at the entrance to the waveguide. A network analyzer Agilent E

4991A was used to generate, and a high frequency analyzer HF-38B (Gigahertz Solutions) was used to receive the electromagnetic signals. More details of this measurement method can be found in [22]. The electromagnetic shielding effectiveness SE [dB] was calculated based on Equation (4).

$$SE = 10 \log \frac{P_t}{P_i} \quad (4)$$

where P_t and P_i is power density (W/m^2) measured in presence of sample (transmitted), and without the sample (incident) respectively.

2.4.2. Coaxial transmission line method

The coaxial transmission line method examined the electromagnetic shielding ability in frequency range of 600 MHz to 1.5 GHz. This device determined electromagnetic shielding effectiveness using the insertion-loss method according to ASTM D 4935-10 standard [22]. The measurement set-up consisted of a sample holder with its input and output connected to the network analyzer. A shielding effectiveness test fixture (Electro-Metrics, Inc., model EM-2107A) was used to hold the sample. The network analyzer (Rohde & Schwarz ZN3) was used to generate and receive the electromagnetic signals.

3.1. Effect of carbonization parameters on properties of activated carbon web

3.1.1. Effect of carbonization temperature

The physical characteristics of activated carbon webs prepared at 800 °C, 1000 °C and 1200 °C of temperature, under 300 °C h⁻¹ heating rate and without any holding time are shown in table 3. The stabilization of acrylic fibers at 250 °C leads to cyclization, dehydrogenation, and oxidation of Polyacrylonitrile structure (Figure 2) [23]. During this stage, nitrile groups form non-meltable ladder structure, which further enhances mechanical properties and final carbon yield. During subsequent carbonization of stabilized web, the ladder polymer further cross links to form turbostatic carbon structure and the orientation of basal planes leads to graphite like structure.

Table 3: Effect of carbonization temperature on physical properties of activated carbon web

Temperature (°C)	Yield (%)	Shrinkage	Flexibility	Dusting
800	61.7	Good	Good	Good
1000	57.12	Good	Average	Average
1200	45	Average	Poor	Poor

From Figure 3, the specific surface area of prepared activated carbon web was found to increase with increase in carbonization temperature. The activated carbon web prepared at 1200 °C, 1000 °C and 800 °C exhibited the specific surface area of 278 m²/g, 190 m²/g and 120 m²/g respectively. This behavior was attributed to gradual reaction of atmospheric oxygen with carbonized acrylic fibrous waste, which resulted

into the opening of previously inaccessible pores through the removal of tars and disorganized carbon [21]. Therefore, the increased surface area at high temperature was indication of increase in porosity due to free spaces created by decomposition of organic matter.

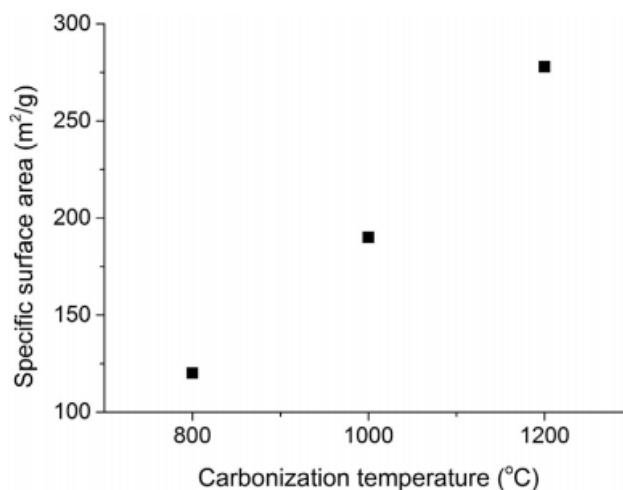


Fig. 3: Effect of carbonization temperature on specific surface area of activated carbon web.

3.1.2. Effect of pre-tension during stabilization

The pre-tension applied on the web during stabilization was found to affect the shrinkage, flexibility and dusting behavior of prepared activated carbon web. Figure 4 shows the significant amount of shrinkage exhibited by carbonized sample (1200 °C temperature, 300 °C h⁻¹ of heating rate and no holding time) when there was no pre-tension applied during the stabilization. This behavior can be explained from higher entropic and chemical shrinkage occurred in absence of pre-tension. The entropic shrinkage resulted from strain relaxation of molecular chains, whereas chemical shrinkage resulted from formation of cyclized ladder structure. The rate and magnitude of this shrinkage depends on various factors such as surrounding atmosphere, applied load and heating rate etc. [23].

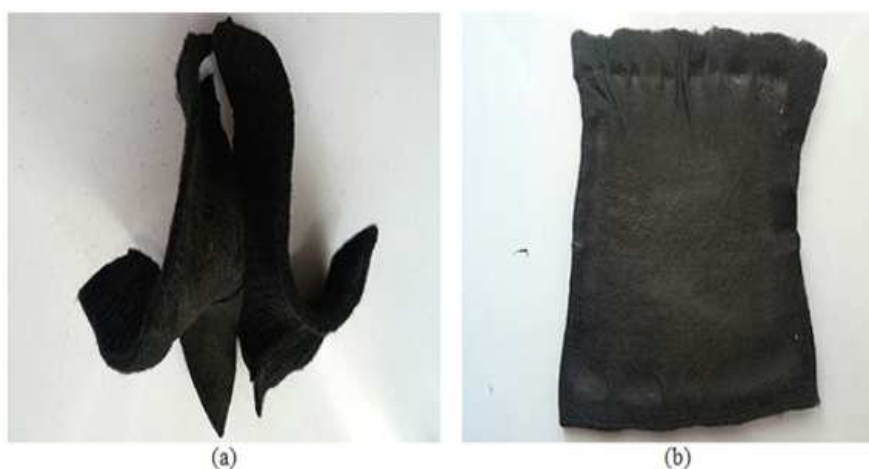


Fig. 4: Activated carbon from stabilization (a) without any pre-tension, (b) with applied pre-tension.

3.2. Characterization of activated carbon web

3.2.1. EDX analysis

Energy disperse x-ray spectroscopy was performed to know the relative proportion of different elements present in the activated carbon webs. From table 4, the increase in carbon content and

reduction in oxygen content was found with increase in carbonization temperature from 800 °C to 1200 °C. The activated carbon web produced at 1200 °C exhibited 92.49 % carbon content and 6.61 % oxygen content. This behavior was attributed to removal of hydrogen, sulfur, nitrogen and other elements due to decomposition at higher temperature.

Table 4: Effect of carbonization temperature on elemental composition of AC web

Element	App conc.	Intensity	Weight (%)	Atomic (%)
800 °C				
CK	0.26	2.12	0.13	91.76
OK	0.01	0.761	0.01	8.24
1000 °C				
CK	0.37	2.12	0.18	91.87
OK	0.02	0.760	0.02	8.13
1200 °C				
CK	0.18	2.10	0.09	92.49
OK	0.01	0.744	0.01	6.61
CaK	0.00	0.902	0.00	0.90

3.2.2. XRD analysis

In order to know the development of crystallinity with increase in carbonization temperature, the XRD analysis was carried out. Fig. 5 shows the XRD pattern of different activated carbon samples produced at 800 °C, 1000 °C and 1200 °C temperature. The crystallinity of material can be identified from nature of peaks present in the XRD pattern. The intensity and sharpness of peak was found to increase with increase in carbonization temperature. This confirmed the development of higher crystallinity in activated carbon samples produced at higher temperature. The strongest diffraction peak was found at 25.5°, which confirmed the presence of hexagonal graphitic structure due to C (002) reflection [13]. The other diffraction peaks found at 43° and 52.5° were associated with C (100) and C (004) diffraction of graphitic structure. The presence of sharp and intense peak for 1200 °C activated carbon sample showed more transformation of amorphous structure into graphitized structure. This is useful observation to support the results of increased electrical conductivity of activated carbon samples described in further sections.

3.2.3. SEM morphology

In order to know the development of porosity after carbonization of acrylic fibrous wastes, the surface morphology of acrylic fibers before and after carbonization was

studied from SEM images. Figure 6 (a-d) show the SEM images of acrylic fibrous web and activated carbon web produced at temperature of 800 °C, 1000 °C and 1200 °C respectively. The activated carbon web showed noticeable rough surface as compared to acrylic fibrous web. The surface roughness was found to increase with increase in carbonization temperature, which indicated the development of more porous structure after physical activation of acrylic fibrous wastes.

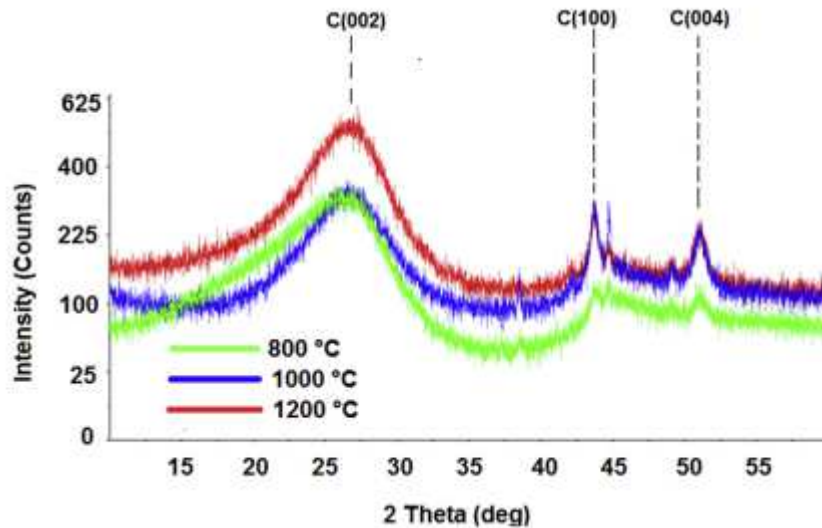


Fig. 5: Effect of carbonization temperature on crystallinity of activated carbon web.

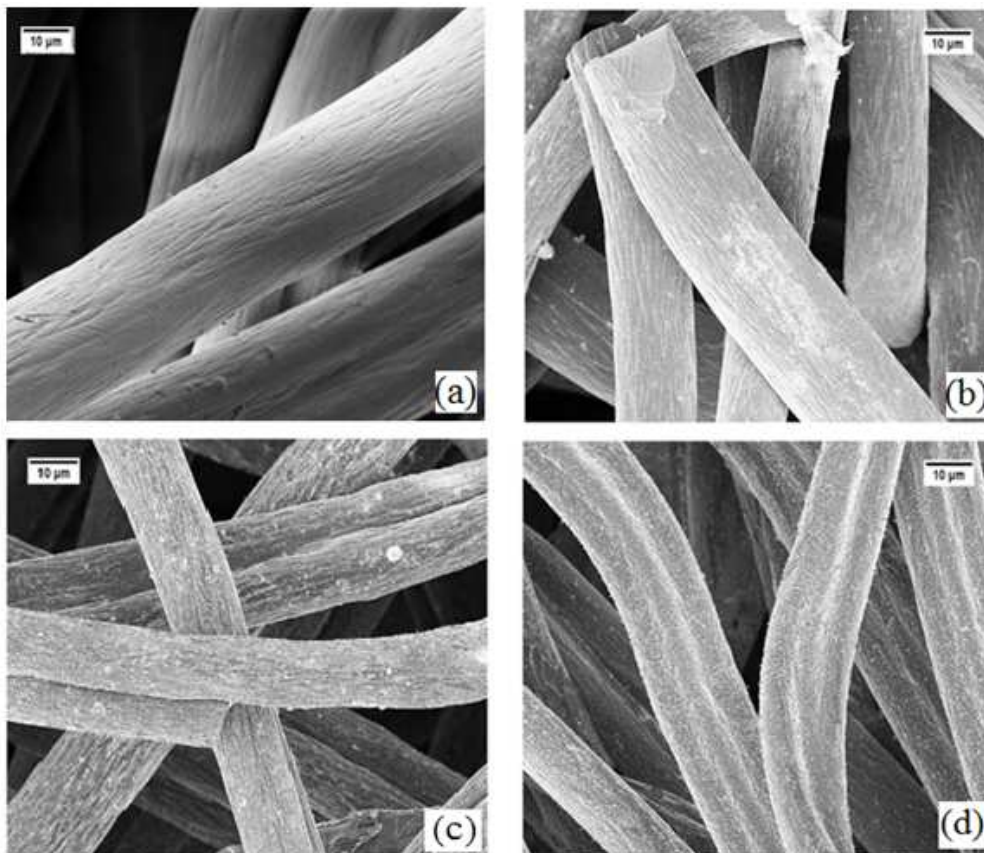


Fig. 6: SEM image of (a) acrylic fibrous web (b) 800 °C activated carbon web (c) 1000 °C activated carbon web (d) 1200 °C activated carbon web

3.2.4. Three dimensional morphology

The three dimensional morphology of acrylic fibrous and 1200 °C activated carbon web can be seen from Figure 7 (a) and (b) respectively. The diameter of individual fibers in the web was found to become thinner after carbonization. For measurement of diameter distribution, the obtained images were processed and analyzed using image analysis software. The background noise was removed and morphological operations were performed using DE speckling function. After careful thresholding of images, the number of fibers for particular range of fiber diameter was examined. Figure 8 shows the diameter distribution of fibers for acrylic fibrous and activated carbon web. The number of smaller diameter fibers in activated carbon web was found in higher quantity than the acrylic fibrous web. This further justified the development of higher surface area after controlled carbonization of acrylic fibers.

3.2.5. BET analysis

For electromagnetic shielding effectiveness to be achieved through absorption of radiations, the knowledge of pore characteristics and specific surface area of samples is necessary. Figure 9 shows the nitrogen adsorption/desorption isotherm of activated carbon web prepared at 1200 °C of carbonization temperature, 300 °C h⁻¹ of heating rate and no holding time.

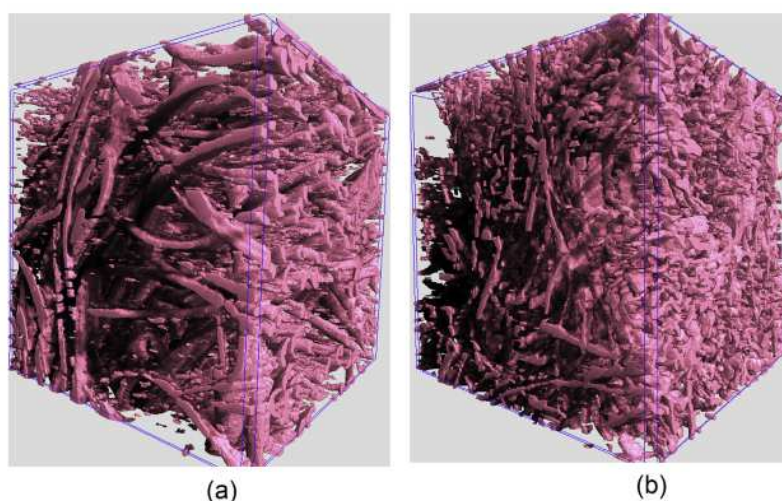


Fig. 7: Three dimensional view at 500 μm scale for (a) acrylic fibrous web (b) 1200 °C activated carbon web.

A rapid rise in the adsorption/desorption isotherm was found at low relative pressures, which was followed by a horizontal plateau at higher relative pressures. This behavior indicated type I isotherm based on the classification of the International Union of Pure and Applied Chemistry (IUPAC) [24, 25]. The type I isotherm confirmed that micropore was developed in the activated carbon web produced at 1200 °C. The pore volume and pore diameter of this activated carbon web was found 0.437 cc/g and 3.062 nm, respectively from BJH analysis. In accordance to IUPAC classification, the adsorbent pores are classified into three groups: micropore (diameter < 2 nm), mesopores (2-50 nm), and macropore (> 50 nm) (26). Therefore, the prepared activated carbon at 1200 °C predominantly exhibited mesoporous nature.

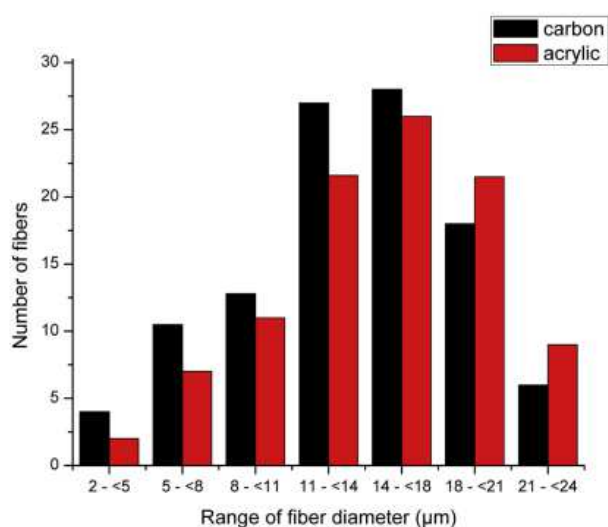


Fig. 8: Distribution of fiber diameter evaluated from computed tomography images

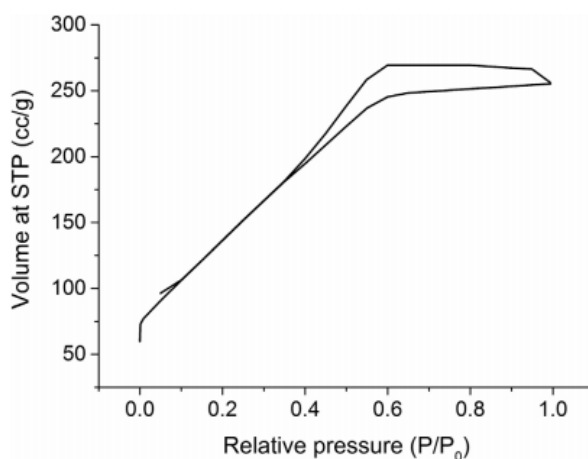


Fig. 9: Nitrogen adsorption-desorption isotherm of 1200 °C activated carbon web.

3.2.6. Electrical conductivity

For electromagnetic shielding effectiveness to be achieved through reflection of EM radiations, the knowledge of electrical conductivity of samples is necessary. Figure 10 shows the average values in 95% confidence interval for electrical resistivity of activated carbon web samples. The electrical resistivity was found to decrease with increase in carbonization temperature. The linear regression model was applied and 76.15% coefficient of determination was found between carbonization temperatures and achieved electrical resistivity. The 1200 °C activated carbon sample exhibited 1000 times reduction in electrical resistivity over 800 °C activated carbon sample. The higher electrical conductivity of 1200 °C activated carbon sample was attributed to more graphitization, which was confirmed from presence of sharp diffraction peak observed in XRD spectra (Figure 10).

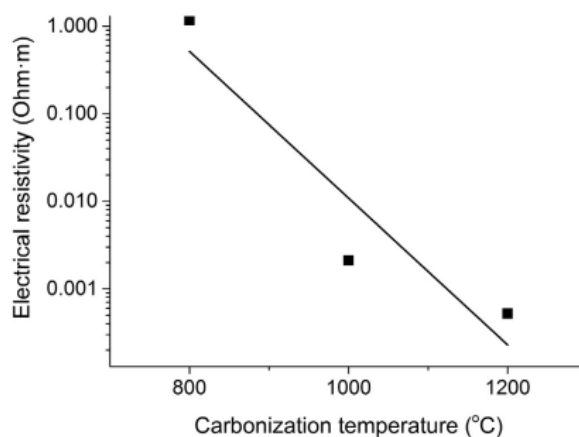


Fig. 10: Effect of carbonization temperature on electrical conductivity of activated carbon web.

3.2.7. Mechanism of charge transport

Figure 11 (a-c) shows the two possible modes of electron transport (i.e., migration and hopping) in the activated carbon web produced at 800 °C, 1000 °C and 1200 °C, respectively. The development of electrical conductivity can be explained from the migration of electrons in one graphite layer or their jumping across the defects/interfaces between disordered graphite layers [27-29]. The higher electrical conductivity indicated relatively easier migration and hopping of electrons in case of 1200 °C activated carbon than 800 °C and 1000 °C activated carbon samples. This behavior can be attributed to their higher graphite content, uniform distribution of graphite layers, reduced fiber diameter, etc. shown in Figure 11, which ultimately resulted into the formation of dense micro-current network in 1200 °C activated carbon structure [30, 8].

3.3. Electromagnetic shielding ability

3.3.1. Waveguide method

Figure 12 (a-b) show the average values in 95% confidence interval for electromagnetic shielding effectiveness of prepared activated carbon web in single and double layers measured at 2.45 GHz frequency. The electromagnetic shielding effectiveness was found to increase with increase in number of layers and increase in carbonization temperature. The electromagnetic shielding effectiveness of 28.29 dB, 26.06 dB and 3.34 dB was exhibited by single layers of activated carbon web produced at 1200 °C, 1000 °C and 800 °C, respectively. At very low carbonization temperature, the shielding effectiveness remained similar to that of non-carbonized Polyacrylonitrile substrate (i.e. zero).

Then, the shielding effectiveness was found to increase dramatically over a very narrow range of carbonization temperature, which was connected to the amount of carbon/graphite phase present in the structure. This point is called the percolation threshold, which showed minimum carbonization temperature required for maximum increase in conductivity for higher shielding effectiveness. In present study, the percolation threshold was found between the range of 800 °C and 900 °C carbonization temperature. The maximum shielding effectiveness in this range was attributed to increased multiple internal reflections and stronger absorption of

electromagnetic radiations due to higher electrical conductivity, higher porosity and higher surface area. The dramatic increase of shielding ability could not be expected with further increase of carbonization temperature ($T > 1100\text{ }^{\circ}\text{C}$). Therefore, the usage of $1000\text{ }^{\circ}\text{C}$ carbonization temperature was considered optimal with regard to its relatively high electromagnetic shielding ability and satisfactory mechanical properties. The similar trend was found for double layers of activated carbon, where shielding effectiveness was increased by 13% in case of $1000\text{ }^{\circ}\text{C}$ activated carbon web.

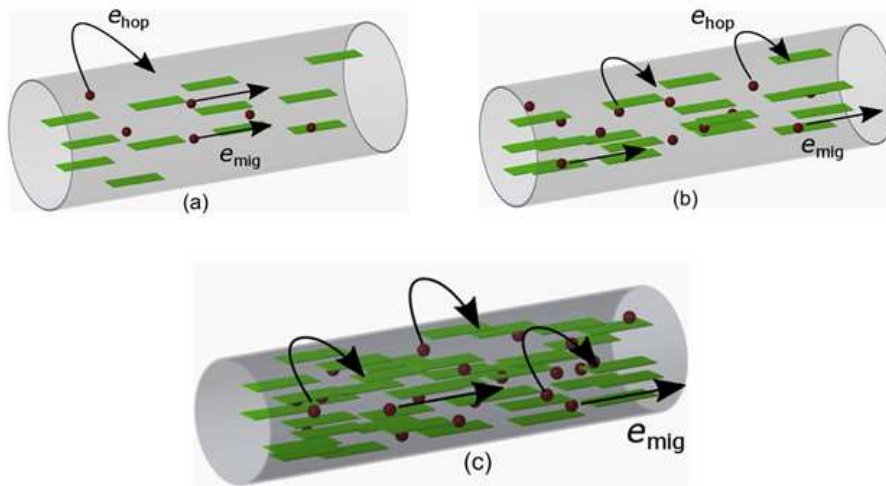


Fig. 11: Mechanism of charge transport in (a) $800\text{ }^{\circ}\text{C}$ activated carbon (b) $1000\text{ }^{\circ}\text{C}$ activated carbon (c) $1200\text{ }^{\circ}\text{C}$ activated carbon

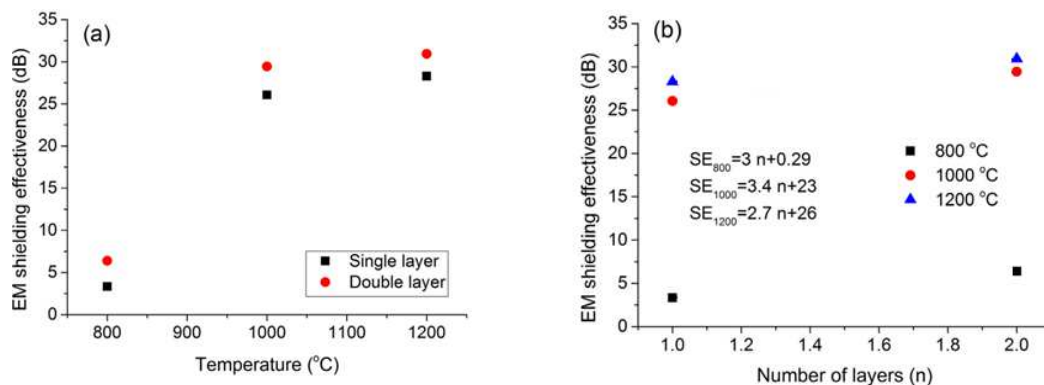


Fig. 12: (a). Effect of carbonization temperature on electromagnetic shielding effectiveness at 2.45 GHz (b). Effect of number layers on electromagnetic shielding effectiveness at 2.45 GHz

This behavior was attributed to increase in thickness with increase in number of layers.

3.3.2. Coaxial transmission line method

Fig.13 (a-b) show the mean values of electromagnetic shielding effectiveness for single layers of activated carbon samples in frequencies of 600 MHz, 1 GHz and 1.5 GHz. The increase in shielding effectiveness with increase in carbonization

temperature was observed. The single layer of 800 °C activated carbon web revealed the lowest electromagnetic shielding effectiveness of about 5 dB in frequency range of 600 MHz to 1.5 GHz. On the other hand, the 1200 °C activated carbon web exhibited the shielding ability of 63.26 dB, 66.75 dB and 75.44 dB for respective frequencies of 600 MHz, 1 GHz and 1.5 GHz.

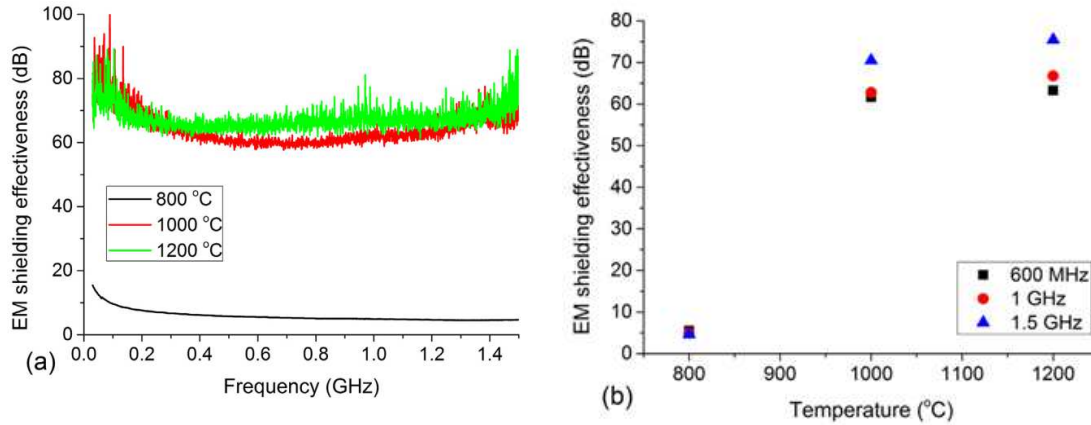


Fig. 13: (a). Effect of frequency on electromagnetic shielding effectiveness. (b). Effect of carbonization temperature on electromagnetic shielding effectiveness in low frequency region

3.3.3. Mechanism of EMI shielding

The phenomena of reflection, absorption and multiple internal reflections of electromagnetic radiations contribute to the EMI shielding efficiency. The reflection is related to the impedance mismatch between air and absorber. The presence of surface nomadic charges or mobile charge carriers (electrons or holes) is considered as the most important factor for the reflection mechanism [27, 8]. Absorption is the second important mechanism and it depends on the thickness of the shield. Absorption arises from Ohmic loss and polarization loss [30]. Ohmic loss comes from the dissipation of energy by nomadic charges through conduction, hopping and tunneling mechanisms, whereas polarization loss originates from the energy required for overcoming the momentum to reorient the dipoles in each half cycle of the EM wave. The polarization is derived from functional groups, defects and interfaces within the material. The third mechanism is multiple internal reflections which represent scattering effect within the shielding material due to its inhomogeneity and huge interfacial area [7]. The 1200 °C activated carbon web exhibited higher EMI shielding properties due to increased multiple internal reflection and stronger absorption of EM waves. This behavior was attributed to the development of heterogeneous surface with increased electrical conductivity and porosity at higher carbonization temperature. This can be explained further from Figures 5, 8, 11 (c), where 1200 °C activated carbon web showed increased graphite content, uniform dispersion of graphite layers, reduced fiber diameter, etc. The greater number of nomadic charges (from increased graphite content in figure 5) coupled with their uniform state of dispersion led to elongated electrons' mean free paths and enhanced conductive network which consequently dissipated more electrical energy and thus higher Ohmic loss. The reduced fiber diameter in figure 8 provided larger conductive

surface area for dissipation of incident EM wave. Moreover, non-homogeneous surface characteristics of 1200 °C activated carbon web in figure 6 (d) could indicate enhanced EMI shielding further from higher polarization loss.

4. Conclusions

The present study was focused on development of porous and electrically conductive activated carbon based electromagnetic shielding materials from acrylic fibrous wastes. The simple and novel approach was employed to introduce absorption and reflection properties of electromagnetic radiations into the shielding materials. This was achieved by physical activation of needle punched nonwoven web of acrylic fibers. The carbonization was performed under the layer of charcoal at 800 °C, 1000 °C and 1200 °C with the heating rate of 300 °C h⁻¹ and without any holding time. Further, the influence of carbonization temperature on physical and morphological properties of activated carbon web was studied from EDX, X-ray diffraction, SEM, X-ray tomography and BET analysis. In the end, the utility of prepared activated carbon web was investigated for electromagnetic shielding ability in high frequency (i.e. 2.45 GHz) and low frequency regions (i.e. below 1.5 GHz) using waveguide method and coaxial transmission line method, respectively. At 2.45 GHz, the electromagnetic shielding effectiveness of 28.29 dB, 26.06 dB and 3.34 dB was exhibited by single layers of activated carbon web produced at 1200 °C, 1000 °C and 800 °C, respectively. On the other hand, for low frequency regions, the 1200 °C activated carbon web exhibited the shielding ability of 63.26 dB, 66.75 dB and 75.44 dB for respective frequencies of 600 MHz, 1 GHz and 1.5 GHz. This behavior was attributed to increased multiple internal reflections and stronger absorption of electromagnetic radiations, which resulted from greater number of nomadic charges (i.e. graphite content), uniform dispersion of graphite layers, reduced fiber diameter, elongated electrons' mean free paths, larger surface area, higher porosity and enhanced conductive network formation in 1200 °C activated carbon.

ACKNOWLEDGEMENT

This work was supported under the student grant scheme (SGS-21198) by Technical University of Liberec, Czech Republic.

References

1. Daniela, N., Cozmin-Toma, B., Dorin, A.: *Electrical Conductivity of Woven Fabrics Coated with Carbon Black Particles*. *Fibres Text East Eur*, 2012, vol. 20, 53–6.
2. Chen, H, C., Lee, K, C., Lin, J, H., Koch, M.: *Comparison of electromagnetic shielding effectiveness properties of diverse conductive textiles via various measurement techniques*. *J Mater Process Technol*, 2007, vol. 192, 549–54.
3. Safarova, V., Tunak, M., Militký, J.: *Prediction of hybrid woven fabric electro-magnetic shielding effectiveness*, *Text Res J*, 2015, vol. 85, 673–86.
4. Safarov, V., Militký, J.: *Electromagnetic shielding properties of woven fabrics*

- made from high performance fibers*. Text Res J, 2014, vol. 84,1255–1267.
5. Chung, D, D, L.: *Electromagnetic interference shielding effectiveness of carbon materials*, Carbon N Y, 2001, vol. 39, 279–85.
 6. Tong, X.: *Advanced materials and design for electromagnetic interference shielding*. CRC press, 2008.
 7. Sano, E., Akiba, E.: *Electromagnetic absorbing materials using nonwoven fabrics coated with multi-walled carbon nanotubes*, Carbon N Y, 2014, vol. 78, 463–468.
 8. Arjmand, M., Sundararaj, U.: *Electromagnetic interference shielding of Nitrogen-doped and Undoped carbon nanotube/polyvinylidene fluoride nanocomposites: a comparative study*, Compos Sci Technol, 2015, vol. 118, 257–263.
 9. Rubeziene, V., Baltusnikaite, J., Varnaite-Zuravliova, S., Sankauskaite, A., Abraitiene, A., Matuzas, J.: *Development and investigation of electromagnetic shielding fabrics with different electrically conductive additives*, J Electrostat, 2015, vol. 75, 90–98.
 10. Wang, L, L., Tay, B, K., See, K, Y., Sun, Z., Tan, L, K., Lua, D.: *Electromagnetic interference shielding effectiveness of carbon-based materials prepared by screen printing*, Carbon N Y, 2009, vol. 12, 905–1910.
 11. Henry, O, O.: *Electromagnetic compatability engineering*. New Jersey: John Wiley & Sons; 2009.
 12. Inagaki, M., Qiu, J., Guo, Q.: *Carbon foam: preparation and application*, Carbon N Y, 2015, vol. 87, 128–152.
 13. Kim, J, H., Jeong, E., Lee, Y, S.: *Preparation and characterization of graphite foams*, J Ind Eng Chem, 2015, vol. 32, 21–33.
 14. Li, Y., Shen, B., Pei, X., Zhang, Y., Yi, D., Zhai, W.: *Ultrathin carbon foams for effective electromagnetic interference shielding*, Carbon N Y, 2016, vol. 100, 375–85.
 15. Farhan, S., Wang, R., Li, K.: *Electromagnetic interference shielding effectiveness of carbon foam containing in situ grown silicon carbide nanowires*, Ceram Int, 2016, vol. 42, 1330–1340.
 16. Fletcher, A., Gupta, M, C., Dudley, K, L., Vedeler, E.: *Elastomer foam nanocomposites for electromagnetic dissipation and shielding applications*, Compos Sci Technol, 2010, vol. 70, 953–958.
 17. Wang, H., Zheng, K., Zhang, X., Ding, X., Zhang, Z., Bao, C.: *3D network porous polymeric composites with outstanding electromagnetic interference shielding*, Compos. Sci. Technol, 2016, vol. 125, 22-29.
 18. Yan, D, X., Ren, P, G., Pang, H., Fu, Q., Yang, M, B., Li, Z, M.: *Efficient electromagnetic interference shielding of lightweight graphene/polystyrene composite*, J Mater Chem, 2012, vol. 22, 187–96.
 19. Chen, Z., Ren, W., Gao, L., Liu, B., Pei, S., Cheng, H, M.: *Three-dimensional flexible and conductive interconnected graphene networks grown by chemical vapour deposition*, Nat Mater, 2011, vol. 10, 424–428.
 20. Song, W, L., Guan, X, T., Fan, L, Z., Cao, W, Q., Wang, C, Y., Cao, M, S.:

- Tuning three-dimensional textures with graphene aerogels for ultra-light flexible graphene/texture composites of effective electromagnetic shielding*, Carbon N Y, 2015, vol. 93, 151–160.
21. Baheti, V., Naeem, S., Militky, J., Okrasa, M., Tomkova, B.: *Optimized preparation of activated carbon nanoparticles from acrylic fibrous wastes*, Fibers Polym, 2015, vol. 16, 2193–2201.
 22. Safarova, V., Tunak, M., Truhlar, M., Militky, J.: *A new method and apparatus for evaluating the electromagnetic shielding effectiveness of textiles*, Text Res J, 2016, vol. 86, 44–56.
 23. Liu, Y., Choi, Y. H., Chae, H. G., Gulgunje, P., Kumar, S.: *Temperature dependent tensile behavior of gel-spun polyacrylonitrile and polyacrylonitrile/carbon nanotube composite fibers*, Polym Guildf, 2013, vol. 54, 4003–4009.
 24. Ghorbani, H., Tavanai, H., Morshed, M.: *Fabrication of activated carbon anoparticles from PAN precursor*, J Anal Appl Pyrolysis, 2014, vol. 110, 12-17.
 25. Jiang, Q., Zhao, Y.: *Effects of activation conditions on BET specific surface area of activated carbon nanotubes*, Microporous Mesoporous Mater, 2004, vol. 76, 215-219.
 26. Zdravkov, B. D., Cermak, J. J., Sefara, M., Janku, J.: *Pore classification in the characterization of porous materials: a perspective*, Cent Eur J Chem, 2007, vol. 5, 1158–1169.
 27. Cao, M. S., Song, W. L., Hou, Z. L., Wen, B., Yuan, J.: *The effects of temperature and frequency on the dielectric properties, electromagnetic interference shielding and microwave-absorption of short carbon fiber/silica composites*, Carbon N Y, 2010, vol. 48, 788-796.
 28. Song, W. L., Cao, M. S., Hou, Z. L., Fang, X. Y., Shi, X. L.: *High dielectric loss and its monotonic dependence of conducting dominated multiwalled carbon nanotubes/silica nanocomposite on temperature ranging from 373 to 873 K in X-band*. Appl Phys Lett, 2009, vol. 94, 1-4.
 29. Wen, B., Cao, M. S., Hou, Z. L., Song, W. L., Zhang, L., Lu, M. M.: *Temperature dependent microwave attenuation behavior for carbon-nanotube/silica composites*, Carbon N Y, 2013, vol. 65, 124-139.
 30. Arjmand, M., Chizari, K., Krause, B., Potschke, P., Sundararaj, U.: *Effect of synthesis catalyst on structure of nitrogen doped carbon nanotubes and electrical conductivity and electromagnetic interference shielding of their polymerich nanocomposites*, Carbon N Y, 2016, vol. 98, 358-372.

Experimental study on compressibility of 3D spacer fabrics for cushioning applications

Veerakumar Arumugam^{1*}, Rajesh Mishra¹, Jiri Militky¹, Dana Kremenakova¹, Jana Salacova, Mohanapriya Venkatraman¹ & Miroslav Vaclavik²

¹ Faculty of Textile Engineering, Dept. of Material Engineering, Studentská 2, Technical University of Liberec 461 17 Czech Republic,

² VUTS, Textile Machinery Research Institute, Liberec, Czech Republic.

1. INTRODUCTION

Foam is an important engineering material used in cushions of mattress, car seats, insole, pillows, packaging, acoustic absorption and upholstery. Foams are typically used under compression, but it is very likely that also shear loading will occur in the foam components of the cushions. It is the primary means used in most modern seats, mattress and insole to achieve static comfort and vibration isolation which also happens to be the application area. It is non-linear and viscoelastic in nature. Its increasing importance as an engineering material has led to a detailed study of its structure and properties [1,2]. The foam has a relatively complex geometry, with curved surfaces and varying thickness in order to provide the desired properties for support and cushioning. The foam material is uniform over the thickness. This means that the thickness is the only parameter to the mechanical cushioning behavior of the foam components. The behavior of foams in general can be described as highly non-linear and strain rate dependent with high energy dissipation characteristics and hysteresis in cyclic loading. For low levels of stress, high levels of strain can be obtained. Low density combined with high energy dissipation capacity make foams attractive for energy absorbing functions in cushioning applications. However, the three-dimensional mechanical response of foam materials is quite difficult to capture in a mathematical model. At small strains, the mechanical behavior is close to linear elastic, followed by a large order of magnitude reduction in slope. Then, there is a long region in which the slope changes gradually. This stage corresponds to the collapse of cells. In this stage, the air is gradually pressed out of the foam. After the cells have collapsed, the final stage of densification is reached in which the cells come in contact with one another causing a sharp increase in the stress [3, 4]. The polyurethane foam (PUF) is characterized by its strongly non-linear and compressible feature. It is a hyper-elastic cellular elastomeric that presents a significant visco-elastic behavior (Fig. 1). A few studies have analyzed the PUF performance in terms of distribution of human-cushioning material interface pressure under static loading. These have established that softer PUF provides the occupant with greater comfort sensation since the contact pressure is more evenly distributed over the contact area of the human body with the seat pan as well as the backrest. Soft foams, however, tend to bottom easily and could thus cause considerable discomfort. Alternatively, relatively harder PUF protect the heavier subjects against bottoming

and yield enhanced sensation of stability; but cause concentrated pressure zones for the lighter subjects. Blair et al. [5] investigated the effect of chemical structure of PUF on dynamic and static characteristics of the seat cushions and concluded that cushions with moderate hardness and high thickness yield lowest vibration transmissibility at low frequencies and near the resonance frequency. It has been further shown that thick PUF cushions yield lower stiffness and higher deflections [6]. However, the hysteresis loss for a thicker PUF sample was observed to be less than that of the thin foam, which led to higher vibration transmissibility.

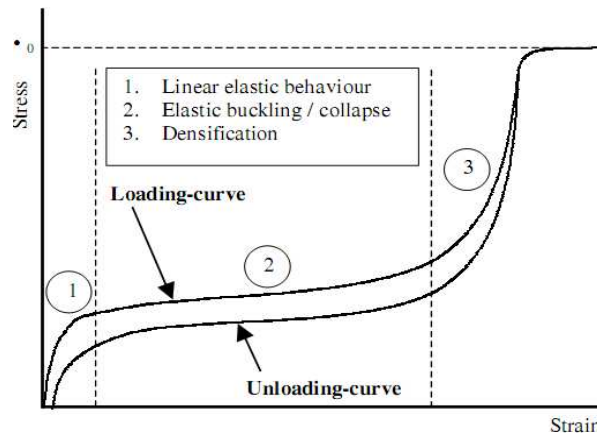


Fig. 1: Compressible feature of polyurethane foam [4]

1.1 Problems and replacement of PU foam for cushions

The PU foam, thanks to its specific characteristics, is the key element of the multilayer fabric in terms of comfort and mechanical behavior especially for the compression ones. The main issue with PU foam is partly the toxic gases it generates during its manufacturing process and recycling [7]. In fact, the recycling processes of such products require a delamination step of the different layers (PET, PU, PA). This operation is not optimal because some PU foam remains on the textile fabrics. It is also important to note that the machines used for the recycling are very expensive. The PU foam has many serious drawbacks such as flammability and gases emissions due to the laminating processes. These problems lead to the question of its replacement by a new product. A key requirement of this new product is not to alter the product functionality. It means that the new product should present at least mechanical properties, especially compression properties close or equal to the actual multilayer fabric. Another key aspect is to propose an environmentally friendly solution for complex fabric composed of a mono material product. This new product should comply with the cushioning application specifications in terms of weight, formability and cost. In this context, industries and researchers all around the world are developing new products which could substitute the PU foam [8, 9]. Analyses of the existing solutions have been carried out by textile industrialists and the obtained results show that the 3D textile technologies offer the best solution in terms of product quality and cost. 3D textiles offer a good solution to the recycling issue of the multilayer products using PU foam because of their specific structure as spacer fabric. In fact, they present a vertical orientation of the yarns (weaving and knitting

technologies) or a vertical orientation of the fibres (nonwoven technology) [10]. This vertical orientation will provide a good mechanical behavior especially in term of compression. It appears that the knitted spacer fabric provides the most interesting solution in terms of mechanical properties, cost and productivity.

1.2 Design parameters of cushions in mattress, seats, insole and mats

Design parameters that affect the local sensation of comfort at the interface between the occupant and cushion are called “Feel” parameters. The effects of “Feel” parameters are detected by nerve receptors in the skin and superficial underlying tissues. Four stimuli applied to the skin surface are important contributors to local tissue discomfort [11].

1.2.1 Compression pressure

It is the force generated directly normal to the skin surface whenever the tissue bears external load. Of course, the skin is continually under hydrostatic pressure from the atmosphere, but this pressure does not cause discomfort. In fact, the skin and underlying tissues are remarkably impervious to hydrostatic pressure (equal components in all directions) as when submerged in water. The physiological effects of surface pressure in seating are due to deformation of the skin and underlying tissues, resulting in occlusion of blood vessels and compression of nerves. Pressure on nerves can cause discomfort immediately, while loss of blood circulation leads to discomfort as cell nutrition is interrupted and metabolites build up in the tissues. The state of stress in body tissues produced by application of external pressure can be decomposed into a combination of hydrostatic and shear stresses. Chow and Odell (1978) point out that since body tissue is relatively impervious to hydrostatic stress; it is the shear stress and accompanying deformation that are harmful [12].

1.2.2 Shear stress

Shear stress results internally whenever a uniaxial load is applied to the skin, as is the case in sitting when pressure is applied to the dorsal surfaces of the buttocks and thighs. The primary cause of discomfort associated with external pressure is the shear stress and deformation that result internally. Shear stresses applied externally (surface friction) have a compounding effect, producing larger tissue deformations than the surface pressure alone. External shear stress often occurs in seating, particularly under the buttock area when the torso is reclined.

1.2.3 Temperature

The temperature can affect the local feeling of discomfort, with both high and low temperatures being perceived as uncomfortable. Both the foam padding and surface material of the mattress, seats, insole and mats affect the skin temperature at the interface [13].

1.2.4 Humidity

Humidity interacts with temperature to influence discomfort. Perspiration that is trapped against the skin by the upholstery can produce a sticky feeling if the skin is warm or a clammy feeling if it is cold. Both the foam padding and the surface covering of the cushion are important determinants of local humidity on the seat [14]. The Feel parameters of compression pressure and shear stress are considered together

because their discomfort causing mechanisms are closely related. Similarly, local temperature and humidity are usually measured simultaneously and are discussed together.

2. LITERATURE REVIEW

Spacer fabrics can be defined as fabrics which have two outer surfaces connected to each other with spacer yarns. Since the middle layer comprised of monofilaments or yarns, the fabrics possess special characteristics. Figure 2 illustrates a kind of spacer fabric in which its third dimension (thickness) is significant. Components in spacer fabrics differ depending on the yarn type and production method [15]. It has excellent compression elasticity and breathability is the greatest advantages of spacer fabric [16]. Admirable compressibility indicated that, crush resistant property and bending performance are excellent. Spacer fabric possesses excellent cushioning and shock absorbing properties [17]. It is because spacer fabric is able to absorb and dissipate kinetic mechanical energy when it is subjected to compression at regular stress over a large extent of displacement [18]. In spacer fabric construction, the two separate outer fabric layers are kept apart by spacer yarns through the thickness direction. A through-thickness property is developed in this 3D textile composite [17]. The spacer yarns act as linear springs, yarn loops are deformed under impact loading and hence created a high damage tolerance characteristic [19]. Besides, the hollow structure created by the spacer yarns between two outer layers resulted in outstanding moisture transmission property since moisture vapour is allowed to transmit freely. Thermal comfort is improved and the chance of skin maceration is reduced in this moisture free environment created by the spacer fabric. The major application areas are automotive textiles, medical textiles, geotextiles, protective textiles, sportswear and composites. This part of review is mainly focuses on knitted spacer fabrics and their production technique, properties and applications.

The three dimensional knitted fabric can be produced in different methods. The classifications of 3D knitted fabrics are given below (Fig. 3). In particular, this review mainly focuses on to discuss about knitted spacer fabrics and their production methods, properties and applications. Spacer fabrics are special types of 3D fabrics which are characterized by two outer fabric surfaces connected with pile yarns. Warp knitting, weft knitting and weaving technologies are suitable for producing this kind of 3D structures. The knitted spacer fabrics can be produced by using either warp or weft knitted technologies.

2.1 Warp knit spacer fabric

Warp knitting spacer fabric is usually knitted on a rib Raschel machine with two needle bars and a number of guide bars (Fig. 4). The warp knitting spacer fabric has a higher thickness [20]. There are two major classes of warp knitting machines: raschel and tricot. Fabric on raschel machines is drawn downward from the needles almost parallel to the needle bar, at an angle of 120-160 degrees. This angle creates a high take-up tension, particularly suitable for open fabric structures such as laces and nets. The warp beams are arranged above the needle bar and centered over the top of the

machine so that the warp yarns pass down to the guide bars on either side of them. The guide bars are numbered from the front of the machine. Raschel machines can accommodate at least four 32-inch diameter beams or a large number of small diameter beams. Raschel machines typically knit with latch needles or compound needles. Machine gauge is expressed as needles per inch. The gauge range can be from 1 to 32. The simple knitting action and the strong and efficient take-down tension makes the raschel machine well suited for the production of coarse gauge open work structures using pillar stitch, inlay lapping variations and partly threaded guide bars (Fig. 5). Raschel sinkers perform the function of holding down the loops while the needles rise [21]. On the other hand, fabric on tricot warp knitting machines is drawn towards the batching roller, almost at right angles to the needle bar. This creates a gentle and lower tension on the fabric being knitted. The maximum number of beams and guide bars on tricot warp knitting machines is limited to four, and the majority of tricot warp knitting machines operate with only two guide bars [22]. The machines have a simple construction and a short yarn path from the beams. Guide bars are numbered from the back of the machine towards the front of the machine. This makes it ideal for the high speed production of simple, fine gauge (28-44 needles per inch), close-knitted, plain and pattern work. For that reason, many lingerie and apparel fabrics are knitted using two guide bar structures with both bars overlapping and under lapping.

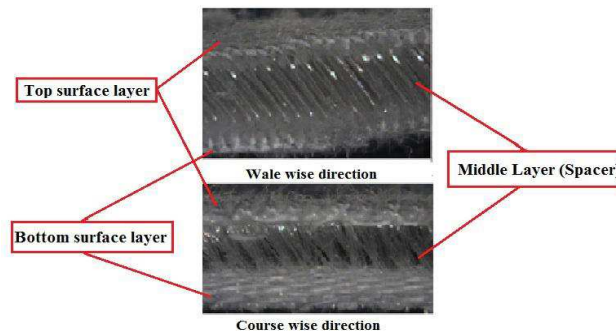


Fig. 2: Structure of spacer fabric

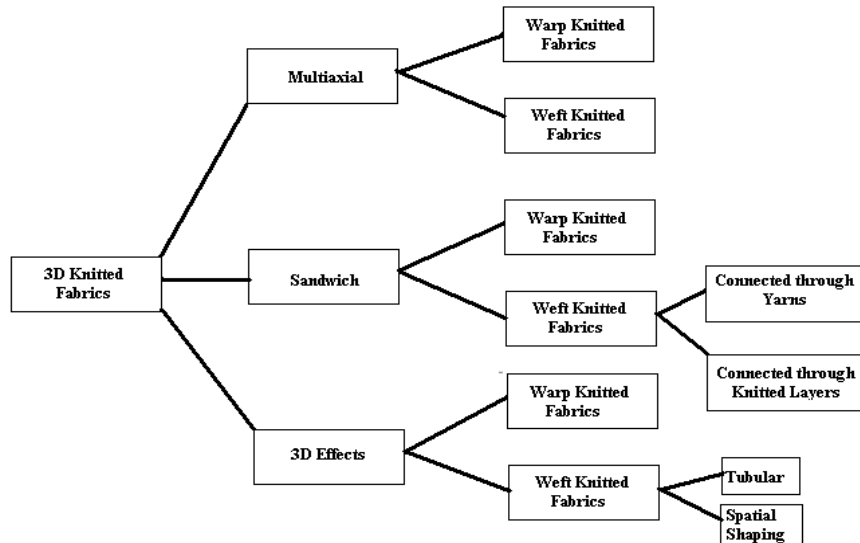


Fig. 3: Classifications of 3D knitted fabrics [21]

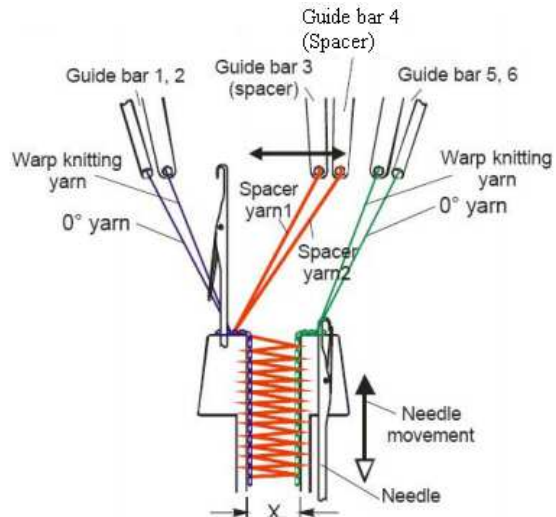


Fig. 4: Warp knitted spacer fabrics in raschel machine

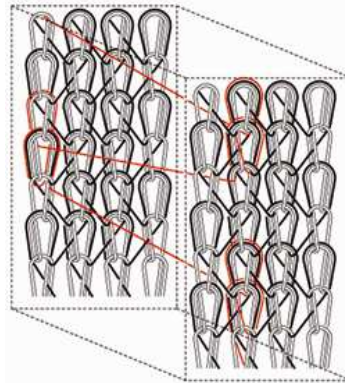


Fig. 5: Structure of warp knitted spacer fabrics

2.2 Mechanism of double needle bar raschel

Double needle bar raschel produced as a plain or semi plain pile structure which utilize up to 48 guide bars and follows the double plush woven model. Two fabrics are knitted at the same time but one behind the other. One is on the front needle bar and one on the back needle bar and they are joined by warp moving between the two and controlled by the guide bars, thus creating double cloth comprising two single cloths with the centre composed of yarn floating between the two cloths. It is possible to refer to the gauge of each needle bar separately or together. The accessibility of the raschel machine is the simple knitting action, and its strong and efficient take down motion [23, 24]. These double needle bar fabrics popularly known as warp knitted spacer fabrics (Fig. 6). Double needle bed Raschel machines designed for spacer fabric are built with varying numbers of guide bars one for each yarn supply beam. The needle bars are operated independently in an up-and-down movement, while the guide bars “shog” alternately back and forth across the needles of each bar. The warp knit fabric design and lapping sequence is controlled by the links, whose height is defined between each course and directs the shogging (back and forth) movement on each of guide bar independently. The shogging movements of the guide bars control different warp knit designs. “Different shogging movements are initiated by varying the radius of a continuously turning pattern shaft, either in the form of different

heights of pattern links that pass over a pattern drum attached to the shaft, or in the form of carefully shaped solid metal circular cams, termed pattern wheels. Figure 7 shows a pattern drum that can be rotated with links of different heights controlling the shogging movements of an associated guide bar [24]. The movement of each guide bar is controlled by a separate sequence of chain links whose height is different in certain order according to the pattern. The height difference produces a thrust against the end of the push rod, resulting in movement of the associate guide bar. An increase in height from one link to the next produces a positive shog in a direction away from the pattern device while a decrease in height produces a negative shog. A constant height will produce no shog and the guide bar will continue to swing through the same needle space, producing a pillar stitch. The guide bars swing or shog in front and at back of needs at the mean while the needles move up and down to form continuous loops. The different structures of face side warp knitted spacer fabrics are shown in Figure 8.

2.3 Weft knit spacer fabrics

Weft knitting spacer fabric is usually knitted on a double jersey circular machine, and fabric width is limited by the needle cylinder in Figure 9 [25]. The two primary forms of weft knitting machines are circular knitting machine and flat knitting machine. Circular machines can be subdivided into single jersey, dial and cylinder, and double cylinder purl machines according to the needle set used and the fabrics made [26, 27]. Weft knitting machines with two sets of needles have the potential to produce two separate covering layers that are held together by tucks. It is considered that dial and cylinder, and purl machines are able to produce spacer fabric. Flat knitting machines can be divided into two types- the V-bed machine and flat Purl machine. V-bed machine is useful in the manufacture of spacer fabrics while flat purl machine is rarely used in today's applications. The dial and cylinder machine can connect two separate layers of fabric together by the use of various combinations of stitches. To produce a dial and cylinder spacer fabric, at least three different yarns are required to form each course of the fabric including yarn for dial needles; yarn for cylinder needles; and spacer yarn. Dial height determines the amount of pile yarn being fed between two surface layers. By adjusting the dial height, producer can alter the distance between the two layers [28].

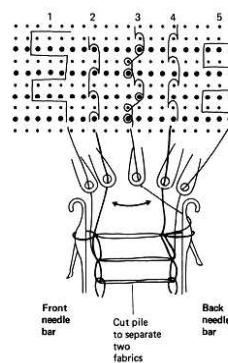


Fig. 6: Structure of the needle bars and guide bars on a double needle bed machine

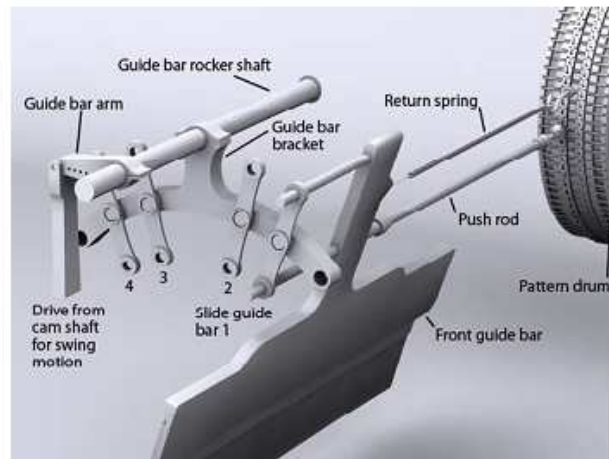


Fig. 7: Design mechanism of pattern drum

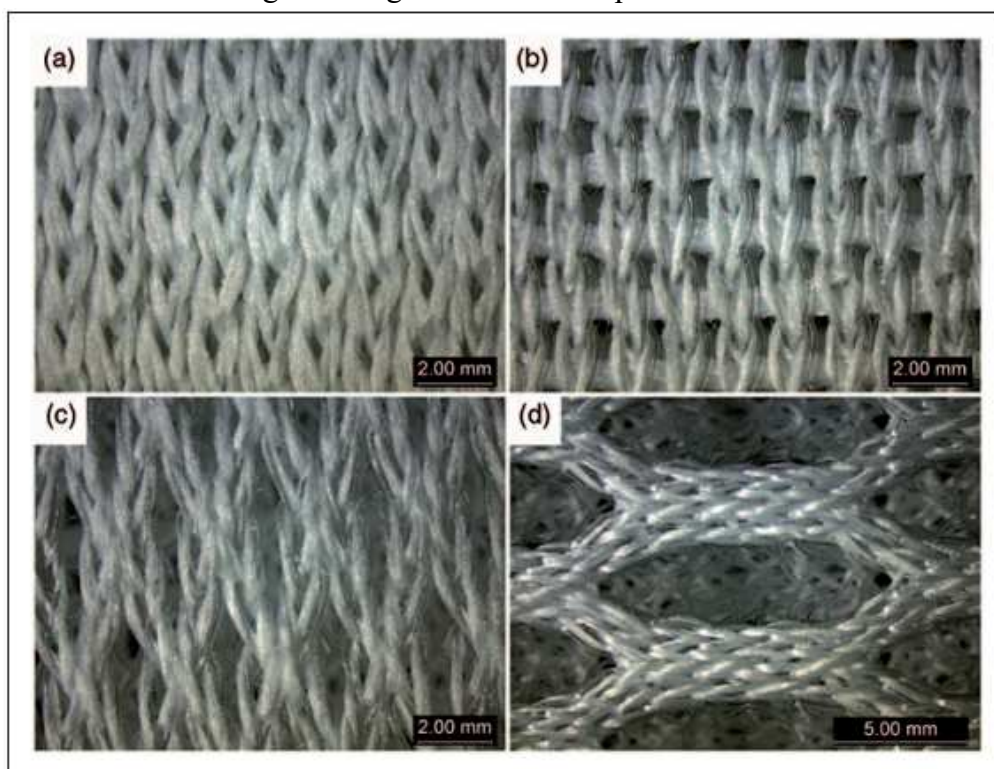


Fig. 8: (a) locknit; (b) chain plus inlay; (c) rhombic mesh and (d) hexagonal mesh [27]

Spacer fabrics can also be produced with a V-bed flat knitting machine as shown in Figure 10. A tubular knitted fabric is connected with mainly mono filament pile connections. Pile yarns are inserted with a zigzag movement between two fabric layers. Angle of connections can be varied, which enables a construction with a localized adjustment of compression stiffness. The distance between the two needle beds determines the spacer fabric thickness. Unlike circular knitting machine, the distance between the two needle beds of a flat knitting machine fixed around 4 mm. By using computerized flat knitting machine with elastomeric yarn, the spacer fabric thickness can vary in a wide range. But the productivity is very low while knitting the thicker spacer fabrics. The mechanism of tucking on two sets of needles leads to ineffective constraints on spacer yarn provided by outer fabric layer stitches. So, the

distance between two needle beds is the cause of limited dimensions [29]. By the use of a V-bed machine, two independent covering layers are knitted on the front and back needle beds respectively. Spacer fabric is created by tucking a pile yarn to link the two separate fabrics together [30].

2.4 Spacer (middle) layer

There are two types of connecting layers [30]:

1. Single layers – the layer is produced on one bed (jersey) or on both beds (rib, interlock) and can have a perpendicular or an inclined disposition between the separate fabrics.
2. Double layers - two layers are knitted separately on the beds, connected at a certain point with a rib evolution; if a specified amount of rib courses will be produced also in the exterior fabrics, then the connection will be "X" shaped, with possibilities to extend more the rib dimensions or to alternate the disposition of the two layers. Figure 11 shows the types of connecting layer (spacer).



Fig. 9: Double jersey circular knitting machine

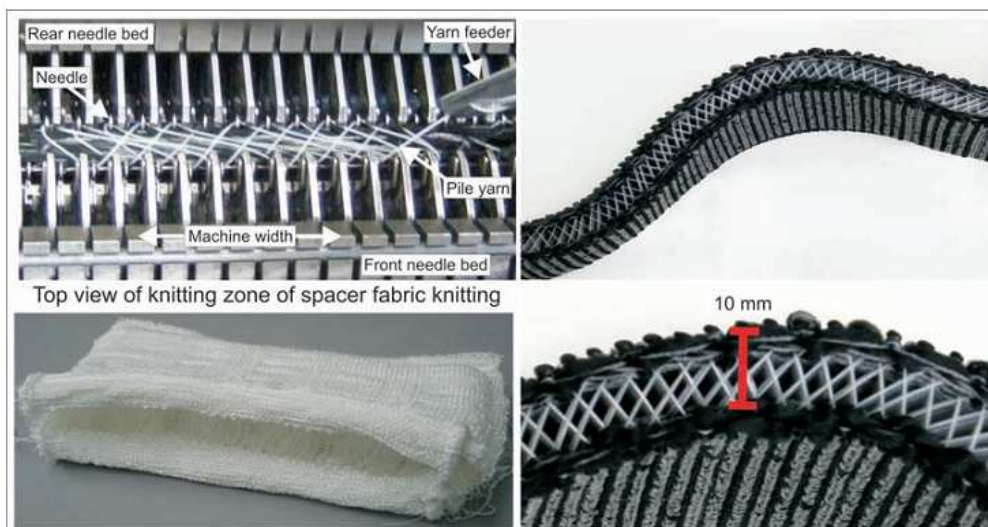


Fig. 10: Flat knitted spacers

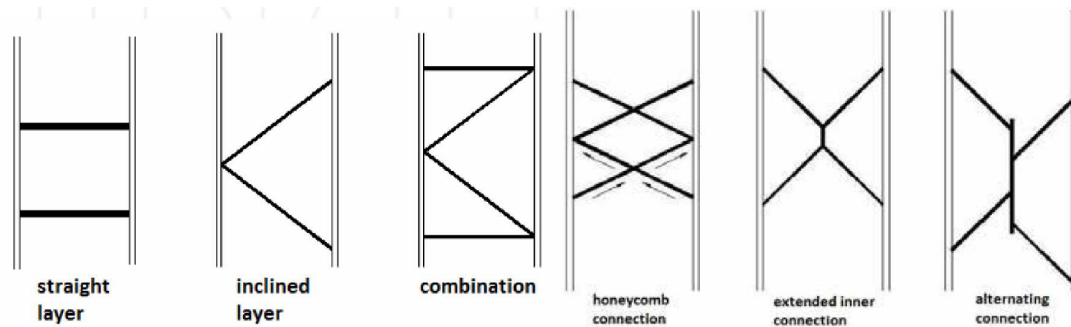


Fig. 11. Types of spacer layers

2.5 Properties of knitted spacer fabrics

2.5.1 Mechanical properties

The critical mechanical properties of spacer fabrics are those related to tensile strength, tear strength and stiffness. Tensile strength of spacer fabrics measures the fabric's ability to resist the tensile forces resulting from pre-stress in combination with external loads and it measures the level of direct pull force required to rupture the fibre of material [31]. Stiffness is of course related to modulus of elasticity of the material and the area of fibres employed, which may vary in the warp and fill directions of the material. In addition, the type of weave employed and the manufacturing process will both effect stiffness variation under load due to crimp interchange.

2.5.2 Impact properties

The structural parameters of a spacer fabric have significantly effect on its protective performance. Among a group of spacer fabrics, the spacer fabric knitted with higher inclination and coarser spacer monofilaments, a bigger fabric thickness, and a more stable outer layer structure will have a better force attenuation capacity, Liu et. al., have studied the impact properties of warp knitted spacer fabric by varying different parameters. First, the thickness and outer layer stitch density of the two fabrics are also kept nearly the same. As shown in Figure 12, it can be seen that the spacer fabric with the coarser spacer monofilament has a lower peak transmitted force and a longer time to the peak point and, therefore, has a better impact force attenuation property [32]. They also investigated, the group of three fabrics with the same outer layer structure (chain plus inlay) and the same spacer monofilament yarn but with different spacer monofilament inclinations (under lapping one needle, two needles, and three needles between the front- and back-needle bars) is used to analyze the effect of the spacer inclination on the impact force attenuation properties of warp-knitted spacer fabrics (Fig. 12). The fabric thickness and stitch density of the outer layers are kept nearly the same. The number of the needles under lapped determines the spacer monofilament inclination and length. The higher the number of the needles under lapped, the longer and more inclined the spacer monofilaments.

As shown in Figure, the transmitted force–time curves of these fabrics in single layer under impact at a kinetic energy of 5Joules are used as an example for discussing the effect of the spacer monofilament inclination with the same impact energy. It can be

seen that while the duration from the beginning point where the striker contacts the fabric upper surface to the peak point where the transmitted force reaches the maximal value increases as the spacer monofilament inclination increases; the peak transmitted force decreases as the spacer yarn inclination increases. This means that the spacer fabric with a higher spacer monofilament inclination and a longer spacer monofilament length more electively resists the impact due to a lower peak transmitted force.

2.5.3 Bending rigidity

Machova et. al., have studied the bending properties of both warp and weft-wise spacer fabrics. It appears that the bending rigidity of a spacer fabric is greatly related to the fabric type. Thus, a weft-knitted spacer fabric has a higher bending rigidity in the weft-wise direction, while a warp-knitted spacer fabric has a higher bending rigidity in the warp-wise direction (Fig. 13). This behavior is mainly due to the directionality of the incorporated yarn [33]. When the samples are of the same fabric type (weft-knitted spacer fabric for example), we can further conclude that the bending rigidity is closely related to the fabric's density, spacer structure and spacer type. They also found that weft-knitted spacer fabrics using interlock structure, monofilament spacer yarn and a higher fabric density have a higher bending rigidity.

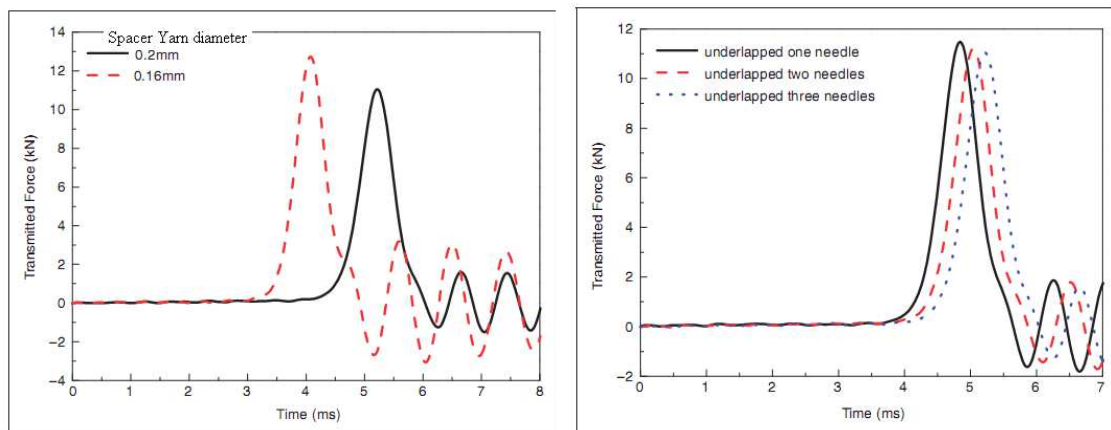


Fig. 12: Effect of spacer yarn characteristics on transmitted force–time curves (fabric layer: 1; impact energy y: 5 J)

2.5.4 Stretch and recovery

Yip and Ng have found and suggest that the stretchability of the spacer fabrics is closely related to their fabric type [31]. The results shown in Figure 14 reveal that the stretchability of a warp-knitted spacer fabric has a high stretchability only in the weft-wise direction, while the stretchability in the warp-wise direction is very low (below 50%). On the other hand, weft-knitted spacer fabrics have similar and high stretchability in both the weft-wise and warp-wise directions. As the spacer fabric is composed of two separate surface fabrics and linked together by a spacer yarn, it can therefore be concluded that spacer fabrics carry the same fabric stretchability as their fabric types (i.e. warp-knitted or weft-knitted). When the results of the weft-knitted

spacer samples were compared, the stretchability in the weft-wise direction of samples 2 and 3 were found to be higher than those of samples 1 and 4. This is due to samples 3 and 4 using multifilament spacer yarns, which have higher stretchability than those corresponding to samples using monofilament spacer yarns.

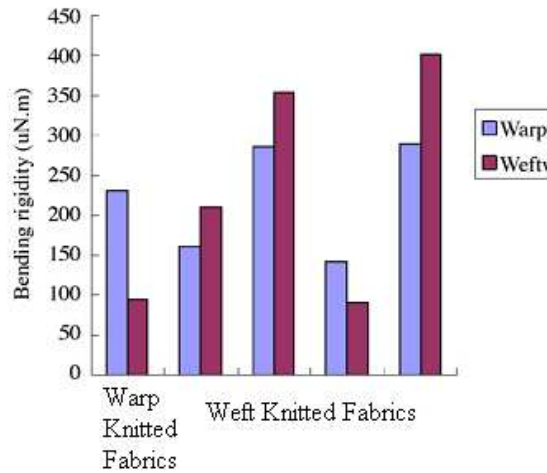


Fig. 13: Bending rigidity of spacer fabrics [38]

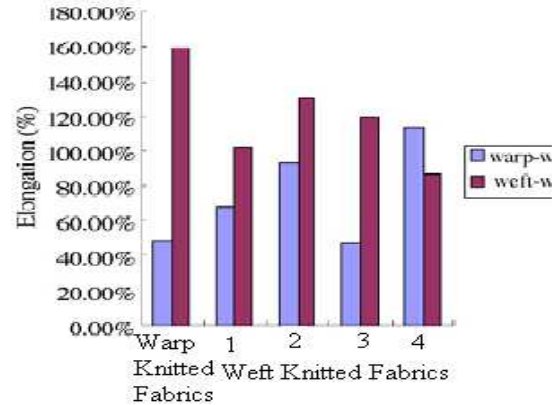


Fig. 14: Elongation of different spacer samples [38]

2.5.5 Compressibility

Spacer fabrics are very resilient and will resist and recover from pressure that may be applied on them thus deformation is not a problem in apparel made using spacer fabrics and this may increase the life of the garment. The stress-strain curve of the spacer fabric reported in article is given in Figure 15. Three distinct regions in this curve can be observed: modulus, collapse and densification regions. The modulus of elasticity is defined as the initial slope in the linear elastic part of the stress-strain curve (modulus region). The initiation of collapse region is characterized by a relatively large deformation that occurs with a constant stress. During this stage, the monofilaments bend, so the thickness of the spacer fabric will decrease. This constant stress is referred to a collapse stress or a collapse plateau. The most compressibility behavior and deformation of 3D fabrics occurs in this region, this is why this region is the subject of many investigations in the cushion fabric mechanical behavior. In the densification region, monofilaments are engaged to each other and the deflection change decreases; the slope of stress-strain curve will decrease [34].

2.5.6 Shear properties

The shearing behavior of a fabric determines its performance properties when subjected to a wide variety of complex deformations during its use. The ability of a fabric to be deformed by shearing distinguishes it from other thin sheet materials such as paper or plastic films. This property enables fabric to undergo complex deformations and to conform to the shape of the body [35]. Shear properties influence draping, flexibility and also the handle of fabric. The shear behavior of 3D spacer fabrics was investigated by using a picture frame fixture. The image analysis

procedure can provide much more information about the shear behavior of the fabric than stroke measurement. The displacement data, and shear angles change during loading process can aid in the understanding of the shear behavior of the fabric. It is found that shear deformations depend very much on the type of spacer yarn and the fabric stitch density. The non-linearity of shear deformation increases after limiting locking angle which initiates the buckling of the sample [35].

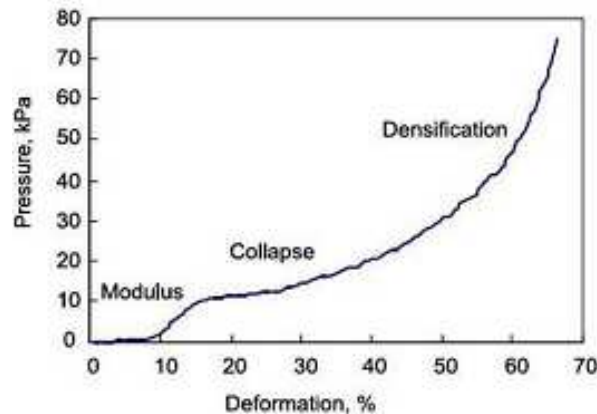


Fig. 15: Stress-strain curves for spacer fabric during compression

2.5.7 Sound absorption

The properties of spacer fabrics such as 3D fibre disposition, possibility to use different materials and single step production system, enable them in different application areas. Dial et al. introduced fabric with spacer fabric structure to improve sound absorption performances. Their studies analyzed and reported that acoustic performance of plain weft knitted spacer is good in middle and high frequency range [36]. Liu and Hu analyzed and compared the effects of different fabric layers and arrangement sequences of both warp and weft knitted spacer fabrics on the noise absorption coefficient. They suggested that sound absorption behavior of spacer fabrics are effective with multilayer arrangements backed up with air cavity. There is only few research studies conducted on acoustic performance of spacer fabrics. Erhan Sancak determined that three factors have a major impact on the sound absorbance behaviour; thickness of fabric, micro porosity between fabric surfaces and yarn linear density in the interconnection of the fabrics (Fig. 16). Arumugam et al deeply discusses that the spacer fabrics have too much air in the pores, hence, sound energy dissipation may weaken when the porosity is higher than 0.9. The air flow resistivity is inversely proportional to the porosity of the fabrics; therefore, the sound absorption can increase with decrease in porosity and increases with air flow resistivity. The 3D spacer fabrics have more tortuous path but still lower sound absorption because incident sound energy may get reflected away from the top layer and does not penetrate in to the fabric. The thickness of the porous material layer has also a great influence on the position of the peak value in the frequency spectrum. But the effect of density is more predominant in terms of sound absorbency as compared to effect of thickness [37].

2.5.8 Air permeability and moisture management

Air permeability is another important factor that should be taken into account when choosing fabrics for certain applications. In this regard, weft knitted spacer fabrics have significantly better air permeability ratings, and are thus more able to resist air penetration, than the warp knit fabric. Although, it should be noted that the density of the fabric, regardless of whether it is a warp knit or a weft knit will have a substantial impact on the air permeability and thermal regulation properties. A spacer fabric that is quite dense will have a higher thermal conductivity value, but a low air permeability value; therefore end use must be taken into consideration to find an optimum density for the fabric [38]. In regard to breathability, moisture wicking, and insulation of spacer fabrics, research at the Institute for Textile and Clothing Technology at the Hohenstein Institutes was conducted in regard to the insertion of a hydrophilic weft yarn on the face of the spacer fabric that is closest to the body, and its effect on the body's microclimate. Using a spacer fabric made of polyester (PES), monofilament for the pile and multifilament for the faces, and various inserted weft yarns, which accounted for about 5% of the total fabric, in the face of the fabric closest to the body, which also had a ribbed construction Machova, Hoffmann, and Cherif found that the inserted weft yarns increased the density of the fabric, and thus lowered the air permeability.

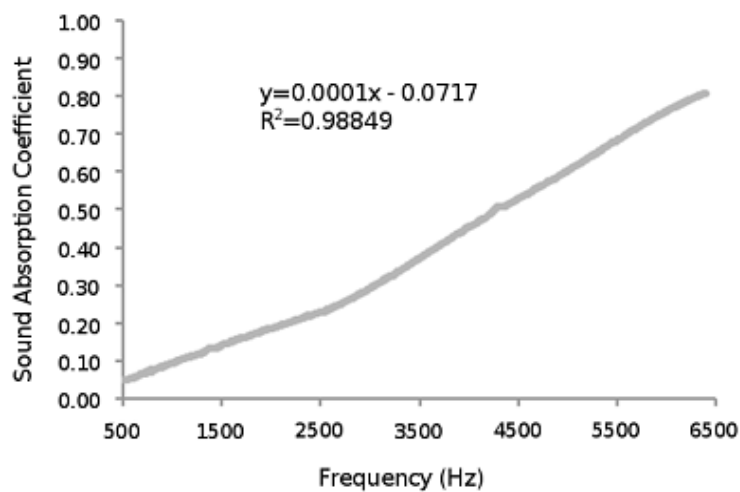


Fig. 16: Sound absorptive knitted spacer fabrics

It was also found that viscose weft yarns increase heat transport by 14.2% when compared to spacer fabrics without inserted weft yarns. The inserted weft yarn, while increasing the thermal insulation properties of the fabric, also can increase the dimension stability of the fabric. Moisture management behavior is a vital factor in evaluating thermal and physiological comfort of functional textiles. Air and water vapour permeability, vertical wicking and moisture management of spacer fabrics with different fibre properties (fibre cross section profile) have been studied quantitatively by various authors. They suggested that these spacer fabrics can be used for protective vest to absorb a user's sweat, to reduce the humidity and improve user's thermal comfort. For this reason, Bagherzadeh et. al., have investigated the

different 3D warp knitted spacer fabrics were produced with functional fibre yarns in the back layer of the fabric (close to the body) and polyester in the front and middle layers (outer surface). Comfort properties such as air and water vapour permeability and wicking and other moisture management properties (MMP) of different fabric samples were measured. It is demonstrated that by using profiled fibres such as Coolmax fibre, moisture management properties of spacer fabrics can be improved significantly (Fig. 17). It is expected that these properties of 3D functional spacer fabrics, beside their good ventilation property, enable them to be used as a snug-fitting shirt worn under protective vests to feel lower humidity and to be dry and comfort [39].

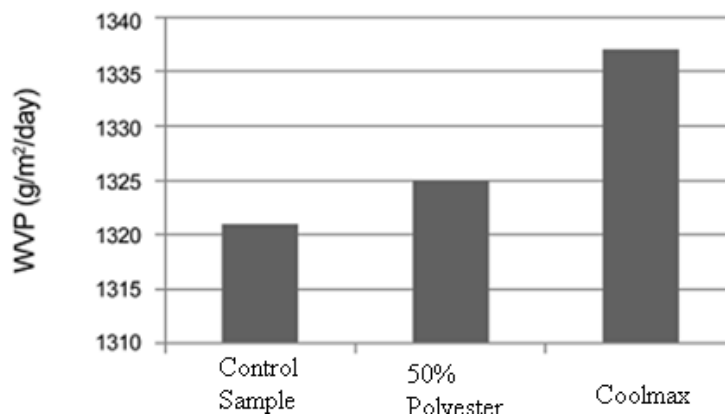


Fig. 17: Comparisons of water vapour permeability

2.6 Applications of knitted spacer fabrics

2.6.1 Cushioning applications

Cushioning materials are used to dissipate the kinetic energy of the impacting mass while keeping the maximum load (or acceleration) below some limit. They generally absorb kinetic mechanical energy under compression actions at a relatively constant stress over a large range of displacement. The works done by compressing these kinds of materials are equivalent to the kinetic energies of a mass that might impact on them. There are a number of materials and structures with the above mentioned feature for cushioning applications. Airbags, bubble films, rubberized fibres cushioning, and polymer-based foams are just a few typical examples. However, despite their promising cushioning properties and low cost, the inferior comfort property makes these materials and structures unsuitable for human body protection. A combination of excellent transversal compressibility and high permeability makes spacer fabrics very suitable for multifunctional clothing and technical applications. Some efforts have already been made to investigate the compression properties of warp-knitted spacer fabrics, and most of the studies have reported that the overall compression load-displacement relationship of these fabrics can be split into three main stages, i.e., linear elasticity, plastic plateau, and densification [40]. This is the typical behavior required by a cushioning material in compression. In the published results, relatively constant loads at the plastic plateau stage were observed. These results have proved that warp-knitted spacer fabrics are a new class of alternative candidate materials for

cushioning applications. However, the plateau stage found in literature is not notable and the zone of the plateau stage reported in literature is too short as well. In other words, the total energy absorbed in the plateau zone by these reported fabrics is not sufficient to identify them as good cushioning materials.

2.6.2 Spacer fabrics for composites

Spacer fabrics are three dimensional textiles. Properties of spacer fabrics such as 3D fibre location, possibility to use different materials and production in one step, provide the spacer fabrics to use in different application areas. Due to inferior mechanical properties, such as elasticity and deformability under applied loads, conventional spacer fabrics are not suitable for high-performance composite applications. Moreover, the restricted distance between the plane layers contributes to the drawbacks of such spacer fabrics. One solution is to connect the planes by means of vertical fabric layers instead of pile yarns. This type of 3D spacer fabric with multi-layer reinforcements in the fabric structures is expected to show superior mechanical properties and be especially suitable as textile preforms for lightweight composite applications [41]. Future applications of composites made from 3D multi-layer spacer fabrics involve the replacement of conventional panel structures that are being used for aircraft, transport vehicles, marine applications and infrastructures, lift cabins, and ballistic protection for buildings and combat vehicles, etc. Verpoest was investigated knitted spacer fabrics as reinforcement material in composite structures [42]. Philips et al., investigated the knitted spacer fabric reinforced composite materials produced with monofilament and multifilament spacer yarns. As a result of the study it was concluded that multifilament spacer yarns provide better resin distribution although it is necessary to use monofilament spacer yarn to provide better compression resistance. Philips and Verpoest, focused on the bending behavior of warp knit spacer fabric reinforced composite materials. Mecit and Marmarali studied on application of spacer fabrics in composites [43]. Flat knitted spacer fabrics offer a strong potential for complex shape preforms, which could be used to manufacture composites with reduced waste and shorter production times. A reinforced spacer fabric made of individual surface layers and joined with connecting layers shows improved mechanical properties for lightweight applications such as textile-based sandwich preforms.

2.6.3 Protective applications

Over the past few decades a wide range of personnel protective equipment (PPE) has been developed to protect wearers from various types of risks or hazards to their health and safety . Impact protectors, which are the most commonly used PPE, are normally manufactured to include energy-absorbing material in the form of pads. They are integrated or inserted into protective clothing or equipment specially designed for protecting the human body from impact, blows or falls. A number of different types of impact protectors are on the market for protecting different areas of the body in a variety of circumstances. The use of warp-knitted spacer fabrics in clothing and equipment providing protection against impact has attracted great attention in recent years due to their combination of protection and comfort in use.

The static and dynamic compression behavior of a series of warp-knitted spacer fabrics has been investigated in our previous studies, and the energy absorption performance and force attenuation capability of these fabrics under flat wise static and impact compression has been analyzed in detail [44]. These studies indicate that these fabrics have the key feature of behaving as cushioning materials, providing three distinct stages in static and dynamic compression, described as linear elasticity, plateau and densification. However, in order to offer an adequate combination of protection and comfort, the protective material must conform to the shape and curvature of the body part being protected. There is no doubt that the impact properties of a protective material of curved shape are different from those of a planar shape, due to the change in boundary conditions during loading. Most recently, Guo et al. have reported an experimental investigation into the impact behavior of warp-knitted spacer fabrics of hemispherical shape. The impact energy and weight of the striker were kept constant, and only the contact forces were measured. The tests were quoted as having been carried out according to European Standard BS EN 1621-1:1998. However, this standard specifies that protectors should be impacted using a striker of 5 kg weight at a kinetic energy of 50 J, and the transmitted forces then measured. Furthermore, their study did not pay attention to the relationship between energy absorption capacity and force attenuation properties, which is very important in designing fabrics to satisfy protective requirements.

2.6.4 Spacer fabrics for thermo-physiological clothing

In last few years, extensive research has been carried out on knitted fabrics for thermo – physiological comfort clothing [45]. Spacer fabrics have ability to trap and hold air and insulate the body because of its nature of spacer yarns between two surface layers. This, along with the ability to wick away moisture, maintains the body's microclimate, and thus keeps the person dry and comfortable. There are many outdoor/ active apparel manufacturers who still employ the layering concept in order to achieve all the desirable properties in active apparel. Warp knitted spacer fabrics tend to have a higher thermal insulation value than weft knitted spacer fabrics regardless to whether the fabric is wet or dry, an important feature for those who may utilize this fabric in the snow. Warp knitted spacer fabrics also have a higher thermal absorptivity value than weft knitted spacer fabrics, and thus the warp knitted will be warmer to touch than weft knitted. Yip and Ng found that warp knit spacer fabrics have a lower thermal conductivity rating than the weft knit fabric, which means the excess heat from the body would not be as quickly transferred if a warp knit spacer fabric is being utilized than if a weft knit fabric is to be utilized with warp knitted spacer fabrics. Spacer fabrics that have a rib construction, and are flocked during the finishing process, have shown to provide better insulation, and better heat and moisture transference, both of which will help maintain the body's micro climate [46]. The ribs of the face fabrics are what actually aid in the movement of heat and moisture; the channels created by ribbed fabric faces thus are better suited to control the microclimate and keep the wearer cool and dry. In regard to the water vapour permeability properties of spacer fabrics, weft knitted spacer fabrics have been found

to have better evaporative heat loss properties and water vapour permeability properties than warp knitted spacer fabrics, thus making the weft knit more comfortable when worn close to the skin of a person who is exerting energy and perspiring. When choosing a fibre type to aid in microclimate regulation, viscose can absorb the perspiration of the wearer and delay the moment at which the air in the spacer layer becomes saturated with moisture. This means that a person who is perspiring heavily, or has varying perspiration levels with high peaks, will remain drier for a longer period of time, and have a more level microclimate, if wearing a garment utilizing spacer fabrics with a viscose inserted weft yarn. An inserted weft yarn, that is hydrophobic, will maintain the body's microclimate more effectively than an inserted weft yarn that is hydrophilic because the hydrophilic yarn will hold the moisture and inhibit it from being transported away from the body [47]. Another, not commonly realized, important factor of spacer fabrics for certain types of active wear is compressibility. Many outdoor activities of athletes are seasonal (i.e. skiing), therefore during the off-season it is likely that the garments are stored away in containers, or other means, where they under a heavy load. During the in season, these garments are packed in suitcases for traveling. The athlete or outdoor enthusiast expects the garments to not be distorted in any way when they are removed from storage, as they should be ready to be utilized for the new season.

2.6.5 Spacer fabrics for medical applications

As a 3D structure, the spacer fabric contains a considerable amount of space inside the fabric, and the spacer yarns oriented in the Z or thickness direction provide superior compression and recovery properties [24]. In addition to having the well-known advantages of knitted structures, such as high bursting strength, high elongation, low Young's modulus and high porosity, the 3D spacer fabric stands out as a one piece multi-layered structure with high volume to weight ratio, softness, breathability, moisture conductivity, compression resistance and excellent recovery properties [48]. This unique architecture with its impressive physical and mechanical performance has been discovered by medical textile researchers and applied to both internal and external end-uses. In various external applications, the spacer layer allows consistent air circulation to reduce heat build-up and increase moisture transfer. Under applied pressure, it shows sustained graduated compression and uniform pressure distribution. So it is ideally suited for use as a compression bandage, for comfort cushioning and shock absorbency. When used as a compression bandage, for example, the spacer fabric provides lightweight, non-fraying and breathable support with enhanced thermo-physiological properties and protective cushioning. In addition, spacer shows excellent transference of pressure and the sub-bandage compression applied to the limb does not appear to be as severely influenced by the number of layers as it is with the traditional 2D bandages (Figure 18). For internal applications, spacer yarns can provide a layered surface area for cell attachment and guide the cell migration through the thickness of the fabric. The numerous interconnecting pores will allow fluids carrying nutrients and waste by-products to flow through the entire structure, hence providing superior fluid transport performance. However, there is no

published research data to support this claim at the present time. Another key advantage of using a spacer fabric as a tissue engineering scaffold is that it is a one-piece multilayer structure with different pore size distributions in the layers but without an inter face. This means that it success fully avoids thermal bonding, toxic organic solvents or chemical adhesives that would be used to assemble traditional foams and combine multi-layer fabrics. The spacer fabric may also facilitate different cell lines so as to generate separate types of tissue in the different layers [86, 88]. The engineered pore size distribution and porosity gradient could also provide physical guidance for the differentiation of progenitor and stem cells. In summary, the future possibilities of applying knitted spacer fabrics to a wide range of different tissue engineering end-uses looks promising, since various properties can be incorporated into the scaffold structure by changing the type of polymer, changing the type of yarns, modifying manufacturing process or activating the fibres with a surface treatment. For instance, the total porosity and the pore size distribution can be controlled by a number of manufacturing parameters, such as the gauge of the needle bed, the number of or the yarn guides, the type or combination of yarns, the gap between the needle beds and the orientation of the spacer yarns to parallel or crossed [49].



Fig. 18: Commercial two layer bandage

2.6.6 Other applications of knitted spacer fabrics

The other applications of knitted spacer fabrics and their products which are available in the market are shown below (Table 1) [50].

Table 1: Applications of knitted spacer fabrics

Application Fields	Spacer Fabric Products
Automotive	Car seat , door paneling, dash board cover, car boot liners, car window shelf, car seat heating, etc.
Medical	Bandage, knee braces, thermal mats, wheelchair cushions, absorbent fleece, neck supports, etc.,
Industrial	Textile antenna, sound absorption, solar thermal collectors, concrete reinforcement, etc.
Sports	Sports shoe, sports protectors, sportswear, mattress, pillows, etc.
Safety &Protection	Cycle helmets, body armor, bullet proof jackets, hip protector, etc.

3. MATERIALS AND METHODS

3.1 Materials

Six different weft knitted spacer fabric samples were developed using computerized Mayer & Cie, circular weft knitting machine with 5 feeders, 14 gauge and 80 cm diameter. These fabrics were developed in co-operation with SINTEX s.r.o., Czech Republic. The first and second feeders were supplied with spacer yarn, third and fourth for technical face side and fifth feeder for technical back. The structure and knit pattern of these samples are given in Figure 19. The six fabric samples were classified into two groups for convenient analysis of results, the first group has been developed using Polyester/Polypropylene blend with three different proportions and second group with Polyester/Polypropylene/Lycra blend having another 3 different compositions. As a spacer yarn, three different types of 88 dtex Polyester monofilament yarn and Polyester multifilament yarns (167 dtex and 14.5 tex) were used. 14.5 tex Polypropylene yarn was used on both the surfaces in group 1 samples. In group 2 samples polypropylene (14.5 tex), without and with lycra (44 dtex) were used for the top and bottom surface of the spacer fabrics (Table 2). The loop length of the fabric without lycra (WES 1) was 2.46 mm and samples (WES 2 and WES 3) were 2.78. The loop length weft knit spacer fabrics with Lycra on the surface (WES 4) was 1.28 mm and for samples (WES 5 and WES 6) were 1.52 mm.

Table 2: Weft knitted Spacer fabric samples particulars

sample No.	Fabric layers	Technical face	Spacer yarn	Technical back	fibre composition (%)
Group 1 - Without Lycra					
WES 1	Type of yarns and linear density	Polypropylene (POP) -14.5 tex	Polyester monofilament) - 88 dtex	Polypropylene (POP) -14.5 tex	58% POP & 42% PES monofilament
WES 2		Polypropylene (POP)-14.5 tex	Polyester (PES) - 14.5 tex	Polypropylene (POP) -14.5 tex	45% POP & 55% PES
WES 3		Polypropylene (POP) -14.5 tex	Polyester (PES) - 167 dtex	Polypropylene (POP) -14.5 tex	41%POP & 59% PES
Group 2- With Lycra					
WES 4	Type of yarns and linear density	Polypropylene (POP)-14.5 tex Lycra - 44dtex	Polyester monofilament - 88 dtex	Polypropylene (POP) -14.5 tex	55%POP 39%PES monofilament 6% Lycra
WES 5		Polypropylene (POP)-14.5 tex Lycra - 44dtex	Polyester (PES) - 14.5 tex	Polypropylene (POP) -14.5 tex	42% POP 52% PES 6% Lycra
WES 6		Polypropylene (POP)-14.5 tex and Lycra - 44dtex	Polyester (PES) - 167 dtex	Polypropylene (POP) -14.5 tex	39% POP 55% PES 6% Lycra

3.2 Methods

The fabric characteristics such as areal density, stitch density, structure, thickness etc. are presented in Table 2. The density (D) of the fabric was calculated using the relationship (eqn. 1)

$$D = \frac{W}{t} \text{ kg / m}^3 \quad (1)$$

Where, W is areal density (weight per unit area) which was determined following the standard method ASTM D 3776. Thickness, t was determined using SDL thickness gauge as per ASTM D 5736 standard.

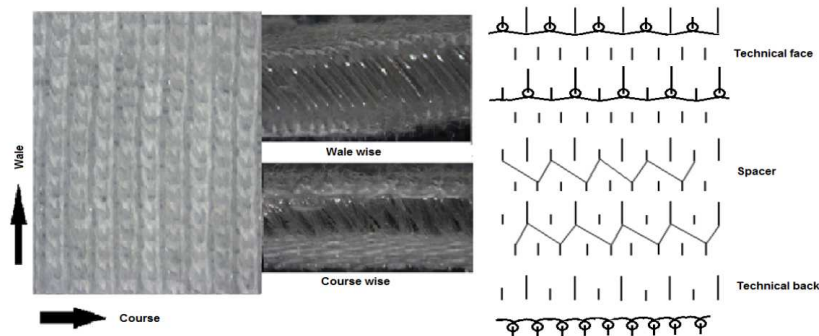


Fig. 19: Structure and knit pattern of weft knit spacer fabric

Table 3: Structural characteristics of weft knitted spacer fabrics

Weft Spacer Samples	GSM (g.m ⁻²)				Thickness (mm)				Density (kg.m ⁻³)	Stitch Density (Stitches/cm ²)				Porosity (%)
	Mean	ME	LL	UL	Mean	ME	LL	UL		Mean	ME	LL	UL	
WES 1	493	0.16	492.84	493.16	4.4	0.88	3.52	5.28	112	200	0.1	199.9	200.1	90.12
WES 2	443	0.12	442.88	443.12	2.62	1.1	1.52	3.72	169.1	150	0.04	149.96	150.04	86.21
WES 3	477	0.2	476.8	477.2	2.74	0.61	2.13	3.35	174.1	150	0.12	149.88	150.12	85.06
WES 4	632	0.1	631.9	632.1	4.4	0.55	3.85	4.95	144.8	350	0.06	349.94	350.06	87.15
WES 5	657	0.12	656.88	657.12	3.5	0.86	2.64	4.36	187.7	280	0.1	279.9	280.1	84.09
WES 6	695	0.22	694.78	695.22	3.4	0.45	2.95	3.85	205.4	280	0.1	279.9	280.1	83.11

3.2.1 Compression behavior

All the compression tests were carried out on a universal testing machine (TIRA) fitted with 5kN load cell. The speed of compression was chosen at 12mm/min in accordance to the ASTM D 575 (Test methods for rubber properties). The compression test was performed on the machine equipped with 2 strictly parallel plates having diameter of 150mm and a smooth surface. The samples were cut with dimensions of 100 mm x 100 mm. All the spacer fabric specimens are compressed up to 80 % of the initial thickness in an atmospheric condition of 20°C and 65% relative humidity. Five tests were carried out for each sample under each testing condition and the average compression stress-strain curves are presented.

3.2.2 Analysis of compression stress- strain curve of spacer fabrics

Overall compressive stress-strain trend of the spacer fabric samples are presented in the Figure 20. Normally the compression behavior of spacer fabrics are classified into

four stages with respect to changes in the slope. The four stages are (1) initial, (2) elastic, (3) plateau and (4) densification (4). In the first stage, the surface layer of spacer fabric undergoes compression, a smaller slope is observed for loose/open structures and slope increases with increase in stitch density. The spacer yarns have very low contribution in constraining the deformation during initial compression. Further compression (2nd stage) leads to rapid increase in stress; it might be due to jamming of surface yarns which allows monofilaments to buckle to a larger extent. In spacer fabrics, third stage is quite complex because the compressive stress and strain have been affected by buckling, shearing and inter-contacting of spacer yarns. A faster increase in stress occurs in 4th stage because the fabric achieves a very high density.

3.2.3 Energy absorption during compression of spacer fabrics

It is necessary to evaluate and analyze the spacer fabrics energy absorbing ability during compression. It would be more useful to get a better understanding about the applicability of spacer fabric for cushion materials. The compression curve suggests that all spacer fabric samples may potentially be good energy-absorbing materials. The area under the load-displacement curve represents the total energy absorbed and it can be calculated by multiplying the area under the stress-strain curve by the volume of the sample. The energy absorption capacity per unit volume, W , can be calculated by integrating the compression stress-strain curve, as given by equation 2 [51].

$$W = \int_0^{\varepsilon} \sigma(\varepsilon) d\varepsilon \quad (2)$$

Where, σ is the compression stress, ε is the compression strain at the end/beginning of densification stage. In order to better understand the energy-absorption capacity of a spacer fabric, the energy-absorption efficiency E can be used to analyze its energy-absorption process. The efficiency E is expressed by Equation (3)

$$E = \frac{Ah \int_0^{\varepsilon} \sigma(\varepsilon) d\varepsilon}{Ah\sigma_1} \quad (3)$$

Where A – area, h – thickness, σ – compression stress at the strain ε and σ_1 – corresponding stress value at nominal strain. The energy-absorption and efficiency of all the spacer fabrics are compared and analyzed to find the suitable material for cushioning applications.

4. SOME RESULTS AND DISCUSSION

4.1 Effect of fabric characteristics on compression behavior of weft knit spacer fabrics

As shown in Fig. 21a, the compressive stress-strain curve reveals that the compressive resistance of spacer fabric without lycra made up of monofilament yarn is low in linear and elastic stage, but sudden increase in compressive stress observed in plateau

and densification stage. From Fig. 21b, spacer fabrics with lycra made up of monofilament spacer yarn constantly offers high compression resistance in all four stages. Among the fabrics made up of multifilament spacer yarn, the compressive stress – strain curve showed that, compressive resistance has indirectly proportional to thickness of the spacer fabrics.

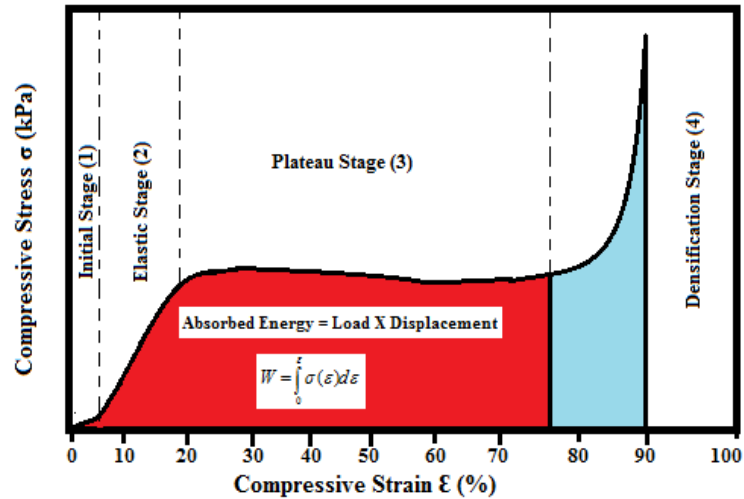


Fig. 20: Compression behavior of 3D spacer fabrics

It was observed that the denser fabrics require higher compressive stress to undergo same compressive deformation than the fabric with low density. It was also observed that the thicker fabric has ability to undergo larger deformation under low loading condition. The thickness of the fabric should be selected according to the amount of the energy to be absorbed and the allowed stress level. In both the set of spacer fabrics (without lycra and with lycra), two types of spacer yarn such as monofilament and multifilament spacer yarns were used for convenient analysis of its effect on compression. Normally the monofilament spacer yarns act as a linear spring which offers more resistance towards compression as compared to other type of materials in cushioning applications. From the Fig. 22, it is observed that, the compressive resistance is high for the fabrics with monofilament yarn for both the groups than that of fabric with multifilament spacer yarn. In plateau region (3rd stage), the marginal differences has been observed between the fabrics made up of monofilament spacer yarn (WES 1 & WES 4) in both the groups. It might be due to the fact that the large differences in density between these two samples. But the fabrics with multifilament spacer yarn (WES 2, 3 & WES 5, 6) don't show significant differences in compressive strength because the densities of these samples have almost closer to each other. It has also been found that the outer layer structures could affects the stitch density of the fabrics. The stitch density on the surface layer directly affects the compressive strength of the spacer fabrics. The compressive resistance increases with increase in stitch density. The lower stitch density on the surface of the fabric results in large surface deformation. In stage 4, a lower deformation was observed in the fabrics with monofilament spacer yarn than the fabrics made up of multifilament

spacer yarn. It might be the fact that the spacer yarns have come in to contact with each other and also makes locking effect with surface structure as quick as possible.

4.2. Compressive energy absorption of weft knit spacer fabrics

Figure 23(a & b) presents the work done of all spacer fabrics under compression load and also it compares the response compressive stress with effect of deformation and structural characteristics. The figures reveal that thicker spacer fabrics with monofilament spacer yarn have higher work done than that of thin fabrics with multifilament spacer yarn when it undergoes compression.

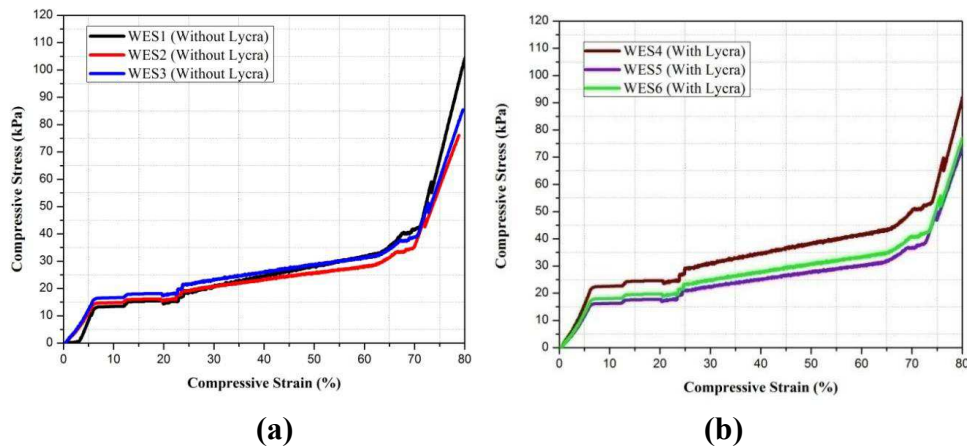


Fig. 21: Influence of thickness on compressive behavior of weft knit spacer fabrics

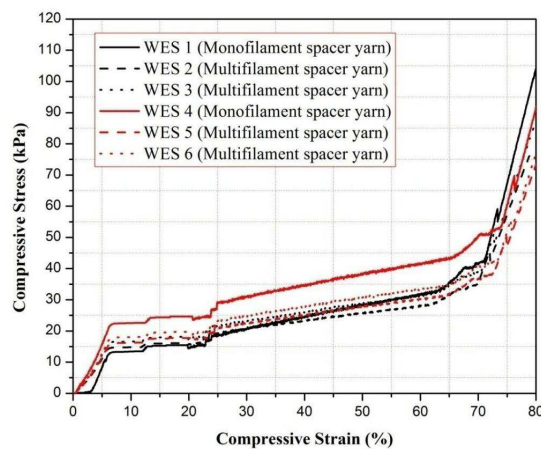


Fig. 22: Influence of spacer yarn on compressive behavior of weft knit spacer fabrics

Irrespective of the structural variations, the compressive work done shows same trend for all the samples. In both the groups, over all work done values are higher for the spacer fabrics made (WES 1 & WES 2) up of monofilament yarn. The density of spacer fabric also plays a vital role in compressive behavior, negative linear correlation was observed between density and compressive work done. Figure 24 presents the graphical analysis of compressive stress – absorbed energy – efficiency. It is observed from the figure that the absorbed energy of weft knit spacer fabrics (WES 1 –WES 6) linearly increases with the stress in the initial stage of compression. The marginal differences in energy absorption between the samples can be seen when

the compressive stress reaches towards the third stage for both the groups. At the start of densification stage, the rapid increases in stress results in small deformation and energy absorption. From the energy absorption graph, it is easy to find the stress associated with the required amount of energy to be absorbed. So, it is more convenient to select the suitable spacer fabrics for car seat and back support application with optimum compressive performance. As noticed from the Figure 24, in the densification stage, efficiency decreases with rapid increase in stress level. It is also because of dramatic increase in volume density of the spacer fabrics. The point at the maximum energy-absorption efficiency can also be considered a critical point between the plateau zone and the densification zone. Overall it is observed that the compressive energy and efficiency is higher for the thicker fabrics made up of monofilament spacer yarn with low density. Also it is found that fabrics with finer spacer yarns undergoes large amount of work done as well as high efficiency during compression mechanism.

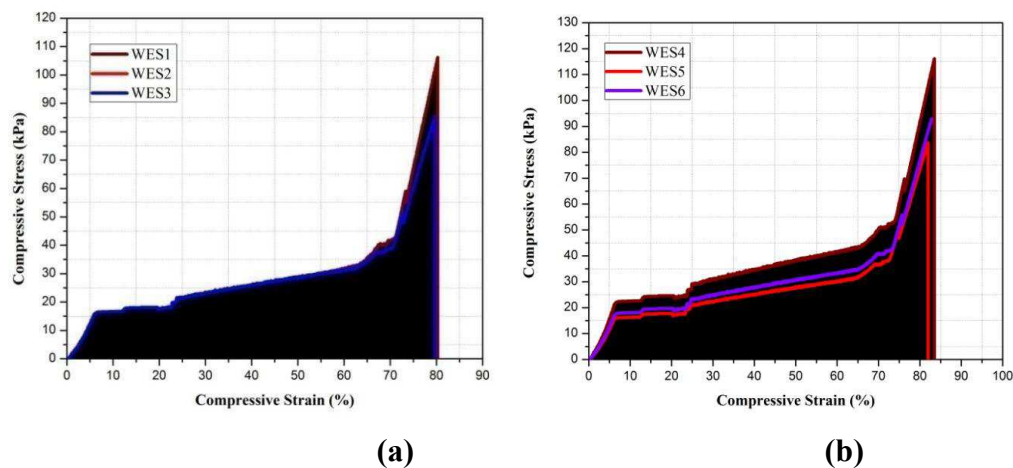


Fig. 23: Compressive energy absorption of weft knit spacer fabrics

4.3 Regression model for compressibility of weft knit spacer fabrics

The average of compressive stress responses against strain obtained for each spacer fabrics samples was fitted in the general form of third order polynomial (Fig. 25). Response fit analyses, regression coefficient estimations and model significance evaluations were conducted. The estimated regression coefficients of the fitted polynomial equation as well as the correlation coefficients for each model are given in Table 4. The adequacy of the models was tested using residuals sum of squares and adjusted coefficient of determination (R^2).

4.4 Statistical evaluation for compressive behavior response of weft knit spacer fabrics

In this section, one-way ANOVA is analyzed and the selected value of significance for all statistical tests in the study is $\alpha = 0.05$ levels. The degree of freedom is 1, 8, the $F_{critical}$ is 5.318, and degree of freedom 3, 16, the $F_{critical}$ is 3.239. If the statistic is smaller than the critical value, we retain the null hypothesis because the p-value must be bigger than α , and if the statistic is equal to or bigger than the critical value, we

reject the null hypothesis because the p-value must be equal to or smaller than α . Also pair wise comparison using Scheffé's method and Z score was calculated and presented in Table 5. The results of the ANOVA are listed in Table 4.12, which analyses the effect of groups of thickness and surface characteristics and types of spacer yarn of spacer fabric samples with compressive stress.

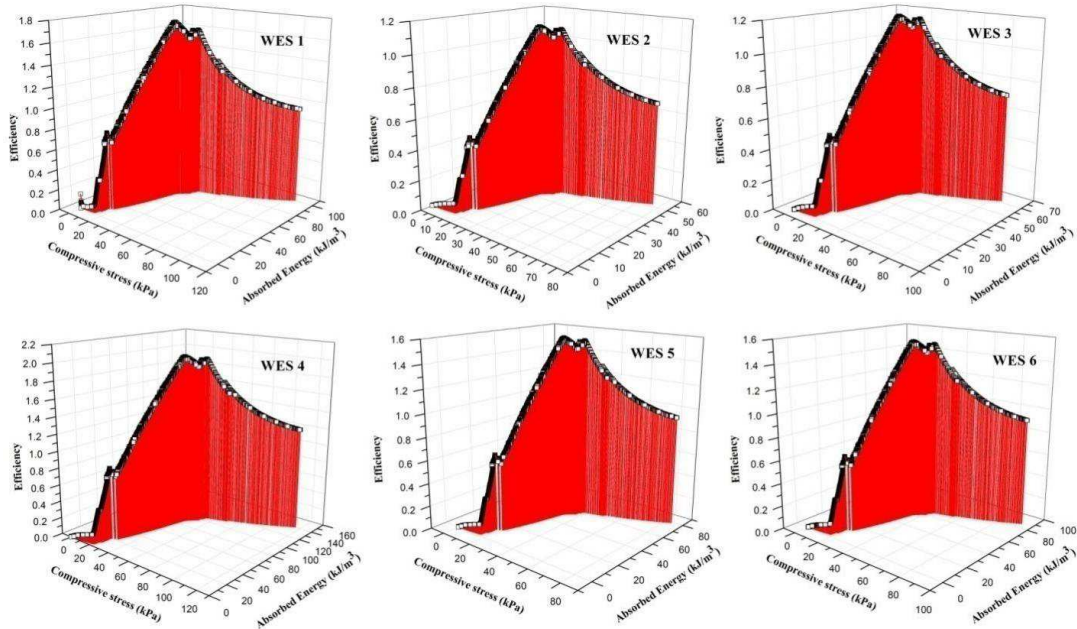


Fig. 24: Energy absorption and efficiency of weft knit spacer fabrics

The value of $F_{critical} < F_{actual}$ proves that the changes in the thickness, types of spacer yarn and surface layer structure (stitch density) of warp-knitted spacer fabric have significant influence on the above-mentioned fabric compressive stress. The insignificant difference in compressive stress is obtained between the pair, sample made up of multifilament spacer yarn without lycra on surface and with lycra. But the quite significant values are obtained in compressive stress between the other samples with multifilament spacer yarn. The box plot and a z-score are also known as a standard score and it can be placed on a normal distribution curve as shown in Figure 26. The box plots show fairly symmetric distributions with fairly equal spread and also observed that the no outliers. Normally Z-scores range from -3 standard deviations (which would fall to the far left of the normal distribution curve) up to +3 standard deviations (which would fall to the far right of the normal distribution curve).

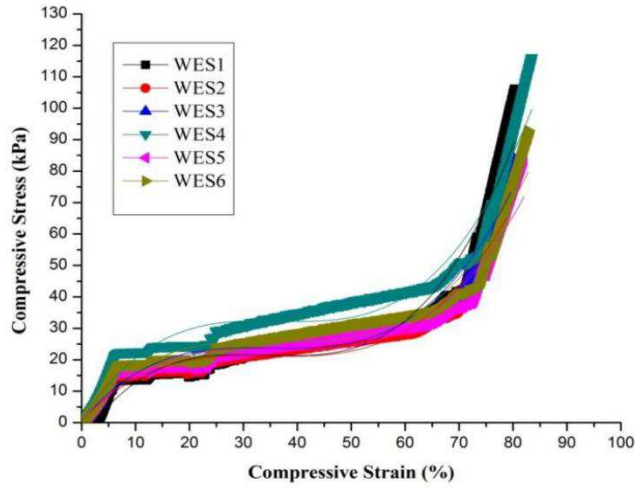
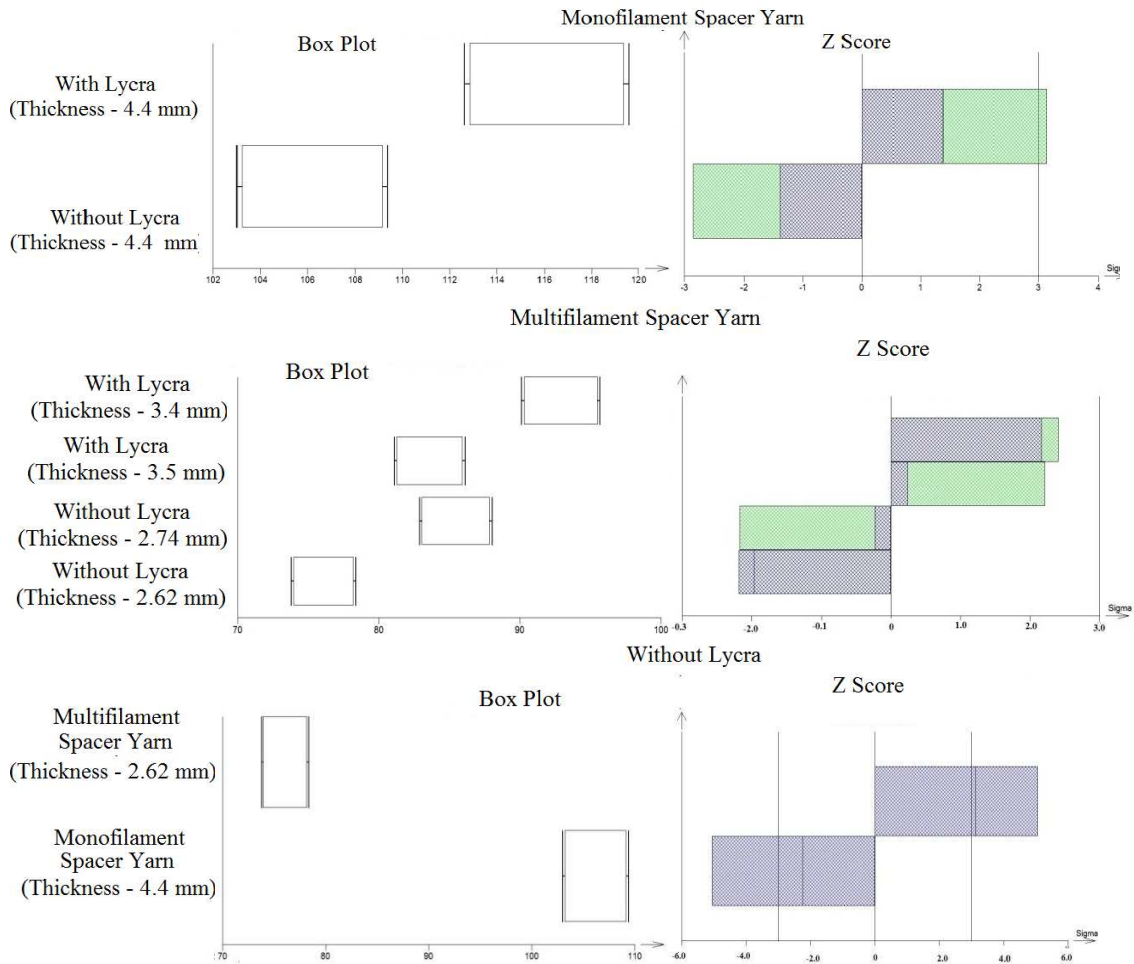


Fig. 25: Third order polynomial regression fit for compressibility of weft knit spacers



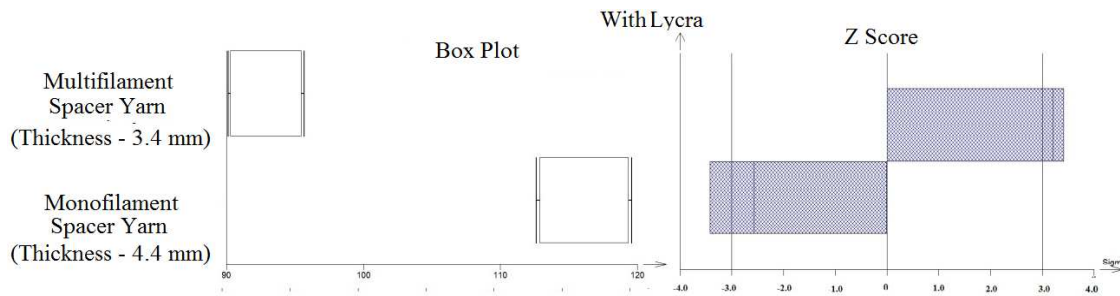


Fig. 26: Graphical outputs – Statistical evaluation for compressive behavior response of weft knit spacer fabrics

5. SUMMARY AND CONCLUSION

Since spacer fabrics have two outer surfaces connected to each other with spacer yarns, they provide light weight and bulkier structure. So, the properties of spacer fabrics such as 3D fiber disposition, possibility to use different materials and single step production system, enable them in different application areas. Components in spacer fabrics differ depending on the yarn type and production method. It has excellent compression elasticity and breathability is the greatest advantages of spacer fabric. Admirable compressibility indicated that, crush resistant property and bending performance are excellent. Spacer fabric possesses excellent cushioning and shock absorbing properties. It is because spacer fabric is able to absorb and dissipate kinetic mechanical energy when it is subjected to compression at regular stress over a large extent of displacement. The above discussion clearly stated that the potential of knitted spacer fabrics in a number of technical applications and hold promises for more applications. Also the spacer fabrics are still under active research for a number of advanced functional applications. Compressive behavior, energy absorption and efficiency of weft -knitted spacer fabrics were studied. The compression deformation mechanism of the fabric was identified based on the analyses of the load-displacement curve. The results showed that the 3D spacer fabrics are more resilient towards compression stress. Indeed, this structure enables a vertical alignment of spacer yarn; this z axis yarn has the effect to provide maximum recovery to the material. On the other hand, it has been shown that the spacer fabrics dissipate more energy in compression than other foam and nonwoven materials. Overall it is observed that the compressive energy and efficiency is higher for the thicker spacer fabrics with low density. Also it is found that fabrics with monofilament spacer yarns undergoes large amount of work done as well as high efficiency during compression mechanism. The spacer fabric with large compressive deformation, high efficiency and energy absorption until plateau stage is the suitable finding for mattress, seats and back supports etc.

ACKNOWLEDGEMENT

The authors gratefully acknowledge the support by project No. L1213 of program NPU from MSMT Czech Republic.

REFERENCES

- [1] Fung, W. and Hardcastle, M.: *Product engineering – Interior trim, Textiles in automotive engineering*, In: *Textiles in automotive engineering*. The Textile Institute, 2001, pp 194-211, Woodhead Publishing Limited, ISBN 1 85573 493 1, Cambridge, England
- [2] Deng, R., Davies, P. and Bajaj. K.: *Flexible polyurethane foam modelling and identification of viscoelastic parameters for automotive seating applications*. Journal of Sound and Vibrations, 2003, vol. 262, no. 3, 391– 417.
- [3] Gibson, L. J. and Ashby, M. F.: *Cellular Solid Structure and Properties*, Pergamon Press, New York, 1988.
- [4] Pajon, M., Bakacha, M. Pignede, D. and Van, P. Effenterre,: *Modeling of P.U. Foam Behavior – Applications in the Field of Automotive Seats*, Bertrand Faure Equipments S.A., SAE 960513, International Congress and Exposition Detroit, Michigan, February 1996
- [5] Blair, G. R., Milivojevic, A. and Van Heumen, J. D.: *Automotive Seating Comfort: Investigating the Polyurethane Foam Contribution - Phase I*, SAE Paper No. 980656, Detroit, Michigan, 1997.
- [6] Ebe, K.: *Effect of Thickness on Static and Dynamic Characteristics of Polyurethane Foam*, International Congress of Noise Control Engineering, Yokohama, 1994.
- [7] Kolich, M., Essenmacher, S. D. and McEvoy, J. T.: *Automotive seating. the effect of foam physical properties on occupied vertical vibration transmissibility*. Journal of Sound and Vibrations, 2005, vol. 281, no. 1– 2, pp. 409–416.
- [8] Hopkins, J.: *A comparative analysis of laminating automotive textiles to foam*. Journal of coated fabrics, 1995, 250-267.
- [9] Pfeifer, R. A.: *Evaluation of textile fabric properties Utilized in foam-in-place head restraints*. Master Thesis, Eastern Michigan University October 12, 2005.
- [10] Njeugna, N., Schacher, L., Adolphe, D. C., Schaffhauser, J. B. and Strehle, P.: *Development of a New 3D Nonwoven for Automotive Trim Applications*, *New trends and developments in automotive industry*, 323 – 346, January 2011, I SBN: 978 - 953 - 307 - 999 - 8, InTech .
- [11] Wu, X., Rakheja, S., Boileau, P.: *Distribution of human-seat interface pressure on a soft automotive seat under vertical vibration*. International Journal of Industrial Ergonomics, 1999, vol. 24, 545-557.
- [12] Hostens, G. Papajoannou, A., Spaepen, and Ramon, H.: *Buttock and back pressure distribution tests on seats of mobile agricultural machinery*. Applied. Ergonomics, 2001, vol. 32, no. 4, 347– 55..
- [13] Cengiz, T.G. and Bablik, F. C.: *In on -the-road experiment into the thermal comfort of car seats*. Applied. Ergonomics, 2007, vol. 38, no. 3, pp. 337– 47.
- [14] Hilyard, N. C. and Collier, P.: *Effect of vehicle seat cushion material on ride comfort*, " Paper presented at Plastic on the Road, The Plastic and Rubber Institute International Conference, London, 1984.
- [15] Liu, Y. and Hu, H.: *Compression property and air permeability of weft knitted spacer fabrics*. Journal of the Textile Institute, 2011, vol. 102, no. 44, 366-372.
- [16] Liu, Y. and Hu, H.: *Compression property and air permeability of weft-knitted spacer fabrics*. Journal of the Textile Institute, 2011, vol. 102, no.4 4, 366-372.
- [17] Liu, Y., Lv, L., Sun, B., Hu, H. and Gu, B.: *Dynamic response of 3d biaxial spacer weft-knitted composite under transverse impact*. Journal of Reinforced Plastics and Composites, 2006, vol. 25, no.15, 1629-1641.

- [18]Liu, Y., Hu, H., Zhao, L. and Long, H.: *Compression behavior of warp-knitted spacer fabrics for cushioning applications*. Textile Research Journal, 2011, vol. 0, no. 00, 1-10.
- [19]Li, M., Wang, S., Zhang, Z. and Wu, B.: *Effect of structure on the mechanical behaviors of three-dimensional spacer fabric composites*. Applied Composite Materials, 2008, vol. 16, 1-14.
- [20]Yip J, and Ng S.: *Study of three-dimensional spacer fabrics: Physical and mechanical properties*. Journal of Materials Processing Technology, 2008, vol. 206, no. 1-3, 359-64.
- [21]Darlington, K. D.: *The production of Raschel crochet fabric*, Knit Outwear Times, 1968, 22 July, 42–45.
- [22]Wheatley, B.: *Development of tricot and Raschel machinery over the past 50 years*. Knit Outwear. Times Y'r Bk, 1968, 242-57.
- [23]Fung, W. and Hardcastle, M.: *Textile and automotive engineering*. The Textile Institute, Woodhead Publishing Ltd., 2001
- [24]Fung, W.: *Coated and laminated textile*. The Textile Institute, Woodhead Publishing, 2002.
- [25]Liu, Y., and Hu, H.: *Vibration Isolation Performance of Warp-knitted Spacer Fabrics*. Fiber Society spring conference, Honkong, China, 2011, 23–25 May, 63–64.
- [26]Smith, G. : *Industrial fabric products review*. Buyers Guide, 2004, vol. 60, no.10, 42-44.
- [27]Iyer, C., Mammel, B: *Circular knitting*. Germany: Meisenbach, 1992.
- [28]Ertekin, G. and Marmarali, A.: *Heat, Air and Water Vapor Transfer Properties of Circular Knitted Spacer Fabric*. Textil ve Konfeksiyon, 2011, vol. 4, 369-373.
- [29]Abounaim, M.: *Process development for the manufacturing of flat knitted innovative 3D spacer fabrics for high performance composite applications*. PhD. Thesis, Technical University of Dresden, Germany, 2011.
- [30]Yip J, and Ng S.: *Study of three-dimensional spacer fabrics: Physical and mechanical properties*. Journal of Materials Processing Technology, 2008, vol. 206, no. 1-3, 359-64.
- [31]Liu, Y., Hu, H. and Au, W. M.: *Effect of structural parameters and lamination Protective properties of warp-knitted spacer fabrics under impact in hemispherical form. Part II*. Textile Research Journal , 2013, DOI: 10.1177/0040517513495942
- [32]Reisfeld, A.: *Warp Knit Engineering*. National Knitted Outerwear Association, New York, 1990.
- [33]Xu-hong, M., Ming-qiao, G.: *The compression behaviour of the warp knitted spacer fabric*. Fiber and Textile in Eastern Europe, 2008, vol.16, no.1, 56-61.
- [34]Arumugam, V., Mishra, R., Militky, J., M. Tunak.: *In-plane shear behavior of 3d knitted spacer fabrics*. Journal of Industrial Textiles, 2016, vol. 46, 868–886.
- [35]Dias, T., Monaragala, R., Needham, P. and Lay, E.: *Analysis of sound absorption of tuck spacer fabrics to reduce auto-motive noise*. Measurement Science and Technology, 2007, vol. 18, no. 8, 2657–2666.
- [36]Arumugam, V., Mishra, R., Militky, J. and Novak, J.: *Thermo - acoustic Behavior of 3D Knitted spacer fabrics*, fibers and Polymers, 2015, vol.16, no.11, 2467-2476.
- [37]Ye, X., Hu, H. and Feng, X.: *Development of the warp knitted spacer fabrics for cushion applications*. Journal of Industrial Textiles, 2008, vol. 37, no. 3, 213-223.
- [38]Bagherzadeh, M., Gorji, M., Latifi, P., Payvandy and Kong, L. X.: *Evaluation of Moisture Management Behavior of High-wicking 3D Warp Knitted Spacer Fabrics*. Fibers and Polymers, 2012, vol.13, no.4, 529-534.

- [39] Ye, X., Fangueiro, R., Hu, H. and Araujo, M.: *Application of warp-knitted spacer fabrics in car seats*. Journal of Textile Institute, 2007, vol. 98, 337–344.
- [40] Mecit, D. and Roye, A.: *Investigation of a testing method for compression behavior of spacer fabrics designed for concrete applications*. Textile Research Journal, 2009, vol. 79, 867–875.
- [41] Savci, S., Curiskis, J. I. and Pailthorpe, M.: *Knittability of glass fiber weft-knitted preforms for composites*. Textile Research Journal, 2001, vol. 71, 15–21.
- [42] Mecit, D. and Marmarali, A.: *Application possibilities of 3d weft knitted spacer fabrics in composite structures*, AUTEX 2011, 8-10 June 2011, Mulhouse, France
- [43] Liu, Y., Au, W. M. and Hu, H.: *Protective properties of warp-knitted spacer fabrics under impact in hemispherical form. Part I: Impact behavior analysis of a typical spacer fabric*, Textile Research Journal, 2014, Vol. 84, no. 4, 422–434
- [44] Pause, B.: *Thermo-physiological comfort provided by knitted spacer fabrics*. Melliand Textileberichte, 2002, vol. 83, no. 3, 134-136.
- [45] Krel, V., Hoffmann, G., Offermann, P., Machova, K. and Hes, L.: *Spacer fabrics for sports clothing with improved comfort*. Melliand Textilberichte, 2005, vol. 86, no. 5, E73.
- [46] Anand, S., and Rebenciuc, C.: *Elaboration of a prediction method of the values for some characteristics of the weft knitted fabrics*, In “5th International Conference TEXSCI 2003 Proceedings, Liberec, Czech Republic, 2003.
- [47] Rajendran, S. and Anand, S.: *Design and development of novel bandages for compression therapy*. British Journal of Nursing, 2003, vol. 12, no. 6, S20-9.
- [48] Davies, A. and Williams, J.: *The use of spacer fabrics for absorbent medical applications*. Fiber Bioengineering and Informatics, 2009, vol. 1, no. 4, 321-329
- [49] Rock, M. and Lohmueller, K.: *Three dimensional knit spacer fabric for bed pads*. US patent No. 5817391, 1998.
- [50] Avalle, M., Belingardi, G. and Montanini, R.: *Characterization of polymeric structural foams under compressive impact loading by means of energy-absorption diagram*. International Journal of Impact Engineering, 2001, vol. 25, 455–472.

Development of cost effective cut resistant gloves by using virgin and recycled PPTA

Haritham Khan, Hafsa Jamshaid, Rajesh Mishra, Jiri Militky, Rudolf Sramek*
Technical University of Liberec, Czech Republic

**VUTS, Textile Machinery Research Institute, Liberec, Czech Republic.*

Abstract

PPTA (p-phenylene terephthalamides) Kevlar, is a high performance fiber with exceptional mechanical and heat resistant properties. Owing to high mechanical properties it is preferred to use in many personal protective equipment (PPE) which include ballistic protection, abrasion, cut, heat resistant etc. This study is focused to develop cost effective gloves by employing recycled PPTA. Gloves are developed with 100% recycled (RK) and combination of virgin and recycled PPTA (100% and 50:50) i.e VK and RK. Usage of recycled PPTA effect performance of gloves cut resistance, although it is cost effective.

Keywords: Gloves, cut resistance, high performance fibre, Personal protective equipment

1. Introduction

Gloves:

The word glove is derived from the word “glof”. It is a type of garment made up of different textile materials. A normal glove usually has separate sheaths for each finger and thumb. Gloves have a long history, they were initially used by Egyptians. A glove can be woven or knitted. There are also two different techniques for manufacturing gloves either seamless or cut and sewn gloves. Seamless gloves are wholly knitted on ultra-fine seamless machines while cut and sewn gloves are cut from woven or knitted fabric and then they are seamed later on in a separate process. Such type of gloves need stitching to make them usable. The gloves can be categorized as aesthetic gloves and functional gloves. The aesthetic gloves are used for ornamentation purposes. These gloves are normally made up of natural fibres like cotton and wool. Initially they were worn to differentiate between different classes of people and social status i.e. the British royal society wear special type of gloves. The functional gloves are used by industrial worker. They fall into the category of personal protective equipment (PPE). These gloves are made from high performance textile material i.e. Kevlar, Dyneema and steel fibres. These gloves are worn for protection purposes from cuts, abrasion, chemicals, heat, frost bite and many more. According to OSHA the PPE are must for employees and employer must provide their employees suitable PPE.

Types of gloves:

Keeping in view their usage, gloves are categorized into two main types, conventional and technical/high performance gloves type [1-13]. The conventional gloves are normally worn to perform daily life tasks. Such as to protect hands from cold in winter, motorbike gloves and to protect hand from dust and oils. These gloves are reusable and washable. These gloves are made from natural fibres that are cheap and enough durable. Although the purpose of conventional gloves is also protection but high performance gloves are used for extreme weather conditions. They are used where chance of hazards is high and severe. These gloves are made from high strength textile materials and they are costly to manufacture. In high performance gloves, we use performance yarns like Kevlar, Dyneema, Spectra, Steel core yarn etc. These high-performance gloves are widely used in different industries like chemical, electrical, textiles, electrical and glass industry. They have much importance as they provide protection from cuts and abrasions, acids, strong alkalies, electrical shocks, frost bite and heat. Technical gloves are further identified by the end application they are used for. Most high-performance gloves include disposable/reusable gloves, chemical resistant gloves, electrically insulated gloves, abrasion resistant gloves, heat resistant gloves, vibration resistant gloves, winter gloves and cut resistant gloves. The focus of study here are cut resistant gloves and these gloves will be discussed in detail.

Cut resistant gloves

Cut resistant glove is class of protective clothing used to protect wearer from all possible cuts. A worker who is handling sharp materials, such as working on a product assembly line, will need gloves that are cut or puncture resistant. Mechanical aggressors, such as knives, metal parts, and sharp objects are responsible for nearly 30% of lost time work injuries and contribute to 80% of the injuries involving the hands[14]. When deciding, which cut resistant glove to choose, use a formal hazard analysis to decide which type of cuts your worker might be most prone to receive. According to certain manufacturers, there are three types of cuts that gloves are designed to protect against. Abrasion cuts are extremely common in many different industries. For example, an abrasive cut occurs when a worker is constantly rubbing his/her glove against the parts of a machine that could be sharp or rugged. Second are slicing cuts, workers who are at risk for this type of cut typically reside in the food industry, or any other workplace that involves the use of knives and sharp blades both manually and mechanically. Third types of cuts are impact cuts, which are least common of the three types of cuts. These occur when a piece of sheet metal or glass suddenly comes in contact with the hands or fingers with heavy force. Gloves that are made from Kevlar® or Dyneema® provide great protection against higher level sharp objects[3], unlike leather and cotton which provide a lower level of protection. It should be remembered that there is no glove that offers complete protection against a circulating or serrated blade; engineering controls must be relied upon for protection from such a motorized blade.

Manufacturing Process

Knitting of gloves

In gloves making process, yarn packages are used as a feed material. Gloves knitting machine is capable to give seamless gloves and does not require manual stitching. The five finger gloves, with the fingers placed horizontally, are usually produced on specialized knitting machines, equipped with special devices, for producing parts as automatic beginning of the tubular finger, connection between fingers, in order to avoid holes, insertion of an elastic yarn in border structure, patterning the gloves palm, with jacquard pattern i.e., narrowing edges of the tubular palm fabric. Knitting methods for manufacturing knitted glove are explained briefly in forthcoming paragraphs.

The knitting action starts with a piece of fabric which holds the knit during finger production. Knitting action for different parts of gloves is carried out in the order 1-2-3-4-5-6-7-8. During its production, the take down is executed by the auxiliary take down, placed under the needle bed while the main take down is deactivated. Fingers no 1 to 4 are knitted in a tubular style, knitted one after the other, on the same number of needles but with different lengths. After the index finger production, the connection between the fingers must be executed, in order to avoid the holes. The connection between fingers it is made by cross linking of the loops from each finger edges. Considering that the finger knitting is done on all needles, there are not any free needles at the edges in order to receive a transferred loop. After connecting the finger, palm and thumb finger will be knitted. The connection between thumb finger and palm by knitting a tubular row with split transfer comes next.

The second part of the palm must be fashioned in both edges, by successive narrowing of the tubular knitted fabric. The narrowing takes place by transferring inside the knitted fabric some loops from the two needle beds. In order to get a designed form of the narrowed fabric, some elements should be considered, i.e., the number of the rows between the two narrowing actions, the number of needle steps toward the inside of the fabric at transfer and the number of transferred stitches.

This knitting method permits full automatic knitting of gloves without requiring manual stitching or drawing-in of the leading end of the yarn. Patterning is also possible on the knitted gloves according to the designer's creativity and machine specifications.

Over Locking the Cuffs of Gloves

A high speed over lock machine is used to perform this function. It features high efficiency, durability, Convenience and so on. It is intended to sewing edges of glove's cuff with a polyester (polypropylene) string of the necessary colour and density.

Packing of Gloves:

Packing of gloves is done by the electronic packing machine. This equipment opens when ready for inputting the gloves, and it is on its level when ready for one

dozen packing. The electronic system controls the whole process. This machine is essential equipment for every glove producer.

General requirements and test methods of Protective gloves:

This standard is designed to ensure that the gloves themselves do not cause harm to the wearer and are comfortable to wear. Tests and requirements include the pH and chrome VI content of leather plus water vapour transmission and absorption of materials. Also procedures to examine the sizing of the glove and its effect on finger dexterity are covered plus general requirements for the information to be supplied with and marked on the glove.

Length

The length of the glove is measured by suspending it from the middle finger with a graduated rule having a rounded tip designed to fit the tip of the finger. The glove is manipulated to remove any wrinkles or folds and the minimum length is recorded. EN 420 includes a list of minimum lengths for each glove size, however, gloves for special purpose are permitted to be below the minimum length but in such situations the manufacturer must demonstrate that they are fit for special purpose by a statement in the user instructions.

Sizing / Dexterity

Gloves are fitted on a hand of the size that they are intended to fit and comments are made regarding comfort and fit. The wearer will then try to pick up pins of varying size to provide an indication of dexterity. Five pins are defined of diameter from 5 mm to 11mm, clearly the smaller the diameter that can be picked up the greater the dexterity result.

Abrasion

Samples are cut from the palm of a glove and rubbed against a 100 grit abrasive paper using a "Martindale" type abrasion machine. The number of cycles for the samples to hole is measured. Four performance levels are defined in EN 388 ranging from level 1 = holing > 100 cycles to Level 4 = holing > 8000 cycles.

Blade Cut

Samples are taken from the palm of a glove and the number of cycles to cut through the full thickness of the test sample by a circular rotating blade is recorded. Blade sharpness will vary and is assessed by using the cut test machine to cut through a standard reference fabric. The cut resistance of the glove is based on a relative index that compares the number of cycles to cut through the glove when compared with the standard fabric. There are three different testing standards and methods to check the cut level of cut resistant gloves. ASTM-F1790 is used in USA industry, the EN-388 is used in Europe and ISO 13997 is used internationally. Each standard has different testing parameter and equipment.

In these test methods a long blade is slide to and fro to cut the sample. The samples are cut five time to determine the loaded required to cut the material. Here are the following charts of cut resistance levels of ASTM F1790 and the ISO 13997.

ISO 13997:1999 Blade Cut Resistance Levels

Level 1 +1.2 N	Level 2 +2.5 N	Level 3 +5.0 N	Level 4 +11.0 N	Level 5 +22.0 N
-------------------	-------------------	-------------------	--------------------	--------------------

ASTM F-1790 Blade Cut Resistance Levels

Level 0 0-199 gm-f	Level 1 200-499 gm-f	Level 2 500-999 gm-f	Level 3 1000-1499 gm-f	Level 4 1500-3499 gm-f	Level 5 above 3500 gm-f
--------------------------	----------------------------	----------------------------	------------------------------	------------------------------	-------------------------------

The EN-388 is the most common and widely used method. The coup test is used to check the cutting level. It consists a circular blade which moves to and fro. The blade has fixed load of 500g. The reference material for this test is neoprene. The sample is cut 5 times to determine the index level. There are 5 index levels of cut. The cutting index (cycles)of sample material is compared with reference material to determine the cut level.

Performance Level	Average Cut Index
0	<1.2
1	1.2 - 2.4
2	2.5 - 4.9
3	5.0 - 9.9
4	10.0 - 19.9
5	> 20

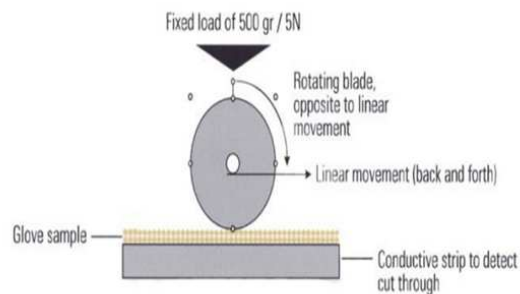


Fig. 1: Coup test for cut resistance

Tear

“Trouser leg” type samples are taken from the palm of a glove and are torn apart using a standard tensile test machine. Four performance levels are defined in EN 388 ranging from level 1 = tear strength > 10 N to Level 4 = tear strength > 75 N.

Puncture

Samples are taken from the palm of a glove and the force required to penetrate the sample with a defined stylus using a tensile test machine is measured. Four performance levels are defined in EN 388 ranging from level 1 = Puncture force > 20 N to Level 4 = Puncture force > 150 N.

Factors affecting cut resistance of a glove

The resistance of a glove depends on many factors[12-13]. These include thickness of fabric, material used, linear density of the yarn, machine used, tightness and looseness of the knitted fabric etc. The thickness of a fabric is directly proportional to the cutting resistance of a glove. Thicker fabric has more cut resistance and vice versa. The count of yarn also effects the cutting and other properties of glove. More the count (indirect system) less will be the cutting resistance. The count also effects the thickness of fabric. The knitting construction also has important role in cutting resistance. The plain construction fabric will have low cutting resistance. The string-knit gloves have inherent cut resistant properties. When we use Kevlar or Dyneema the cut resistance is much improved. Cover factor also influences cut resistance of the fabric. Performance characteristics can also be affected by a materials weight and coatings applied to the outside surface. Lighter weight styles are typically more flexible, resulting in less hand fatigue, while their heavier counterparts will generally provide the wearer with more cut and abrasion protection. Coated gloves enhance grip, especially on slippery surfaces. However, some coated gloves may not be appropriate for food handling applications. The cut resistance gloves are manufactured using different type of fibres for various end uses. Some of these are given below;

Spectra Fiber:

Ultrahigh molecular-weight polyethylene fibre that offers high cut-resistance, even when wet. It's 10 times stronger than steel per unit weight. Spectra gloves are cut and abrasion resistant, often lightweight, flexible and used for food processing, appliance assembly, food service, automotive assembly and the paper industry [4].

Dyneema:

It is a super strong polyethylene fibre that offers maximum strength combined with minimum weight. It is up to 15 times stronger than quality steel and up to 40% stronger than aramid fibres, both on weight for weight basis. Dyneema® floats on water and is extremely durable and resistant to moisture, UV light and chemicals.

Aramid Fiber:

Kevlar is an aramid fibre. It is a propriety material made by Dupont. Aramid fiber (Kevlar®) is five times stronger than steel per unit weight. Inherently it is flame resistant it begins to char at 800°F (427°C). The thread made of Kevlar fibre is used to sew seams on temperature-resistant gloves. Kevlar gloves offer cut- and heat-resistance. Typically, a lightweight flexible material that is used for many applications relating to automotive assembly, sheet metal handling and glass handling[13]. The Kevlar is made by polymerization. It is a synthetic fibre and widely different properties from other textiles materials. There are two different types of Kevlar i.e Kevlar 29 and Kevlar 49. The other varieties are made for special use. The Kevlar is a super strong plastic and its properties are partially due to the inherent

properties of material and some properties are imparted by the way of manufacturing. The chemical name of Kevlar is Poly-para-phenylene terephthalamide (PPTA). In Kevlar the ring like structures are interconnected to make long chains. The identical molecules are connected to each that make Kevlar a polymer compound. These aromatic molecules run parallel along the length of fibre. The Kevlar is from nylon family. Kevlar was introduced in 1971, having been discovered in the early 1960s by chemist Stephanie Kwolek, who earned a patent for her invention with Paul Morgan in 1966. Here is the structure of Kevlar fibre.

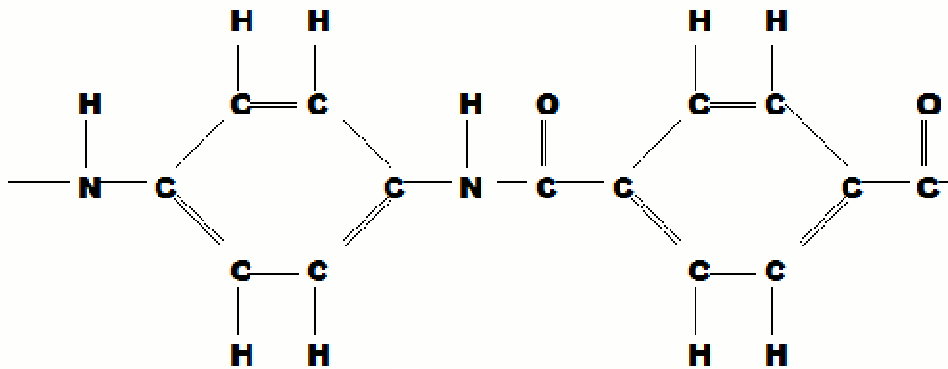


Fig. 2: Structure of PPTA

The chemical structure of Kevlar make it like tiny rods as shown in Figure 2. These tiny rods make bonds (hydrogen bonding) with each other. This behaviour of Kevlar structure gives it amazing properties like no other one have such properties i.e. high chemical resistance, high tensile strength and excellent heat resistance.

The aramid fibre are spun into yarns by wet spinning. In wet spinning the hot and concentrated solution of poly-para-phenylene is passed through spinneret. While the material is passed they are drawn to make fibres parallel along the length yarn. These yarns are wound on drum. The fibres are cut to the required length and woven or knitted to make end product.

Fiber-Metal Blends:

Many durable, abrasion-resistant gloves are made of a woven fabric blend of Spectra, Kevlar and stainless steel.

Metal Mesh:

Interlocked stainless steel mesh offers superior cut and puncture protection due to its strength. Metal Mesh gloves are very cut- and abrasion-resistant and are used often in meat/poultry applications.

Super Fabric:

Combinations of the number of layers, thickness, substrates, surface coatings, etc., lead to fabrics which have varying levels of puncture, cut and abrasion resistance, grip and flexibility. Tactile surface offers improved grip of wet and oily surfaces.

Steel Core:

These Gloves are cut- and abrasion-resistant and are often used for meat/poultry processing, glass handling, metal fabrication, automotive manufacturing as well as being used in the paper industry.

Significance of the cut resistant gloves:

The world market demand of all categories of protective gloves including cut resistant is, increasing day by day. Total annual worldwide demand of protective gloves is estimated near about 13.5 billion pairs. Demand of protective gloves split among Europe, North America, Asia and rest of the world is about 20 to 30% of total consumption. In 2006, total industrial demand for protective gloves amounted to € 1,972 million. The market size grew 2.9% annually during the period 2003-2008 and a further growth of the same level is expected in 2009 and 2011. The share of developing country imports increased 20% (in absolute terms) to 68% of the EU imported value of protective gloves in the period 2005 -2007 and accounted for 95% of imports from outside the EU in 2007. Developing countries, in particular Asian countries dominate EU imports of protective gloves. Malaysia and China (each country 21% of total imports) remained by far the most important suppliers of protective gloves, followed by Thailand (8%), India and Sri Lanka. China dominates EU imports of protective gloves, made of leather, textiles and plastic.

Handling injuries Statistics:

Personal protective equipment, commonly used as "PPE", are the equipment that protect from serious hazards. The hazards can be from chemicals, sharp edge objects, mechanical and electrical systems. To maximize the protect worker must wear safety equipment. The PPE may include gloves, glasses, shoes, clothes, helmet, ear plugs, and bullet proof jacket to full body suits [1]. Employer is the responsible for the safety of his workers. He must provide personal protective equipment to their workers and ensure its proper use. Employers are also required to train each worker required to use personal protective equipment to know:

- When it is necessary
- What kind is necessary
- How to properly put it on, adjust, wear and take it off
- The limitations of the equipment
- Proper care, maintenance, useful life, and disposal of the equipment

If we have to use PPE, a PPE training must be done. This program or training should address the hazards present; the selection, maintenance, and use of PPE; the training of employees; and monitoring of the program to ensure its ongoing effectiveness. Our hands and fingers are used to perform countless daily tasks.

According to the Bureau of Labour Statistics in the USA, injuries to the hand, wrist and finger account for 23% of total workplace injuries. The Bureau 'guesstimates'

there are about 110,000 lost-time hand injuries annually. Some of the most common hand injuries included lacerations or cuts, amputations, loss of finger(s), burns by chemical or fire, broken pieces of material becoming lodged in the hand, and crush injuries resulting in broken bones.

A report released in October 2009 by Safe Work Australia reported that construction industry workers experienced 86 injuries per 1,000 workers from 2005 to 2006, nearly 25 percent higher than the rate for all other Australian workers, of 69 injuries per 1,000 workers. Additionally, a study commissioned by the Australian Safety and Compensation Council (ASCC, 2008) acknowledged the prevalence of hand related injuries in the construction industry. The range considered minor to very severe injuries, with the most common found to involve the fingers. Open wounds were found to be the most common injury type and amputations the most severe [2]. The report concluded that work related hand and wrist injuries are the most common injury type and pose a problem to Australia's workforce. Resulting in about 8,400 admissions to hospital every year, they are a very common cause of work related injury presentation to emergency departments in Australia.

Figures for hand injuries are high across all industries. A review of hospitalizations due to work related injuries in Australia, conducted by the National Occupational Health and Safety Commission (NOHSC), found that in 2004 hand injuries represented 37.17% of the total of 15,902 work related hospital treated cases. This location on the body was the most frequent occupational injury. This trend is especially true of the construction and mining industries, particularly when it comes to workshops and workshop related activities. Indeed, a 2013 Australian government mines safety bulletin reported that "Hand injuries are the second most commonly reported lost time injuries in the Queensland mining industry." In many ways, this data is not surprising, since the hands are often central to work tasks. Consequently, they are often the closest part of the body to the work hazard such as the hammer impact point, vibrating tool, hot pipe or sharp object.

Analysis of workplace incidents shows that some of the main reasons for hand injuries are:

- Hands being caught or pinched between objects
- Hands being hit by flying, moving or falling objects
- Hands striking objects or making contact with a sharp object

Most hand injuries occur during maintenance activities when carelessness or complacency can ensue, resulting in:

- The use of incorrect tools
- Failure to use appropriate hand protection
- Adoption of hazardous body positions or work methods

Here are the following statistic for handling injuries between 2013 and 2014.

Table 1: Handling, lifting and carrying injuries

<i>Injury</i>	<i>Employee</i>	<i>Self-employed</i>	<i>worker</i>
<i>Fatal</i>	0	0	0
<i>Major</i>			
<i>Over seven days</i>	1431	59	1490
<i>Total</i>	18354	221	18575

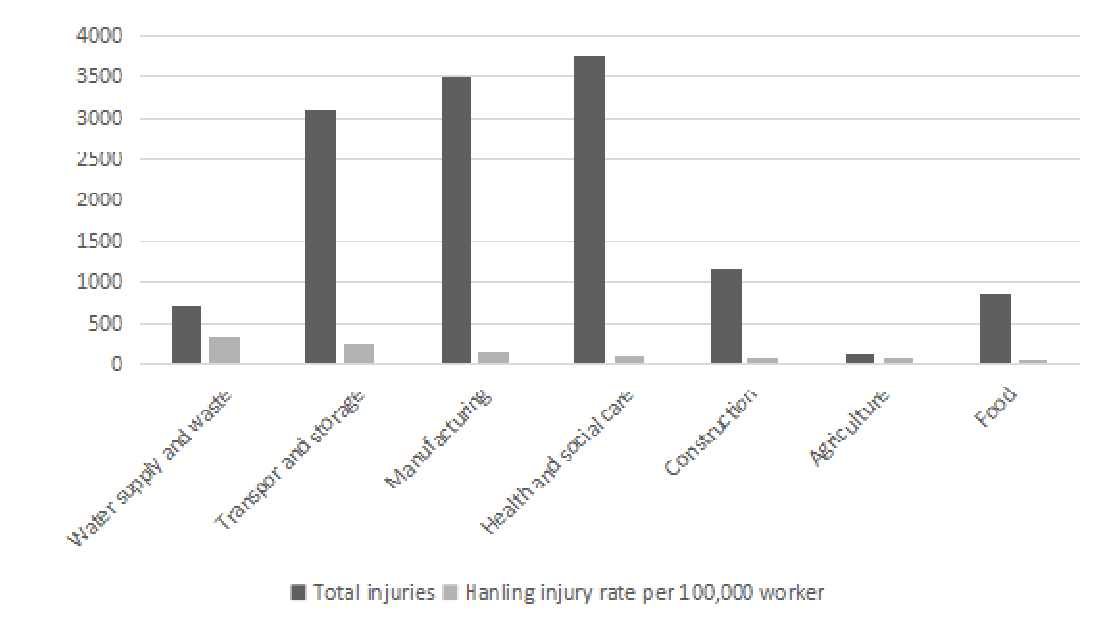


Fig. 3: Industry wise distribution of injury statistics

OSHA Hand protection standard

Standard: OSHA 29 CFR 1910.138 Hand Protection

Employers must select and require employees to wear hand protection when their hands are exposed to hazards such as harmful substances, severe cuts or lacerations, severe abrasions, punctures, chemical burns, thermal burns and harmful temperature extremes. Selection of hand protection should be based on an evaluation of the performance characteristics of the hand protection in relation to the tasks to be performed, conditions present, duration of use and potential hazards.

Other sections of the OSHA standard require hand protection to:

- Offer reasonable comfort
- Fit securely without interfering with dexterity
- Be durable and able to be disinfected or cleaned

It is also important to note that the gloves should be comfortable. If the worker finds the gloves uncomfortable, they may be less likely to keep them on, thus leaving unprotected hands that are much more at risk for injury, which can lead to an increase in medical expenses and workers' compensation.

Why we are developing cost effective cut-resistant gloves:

The question is why we choose Kevlar for cut resistant gloves over other materials like steel and Dyneema. Kevlar is 10 times stronger than steel by weight. It has excellent chemical resistance while providing excellent cut and abrasion resistance. The drawback of steel that it is bulky and do not provide required level of dexterity. Secondly it absorbs heat and transfer it to the hand which is uncomfortable. The Dyneema is 15 times stronger than steel. Although the Dyneema is strongest fibre against cuts and abrasions, it has poor heat resistance which may reduce its life span. The price of Dyneema is also much higher than Kevlar yarn. As the cut, resistant gloves have high prices. The rate of Kevlar yarn is Rs. 5000 to Rs. 7000 per kg. Gloves made from these high performances are high and its price is required to be economical. So, there is a high need of low cost gloves without compromising its cutting resistance level. Balance of price and cut resistance will be an attractive feature in a glove to gain market value. During our study efforts are being made to develop gloves by blending virgin and recycled material. The cost of gloves decreased up to 2 to 3 times as compared to gloves manufactured from 100% virgin Kevlar. We compared performance of 50/50 % Kevlar gloves and 100% recycle Kevlar. Different studies have been conducted[9] to investigate performance of different high performance fibres, both organic and inorganic, in pure form so there is strong need to check recycled or combination of high cost and low cost fibres in order to reduce cost without compromising cut resistance.

Material and Methods

Kevlar yarn is used to produce gloves. We use 100% virgin and 50 virgin/50 recycle % composition of Kevlar yarn. We tested 100% virgin and 50/50 percent composition of Kevlar yarn. The “Uster tester 5-S400” and “Uster Tesnsorapid” machines was used to test the yarn. Properties are mentioned in Table 2. The machine used to knit the gloves was used Shima sieki SFG-I. This machine used the seamless garment technology. As we have to make seamless gloves so we choose this machine. The SFG-I uses the sinker mechanism to knit the glove. It has three two feeders for main yarn, one for elastic yarn and one for pattern yarn. On machine we can change stitch density and other yarn related parameters. The machine has centralized lubrication system. The moving parts of machines are automatically get lubricated. In case of error or yarn breakage the machine stops automatically. The gauge of machine was 13 E. The tension and stich density was optimum. First the 20/1 yarn was used to knit the glove. But the structure of glove was much loose and yarn breakage occurs frequently. Then 20/2 or two ply yarn was used knit the glove. Although the yarn breakage reduced but the gloves structure was still loose. Finally the 3-ply yarn was used. The gloves structure was fine and no yarn breakage occurred. We made six pairs of gloves of each yarn (100% RK and 50VK/50 RK%Kevlar).For testing cut resistance, the most widely used standard EN-388 was used.

Table 2: Properties of 100 %RK and VK/RK Kevlar yarn

Test	100% recycled Kevlar	50VK/50 RK % Kevlar
Count	20/1	20/1
Elongation %	3.75	3.61
Tenacity(CN/Tex)	66.05	67.13
Time to break (S)	0.29	0.27
Thick +50%	209.2	27.5
Thin -50%	66.7	37.5
Neps +200%	670.0	60.0

Results and discussions

The cut resistant of gloves was tested by using BS: EN: 388:2003 6.2 standard. Two pairs of each 100% RK and 50VK/50RK % gloves were tested to get the average value of cut level. There are four sample test for each glove category.

Sample 1

Indexes	Levels
9.45	3
8.57	3
8.94	3
9.15	3
8.87	3
Mean=8.99	3

Sample 2

Indexes	Levels
9.19 3	3
10.13	4
10.24	4
9.15	3
9.79	3
Mean=9.70	3

Sample 3

Indexes	Levels
7.71	3
7.84	3
8.16	3
8.36	3
8.63	3
Mean= 8.14	3

Sample 4

Indexes	Levels
6.98	3
7.18	3
7.24	3
6.90	3
7.88	3
Mean= 7.23	3

Test report of 100% RK gloves

Colour: Yellow

Environmental Conditions: 23±1°C, 52±3% RH

Performance level: 3

Test report of 50VK/50RK Kevlar gloves

Colour: Yellow

Environmental Conditions: 23±1°C, 52±3% RH

Performance level: 4

Sample 1

Indexes	Levels
9.75	3
10.17	4
10.94	4
10.95	4
10.47	4
Mean= 10.45	4

Sample 3

Indexes	Levels
10.86	4
9.94	3
10.18	4
10.15	4
13.00	4
Mean= 10.82	4

Sample 2

Indexes	Levels
10.72	4
9.15	3
10.99	4
10.55	4
9.04	3
Mean= 10.09	4

Sample 4

Indexes	Levels
10.98	4
10.18	4
9.24	3
10.90	4
8.88	3
Mean= 10.03	4

The pair of gloves were tested according to the standard. The cut level of 100% recycled Kevlar (RK) gloves was 3 and cut level of 50%VK/50%RK was 4. The result difference is obvious. The gloves made from 100% recycled Kevlar have low cut resistance. Because they have lost their strength. While the gloves that are made from 50% virgin Kevlar (VK) and 50% recycled Kevlar (RK) has higher cut level. This is because of virgin Kevlar strength.

Conclusion:

The research showed that the gloves made from 50%VK/50%RK Kevlar has better performance as compared to gloves just made from 100% recycled Kevlar. Although there is no big difference but it matters when it comes to personal protect equipment. Overall cost is reduced .So these types of gloves can be used for less intense applications .Usage of recycle material will be helpful for environmental protection.In future different % of RK can be used for improvement in performance level and cost. The Kevlar gloves can also be layered with extra material to improve their cut level.

ACKNOWLEDGEMENT

The authors gratefully acknowledge the support by project No. L1213 of program NPU from MSMT Czech Republic.

References

- [1] M. Awais, M. Tausif, F. Ahmad, A. Jabbar, and S. Ahmad, "Inclusion of recycled PPTA fibre in development of cut-resistant gloves," *J. Text. Inst.*, vol. 106, no. 4, pp. 354–358, 2015.
- [2] M. Stirling, *Ergonomics of protective clothing*. 2000.
- [3] M. Afshari, D. J. Sikkema, K. Lee, and M. Bogle, "High performance fibers based on rigid and flexible polymers," *Polym. Rev.*, vol. 48, no. 2, pp. 230–274, 2008.
- [4] S. Pal, "High performance fibers and their application," *Man-Made Text. India*, vol. 52, no. 11, pp. 376–388, 2009.
- [5] X. Flambard, M. Ferreira, B. Vermeulen, and S. Bourbigot, "Mechanical and thermal behaviors of first choice, second choice and recycled p-aramid fibers," *J. Text. Apparel, Technol. Manag.*, vol. 3, no. 2, pp. 1–5, 2003.
- [6] R. Vajko, *Making Sense of Cut Resistance*. 2008, p. 9.
- [7] F. Kajiyama, Y. Nakamura, and S. Control, "Development of an advanced personal protection equipment fabric for protection against slashes," 2010.
- [8] R. Shishoo, "Recent developments in materials for use in protective clothing," *Int. J. Cloth. Sci. Technol.*, vol. 14, no. 3/4, pp. 201–215, 2002.
- [9] J. Mayo and E. Wetzel, "Cut resistance and failure of high-performance single fibers," *Text. Res. J.*, vol. 84, no. 12, pp. 1233–1246, 2014.
- [10] P. I. Dolez and T. Vu-Khanh, "Recent developments and needs in materials used for personal protective equipment and their testing," *Int. J. Occup. Saf. Ergon.*, vol. 15, no. 4, pp. 347–362, 2009.
- [11] J. B. Mayo, E. D. Wetzel, M. V. Hosur, and S. Jeelani, "Stab and puncture characterization of thermoplastic-impregnated aramid fabrics," *Int. J. Impact Eng.*, vol. 36, no. 9, pp. 1095–1105, 2009.
- [12] E. Silva, *Protective clothing for law enforcement personnel*. 2010, pp. 1–15.
- [13] M. Ertekin and H. Erhan Kirtay, "Cut resistance of hybrid para-aramid fabrics for protective gloves," *J. Text. Inst.*, vol. 107, no. 10, pp. 1276–1283, 2016.
- [14] M. Lucas, "Injuries in Australian Veterinarians," no. 7817538, 2012.

Development of electrical conductive films of polylactic acid reinforced with carbon particles derived from waste acrylic fibers

Muhammad Salman Naeem¹, Vijay Baheti¹, Jiri Militky¹, Zafar Javed², Abher Rasheed²
Saima Javed³, M. Tahir Siddique²

¹*Faculty of Textile Engineering, Department of Material Engineering, Technical University of Liberec, Czech Republic.*

²*Faculty of Textile Engineering, Department of Garments Manufacturing, National Textile University, Faisalabad, Pakistan.*

³*Department of Microbiology and Molecular Genetics, Punjab University Lahore, Pakistan.*

ABSTRACT

The acrylic fibrous waste was successfully converted into activated carbon through single stage carbonization and physical activation using high temperature furnace at different carbonization temperatures 800 °C, 1000 °C and 1200 °C. The carbonized fibers were characterized by using EDX and XRD in order to find the proportion of carbon element and degree of crystallinity in carbonized fibres prepared at different temperatures. Later on, the carbonized acrylic fibrous waste was pulverized in dry conditions by high energy planetary ball milling to get activated carbon micro/nano particles. In addition to refinement of size, the electrical conductivity of pulverized carbon particles was found to increase with increase in milling time. Subsequently, the particles were incorporated into poly lactic acid (PLA) in different loadings from 1 % to 10 % to develop conductive green composite films. The composite films were then characterized for electrical, thermo-mechanical and thermal properties.

1 INTRODUCTION

Nowadays electrically conductive textiles are of great interest due to numerous applications in various fields like military and medical fields, as actuators and sensors and for electromagnetic shields etc. Electrically conductive fabrics can be obtained through different means like metallization, chemical coating, deposition of thin layers of conductive fillers like carbon black particles or through the insertion of metallic yarns [1]. Most of the synthetic fibers used in textiles are insulating materials with resistivity around $10^{15} \Omega/\text{cm}^2$. This resistivity is much higher than the desired for anti-electrostatic and electromagnetic shielding applications. The desired resistivity for electromagnetic shielding materials should be lower than $10^2 \Omega/\text{cm}^2$ and for anti-electrostatic materials it should be in the range of 10^9 - $10^{13} \Omega/\text{cm}^2$ [2]. Conductive fibers are classified as naturally conductive and those that are specially treated to make conductive. Natural conductive fibers are carbon fibers or fibers developed from inherently conductive polymers or metallic fibers [3][4]. Carbon black particles and nano-tubes incorporation causes substantial impact on electrical and thermal

properties. The well-known extra-ordinary properties like high electrical conductivity, large surface area and low percolation threshold makes them superior candidate over other conventional conductive fillers. Compared with granular form of activated carbon, the pore length and pore diameter in activated carbon fibers are more easily controlled which makes it attractive choice to be used in electrical applications. Hence the focus is now shifted from adsorption characteristics to electrical properties. Different precursor materials are available for the formation of activated carbon but acrylic fibers are better choice due to more yield, excellent natural structure, dust free nature and less ash content. In addition to high porosity, the electrical conductivity of activated carbon fibers is a key factor that has shifted the focus of studies from adsorption characteristics to electrical properties. Kuriyaman found that electrical conductivity of activated carbon fibers (ACF) increases as temperature increases, this behavior is similar to semi-conductors. The similar kind of trend was seen in active rods, saran carbon and glassy carbon heated at 1000 ~ 1100 k [5]. Much work is done on modelling of electrical conductivity ACF with temperature dependence. Fung is of the view that electrical resistivity of activated carbon fibers follow Mott's law with exponent of 1/2 as can be seen from equation 1 [6].

$$\sigma(T) = \sigma_0 \exp \left[- \sqrt{\frac{T_0}{T}} \right] \quad (1)$$

Here σ_0 is characteristic constant for conductivity, T is measuring temperature and T_0 is fitting parameter which is sensitive to energy required for hopping. However, Di Vittorio found that exponent 1/3 is more appropriate than 1/2 [7]. The electrical properties of activated carbon fibers vary widely and depend mainly on the structure of fibers. As far as carbon fibers are concerned, higher degree of crystallinity results in increase of thermal and electrical conductivity. When the carbonized fibers are further activated, the porous structure is greatly developed which has a major impact on lowering thermal and electrical properties. Di Vittorie made a comparison of electrical conductivity of activated carbon fibers from ex-pitch fibers and pitch based ACFs at 1000 °C. The electrical resistivity at room temperature of earlier was $7 \times 10^{-5} \Omega \text{ m}$, while that of latter was $2 \times 10^{-3} \Omega \text{ m}$. According to him the difference in electrical resistivity is because of difference in porosity of fibers [7]. Narrow micropores were developed during the start of activation process causing higher surface area of ACFs. But as the burn off increases during the activation process causes conversion of micropores to mesopores hence decrease in electrical conductivity. Hashisho also found that higher degree of activation removes material from ACF which increases the porosity but correspondingly decreases the conductivity. As with higher surface, the available cross-section for current to pass through the activated carbon fiber decreases [8]. During the beginning of activation process only narrow micro pores are developed which results in higher surface area [9]. As the time proceeds during activation process micro pores collapsed that is enlarged to mesopores due to burn off and hence electrical conductivity is decreased

correspondingly. The same trend has been proved by Hashisho and others who analyzed electrical resistivity of activated carbon fiber cloth by varying degree of porosity. It is clear that increasing activation causes increase in electrical resistivity due to increased amount of material removed from the surface of carbon fibers. Hence due to reduction of cross section area available for the electric charge to pass through the fiber and reduction of graphitic organization caused a reduction of electrical conductivity [8]. The ACF produced at higher temperatures favors production of turbostratic structure in inner regions of fiber which resulted in higher electrical conductivity at higher temperatures. Liu also showed that electrical resistivity of ACF increases by increasing activation time at a particular temperature due to reason that prolonged activation time ruined structural order formed during carbonization process. The electrical conductivity of activated carbon fiber is major concern for electrical applications and ohmic heating [10]. The electrical conductivity of ACFs can be improved by different methods like physical adsorption, surface functional groups incorporation and heat treatment. As already stated electrical conductivity increases by increasing carbonization temperature. As heat treatment of activated carbon fibers affect the electrical conductivity by changing the chemical and physical structure. High temperature during carbonization graphitizes carbon by aligning non-graphite domains thereby helps in generation of more ordered structure of nanographites [11]. Surface functional groups help in charge transfer hence have a strong influence on electrical properties of resulting activated carbon fibers. As doping of carbon fibers with electron acceptors or donors decreases or increase concentration of electrons. Oxygen is electron acceptor and it creates oxygen functionalities after reacting with edges of nano graphene sheets because edges of nano-graphene sheets are more reactive. Oxygen functional groups can be introduced in many ways like acid treatment of activated carbon fibers, which reduces electron hopping thereby increasing electrical conductivity of ACFs. On the other hand hydrogen treatment is used to reduce electrical resistivity by removing oxygen functional groups. Hashisho and Johnsen in their separate studies proved that electrical conductivity of activated carbon fibers increased by reducing oxygen functional groups although the ACFs did not change their crystalline structure and inter layer spacing of nano-graphitic layers [8, 12].

Theoretically any source material rich in carbon content can be used for the formation of carbon. Practically wood, coconut shells, peat and fruit stones and a number of other materials are also used, in laboratories municipal wastes [13], synthetic polymers [14], tyres and acrylic fibres [15] are also used to produce carbon fibres. However on industrial scale different kinds of synthetic and natural materials are in use for precursor materials like Polyacrylonitrile, phenolic resins, polyamides, pitch and cellulose. Literature shows that PAN based precursors are better than other precursors like rayon and pitch etc. due to greater carbon yield and higher melting point. The polyacrylonitrile (PAN) based precursors are dominant as compared with other precursors for the formation of carbon fibers. The PAN polymer is high melting polymer, relatively hard and insoluble in which carbon chains are connected to one another as shown in figure 1.

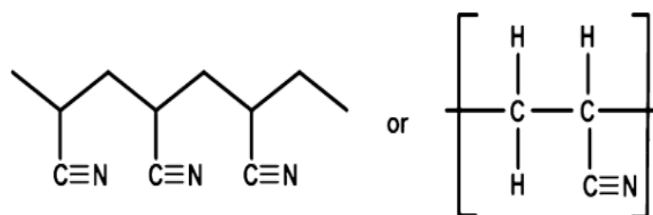


Fig. 1: Molecular structure of polyacrylonitrile [16]

PAN based carbon fibers have dominant edge over pitch and viscose rayon due to the following reasons.

- Because of its structure as shown in figure 5, it permits pyrolysis at faster rate without much disturbance in its basic structure as well as preferred orientation in molecular chains along the fiber axis as present in original fiber.
- The polymer decomposes before melting.
- When pyrolyzed at 1000 °C and above, high yield of carbon becomes possible.
- Improvement in molecular chains is possible during thermal stabilization as it becomes plastic around 180 °C and by different post spinning modifications [17].

The researchers are now trying to reduce the cost of carbon materials for using different cheap and alternate materials. In this context the idea of using acrylic fibrous waste is a favorable approach not only to reduce the cost of carbon but also for helping eco-friendly environment. Recently, the development of low cost, high performance and functional composites has gained much importance. In this context, biopolymers are an attractive materials because they can be easily biodegraded by microorganism even in local environment to their component elements[18][19]. Biopolymer is a type of polymer that is produced by living organisms like RNA, DNA, cellulose, starch and protein. Amongst these cellulose is the most common organic compound and biopolymer found on the earth. From structural point of view, biopolymers are not same as polymers. Biopolymers have a well-defined primary structure that folds to form compact shapes, however polymers have simple and random structure. The biopolymers and bioplastic market is rapidly increasing and is witnessed a current annual growth rate of 12.0 % from 2016 to achieve a market size around 5.08 US billion dollars by the year 2021 [20]. Polylactic acid is biodegradable thermoplastic aliphatic polyester produced from renewable resources like tapioca roots, corn starch or sugarcane. Since 2010, its consumption was second highest in terms of volume as compared with other biopolymers [21]. PLA biopolymer films accounted for roughly around 25% of the global industry share in 2015. It has become popular over other biopolymers due to its easy process ability, high mechanical strength and faster rate of decomposition. As a result, its use is increased in applications of food packaging, milk and water bottles, biodegradable plastics [22][23]. Besides its advantages, it has some drawbacks as well like its thermal and mechanical properties are not stable at high temperature [24]. To improve

performance and to incorporate functional characteristics, the addition of nano-fillers seems to be a favorable approach [25]. Keeping in view the above described advantages different group of researchers are in search to explore and improve properties by incorporating different particles. For instance, the addition of cellulosic nano particles improved the mechanical and thermo-mechanical properties of Polylactic acid significantly. Likewise addition of conductive particles in insulating polymers generate a new kind of intelligent materials called as conductive polymer nano-composites [26-29]. Millions of tons of textile waste is being landfilled every year. Last year Turkey landfilled around two hundred eighty thousand tons of textile waste which is only 2.62% of municipal solid waste. Environmental protection agency states that on average 31 kg of textile and clothing waste is generated by one person. The results are not too much difference in Europe where on average one UK citizen discards 30 kg of textile waste every year with a population of more than 500 million for the 27 countries of EU, this equates to approximately more than 18.3 million tons of clothing and textile waste generated every year. Textile waste is considered as one of the fastest growing sectors in terms of household waste and the amount of waste is forecast to continue growing as sales of new textiles and clothing continue to increase [30]. The main categories of clothing and textile waste are composed of synthetic materials such as acrylic, nylon and polyester and natural fibres such as wool, flax and cotton [31]. Due to strict rules and regulations for conserving nature, it is preferred and encouraged to utilize the fibrous wastes in value added applications. In recent years, research on recycling and reuse of textile wastes, instead of landfilling or incineration, has gained a lot of importance due to the increased awareness of environmental concerns [32][33]. This is because, textiles in landfill biodegrade to form methane gas and release it into the air which is not suitable for human consumption. Similarly incineration of textile wastes lead to release of toxic fumes which are hazardous in nature. European Union (EU) typically being more progressive on environmental issues have implemented laws (Directive 2000/53/CE) to prevent the landfilling of waste materials [34][35].

In the context of environment protection and current disposal of the textile wastes, it becomes essential to recover useful products from them for economic reasons. Traditionally, textile wastes are converted into individual fiber stage through cutting, shredding, carding, and other mechanical processes. However, due to increase in competition and reduced profit margins in these industries, it has become important to search for new recycling techniques to utilize them for high end applications. In this work, waste of acrylic fibers was converted into activated carbon by using high temperature furnace. The waste acrylic fibers were first stabilized at 250 °C under the application of tension. The stabilized fibers were then carbonized at different temperatures for getting higher values of electrical conductivity. Later these fibers were converted to carbon nano-particles through the action of ball milling process. After making the particles these were incorporated into PLA films with different proportions in order to develop green conductive composites.

2 EXPERIMENTAL

2.1 Material and method

The acrylic fibrous waste was provided by Grund Industries, Czech Republic in the form of bath mats. Every year abundant of acrylic fibrous waste is produced by Czech Republic in the form of bath mats. Traditionally these wastes are discarded or recycled by industries. However the cost of discarding or recycling has increased significantly in recent years due to the new regulations of European Union. These fibers were removed from bath mats by using mechanical cutting method. The physical characteristics of acrylic fibers as shown in table 1.

Table 1: Physical properties of acrylic fibers

Fineness [tex]	117
Tenacity [cN/tex]	23.84
Elongation [%]	45
Wet Shrinkage [%]	2.5

Polylactic acid was taken from NatureWorks LLC, USA, it has average molecular weight of 200,000 and a density of 1.26 g cm^{-3} . Chloroform was used as a solvent for dissolving PLA. It was purchased from Sigma Aldrich, Czech Republic.

2.2 Stabilization and carbonization of acrylic fibrous wastes

The acrylic fibers were first stabilized at $250 \text{ }^\circ\text{C}$ at the heating rate of $50 \text{ }^\circ\text{C h}^{-1}$. The stabilized fibers were then pyrolysis in order to have gradual reaction of atmospheric air with carbonized acrylic fibrous waste. The carbonization behavior was studied under two variables:

- Final pyrolysis temperature (FPT)
- Heating rate per hour (HRPH)

Three levels of final temperature were selected that is $800 \text{ }^\circ\text{C}$, $1000 \text{ }^\circ\text{C}$ and $1200 \text{ }^\circ\text{C}$. Heating rate was varied from $150 \text{ }^\circ\text{C h}^{-1}$ to $450 \text{ }^\circ\text{C h}^{-1}$. These variables were optimized to get higher electrical conductivity.

2.3 Effect of carbonization temperature on the properties of activated carbon fibers

Later the stabilized fibers were further heated to high temperature for single stage carbonization and activation. The carbon fibers were prepared at final temperature of $800 \text{ }^\circ\text{C}$, $1000 \text{ }^\circ\text{C}$ and $1200 \text{ }^\circ\text{C}$, with no holding time and heating rate of $300 \text{ }^\circ\text{C h}^{-1}$. The stabilization of acrylic fibers at $250 \text{ }^\circ\text{C}$ leads to cyclization, dehydrogenation, and oxidation of Polyacrylonitrile structure [37]. During this stage, nitrile groups form non-melttable ladder structure, which further enhances mechanical properties and final carbon yield. During subsequent carbonization of stabilized fibers, the ladder polymer further cross links to form turbostatic carbon structure and the orientation of basal

planes leads to graphite like structure. After carbonization physical and analytical characterization was done on the prepared activated carbon fibers. Physical characterization included yield %, shrinkage, flexibility and dusting properties.

The shrinkage of activated carbon fibers was measured as per ASTM D 2259 standard available for testing textile fibers. The shrinkage was evaluated from change in length of web before and after carbonization. Similarly like shrinkage, yield of activated carbon before carbonization and after carbonization at different temperatures was calculated by using the equation 2.

$$Yield = \frac{\text{Final weight of activated web}}{\text{Initial weight of acrylic web}} \times 100 \quad (2)$$

The flexibility or stiffness was evaluated from bending length by employing the principle of cantilever bending of the web under its own weight as per ASTM D 1388 standard.

2.4 Effect of carbonization temperature on electrical conductivity

Hewlett Packard 4339 B high resistance meter was used to measure the surface electrical resistance of carbonized fibres. The environmental condition for the measurement was kept at 22 °C temperature and 29.5 % relative humidity and voltage used was 100 V. Due to high electrical conductivity of carbonized fibres, alternative method of characterization using multimeter was also used.

2.5 Preparation of nanoparticles from carbonized acrylic fibrous wastes

After getting the optimum pyrolysis parameters, dry pulverization of carbonized acrylic fibrous waste was carried out using high energy planetary ball milling of Fritsch pulverisette 7, Germany. The sintered corundum container of 80 ml capacity and zirconium balls of 10 mm diameter were chosen for 3 hours of dry milling. The ball to material ratio (BMR) was kept at 10:1 and the speed was kept at 850 rpm.

2.6 Characterization of activated carbon nanoparticles

Particle Size. Particle size distribution of dry milled activated carbon particles was studied after each hour of milling on Malvern zetasizer nano series based on dynamic light scattering principle of brownian motion of particles. Deionized water was used as dispersion medium and it was ultrasonicated for 5 min with bandelin ultrasonic probe before characterization. In addition, morphologies of dry milled activated carbon particles were observed on scanning electron microscope (SEM) of TS5130-Tescan at 30 kV accelerated voltage and on field emission scanning electron microscope (FESEM) of Zeiss at 5 kV accelerated voltage. The amount of 0.01 g of carbon black particles was dispersed in 100 ml acetone and then a drop of the dispersed solution was placed on aluminum foil and gold coated after drying.

Electrical Conductivity. The pulverized activated carbon particles were taken out after every 30 min of dry milling and dispersed in distilled water using Bandelin SONOPLUS ultrasonic probe. The electrical conductivity of dispersion was measured by conductometer under different concentrations of activated carbon particles from 0.5 to 4.0 wt %.

EDX analysis. Energy dispersive X-ray spectroscopy (EDX) analysis is an analytical technique used for the elemental analysis or chemical characterization of a sample. EDX analysis was done to find out the different elements and their concentrations in carbonized samples prepared at 800 °C, 1000 °C and 1200 °C.

XRD analysis. In order to know the development of crystallinity with increase of temperature, the XRD analysis was carried out by using PAN analytical X pert MPD diffraction system. X-ray diffraction (XRD) is a technique used for the identification of crystalline material and analysis of unit cell dimensions. Degree of crystallinity can be calculated by using equation 2 [38].

$$I_c = 1 - \frac{I_1}{I_2} \quad (2)$$

I_1 is intensity at minimum peak

I_2 is intensity at maximum peak

2.7 Preparation of Poly-lactic acid films

Firstly, 5 % by weight Polylactic acid was dissolved into chloroform to make a solution of 100 g L⁻¹. The pre-weighted amounts of carbon nano-particles derived from acrylic fibrous waste (1-10 wt% related to mass of films) were mixed in 100 ml solution of PLA and chloroform. The mixture was first stirred by the help of magnetic stirrer for 3 hours at room temperature then ultra-sonicated for 15 minutes on BANDELIN Ultra Sonic Probe Mixer with 50-horn power. The prepared homogenous solution was poured in mould (6 cm × 4 cm) on a Teflon sheet. The films were kept at room temperature and after 20 hours the prepared film were removed from moulds, folded and hot pressed at 140 °C. This helps to improve uniform dispersion of particles in the polymer. The process of hot press was repeated three times to ensure uniform distribution of particles in the polymer.

2.8 Characterization of Poly-lactic acid films

Dynamic mechanical analysis (DMA). Dynamic mechanical analysis was carried out on DMA DX04T RMI instrument, Czech Republic in tensile mode. The measurements were carried out at constant frequency of 1 Hz, strain amplitude of 0.05 %, temperature range of 35–100 °C, heating rate of 5 °C/min and jaw distance of 30 mm. The samples were prepared by cutting strips from the films with a width of 10 mm. The total of three tests was done to characterize each composite sample.

Differential scanning calorimetry (DSC). The melting and crystallization behavior of neat and composite films was investigated on DSC 6 Perkin Elmer instrument under

nitrogen atmosphere with sample weight of 7 mg. The sample was heated from 25 °C to 200 °C at a rate of 5 °C/min.

Thermo gravimetric analysis (TGA). Thermo gravimetric analysis (TGA) TGA/SDTA 851, Metler Toledo is used to study the desorption rate. The weight of PLA film used was approximately 9 mg and films were heated to 900 °C at a rate of 10 °C min⁻¹ in the presence of nitrogen atmosphere.

Electrical properties. The resistivity of PLA carbon films prepared was measured according to ASTM D 257-14 at temperature 22 °C and relative humidity 40 %. The specific voltage potential of 1V using direct current was applied across opposite ends of activated carbon web and resultant current flowing across the sample was measured after 15 ± 1 s. Electrical conductivity of activated carbon webs was measured by two different techniques.

- Parallel electrode method
- Concentric electrode method

Electrical conductivity or specific conductance is the reciprocal of electrical resistivity and measures the ability of a material to conduct electric current. Electrical conductivity is commonly represented by Greek letter σ (*sigma*). *S.I unit of conductivity is Siemens per meter (S/m)*. The parallel electrode instrument is shown in figure 2. By using this apparatus surface resistance was determined.

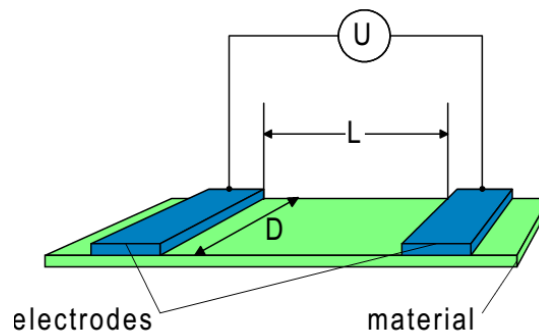


Fig. 2: Surface resistivity measurement set up for parallel electrode

Surface resistivity is calculated by using the equation 3.

$$\rho = R \times \frac{D}{L} \quad (3)$$

ρ = Surface resistivity(Ω), D = Width of electrode (5 cm), R = Electrical resistance (Ω), L = Distance between electrode (2 cm)

The second method used for measuring conductivity is shown in figure 3. In this method conductivity was measured at 22 °C temperature with relative humidity of 62 %. The specific voltage potential of 1 volt was applied across the webs of activated carbon webs and readings were measured at 15 seconds. The conductivity was calculated by using equation 4.

$$\text{Surface resistivity} = \rho = R \times 9.99 \quad (4)$$

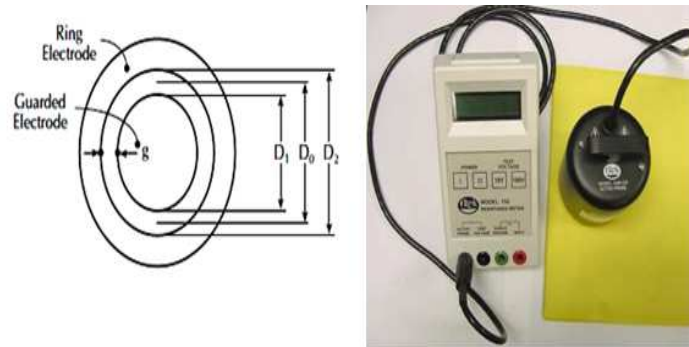


Fig. 3: Surface resistivity measurement set up for concentric ring electrode

3. RESULTS AND DISCUSSIONS

3.1 Effect of carbonization temperature on the properties of activated carbon fibers

When the temperature is increased from 800 °C to 1200 °C, the reaction of newly formed carbon with available oxygen increased which resulted in decreasing yield of carbon and consequently shrinkage was increased and more rigid structure of activated carbon was achieved.

Table 2: Effect of carbonization temperature on physical properties of activated carbon fibers

Run	Final pyrolysis temperature [°C]	Heating rate [°C hr ⁻¹]	Resistivity [Ohm.mm]	Yield [%]	Flexibility
1	800	150	169.65	60.33 ± 3.13	Good
2	800	300	1174.50	61.27 ± 3.63	Good
3	800	450	323.11	63.33 ± 2.55	Average
4	1000	150	4.69	55.88 ± 2.33	Average
5	1000	300	3.21	57.12 ± 1.83	Poor
6	1000	450	2.08	58.55 ± 1.98	Poor
7	1200	150	0.67	46.45 ± 1.89	Poor
8	1200	300	0.52	45.11 ± 1.60	Poor
9	1200	450	0.65	49.11 ± 2.12	Poor

Because of this reason activated carbon fibers at high temperature showed poor flexibility and dusting behavior as can be seen from table 2. When the heating rate is increased from $150\text{ }^{\circ}\text{C hr}^{-1}$ to $450\text{ }^{\circ}\text{C hr}^{-1}$ the yield of carbon fibers increased to some extent because at slow heating rate carbonized fibers remain to high temperature for longer time causing reduction of yield and also adversely effects on flexibility of carbon fibers. Figure 4 shows two possible modes of electron transport (i.e. migration and hoping) in the activated carbon fibers produced at $800\text{ }^{\circ}\text{C}$, $1000\text{ }^{\circ}\text{C}$ and $1200\text{ }^{\circ}\text{C}$ respectively. The development of electrical conductivity can be explained from the migration of electrons in one graphite layer or their jumping across the defects/interfaces between disordered graphite layers [39-40]. The higher electrical conductivity indicated relatively easier migration and hoping of electrons in case of $1200\text{ }^{\circ}\text{C}$ activated carbon fibers than $800\text{ }^{\circ}\text{C}$ and $1000\text{ }^{\circ}\text{C}$. At high temperature more conductivity is because of higher crystallinity and more parallel arrangement of carbon layers and carbon content as can be seen from figure 4.

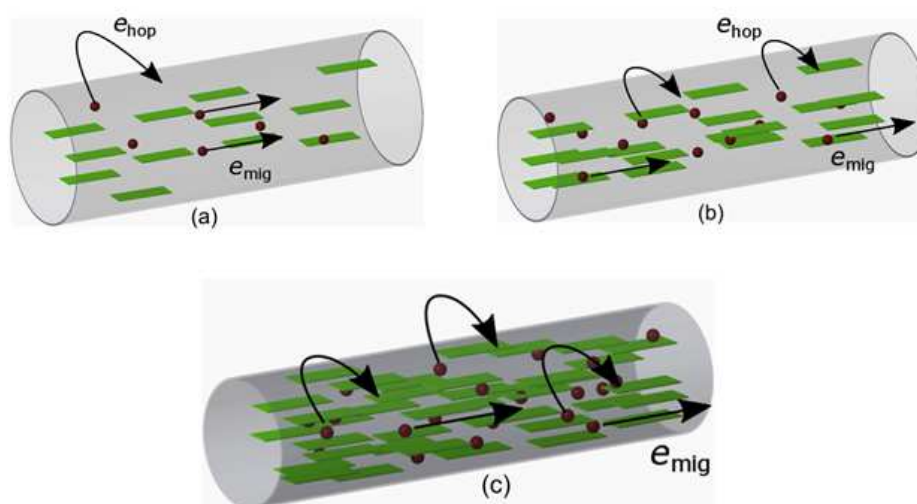


Fig. 4: Mechanism of charge transport in (a) $800\text{ }^{\circ}\text{C}$ activated carbon (b) $1000\text{ }^{\circ}\text{C}$ activated carbon (c) $1200\text{ }^{\circ}\text{C}$ activated carbon

3.2 CHARACTERIZATION OF CARBON NANO PARTICLES

Particle size. Figure 5(a), Figure 5(b) and Figure 5(c) show the particle size distribution results of dry milled activated carbon particles for different time of milling from one hour to three hours. It can be seen from Figure 5(a) that the rate of particle size reduction is higher during the initial one hour of milling during which the characteristic particle diameter Z-average reduced to 1563 nm . However, the particle size was gradually reduced later and reached to 521 nm after three hours of dry milling as shown in Figure 5(c). When milling was performed for longer time, particle size distribution changed from multimodal distribution to near unimodal distribution. The reason behind multimodal distribution of particles is due to increase in temperature within the mill because of continuous impact of balls [41-42]. The increased temperature of mill rendered the activated carbon particles to undergo cold welding and deposited a layer on the surface of milling media. The growth of deposited layer changed the impact force of balls on the material with least impact on

particles at bottom of layer. The morphology of activated carbon particles after three hours of dry milling was further investigated with the help of SEM images shown in Figure 6 (a), Figure 6 (b) and Figure 6 (c). The shape of activated carbon particles was observed in the form of mixture of both nanoparticles and nano-segments. The few carbon particles with higher aspect ratio were found due to inability of milling process as a result of increased temperature.

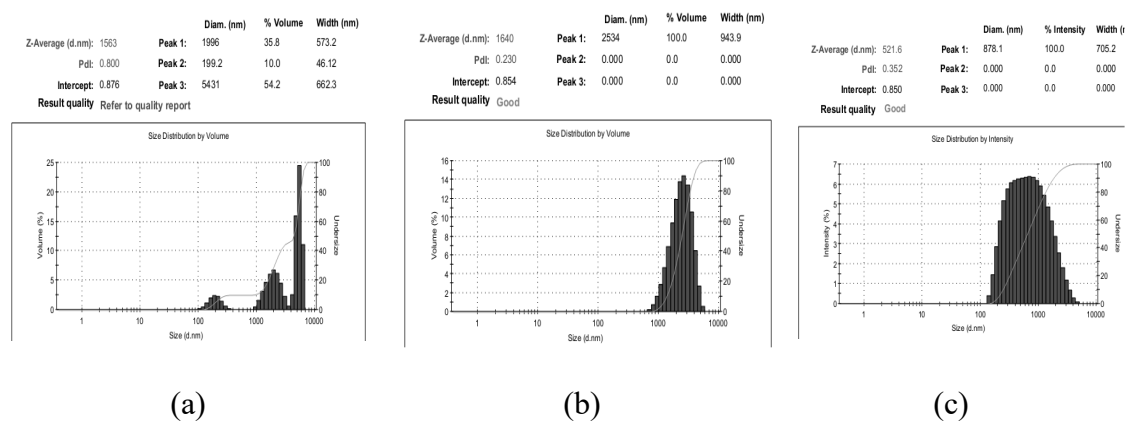


Fig. 5: Particle size distribution after milling (a) one hour (b) two hour (c) three hour

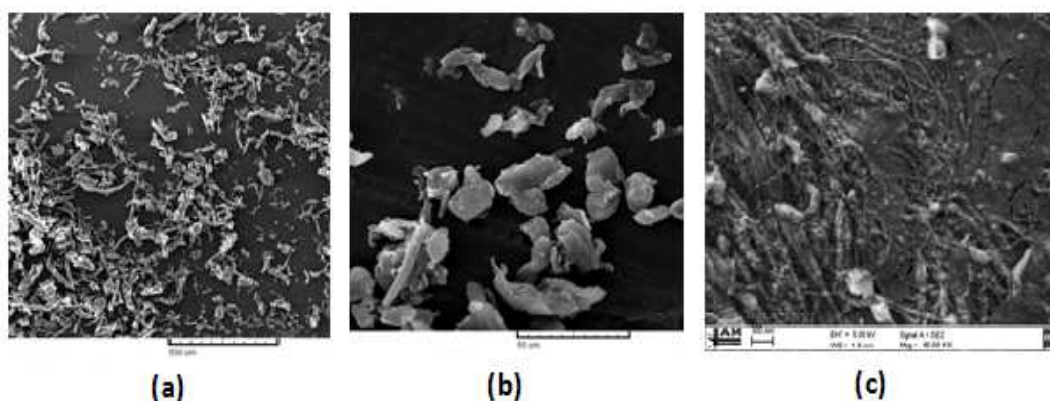


Fig. 6: Activated carbon particles after (a) one hour milling (b) Two hour milling (c) three hour milling

Electrical Conductivity. Figure 7 shows the electrical conductivity of aqueous dispersion of activated carbon particles measured under different concentrations from 0.5 to 4.0 wt %. The influence of dry milling time on electrical conductivity is clearly observed under lower concentration of carbon particles at 1 wt % and below, where electrical conductivity of aqueous dispersion of carbon particles increased significantly with increase in dry milling time.

This behavior was attributed to increase in surface area and reduction in size of activated carbon particles at extended milling time. For higher concentration of carbon particles (i.e. 2 wt % and 4 wt %), there is gradual increase in electrical conductivity with increase in dry milling time. This behavior is attributed to early achievement of percolated network of carbon particles due to their higher loading in aqueous dispersion.

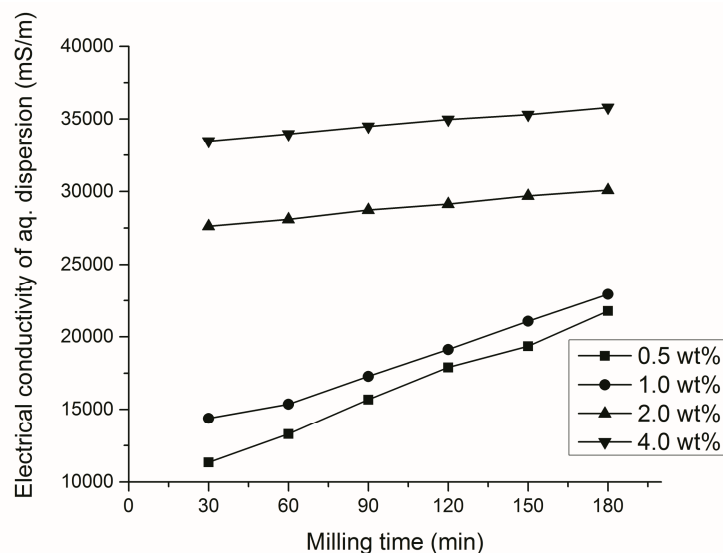


Fig. 7: Effect of milling time on electrical conductivity of activated carbon particles

EDX analysis. EDX analysis was done to find out the different elements and their concentrations in activated carbon fibers. From table 3, the increase in carbon content and reduction in oxygen content was found with increase in carbonization temperature from 800 °C to 1200 °C. The activated carbon web produced at 1200 °C exhibited 92.49 % carbon content and 6.61 % oxygen content because of more removal of hetero atoms and as the temperature kept on increasing the proportion of carbon also increased [25].

XRD analysis. In order to know the development of crystallinity with increase in carbonization temperature, the XRD analysis was carried out. Figure 8 shows the XRD pattern of different activated carbon particles prepared at 800 °C, 1000 °C and 1200 °C temperature. The degree of crystallinity is increased from 82.21 % to 86.7 and then finally reached to 92.41% by increasing temperature from 800 °C to 1000 °C and then finally to 1200 °C. The higher degree of crystallinity at higher temperature indicates more parallel orientation of chains.

3.3 Characterization of polylactic acid films

Electrical conductivity. Poly(lactic acid)/carbon films were produced by adding different amounts of acrylic-derived carbon particles prepared in this study into the solution of PLA with chloroform and later evaporating the solvent. The obtained composite films of PLA carbon showed conductivity at the loading of 10 % by weight of carbon particles prepared at 1200 °C after 3 hour of dry milling. In another study it was revealed that by the addition of 10 % carbon particles, PLA films showed conductivity lower than 1 Ω m [43]. However by the addition of 3 % carbon black particles, electrical conductivity was achieved in high density polyethylene (HDPE) [44]. The electrical conductivity of carbon particles prepared from acrylic fibrous waste can be seen from table. The contact resistance between carbon particles decreases when the surface area between them is increased due to which particles

prepared at 1200 °C with three hours of milling was selected for making the films.

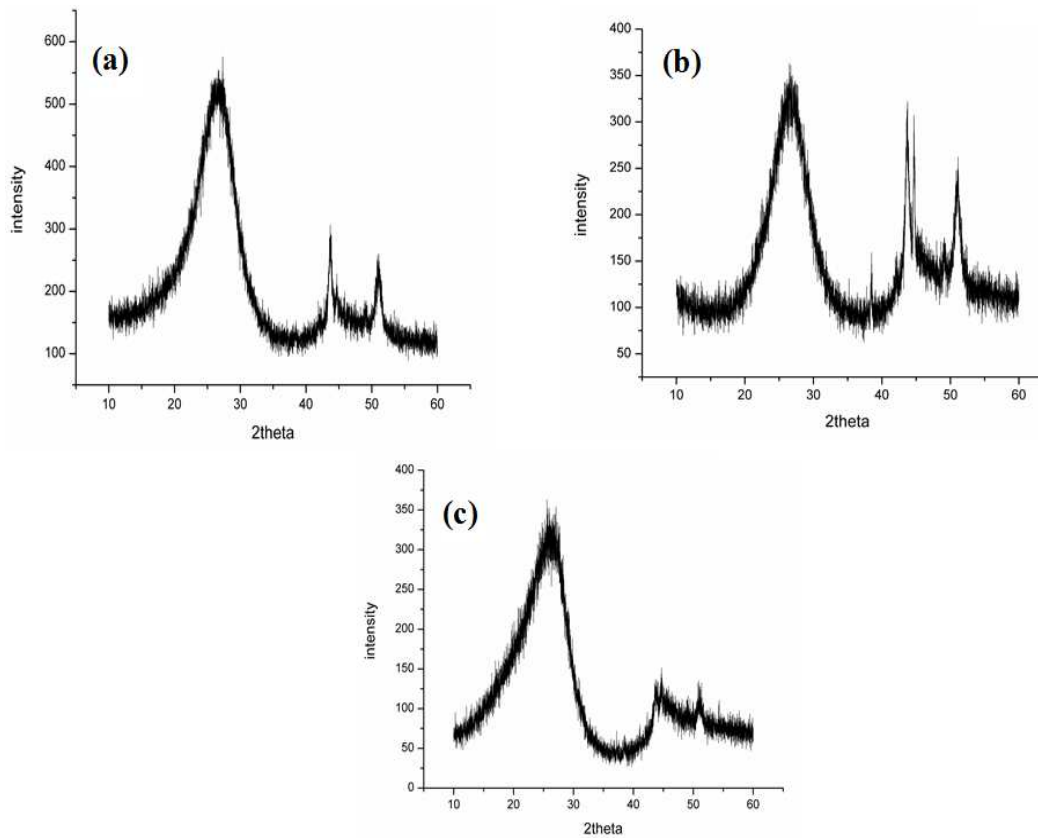


Fig. 8: Effect of carbonization temperature on crystallinity of activated carbon web prepared at 800 °C (a), 1000 °C (b) and 1200 °C (c)

The origin of electrical-conduction process is explained because of conductivity at high concentration of carbon particles which enables transport of electrical charges across micro contacts between the carbon particles dispersed in a homogenous way in PLA films. The path of electrical conduction is established because of particle to particle network which creates a network of channeling extending throughout the film. Both the instruments gave similar values of conductivity as show. The films prepared at 5 % showed very less conductivity but the film prepared at 10 % by weight showed increase in conductivity due to more establishing of electrical network as can be seen from table 4.

Table 4. Electrical resistivity of PLA-carbon films

1	PLA-5% carbon	$230 \pm 2.33 \Omega\text{m}$
2	PLA-10% carbon	$1.8 \pm 1.90 \Omega\text{m}$

Dynamic mechanical analysis. The load bearing capacity of neat PLA and activated carbon particles (ACP)/PLA composite films was studied from the storage modulus results shown in the Figure 9 (a) and Table 5. The storage modulus of the ACP /PLA composite films was improved over the entire temperature span compared to neat

PLA. The maximum improvement was observed in case of 5 wt % composite where storage modulus was increased from 2.04 to 3.84 GPa at 30 °C. This increase in storage modulus value is attributed to the higher stiffness of ACP during the transfer of stress from the matrix to carbon particles. However, with further increase in loadings of ACP to 10 wt %, storage modulus reduced to 2.46 GPa because of poor dispersion and agglomerations of particles which increased the stress concentration points. With the increase in temperature from 30 to 60 °C, the storage modulus of neat PLA dropped at faster rate than PLA composite films. The storage modulus was dropped by 14 times in neat PLA, whereas the drops of 5 and 9 times were observed in case of 1 and 10 wt% composites films, respectively. The significant drop in storage modulus of neat PLA at 60 °C is due to the softening of matrix and easier movement of PLA chains. The relatively smaller drop in case of composite films is attributed to the presence of ACP, which restricted the motion of PLA chains. At 60 °C, PLA composite films of 1 and 10 wt% ACP showed 271 %, and 85.00% respective increase in storage modulus as compared to neat PLA films. The higher storage modulus values of PLA composite films compared to neat PLA above 60 °C are attributed to the nucleating behavior of ACP, which improved crystallinity of PLA through trans-crystallization. The development of crystallinity after addition of ACP is explained later in section of differential scanning calorimetric analysis. The ratio of loss modulus to storage modulus is defined as mechanical loss factor or tan delta. Figure 9 shows that the tan delta peak of PLA was positively shifted with increased content of ACP in composites. The shift of 13 and 11 °C was observed in case of 1 and 5 wt % ACP/PLA composites, respectively. The positive increments in shift of tan delta are attributed to the increased surface area of interaction between the matrix and particles, which restricted the segmental mobility of the matrix chains around them. The indistinct or negligible peak in 10 % ACP/PLA composites showed their inability for damping properties due to compact filling of carbon particles.

Differential scanning calorimetry analysis. The behavior of neat PLA and PLA films reinforced with carbon nanoparticles on the application of heat is studied from DSC thermograms as shown in figure 10. The glass transition (T_g), followed by the polymer cold crystallization (T_{cc}), and the polymer melting (T_m) can be observed on the thermograms of all samples. These three parameters are typical for semi crystalline PLA. Table 6 shows that T_g value of PLA increased with the increased loading of ACP. The maximum improvement was observed in case of 10 wt % of ACP where T_g was increased from 42 to 47 °C as compared to the neat PLA film. The T_g is a complex phenomenon, which depends on intermolecular interactions, steric effects, chain flexibility, molecular weight, branching, and the cross linking density. The corresponding increase in value of T_g by 2%, 7%, and 12% over neat PLA film can be attributed to the reduced PLA chain flexibility after addition of 1, 5, and 10 wt% ACP, respectively. With the addition of ACP, the cold crystallization peak found to become broader and shifted to higher temperatures as compared to the cold crystallization of neat PLA. The higher T_{cc} observed in the heating run can be an

indication of slower crystallization induced by ACP. It is clear from Table 6 that T_m of PLA improved at lower loading of ACP and then remained constant till 5 % ACP.

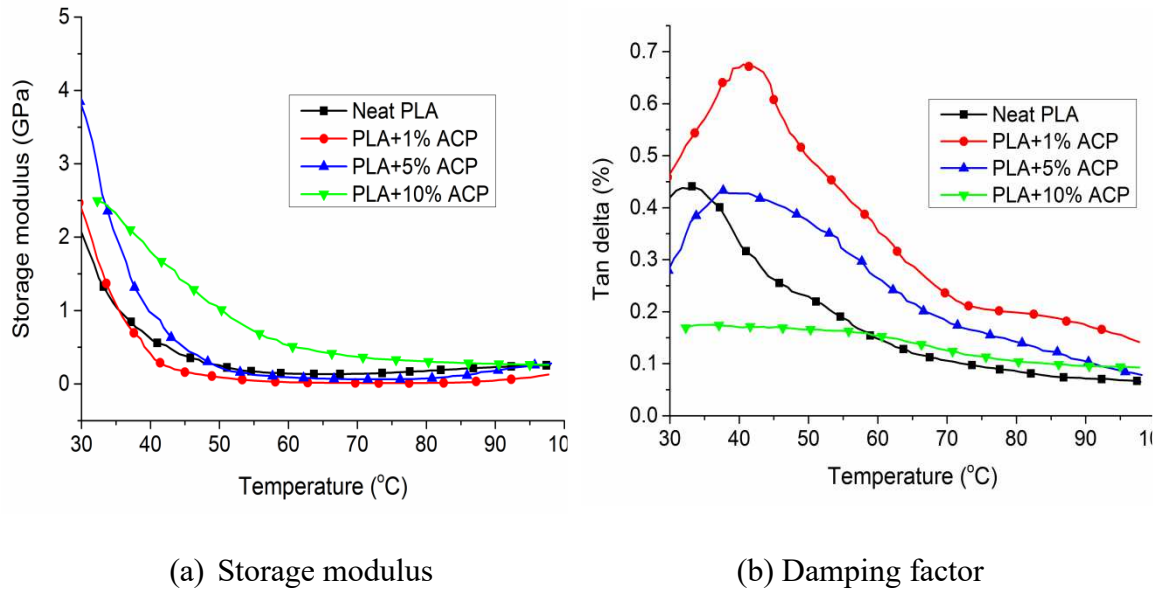


Fig. 9: Dynamic mechanical properties of PLA composite

Table 5: Storage modulus of ACP/PLA composites films at different temperature

Sample name	E' [30°C] GPa	E' (60 °C) (GPa)	E' (90 °C) (GPa)
Neat PLA	2.04±0.15	0.14±0.20	0.22±0.02
PLA+1% ACP	2.49 ± 0.50	0.52 ± 0.80	0.27 ± 0.21
PLA+5% ACP	3.84 ± 0.35	0.09 ± 0.46	0.18 ± 0.04
PLA+10% ACP	2.46 ± 0.24	0.26 ± 0.55	0.04 ± 0.26

The increase in T_m from 147 to 151 after addition of 1-5 wt% ACP can be attributed to the adhesion between particles and PLA matrix. A more careful observation of the thermograms of the composites reveals the presence of small endotherms just before the main melting peaks. The melting peak at higher temperature (T_{m2}) was attributed to a more perfect crystalline structure of PLA and the shoulder peak at lower temperature (T_{m1}) to a less perfect crystalline structure. This indicated that PLA develops more heterogeneous crystalline morphology after addition of ACP.

Table 6: Behavior of neat and ACP/PLA composite films on application of heat

Sample	T_g [°C]	T_{cc} [°C]	T_m [°C]
Neat PLA	42± 0.3	80 ± 1.1	147 ± 0.1
PLA+1% ACP	43 ± 0.5	107± 1.2	151 ± 0.1
PLA+5% ACP	45 ± 0.6	111 ± 1.4	151 ± 0.2
PLA+10% ACP	47 ± 1.2	96 ± 1.5	153 ± 0.5

Thermogravimetric analysis. For analysis of thermal stability of pure PLA films and PLA reinforced with carbon particles at different loadings, thermogravimetric analysis was performed. TGA of PLA with carbon particles showed thermal and oxidative stability, mass loss and decomposition temperature during heat treatment as shown in figure 11. The start of mass loss observed in all three films around 80 to 90.

The neat PLA-film degraded with negligible residue while PLA-carbon films left with residue related to carbon. The residue kept on increasing when the content of carbon was increased from 1% to 5% and finally to 10 % which is clear indication that thermal stability of PLA films increased after addition of carbon particles. The 20.19 % increase in mass was achieved by adding 10 % loading of carbon particles. The increase in thermal stability is because of more homogenous distribution of carbon in PLA matrix which caused positive impact on the volatile products of PLA. The results are very much similar with previously reported thermal stability of PLA with halloysite and silica nano-particles[45][46].

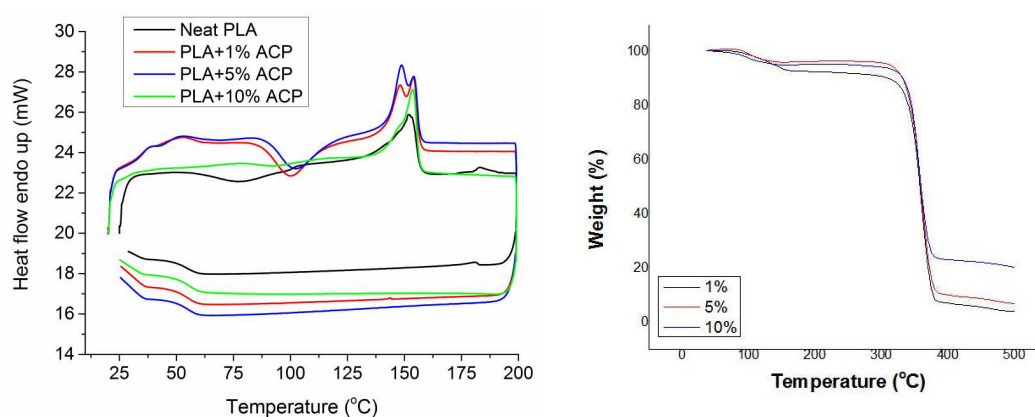


Fig. 10: Differential scanning calorimetry of PLA composites

4. CONCLUSIONS

The objective of this study was to successfully utilize acrylic fibrous waste for the formation of activated carbon and later on incorporated with biopolymer to get functional characteristics of PLA composites. As the temperature of carbonization was increased from 800 °C to 1000 °C and finally to 1200 °C, electrical conductivity also kept on increasing due to more parallel orientation of carbon basal planes. The higher electrical conductivity of activated carbon sample prepared at 1200 °C was attributed to more graphitization, which was confirmed from presence of sharp diffraction peak observed in XRD spectra and higher degree of crystallinity. As the temperature during carbonization was increased, the degree of crystallinity along with carbon content in carbonized fibres also increased, which is the main cause for decrease in resistivity. Hence carbon fibres produced by carbonization at 1200 °C were dry pulverized through the use of high energy planetary ball milling process. The carbon nanoparticles produced after three hours of ball milling showed more uniform distribution of size. These particles were mixed with PLA to get conductive biopolymer films. The electrical conductivity not only depends on uniform distribution of particles but also to higher loading of particles. Not only electrical properties of PLA films increased by the addition of carbon nanoparticle but also

thermal stability of films also increased due to more homogenous distribution and high temperature bearing characteristics of carbon particle. Furthermore the presence of activated carbon particles in the PLA films favors for improvement in thermal stability of PLA. Hence on the basis of above discussion it is clear that technique for dry milling of carbonized fibres from acrylic fibrous waste is simple, economical and environment friendly approach for the formation of conductive biopolymer films.

References

- [1] D. Negru, C. Buda, and D. Avram, "Electrical Conductivity of Woven Fabrics Coated with Carbon Black Particles," *Fibres Text. East. Eur.*, vol. 20, no. 1, pp. 53–56, 2012.
- [2] H. Chen, K. Lee, J. Lin, and M. Koch, "Comparison of electromagnetic shielding effectiveness properties of diverse conductive textiles via various measurement techniques," *J. Mater. Process. Technol.*, vol. 192, pp. 549–554, 2007.
- [3] M. Lennox and R. Kerr, "Current State of Electrically Conductive Materials," *High Perform. Text.*, vol. 11, pp. 6–7, 1990.
- [4] B. Mahltig, D. Darko, K. Günther, and H. Haase, "Copper Containing Coatings for Metallized Textile Fabrics," *J. Fash. Technol. Text. Eng.*, vol. 3, no. 1, pp. 1–10, 2015.
- [5] K. Kuriyama and M. Dresselhaus, "Photoconductivity of activated carbon fibers," *J. Mater.*, vol. 6, no. 5, pp. 1040–1047, 1991.
- [6] J. Chen, *Activated carbon fiber and textile*. UK: Woodhead Publishing, 2016.
- [7] S. Di Vittorio, M. Dresselhaus, M. Endo, J. Issi, L. Piraux, and V. Bayot, "The transport properties of activated carbon fibers," *J. Mater. Res.*, vol. 6, no. 4, pp. 778–783, 1991.
- [8] Z. Hashisho, M. Rood, S. Barot, and J. Bernhard, "Role of functional groups on the microwave attenuation and electric resistivity of activated carbon fiber cloth," *Carbon N. Y.*, vol. 47, no. 7, pp. 1814–1823, 2009.
- [9] S. Ryu, S. Kim, N. Gallego, and D. Edie, "Physical properties of silver-containing pitch-based activated carbon fibers," *Carbon N. Y.*, vol. 37, no. 10, pp. 1619–1625, 1999.
- [10] C. Liu, W. Dong, G. Cao, J. Song, and L. Liu, "Capacitance limits of activated carbon fiber electrodes in aqueous electrolyte," *J. Electrochem. Soc.*, vol. 155, no. 1, pp. 1–7, 2008.
- [11] S. Mrozowski, "Semiconductivity and diamagnetism of polycrystalline graphite and condensed ring systems," *Phys. Rev.*, vol. 85, no. 4, pp. 609–620, 1952.
- [12] D. Johnsen, Z. Zhang, H. Emamipour, Z. Yan, and M. Rood, "Effect of isobutane adsorption on the electrical resistivity of activated carbon fiber cloth with select physical and chemical properties," *Carbon N. Y.*, vol. 76, pp. 435–445, 2014.
- [13] P. Williams and A. Cunliffe, "Properties of chars and activated carbons derived from the pyrolysis of used tyres," *Environ. Technol.*, vol. 19, no. 1, pp. 1177–1190, 1998.
- [14] P. Williams and W. Buad, "Activated carbons prepared from refuse derived fuel

- and their gold adsorption characteristics,” *Environ. Technol*, vol. 31, no. 2, pp. 125–137, 2010.
- [15] J. Nabais, M. Ribeiro Carrot, Pajares, and P. Carrott, “Preparation of activated carbon fibres from acrylic textile fibres,” *Carbon N. Y.*, vol. 39, no. 10, pp. 1453–1555, 2001.
- [16] M. S. A. Rehman, A. Ismail, and A. Mustafa, “A review of heat treatment on polyacrylonitrile fiber,” *Polym. Degrad. Stab*, vol. 92, no. 8, pp. 1421–1432, 2007.
- [17] J. Donnet and T. Wang, *Carbon Fibers*, 3rd ed. London: London: CRC Press, 1998.
- [18] G. Charles, C. Gebelein, and J. Carraher, *Biotechnology and bioactive polymers*. New York: Plenum, 1994.
- [19] G. Scott, *Biodegradable Plastics and Polymers*. London, U.K: Elsevier, 1994.
- [20] “Global markets and technologies for bioplastics,” 2016.
- [21] L. Wang, B. Tay, K. See, Z. Sun, L. Tan, and D. Lua, “Electromagnetic interference shielding effectiveness of carbon-based materials prepared by screen printing,” *Carbon N. Y.*, vol. 47, pp. 1905–1910, 2009.
- [22] M. Inagaki, J. Qiu, and Q. Guo, “Carbon foam: preparation and application,” *Carbon N. Y.*, vol. 87, pp. 128–152, 2015.
- [23] J. Kim, E. Jeong, and Y. Lee, “Preparation and characterization of graphite foams,” *J. Ind. Eng. Chem*, vol. 32, pp. 21–33, 2015.
- [24] H. Wang, K. Zheng, X. Zhang, X. Ding, Z. Zhang, and C. Bao, “3D network porous polymeric composites with outstanding electromagnetic interference shielding,” *Compos Sci. Technol*, vol. 125, pp. 22–29, 2016.
- [25] D. Yan, P. Ren, H. Pang, Q. Fu, M. Yang, and Z. Li, “Efficient electromagnetic interference shielding of lightweight graphene/polystyrene composite,” *J. Mater Chem*, vol. 22, pp. 37-46, 2012.
- [26] V. Safarova and J. Militky, “Comparison of methods for evaluating the electromagnetic shielding of textiles,” *Vlakna a Text.*, vol. 2, pp. 12–18, 2012.
- [27] P. Wang, Z. Yue, and J. Liu, “Conversion of polyacrylonitrile fibers to activated carbon fibers: effect of activation,” *J. Appl. Polym. Sci.*, vol. 60, no. 7, pp. 923–929, 1996.
- [28] S. Qu, F. Huang, S. Yu, G. Chen, and J. Kong, “Magnetic removal of dyes from aqueous solution using multi-walled carbon nanotubes filled with Fe₂O₃ particles,” *J. Hazard. Mater.*, vol. 160, pp. 643–647, 2008.
- [29] V. Baheti, S. Naeem, J. Militky, M. Okrasa, and B. Tomkova, “Optimized preparation of activated carbon nanoparticles from acrylic fibrous wastes,” *Fibers Polym.*, vol. 16, pp. 2193–2201, 2015.
- [30] D. Negru, C. Buda, and D. Avram, “Electrical Conductivity of Woven Fabrics Coated with Carbon Black Particles,” *Fibres Text. East. Eur.*, vol. 20, no. 1, pp. 53–56, 2012.
- [31] H. Chen, K. Lee, J. Lin, and M. Koch, “Comparison of electromagnetic shielding effectiveness properties of diverse conductive textiles via various measurement techniques,” *J. Mater. Process. Technol.*, vol. 192, pp. 549–554, 2007.
- [32] W. Youjiang, *Recycling in Textiles*, 1st ed. UK: Woodhead Publishing, 2006.

- [33] H. Richard, *Recycling textile and plastic waste*, 1st ed. UK: Woodhead publishing, 1996.
- [34] P. Soraia and T. Silvestre, "Recycling carbon fibre reinforced polymers for structural applications: Technology review and market outlook," *Waste Manag.*, vol. 31, pp. 378–392, 2011.
- [35] R. Witik, R. Teuscher, V. Michaud, C. Ludwing, and J. A. Manson, "Carbon fibre reinforced composite waste: An environmental assessment of recycling, energy recovery and landfilling," *Compos. part A*, pp. 89–99, 2013.
- [37] Y. Liu, Y. Choi, H. Chae, P. Gulgunje, and S. Kumar, "Temperature dependent tensile behavior of gel-spun polyacrylonitrile and polyacrylonitrile/carbon nanotube composite fibers," *Polym.*, vol. 54, no. 15, pp. 4003–4009, 2013.
- [38] G. Siqueira, H. Abdillahi, J. Bras, and A. Dufresne, "High reinforcing capability cellulose nanocrystals extracted from *Syngonanthus nitens*," *Cellulose*, vol. 17, pp. 289–298, 2010.
- [39] W. Song, M. Cao, Z. Hou, X. Fang, X. Shi, and J. Yuan, "High dielectric loss and its monotonic dependence of conducting-dominated multiwalled carbon nanotubes/silica nanocomposite on temperature ranging from 373 to 873 K in X-band," *Appl. Phys. Lett.*, vol. 94, pp. 1–4, 2009.
- [40] M. Wen, Z. Cao, W. Hou, L. Song, Zhang, and M. Lu, "Temperature dependent microwave attenuation behavior for carbon-nanotube/silica composites," *Carbon N. Y.*, vol. 65, pp. 124–139, 2013.
- [41] B. Kumar, M. Castro, and J. . Feller, "Poly(lactic acid)–multi-wall carbon nanotube conductive biopolymer nanocomposite vapour sensors," *Sensors Actuators B Chem.*, vol. 161, pp. 621–628, 2012.
- [42] B. Philip, J. Abraham, A. Chandrasekhar, and V. Varadan, "Carbon nanotube/PMMA composite thin films for gas-sensing applications," *Smart Mater. Struct.*, vol. 12, pp. 935–939, 2003.
- [43] H. Tsuji, Y. Kawashima, H. Takikawa, and S. Tanaka, "Poly(L-lactide)/nano-structured carbon composites: Conductivity, thermal properties, crystallization, and biodegradation," *Polym.*, vol. 48, pp. 4213–4225, 2007.

Equilibrium and kinetic studies of acid red adsorption on activated carbon web derived from acrylic fibrous waste

Muhammad Salman Naeem, Vijay Baheti, Jiri Militky, Saima Javed, Qummer Zia Gilani, Syed Zameer Ul Hassan, Hafiz Affan, Zafar Javed, Zuhaib Ahmed

*Faculty of Textile Engineering, Dept. of Material Engineering, Studentská 2,
Technical University of Liberec 461 17 Czech Republic*

1. INTRODUCTION

Rapid industrialization because of development in the field of science and technology along with huge burden of population is causing a severe threat to environment. One of the most important sources of pollution these days is the excessive use of dyes which is increasing day by day due to increased demand in leather, tanning, paper production and textile industries. Dyes are used to give colors and currently more than 10,000 dyes with a production of 1 million tons under different trade names are used [1]. The use of synthetic dyes is increasing in textile industries due to their low cost. However, the synthetic dyes are very stable against photo and biodegradation due to their complex structure [2].

The most oftenly used synthetic dyes in textile industries are basic dyes, reactive dyes, vat dyes and direct dyes. Acid red 27 is anionic dye used to color synthetic and natural fibers. But this dye has been banned in many countries due to suspected carcinogenic, however it is still used in many countries. The colored solutions of synthetic dyes discharged from textile industries are aesthetically unpleasant, damage the ecosystem and disturb the biological processes in water. The colored solutions not only reduce the process of photosynthesis by absorbing sunlight but serious health risks are also associated with synthetic dyes. Hence the removal of these dyes from waste water is very important before discharging them to main stream water. Different water treatment methods are successfully used like chemical, physical and biological methods. Physical methods like membrane filtration, ozonation and irradiation are not only expensive but also accompanied with the production of sludge and hazardous by products [3].

Chemical methods such as flocculation and coagulation are not desirable due to high solubility of dyes in water and consequently higher yield of sludge. The biological method is not preferred in case of synthetic dyes due to their low bio-degradation behavior [4]. Among the various techniques described, adsorption is better method due to high efficiency, simple operation, cost effectiveness and easy recovery of adsorbent [5, 6]. The dye molecules present in water are adsorbed onto the surface of activated carbon either by physical or chemical attraction. Two mechanisms are involved in adsorption of chemicals onto surface of activated carbon that is either dye molecules are attracted onto the surface of activated carbon or dislike water. The

porosity, pore structure and surface area are different structural factors that determine adsorption capacity of adsorbent [7][8]. Activated carbon is popularly used adsorbent in solid/gas separation and to remove odor/taste and other impurities from waste water. For further improving its structural characteristics, different surface modification techniques of activated carbon like physical, chemical and biological methods are also used [9]. Around 80% of produced activated carbon (AC) is used worldwide in liquid phase application for the removal of organic and inorganic compounds, however 20% is used in gas phase applications. All the carbonaceous materials can be transformed into active carbons, however the final properties of activated carbon like surface area, porosity will be different depending upon the selection of raw material, conditions at which activation is done and nature of activating agent.

During the process of activation most of the elements other than carbon are eliminated as volatile products by pyrolytic decomposition of source material. The residual carbon atoms group themselves in the form of stacks of aromatic sheets which then cross-linked in random way. The mutual arrangement and rearrangement of aromatic sheets is irregular and hence leaves or creates free interstices between aromatic sheets. These free interstices are partially filled with products of decomposition or tarry matter or blocked to some extent by disorganized carbon. These interstices are responsible for creation of porosity and make activated carbons excellent adsorbents. Different precursors are used for the formation of activated carbon like phenolic resins [10][11], polyacrylamides, polyimides, pitch, cellulose based fibers and Polyacrylonitrile based fibers [12]. It has been found that carbon fibers made from PAN precursor are stronger than other types of precursor based carbon fibers (rayon, pitch etc.) because of its greater carbon yield and higher melting point, dust free nature, better purity and high density [13].

In this context, the idea of using acrylic fibrous waste for the formation of activated carbon would be a favorable approach. Nowadays focus has been shifted towards the use of waste materials for effective utilization in order to keep environment more safe and protective. The statistics showed that generation of textile and clothing waste in UK is of the order of 2 million tons per year. This means 33 kg of clothing and textile waste per person in UK with a population of 500 million for the 27 countries of European Union equates to approximately 16.5 million ton. Textile waste is mainly categorized in two ways, natural fibers (cotton, wool, flax etc.) and synthetic fibers (polyester, acrylic, nylon etc.) [14].

In this context the idea of using acrylic fibrous waste for the formation of activated carbon is attractive as cost of activated carbon can be reduced along with effective utilization of textile waste. In this work, acrylic fibrous waste after converting into non-woven web was carbonized to activated carbon web by physical activation in high temperature furnace. Later, the yield %, specific surface area, shrinkage, flexibility and dusting tendency of carbonized samples were determined. The study presented the utility of prepared activated carbon web for the removal of acid red 27 dyes from aqueous solution using adsorption kinetics.

2 Experimental Methods

2.1 Materials

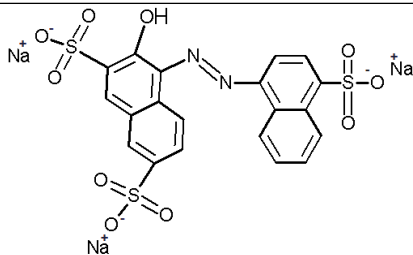
The acrylic fibrous waste was taken from Grund Industries of Czech Republic in the form of bath mats. These fibers have acrylonitrile copolymer 85-89%. The physical characteristics of acrylic fibers are shown in table 1.

Table 1: Physical properties of acrylic fibers

Physical Properties	
Tenacity (g/D)	0.3
Fineness (D)	9
Elongation (%)	50-52
Shrinkage (%)	2.5

Acid red 27 was purchased from Sigma Aldrich, Czech Republic. The structure and properties of acid red are given in table 2.

Table 2: Structure and properties of acid red 27

Acid red 27	
Chemical Structure	
Molecular formula	$C_{20}H_{11}N_2Na_3O_{10}S_3$
Molecular weight	604.47
Color index number	16185

2.2 Conversion of acrylic fibrous waste into AC web

The acrylic fibers were separated from bath mats by using mechanical cutting. The fibers were further opened on laboratory roller card (Befama, Poland) and converted into compact structure of non-woven web by using needle punching machine. The speed of feeding the carded web to needle punching machine was fixed at the rate of 0.4 m/sec. The frequency of strokes was maintained at 200 strokes per minute with 5 mm depth of needle penetration. This produced the web having thickness of 11.6 mm and density 2.78 g/cm³. The schematic diagram for the formation of activated web is shown in figure 1. The acrylic fibrous web was then cut into 30 cm (length) and 30 cm (width) for subsequent high temperature treatment using high temperature furnace. The acrylic non-woven web was initially stabilized with 35 °C hr⁻¹ up to 250 °C to minimize the shrinkage during carbonization. During stabilization, predetermined tension was applied to avoid shrinkage. Later, the stabilized web was carbonized to 800 °C, 1000 °C and 1200 °C with different heating rate (150, 300 and 450 °C hr⁻¹) and no holding time (holding time means for how much time the web was placed at high temperature) under the layer of charcoal to find better values of yield and surface area as can be seen from table 3.

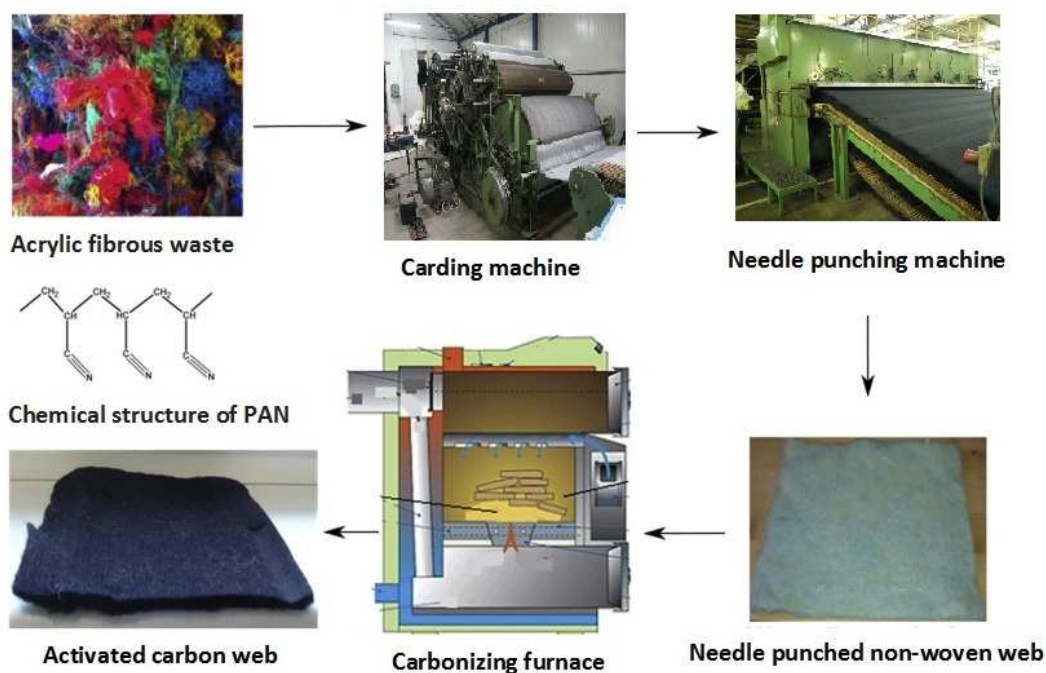


Fig. 1: Schematic diagram of AC web from acrylic fibrous waste

Table 3: Carbonization parameters for acrylic fibrous waste

Sample No.	Final pyrolysis temperature (°C)	Heating rate (°C hr ⁻¹)
1	800	150
2	800	300
3	800	450
4	1000	150
5	1000	300
6	1000	450
7	1200	150
8	1200	300
9	1200	450

2.3 characterization of prepared AC web

The activated carbon webs prepared at different temperatures were characterized for determining their flexibility, yield, dusting, specific surface area and elemental analysis. The yield of activated carbon web was determined by using equation 1.

$$Yield(\%) = \frac{Final\ weight\ of\ ac\ web}{Initial\ weight\ of\ acrylic\ web} \times 100 \quad (1)$$

The flexibility of carbonized webs was determined by using cantilever bending principle (ASTM D 1388). The dusting behavior of activated carbon webs was determined by rubbing the webs after certain time (ASTM D 3884). The specific surface area of activated carbon webs was determined by nitrogen adsorption

desorption isotherms at 77.3 K using Quantachrome instrument. The isotherms measured were taken in relative pressure P/P₀ (range from 0.02 to 1). Energy dispersive x-ray (EDX) analysis was done to find out the different elements and their concentrations. X-ray diffraction (XRD) is a technique used for the identification of crystalline material and analysis of unit cell dimensions. Degree of crystallinity can be calculated by using equation 2.

$$I_c = 1 - \frac{I_1}{I_2} \quad (2)$$

I_1 is intensity at minimum peak

I_2 is intensity at maximum peak.

2.4 Adsorption of acid red 27 on to AC non-woven web

The aqueous solution of acid red with different concentrations was prepared by dissolving the required amount of dye in distilled water. For determining adsorption performance different concentrations (5.0, 10.0, 15.0, 20.0 and 25.0 mg L⁻¹) of acid red were used. The adsorption performance was investigated by using batch method. A constant amount of AC web (i.e. 0.1 g) was introduced in each flask having 50 ml of dye solution and was placed on water bath shaker for 200 rpm to ensure that equilibrium was achieved. After set intervals of time, the dye solution was examined with the help of UV-visible spectrophotometer (UV-1600 pc spectrophotometer). The dye removal efficiency was calculated by using equation 3.

$$\text{Dye removal efficiency} = \left[\frac{(C_0 - C_e)}{C_0} \times 100 \right] \quad (3)$$

Where C_0 (mg L⁻¹) and C_e (mg L⁻¹) are initial and final concentrations of dye before and after the addition of adsorbent (activated carbon web). The adsorption capacity of activated carbon web was calculated from equation 4.

$$\text{Adsorption capacity } (q_e) = (C_0 - C_e) \frac{V}{W} \quad (4)$$

Where q_e (mg g⁻¹) is the amount of dye adsorbed or accumulated on adsorbent, V is the volume of solution in liters and W is the mass of adsorbent in grams.

2.5 Morphology of AC web after dye adsorption

The morphology of activated carbon and dye adsorbed activated carbon web was studied by the help of Scanning electron microscope (SEM) at 30 kV accelerated voltage.

2.6 Adsorption isotherms

The adsorption isotherms explain the distribution of adsorbate (dye molecules) in liquid phase and adsorbent, when the equilibrium is achieved [15]. Langmuir and Freundlich isotherms were used to explain the distribution of adsorbate molecules and their adsorption mechanism on activated carbon. The Langmuir believes in monolayer adsorption while Freundlich endorses heterogeneity of adsorbent surface and multi-layer adsorption capacity [16].

2.6.1 Langmuir isotherm

The Langmuir isotherm is described by the equation 5.

$$q_e = \frac{q_{max}K_L C_e}{1 + K_L C_e} \quad (5)$$

After linearization the Langmuir equation becomes as given in equation 6.

$$\frac{C_e}{q_e} = \frac{1}{q_{max}K_L} + \frac{C_e}{q_{max}} \quad (6)$$

Here K_L is Langmuir constant for rate of adsorption ($L\ mg^{-1}$), q_{max} is Langmuir constant for maximum dye adsorption capacity ($mg\ g^{-1}$), q_e is the amount of dye adsorbed per unit mass of adsorbent ($mg\ g^{-1}$) and C_e is the concentration of dye at equilibrium ($mg\ L^{-1}$).

2.6.2 Freundlich isotherm

The non-linear form of Freundlich isotherm is given by equation 7.

$$q_e = K_f C_e^{1/n} \quad (7)$$

The linear form of Freundlich equation is given by equation 8.

$$\log q_e = \log k_f + \frac{1}{n} \log C_e \quad (8)$$

Here, $1/n$ is Freundlich constant for intensity of adsorption ($L\ mg^{-1}$), k_f is Freundlich constant for adsorption capacity ($mg\ g^{-1}$).

2.7 Kinetic mechanisms

The adsorption mechanism on activated carbon was analyzed by using pseudo first order and pseudo second order model. The pseudo first order model is described by equation 9.

$$\frac{dq_t}{dt} = K_1 (q_e - q_t) \quad (9)$$

Where k_1 is the equilibrium rate constant of adsorption (min^{-1}), q_e and q_t are the amounts of dye adsorbed at equilibrium and at time t (min) respectively. After integrating above equation with boundary conditions from $q_t=0$ to $q_t= q_e$ and $t=0$ to t the above equation becomes.

$$q_t = q_e (1 - e^{-k_1 t}) \quad (10)$$

The equation 9 after linearization becomes as shown in equation 11.

$$\log(q_e - q_t) = \log q_e - \frac{k_1 t}{2.303} \quad (11)$$

Pseudo second order kinetics is expressed as

$$\frac{dq_t}{dt} = k_2 (q_s - q_t)^2 \quad (12)$$

After integrating the above equation becomes.

$$q_t = \frac{k_2 q_s^2 t}{1 + k_2 t} \quad (13)$$

After linearization the above equation becomes equation 14.

$$\frac{t}{q_t} = \frac{1}{k_2 q_s^2} + \frac{t}{q_s} \quad (14)$$

3 Results and discussions

3.1 Effect of carbonization parameters on the properties of AC web

The physical properties of activated carbon webs prepared at different temperatures (800 °C, 1000 °C and 1200 °C) with different heating rates (150, 300 and 450 °C hr⁻¹) and no holding time are shown in table 4. Initially the acrylic webs were stabilized at 250 °C with slow heating rate (35 °C hr⁻¹). Black color after stabilization indicated that web was properly stabilized due to cyclization, dehydrogenation and oxidation of PAN structure[17]. During stabilization nitrile groups assisted in formation of ladder structure which enhanced mechanical properties and yield of final carbon web. During carbonization process, further crosslinking converted stabilized web into turbostratic carbon structure with more orientation of carbon basal planes. The activated carbon web prepared at 800 °C with heating rate 150, 300 and 450 °C hr⁻¹ provided surface area of 104, 120 and 90 m²g⁻¹. Similarly at 1000 °C it give 170, 190 and 140 m²g⁻¹. Whereas at 1200 °C, the achieved surface area were 240, 278 and 210 m²g⁻¹ at heating rate of 150, 300 and 450 °C hr⁻¹ respectively.

Table 4: Effect of carbonization parameters on AC web properties

Temperature (°C)	Yield (%)	Flexibility	Dusting
Heating rate (150 °C hr⁻¹)			
800	56.62	Good	Good
1000	49.32	Good	Good
1200	37	Poor	Poor
Heating rate (300 °C hr⁻¹)			
800	61.70	Good	Good
1000	57.14	Average	Average
1200	45.33	Poor	Poor
Heating rate (450 °C hr⁻¹)			
800	63.47	Good	Good
1000	61.38	Poor	Poor
1200	51.56	Poor	Poor

Literature also showed almost similar surface area by using physical activation with different precursor materials [18][19]. The increase in surface area at high temperature was due to more reaction of atmospheric oxygen with carbonizing structure, which caused elimination of different elements from structure and rearrangement of basal planes. These two reasons were main driving forces for creation of porous structure. With increase of temperature, more reactions of carbonizing material caused more elimination of volatile gases and tarry matter resulted in higher carbon content although a decrease in the yield of carbon. At high heating rate sudden rise of temperature caused fusion of carbonized structure due to which surface area was reduced and poor behavior of flexibility and dusting can be seen. However, the reduction of surface area at slow heating rate was due to prolonged carbonization which caused more oxidation of carbon and resulted in lesser yield. From the results achieved, the heating rate $300^{\circ}\text{C hr}^{-1}$ was found more appropriate for getting more value of surface area along with appropriate yield. Figure 2 showed the increase of surface area with rise of temperature from 800 to 1200°C at heating rate of $300^{\circ}\text{C hr}^{-1}$.

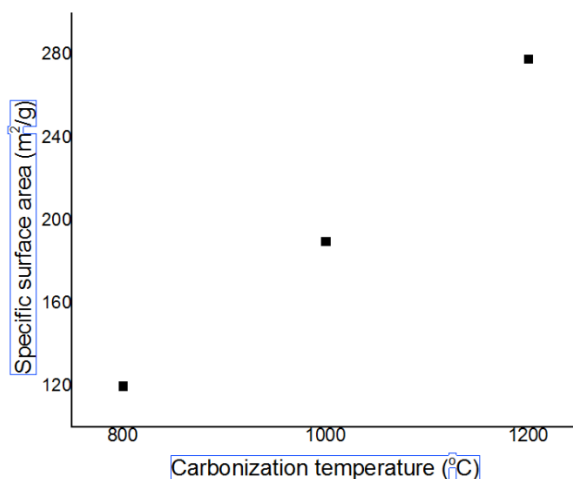


Fig. 2: Effect of carbonization temperature on specific surface area of AC web

3.2 Energy disperse x-ray spectroscopy analysis

Energy disperse x-ray spectroscopy analysis (EDX) gave the relative proportion of different elements present in carbon webs prepared at different temperatures (800 , 1000 and 1200°C) with heating rate $300^{\circ}\text{C hr}^{-1}$ as can be seen from table 5. It is clear from table 5 that by increasing carbonization temperature from 800°C to 1200°C the carbon content was increased however with reduction in concentration of oxygen. The AC web produced at 1200°C showed 92.49% and 6.61% content of carbon and oxygen respectively, due to elimination of nitrogen, sulfur, hydrogen and other elements [20].

3.3 SEM morphology

For determination of porosity the surface morphology of activated carbon webs prepared at different temperatures was analyzed. Figure 3 (a-d) showed the SEM images of pure acrylic and AC webs produced at 800°C , 1000°C and 1200°C . It was

clear from SEM images that as temperature of carbonization increased, roughness of surfaces also increased. The increased in surface roughness indicated the more porous structure at high temperature.

Table 5. Effect of carbonization temperature on elemental composition of AC web

Element	App conc.	Intensity	Weight (%)	Atomic (%)
800 °C				
CK	0.26	2.12	0.13	91.76
OK	0.01	0.761	0.01	8.24
1000 °C				
CK	0.37	2.12	0.18	91.87
OK	0.02	0.760	0.02	8.13
1200 °C				
CK	0.18	2.10	0.09	92.49
OK	0.01	0.744	0.01	6.61
CaK	0.00	0.902	0.00	0.90

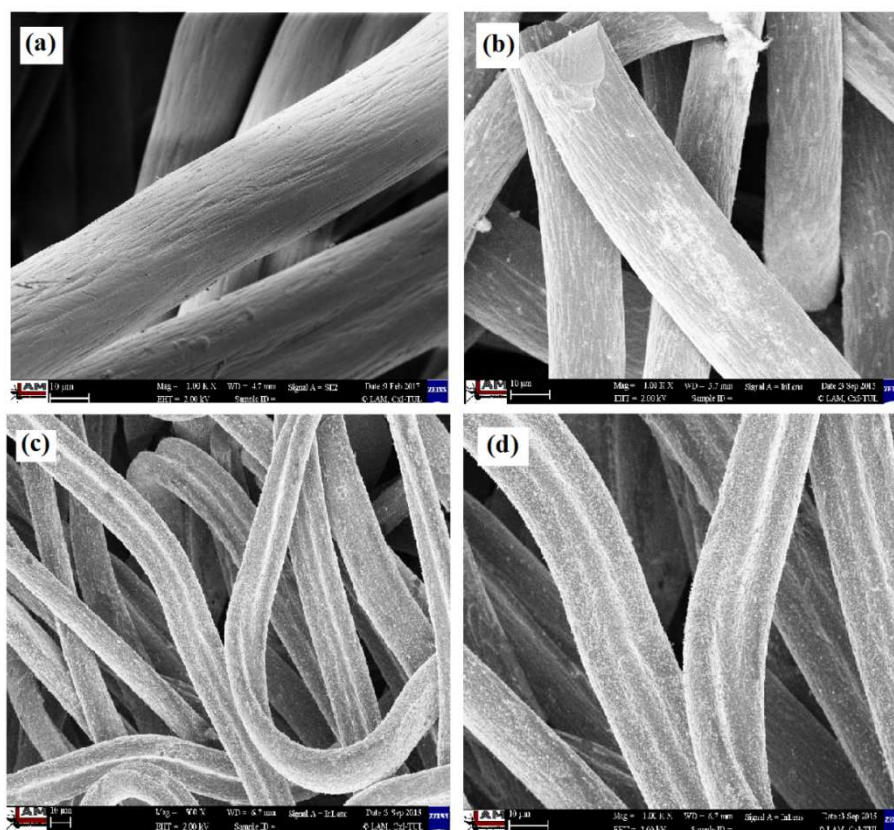


Fig. 3: (a) SEM image of acrylic web (b) SEM image of AC prepared at 800 °C (c) SEM image of AC prepared at 1000 °C (d) SEM image of AC prepared at 1200 °C

3.4 Effect of process parameters on dye removal efficiency

3.4.1. Effect of initial concentration of dye

The dye adsorption performance of activated carbon was investigated by varying the initial concentration of dye from 5 mg L⁻¹ to 25 mg L⁻¹. It is clear that dye removal percentage increased by increasing contact time and then achieved a constant value

when the process reached at equilibrium as can be seen from figure 4 (a). At low concentration of dye the equilibrium process achieved earlier because of more available active sites for adsorption of dye molecules [16]. As far as dye removal efficiency was concerned, it decreased from 92.59 % to 76.31 % when the concentration of dye was increased from 5 mg L⁻¹ to 25 mg L⁻¹ while keeping other factors constant like dosage of activated carbon, stirring speed and temperature. Similarly, when the dye concentration was increased from 5 mg L⁻¹ to 25 mg L⁻¹, the dye accumulated on activated carbon was also found to increase from 0.95 mg g⁻¹ to 6.48 mg g⁻¹ as can be seen from figure 4(b).

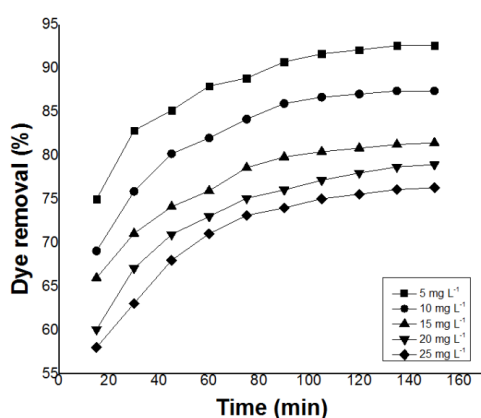


Fig. 4 (a): Effect of dye concentration on dye removal efficiency

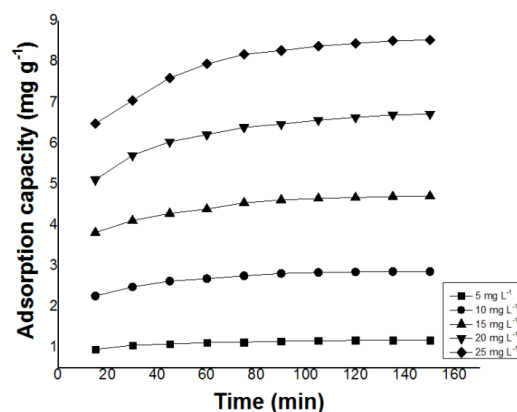


Fig. 4 (b): Effect of initial concentration of dye on adsorption capacity

However, with the increase of contact time at a particular dye concentration, the adsorption capacity was reduced. The adsorption capacity decreased as it was related to the capacity of adsorbent material which decreased by accumulation of dye molecules on the activated carbon.

3.4.2 Effect of adsorbent dosage

The effect of adsorbent dosage on dye removal efficiency and adsorption capacity was analyzed by changing the adsorbent dosage from 1 mg L⁻¹ to 5 mg L⁻¹ while keeping other factors same like contact time 150 minutes, temperature 25 °C, 15 mg L⁻¹ acid red concentration and a stirring speed of 200 rpm. From figure 5, it was clear that dye removal efficiency increased as the quantity of activated carbon was increased. The acid red removal percentage was 81.46 % when 1 g L⁻¹ adsorbent (activated carbon) was used. However this trend of dye removal efficiency kept on increasing to 84.72 %, 87.98 %, 91.64 % and 95.51 % when the quantity of activated carbon was increased to 2 g L⁻¹, 3 g L⁻¹, 4 g L⁻¹ and 5 g L⁻¹ respectively. This increase in dye removal efficiency is attributed due to increased surface area of adsorbent and more availability of active sites resulting due to increased adsorbent dosage. Similar results have been reported by removal of acid dye on granular AC [21]. However there was an inverse trend when the adsorbent dosage and adsorption capacity of activated carbon was analyzed. This is probably due to the reason that adsorption sites present

on activated carbon remained unsaturated in adsorption process, hence a fall in adsorption capacity was analyzed [22][23].

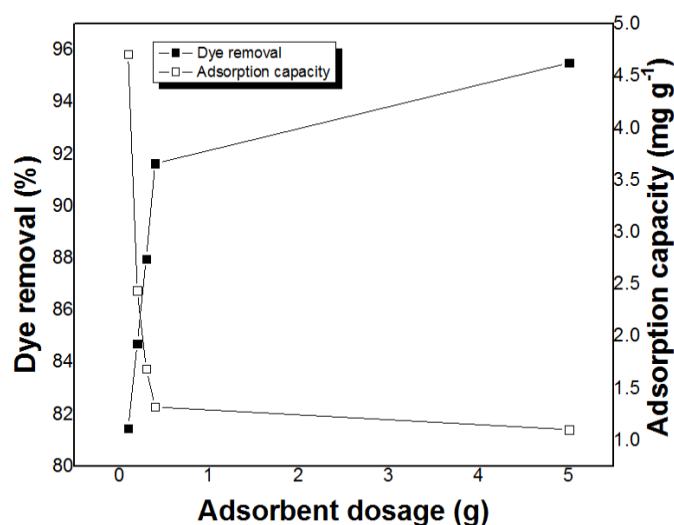


Fig. 5: Effect of adsorbent dosage on dye removal and adsorption capacity

3.4.3 Effect of stirring speed

The effect of stirring speed on dye removal efficiency and adsorption capacity was investigated by keeping acid red concentration 6 mg L^{-1} , temperature $25 \text{ }^\circ\text{C}$, adsorbent dosage 2 g L^{-1} and contact time 150 minutes to ensure that equilibrium point was achieved. The stirring speed was changed from 50 rpm to 200 rpm. One sample was used without the stirring speed for comparing the results. From figure 6 it was clear that only 2.44 % dye was removed without any stirring. However as the stirring speed was increased dye removal efficiency was found to increase to 30.75 %, 57.23 %, 71.89 % and 81.78 % respectively. As far as adsorption capacity was concerned it also increased as the stirring speed was increased. The adsorption capacity of activated carbon increased from 1.78 mg g^{-1} to 3.31 mg g^{-1} , 4.155 mg g^{-1} and 4.71 mg g^{-1} when the stirring speed was increased from 50 rpm to 100 rpm, 150 rpm and 200 rpm respectively. This trend is obvious due to more interaction of dye solution with the adsorbent at high stirring speed [23].

3.4.4 Effect of pH

The pH of solution has significant effect on the dye removal efficiency and adsorption performance of activated carbon. For analyzing dye removal efficiency of acid red, pH of solution was varied from 2 to 11, while keeping other parameters constant like adsorbent dosage 2 mg L^{-1} , dye concentration 15 mg L^{-1} , stirring speed of 200 rpm temperature 25°C and contact time 150 minutes to ensure that equilibrium was achieved. The point of zero charge of AC web prepared by pyrolysis of acrylic fibrous waste was found to be 5.90. It is the point at which the net charge on the surface of activated carbon is zero [24]. At $\text{pH} > \text{pH}_{\text{ZPC}}$ the surface of adsorbent is negatively charged while at $\text{pH} < \text{pH}_{\text{ZPC}}$ the surface becomes positively charged [25][26]. The pH of solution was varied by the help of sodium hydroxide (NaOH) and hydrochloric acid (HCL). It is clear from figure 7 that maximum dye removal efficiency (93.27%)

was observed at pH 2, while minimum dye removal (67.82%) was observed at pH 11. At pH value lower than the point of zero charge of activated carbon the surface of activated carbon becomes positively charged due to accumulation of positive ions (H^+). Therefore, as the pH value was reduced, the adsorption capacity and dye removal efficiency was increased due to electrostatic attraction between positively charged activated carbon and anionic dye molecules (AR^-). This force of attraction is mainly responsible for the removal of dye molecules from the solution. However as the pH of solution was increased further, the dye removal efficiency and adsorption capacity decreased due to accumulation of negatively charge on the surface of adsorbent. This force of repulsion between anionic dye molecules and surface of activated carbon was mainly responsible for less removal of dye at high pH. Similar results have been reported by Shah and coworkers [27] where they found that electrostatic force of attraction and repulsion played significant effect in dye removal from solution.

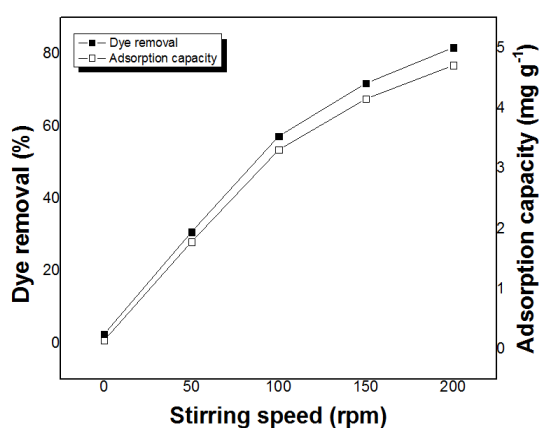


Fig. 6: Effect of stirring speed on dye removal and adsorption capacity

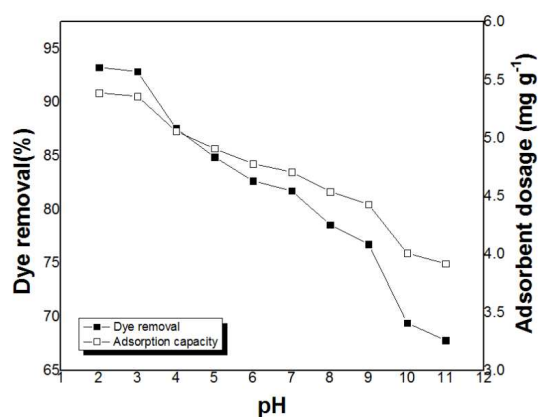


Fig. 7: Effect of pH on dye removal efficiency and adsorption capacity

3.5 Adsorption isotherms

3.5.1 Langmuir isotherm

Langmuir model believes in monolayer adsorption of adsorbate (dye molecules) because of uniform energies of adsorption sites [28]. For determining Langmuir isotherm the non-linear plot of C_e versus q_e for adsorption of acid red onto activated carbon derived from acrylic fibrous waste at 25°C are shown in figure 8. The intercept and slope from the non-linear plot of C_e versus q_e were used to estimate K_L and q_{max} in table 6 along with their standard errors. The value of R^2 (coefficient of determination) from Langmuir isotherm was found to be .995 with SSE (0.005).

Here, R_L is dimensionless equilibrium parameter which gives the information about the shape of isotherm as $R_L=0$ (irreversible), $R_L=1$ (linear), $0 < R_L < 1$ (favorable) and $R_L > 1$ (unfavorable). The value of R_L calculated to be 0.49 which showed favorable adsorption of acid red on activated carbon.

Table 6: Parameters for adsorption isotherms

Langmuir adsorption isotherm	
q_{\max} (mg g ⁻¹)	21.68 ± 2.12
K_L (L mg ⁻¹)	0.067 ± 0.009
R_L	0.49
R^2	0.995
SSE	0.057
Freundlich adsorption isotherm	
K_F	0.50 ± 0.02
1/n	1.35 ± 0.012
R^2	0.999
SSE	0.017

The value of R_L was calculated by using equation.

$$R_L = \frac{1}{1 + K_L C_e}$$

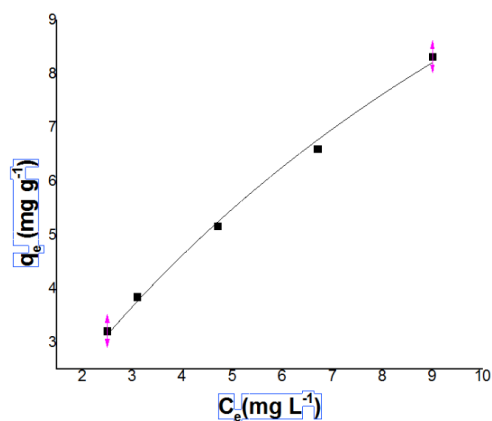


Fig. 8: Non-linear form of Langmuir adsorption isotherm

3.5.2 Freundlich isotherm

The Freundlich isotherm for the adsorption of acid red on activated carbon is shown in figure 9 by plotting C_e versus q_e . From the respective plot of C_e versus q_e the values of slope and intercept were found out which were used to calculate $1/n$ and K_F as given in table 6. The value of SSE is more in Langmuir isotherm than Freundlich isotherm which showed closer fit of results in Freundlich isotherm. This showed heterogeneous surface nature of activated carbon with non-homogenous presence of active groups. However the value of $1/n$ obtained is 1.35. The value of $1/n$ is a function that gives the strength of adsorbent material. When the value of $1/n$ is more than 1, it shows the adsorption coefficient increases by increasing the concentration of solution which led to increase in hydrophilic surface characteristic after mono layer adsorption. Therefore both Freundlich and Langmuir models could be used for the utility of present study.

3.6 Adsorption Kinetics

The adsorption kinetics is important in determining the adsorbate uptake by adsorbent and time required for the completion of process of adsorption [29]. The adsorption kinetics for acid red onto activated carbon was studied by using experimental data for linear and non-linear forms of pseudo first and second order models. The linear and non-linear forms of pseudo first order model were plotted by taking $\log (q_e - q_t)$ on y-axis and time on x-axis respectively as can be seen from figure 10 and 11. Similarly the linear and non-linear forms of pseudo second order model were plotted by taking t/q_t on y-axis and time on x-axis and for non-linear q_e (y-axis) was plotted against time (x-axis) respectively as shown in figure 12 and 13.

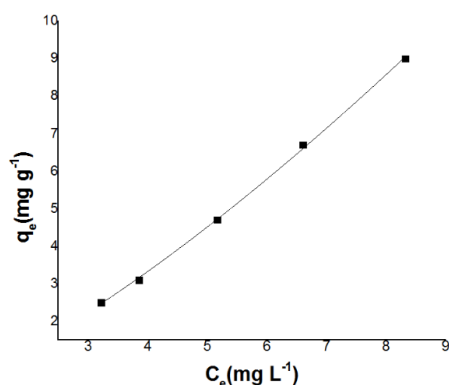


Fig. 9: Non-linear form of Freundlich adsorption isotherm

From the intercept and slope of linear forms of pseudo first and second order model, the respective values of adsorption capacity (q_e) and rate constants (k_1 and k_2) were calculated. Table 7 and 8 gives values of dye uptake and rate constants at different concentrations of dye. In linear form although correlation coefficient of pseudo second order was more appropriate but the values predicted by both the models were far away from actual results and did not follow any trend. For getting values more close to practical results the non-linear curve fitting by using origin pro was used. In non-linear curve fitting both models predicted values very much close to practical values. However the higher values of R^2 for pseudo second order model suggested this model to be more effectively employed for the adsorption behavior of acid red on activated carbon.

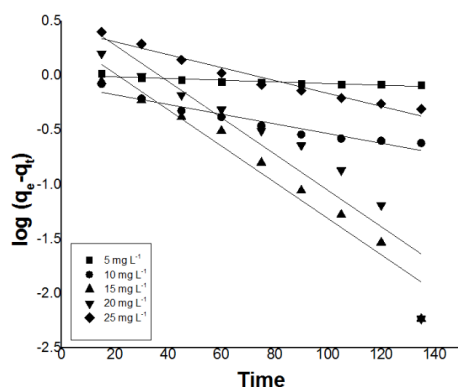


Fig. 10: Linear form of 1st order model

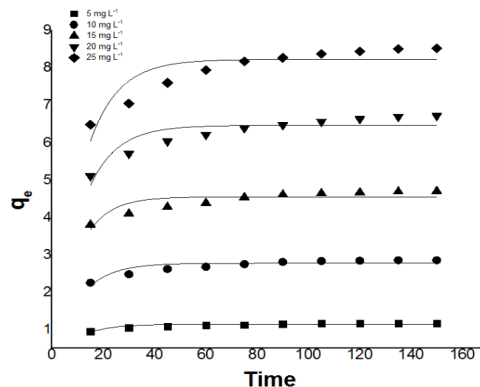


Fig. 11: Non-linear form of 1st order

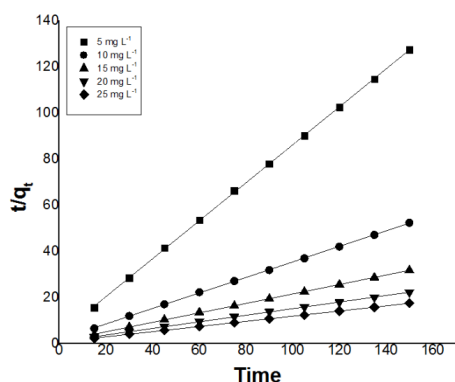


Fig. 12: Linear form of 2nd order

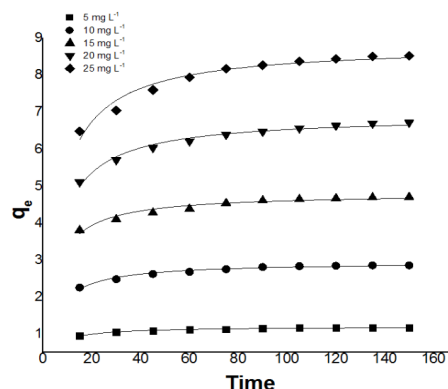


Fig. 13: Non-linear form of 2nd order

4 Conclusion

The acrylic fibrous waste was successfully converted into activated carbon web by physical activation at different temperatures (800°C, 1000 °C and 1200 °C) with different heating rates of 150, 300 and 450 °C hr⁻¹ with no holding time under the layer of charcoal. The higher surface area 278 m²/g was achieved at higher temperature 1200 °C with 300 °C hr⁻¹ due to more elimination of different elements from carbonized material and due to mutual arrangement of carbon sheets. Later the adsorption performance of acid red on activated carbon was examined by varying different parameters like varying the initial concentration of dye from 5 mg L⁻¹ to 25 mg L⁻¹, adsorbent dosage, stirring speed and different pH of solutions. From the results, it was clear that more equilibrium time was required when the concentration of dye was increased. However, when the adsorbent dosage and stirring speed was increased, it took less time to remove dye. When the experimental results were analyzed by using non-linear forms of adsorption isotherms (Langmuir and Freundlich isotherm), the Freundlich isotherm showed more better fitting of results due to heterogeneous surface nature of activated carbon.

Acknowledgement

This work was supported under the student grant scheme (SGS-21198) by Technical University of Liberec, Czech Republic.

References

- [1] V. K. Gupta and Suhas, *J. Environ. Manag.*, **90**, 2313 (2009).
- [2] A. Slampova, D. Smela, A. Vondrackova, I. Jancarova, and V. Kuban, *Chem. List.*, **95**, 163 (2001).
- [3] E. L. Grabowska and G. Gryglewicz, *Dye. Pigment.*, **74**, 30 (2007).
- [4] V. K. Gupta, P. J. M. Carrott, and M. M. L. S. Ribeiro Carrott, *Environ. Sci. Technol.*, **39**, 783 (2009).
- [5] Z. Boubarka, A. Khenifi, F. Sekrane, N. Bettahar, and N. Derriche, *Chem. Eng. J.*, **136**, 295 (2008).
- [6] V. K. Gupta, I. Ali, T. A. Saleh, A. Nayak, and A. Agarwal, *RSC Adv.*, **2**,

- 6380 (2012).
- [7] H. Y. Shan, R. Malarvizhi, and N. Sulochana, *J. Environ. Prot. (Irvine,. Calif)*, **3**, 111 (2009).
- [8] G. Ciardelli and N. Ranieri, *Water. Res*, **35**, 567 (2001).
- [9] G. Zelmanov and R. Semiat, *Desalination*, **333**, 107 (2014).
- [10] C. Mangun, J. Barr, S. Riha, A. Lizzio, G. Donnals, and M. Daley, *Carbon N. Y.*, **35**, 411 (1997).
- [11] M. Daley, R. Braatz, J. Economy, and C. Mangun, *Carbon N. Y.*, **36**, 123 (1998).
- [12] M. Coleman and G. . Sivy, *Carbon N. Y.*, **19**, 137 (1981).
- [13] V. Baheti and J. Militky, *Fiber. Polym*, **14**, 133 (2013).
- [14] M. A. Nahil and P. T. Williams, *J. Anal. Appl. Pyrolysis*, **89**, 51 (2010).
- [15] U. Gecgel, G. Ozcan, and G. C. Gurpinar, *J. Chem.*, **201**, 1 (2013).
- [16] Z. Z. Chowdhury, S. M. Zain, R. A. Khan, and K. Khalid, *Orient. J. Chem.*, **1**, 405 (2011).
- [17] Y. Liu, Y. H. Choi, H. G. Chae, P. Gulgunje, and S. Kumar, *Polym. Guildf.*, **54**, 4003 (2013).
- [18] M. A. Zaini, Y. Amano, and M. Machidaa, *J. Hazard. Mater*, **180**, 552 (2010).
- [19] S. Jagannathan, H. G. Chae, R. Jain, and S. Kumar, *J. Power Sources*, **185**, 676 (2008).
- [20] S. Naeem, V. Baheti, V. Safarova, J. Militky, B. Tomkova, and D. Karthik, *Carbon N. Y.*, **111**, 439 (2017).
- [21] S. Marius, C. Benoit, C. Igor, D. Mariana, and P. Stelian, *Sci. Study Res.*, **12**, 307 (2011).
- [22] D. C. Sharma and C. F. Forster, *Water Res*, **27**, 1201 (1993).
- [23] S. Naeem, V. Baheti, J. Militky, J. Wiener, P. Behera, and A. Ashraf, *Fiber Polym.*, **17**, 1245 (2016).
- [24] M. A. Rahman, S. M. R. Amin, and A. M. S. Alam, *Dhaka Univ. J. Sci.*, **60**, 185 (2012).

Theoretical and experimental investigation on shear performance of 3D spacer fabrics

Veerakumar Arumugam^{1*}, Rajesh Mishra¹, Maros Tunak²,
Jiri Militky¹, Dana Kremenakova¹, Mohanapriya Venkatraman¹, Blanka Tomkova¹ &
Miroslav Vaclavik³

¹ Faculty of Textile Engineering, Dept. of Material Engineering, Technical University of Liberec, , Studentská 2 461 17 Czech Republic,

² Faculty of Textile Engineering, Dept. of Textile evaluation, Technical University of Liberec, Studentská 2, Liberec 461 17 Czech Republic

³ VUTS, Textile Machinery Research Institute, Liberec, Czech Republic.

1. INTRODUCTION

The shearing behavior of a fabric determines its performance properties when subjected to a wide variety of complex deformations during its use. The ability of a fabric to be deformed by shearing distinguishes it from other thin sheet materials such as paper or plastic films. This property enables fabric to undergo complex deformations and to conform to the shape of the body. Shear properties influence draping, flexibility and also the handle of fabric. Shear properties are important not only for standard fabrics but for textile reinforced composites preforming as well. Automated manufacturing of textile composite shell-like products typically requires draping of dry or pre-impregnated textile sheets. Large local deformations occur in the textile sheet in order to adapt to the curved shape [1-3]. These deformations affect the local fiber directions, volume fractions, and thickness. Several factors together with the consolidation level and the occurrence of flaws (e.g. wrinkling and tearing) determine the product quality. Simulation tools that link product quality to material, mold and process parameters are being developed to support design and process optimization [4,5].

The prediction of local deformations is an essential task within this objective. Although the composites have excellent in-plane mechanical properties, the application range of laminated composites is limited by the through-thickness failure due to the poor interlaminar properties. Three dimensional (3D) textile structural composites provide excellent strength through thickness, outstanding damage tolerance and good impact and fatigue resistance [6]. As one type of the 3D textile structural reinforcements for composites, the 3D spacer fabric has been widely used in engineering field owing to its easy and efficient processing in warp and weft knitting. In addition, the most attractive advantage of spacer fabric is the three dimensional shape forming capacity to manufacture composites. The 3D spacer fabric preforms have excellent mechanical properties and good formability. With the development of the preforming technology, complex shape and different size of the structural parts

can be produced. In the structure integrated manufacture of composites, the 3D spacer fabric is preformed according to the shape of the final composite that can be complex [7]. The in-plane behavior and the inter-laminar behavior are the most important deformations in 3D fabrics, and also shear behavior predominates the deformation mode of the material [8].

It is necessary to study the inter/intra-ply shear behavior of 3D fabric because of their wide application in production especially in the case of forming process. The in-plane shear behavior of 2D fabric has been comparatively well investigated. Zhu et al. [9] carefully investigated the in-plane shear characterization of 2D fabric by experimental test, and found that the reduction of yarn was a key to wrinkling. Xiaohua et al. [15] studied the shear property of 2D fabrics using picture-frame test method, and pointed out that the shear results were sensitive to the tensions in the yarns during the experiment. The tensile force increased with the increase in shear angle. Lomov et al. [10] presented shear tests of unbalanced 2/2 twill glass/PP fabric on picture frame in three different pretension states and studied the influence of tensile load in the yarn direction on the shear resistance for the fabric and the repeatability of the test method. Lin et al. [11] established the finite element model based on the geometry of 2D fabric to simulate the in-plane shear deformation, the simulation results were identical with experiments. Cao et al. [12] compared the picture frame shear test results from seven different labs for developing a standard test setup and obtaining accurate and appropriate material properties. Chen et al. [13] developed a FEM model to predict in-plane and interlaminar shear properties of laminates. However, the in-plane shear behavior of 3D spacer fabric was rarely reported. Charmetant et al. [14] built a hyperelastic model to simulate the formability of 3D fabric.

In this work, a picture frame shear fixture was developed and a careful study was made on its applicability in testing the in-plane shear behavior of 3D spacer fabrics with different fabric density, thickness and structure. The shear force versus shear angle curves and position of wrinkles during in-plane shear test are recorded by considering two different frame lengths in order to compare with each other and load–displacement curves of inter-ply shear test were also analyzed. In addition, suitable program was developed in MATLAB using Hough transform to analyze the shear angle during deformations. The results of image analysis were compared with the actual experimental data. It can provide the foundation for investigating the performance of picture frame to study formability and theoretical analysis of in-plane shear in 3D spacer fabrics.

2. LITERATURE REVIEW

The following literature review focuses on 3D spacer fabric materials and in particular the intra-ply shear that tends to occur when the material is subjected to in plane shear. The issues of the review include intra-ply test methods, material characterization during the picture frame and bias extension test and onset of wrinkling during the shear deformation. The intent is not to cover all the past literatures but to give necessary works performed regarding to the intra-ply shear.

2.1 Shear deformation modes

There are two types of shear deformation occurs when the fabric is subjected to shear stress. They are 1. Intra-ply Shear (In-plane) 2. Inter-ply Shear

The intra-ply shear involves rotation between the parallel tows within the fabric layers at its crossover points, followed by compaction [16, 17], as represented in Fig. 1. There is no standard ASTM test to measure the intra-ply shear behavior of the composite [18,19]. However, the two most common tests (picture frame and bias extension test) used to characterize the in-plane shear behavior of the fabric is discussed below in detail. The inter-ply slip, considered as an important deformation, tends to occur during the forming of the single curvature and double curvature contours [20]. The plies tend to slip over each other, resulting in inter-ply slippage. In turn, if the slippage is restricted, as in Figure 2, the inner- most ply might tend to buckle out of the plane, as a result of high compressive strain [20]. The inter/ply friction is also termed as ply-ply friction and it also plays an important role in transferring of loads between the plies. In addition, researches by Vancalooster [20] and Konstantine et al. [21] revealed that friction between the tools and fabric plays an important role in the composites. If the friction is too much it might result in the tearing off of the material, whereas if it is too low it might lead to wrinkling of the material. Similar to intra-ply shear, there is no standard ASTM test to measure the ply-ply friction. However, a similar setup, as in Fig. 2 has been used for years by researchers [22-24] (with some modifications) to measure the inter-ply friction. The set-up works by placing a layered or 3Dimensional fabric in between two plates (which are pressurized using compressed air) and pulling them in the opposite directions to measure the frictional resistance of the fabrics [56].

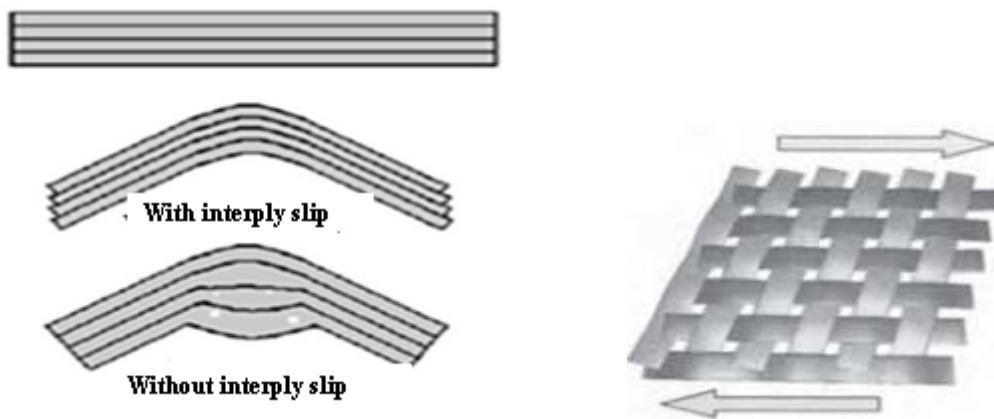


Fig. 1: Intra –ply shear deformation mode Fig. 2: Inter –ply shear slip during double curvature

2.2 Intra-ply shear

Intra-ply shear is inferred to be the predominant deformation mechanism which tends to occur when the material is subjected to in-plane shear. The two different mechanisms of intra-ply deformations: the in-plane deformation and through thickness deformation [25] are shown in Fig. 3.

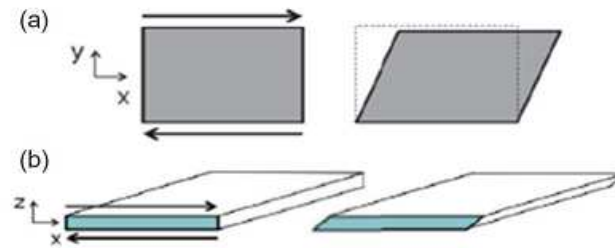


Fig. 3: Types of intra-ply shear; (a) in-plane shear and (b) through thickness shear

The many variations of shear experiments can be classified into three broad types,

1. Direct Shear Measurement
2. Bias Extension Test
3. Picture Frame Test

2.2.1 Direct shear measurement

Direct shear force experiments originate from the textile industry [26]. Opposite sides of a rectangular specimen are clamped parallel to one of the fibre directions. Displacement of one of the clamp edges is in the direction of the fibres, so that a direct shear force is exerted as shown in fig. 4. A force is applied normal to the fibre direction in order to keep the fabric taut. This ensures that shear rather than wrinkling is measured. This was adapted for engineering fabrics by the likes of Kawabata [27], who used a biaxial testing machine to measure the direct shear response. Force was applied in one direction to keep the specimen taut, while a centre clamp applied the shear stress in the other direction. Later variations [28] on this method included more than one specimen pulled by the central clamp so that out of plane reactions would cancel. This also allows, with careful placement of the specimens, measurement of shear strain in only one direction, an important factor in textiles that exhibit different shear characteristics according to the shear direction. Kawabata's work led to the Kawabata Evaluation System for Fabrics (KES-F), now available commercially for fabric characterization, and is used for the characterization of technical textiles including reinforcements [29]. The KES-F system presents difficulties as a shear measurement system for reinforcements. It is very expensive and hard to obtain and is limited to the low shear strains and loads characteristic to the textiles industry. Furthermore, Hu and Zhang [30] suggested that the specimen in the KES-F was not subjected to pure shear. Their finite element simulation of the shear test suggested a shear distribution from zero at the corners to a maximum at the centre of the specimen.

2.2.2 Bias extension test

The bias-extension test is a tensile test with the material initially in the $\pm 45^\circ$ -direction, in relation to the direction of tension. An advantage is that it requires no specialized rig, only a clamping suitable for the tested material. To obtain a uniform shear zone the samples length should be larger than twice the width [31]. The test does not force the sample into pure shear mode and the free edges enable slippage between the layers,

which is important when investigating preferred deformation modes. A problem with bias-extension is that the shear rate in the sample is not uniform, but instead the level of shear is divided in different zones [32]. A bias-extension sample is divided into three types of regions; A, B and C, see Fig. 5. According to the theory of Pin Jointed Net (PJN) region A is supposed to undergo pure shear, where the shear angle, θ , can be extracted from this area. The shear angle in region B is $\theta/2$. Region C is by geometrical constraints kept undeformed and not contributing to the total load.

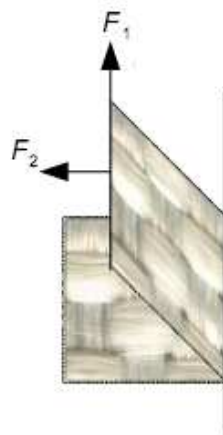


Fig. 4: Direct shear measurement

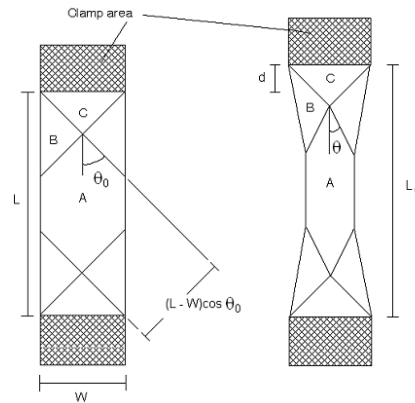


Fig. 5: Bias-extension test specimen with shear region and shear angle description

To register deformation and follow the rotation of fibres, some type of visual registration is required. Previously, rigorous marking of the sample in combination with a camera was used to capture the behaviour. Today, an image processing technique called digital image correlation (DIC) can be used [33]. An example is Aramis system for optical 3D and 2D deformation analysis provided by GOM. The system is suited to measure three-dimensional deformation and strain with a high accuracy.

2.2.3 Picture frame test

The picture frame shear test method achieved some popularity in the early days of composite materials development when few other shear test methods existed. But as the two- and three-rail shear test methods, and later the Iosipescu shear test, were introduced for characterizing basic shear properties, picture frame shear testing became less popular for three reasons: It used a relatively large specimen; test preparation required that a number of holes be drilled in the specimen; and the method required a complex fixture. Despite these disadvantages, the picture frame shear test continued to be an attractive option for composite laminate panel testing because the method accommodates large specimens. As shown in Fig. 6, the picture frame is an effective way for characterizing intra-ply shear property of fabrics [34]. The picture frame test is preferred by many researchers for shear testing since it has pure state of strain can be imposed on the test specimen [35-37]. Shearing is induced by restraining the textile reinforcement in a rhomboid deformation frame with fibers constrained to

move parallel to the frame edges. The frame is extended at diagonally opposing corners using simple tensile testing equipment. The description of this test method and the modifications done in the frame for this work has been in detail discussed in the materials and methods section.

2.3 Spacer Fabrics

Since spacer fabrics have two outer surfaces connected to each other with spacer yarns, they provide light weight and bulkier structure. The middle layer comprises of mono or multifilament yarns. Fig. 7 illustrates a kind of spacer fabric in which its third dimension (thickness) is significant. Components in spacer fabrics differ depending on the yarn type and production method [38]. There are two types of knitted spacer fabrics: warp-knitted spacer fabrics and weft-knitted spacer fabrics. The first type can be produced on rib raschel machine having two needle bars [39], while the second type can be produced on double jersey circular knitting machine having a rotatable needle cylinder. It can be produced by flat knitting too [40].

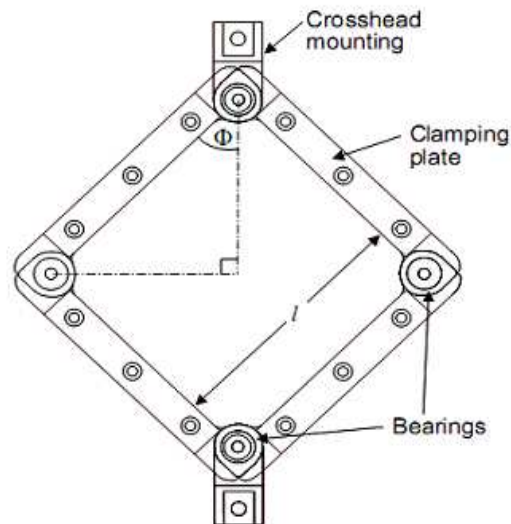


Fig. 6: Picture frame fixture design.

The properties of spacer fabrics such as 3D fiber disposition, possibility to use different materials and single step production system, enable them in different application areas. Figure 7 illustrates a kind of spacer fabric in which its third dimension (thickness) is significant. Components in spacer fabrics differ depending on the yarn type and production method. It has excellent compression elasticity and breathability is the greatest advantages of spacer fabric [41]. Admirable compressibility indicated that, crush resistant property and bending performance are excellent. Spacer fabric possesses excellent cushioning and shock absorbing properties [42]. It is because spacer fabric is able to absorb and dissipate kinetic mechanical energy when it is subjected to compression at regular stress over a large extent of displacement [43].

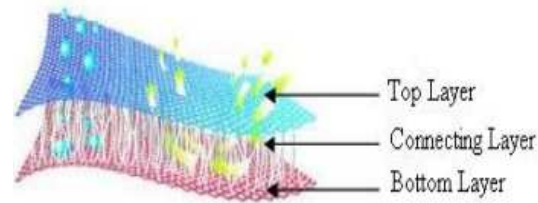


Fig. 7: Structure of spacer fabric

In spacer fabric construction, the two separate outer fabric layers are kept apart by spacer yarns through the thickness direction. A through-thickness property is developed in this 3D textile composite [42]. The spacer yarns act as linear springs, yarn loops are deformed under impact loading and hence created a high damage tolerance characteristic [44]. Besides, the hollow structure created by the spacer yarns between two outer layers resulted in outstanding moisture transmission property since moisture vapor is allowed to transmit freely. Thermal comfort is improved and the chance of skin maceration is reduced in this moisture free environment created by the spacer fabric. The major application areas are acoustics and automotive, aerospace, civil engineering, medical field, geotextiles, protective textiles, sportswear and composites [45, 46]. Further promising application of these spacer fabrics using favorable materials include the protective textiles as “Active Protection System (APS)” [47]. Nevertheless, because of the extreme elasticity and deformability due to applied forces along with limited reinforcing possibilities, these pile yarns connected conventional spacer fabrics are not considered as load-adapted 3D spacer textile preforms for high performance lightweight composites applications. Lack of knowledge on shear behavior of knitted spacer fabrics during compression, tensile and composite forming are the main reasons to make this study. In this work, a picture frame shear fixture was developed and a careful study was made on its applicability in testing the intra-ply shear behavior of 3D knitted spacer fabrics with different fabric density, thickness and structure.

3. MATERIALS AND METHODS

The details on the materials used and the methods followed in the present study are explained below.

3.1 Materials

Twelve different spacer fabrics made up of polyester filament yarn were knitted using Raschel warp knitting machine with gauge of E22 and 6 guide bars. The surface layer of spacer fabrics were produced with polyester multifilament yarn with same linear density, the spacer layer (connecting) was knitted using polyester monofilament with different diameters and linear densities. By adjusting guide bar movements, the fabrics were produced with two different surface structures. The first group (6 samples) was knitted using lock-knit on both the surfaces and the second group (6 samples) was produced with face layer hexagonal net and base with lock-knit structure. Among these samples, spacer fabrics with different thickness were manufactured by adjusting two needle bars. In each group, former set was developed with 1.5, 2.5 and 3.5 mm thickness and spacer yarn diameter of 0.055 mm, latter set

was constructed with same thickness with different spacer yarn diameter (0.1mm). The loop length of the all twelve warp knit spacer fabrics were kept at 2.12 mm. The samples classification is clearly presented in Table 1.

Table 1: Description of warp knitted spacer fabrics

S.No.	Structure	Fibre Composition (%)	Face Layer (dtex)	Middle Layer (Spacer) (dtex)	Back Layer (dtex)	Spacer Yarn Dia (mm)		
WAS 1	Lock knit	100% Polyester	83f36 (linear density – 83 dtex, number of filaments – 36)	33f1	83f36 (linear density – 83 dtex, number of filaments – 36)	0.055		
WAS 2								
WAS 3								
WAS 4								
WAS 5							108f1	0.1
WAS 6								
WAS 7	Hexagonal net			33f1		0.055		
WAS 8								
WAS 9								
WAS 10								
WAS 11								
WAS 12								

Structural properties including the yarn linear density and fabric weights per unit area were determined according to ASTM D1059 standard using electronic weighing scales. The thickness of the fabrics was measured according to ASTM D1777-96 standard with the SDL digital thickness gauge at a pressure of 200 Pa. The stitch density was calculated from Wales per centimetre (WPC) and course per centimetre (CPC) with the help of optical microscope. The density (D) of the fabric was calculated using the relationship in (eqn. 1)

$$D = \frac{W}{t} \text{ kg / m}^3 \quad (1)$$

Where, W is areal density (weight per unit area) and t is thickness. Porosity, H, was calculated using the equation 2,

$$H = 1 - \frac{\rho_a}{\rho_b} \quad (2)$$

where, ρ_b is bulk density of spacer fabrics, ρ_a is weighted average absolute density of fibres in the spacer fabric, expressed in kg/m^3 .

3.2 Shear test

The in-plane shear behavior of warp knitted spacer fabrics are carefully measured and analyzed using picture frame test and image analysis methods. The picture frame shear test method achieved some popularity in the early days of composite materials development when few other shear test methods existed. But as the two- and three-rail shear test methods, and later the Iosipescu shear test, were introduced for

characterizing basic shear properties, picture frame shear testing became less popular for three reasons: It used a relatively large specimen; test preparation required that a number of holes be drilled in the specimen; and the method required a complex fixture. Despite these disadvantages, the picture frame shear test continued to be an attractive option for composite laminate panel testing because the method accommodates large specimens.

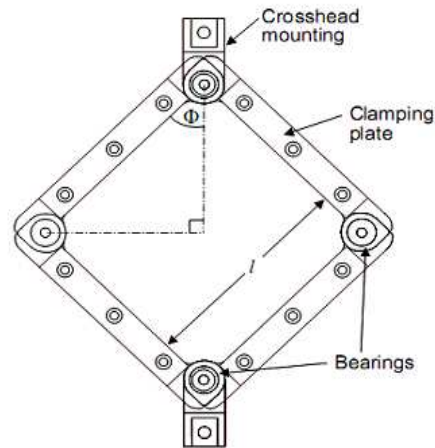


Fig. 8: Picture frame fixture design

As shown in Figure 8, the picture frame is an effective way for characterizing intra-ply shear property of fabrics. The picture frame test is preferred by many researchers for shear testing since it has pure state of strain which can be imposed on the test specimen. Shearing is induced by restraining the textile reinforcement in a rhomboid deformation frame with fibres constrained to move parallel to the frame edges. The frame is extended at diagonally opposing corners using simple tensile testing equipment. The description of this test method and the modifications done in the frame for this work has been discussed in detail in the following section.

3.2.1 Description of the test method

A 3-dimensional view of developed picture frame fixture for shear testing is given in Figure 9. The apparatus has four legs which are hinged to form a picture frame. Further, there is a rod which runs across one of the diagonal of the frame. It should be noted that this rod is not in the plane of the frame but runs behind the frame. The lower end of the rod is hinged with the common hinge of the two legs meeting in that corner. The other opposite corner hinge is resting in the slot provided in the rod. The slot is about 6 cm long for maximum deformation of frame. Further, at the lower end the rod is again hinged to individual legs of the frame. The lower end of the rod is fixed in crossheads of the loading machine. By adjusting the distance between the upper and lower crossheads, the angles between the arms of fixture reach 90°.

The distance can be set as the original reference value, i.e., the zero displacement position, in computer, so that later on, all the experiments can automatically begin from this zero point. Also, the force can be set to zero at this position. Thus, when the load is applied through the upper end of the rod, it pushes these two legs apart and

deforms the frame. These two legs in turn push their adjacent legs making their common hinge to slide in the slot of the rod. The plate deforms into a diamond shape. The spacer fabric is clamped to the frame with the help of clamping plates as shown in Figure 10. These clamping plates are 3cm in width and it has diamond knurled surface for better gripping. The empty frame is tested under the same condition to find the frictional effects between bearings and slots, after several trials of this test; the average value of load at each displacement point is calculated. This is to record the load-displacement behavior of the empty fixture under the same condition as in the real shear experiment. So, it is mainly considered and optimized during sample testing. To eliminate the error caused by the weight and inertia of the fixture, the net load obtained was subtracted from the machine-recorded load when the fabric is being deformed in the picture frame. This resultant load is considered and accounted as an actual load. In order to prevent the pressures from imposing on test samples by the fixture during the large deformation, the central area of shear deformation was 100 mm X 100 mm, and the four corner parts were cut off in order to avoid edge buckling. Shear tests were conducted on a TIRA - universal tensile testing machine with a crosshead speed of 10 mm/min. The test was repeated for 5 samples of each type under the same conditions.

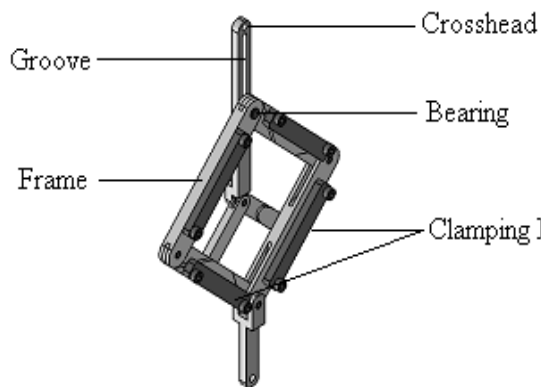


Fig. 9: 3-dimensional view of picture frame shear fixture

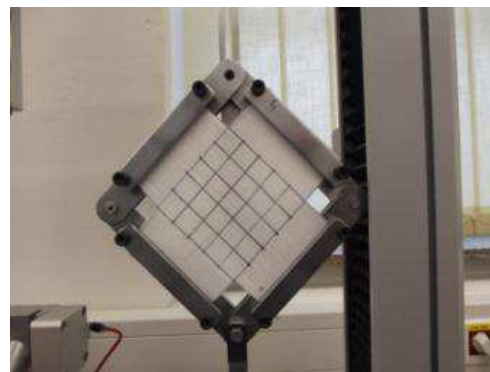


Fig. 10: Clamping of sample in fixture

3.2.2 Deformation kinematics of fixture

A tensile force is applied at the crosshead mounting. The rig is jointed at each corner such that its sides can rotate and the interior angle between adjacent sides can change. The initially square frame thus becomes of rhomboid (or diamond) shape as shown in Figure 11. Material inside the rig is subjected to pure shear deformation kinematics (Fig. 11). The force required to deform the material is recorded at the crosshead mounting as a function of crosshead displacement. The 3D spacer fabrics for shear tests were prepared according to the size of the picture frame and the characteristics of samples are described in the Figure 12. Direct measurement of axial load and shear angle is possible through the following relationship (eq. 3).

$$F_s = \frac{F_x}{2 \cos \varphi} \quad (3)$$

Shear force (F_s) is determined by the axial force (F_x) frame rig length or sample length (L) and the frame angle (φ). In this study, both sample length and frame length are considered for calculation of shear angle and to find the correlation with the image analysis method. Meanwhile frame angle can be determined directly from cross head displacement (d). Shear angle (γ) can be obtained from frame angle by using the following equations 4 and 5.

$$\varphi = \cos^{-1} \left[\frac{L\sqrt{2} + d}{2L} \right] \quad (4)$$

$$\gamma = \frac{\pi}{2} - 2\varphi \quad (5)$$

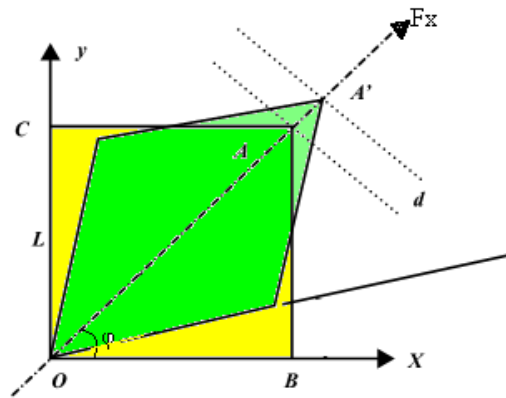


Fig. 11: Deformation kinematics of picture frame

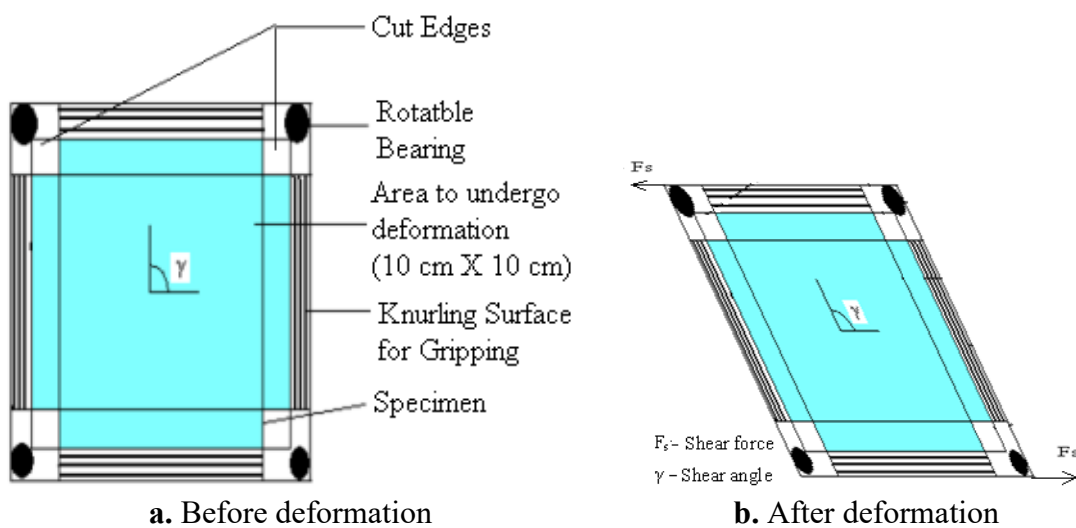


Fig. 12: Shear deformation of frame and specimen

3.2.3 Analysis of in-plane shear stress- strain curve of spacer fabrics

Overall shear stress-strain trend of the spacer fabric samples are presented in the Figure 13. Normally the shear behaviour of spacer fabrics are classified into three stages with respect to changes in the slope. The three stages are surface elongation and lateral compression (1), inter fibre compaction and buckling (2) and densification (3). In the first stage, the surface layer of spacer fabric undergoes elongation; also the inter-fibre slippage takes place in this stage. In this stage, the initial lateral compression occurs in the fabrics due to shearing, a lower slope is observed for loose structures and slope increases with increase in stitch density. Here the spacer yarn has low contribution in constraint during initial compression. Further inter-fibre compaction and extended compression (2nd stage) leads to rapid increase in stress, it might be due to jamming of surface yarns which allows both surface yarn and spacer yarn to buckle to a larger extent. In spacer fabrics, the next stage is quite complex because the compressive stress and strain have been affected by buckling, shearing and locking of spacer yarns. It is also noticed that there is sharp increase in stress in the 3rdstage because the fabric attains a very high density.

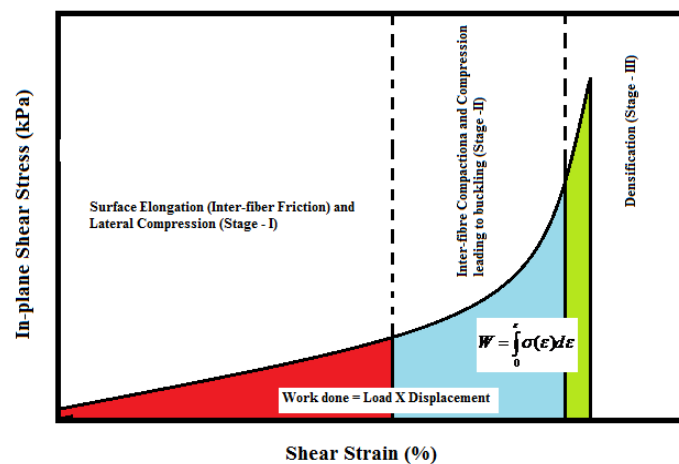


Fig. 13: In-plane shear behavior of 3D spacer fabrics

3.2.4 Energy absorption during in-plane shear of spacer fabrics

It is necessary to evaluate and analyze the spacer fabrics energy absorbing ability during shear. It would be more useful to get a better understanding about the applicability of spacer fabric for cushion materials. The shear curve suggests that all spacer fabric samples may potentially be good energy-absorbing materials. The area under the load-displacement curve represents the total energy absorbed and it can be calculated by multiplying the area under the stress-strain curve by the volume of the sample. The energy absorption capacity per unit volume, W , can be calculated by integrating the shear stress-strain curve, as given by equation 6 :

$$W = \int_0^{\epsilon} \sigma(\epsilon) d\epsilon \quad (6)$$

Where, σ is the shear stress, ϵ is the shear strain at the end/beginning of densification stage. In order to better understand the energy-absorption capacity of a spacer fabric, the energy-absorption efficiency E can be used to analyze its energy-absorption process. The efficiency E is expressed by Equation (7)

$$E = \frac{Ah \int_0^{\epsilon} \sigma(\epsilon) d\epsilon}{Ah\sigma} \quad (7)$$

Where A – area, h – thickness, σ – shear stress at the strain ϵ . The energy-absorption and efficiency of all the spacer fabrics are compared and analyzed to find the suitable material for hi-end applications.

3.3 Image analysis using MATLAB

Image analysis can aid in the determination of the shear angle and displacement at any particular point on the surface of fabric specimen. Grid pattern was applied on the specimen surface before the test and used as the reference points of image analysis. The complete displacement of the specimens during loading process was obtained by image analysis method. The images were captured at certain regular interval of time using digital camera. A special program is developed in MATLAB 7.10 (R 2010a) using Hough's transform to find the angle between the lines on the specimens. The results of experimental methods and image analysis were compared with each other.

3.3.1 Hough Transformation

The Hough Transform patented by Paul Hough in 1962 is basically a feature extraction method used to detect lines and finding position of arbitrary shapes in the image and is widely used in the field of computer vision and image processing. Related to this patent, Richard Duda and Peter Hart in 1972 invented the Hough Transform which is used in modern times and they named it generalized Hough Transform. The simplest case of Hough transform is the linear transform for detecting straight lines. In the image space, the straight line can be described as $y = mx + c$ and can be graphically plotted for each pair of image points (x, y) . In the Hough transform, the main idea is to consider the characteristics of the straight line not as image points x or y , but in terms of its parameters, here the slope parameter m and the intercept parameter c . Figure 3.9 shows the main idea in Hough transform. All straight lines passing through point (x, y) satisfy that equation but the values of slope m and intercept c may vary. Now instead of considering the point (x, y) , parameters (m, c) are considered to understand the characteristics of straight lines in the image. This is the main idea in Hough Transform. If vertical lines are present in the image the values of m will be infinity, so parameters (ρ, θ) are used. The parameter ρ represents the distance between line and origin, θ is the angle of the vector from origin to this point. So the new rearranged equation becomes (eqn. 8),

$$\rho = x \cos \theta + y \sin \theta \quad (8)$$

This forms a sinusoidal curve in the (ρ, θ) plane, which is unique for that particular point. Now, more generally a set of points which form a straight line will produce curves which cross at the (ρ, θ) . The result of the Hough transform is stored in a matrix that is often called an accumulator. One dimension of this matrix is the θ values (angles) and the other dimension is the r values (distances), and each element has a value telling how many points/pixel lie on the line with the parameters (ρ, θ) . So the element with the highest value tells which line is most represented in the input image. Hough Transform has an advantage that the points need not all be continuous. This can be really helpful if line is broken due to noise. One more factor to be considered is the efficiency which depends on the quality of input data. It also has an importance in the skew correction of documents and characters, finding shapes like rectangle, circle, ellipse etc. in the image.

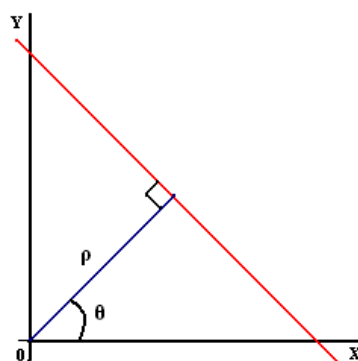


Fig. 14: Line showing parameters ρ and θ

3.4 Finite Element Analysis of shear behavior

The spacer fabric geometry was created using solidworks and was imported into ANSYS platform for finite element analysis of shear stress. SOLID45 is used for the 3-D modelling of spacer structures. The element is defined by eight nodes having three degrees of freedom at each node: translations in the nodal x, y, and z directions. The element has plasticity, creep, swelling, stress stiffening, large deflection, and large strain capabilities. The mesh size and number of nodes were determined in order to minimize processing time and yet have accurate results.

4. RESULTS AND DISCUSSIONS

4.1 In-plane shear behavior of 3D spacer fabrics

The in-plane shear properties of warp knitted spacer fabrics have been carefully evaluated using experimental and image analysis method and discussed in this section.

4.1.1 Image analysis method

The picture frame test method was verified for the 3D spacer fabrics under consideration.

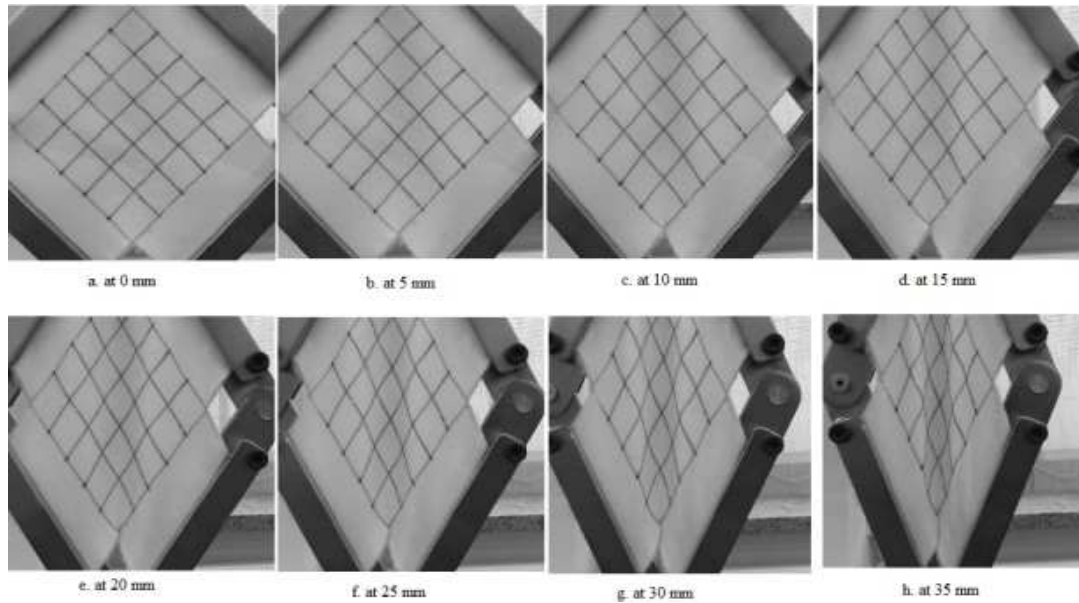


Fig. 15: Shear deformation of specimen at different displacement levels

Figure 15 shows the array of images for a 3D spacer fabric specimen captured during the loading process at each 5mm displacement for every 30 sec. In the beginning, (Fig. 15a), there is no shearing. Subsequently the shear deformation resistance was mainly from the friction between the wale and course direction loops before reaching the limiting locking angle. The limiting locking angle was the ultimate shear deformation observed by means of local wrinkling. Based on the deformed configuration of the fixture, shear angle was calculated using the relationship shown in equation 3. A vertical displacement of 40 mm, which corresponds to a shear angle of around 45° was found to be the maximum displacement but the pre-buckling occurs after 20 mm displacement with shear angle ranging between $20\text{-}30^\circ$ (Figure 15e). The local buckling is calculated using image analysis software. Figure 16 presents the linear fit curve between time and displacement.

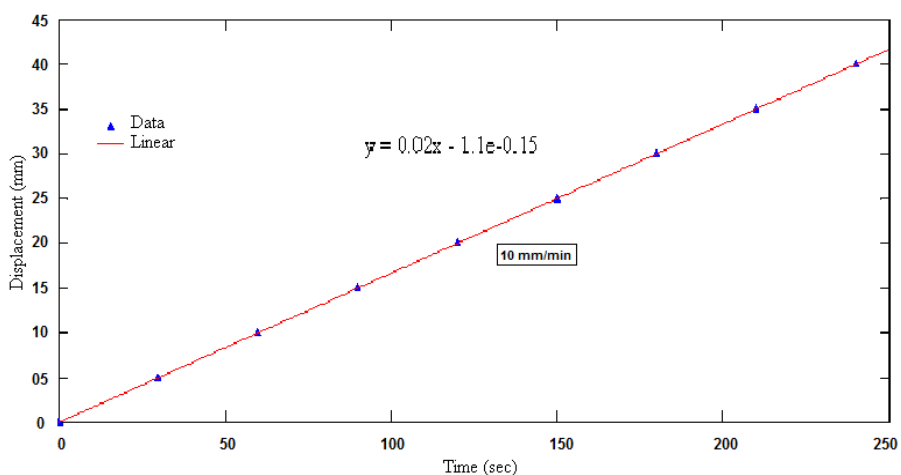


Fig. 16: Linear fit curve between time and displacement (10 mm/min)

Figure 17 shows the image of a fabric specimen captured during the loading process without displacement. This image was analyzed to obtain shear angle of the specimen

during the shear displacement. The image file string was examined and then the appropriate image reading function was called by MATLAB `imread`. The image was then converted to a gray image and then normalized to a matrix of values ranging from zero to one. This matrix was returned by the function in the variable `I`. Image analysis can aid in the determination of the shear angle and displacement at any particular point on the surface of fabric specimen. Grid pattern was applied on the specimen surface before the test and used as the reference points of image analysis. Around 16 points (25 square cells (4cm² each) with 90° angle at 4 points) can be chosen on a 100 mm x 100 mm specimen for image analysis to determine the displacements and shear angles at the chosen points. First, by manually choosing the points on a reference image, the X and Y coordinates of each point can be determined in pixel as shown in Figure 18. The difference of X and Y coordinates of each chosen point between the reference image and the image chosen for analysis represents the displacements in X and Y directions. Figure 4.4 shows the main idea of Hough transform applied to find the shear angle in image analysis technique. The Hough transform is widely used in image analysis, computer vision and digital image processing. It is a technique used to find shapes in a binary digital image. This approach is preferred when the objective is to find lines or curves in an image. The parameter ρ represents the distance between line and origin, θ is the angle of the vector from origin to this point. Figure 18 shows the points where the lines intersect giving the distance and angle. This distance and angle indicate the line which bisects the points being tested after each 5 mm displacement at every 30 sec interval. It helps researchers to understand more about detection of angles using Houghs transform. It clearly shows that detected points for two different levels of displacement are widely different, at 0 mm ($\theta=90^\circ$) and at 10 mm ($\theta=$ around 80°). Figure 19(a & b) show behavior of specimen during application of axial force by considering buckling effects. At 10 mm displacement the lines detected on surface of the specimen clearly indicate that the buckling has not happened because of regular intersection of lines (Fig 4.4a). But in case of 25 mm displacement, the irregular intersections of lines have occurred due to its wrinkling effects (buckling). The buckling starts at 20 mm displacement and having maximum buckling at 35 mm. The determination of shear angle for both warp and weft knitted spacer fabrics using image analysis are discussed and presented clearly in the following section.

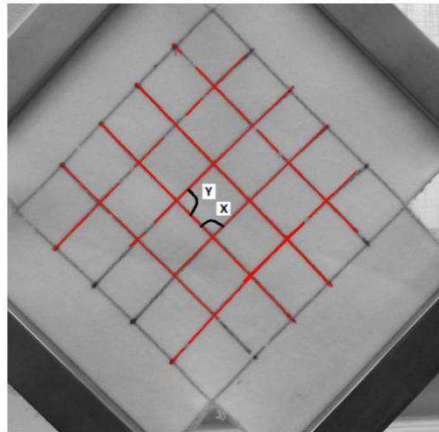


Fig. 17: Determination of shear angle using image analysis

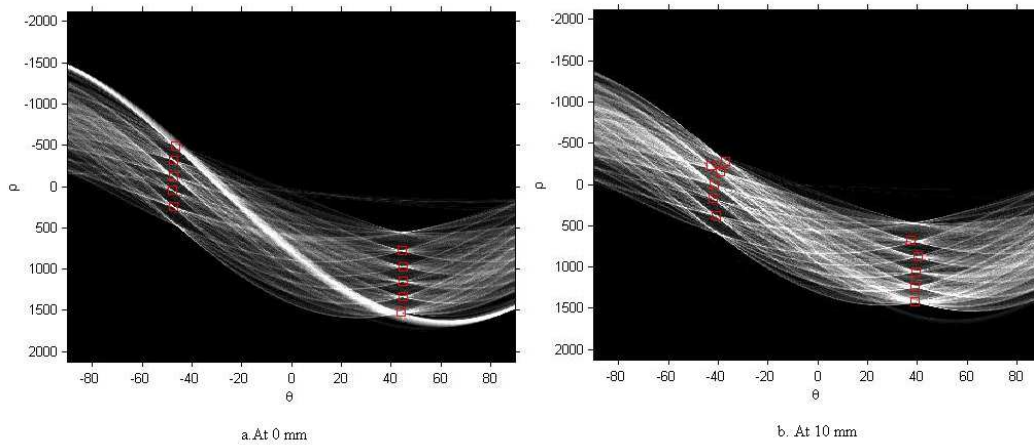
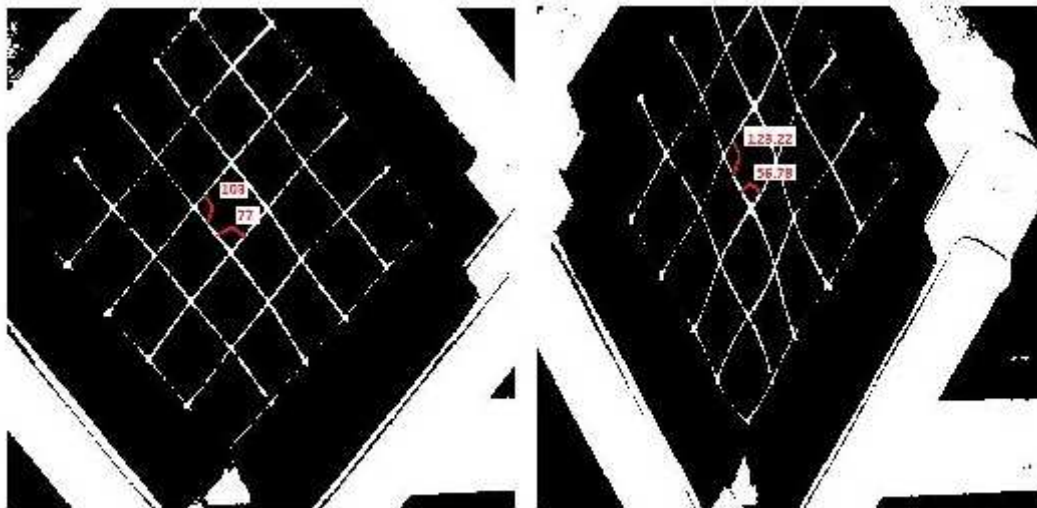


Fig. 18: Detected lines and points in Hough's histogram at two displacement levels



a. At 10 mm (Without Buckling)

b. At 25 mm (With Buckling)

Fig. 19: Gray image of shear angle at two displacement levels, considering buckling effects

4.1.2 Experimental evaluation of in-plane shear behavior of warp knitted spacer fabrics

The experimental evaluation of shear stress, shear strain and shear angle of warp knitted spacer fabrics are explained in this section.

4.1.2.1 Influence of thickness on in-plane shear behavior of warp knitted spacer fabrics

In this section, the effect of thickness on in-plane shear behavior of warp knitted spacer fabrics has been evaluated with respect to different structural parameters. First group of six spacer fabrics (WAS 1 – WAS 6) were produced with same outer layer structure (Lock knit) and stitch density but with different thickness (1.5, 2.5 & 3.5mm). As shown in Figs. 206a & b, the stress-strain curve reveals that the shear resistance decreases with increase in thickness. It can be seen that, the samples have almost similar behavior as they behave linearly in surface extension stage due to same surface structure and density. In next stage of shear deformation, the compressive stress also played a vital role to make the fabrics resist shear force. It was also observed that the thicker fabric has ability to undergo larger deformation in both shear and compression conditions. It was found that the hexagonal net structure fabrics (WAS 7 - WAS 12) show similar trend as the lock knit structures (Figs. 20c & d). The stress–strain curves show that, shear resistance is indirectly proportional to thickness of the spacer fabrics. From this observation, it is suggested that the fabrics with different thicknesses have different ranges of applications. The thickness of the fabric should be selected according to the amount of the energy to be absorbed and allowed shear stress level. The shear stress–strain behavior of spacer fabrics appears to change significantly with an appreciable decrease in spacer thickness.

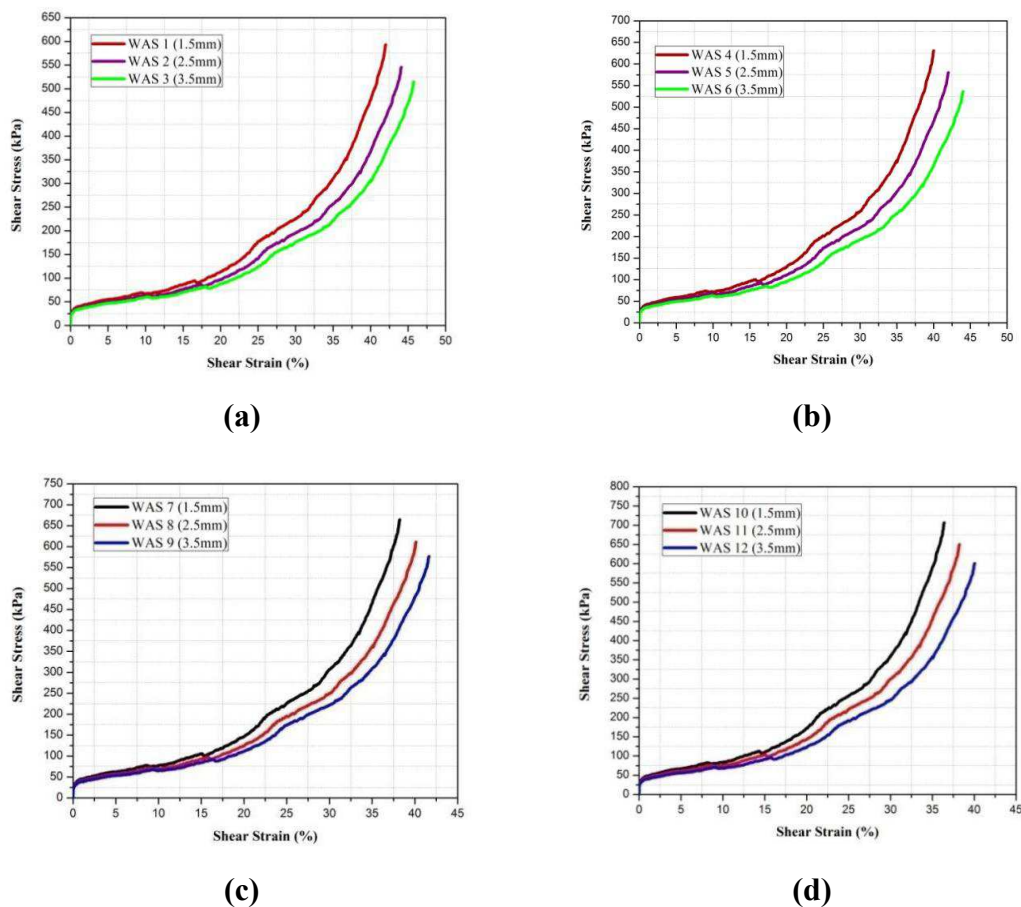


Fig. 20: Influence of thickness on shear behavior of warp knitted spacer fabrics

4.1.2.2 Influence of spacer yarn on in-plane shear behavior of warp knitted spacer fabrics

In both sets of spacer fabrics (lock knit and hexagonal net), two types of spacer yarn with different linear density (33 & 108 dtex) and diameter (0.055 & 0.1 mm) were used for convenient analysis of its effect on in-plane shear. Normally the spacer yarns are monofilament which connect surface layers and keep them apart. The spacer yarns act as linear springs which offer more resistance towards compression, result in higher shear stress as compared to other type of materials in specific applications. The angles between spacer yarn and surface layer can be varied by means of needle under lapping. In this study, spacer yarn angles ($84^\circ - 86^\circ$) of different samples have been maintained. From the Figures 21(a)&4.7(b), it is observed that, the shear stress is high for the fabrics with coarser spacer yarn for both types of structures. In surface elongation and compression (1st stage), a higher shear force was observed in the fabrics with coarser spacer yarn as compared to the fabrics made up of finer spacer yarns. It might be the fact that the large diameter and linear density of the coarse spacer yarns have higher ability to resist compressive stress than the fabrics made up of finer spacer yarn. In stage 2, the pre-buckling was observed after 20% of shear strain because the surface layers come in contact with each other leading to a locking effect. The fabrics have almost identical stress-strain curves with same thickness for both lock knit and hexagonal spacers in stage 1 region. However, a significant difference in the shear stress-strain behavior was obtained in the densification stage. It was due to the fact that the internal surface and spacer layer experience a closer compaction which depends on the thickness, the surface structure and spacer yarn properties.

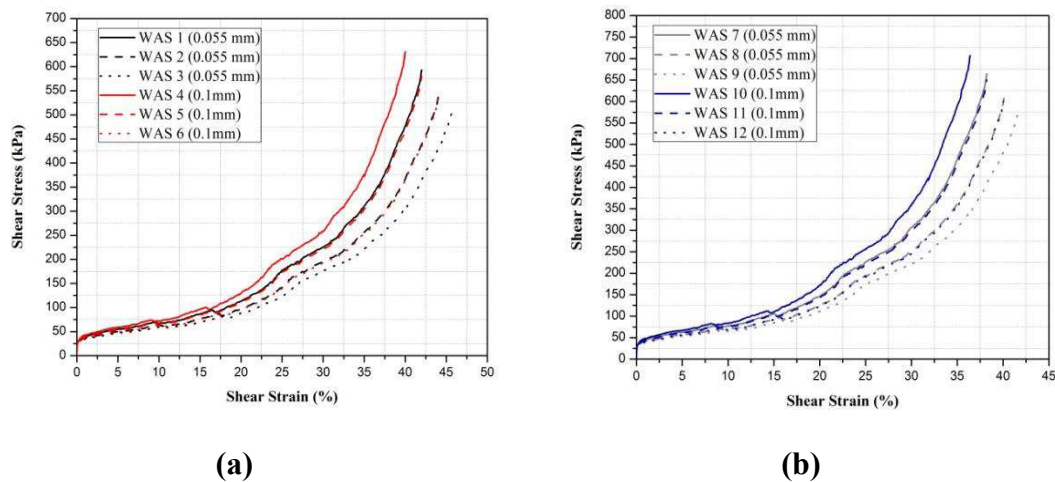


Fig. 21: Influence of spacer yarn linear density on shear behavior of warp knit spacer fabrics

4.1.2.3 Influence of surface structure on shear behavior of warp knit spacer fabrics

The in-plane shear behaviors of spacer fabric are also greatly influenced by their surface structures. The outer layer structure affects the monofilament yarn inclination, binding condition with surface, distribution and multifilament stitches in surface layers. The surface layers with these structures are shown in Table 1, from which the

stitch density, spacer yarn angle and size of the stitches in the outer layers can be clearly observed. It has been found that the surface structures could slightly affect the stitch density of the outer layers and the spacer yarn inclination angle, although these parameters are maintained the same during knitting.

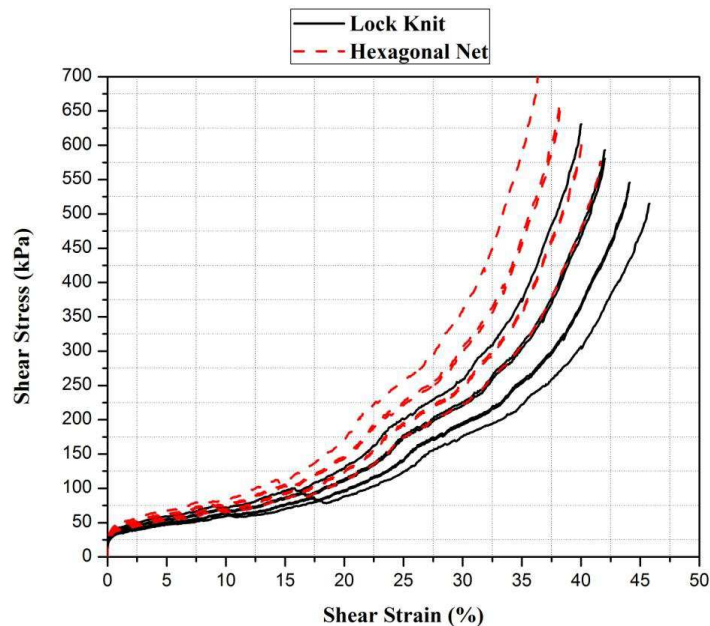


Fig. 22: Influence of surface structure on shear behavior of warp knit spacer fabrics
 As shown in Figure 22, the shear stress-strain behavior for both the structures (Lock knit and Hexagonal net) exhibits almost same load and deformation in stage 1. In stage 2, it is found that the Hexagonal-mesh fabric offers higher shear resistance than that of lock knit structures. All the samples have almost close value in the surface elongation region and the differences could be observed when the fabric undergoes lateral compression in stage 2. It might be due to those insignificant differences in the stitch density in surface deformation stage and thickness and spacer yarn properties influences in compression stage. In stage 3, the lock knit fabrics (WAS 1 – WAS 6) undergo large shear deformation for the same shear stress.

4.1.2.4 In-plane shear work done of warp knit spacer fabrics

Figure 23 (a – d) presents the work done on all spacer fabrics under in-plane shear load and it also compares the response shear stress with effect of deformation and structural characteristics. The figures reveal that thicker fabrics have higher work done than that of thin fabrics when it undergoes compression. Irrespective of the structural variation (lock knit and hexagonal net), the shear work done shows same trend for all the samples. Overall, the work done values were higher for the fabrics made up of hexagonal net structure on face side than that of lock knit fabrics. Also, it can be seen that fabrics with finer spacer yarn have low work done when compared to other fabrics; it might be due to finer spacer yarn offers low resistance towards compression. Figure 24 and Figure 25 present the graphical analysis of shear stress versus absorbed energy versus efficiency. It is obtained from the Figure 6, the shear work done of lock knit spacer fabrics (WAS 1 – WAS 6) linearly increases with the

stress in the surface extension and compression stage. The marginal differences in work done between the samples can be seen when the shear stress reaches towards the stage 2 for both the structures. At the start of densification stage, the rapid increases in stress results in small deformation and work done. From the energy absorption graph, it is easy to find the stress associated with the required amount of energy to be absorbed. So, it is more convenient to select the suitable spacer fabrics for car seat and back support application with optimum in-plane shear performance. As it is observed from the Figure 24, the fabric with hexagonal net structure shows similar tendency in energy absorption and efficiency with regards to thickness and spacer yarn. The maximum energy-absorption efficiency is obtained at the end of the densification stage. As noticed in the densification stage from Figures 24 & 25, efficiency becomes almost constant with increase in stress level. It may also be because of locking of the spacer yarn and with the yarns in the surface structure of spacer fabrics. The point at the maximum energy-absorption efficiency can be considered a critical point in the densification zone. Overall, it was observed that the shear work done and efficiency is higher for the thin fabrics with low density. Also, it was found that fabrics with finer spacer yarns undergoes large amount of work done as well as high efficiency during shearing mechanism.

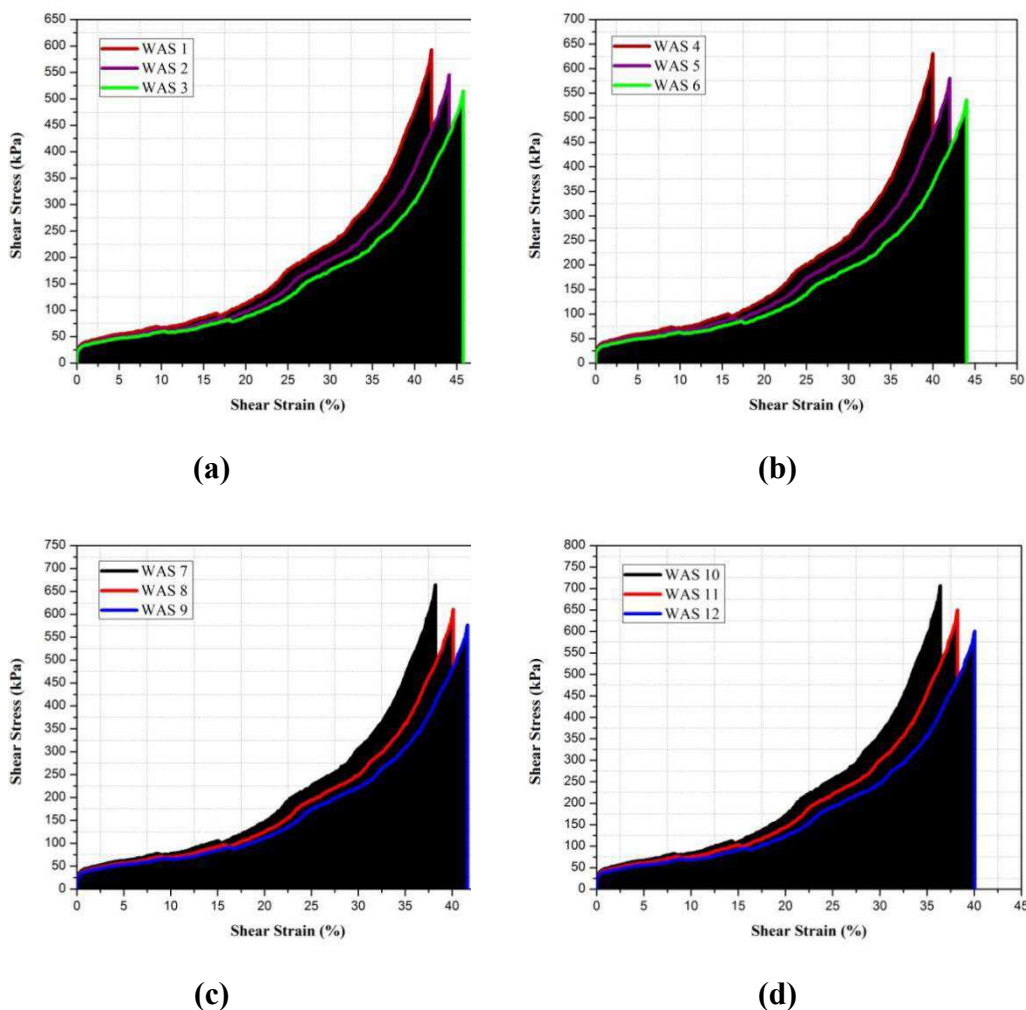


Fig. 23: Work done during shearing of warp knit spacer fabrics

4.1.2.5 Relation between shear angle versus shear force of warp knit spacer fabrics

The in-plane shear angle versus shear stress of 12 warp knitted spacer fabrics were carefully evaluated and presented in the Figure 26. It is observed from the graph that the thin hexagonal net spacer fabric with coarser spacer yarn (WAS 10) offers more resistance towards shear deformation than that of other fabrics. The thick lock knit fabrics with low linear density spacer yarn (WAS 3) have ability to undergoes high shear angle with low shear stress

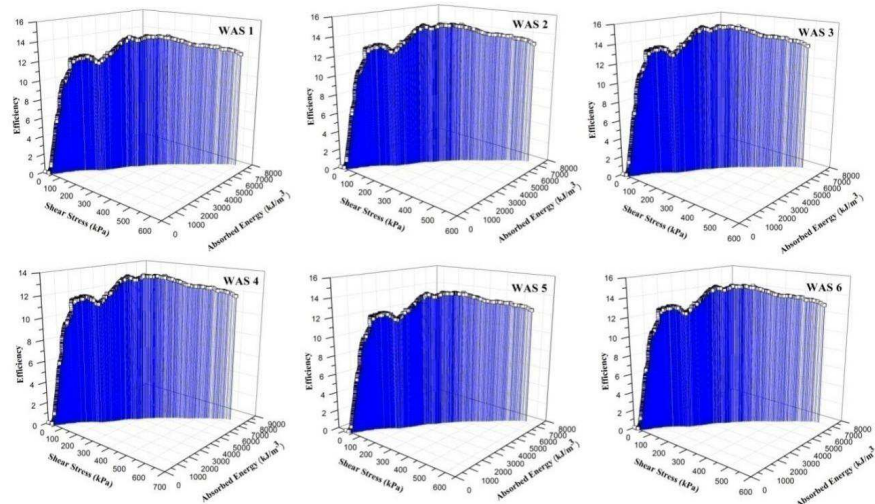


Fig. 24: In-plane shear energy absorption and efficiency of lock knit spacer fabrics

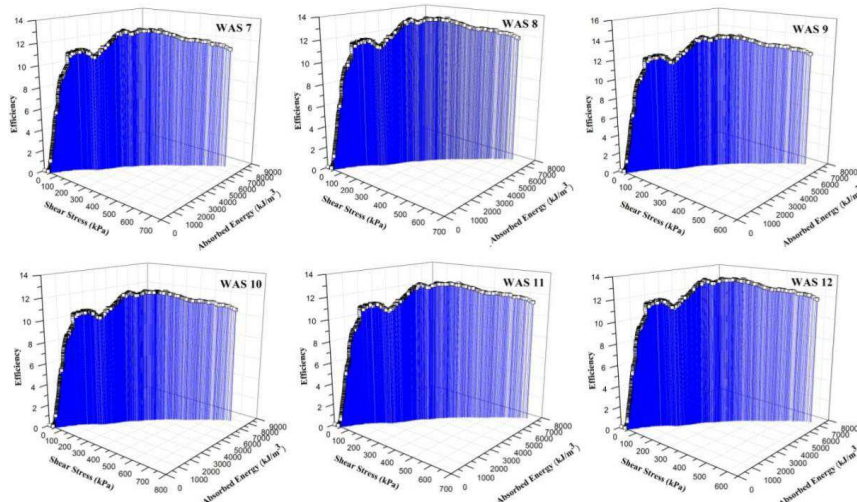


Fig. 25: In-plane shear energy absorption and efficiency of hexagonal net spacer fabrics

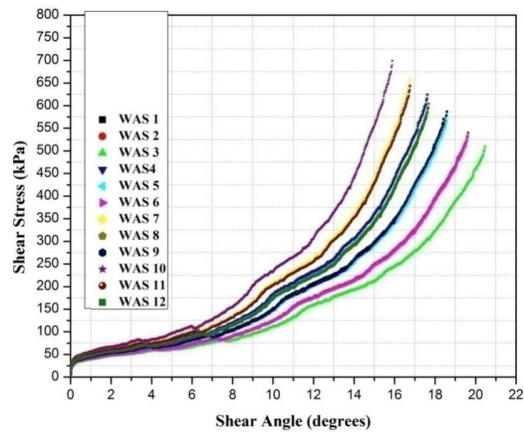


Fig. 26: Experimental determination of shear force and shear angle of warp knit spacer fabrics

4.1.2.6 Regression model for shear deformation of warp knitted spacer fabrics

Linear relationship between two variables x and y is a common concept, in which effective and easy assumptions helps to deduct relationship between them.

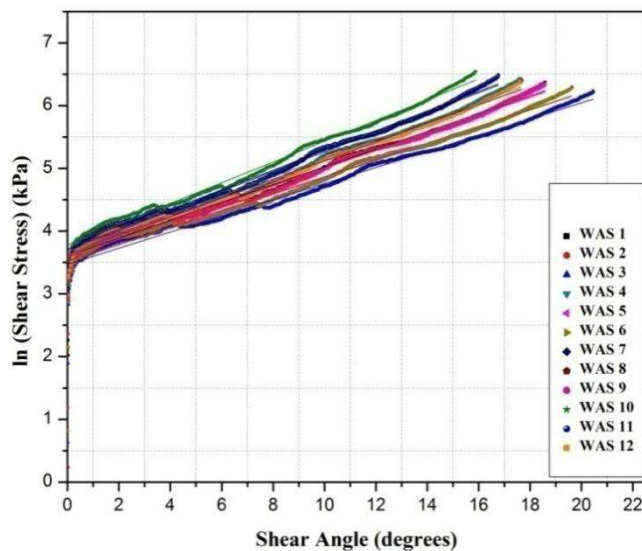


Fig. 27: Linear regression fit of experimental shear stress of warp knit spacer fabrics as a function of shear angle

The average of in-plane stress responses against shear angle obtained for each spacer fabrics samples was fitted in the general form of linear fit (Figure 27). To obtain highly fitted linear equation and R^2 value, the dependent variable values (shear stress) were transformed using log-transformation. Response fit analyses, regression coefficient estimations and model significance evaluations were conducted.

4.1.2.9 Comparative discussion of shear behavior of warp knitted spacer fabrics using different methods

The shear angles are calculated by considering sample length as a substitute for L in Equation 2 and it is further used for calculation of shear force. Figure 31 shows the comparison of shear angles between image analysis and both experimental

measurements for all 12 specimens. The differences between image analysis and calculated shear angle using sample length at the chosen points are relatively small. It does not show any significant difference until pre-buckling occurs but significant difference occurs after 20 mm displacement. It was also believed that during image processing in MATLAB, detection of X and Y coordinates on the image was not accurate due to wrinkling in the central zone of samples. Also, it was noted that dimension of the frame rig length can cause big difference in shear angle as shown in Figure 31. Further study is required on the effect of different frame rig length and ratio of frame length to specimen size on in-plane shear behavior of 3D warp spacer fabrics. The comparative linear regression is given in the Table as a function of shear strain. The regression equations for all three methods are also given with the coefficient of determinant (R^2) to find the degree of linear fit.

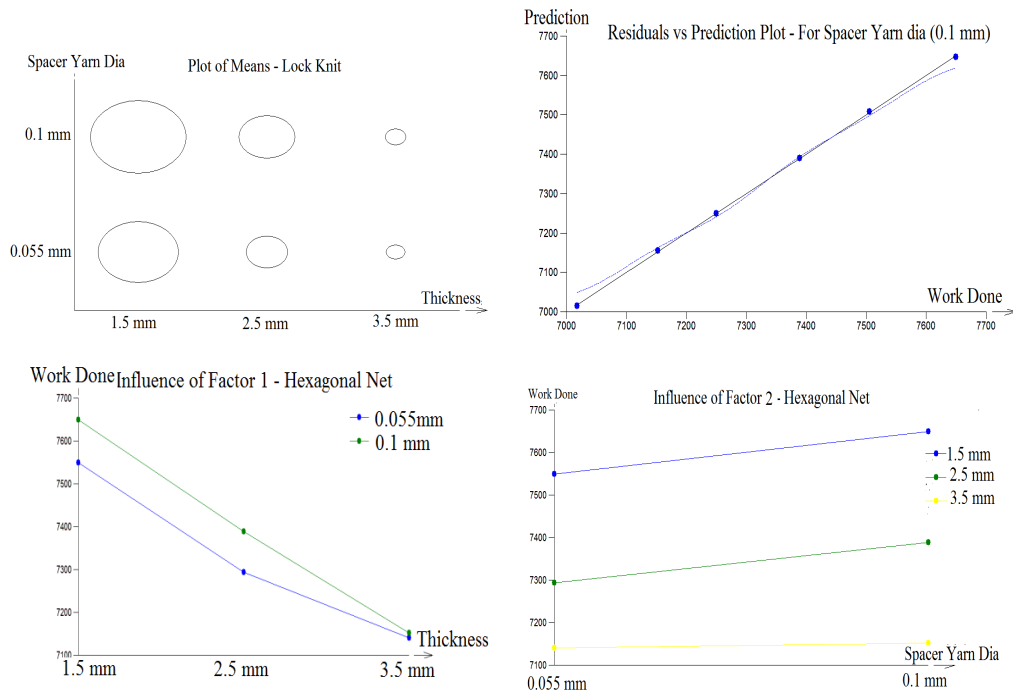


Fig. 28: Graphical output – Statistical evaluation for in-plane shear behavior response of warp knit spacer fabrics

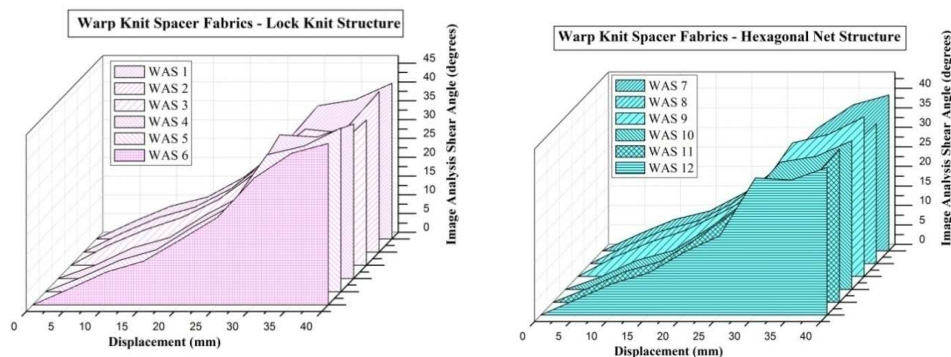


Fig. 29: Determination of shear angle of warp knit spacers using Image Analysis method

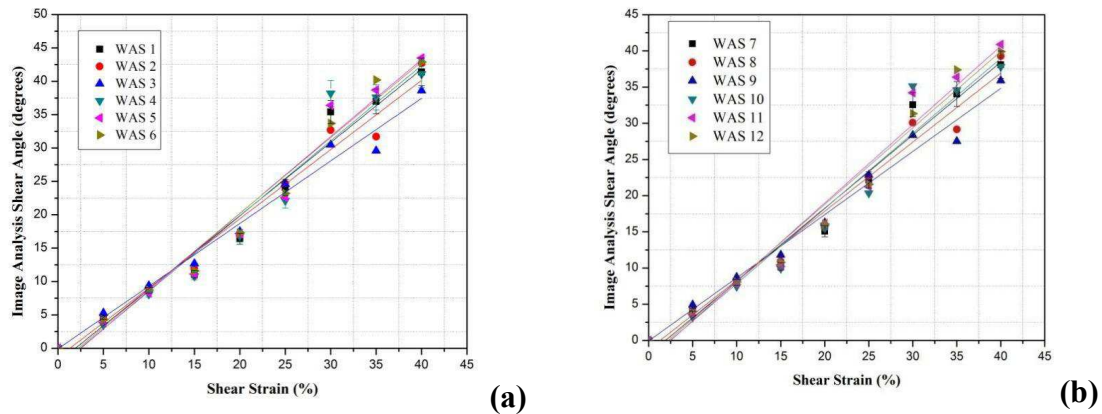


Fig. 30: Linear regression fit of shear angle using image analysis as a function of strain of warp knit spacer fabrics (a) Lock knit structure (b) hexagonal net structure

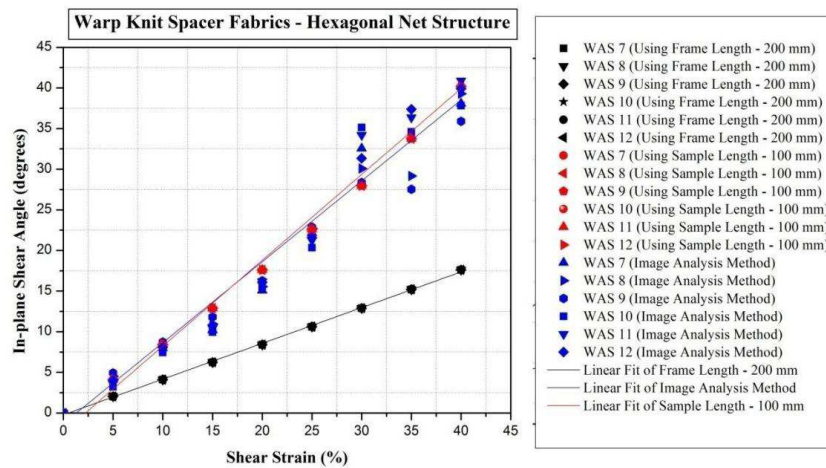
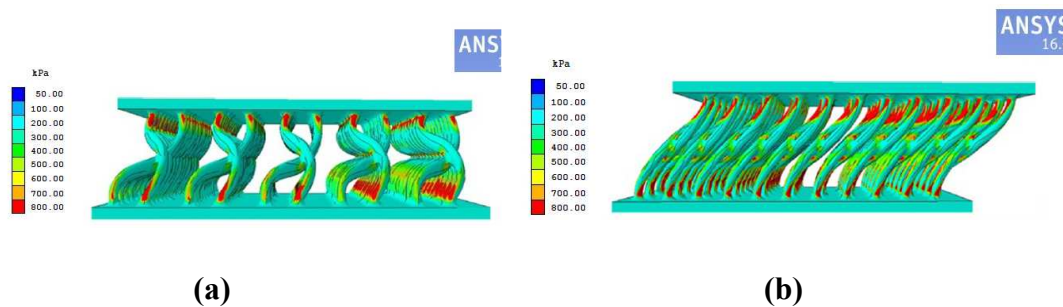


Fig. 31: Comparison of shear behavior of warp knit spacer fabrics using different test methods

4.1.2.10 Prediction of shear stress using Finite Element Method

The spacer structures were made using solidworks45 and were imported into ANSYS platform for mesh generation. The number of nodes in unit cell was 2130. Material properties e.g. tensile modulus, tensile strength, strain rate, Poisson’s ratio etc. were used. Shear stress at various displacements were simulated. The results are shown in figure 32 and 33.



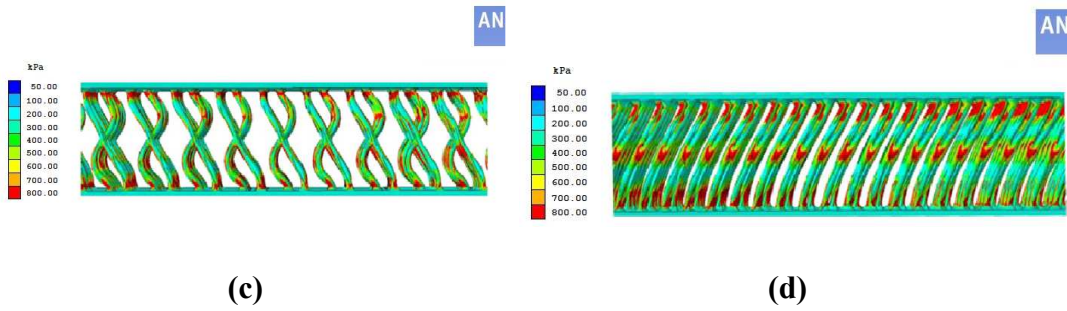


Fig. 32: (a) Lock knit spacer before shear, (b) Lock knit spacer after shear, (c) Hexagonal net spacer before shear and (d) Hexagonal net spacer after shear

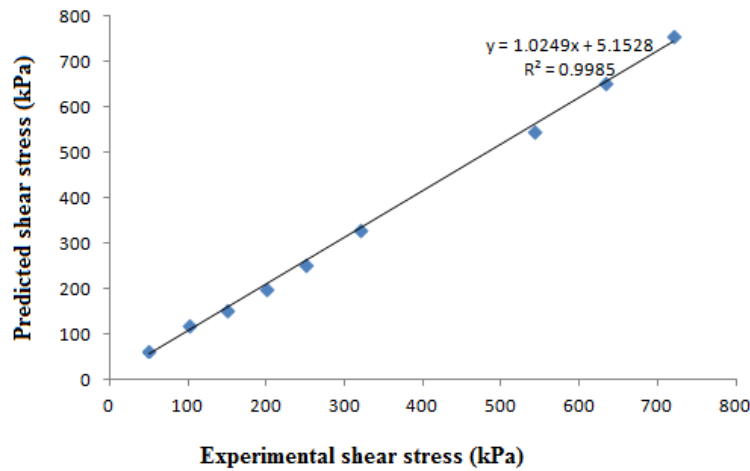


Fig. 33: Correlation of simulated and experimental shear stress
The predicted shear stress was well correlated with experimental values obtained.

5. CONCLUSION

3D warp-knitted spacer fabrics with varying thicknesses, spacer yarn linear density and face structures resulted in significant shear performance. In-plane shear behavior of spacer fabrics are greatly influenced by their surface structures, type of spacer yarn and the fabric stitch density. The nonlinear behavior of shear stress versus shear angle and the deformation mechanism were analyzed and it was established that shear deformation increases after limiting locking angle which initiates the buckling of the sample. The work done is higher for the fabrics made up of hexagonal net structure on face side than that of lock knit fabrics. Shear stress is higher for the fabrics with coarser spacer yarns among all the fabrics samples. Significant differences in the shear stress-strain curve were obtained in the densification stage. The outer layers and spacer layer lead to higher compaction depending on thickness, density, surface structure and spacer yarn properties. Even minor change in the spacer fabric thickness results in significant change in the shear behavior. The image analysis procedure provided much detailed information about the shear behavior of the fabric than stroke measurement. The displacement data, and change in shear angles during loading process explain the excellent shear behavior of the warp knitted spacer fabrics. The significant regression equations accurately predict the in-plane shear behavior, and

identify the most significant factors influencing the spacer fabric shear properties. The outer layer structure affects the monofilament yarn inclination, binding condition with surface, distribution and multifilament stitches in surface layers. Suitable models can be developed to inter-relate shear behavior with compression and related deformations. Such an approach can enable attaining the needed performance based on constructional parameters with sufficient accuracy.

ACKNOWLEDGEMENT

The authors gratefully acknowledge the support by project No. L1213 of program NPU from MSMT Czech Republic.

REFERENCES

- [51]Chen, X. G., Taylor, L. W. and Tsai, L. J.: *An overview on fabrication of three-dimensional woven textile preforms for composites*. Textile Research Journal, 2011, vol. 81, 932–944.
- [52]Bilisik, K.: *Multiaxis 3D woven preform and properties of multiaxis 3D woven and 3D orthogonal woven carbon/epoxy composites*. Journal of Reinforced Plastic Composite 2010, vol. 29, 1173–1186.
- [53]Boisse, P.: *Meso–macro approach for composites forming simulation*. Journal of Material Science, 2006, vol. 41, 6591–6598.
- [54] Behera, B. K. and Mishra, R.: *Artificial neural network-based prediction of aesthetic and functional properties of worsted suiting fabrics*. International Journal of Clothing Science and Technology, 2007, vol. 19, 259-276.
- [55]Mishra, R., Militky, J., Behera, B. K. and Banthia, V.: *Modeling and simulation of 3D orthogonal fabrics for composite applications*. Journal of Textile Institute, 2012, vol. 103, 1255-1261.
- [56]Bilisik, K.: *Multiaxis three-dimensional weaving for composites: a review*. Textile Research Journal, 2012, vol. 82, 725–743.
- [57]El Abed, B. and Msahli, S.: *Numerical simulation of woven fabric wrinkling*. Journal of Textile Institute, 201, vol.102, 77–86.
- [58]Vanclouster, K., Lomov, S. V. and Verpoest. I.: *Investigation of interply shear in composite forming*. International Journal of Material Formation, 2008, vol. 1, 957–960.
- [59]Zhu. B., Yu, T. X. and Tao, X. M.: *Large deformation and slippage mechanism of plain woven composite in bias extension*. Composite Part A- Applied Science, 2007, vol. 38, 1821–1828.
- [60] Willems, A., Lomov, S. V., Verpoest, I. and Vandepitte, D.: *Picture frame shear tests on woven, textile composite reinforcements with controlled pretension*. In: 10th ESAFORM conference on material forming, Parts A and B 2007: 999–1004.
- [61] Lin, H., Clifford, M. J., Long, A. C. and Sherburn, M.: *Finite element modelling of fabric shear*. Model Simulation Material Science, 2009, vol. 17, 1–16.
- [62] Cao, J., Akkerman, R., Boisse, P., Chen, J., Cheng, H. S., de Graaf, E. F., et al. *Characterization of mechanical behavior of woven fabrics: experimental methods and benchmark results*. Compos Part A- Applied Science, 2008, vol. 39, 1037–1053.
- [63] Chen, Q. Q., Boisse, P., Park, C. H., Saouab, A. and Bréard, J.: *Intra/inter-ply shear behaviors of continuous fibre reinforced thermoplastic composites in thermoforming processes*. Composite Structure, 2011, vol. 93, 1692–1703.

- [64] Charmetant, A., Orliac, J. G., Vidal-Sallé, E. and Boisse, P.: *Hyperelastic model for large deformation analyses of 3D interlock composite preforms*. Composite Science and Technology, 2012, vol. 72, 1352–1360.
- [65] Ye, X., Hu, H. and Feng, X.: *Development of the warp knitted spacer fabrics for cushion applications*. Journal of Industrial Textile, 2008, vol. 37, 213-223.
- [66] Long, A. C.: *Design and manufacture of textile composites*, CRC press. 2005.
- [67] Long, A. C.: *Composites forming technologies*, CRC press. 2007 .
- [68] Lebrun, G., Bureau, M. N. and Denault, J.: *Evaluation of bias-extension and picture frame test methods for the measurement of intra-ply shear properties of PP/glass commingled fabrics*, Composite Structures, 2003, vol. 61, no. 4, 341– 352.
- [69] Potter, K.: *Beyond the pin-jointed net: maximising the deformability of aligned continuous fibre reinforcements*, vol. 33, 2002.
- [70] Vanclooster, K.: *Forming of Multilayered Fabric Reinforced Thermoplastic Composite*, PhD. Thesis, Katholieke University, Belgium, 2009.
- [71] K. a. Fetfatsidis, K. A., Jauffrès, D., Sherwood, J. A. and Chen, J.: *Characterization of the tool/fabric and fabric/fabric friction for woven-fabric composites during the thermo stamping process*, International Journal of Material Forming, 2011, vol. 6, no. 2, 209– 22.
- [72] Larberg, Y. R. and Åkermo, M.: *On the interply friction of different generations of carbon/epoxy prepreg systems*, Composites Part A: Applied Science and Manufacturing, 2011, vol. 42, no. 9, 1067– 1074.
- [73] Sun, J., Li, M., Gu, Y., Zhang, D., Li, Y. and Zhang, Z.: *Interply friction of carbon fiber/epoxy prepreg stacks under different processing conditions*, Journal of Composite Materials, Feb. 2013.
- [74] Ersoy, N., Potter, K., Wisnom, M. R. and Clegg, M. J.: *An experimental method to study the frictional processes during composites manufacturing*. Composites Part A: Applied Science and Manufacturing, 2005, vol. 36, 1536-44.
- [75] Larberg, Y.: *Forming of Stacked Unidirectional Prepreg Material*. PhD. Thesis, KTH Royal Institute of Technology, Sweden, 2012.
- [76] Spivak, S. M.: *The behavior of fabrics in shear, part 1: The instrumental method and the effect of test conditions*. Textile research journal, 1966, vol. 36, no. 12.
- [77] Kawabata, S., Niwab, M. and Kawai, H.: *The finite-deformation theory of plain weave fabrics part iii: The shear- deformation theory*. Journal of the Textile Institute, 1973, vol. 64, no. 2, 61–85.
- [78] Kawabata, S., Inoueb, M. and Niwab, M.: *Theoretical analysis of the non- linear deformation properties of a triaxial weave under biaxial stress fields*. Composites Science and Technology, 1996, vol. 56, 261–271.
- [79] Lomov, S. V., Verpoest, I., Barburski, M. and Laperre, J.: *Carbon composites based on multiaxial multiply stitched preforms. part 2. kes-f characterization of the deformability of the preforms at low loads*. Composites Part A, 2003, vol.34, no.4, 359– 370.
- [80] Hu, J. L. and Zhang, Y. T.: *The kes shear test for fabrics*. Textile research journal, 1997, vol. 67, no. 9, 654–664.
- [81] Wang, J., Page, J. R. and Paton, R.: *Experimental investigation of the draping*

- properties of reinforcement fabrics*, Composites Science and Technology, 1998, vol. 58, 229-237.
- [82] Lebrun, G., Bureau, M. N. and Denault, J.: *Evaluation of bias-extension and picture-frame test methods for the measurement of intraply shear properties of PP/glass commingled fabrics*. Composite structures, 2003, vol. 61, 341-352.
- [83] Digital image correlation (DIC) provided by “GOM-optical measuring techniques” with Aramis v. 6.2.0 software.
- [84] Zhang, Y., Sun, F., Wang, Y., Chen, L. and Pan N.: *Study on intra/inter-ply shear deformation of three dimensional woven performs for composite materials*. Materials and Design, 2013, vol. 49, 151–159.
- [85] Willems, A., Lomov, S., Verpoest, I. and Vandepitte, D.: *Picture frame shear tests on woven, textile composite reinforcements with controlled pretension*. In: 10th Esa form conference on material forming, Parts A and B, 2007, 999–1004.
- [86] Dash, B. P., Behera, B. K., Mishra, R. and Militky, J.: *Modeling of internal geometry of 3D woven fabrics by computation method for structural composites*. Journal of Textile Institute, 2013, vol. 104, 312-321.
- [87] Mishra, R.: *Impact tolerance of 3D woven nanocomposites: A simulation approach*. Journal of Textile Institute, 2013, vol. 104: 562-570.
- [88] Mecit, D., Marmarali, A.: *Application of spacer fabrics in composite production*, Usak University Journal of Material Sciences, 2012, vol. 1, 71 – 78.
- [89] McCartney, P. D., Allen, H. E., Donaghy, J. G.: *Underwire brassiere, warp-knitted textile fabric for use in fabricating same, and method of warp knitting such fabric*. USPTO Patent Full Text and Image Database, U S Patent No. 5669247, 1999.
- [90] Shepherd, A. M.: *Weft-knitted spacer fabrics*. USPTO Patent Full Text and Image Database, U S Patent No. 6779369 B2, 2004.
- [91] Liu, Y., and Hu, H.: *Compression property and air permeability of weft-knitted spacer fabrics*. Journal of the Textile Institute, 2011, vol. 102, no. 4, 366-372.
- [92] Liu, Y., Lv, L., Sun, B., Hu, H., and Gu, B.: *Dynamic response of 3d biaxial spacer weft-knitted composite under transverse impact*. Journal of Reinforced Plastics and Composites, 2006, vol. 25, no. 15, 1629-1641.
- [93] Liu, Y., Hu, H., Zhao, L., and Long, H.: *Compression behavior of warp-knitted spacer fabrics for cushioning applications*. Textile Research Journal, 2011, 0(00), 1-10.
- [94] Gross, D.: *3D spacer knit fabrics for medical applications*, Journal of Textile Apparel Management, 2003, vol. 4, 26-28.
- [95] Walker, K., Robson, S., Ryan, N., Malien, L., Sibbick, R., Budden, G., Mephram, A.: *Active protection system*. In: Advanced materials processes, 2008, S. 36.

Compressibility of sandwich composite structures for impact absorbance

Kasthuri R Venkatesh, Jana Novotna, Rajesh Mishra and Jiri Militky
*Faculty of Textile Engineering, Dept. of Material Engineering, Studentská 2,
Technical University of Liberec 461 17 Czech Republic*

1. INTRODUCTION

From ancient times, mankind has used textiles and compliant laminates, not only for clothing and protection against the elements, but for bodily protection. From the use of leather on Grecian shields, layered silk in ancient Japan, to chain mail and suits of armor in the Middle Ages, personnel protection has sought to protect its wearer from the corresponding advances in armaments [1]. With the advent of high performance polymer fibers in the 1960s, such as aramid fiber (aromatic polyamide), ultra-high molecular weight polyethylene (UHMWPE) fibers and Zylon, there has been remarkable properties achieved in the protective equipment. High performance fibres used in ballistic products are characterized by: low density, high strength, and high energy absorption capability. But the quest for attaining the light weight and high strength protective garments with the aid of such fibres depends on the engineering design of the material used and architectural concepts. Jackets made from high-strength aramid Kevlar-49 and Armor are used for bullet protection [2]. A jacket must fulfill two major requirements. First, the jacket must stop a bullet. In addition, the height of a bullet bulge on the inside lining should not exceed some value. If the bulge height exceeds this value, the bullet may result in injury even if it is stopped.

With the requirement of light weight body armors, the need for performance improved fiber reinforced composites is significantly increasing. The architecture of the fabric plays a significant role in the protection against ballistic impact and provides a unique ballistic penetration resistance for varied orientations. The main structural parameters of the fabric, which shows the effect on the ballistic performance, are type of weave (with a twist in the yarns), yarn crimp, fabric structure, projectile geometry, impact velocity and friction [3].

With the established high performance fibres and materials in market, to achieve advancements in body armor performance levels, the use of models and simulations to develop innovative system designs[4]. The application of impact resistance materials can be broadly classified into high-velocity impact response and low-velocity impact response. In the former, the response is dominated by the stress wave propagation through the material. The latter deals with the absorption of the impact energy. Cushioning is thus important for low-velocity impact resistance. Non-penetrated damage is a main index that expresses the safety of bulletproof cloth in use. In this work, the novel cushion material of the sandwich structure, made of the filament-laying layer and nonwoven fabric, is used to improve the properties of

ballistic resistance. [5] The kinetic energy of the bullet needs to be dissipated and dispersed by the bulletproof cloth after shooting to prevent excessive impact indentation. The nonwoven cushion structure is useful for improving the non-penetrating damage of the bulletproof cloth after a bullet is shot into it. The works done by compressing these kinds of materials are equivalent to the kinetic energies of a mass that might impact on them. If properly designed with extended displacement and appropriate level of the constant stress, a cushioning material could absorb most of the energy of the mass impacting on it. Thus, by means of absorbing the impact energy with an increased displacement and a constant stress, the protected object would not have to endure a concentrated high-energy or high-load impact that would occur if a mass directly impacts on it.

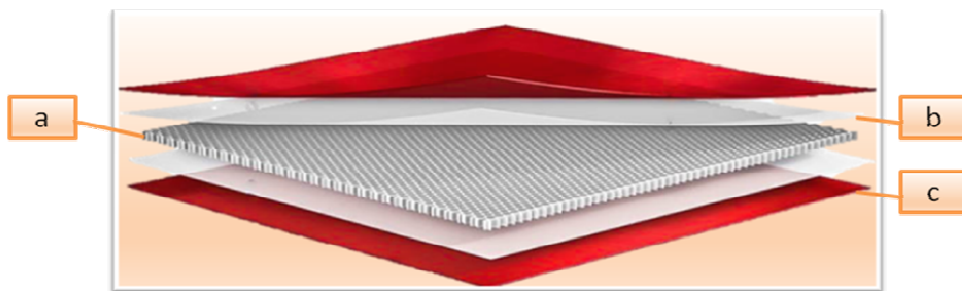


Fig. 1: Components of a sandwich composite a) Core layer, b) Adhesives/resin, and c) Face/ Skin

Therefore, in the current study sandwich composites were prepared with 3 Dimensional spacers and struto nonwovens are used as the core layers to absorb the impact energy. They are used as the cushioning layer. The outer layer or face is woven Kevlar fabric. The sandwich was fabricated together with epoxy resin by vacuum bagging technique. It was then measured for its compression resilience.

2. MATERIALS

Several different types of fibres have been used in different combinations of fabric construction and thereby in the production of composites or laminates for impact resistance property.

2.1 Fibre properties

The advent of the High performance polymeric fibres has led to a new era of impact resistance materials that offered protection against small arms munitions. High performance fibres used in ballistic products are characterised by: low density, high strength, and high energy absorption capability [6]. As seen in above figure, Dyneema has a very high score. By using a numerical model, it was established that higher modulus fibre gives higher wave velocity, which leads to a rapid energy absorption rate. As the modulus is decreased, the wave velocity is decreased and the strain is more concentrated in the vicinity of the impact zone. Fabric with high modulus can

spread load onto other fibres and layers more quickly, which is beneficial in ballistic applications.

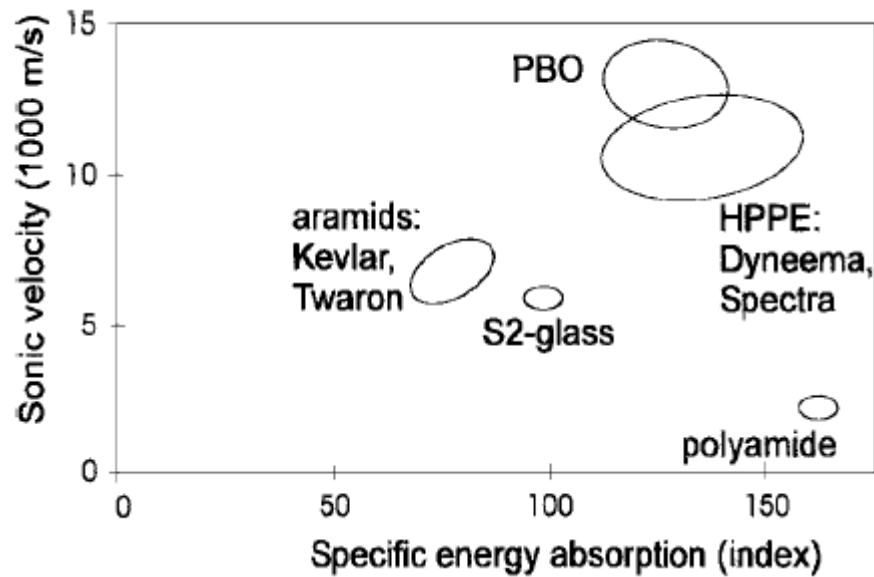


Fig. 2: Primary ballistic figures of merit for various fibres [6]

The impact process in effect requires two things from the fabric or yarns; firstly they should not break so they should be strong (or tough) and secondly the imposed load and the resulting stress waves need to move quickly from the impact point. This has led the combined performance factor U^* which states that the performance of fabric is the product of the specific yarn toughness and longitudinal wave speed of the yarn.

Many studies have been carried out to find the contribution of aramid fibers[8] in a hybrid carbon–aramid composite. Effect of type of weave also plays an important role. Twill weave was widely used with epoxy resin for impregnation. To evaluate the influence of the aramid fibers, a comparative study between carbon and carbon–aramid woven–reinforced composites was undertaken. The mechanical tests performed indicated that the aramid phase present in the hybrid carbon–aramid composite induced an important enhancement on the impact (37.9% in energy absorption) and fracture resistance (12.7% for fracture initiation and 43% for steady state regime), compared to small reductions on the material stiffness.

2.2 Fabric construction

2.2.1 Woven fabric

Weave density of fabric, which is known as “cover factor”, is a function of the number of warp picks and weft ends in a unit of length of fabric and indicates the percentage of area covered by the fabric. High cover factor will increase the available dissipation of strain energy capability by getting more fibres and yarns engaged with a projectile. [9] It has been suggested that the cover factor should be in the range of 0.6 to 0.95 for ballistic applications. When cover factors are greater than 0.9, yarn properties degrade in the process of weaving and when the cover factor fall below

0.65, the fabric will become too loose. The ‘wedge through’ effect is more likely to occur on loosely woven fabrics.

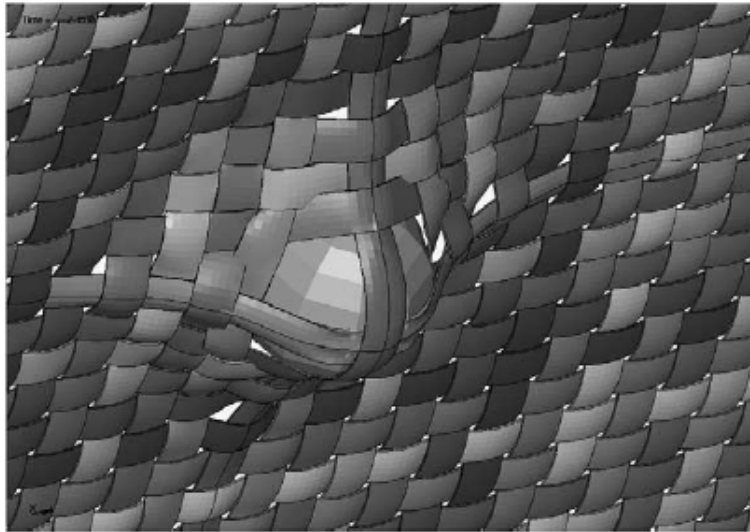


Fig. 3: A depiction of the “wedge through” phenomenon associated with fabric impact [9]

2.2.2 Weave Character of woven fabric

The effects of the weave structure [10] and hybridization on the low velocity impact properties were investigated. Between the weaves, plain and 2×2 twill, 2×2 Twill was found to represent a better weaving structure than plain fabric. However,[3] when the 2D plain woven armors were compared to 3D orthogonal and 3D interlock armors, the 2D plain woven failed. The increase in the ballistic limit from 2D plain woven armor to 3D orthogonal and 3D angle interlock armors was 16.44% and 20%, respectively, indicating the effect of fabric architecture. In another study, [11] which also compared the 2D woven against the 3-D interlock, the results showed that the 3-D interlock woven composites exhibited a smaller impact damage area and higher % residual strength than the 2-D woven laminated composites. The improvements were attributed to the larger crimp-angle and interlacing structure of the 3-D interlock woven composites, which inhibits delaminated propagation along the plane direction. al compression strength of three-dimensional (3-D) interlock carbon woven/epoxy composites. Comparative evaluations were also contrasted with those for conventional two-dimensional (2-D) plain woven/epoxy laminated composites. Besides, the fact that the 3-D interlock woven structure prevents buckling of the fibre tows under compressive load also contributes to the compression-after impact test performance.

2.2.3 Unidirectional

In a study by Karahan[12] the performance of ballistic protection panels formed with 100% woven and 100% unidirectional nonwoven para-aramid fabrics at different fabric ply numbers was compared. The UD Kevlar is not a woven fabric structure. It is a nonwoven fabric which is formed by placing Kevlar 129 yarns at right angle (at 0

and 90 degrees) on top of each other and then by sticking them with the help of pressure and temperature using polyethylene films.

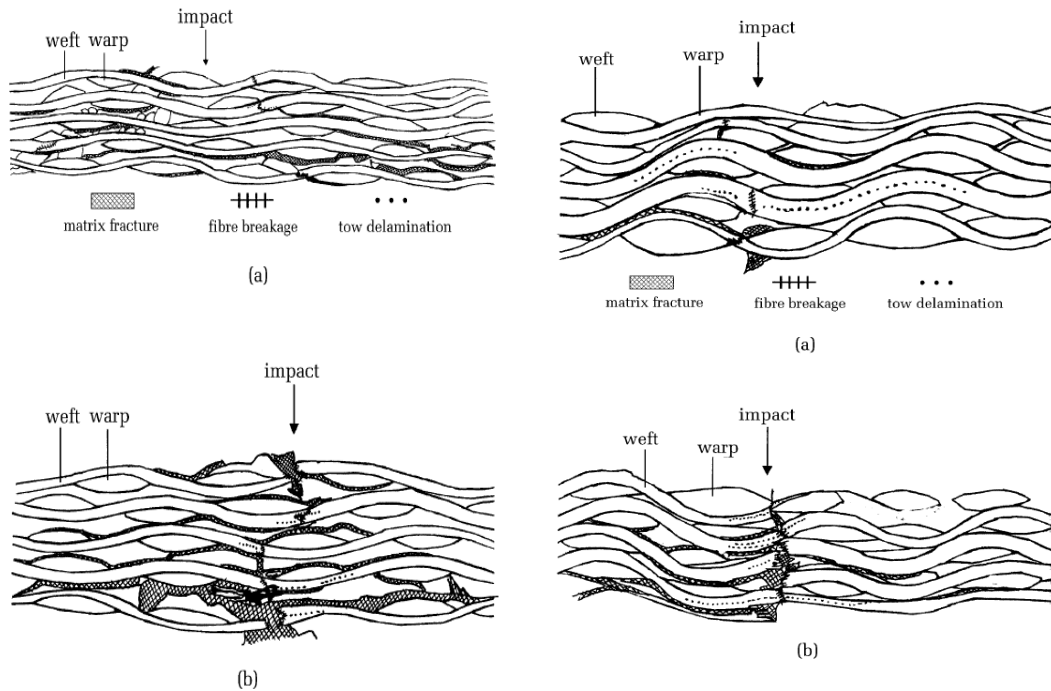


Fig. 4: Schematic illustration of the impacted modes of the 2-D (left) and 3D (right) woven composite subjected to a) 15J and b) 20J impact energy, respectively.

No interlacing exists between the yarns perpendicular to each other and, therefore, UD Kevlar fabric is a laminate comprising orthogonal layers of UD nonwoven yarns sandwiched between polymer films. Due to this, no crimp is induced in the yarns. It was found that that the unidirectional fabric panels absorbed around 12.5–16.5% more energy than woven fabric panels for the unit panel weight. This is due to better propagating of ballistic impact energy on the fabric plane because of absence of crimp.

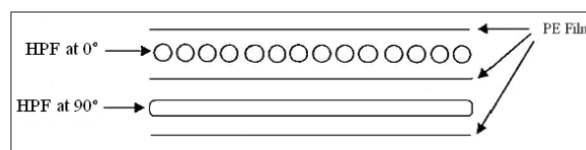


Fig. 5: Schematic representation of UD nonwoven fabric structure formed by placing the yarns at right angles (0 and 90 degrees) and sticking them using polyethylene (PE) film (HPF- High Performance Fibre)

2.3 Composite construction

With new engineering designs and concepts there are different type of composite structures that varies with the number of layers, method of bonding, different structures incorporated, etc.

2.3.1 Hybrid composites- based on fibers used

In the first case, [13] the intermediate aramid fabric layer was replaced by an equal thickness layer of 30 vol% jute fabric reinforced epoxy composite. Ballistic impact test with 7.62 caliber ammunition revealed that both the plain epoxy and the jute fabric composite have a relatively similar performance of the Kevlar™ and also attended the NIJ standard for body protection. The energy dissipation mechanisms of jute fabric composite were analyzed by scanning electron microscopy and found to be the rupture of the brittle epoxy matrix as well as the interaction of the jute fibers with the post-impact fragments. This latter is the same mechanism recently disclosed for aramid fabric. However, the lightness and lower cost of the jute fabric composite are additional advantages that favor its substitution for the aramid fabric.

A similar study was conducted replacing the jute with sisal[14]. The front ceramic layer was a 15 mm thick hexagonal plate with 31mm of side dimension and made of 4 wt% Nb2O5 doped Al2O3 (ceramic). The intermediate layer, with 10 mm in thickness and square sides with 150 mm, was either: (i) 16 plies of aramid fabric (aramid), or (ii) 30 volume % of continuous and aligned sisal fibers reinforced epoxy matrix composite (sisal composite) plates, or (iii) plain epoxy plate. The ballistic performance of the sisal composite was found to be 20% more ballistic effective (smaller indentation in clay witness) than the aramid with the additional advantage of being 5% lighter and 31% cheaper.

Plenty of investigations were done on effects of stacking sequence layers of hybrid composite materials on ballistic energy absorption by running the ballistic test at the high velocity ballistic impact conditions. For instance, the work carried out [15] preparing composites given in the table 1.

The results show, that Hybrid 2 has the superlative energy absorption of 95.17 J. Second, it can be concluded that stacking the first layer with glass fibre is better than to use the Kevlar fibre, according to Hybrid 2 and Hybrid 4 impact specimens with ballistic impact energy absorption of 95.17 J and 95.15J, respectively.

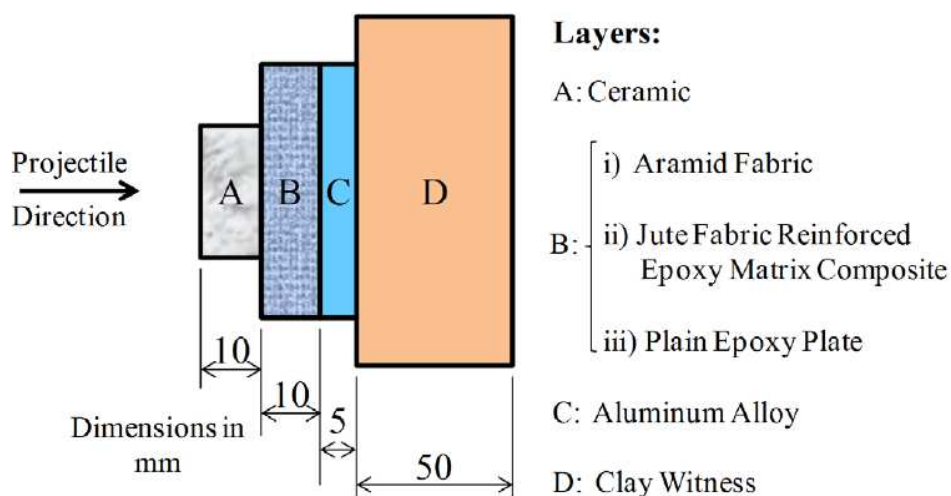


Fig. 6: Schematic diagram of the multilayered armor [13]

Table 1: Different sequence of fibre layers for hybrid composites construction

HYBRID 1	HYBRID 2	HYBRID 3	HYBRID 4	HYBRID 5
Kevlar	Glass	Kevlar	Glass	Kevlar
Carbon	Carbon	Glass	Kevlar	Carbon
Glass	Kevlar	Carbon	Carbon	Glass
Glass	Kevlar	Carbon	Glass	Carbon
Kevlar	Carbon	Glass	Carbon	Glass
Carbon	Glass	Kevlar	Kevlar	Kevlar

Moreover, the results indicated that using the combination of carbon and glass is more efficient in the central layers due to its excessive brittleness under impact loads. In another study on hybrid composite[10], the effects of the weave structure and hybridisation on the low velocity impact properties were investigated. 100 % Carbon and carbon-aramid hybrid woven fabrics of different constructions, produced from the same yarn and under the same production conditions, was determined. Depending on the weaving structure, the best results were obtained for twill woven composites. This study shows that through proper fabric construction and hybridisation, the impact resistance of the composite structure can be improved and adjusted to different performance levels. Between the weaves, plain and 2 × 2 twill, 2 × 2 Twill was found to represent a better weaving structure than plain fabric. Also, 100% carbon composites are quite limited in their energy absorption capacity; however, this was found to improve by about 9 – 10% via hybridization

2.3.2 Thermoplastic Composite

A lot of study has been carried out on composites constructed using thermoplast as binding agent or matrix. For instance, Kevlar® fabrics of different architectures, namely 2D plain woven, 3D orthogonal and 3D angle interlock fabrics, were produced and used as reinforcements to fabricate composite armor panels, using compression molding technology. Interfacial property between PP and Kevlar® was improved by adding a coupling agent called maleic anhydride grafted PP. Reduced density was observed in Kevlar® thermoplastic based composites as compared to that of the thermoset-based laminates. The ballistic limit velocity was increased with the change in the fabric architecture from 2D-P to 3D-O and 3D-A. The ballistic limit velocity of 3D-A laminates was 20% higher than that of the 2D-P laminates and 4.2% higher than that of the 3D-O laminates. However, the 2D plain woven armors failed. The increase in the ballistic limit from 2D plain woven armor to 3D orthogonal and 3D angle interlock armors was 16.44% and 20%, respectively, indicating the effect of fabric architecture. The ballistic behavior of multi-layer Kevlar [16] aramid fabric/polypropylene (PP) composite laminate (CL) and plain layered aramid fabric (AF) impact specimens was investigated. It was found that the thermoplastic PP matrix increases the ballistic performance of CL targets when compared to AF targets with similar areal density, resulting in less aramid fabric needed to obtain the same level of protection when the PP matrix is incorporated. It was found that the improved

ballistic performance of CL targets is due to the fact that the thermoplastic matrix enables energy absorbing mechanisms such as fabric/matrix debonding and delamination. The ballistic limit and penetration threshold energy of the CL configurations, which were predicted using an empirical model, were found to be higher than those of the AF targets. These results show that aramid fabric/PP laminates should be further studied for improved ballistic performance at lower costs.

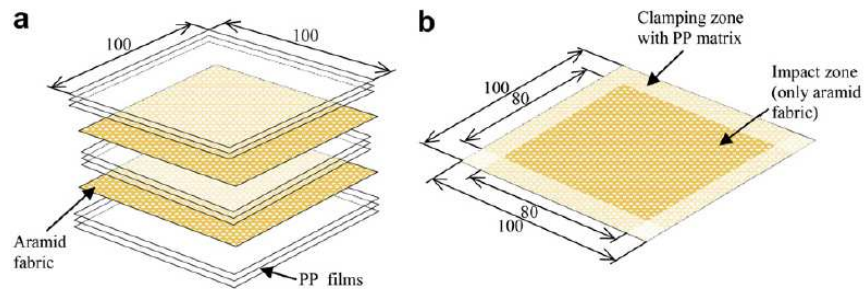


Fig. 7: Geometric details of target configurations (a) composite laminates, and b) plain multi-layer aramid fabric.[16]

2.3.3 Epoxy composites

Epoxy resin is widely used in the composite preparation. Many studies have been carried out using epoxy as matrix. [17]The E-glass/epoxy/nanoclay composite is a laminate with 12 layers and 50% fiber mass fraction. This type of laminate configuration is prepared using a hand lay-up method which leads to an average thickness of 2.6 mm. A flat rectangular glass mold was used to prepare the glass/epoxy nanoclay plate. Curing of the glass/epoxy nanoclay plate is performed for 150 min at 80°C under pressure 0.25MPa followed by 150 min at 120°C under pressure 0.4MPa in an autoclave. The best ballistic resistance is observed with 3wt% nanoclay content in an impact velocity of 134 m/s (near to the ballistic limit) and with 10wt% nanoclay content in an impact velocity of 169 m/s.

In this chapter, a theoretical model to investigate the ballistic impact behavior of two-dimensional woven glass/epoxy/nanoclay nanocomposites is presented, developed on the basis of dividing of the impact duration into several time intervals and calculation of the energy absorbed during each time interval. The major components of energy lost by projectile during ballistic impact were identified, namely the primary yarns tensile failure energy, the secondary yarns deformation energy, the cone kinetic energy formed on the back face of the target, the delamination of layers of nanocomposite and the matrix cracking. Ballistic tests were performed by a flat-ended projectile by a gas gun. Finally, a good correlation has been observed, comparing the theoretical model presented in this chapter to the experimental results. In a study, [11] the impact performance, compression failure mechanisms and residual compression strength of three-dimensional (3-D) interlock carbon woven/epoxy composites was studied. Comparative evaluations were also contrasted with those for conventional two-dimensional (2-D) plain woven/epoxy laminated composites. The results show that the 3-D interlock woven composites exhibited a smaller impact damage area and higher % residual strength than the 2-D

woven laminated composites. The improvements were attributed to the larger crimp-angle and interlacing structure of the 3-D interlock woven composites, which inhibits delaminated propagation along the plane direction. Besides, the fact that the 3-D interlock woven structure prevents buckling of the fibre tows under compressive load also contributes to the compression-after impact performance. This chapter investigates the ballistic impact mechanism of multi-ply aramid/epoxy composites with different laying up structures. The effect of ply angle and number of ply was studied. Ballistic impact behaviour of the composites was evaluated by their energy absorption capacity and high-speed video observation and analysis. Angle-laid dry fabric assemblies were used as reinforcements in parallel to the align-laid fabric assemblies. The energy loss during penetration process was used to characterise the ballistic performance of the composites experimentally. The results of the investigation indicate that for three-layered composites, $[0/45/0]$ and $[0/30/60]$ angle-laid constructions absorb 3% and 10% more energy than the composite with align-laid reinforcement. However, for the four-layered composites, angle-laid composites demonstrate lower ballistic resistance than the align-laid composites, which calls for further investigation.

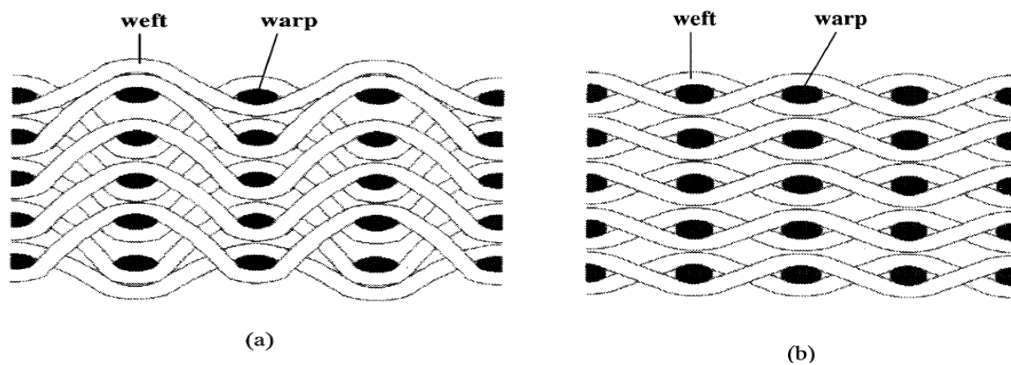


Fig. 8: Schematic illustration of the perform construction. a) 3-D interlock woven perform b) 2-D plain woven perform [11]

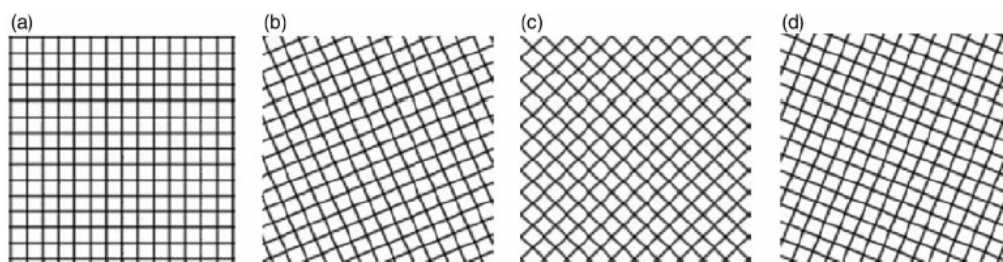


Fig. 9: The top view of each ply in a 4-ply panel a) 1st ply 0°, b) 2nd ply 22.5°, c) 3rd ply 45° and d) 4th ply 67.5° [18]

Aramid/epoxy composites with three- and four-layers of fabrics were penetrated by projectile at the high impact velocity ranging from 460 m/s to 510 m/s. It was found that the strain wave propagation is with a circular wave front both aligned and angled ply composites. This is different to the strain wave front observed and reported for dry fabric panels. The main energy absorbent mechanisms of ballistic resistance before

the failure of composite are matrix cracking and delamination while the mechanisms during the failure are matrix cracking, delamination and fibre fracture and pull-out. Pull-out effect of fractured fibre is apparent. Differences with various constructions become unapparent for more fabric layers.

Table 2: Multi-layered composite materials construction.

Layup Type Rotate angle	3-ply panel			4-ply panel		
	Model 1	Model 2	Model 3	Model 4	Model 5	Model 6
Layer 1	0°	0°	0°	0°	0°	0°
Layer 2	0°	30°	45°	0°	22.5°	45°
Layer 3	0°	60°	0°	0°	45°	0°
Layer 4	—	—	—	0°	67.5°	45°

3.3.4 Cushion layer in composite

A cushion layer is incorporated composite to absorb the impact energy. [19] Studies have been carried out on comparison between the composite fabrics with and without the cushion layer Reducing the non-penetrating damage is crucially important in avoiding serious harm to users. The sandwich structure was made from nonwoven fabric and laid filament layer to produce a cushion layer. The construction of composite design is shown in figure below. The experiment's results showed that the cushion layer of the composite nonwoven fabric was useful for the Kevlar laminated fabrics to dissipate the impact energy and transmit the impact stress. The dropping impact test results demonstrated polyester filament rather than polyamide filament in cushion effect of the bullet-shooting test. The experimental results also revealed that the composite nonwoven fabric was suitable for a cushion material of ballistic-resistant cloth and was useful in decreasing the nonpenetration damage of ballistic-resistant cloth after shooting of bullets. The addition of the cushion layer could reduce both number of layers and manufacturing cost. Non-penetrated damage is a main index that expresses the safety of bulletproof cloth in use. The kinetic energy of the bullet needs to be dissipated and dispersed by the bulletproof cloth after shooting to prevent excessive impact indentation. The nonwoven cushion structure is useful for improving the non-penetrating damage of the bulletproof cloth after a bullet is shot into it. In this work, the novel cushion material of the sandwich structure, made of the filament-laying layer and nonwoven fabric, is used to improve the properties of ballistic resistance. The design of the nonwoven cushion structure is expected to be suitable for reducing the impact indentation of the bulletproof cloth after a bullet is shot; it must be able to replace the original cushion material. The impact indentation of the bullet-shooting test can express the ability of the ballistic resistance or the resistance of the non-penetrating damage. The analytical results show that the design of the nonwoven cushion structure is effective in improving the non-penetrating damage of the bulletproof cloth after the bullet has been shot. The analytical results show that the sandwich structure is useful for the cushion material of the bulletproof

cloth. Through structural design, the impact indentation of the bulletproof cloth after bullet shooting is improved to decrease the non-penetrating damage to the human body. Additionally, the performance of the ballistic resistance can be raised. The better cushioning effect is expected at a lower cost. use that is simulated by the oil clay. The result shows that the compound nonwoven fabric is more suitable than the original cushion material, which is made of a polyamide plain-woven fabric, for use as the cushion material of the bulletproof vest, as shown in Table 2.

In this current study, the sandwich composite was made with three types of core layers and they are,

- a. Warp knit spacers
- b. Weft knit spacers and
- c. Struto nonwovens.

Eleven different types of sandwich composites were made for this study. The composition of sandwich composites is given in table 1.

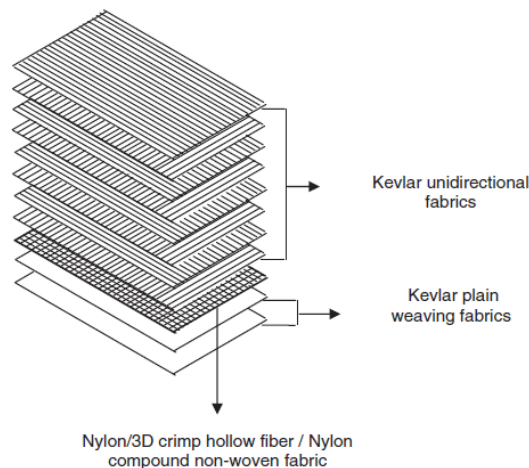


Fig. 10: Dropping impact test sample diagram

In addition, the compound nonwoven fabric shows a better expanding area of energy transmission after the bullet shooting test (shown in Fig.11). The result shows that the compound nonwoven fabric has a better cushioning effect as compared with original cushion material (Nylon plain woven fabric). Therefore, we can use the compound nonwoven fabric to replace the original cushion material.

a. Warp knit spacer

Warp-knitted spacer fabrics are three-dimensional textile structures consisting of two separate outer fabric layers joined together but kept apart by spacer yarns, which are generally monofilaments[5]. They are produced on high-speed double-needle bar Raschel machines and their three elements, namely outer fabric layers and spacer yarns, are knitted together in a single process. Typical compression stress strain curve is given by the author in figure below. The compression process is divided into four different stages, i.e., initial stage (stage I), elastic stage (stage II), plateau stage (stage III), and densification stage (stage IV) according to the changes in the slope of the curve. At the initial stage, a lower slope is observed due to the compression of the

loose outer layers and their ineffective constraint for the monofilaments. However, when the fabric is further compressed into stage II, all the compressed multifilament stitches are changed to a fastened microstructure.

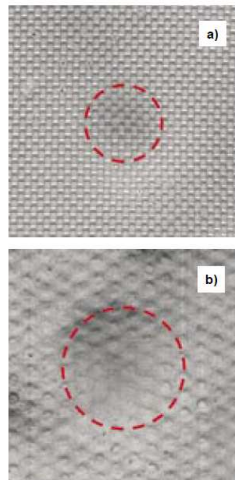


Fig. 11: The comparison of the indentation deformation between the original cushion material (nylon plain woven fabric) and the compound nonwoven fabric after shooting test; a) the original cushion material, b) the compound nonwoven fabric.

[20]

Table 3: Composition of sandwich composites

Sample No.	Type of Core	Composition of Core	Thickness of Core (mm)	Areal Density of Core (GSM)	Weave of outer layer	Thickness of outer layer (mm)
1	Weft knitted Spacer	Meta-Aramid	5.29	1260	Plain	0.55
2		Meta-Aramid	3.3			
3		Meta-Aramid	3.2	830		
4	Warp knitted spacer	Polyester	27	280	Plain	0.55
5		Polyester	27		Twill	0.51
6		Polyester	27		Satin	0.6
7		Polyester	27		Plain	0.2
8	Nonwoven	Polyester	27	465	Plain	0.55
9		Polyester	27		Twill	0.51
10		Polyester	27		Satin	0.6
11		Polyester	27		Plain	0.2

In this stage, the monofilaments buckle at a larger scale and they are better fastened by the multifilament stitches. Consequently, a rapid increase of the compression

stress, i.e., a stiffer mechanical behavior of the fabric is observed. A nearly constant stress is obtained in stage III. The deformation mechanism of the fabric in this stage is very complicated. The compression at stage IV shows a rapid increase in the stress due to the swift densification of the entire fabric. At this stage, the monofilaments within the fabric collapse and contact each other, and therefore a really high stiffness is obtained.

b. Weft knitted spacer:

The two outer layers are formed by intermeshing loops, while the spacer yarns tuck the loops of the two outer layers alternately in the course-wise direction to form a sandwich structure without intermeshing. The typical stress-strain curve for the weft knitted spacer is below. There are 4 stages. Figure below shows a typical compression stress–strain curve of a spacer fabric. The compression process can be divided into four different stages, i.e. initial (stage I), linear elasticity (stage II), plateau (stage III), and densification (stage IV) according to the changes in the slope of the curve.

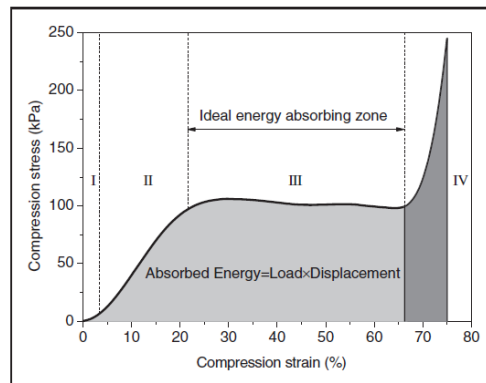


Fig. 12: Typical compression stress-strain curve of a spacer fabric

c. Struto Nonwoven

The Struto nonwoven made up of polyester fibres was produced in the university. A vibrating perpendicular lapper was used to produce Struto nonwovens. The struto technology is patented in Czech Republic and a schematic is shown in figure 13.

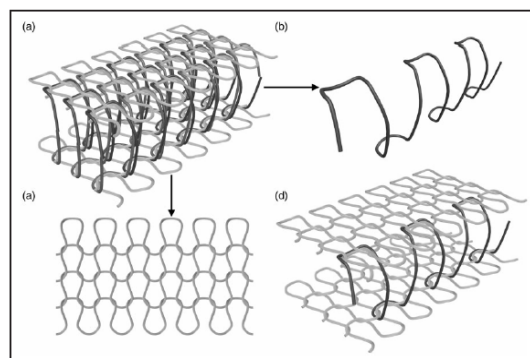


Fig. 13: Loop structure of a weft knitted spacer fabric a) fabric structure; b) spacer (core) yarn; c) outer or sheath layer; d) a spacer yarn tucking outer layers

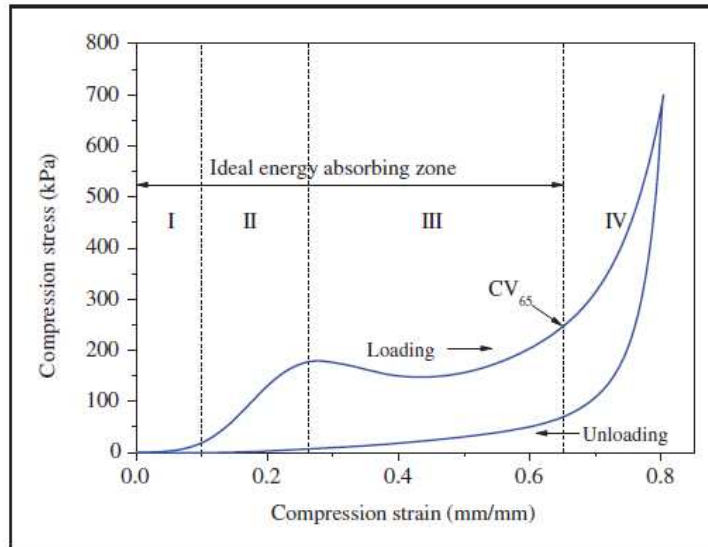


Fig. 14: Typical compression stress-strain curve of a warp knit spacer fabric

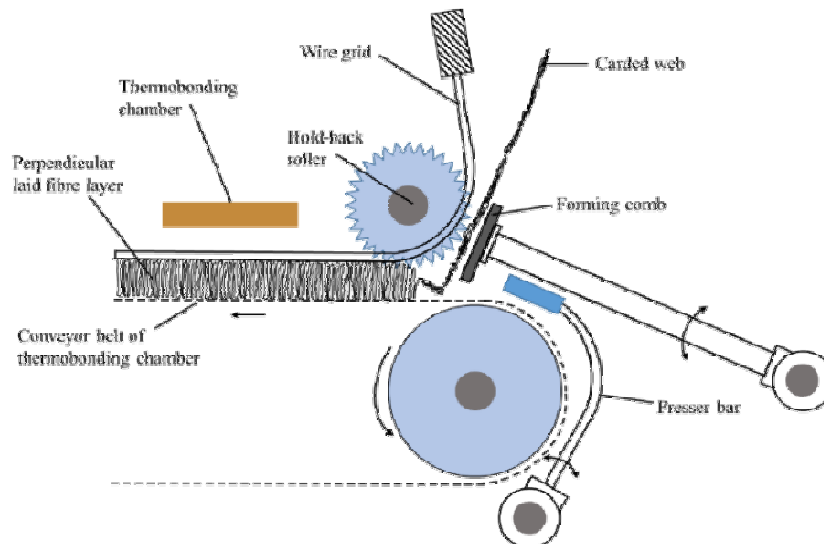


Fig. 15: Vibrating perpendicular lapper.

The carded web is fed onto conveyor belt and a reciprocating forming comb pulls the carded web towards the hold back roller to form a fold. The fold is pulled off the comb by a system of needles placed on a reciprocating compressing bar and pushed to the fiber layer which is created and moved between the conveyor belt and a wire grid. The fiber layer is bonded by melt-bonding fibers present in the fiber blend when it passes through thermobonding chamber. The skin or outer layers are made of kevlar woven fabric of different weave structures, such as plain, 2x2 twill and satin. The woven kevlar fabrics were obtained from an industry. The core or middle layer was of three different material, weft knit spacers, warp knit spacers and, struto nonwoven. Weft knit spacers was made up of meta-aramid fibers. Three different thickness or space between the two fabrics was obtained by changing the dial height relative to machine cylinder. Warp knit spacers are made up of polyester fibres. Both the warp and weft knit spacers were obtained from an industry.

3. METHODOLOGY OF PREPARATION AND TESTING OF SANDWICH REINFORCED COMPOSITES

3.1 Preparation of sandwich composites

Sandwich composite manufacturing

The composites were prepared using epoxy resin L180 from the industry Havel's composites. The resin to hardener ratio was 40:16 per 20 cm X 20 cm sample.

Vacuum bagging technique was used to improve the quality of sandwich composite produced by wet lay-up method. Initially, the resin and hardener are mixed with the help of a magnetic stirrer. The mixture is then applied onto the surface of the woven kevlar fabric by help of a roller. In-laboratory set up of vacuum bagging technique is shown in figure 2. A perforated layer of nonwoven on the glass makes the first layer. The sample is placed on the release film. The whole set up is covered with a flexible vacuum bag. Edge of the bag is sealed with vacuum sealing compounds or sealant. Vacuum pressure of 600bar is applied. When vacuum is applied, the trapped air and excess resin escapes out which further consolidates the laminate and eliminates voids. The vacuum pressure was set for 24 hours. After which the sample is put into oven at 60°C for 15hours.

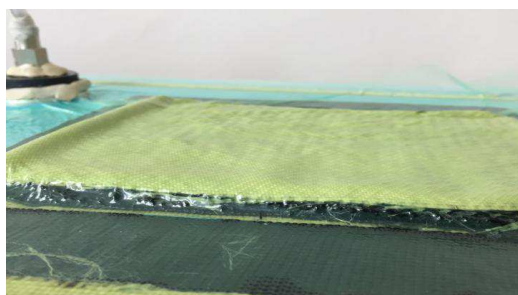


Fig. 16: Vacuum bagging for sandwich composite preparation.

3.2 Testing of sandwich composites

Measurement of compression

The measurement of compression for the prepared sandwich composites was done as shown in figure 3. The sandwich composite samples were tested according to the Standard ASTM D 575 on a TIRA Tester device set up with two compression circular plates. The size of all the specimens was 20cm X 20cm. The compression tests were conducted at a speed of 10 mm/min up to a deformation 40% and 80% of the initial thickness for each composite sample in an environment of 20 °C and 65% relative humidity.

4. A FEW EXPERIMENTAL RESULTS

In samples 1-3, the core material used was weft knit spacer of different thickness with plain woven kevlar as skin. The warp knit spacers as core showed better load bearing capacity. The composite made of warp spacer as core showed better performance in comparison to nonwoven and weft knit spacer. However, in the composite where warp knit spacer is used, there is no significant plateau region that is ideal for energy absorption. It is also clear from the figures 18 & 19, the composite is flexible.

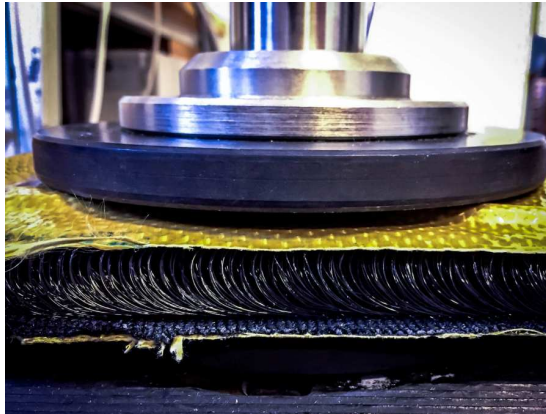


Fig. 17: Compression testing set-up for sandwich composites

The recovery of the composites is also to be noted from the curves.

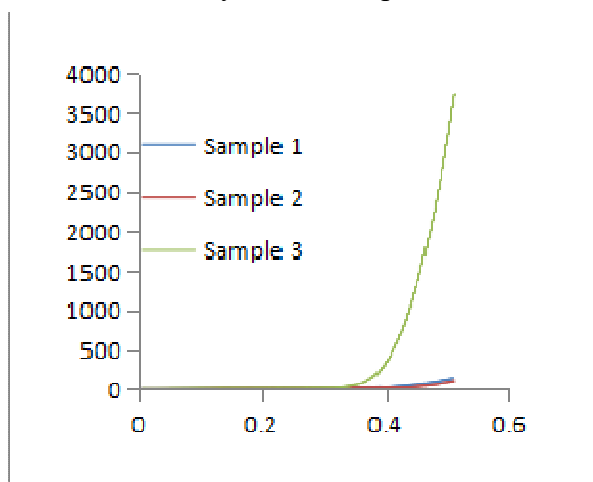


Fig. 18: Compression upto 40% for sample with weft knitted core

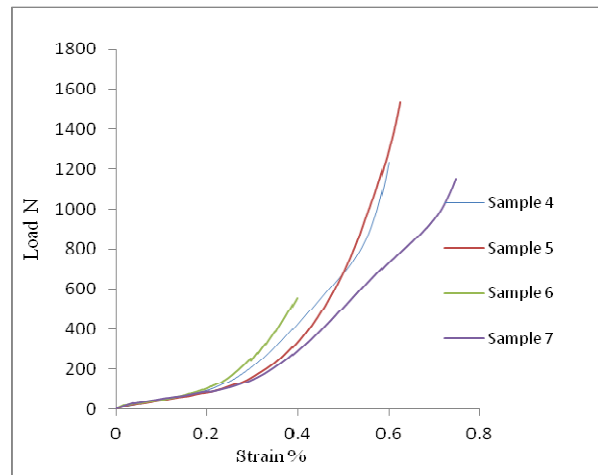


Fig. 19: Compression upto 40% for sample with warp knitted core

Effect of Struto non-woven as core material:

The compression behavior of struto based nonwovens is shown in figure 20.

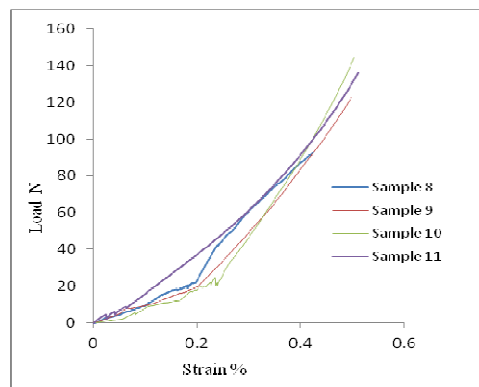


Fig. 20: Compression curves for sample 8-11 at 40% deformation

The nonwoven samples show almost similar behavior with respect to compression. They are compressible to almost 80% of initial thickness.

Conclusions

The sandwich composites having core of knitted spacers as well as struto nonwovens were evaluated for their compression properties. It is evident that the compression and recovery is largely dependent on the thickness and density of the core material. Knitted spacers based sandwich composites are less compressible but more resilient or elastic to recovery. The struto nonwoven based sandwich composites are compressible to almost 80% of initial thickness. However, their resilience is lower than that of spacer based sandwich composites. Between weft and warp knitted spacer fabric based composites, the warp knit spacer based sandwiches exhibit higher compressional resiliency. The sandwich composites will be evaluated for impact performance and the overall utility for load bearing as well as protective applications will be further investigated.

Acknowledgement

This work was supported by the research project of Student Grant Competition of Technical university of Liberec no. 21197/2017 granted by Ministry of Education Youth and Sports of Czech Republic.

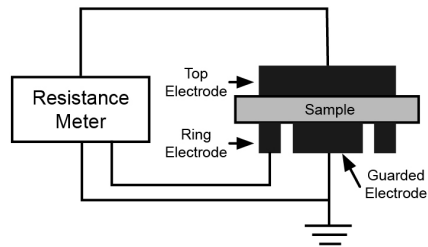
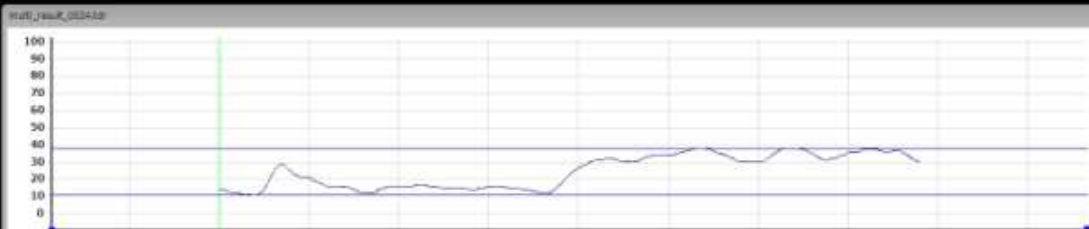
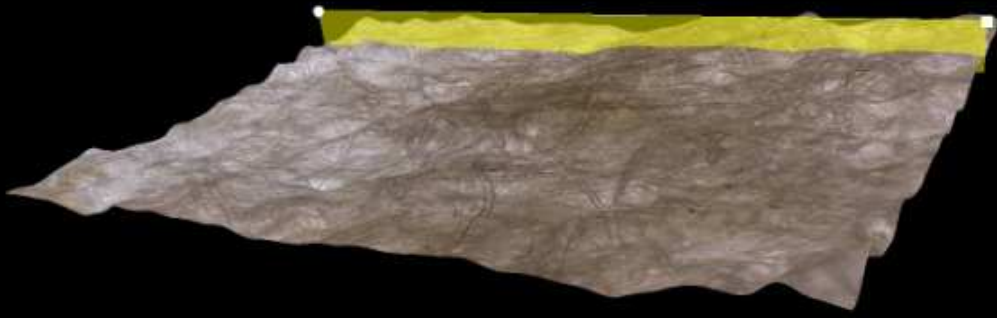
References

1. Bryan A. Cheeseman, T.A.B., Ballistic impact into fabric and compliant composite laminates. *Composite Structures* 2003. **61**: p. 161–173.
2. Bazhenov, S., Dissipation of energy by bulletproof aramid fabric. *Journal of Materials Science*, 1997. **32**: p. 4167-4173.
3. Aswani Kumar Bandaru, V.V.C., Suhail Ahmad , R. Alagirusamy, Naresh Bhatnagar, Ballistic impact response of Kevlar® reinforced thermoplastic composite armors. *International Journal of Impact Engineering* 2016. **89** p. 1–13.
4. Jia-Horng Lin, C.-H.H., Hsien-Hui Meng, Process of Preparing a Nonwoven/Filament/Woven-Fabric Sandwich Structure with Cushioning Effect of Ballistic Resistance. *Fibres and Textiles in Eastern Europe* 2005. **13**: p. 43-57.
5. Yanping Liu, H.H., Li Zhao and Hairu Long, Compression behavior of warp-knitted spacer fabrics for cushioning applications. *Textile Research Journal*, 2011. **82**(1): p. 11–20.
6. M.J.N. Jacobs, J.L.J.V.D., Ballistic protection mechanisms in personal armour. *Journal of Materials Science*, 2001. **36**: p. 3137 – 3142.
7. PM., C., Dimensionless parameters for optimization of textilebased body armor systems. In: *Proceedings of the 18th International Symposium on Ballistics*, San Antonio, Texas, 15–19, 1999: p. 1303-1310.
8. Gonzalo Pincheira, C.C., Carlos Medina, Eduardo Fernandez and Paulo Flores, Influence of aramid fibers on the mechanical behavior of a hybrid carbon-aramid-reinforced epoxy composite. *Proc IMechE Part L: J Materials: Design and Applications*, 2015: p. 1-19.
9. Chitragad., Hybrid ballistic fabric. 16 February 1993: United States

10. Mehamat Karahan, N.K., Effect of Weaving Structure and hybridization on the Low-Velocity Impact Behavior of Woven Carbon-Epoxy Composites. *Fibres & Textiles in Eastern Europe*, 2014. **22**: p. 109-115.
11. C. H. Chiu, M.H.L.a.C.M.W., Compression Failure Mechanisms of 3-D Angle Interlock Woven Composites Subjected to Low-energy Impact. *Polymers & Polymer Composites*, 2004. **12**(4): p. 309-320.
12. Karahan, M., Comparison of Ballistic Performance and Energy Absorption Capabilities of Woven and Unidirectional Aramid Fabrics. *Textile Research Journal*, 2008. **78**(8): p. 718–730.
13. Appleby-Thomas, P.J.H.a.G.J., The impact of structural composite materials. Part 1: ballistic impact. *Journal of Strain Analysis*, 2012. **47**(7): p. 396-405.
14. Lazaro Araujo Rohena, F.M.M., Sergio Neves Monteiro, Carlos Maurício Fontes Vieira et al, Ballistic Efficiency of an Individual Epoxy Composite Reinforced with Sisal Fibers in Multilayered Armor. *Materials Research*, 2015. **18** (2): p. 55-62.
15. Elias Randjbaran, R.Z., Nawal Aswan Abdul Jalil, and Dayang Laila Abang AbdulMajid, Hybrid Composite Laminates Reinforced with Kevlar/Carbon/Glass Woven Fabrics for Ballistic Impact Testing. *Scientific World Journal*, 2014: p. 1-7.
16. J.G. Carrillo , R.A.G., E.A. Flores-Johnson, P.I. Gonzalez-Chi, Ballistic performance of thermoplastic composite laminates made from aramid woven fabric and polypropylene matrix. *Polymer Testing* 2012. **31**: p. 512–519.
17. M Hossein Pol, G.L., E Zamani and A Ordys, Investigation of the ballistic impact behavior of 2D woven glass/epoxy/ nanoclay nanocomposites *Journal of Composite Materials*, 2014: p. 1-12.
18. Chen, R.Y.a.X., Aramid/epoxy composites with angle-laid reinforcement constructions for ballistic protection. *Journal of Industrial*, 2014: p. 1-12.
19. Chia-Chang Lin, C.-M.L.a.C.-C.H., Elucidating the Design and Impact Properties of Composite Nonwoven Fabrics with Various Filaments in Bulletproof Vest Cushion Layer. *Textile Research Journal*, 2009. **79**(3): p. 268–274.
20. CHIA-CHANG LIN, C.-W.L., CHIEN-TENG HSIEH, CHIN-MEI LIN, PAI CHEN AND JIA-HORNG LIN, Process and Ballistic-resistant Buffer Effect of Cushion Composite Layer Made of Three-dimensional Crimped Hollow Fiber. *Journal of REINFORCED PLASTICS AND COMPOSITES*, , 2010. **29**(11): p. 1681-1687.

PART - III

Miscellaneous Functional Fibrous Materials



Investigation on performance of nanoporous fibrous composites

Xiaoman Xiong, Tao Yang, Mohanapriya Venkataraman, Rajesh Mishra and Jiří Militký

*Faculty of Textile Engineering, Dept. of Material Engineering, Studentská 2,
Technical University of Liberec 461 17 Czech Republic,*

1. INTRODUCTION

Nonwoven fabric, a manufactured sheet or web structures bonded together by entangling fibers or filaments, possess plenty of functional properties such as high bulkiness and resilience, great compressional resistance, good filling properties and excellent thermal-insulating properties [1]. As conventional thermal insulators used in technical applications, their impact on thermal insulation performance is determined by the physical and structural parameters of fibrous structures. Especially, their thermal insulation ability strongly depend on the fabric thickness. Generally, the thermal insulating properties increase with the increasing in thickness. However, when this thickness is limited to few centimeters, the insulating properties are quite limited. Silica aerogel, synthesized via sol-gel process and supercritical drying of the wet gel in an autoclave, is open-celled solid foam of silica dioxide that is composed of a network of interconnected nanostructures [2, 3]. Due to its extraordinary small pore size and high porosity, silica aerogel exhibits superior thermal insulation performance with extremely low thermal conductivity (0.015 W/mK), low bulk density (0.1 g/cm³) and high specific surface area (1000 m²/g) [4-6]. Nowadays, silica aerogel has well been acknowledged as one of the most attracting thermal insulating materials for applications in heat-protective clothing, automotive industry, building and construction products [7-10]. Recently, the successful and cost effective production of silica aerogels by use of inexpensive precursors and ambient pressure drying method has been achieved [11-13], this raises the possibility of continuous production with lower operating costs for industrial application. The excellent thermal insulation properties of aerogels are determined by their nanoporous structure, which can provide a barrier to the collision of gas molecules. It is well known that heat transfers in a still gas by means of molecular collisions, faster (hot) moving molecules collide with slower (cold) moving molecules and pass on some of their heat energy. In an aerogel, since the mean free path of gas molecules, the average distance which a gas molecule travels before it collides with another molecule, is smaller than that in free space, the motion of the gas molecules in the aerogel is retarded, this can act as a barrier to prevent the collision process. Thus, the molecules will not collide with each other but rather collide with the barrier from which they rebound and therefore, retain their heat energy and reduce heat transfer [14].

Aerogel can be used as loose bulk material for thermal insulation, but for the majority of applications a bound form such as aerogel containing sheet is required. For this

purpose, aerogels are usually incorporated into lightweight textile structure such as nonwoven fabric, with the assistant of proper binding material. At present, combining nonwoven fabric with silica aerogel to enhance thermal insulation ability has gained increasing interest during the past several decades. A lot of contributions have been devoted to explore the combination of silica aerogel with available supporting materials as thermal insulator, but only a few investigation regarding the incorporation of aerogel with textile structure for thermal insulation enhancement can be found in existing literature. Aspen Aerogels Inc., USA, produced an "Aerogel blanket" for winter apparel products application by using a fiber matrix impregnated with an aerogel forming precursor and supercritical drying method [15]. Aerogel particles have been embedded into the thermal barrier layer of firefighters' protective clothing (FPC), the backside temperature of the FPC samples with aerogel was about 100°C lower than that of samples without aerogel when exposed to radiant heat [16]. A study on incorporated super hydrophobic silica aerogel nanoparticles in 65/35 wool-Aramid blended fabrics indicated that only 2% coating of aerogel nanoparticle increases thermal resistance by up to 68.64% [17]. Some researcher applied silica aerogel on the surface of cotton woven fabrics by coating and found that pique showed the lowest values in thermal resistance and satin had the highest values while plain weave lied in between. Furthermore, it was also reported that the thermal properties of treated high-density cotton plain weave fabric were strongly influenced by finishing agent concentration [18]. With respect to aerogel-treated nonwoven fabrics, the fibrous structure density and the aerogel present in the polyester/polyethylene fibrous nonwovens with silica aerogel impregnation were believed to have significant effect on thermal properties of the overall structures [19]. Meanwhile, thermal insulation of aerogel-treated nonwoven was observed to strongly dependent on the weight and compressional properties of the fabric [20]. The modeling and simulation of heat transfer for aerogel-treated nonwoven fabric indicated that thermal behaviour of the fabric improved when treated with aerogel [21]. University of Leeds developed Hydrospace™ fabric from a carded and cross-laid web. This fabric enables the formation of moulded voids within the cross-section of hydroentangled fabrics and simultaneous filling of these voids with loose aerogel particles composed of amorphous silica [14]. The size, shape and frequency of the filled voids can be varied depending on the dimensions of the encapsulated materials. However, the details of fabrication method was not given. Although all these studies confirmed that the present aerogel in textile structure would significantly improve the thermal performance of composite textiles, however, the application of aerogel granules has so far been limited in a few methods such as coating, padding and impregnation. In these obtained aerogel-containing composites, aerogel granules are exposed or filled into the void space in textile structure, the porous space of the loose textile structure is partly filled by additive agent, the thermal performance of the final product is thus reduced since the porous space which is essential to entrap air pockets for thermal insulation enhancement is decreased. Meanwhile, the nanopores of aerogel granules are filled or covered by binding materials, this would blunt their advantage in thermal insulation ability. Furthermore,

the prepared composite may lack compressibility and compression resilience, causing less recovery after exposed to external forces, which may influence the final use and the durability of thermal-insulating function. The above mentioned problems were not considered in existing literature. Some researchers stated that the application of aerogel in textile structure may cause some adverse effect on thermal insulation enhancement since the porosity of textile fabric is reduced by the adhesive, but how much is the reduction was not experimentally studied. In this research, aerogel-containing composites were prepared by using thermal adhesive powder and laminating method to investigate the effect of aerogel and thermal adhesive on transport properties of these composite textiles. Especially, their influence on thermal insulation performance were analyzed and discussed. Moreover, a series model was considered for the thermal resistance of this layered system. To make the final insulating material more effective and flexible, use less or even no binder to combine silica aerogel with high porous textiles could be a better consideration to develop aerogel-based composite fibrous structure. In this work, a new approach to apply silica aerogel into textile without using any binder to bond aerogel particles was proposed. To take benefit of air trapping potential in porous materials, high porous nonwoven fabrics as well as sponge foam were selected as support layers to produce perforations by laser engraving, aerogel granules could be applied into these holes, together with laminating thin fabric sheet onto two surfaces of the support layer. Since both sides of the support layer were covered by soft fabric sheet to achieve a closed fibrous system and the adhesion of aerogel with this support structure was not involved, the resultant multi-layered composites will have light weight, excellent thermal insulation ability and good flexibility simultaneously. This work is an attempt to explore the potential of using laser engraving to develop flexible aerogel-encapsulated fibrous composite systems for cold condition use. Thus, thermal insulation function of these novel developed composites is the main point we have to concern. Thermal performance were studied in terms of thermography, thermal conductivity, thermal resistance and thermal diffusivity to further evaluate their effectiveness in thermal insulation. Meanwhile, our aerogel-encapsulated composites are quite different with regular aerogel-containing textiles because our new technique used to combine aerogel with textiles enables the final products to be more flexible, which could be more advantageous for potential application in clothing field. In this case thermal contact property as well as compression performance such as compression resistance, compression resilience and thickness loss after compression test were evaluated. The findings in this work could contribute to new developments in flexible aerogel-treated high performance composites for both industrial and clothing applications.

2. METHODOLOGY OF INVESTIGATION ON THERMAL PERFORMANCE OF SILICA AEROGEL-BASED COMPOSITES

2.1 Materials

PAN nanofiber web with areal density of 1.17 g/m² from CXI lab (nanocenter, TUL, Czech Republic) and silica aerogel granules purchased from Cabot aerogel Corp., as

well as nonwoven fabric were used to prepare aerogel-containing composite textiles. The Polyacrylonitrile (PAN) nanofiber web were prepared by electrospinning of 12 wt% PAN/DMF solution in a horizontal electrospinning setup as shown in Figure 1. The specifications of aerogel granules are listed in Table 1.

Table 1: Specifications of aerogel granules

Properties	Value range
Particle size (mm)	0.1-0.7
Pore diameter (nm)	~ 20
Particle density (kg/m ³)	About 120
Surface chemistry	Fully hydrophobic
Thermal conductivity (W/m·K)	0.012 (at 25°C)

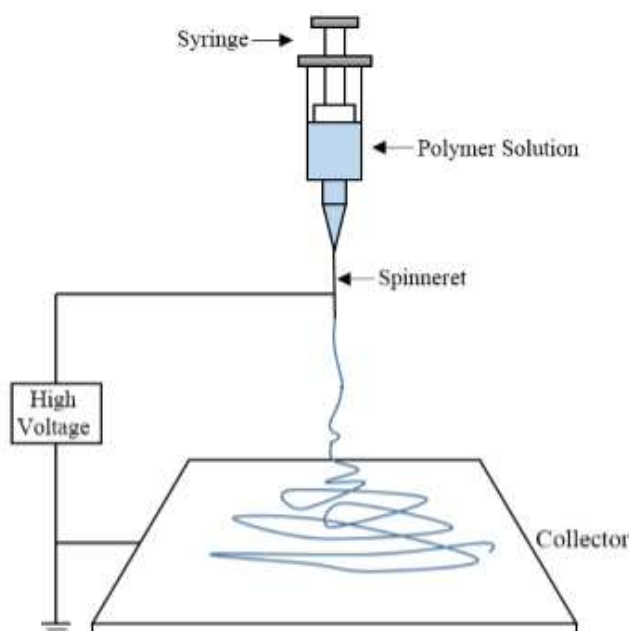


Fig. 1: Schematic diagram of set up of electrospinning apparatus

The nonwoven used was 100% polyester, light-weight and highly porous needle punched. The thickness of nonwoven fabric was 1.22 mm, weight 87.02 g/m². Low melting powder with melting temperature 92°C was used as thermal adhesive for laminating. Three types of Struto nonwoven fabrics prepared at Technical University of Liberec and a polyurethane (PU) sponge foam purchased from Shijiazhuang Chuanghong Technology Co., Ltd were selected as support layers to hold silica aerogels for the development of aerogel-encapsulated composites, their characterizations are presented in Table 2. All these Struto nonwoven fabrics were made by 70 % polyethylene terephthalate (PET) and 30 % bi-component PET fibers, the fiber specifications are given in Table 3. The sheath part of bi-component fibers is low-melting PET with melting temperature 120°C, the core part is polyethylene terephthalate PET with melting temperature 160-180°C. A thermo-bonded nonwoven fabric sheet with thickness 0.16 mm and GSM 49.55 g/m² was used as cover layer.

Table 2: Structural parameters of materials used as support layers

Sample codes	Structure	Porosity %	Bulk density kg/m ³	Thickness mm	GSM g/m ²
P	Struto nonwoven	96.69	25.56	12.42	317.51
Q	Struto nonwoven	97.93	26.79	9.68	259.28
X	Struto nonwoven	99.19	16.48	12.05	198.64
Y	PU sponge	92.72	29.54	6.67	197.01

Table 3: Specifications of polyester fibers in Struto nonwovens

Fiber type	Diameter μm	Fineness dtex	Fiber length mm	Ratio of core and sheath
PET	26.91	6.70	57.00	-
Biocomponent PET	14.58	2.20	38.00	3:1

2.2 Fabrication of aerogel-containing composite textiles

The layered nanofiber web/nonwoven system were prepared by manual laminating technique, using low melting powder as thermal adhesive to provide proper bond strength. Aerogel granules were uniformly applied between the two layers before the laminating process. The low melting powder used here was 10g/m². The layered system was subsequently held together on a heated plate at 110°C at a given pre-tension and continuous pressure, the aerogel-containing composite textile was obtained as it cools down. In order to investigate the effect of aerogel areal density on transport properties, composite textiles containing varying content of aerogel were prepared. A layered system without aerogel granules was prepared as control sample.

2.3 Characterization of aerogel-containing composite textiles

Cross sectional morphology of composite textiles were examined using a Dino-lite digital microscope. In order to observe the overall structure of their cross section, the magnification was chosen to be 50. Air permeability tests were performed according to ISO 9237, Determination of the Permeability of Fabrics to Air, using a Tex test FX-3300 air permeability tester. Two pressure drops 100 Pa and 200 Pa were chosen for the measurement to investigate the effect of pressure gradient on air permeability. Alambeta Instrument was used to measure thermal conductivity and thermal resistance, according to EN 31092 Standard.

2.4 Laser engraving based application of silica aerogel into nonwovens

In this part, the support layers (P, Q, X and Y) were treated by a commercial pulsed CO₂ laser system GFK Marcatex FLEXI-150 to remove certain materials as the laser beam vaporizes the surface [22]. During the laser engraving process, the laser head moves back and forth to engrave a series of dots in one line at a time, the dot pattern will form the designed image [23]. The generated wavelength of laser beam was set at 10.6 μm and the input voltage was 100 V. For each material, different duty circle, pixel time and resolution were used for testing to determine optimized parameters.

The specifications of optimized parameters are listed in Table 4. P', Q', X' and Y' refer to laser-engraved support layers, corresponding to regular materials P, Q, X and Y respectively.

Table 4: Specifications of parameters for laser engraving

Parameter	P'	Q'	X'	Y'
Duty circle %	50	50	45	45
Pixel time μs	100	50	50	80
Resolution dpi	96	96	96	96

The dot pattern file designed in grey scale by Photoshop CS4 graphic software and typical image of laser-engraved sample are shown in Figure 2.

The covering fabric sheet was laminated with support layers using textile adhesive film. This adhesive film was inserted between the covering fabric (M) and laser-engraved support layer, proper pressure was applied to bring sufficient adhesive effect, aerogel granules were subsequently injected into these laser-engraved holes using a syringe barrel, the amount of aerogel in each hole was kept the same by controlling the plunger. After that, another covering fabric was combined to form a closed fibrous composite system. The fabrication process is illustrated in Figure 3. Different cases of middle layers including untreated support materials (P, Q, X and Y) and support layers with only air pockets (P', Q', X' and Y') were prepared as control samples. The details of the prepared composites are listed in Table 5.

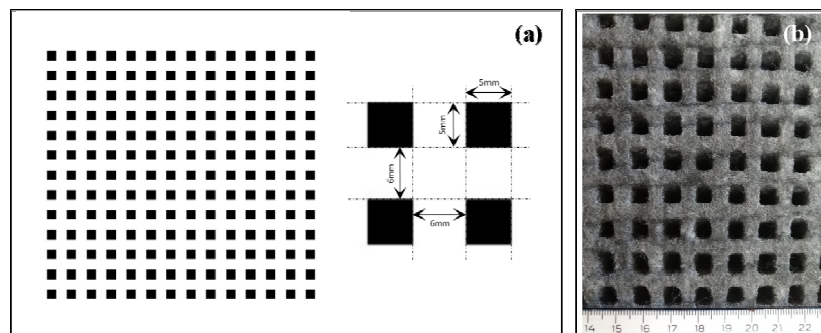


Fig. 2: Dot pattern used for laser engraving: (a) - Designed dot pattern, (b) - Typical image of laser engraved sample

2.5 Investigation on thermal and compression properties of novel developed composites

Thermography measurement was conducted by FLIR TVS300 thermal camera. Tests were carried out in a test chamber with the dimension 45 cm \times 32 cm \times 12 cm. A guard hot plate with constant temperature 33°C was located in the chamber to provide uniform thermal radiation, the thermal camera was fixed with a distance of 40 cm from the hot plate. When the specimen was placed on the hot plate, pictures were taken every 5 second up to when the heat transfer reaches steady state. The temperature value of composite surface was calculated from infrared image by using Avio Thermography Studio 2007 software.

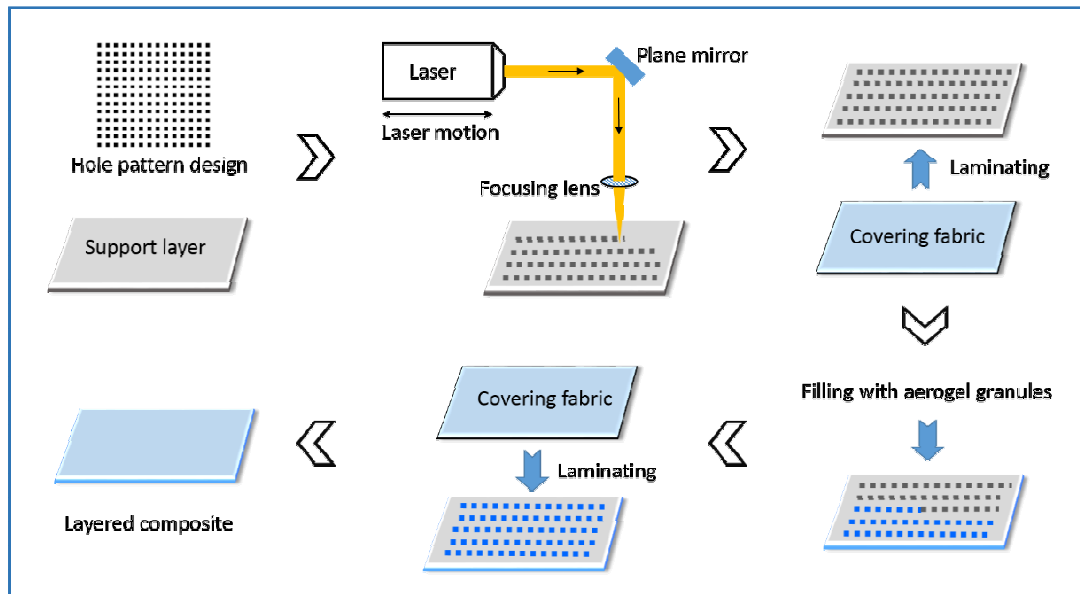


Fig. 3: Fabrication process of aerogel-encapsulated composite.

Table 5: Characterizations of novel developed composites

Sample codes	Composite structure	Aerogel content g/m ²	Thickness mm	GSM g/m ²
P1	MPM	-	12.80	420.32
P2	MP'M	-	12.92	386.58
P3	MP''M	31.89	12.88	415.25
Q1	MQM	-	9.88	363.41
Q2	MQ'M	-	10.11	344.75
Q3	MQ''M	42.35	9.93	391.36
X1	MXM	-	12.50	299.57
X2	MX'M	-	12.64	279.38
X3	MX''M	34.68	12.64	322.65
Y1	MYM	-	7.09	287.81
Y2	MY'M	-	7.15	272.15
Y3	MY''M	18.76	7.13	292.08

Thermal conductivity, thermal resistance and thermal diffusivity were examined by Alambeta Instrument. Heat retention ability and thermal contact property were determined by KES-FT-II Thermolab Tester. All the tests were carried out in the standard atmospheric condition of $65 \pm 4\%$ and $23 \pm 2^\circ\text{C}$. All the samples were conditioned under the standard condition at 23°C and 65% relative humidity for 24 h before testing. The mean value of six measurements for each type of sample was calculated. Compression property plays an important role in textile insulators because compressibility has a linear relationship with thermal conductivity. Compression can be defined as a decrease of initial thickness that occurs with an appropriate increase of force. Compression behaviour of a fabric is generally described by the relationship

between the applied force per unit area and the resulting fabric thickness, in the form of compression load–displacement curve. Compression properties of the novel developed composites were tested by ORIENTEC STA-1225 Universal Testing Machine. The sample size used in compression test was 20 cm × 20 cm, the loading speed was set at 2 mm/min. The maximum pressure used was 560 gf/cm², the pressure foot area was 36.3 cm² with diameter 68 mm. The compression resistance, compression resilience and thickness loss of all the fabrics were calculated from compression hysteresis curves

3. RESULTS AND DISCUSSIONS

3.1 Cross sectional morphology of aerogel-containing composite textiles

The images are shown in Figure 4. Sample codes show the arrangement of layered systems. For example, code NTS refers to layered system composed of nanofiber web (N) and nonwoven substrate (S) laminated by thermal adhesive. For codes NA₁S, NA₂S, NA₃S, NA₄S and NA₅S, A₁, A₂, A₃, A₄ and A₅ refer to aerogel granules of varying areal density, 1.25 g/m², 2.50 g/m², 3.75 g/m², 5.00 g/m² and 6.25 g/m² respectively. It was observed that nanofiber web was well laminated onto the upper surface of nonwoven fabric and silica granules were deposited on the nonwoven fabric under the nanofiber web. Remarkably, significant increase in thickness was observed for sample NA₄S and NA₅S in comparison with other samples.

3.2 Air permeability of composite textiles

The results of air permeability of different composite textiles under different pressure gradients are given in Table 6. Air permeability of nonwoven fabric was found to sharply decrease when a nanofiber web was laminated onto its surface. This is mainly because nanofiber web has a large number of microscopic pores and very low porosity, which covers the open pores of nonwoven fabric and prevents the air flow go through [24]. Moreover, the thermal adhesive would reduce the pores of nonwoven fabric in some degree, this may also account for the decrease in air permeability. Aerogel showed limited influence on air permeability of these composite textiles. For a specified layered system, air permeability had a strong correlation with air pressure gradient, very small difference can be observed between two slopes under different pressure gradients. This indicated that the rate of air flow was directly proportional to the pressure gradient, which consisted well with Darcy's law.

The effect of aerogel areal density on air permeability of these layered systems under different pressure gradients are illustrated in Figure 5. Air permeability directly depends on pore size and porosity, since the aerogel granule can be approximately considered as air-proof material due to its nano scale pores, the air permeability of prepared composite textiles tended to decrease as the increase of aerogel. It was also found that there was a critical value in aerogel areal density, 3.75 g/m² in this study, above which the air permeability showed an increasing trend with the increasing of aerogel content. The reason could be that there may appear more air gap between nanofiber web and nonwoven fabric due to the much bigger size of aerogel granules compared to the thickness of nanofiber web, the enlarged air gap in this layered

system will allow more air to flow through. This was also indicated by the significant increase in fabric thickness (sample NA₄S and NA₅S).

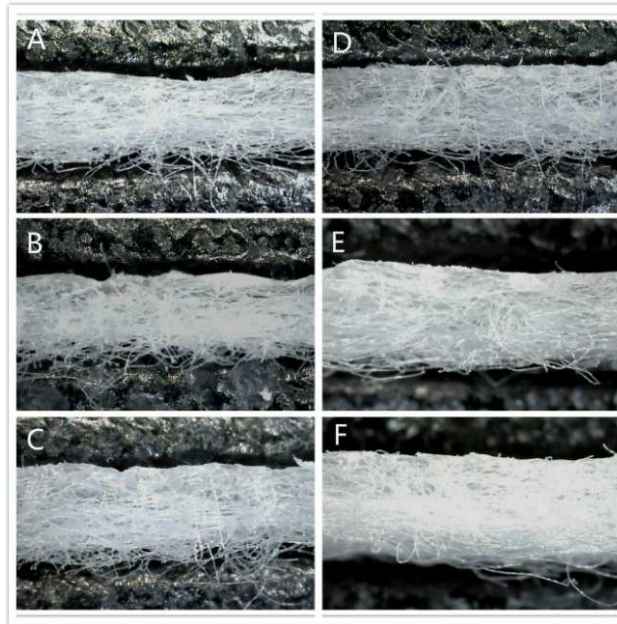


Fig. 4: Cross sectional images of different layered systems (50 ×): A-NTS, B-NA₁S, C-NA₂S, D-NA₃S, E-NA₄S, F-NA₅S

Table 6: Air permeability of samples under different pressure gradients

Samples	Thickness mm	100 Pa mm/s	Slope mm/Pa·s	200 Pa mm/s	Slope mm/Pa·s
S	1.22	2160±54.57	21.60	3743±189.15	18.71
N	0.04	32.22±0.88	0.32	73.48±1.09	0.37
NTS	1.25	32.59±3.01	0.33	61.01±5.93	0.31
NA ₁ S	1.39	39.55±2.02	0.40	84.52±3.25	0.43
NA ₂ S	1.41	33.08±2.73	0.33	67.28±4.73	0.34
NA ₃ S	1.42	30.58±2.10	0.31	54.97±5.12	0.27
NA ₄ S	1.48	36.71±2.46	0.37	74.77±3.73	0.37
NA ₅ S	1.53	41.28±1.13	0.41	84.21±1.90	0.42

Note: slope is the quotient of air permeability and pressure gradient.

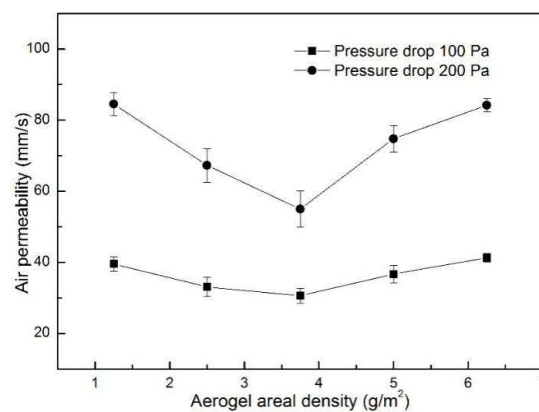


Fig. 5: Effect of aerogel areal density on air permeability

3.3 Thermal performance of composite textiles

Thermal conductivity, k (W/m·K), measures the rate at which heat is transferred through unit area of the fabric across unit thickness under a specified temperature gradient. Thermal resistance, R (m²·K/W), expresses the ability of material to prevent heat flow through the thickness over unit surface area. Thermal resistance is related to thermal conductivity and the fabric thickness L (m):

$$R = \frac{L}{k} \quad (1.1)$$

Amount of stagnant air within the fabric and fabric density are the most important factors governing thermal insulation of textiles. The higher the thermal resistance, the lower in the heat loss [25]. The measured thermal properties of nonwoven substrate, nanofiber web and the integrated fabric of these two materials are given in Table 7. An obvious difference was observed in thermal resistance of samples NTS and S, this is attributed to the thermal adhesive which block the open pores throughout the nonwoven substrate and reduce the trapped air in this layered fabric. Since the thermal performance of high porous textile is determined by the stagnant air present in textile structure, more heat flowed through the layered system NTS due to its decreased air volume fraction.

Table 7: Thermal conductivity and thermal resistance values

Samples	Thermal conductivity 10 ⁻³ W/m·K	Thermal resistance 10 ⁻³ m ² ·K/W
Nanofiber web (N)	-	0.90±0.04
Nonwoven substrate (S)	34.63±0.32	35.40±1.61
Layered system (NTS)	36.98±0.97	31.94±0.80

For multilayered fabric systems, the layers are considered to set as a series of thermal resistance, according to electrical analogy with conduction heat transfer, the following equation can be used for calculating the total thermal resistance [26]

$$R_t = \sum R_i \quad (1.2)$$

However, the use of thermal adhesive in this layered structure will improve thermal conductivity as mentioned before, this will cause some loss in total thermal resistance since the fabric thickness is not proportionally decreased. This loss in thermal resistance, ΔR , can be obtained by

$$\Delta R = R_S + R_N - R_{NTS} \quad (1.3)$$

In this study, the loss in thermal resistance is 4.36×10^{-3} m²·K/W, which accounts for 13.65% of the total thermal resistance value. This indicated that the use of adhesive in textile structure has significant effect on the final thermal insulation performance, which is noteworthy for the development of textile composites as thermal insulators.

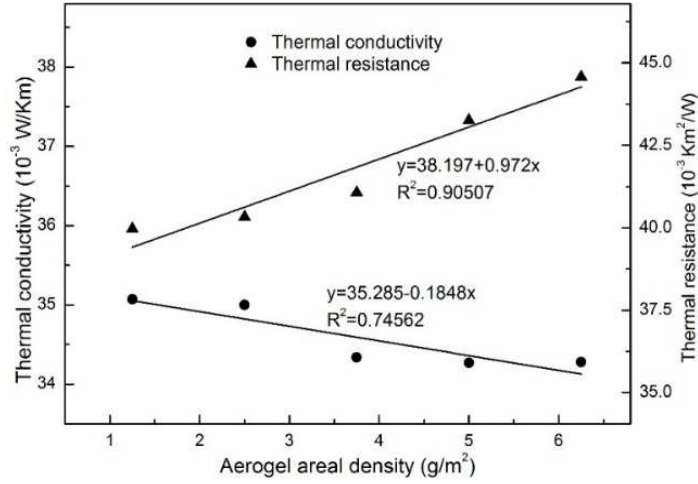


Fig. 6: Effect of aerogel areal density on thermal insulation performance.

The effect of aerogel areal density on thermal conductivity and thermal resistance of these layered systems are presented in Figure 6. The aerogel-containing composites showed lower thermal conductivity and much higher thermal resistance in comparison with sample NTS, indicating that the present of aerogel had significant effect on improving thermal insulation performance. For silica aerogel granules, more than 93% of their volume is occupied by air, thus, the layered system would get more trapped air as the aerogel granules were applied between these two layers. It was observed that the thermal resistance of layered systems was directly proportional to the areal density of silica aerogel since the increment of trapped air was determined by the amount of aerogel, the correlation coefficient between thermal resistance and aerogel areal density was about 0.91. However, this value was only 0.75 for thermal conductivity.

3.4 Series model for thermal resistance of composite textiles

The decrease of thermal resistance induced by adhesive is believed to strongly depend on the amount of adhesive and its distribution. In this study, the amount of thermal adhesive in each layered system is totally identical, if the adhesive is assumed to uniformly spread only in the middle layer consisted by aerogel granules and air, then the loss of total thermal resistance in each composite can be approximately considered to be the same. Therefore, the total thermal resistance of aerogel-containing composite textile can be calculated by

$$R_t \approx R_S + R_M + R_N - \Delta R \quad (1.4)$$

where R_M is thermal resistance of the middle layer.

The thermal performance of this middle layer is determined by aerogel granules and the air space. Assuming it is a homogeneous structure without aerogel loss from this layer, the effective thermal conductivity of middle layer can be obtained by using

$$\frac{k_{eff}}{k_0} = (1 - \phi) + \phi \frac{k_a}{k_0} \quad (1.5)$$

$$\phi = \frac{\rho_s}{\rho_v \cdot L} \quad (1.6)$$

where k_0 is the thermal conductivity of stagnant air (0.024 W/K·m at 25°C), k_a is the thermal conductivity of aerogel granules, ϕ is the volume fraction of aerogel granules, ρ_s is the areal density of aerogel in layered system (kg/m²), ρ_v is the bulk density of aerogel (kg/m³) and L is the thickness of middle layer. Thus, the total thermal resistance of layered system can be expressed as

$$R_t = R_s + R_N + \frac{\rho_v L^2}{k_0(\rho_v L - \rho_s) + k_a \rho_s} - \Delta R \quad (1.7)$$

Table 8: Comparison of theoretical and experimental values of thermal resistance

Samples code	From experiment (R) $10^{-3} \text{ m}^2 \cdot \text{K/W}$	From series model (R') $10^{-3} \text{ m}^2 \cdot \text{K/W}$	Error (%) $\frac{ R-R' }{R} \times 100$
NA ₁ S	39.97	38.00	4.93
NA ₂ S	40.33	39.07	3.12
NA ₃ S	41.07	39.74	3.23
NA ₄ S	43.26	42.48	1.80
NA ₅ S	44.58	44.80	0.50

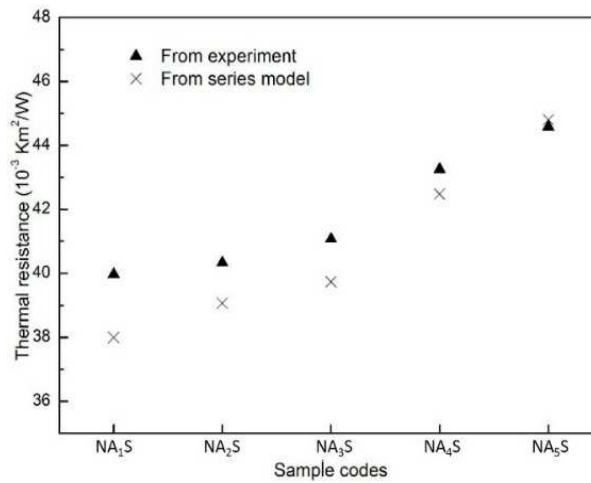


Fig. 7: Theoretical and experimental values of thermal resistance

Thermal resistance values obtained from experiment and series model are shown in Table 8 and Figure 7. Results showed a good agreement between thermal resistance from experiment and those of series model for the layered systems. Average error was about 2.07%. The error showed a decreasing trend with the increasing of aerogel content, the reason could be that the series model is based on the assumption that the middle layer between nanofiber web and nonwoven substrate is an uniformly continuous structure, if aerogel is too less to form a continuous layer, the thermal resistance will be underestimated by theoretical model since the thickness of the middle layer is decreased.

3.5 Series model for thermal resistance of composite textiles

For the novel developed composites prepared by laser engraving, their infrared thermography images under steady state are shown in Figure 8. It is clear that for each group, the detected temperature from samples with air pockets are lower than that from regular samples, the lowest values are observed from aerogel-encapsulated composites, indicating that aerogel-encapsulated samples exhibit best thermal insulation ability.

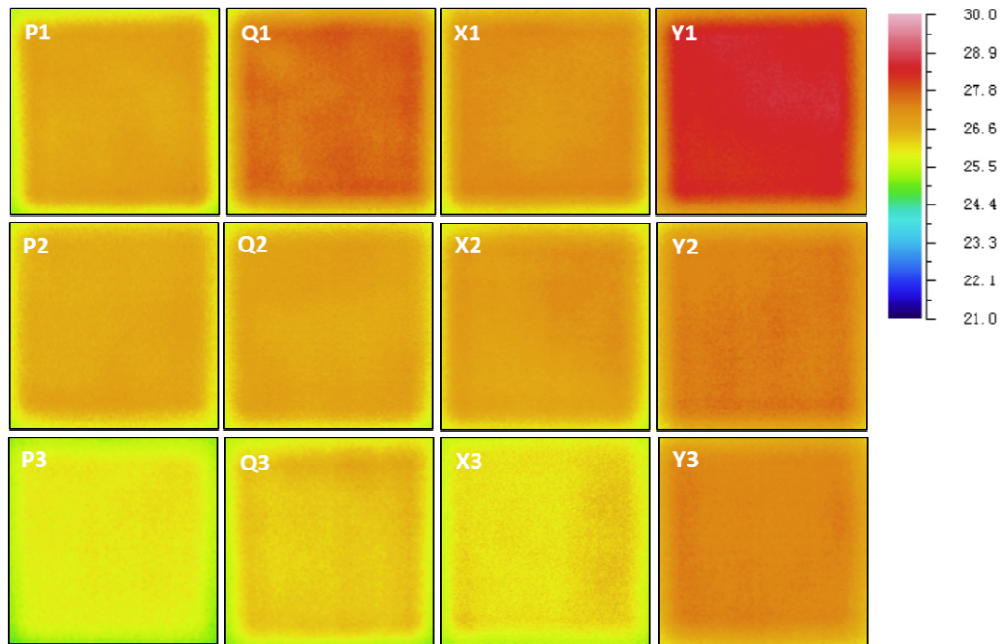


Fig. 8: Infrared thermography images under steady state

Table 9: Temperature of different multi-layered composites under steady state

Sample codes	Max. temperature °C	Min. temperature °C	Mean temperature °C
P1	27.5	27.1	27.3
P2	27.0	26.7	26.8
P3	26.0	25.5	25.8
Q1	27.8	27.5	27.7
Q2	27.3	26.7	27.0
Q3	26.6	26.3	26.5
X1	27.7	27.2	27.5
X2	27.2	26.9	27.0
X3	26.5	26.0	26.2
Y1	28.5	27.9	28.3
Y2	27.7	27.2	27.5
Y3	27.3	26.9	27.1

The obtained temperature values from Avio Thermography Studio 2007 software are listed in Table 9. The average temperature detected from regular composites P1, Q1, X1 and Y1 are 27.3°C, 27.7°C, 27.5°C and 28.3°C respectively, whereas those for samples with air pockets (P2, Q2, X2 and Y2) are only 26.8°C, 27.0°C, 27.0°C and 27.5°C while these values for aerogel-encapsulated structure (P3, Q3, X3 and Y3) are 25.8°C, 26.5°C, 26.2°C and 27.1°C respectively. Generally, a temperature gap of 1°C to 1.5°C was observed between aerogel-encapsulated composites and regular ones under the condition of temperature difference 10°C between hot plate and the environment. Normally, this temperature gap will be enlarged under greater temperature gradient condition.

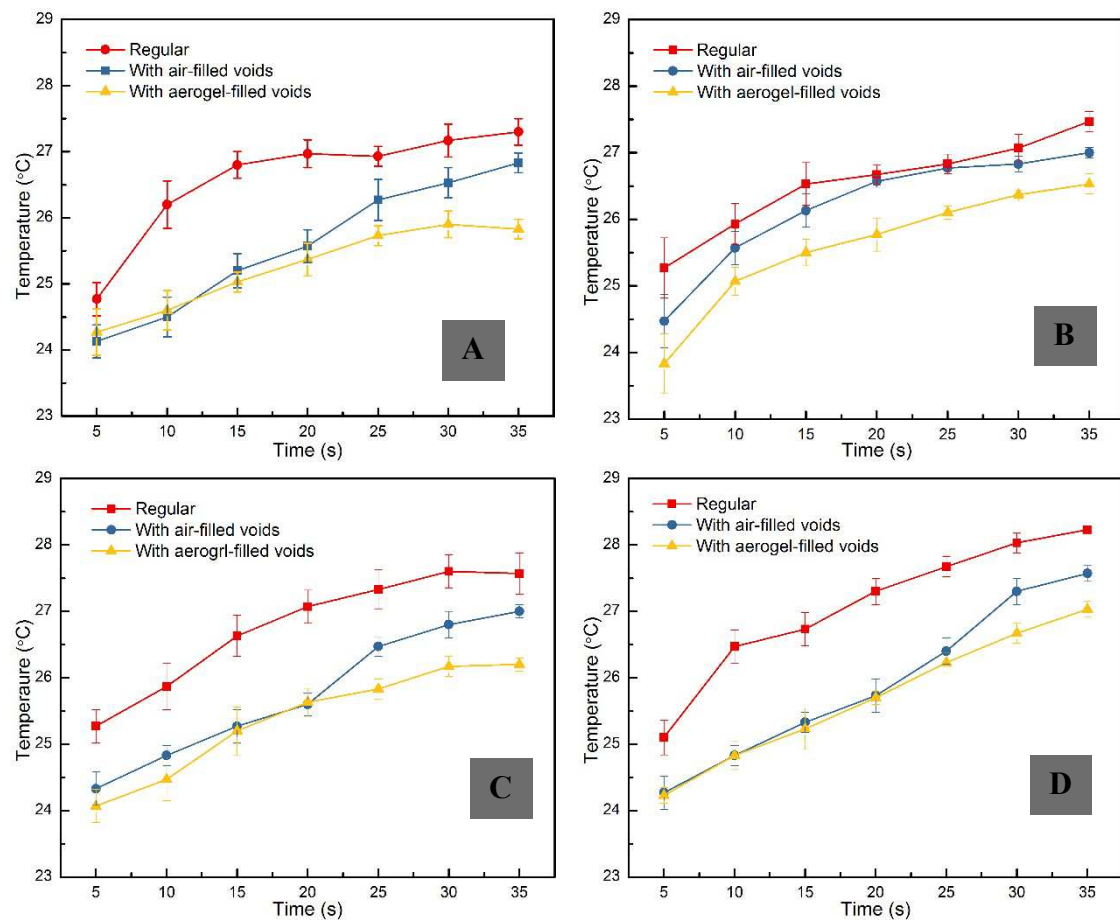


Fig.9: Dependence of detected temperature on time

In order to further observe the heat transfer behavior of different samples under infrared energy, the detected temperatures at different time were recorded with a time interval 5s until steady state. The dependence of detected temperature on time was illustrated in Figure 9. Each value is the mean average of three measurements. It is obvious that the surface temperature of all the samples shows an increasing trend with the time. However, for regular samples, the detected temperature sharply increases with the time, much slowly temperature increasing are observed for samples with aerogel-filled holes and with air-filled holes. Meanwhile, as the placement of

composites, the detected initial temperature is much lower than that from regular samples. These may account for the lower temperature of composites under steady state. This agrees well with the above data of infrared thermography images.

3.6 Thermal conductivity, thermal resistance and thermal diffusivity of novel developed composites

Nonwoven fabrics possess a large amount of void space, their thermal insulation performance is determined by the trapped air in the inter-fiber spaces due to the much lower conductivity of still air compared with textile fibers. The measured thermal conductivity, thermal resistance and thermal diffusivity of prepared composites are shown in Figure 10, Figure 11 and Figure 12 respectively.

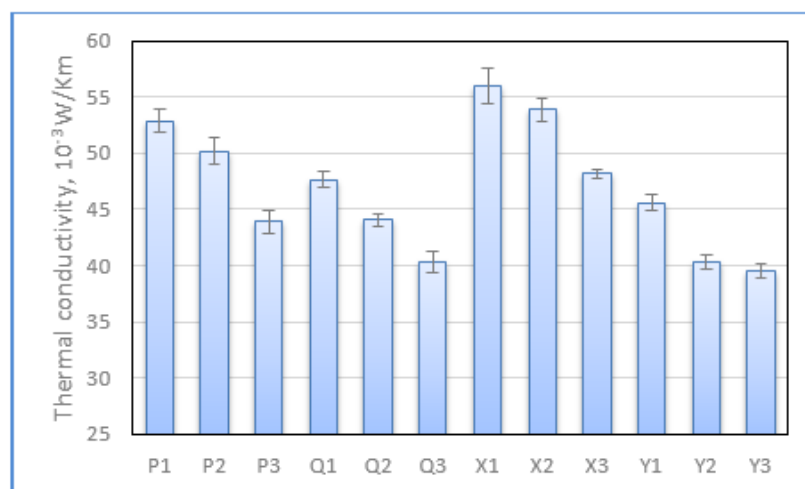


Fig. 10: Thermal conductivity of different composites

In each group, air pockets give slightly decrease to thermal conductivity value and small rise to thermal resistance as compared to regular composites. This is because the large voids formed by laser treatment will enlarge the amount of still air in the composites structure, causing less heat transfer through the fabrics by conduction. Heat transfer by free convection in nonwoven materials has been reported to be negligible because the fibers subdivide the gas into sufficiently small pores and the tortuous nature of air channels present prevent any heat transfer by convection [27]. Studies were conducted on melt blown and needle-punched nonwovens for apparel thermal insulation and found no evidence to indicate convective heat transfer even in low density nonwoven fabrics [28]. Some tests were carried out using low-density samples with fiber volume fractions of 0.2% and 0.4% and the result also revealed that the convection mode of heat transfer was non-existent [29]. Thus, the regular samples can be assumed to be free of convection. These samples gained lots of huge air-filled voids with a size about $5\text{mm} \times 5\text{mm}$ after laser treatment, which may allow air flows through and cause heat transfer by convection. However, the laminating of covering fabrics on the surfaces could minimize this heat convection.

Aerogel-encapsulated structure give decrease to thermal conductivity while the thermal resistance significantly increases. For the aerogel-encapsulated composite, the

large open voids are filled by nanoporous structural aerogel, this will further prevent the convection current transfer through the composites. Furthermore, since the pore size in the aerogel granules is lower than the mean free path of air molecules, according to Knudsen effect [4] these extremely small pore size will cause a very low gaseous thermal conductivity, resulting in less heat transfer through the composite and significant improvement of thermal insulation performance.

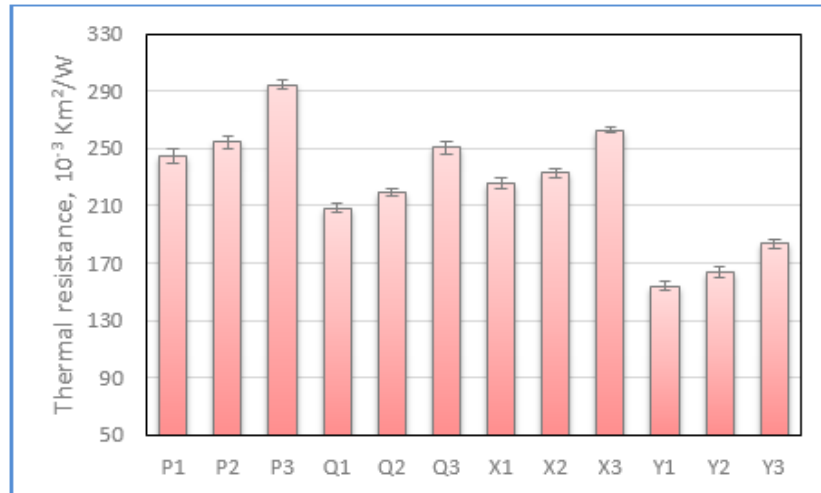


Fig. 11: Thermal resistance of different composites

Analysis of variance was performed for each group using T test method to determine whether there are any significant differences in thermal insulating properties. Results showed that for nonwoven composites the variance of thermal conductivity values within groups are all significant ($p < 0.05$), the differences between air pockets and aerogel-encapsulated structure are found to be very significant ($p < 0.01$). For foam-based composites the thermal conductivity difference between regular sample and laser-engraved one is observed to be highly significant ($p < 0.00001$), however, the values between air pockets and aerogel-encapsulated structure shows insignificant difference. This may be attributed to the least content of silica aerogel in sample Y3. With respect to thermal resistance, in each group all the values from different structures show very significant difference ($p < 0.01$). Variance analysis indicates that the aerogel-encapsulated structure has significant effect on thermal insulation enhancement while the air pockets can improve thermal insulating properties to some degree. Thermal diffusivity describes the rate of temperature spread through a material. The comparisons of thermal diffusivity values (as seen in Figure 12) show that the aerogel-encapsulated materials have the lowest thermal diffusivity values whereas the regular composites have the highest values of this parameter. These further indicated that the aerogel-encapsulated structure has significant effect on the heat transfer behavior of fibrous porous insulators.

3.7 Heat retention ability of novel developed composites

The heat retention ability of different composites are illustrated in Figure 13. It is apparent that composites with air pockets (P2, Q2, X2 and Y2) had better ability to retain heat compared to regular samples P1, Q1, X1 and Y1. The highest heat

retention ability were observed from composites with aerogel-encapsulated structure (P3, Q3, X3 and Y3). The heat transfer in aerogel is effected through its solid-state component, the air occupying the pores is a bad heat conductor. Moreover, as a result of the micro-porous structure, the gas conductivity in silica aerogel becomes substantially lower than that for a free gas [30]. Evacuating air from the aerogel pores additionally reduces its heat transfer. The increasing of heat retention ranged from 3.15% to 5.19 % for samples with air pockets, and this value for aerogel-encapsulated composites lied between 8.42 % and 11.55 %.

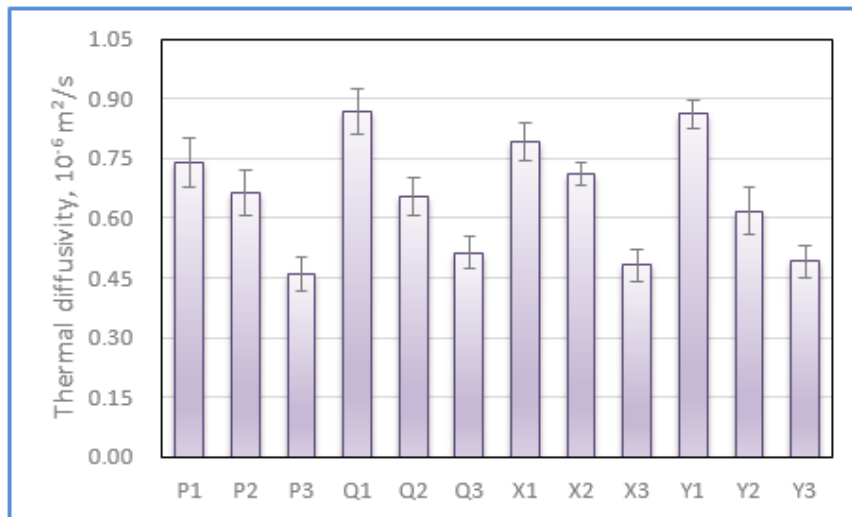


Fig.12: Thermal diffusivity of different composites

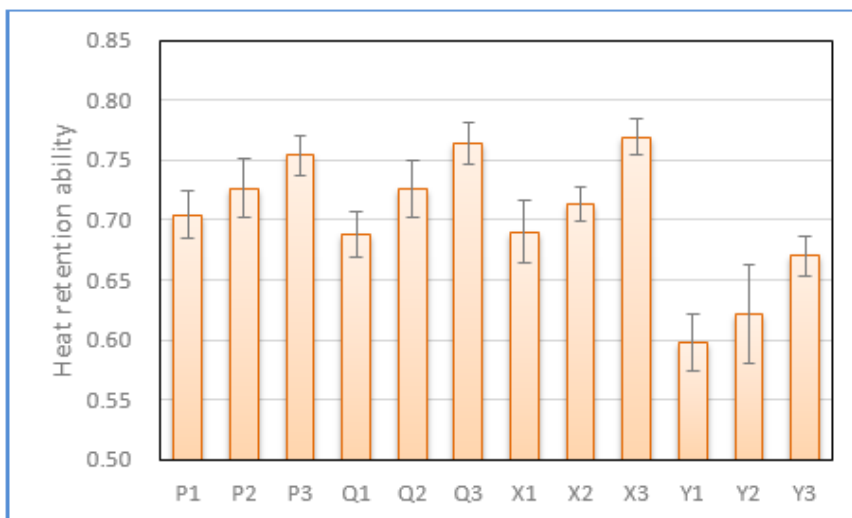


Fig. 13: Heat retention ability of different composites

3.8 Thermal contact property of novel developed composites

Maximum heat flux (q_{\max}) is the transitional thermal exchange at the time of contact between skin and the fabric. The warm/cool feeling, as the result of rapid transfer of heat flux from the skin to the fabric surface immediately after the fabric is placed in contact with the skin, is a transient heat conduction phenomenon. This sensation that arises from thermal contact property is essential for engineering fabrics to provide clothing comfort. The measured values of q_{\max} are presented in Figure 14. The q_{\max}

value of aerogel-encapsulated composites was noticed to be slightly lower than regular samples, indicating a slower heat transfer and a thermal feeling. The warm/cool sensation, resulted as heat flow from the skin to a fabric, is strongly related to the surface condition especially the surface contour of the fabric [31]. Since the contact between skin simulating heat source and fabric surface is reduced by an irregular surface contour for the aerogel-encapsulated composites, it will result in the lowering of q_{\max} value and warmer feeling.

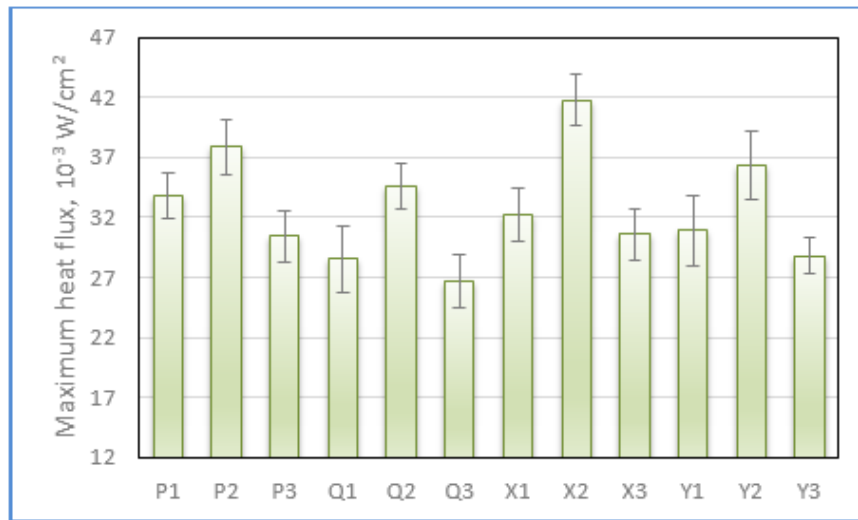


Fig. 14: Measured maximum heat flux of different composites

The highest q_{\max} values were observed from composites with air pockets, revealing more heat flux transferred and a cooler sensation. The reason could be that due to the existence of many air pockets in their structure these samples have more flattened surface when the measuring T box was placed onto fabric surface during the cool/warm feeling testing, resulting in a smoother surface. A smoother surface profile leads to an increased thermal contact between heat source and fabric [32]. Therefore, more heat flux transferred by heat conduction. Meanwhile, for the composites with air pockets, samples with higher thickness (P2 and X2) had higher q_{\max} values, with an increasing of about 32% compared to regular structure (P1 and X1). Thinner samples Q2 and Y2 showed lower q_{\max} value, their increasing rate in q_{\max} was less than 4%, much lower than those of sample P2 and X2.

3.9 Compression performance of novel developed composites

The compression resistance of different fabrics under 560 gf/cm^2 pressure in terms of the percentage change in thickness, is shown in Figure 15. Nonwoven-based composites with air pockets (P2, Q2, X2) or aerogel (P3, Q3, X3) generally have lower compression resistance than regular samples (P1, Q1, X1). During the process of fabric compression, the inter-fiber spaces decrease continuously, the resistance force necessary to compress a fabric has to overcome the internal stresses of the fibers and the inter-fiber frictional force [33]. Thus, the compression resistance is closely related to fiber quantity, composites with less fibers have a lower compression resistance if the fiber arrangement of the fabrics are assumed to be the same.

However, it is found that for foam-based composites the air pockets have insignificant effect on compression resistance while the encapsulated aerogel give slightly increase to compression resistance. The reason could be that in foam structure the deformed networks are easy to return back to their earlier position because of no fiber-to-fiber slippage and fiber entanglement happening during the process of compression. The compression resilience values of regular composites (P1, Q1, X1 and Y1), as shown in Figure 16, are found to lie in the range of 66.11% -76.82%, samples with air pockets (P2, Q2, X2 and Y2) and encapsulated aerogel (P3, Q3, X3 and Y3) are observed to recover slightly less than regular structures. This may be attributed to the fact that the amount of fibers per unit area of laser-engraved nonwovens is much lower, the compressive load will be shared by a fewer number of fibers, resulting in a stronger fiber-to-fiber slippage, fiber bending and fiber entanglement during the compression phase, this may lead to higher energy loss and reduced percentage compression resilience [34]. Results also indicates that the decrease in compression resilience induced by air pockets and aerogel-encapsulated structure are respectively ranging from 4.50% to 12.76% and 7.49% to 11.38%.

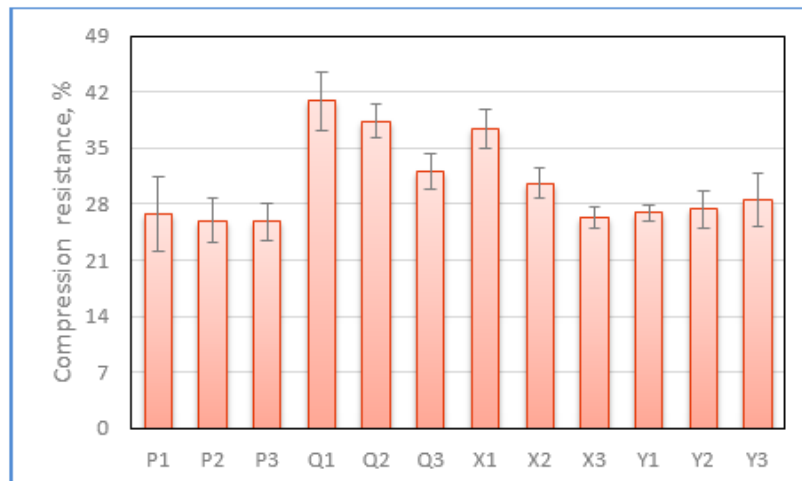


Fig. 15: Compression resistance of different composites

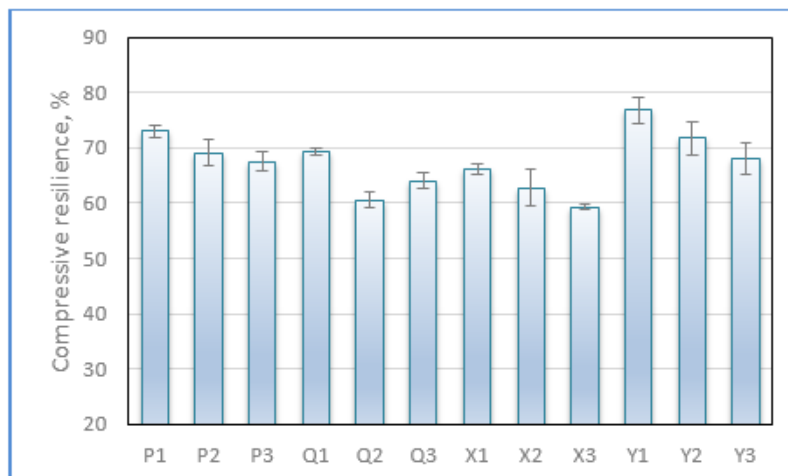


Fig. 16: Compressive resilience of different composites

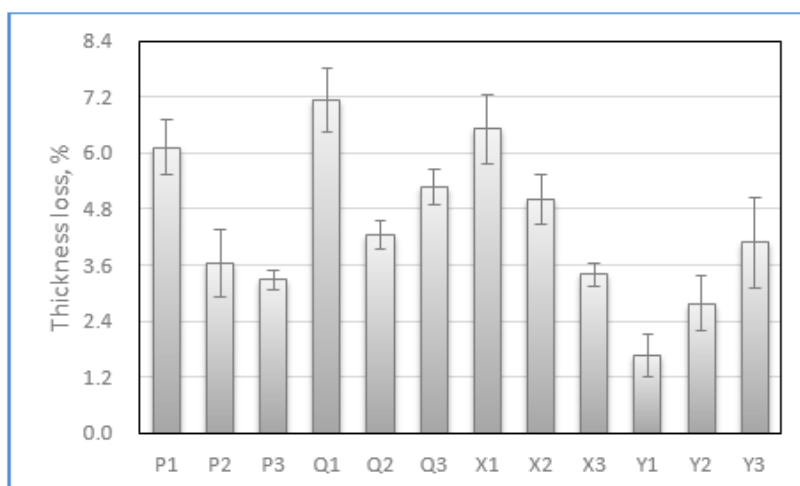


Fig.17: Thickness loss after compression test

Nonwoven composites with air pockets and encapsulated aerogel exhibit lower thickness loss in comparison with regular samples (as shown in Figure 17), indicating these two kinds of nonwoven-based structure are able to maintain relatively higher thermal insulating ability after exposed to external forces. This is because during compression process all the fibers get compressed and trapped to each other, which will restrict the thickness recovery when the load is released. Thus, the percentage thickness loss is much higher in the case of regular composites. The sponge foam is in a reasonably consolidated state, with compression the material gets denser, resulting in better recovery after the compression pressure is released. However, this consolidated state may be partly destroyed by laser engraving treatment, which will reduce its ability to recover back to initial thickness. This is also reflected by the trend with compression resilience percentage.

5. CONCLUSION

It was found that for the aerogel-containing composite textiles, silica aerogels present in layered structure had limited influence on air permeability. Aerogel areal density has a critical value, 3.75 g/m^2 in this work, above which the air permeability showed an increasing trend with aerogel. Thermal resistance of layered systems is directly proportional to aerogel content, the correlation coefficient was about 0.91. Remarkably, the loss in thermal resistance induced by adhesive is $4.36 \times 10^{-3} \text{ m}^2 \text{ K/W}$, accounting for 13.65% of the total thermal resistance value. This indicated that the use of adhesive in textile structure could have significant effect on thermal insulation enhancement. Thus, to make the final insulating material more effective, use less or even no binder to combine silica aerogel with high porous textiles could be a better consideration. The measured thermal resistance values of these layered systems have a good agreement with those calculated from theoretical model.

For the laser engraving-based composites, aerogel-encapsulated structure gave remarkable rise to thermal insulation ability while air pockets could marginally improve the thermal resistance. A temperature gap of 1°C to 1.5°C was observed between aerogel-encapsulated composites and regular ones. Meanwhile,

aerogel-encapsulated structure showed slightly lower q_{\max} value and a thermal feeling, thicker composites with air pockets had higher q_{\max} values, with an increase of about 32% compared to regular samples. Composites with aerogel-encapsulated structure were observed to have the highest heat retention ability.

As for compression properties, it is found that nonwoven composites with air pockets or aerogel-encapsulated structure generally have lower compression resistance. However, for foam-based composites the air pockets have insignificant effect on compression resistance and the aerogel-encapsulated structure lead to slight increase in this value. Composites with air pockets and aerogel granules can recover to a smaller extent than regular samples, the decrease in compression resilience induced by air pockets and encapsulated aerogel are respectively ranging from 4.50 % to 12.76 % and 7.49 % to 11.38 %. Nonwoven composites with air pockets and aerogel are observed to have lower thickness loss after compression test. It can be concluded that the multilayered aerogel-encapsulated composites have good compression properties as well as good thermal insulation ability.

ACKNOWLEDGEMENT

This work was supported by the research project of Student Grant Competition of Technical University of Liberec no. 21195/2017 granted by Ministry of Education Youth and Sports of Czech Republic.

REFERENCES

- [1] Jirsak, O., Sadikoglu, T. G., Ozipek, B. and Pan, N.: *Thermo-insulating Properties of Perpendicular-laid versus Cross-laid Lofty Nonwoven Fabrics*. Textile Research Journal, vol. 70, no. 2, pp. 121-128, 2000.
- [2] Błaszczynski, T., Ślosarczyk, A. and Morawski, M.: *Synthesis of Silica Aerogel by Supercritical Drying Method*. Procedia Eng., vol. 57, pp. 200-206, 2013.
- [3] Bheekhun, N., Abu Talib, A. and Hassan, M. R.: *Aerogels in Aerospace*. Advances in Materials Science and Engineering, 2013.
- [4] Pierre, A. C. and Pajonk, G. M.: *Chemistry of Aerogels and Their Applications*. Chemical Reviews, vol. 102, no. 11, 4243-4265, 2002.
- [5] Mulder, C. A. M., Lierop, J. G.: *Preparation, densification and characterization of autoclave dried SiO₂ gels*. Berlin, Germany, pp. 68-75, 1986.
- [6] Hrubesh, L. W.: *Aerogels: the World's Lightest Solids*. Chemistry and Industry, vol. 24, pp. 824-827, 1990.
- [7] Hostler, S. R., Abramson, A. R. and Gawryła, M. D. et al.: *Thermal Conductivity of a Clay-based Aerogel*. International Journal of Heat and Mass Transfer, vol. 52, no. 3-4, pp. 665-669, 2009.
- [8] Wei, G., Liu, Y. and Du, X. et al.: *Gaseous Conductivity Study on Silica Aerogel and Its Composite Insulation Materials*. Journal of Heat Transfer, vol. 134, no. 4, 2012.
- [9] Zhao, J.-J., Duan, Y.-Y. and Wang, X.-D. et al.: *A 3-D Numerical Heat Transfer Model for Silica Aerogels Based on the Porous Secondary Nanoparticle Aggregate Structure*. Journal of Non-Crystalline Solids, vol. 358, no. 10, pp. 1287-1297, 2012.

- [10] Zhao, J.-J., Duan, Y.-Y. and Wang, X.-D. et al.: *An Analytical Model for Combined Radiative and Conductive Heat Transfer in Fiber-loaded Silica Aerogels*. Journal of Non-Crystalline Solids, vol. 358, no. 10, pp. 1303-1312, 2012.
- [11] Prakash, S. C., Brinker, J., Hurd, A. J., Rao, S. M.: *Silica Aerogel Films Prepared at Ambient Pressure by Using Surface Derivatization to Induce Reversible Drying Shrinkage*. Nature, vol. 374, pp. 439-443, 1995.
- [12] Kang, S. K., Choi, S. Y.: *Synthesis of Low-density Silica Gel at Ambient Pressure: Effect of Heat Treatment*. Journal of Materials Science, vol. 35, no. 19, pp. 4971-4976, 2000.
- [13] Wei, T. Y., Chang, T. F., Lu, S. Y., Chang, Y. C.: *Preparation of Monolithic Silica Aerogel of Low Thermal Conductivity by Ambient Pressure Drying*. Journal of the American Ceramic Society, vol. 90, no. 7, pp. 2003-2007, 2007.
- [14] Höffele, S., Russell, S. J., and Brook, D. B.: *Light-weight Nonwoven Thermal Protection Fabrics Containing Nanostructured Materials*. International Nonwovens Journal, vol. 14, no. 4, pp. 10-16, 2005.
- [15] Ryu, J.: *Flexible aerogel superinsulation and its manufacture*. United State Patent, 6068882, 2000.
- [16] Qi, Z., Huang, D., He, S., Yang, H., Hu, Y., Li, L. and Zhang, H.: *Thermal Protective Performance of Aerogel Embedded Firefighter's Protective Clothing*. Journal of Engineered Fibers and Fabrics, vol. 8, no. 2, pp. 134-139, 2013.
- [17] Shaid, A., Fergusson, M. and Wang, L.: *Thermo-physiological Comfort Analysis of Aerogel Nanoparticle Incorporated Fabric for Fire Fighter's Protective Clothing*. Chemical and Materials Engineering, vol. 2, pp. 37-43, 2014.
- [18] Rosace, G., Guido, E., Colleoni, C., and Barigozzi, G.: *Influence of Textile Structure and Silica based Finishing on Thermal Insulation Properties of Cotton Fabrics*. International Journal of Polymer Science, 2016, Article ID 1726475, 10 pages.
- [19] Venkataraman, M., Mishra, R., Militky, J. and Hes, L.: *Aerogel based nanoporous fibrous materials for thermal insulation*. Fibers and Ploymers, vol. 15, no. 7, pp. 1444-1449, 2014.
- [20] Venkataraman, M., Mishra, R., Kotresh, T. M., Sakoi, T. and Militky, J.: *Effect of Compressibility on Heat Transport Phenomena in Aerogel-treated Nonwoven Fabrics*. The Journal of The Textile Institute, vol. 107, no. 9, pp. 1150-1158, 2015.
- [21] Venkataraman, M., Mishra, R., Militky, J. and Behera, B.K.: *Modelling and Simulation of Heat Transfer by Convection in Aerogel Treated Nonwovens*. The Journal of The Textile Institute, vol. 108, no. 8, pp. 1442-1453, 2016.
- [22] Ghorannevissa, M., Shahidia, S., and Moazzenchia, B.: *Comparison between Decolorization of Denim Fabrics with Oxygen and Argon Glow Discharge*. Surface & Coatings Technology, vol. 201, pp. 4926-4930, 2007.
- [23] Yuan, G., Jiang, S., Newton, E., Fan, J., and Au, W.: *Application of Laser Treatment for Fashion Design*. The Journal of The Textile Institute, vol. 103, no. 1, pp. 48-54, 2012.

- [24] Lee, S. and Obendorf, S. K.: *Transport Properties of Layered Fabric Systems Based on Electrospun Nanofibers*. *Fibers and Polymers*, vol. 8, no. 5, pp. 501-506, 2007.
- [25] Venkataraman, M., Mishra, R., Jasikova, D., Kotresh, T. and Militky, J.: *Thermodynamics of Aerogel-treated Nonwoven Fabrics at Subzero Temperatures*. *Journal of Industrial Textiles*, vol. 45, no. 3, pp. 387-404, 2015.
- [26] Ziaei, M., Ghane, M.: *Thermal Insulation Property of Spacer Fabrics Integrated by Ceramic Powder Impregnated Fabrics*. *Journal of Industrial Textiles*, vol. 43, no.1, pp. 20-33, 2013.
- [27] Bhattacharyya, R. K.: *Heat-transfer Model for Fibrous Insulations, Thermal Insulation Performance*, edited by D. L. McElroy and R. P. Tye, ASTM Special Technical Publication 718, American Society for Testing and Materials, Philadelphia, pp. 272-286, 1980.
- [28] Sang, S. W., Itzhak, S. and Roger, L. B.: *Heat and Moisture Transfer through Nonwoven Fabrics Part I: Heat Transfer*. *Textile Research Journal*, vol. 64, no. 3, pp. 149-162, 1994.
- [29] Farnworth, B.: *Mechanisms of Heat Flow through Clothing Insulation*. *Textile Research Journal*, vol. 3, pp. 717-724, 1983.
- [30] Akimov, Y. K.: *Fields of Application of Aerogels (Review)*. *Instruments and Experimental Techniques*, vol. 46, no. 3, pp. 287-299, 2003.
- [31] Schneider, A. M. and Holcombe, B. V.: *Properties Influencing Coolness to the Touch of Fabrics*. *Textile Research Journal*, vol. 61, no. 8, pp. 488-494, 1991.
- [32] Vivekanadan, M. V., Raj, S., Sreenivasan, S. and Nachane, R. P.: *Parameters Affecting Warm-cool Feeling in Cotton Denim Fabrics*. *Indian Journal of Fibre & Textile Research*, vol. 36, pp. 117-121, 2011.
- [33] Huang, W. and Ghosh, T. K.: *Online Measurement of Fabric Mechanical Properties: Compressional Behavior*. *Textile, Fiber and Film Industry Technical Conference*, 1, 1999.
- [34] Debnath, S. and Madhusoothanan, M.: *Compression Properties of Polyester Needle-punched Fabric*. *Journal of Engineered Fibers and Fabrics*, vol. 4, pp. 14-19, 2009.

Multicriteria decision making in clothing

Srabani Misra¹, Jana Salacova¹, Bibhu Prasad Dash² and Jiri Militky¹

¹*Dept. of Material Engineering, Textile Faculty, Technical University of Liberec, Studentská 2, 46117 Liberec, Czech Republic*

²*Dept. of Textile Engineering, College of Engineering and Technology, Bhubaneswar, India*

Abstract

In multiple criteria design problems (multiple objective mathematical programming problems) the alternatives are not explicitly known. An alternative (solution) can be found by solving a mathematical model. The number of alternatives is either infinite or not countable (when some variables are continuous) or typically very large if countable (when all variables are discrete). But both kind of problems are considered as a subclasses of Multi Criteria Decision Making problems. The MCDM problems can also be divided into two major classes with respect to the way the weights of the alternatives are determined: Compensatory and Outranking Decision Making. Although new product development management is a new successful, challengeable and important strategy in modern society, understanding the key success factors in this approach is not only helpful, but also productive in reducing managerial decision-making risks. In this chapter, after expanding the related literature review, consulting with experts on identifying key factors affecting NPD, the researcher provided the basic questionnaire, and then identified key success factors and their indicators in MCDM process management. Findings showed that improving competitive position, reducing managerial and production failure risks and enhancing success of the MCDM process would improve MCDM by determination of priorities and identification of the key factors in new clothing product development. For developing sustainable clothing products design engineers need to foresee diverse interrelations between a product's characteristics and its economic, social and environmental impacts. In order to support this complex task a wide range of design methods have been developed. Retrospective analytical methods require a large amount of information and are thus utilized when important design decisions are already made. Prospective methods are rather generic (e.g. checklists) and too broad to be helpful in concrete clothing design decisions. In this chapter, the integration of discrete decision trees is proposed for shifting multi-criterial quantitative analysis to clothing product development. Resulting benefits and obstacles are illustrated by evaluating value creation options of a clothing product.

Keywords

Multicriteria decision, marginal utility, clothing quality, total hand value, thermal comfort, total appearance, degree of satisfaction

Introduction

Multi-criteria decision making problems comprise of an underlying space of feasible solutions and several objectives that can be evaluated with regard to the feasible solutions. In general, for this kind of problem there does not exist a generic solution approach and unambiguous concept of optimality, but different approaches depending on the viewpoint of the decision maker towards the underlying problem. The optimization assumes that the given objectives can be ranked a priori and that the decision maker is interested in an optimal solution with respect to this ranking. Reference point methods assume that the decision maker is interested in a solution that minimizes a certain distance function to a given reference point. If the objectives are considered to be equally important and cannot be ranked a priori, a decision maker might also be interested in the entire set of solutions which cannot be improved with respect to one objective without worsening the value of another objective leading to the concept of non-dominance and efficient solutions. These different premises and notions of optimality will generally lead to different (desired) solutions. In sustainable product development problems the objective cannot be ranked a priori since the economic, environmental and social dimension is considered to be equally important. In recent years, understanding the structure and function of complex clothing functions has become the foundation for explaining many different real-world complex biological, technological and informal social phenomena. Techniques from statistical physics have been successfully applied to the analysis of these networks, and have uncovered surprising statistical structural properties that have also been shown to have a major effect on clothing functionality, dynamics, robustness, and fragility. This chapter examines, for the first time, the statistical properties of strategically important clothing properties identified by people engaged in distributed product development (PD) in clothing industry and discusses the significance of these properties in providing insight into ways of improving the strategic and operational decision-making of the product quality. We show that the structure of information flow networks that are at the heart of large-scale clothing product development efforts have properties that are similar to those displayed by other social, biological and technological networks. In this context, we further identify novel clothing properties that may be characteristic of other information-carrying attributes. We further present a detailed model and analysis of clothing dynamic properties on complex analysis, and show how the underlying network topologies provide direct information about the characteristics of this dynamics. We believe that our new analysis methodology and empirical results are also relevant to other product development in textile area.

This chapter develops a set of management and production criteria needed to be used in order to maximize clothing product values. If these criteria are achieved, the clothing product may achieve and sustain “supernormal” characteristics. The criteria developed here are all related to the stream of information value from the consumer, and the velocity of the resulting flow of information through the product development, production and application processes. These streams are constructed in terms of their “Shannon information velocity” which provides a new way to derive the set of variables that effect (and maximize) the value. Rather than equating demand and

supply at each point in time, the decision criteria is based on the information. In addition, the chapter derives the requisite valuation procedures for product and offering creation.

To fulfill their role in maximizing product value, consumer's decision rule is based on analyzing the possible reduction of the internal process. The rule of maximizing Information Velocity leads to the most cost-effective product management in time and money and market responsiveness. With the above derivation, it is shown that the shareholder value of all business processes are driven by the rate at which the information is generated by the market is matched by the responsive acceleration of information within the business processes. Empirical examples are provided which confirm that superior Information Velocity in all processes achieves and sustains supernormal returns.

Steps of Decision Making

A decision making process involves the following steps to be followed:

1. Identifying the objective/goal of the decision making process
2. Selection of the Criteria/Parameters/Factors/Decider
3. Selection of the Alternatives
4. Selection of the weighing methods to represent importance
5. Method of Aggregation
6. Decision making based on the Aggregation results

Working Principle

The MCDM process follows a common working principle as described below:

1. Selection of Criteria

Selected criteria must be:

1. Coherent with the decision
2. Independent of each other
3. Represented in same scale
4. Measurable
5. Not unrelated with the alternatives

2. Selection of Alternatives

Selected alternatives must be:

6. Available
7. Comparable
8. Real not Ideal
9. Practical/Feasible

3. Selection of the Weighing Methods to Represent Importance

The weight determination methods can be either compensatory or outrankable.

Example of Compensatory Method:

Analytical Hierarchy Process (AHP), Fuzzy Multi-Criteria Decision Making Process (FDM) etc.

Classification of discrete multiple criteria methods

There are a lot of MCDM methods (Guitoni and Martel 1998). MCDM approaches are major parts of decision theory and analysis. Hwang and Yoon (1981) grouped the MCDM methods according to the available information. Real-world decision making problems are usually complex and no structures are to be considered through the examination of a single criterion, or point of view that will lead to the optimum decision. Operation in the marketplace requires some knowledge of areas generating critical situations and insolvency.

It is necessary to learn the criteria determining both development and downfall of feasible alternatives. In a mono-criterion approach, the analyst builds a unique criterion capturing all the relevant aspects of the problem. Such a one-dimensional approach is an oversimplification of the actual nature of the problem. In many real-world decision problems, the decision-maker has a set of multiple conflicting objectives.

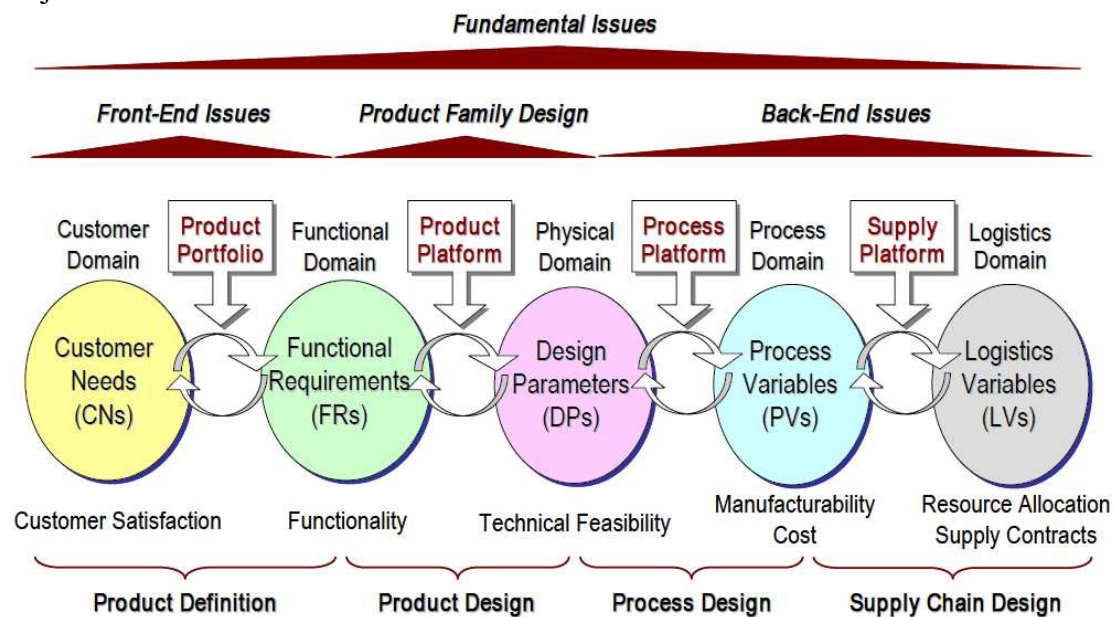


Fig. 1: Issues of product decision making

Most of MCDM methods deal with discrete alternatives, which are described by a set of criteria. Criteria values can be determined as a cardinal or ordinal information. Information could be determined exactly or could be fuzzy, determined in intervals. Modern MCDM methods enable decision makers to deal with all above mentioned types of information. One of the problems encountered during multiple criteria decision making process is the choice of the aggregation procedure for solving the decision problem.

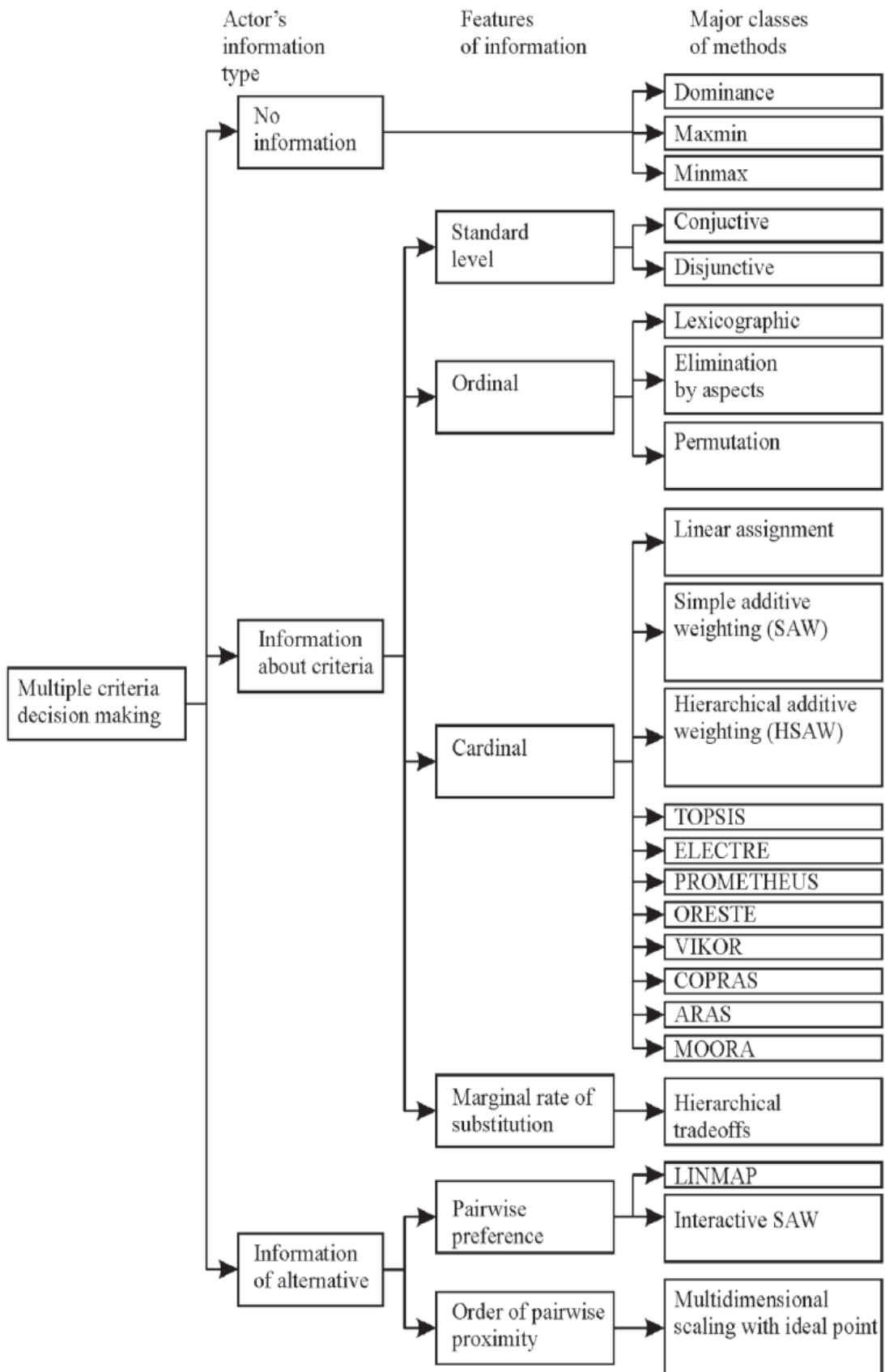


Fig. 2: Grouping of multiple criteria decision making methods

In general multiple criteria decision analysts provide a variety of aggregation procedures. MCDM methods have become increasingly popular in decision making for economics because of the multi-dimensionality of the sustainability goal and the complexity of socio-economic, environment and technical/scientific problems.

Economic analysis of product quality

Equilibrium

Equilibrium price and quantity occur where quantity demanded equals quantity supplied or where the downward-sloping demand curve intersects the upward sloping supply curve. Furthermore, on the one hand, a surplus occurs at a price above equilibrium. It is the result of the quantity supplied being greater than the quantity demanded. On the other hand, a shortage occurs at a price below equilibrium. It results from the quantity demanded exceeding the quantity supplied. In order to move price and the situation toward equilibrium, two forms of movement may occur on the graph: A movement along the curve and a shift in the curve. Students frequently confuse those two forms. In order to keep them clear, students need to remember that a change in price initiates movement along the curve whereas a change in a determinant initiates a shift in the curve. In addition, the curve illustrates the relationship between the axis variables thus any change in them will result in movement along the curve. An equilibrium point is static at one instance, but it is also dynamic in nature by virtue of a curve shift that results in a different intersection of the demand and supply curve. New intersections and new equilibrium prices and quantities often result from any inward or outward curve shift. The demand curve will shift in accordance with a change in a determinant and so will the supply curve. In the pages ahead, readers will gain valuable insights into studying microeconomic concepts and learning how to apply them successfully.

Curve Shifts

Five determinants exist each for demand and for supply and any change in them will prompt the curve to shift. Increases or decreases in demand or supply occur in accordance with a change in a determinant. A rightward, outward, or upward shift in the demand curve is an increase in demand whereas an opposite shift is a decrease in demand. By extension, an increase (decrease) in demand means consumers will purchase a larger (smaller) quantity of an item at any given price. A rightward, downward, or outward shift in the supply curve is as an increase in supply whereas an opposite shift is a decrease in supply. Likewise, an increase (decrease) in supply means producers will supply a larger (smaller) quantity of an item at any given price. In contrast to curve shifts, any movement along a demand curve or a supply curve is respectively a change in quantity demanded or quantity supplied to which there is a corresponding change in price. The list of five determinants for demand and those for supply is as follows:

Marginal Utility

In terms of those individual-level demand schedules, the ability to purchase an item is a function of a consumer's income and the willingness to purchase is a function of the satisfaction that originates from the item's consumption. In other words, consumers maximize their utility subject to their budget constraints. Utility is another word for the satisfaction an individual receives when consuming the item. Marginal utility then, by definition, is the additional unit of satisfaction from consuming an additional amount of the item. However, marginal utility increases but it becomes smaller with additional amounts until a point is reached at which it is zero. Afterwards, marginal utility then becomes negative and it decreases at an increasing rate as a consumer begins to regret overindulgence. This pattern illustrates the diminishing marginal utility concept. One example of this concept is how the feeding frenzy that accompanies a buffet-style meal often results in regrets as the diner attempts to get the most out of each dollar spent. Income constraints, marginal utility, and item prices jointly influence a consumer's purchase plans. Income and item price are primary factors in determining how much the consumer will purchase. With a simplifying assumption that only two items are available for purchase, it is useful to ponder for a moment what combination of them is attainable for a given amount of income and is desirable for achieving an equal amount of utility. Consumer equilibrium is, by definition, a point at which the marginal utility per dollar spent is equal across all.

The product decision process

Effective supply chain design calls for robust analytical models and design tools. Previous works in this area are mostly Operation Research oriented without considering manufacturing aspects. Recently, researchers have begun to realize that the decision and integration effort in clothing supply chain design should be driven by the manufactured product, specifically, product characteristics and product life cycle. In addition, decision-making processes should be guided by a comprehensive set of performance metrics. In this chapter, we relate product characteristics to supply chain strategy and adopt supply chain operations reference (SCOR) model level I performance metrics as the decision criteria. An integrated analytic hierarchy process (AHP) and preemptive goal programming (PGP) based multi-criteria decision-making methodology is then developed to take into account both qualitative and quantitative factors in supplier selection. While the AHP process matches product characteristics with supplier characteristics (using supplier ratings derived from pairwise comparisons) to qualitatively determine supply chain strategy, PGP mathematically determines the optimal order quantity from the chosen suppliers. Since PGP uses AHP ratings as input, the variations of pairwise comparisons in AHP will influence the final order quantity. Therefore, users of this methodology should put greater emphasis on the AHP progress to ensure the accuracy of supplier ratings.

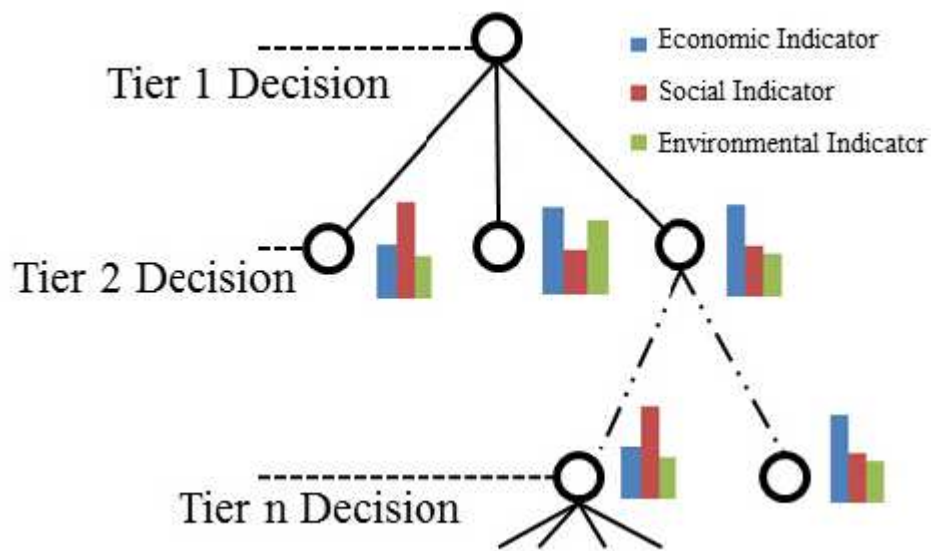


Fig. 3: Decision tree

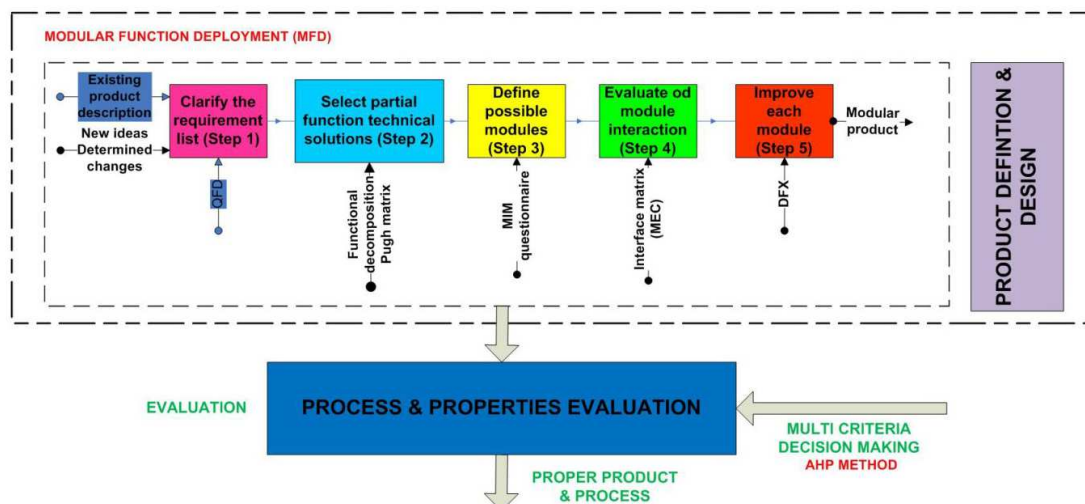


Fig. 4: Product decision process

Quality aspects of clothing

The quality of clothing is categorized into

1. Physiological properties (Heat, moisture and air transmission)
2. Physical properties (Mechanical properties)
3. Psychological properties (Appearance, acceptability, fashion)

The physiological properties

Various types of instruments have been used for measuring the thermal insulation of fabric in the steady state mode and contact transient mode. In practice the measurement of the rate of heat flow in particular direction is difficult as a heater, even when supplied with a known amount of power, dissipates its heat in all directions. Togmeter and guarded hot plate which are most commonly used for

evaluation steady-state thermal insulation characteristics (mainly thermal resistance and thermal conductivity) have several disadvantages such as the length of time required for testing, the size of the samples and cumbersome sample insertion in the apparatus. In the present days, the transient state characteristics of fabrics have become important. Alambeta instrument developed at the Technical University of Liberec, Czech Republic is able to determine these characteristics. Thermal manikins are most important for clothing study due to their anatomic shape and their ability to sweat and move. The interest in using thermal manikins in research and product development has increased continuously over the past 20 years as indicated by the number of manikins being developed and manufactured. In addition, the level of advancement has also increased either for improved precision of the device or for reduced costs. Furthermore, these versatile evaluation instruments are implemented nowadays in a wide range of disciplines including clothing research and manufacturing, automobile industry, environmental engineering of artificial microclimates for human occupancy.

Physical properties for clothing

Fabric physical properties assessment can be done in 2 particular ways:

1. Subjective assessment
2. Objective assessment

Subjective assessment

Subjective assessment treats fabric hand as a psychological reaction obtained from the sense of touch. Apparently it is a valuable method that has traditionally been used by textile technologists and researchers. Although it is probably the most widely discussed aspect of fabric assessment, it is not so well understood due to the reliance on subjective judgments. The first attempts of hand evaluation of textiles in an organized and quantitative manner were published as early as 1926 and have continued up to the present time. Extensive studies have been made by Binns (1934) of the subjective assessment of hand, with particular reference to rank correlation between judges from varying technical and sociological backgrounds. In the study two wool fabric categories (milled and clear) were investigated, with six cloths in each category. Because small numbers of cloths were involved, all samples in a particular category were presented together for ranking. The judges were asked to rank the samples directly according to hand, from best to worst, without any suggestion of what primary hand qualities to look for.

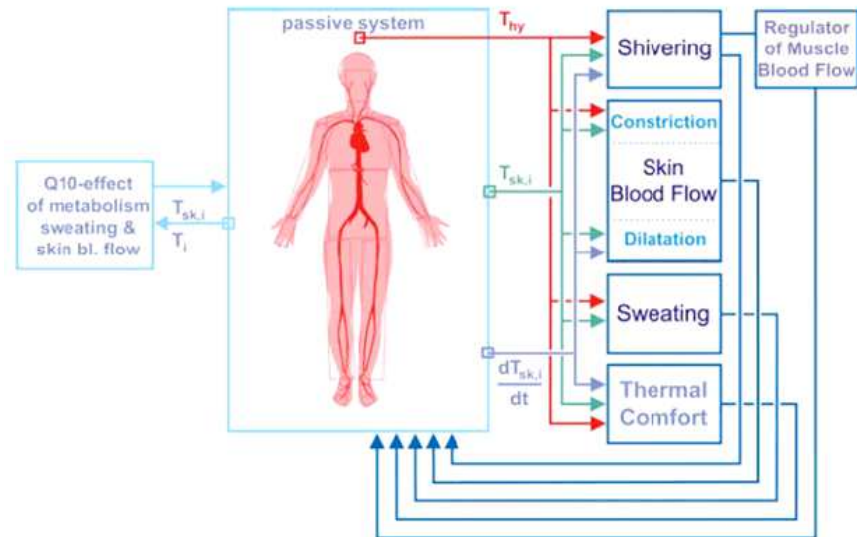


Fig. 5: Heat transfer in a manikin

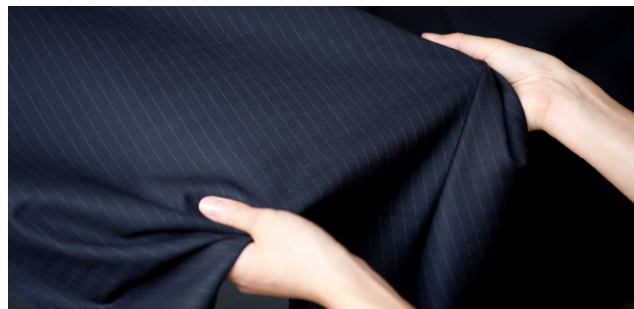


Fig. 6: Subjective assessment of mechanical properties

Hand evaluation by physical testing

The following properties are responsible for hand of clothing.

- Bending Properties
- Shear Properties
- Tensile Properties
- Compression Properties
- Surface Properties
- Weight Property

Kawabata Evaluation System (KES)

The Kawabata Evaluation System (KES) is a series of instruments used to measure those textile material properties that enable predictions of the aesthetic qualities perceived by human touch. KES instruments quantify garment material tactile qualities through objective measurement of the mechanical properties related to comfort perception. With low forces applied, as in manipulating / touching fabrics, the Kawabata instruments define the role played by tensile (stretch), shear stiffness (drape), bending rigidity (flexing), compression (thickness, softness), and surface

friction and roughness (next to skin) on tactile sensations (Behera, Chowdhry, & Sobti, 1998; Behera, 2007). This analytical power, combined with the capability to characterize energy loss in mechanical deformation and recovery processes, provides an unparalleled tool for use in fabric hand analysis. KES provides a unique capability, not only to predict human response, but also to provide an understanding of how the variables of fiber, yarn, fabric construction and finish contribute to perceptions of comfort (Kawabata, 1973; 1980).

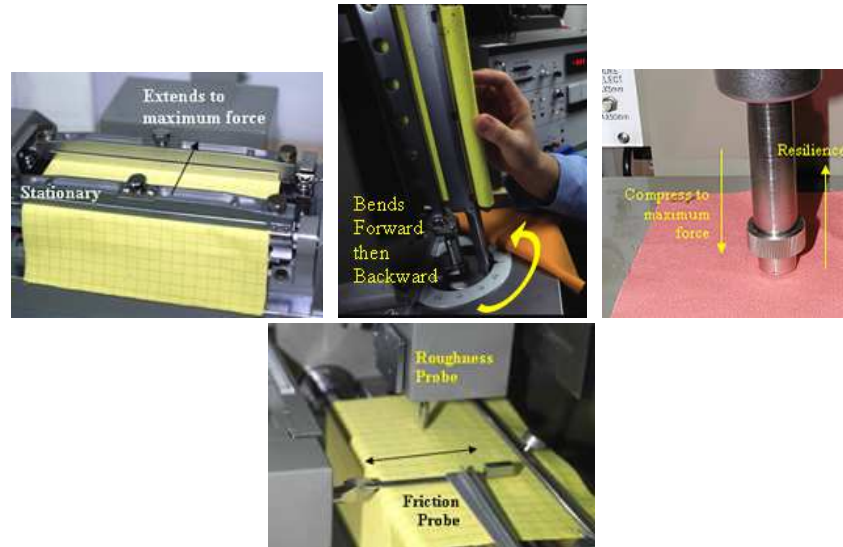


Fig. 7: Kawabata Evaluation System

Calculation of Primary Hand Value

Primary hand values are calculated by KES from the above 16 parameters. These are *koshi* (stiffness), *numeri* (smoothness), *fukurami* (softness and fullness) for the winter fabrics; and *koshi* (stiffness), *shari* (crispness), *hari* (anti-drape stiffness), and *fukurami* (softness and fullness) for the summer fabrics (Kawabata, 1986; 1988; Kawabata, & Niwa, 1989).

Total Hand Value (THV) Calculation

$$THV = C_0 + \sum_{i=1}^8 [C_{1i} (P_i - m_{1i}) / \sigma_{1i} + C_{2i} (P_i - m_{2i}) / \sigma_{2i}] \quad (1)$$

Where,

C_0 , C_{1i} and C_{2i} are coefficients/constants for the i^{th} parameter

P_i is the primary hand value of the i^{th} variable term

m_{1i} & σ_{1i} are the population mean and standard deviation

m_{2i} & σ_{2i} are the square mean and standard deviation.

Total hand value is calculated separately for summer and winter applications and are denoted as THV(s) & THV(w) respectively.

Psychological quality attributes

The appearance of a fabric mainly depends on the fabric design and characteristics of raw material used for it. The design of a fabric could be an artistic design and/or engineering design. The artistic design includes weave structure, pattern and color of the material whereas the engineering design is mainly concerned with constructional details (Behera, 2004). The weave design is also an integral part of the engineering design. However, the color selection for a given end use mainly depends on the user's choice. The weave design, pattern and fabric sett combined together attribute to texture of the cloth. Material characteristics along with engineering design specification determine fabric mechanical prosperities. The properties that directly linked to the aesthetic appearance are therefore drape (mechanical properties), texture (constructional parameters), wrinkle (irregular surface deformations) and pilling (surface abrasion).

Fabric appearance

Fabric appearance is normally evaluated from the traditional appearance attributes such as wrinkling, staining, creasing, texture, pilling, drapes and color. There is no method available which can combine all aesthetic attributes to express the fabric quality from appearance point of view. In this work a computer vision system is proposed to measure and integrate most important aesthetic attributes of an apparel fabric such as pilling, drape, texture and wrinkle so as to develop an index called fabric appearance index.

Drape coefficient

Fabric drape can be defined as a description of the deformation of a fabric produced by the gravity when only part of it is directly supported. It is also one of many factors that influence the aesthetic appearance of a fabric and has an outstanding effect on the formal beauty of the cloth. The drapability of a fabric is quantified into a dimensionless value called 'drape coefficient', which is defined as the percentage of the area from an angular ring of the fabric covered by a vertical projection of the draped fabric. In this image analysis system, the shadow projected from the fabric is quantified into a binary image after being digitized. The threshold value that sets the criteria for converting a grey scale image into a black and white image can be controlled at the user interface of the system. For this reason, this image analysis method is not influenced by the fabric color. The digitized binary image is processed with a closing operation, which removes noise and segmentizes the shadow image of the draped fabric from the background image. The closing operation is a dilation operation followed by an erosion operation. This operation fills in single pixel object abnormalities. After digitizing the image of the draped fabric, the image analysis system searches the boundary between the fabric shadow and the central disc on the drapemeter (between A_d and A_1 of Fig. 8) and the boundary between the fabric shadow and the outer region of the fabric shadow (between A_2 and A_d).

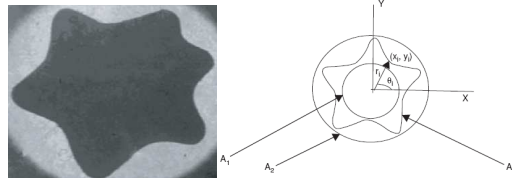


Fig. 8: Drape coefficient of fabric.

$$\text{Drape coefficient} = \frac{A_d - A_1}{A_2 - A_1} \times 100 \quad (2)$$

Pilling evaluation

In digital image processing terms, pills are localized minor disturbances, randomly distributed on the surface, whereas yarn floating points, which are part of the fabric structure, appear to be periodical and associated only with the pattern of interlacing. The periodic structure of a fabric will result in prominent peaks in its power spectrum, and non-periodic components such as pills will generate frequency terms spreading in the background of the spectrum. Here in this research, the Fast Fourier Transform (FFT) technique is used to determine the pills by image processing. Pills often appear in comparable brightness and size to those of floating yarns. Peaks are small, bright regions that can be detected by using a power threshold. The threshold usually needs to be set to a reasonably high value to prevent noisy areas from being detected.

The pixels whose power is above the threshold are considered as the core part of peaks. The spectrum is now divided into two portions; peak portion and the non-peak portion, which can be used in the inverse FFT to reconstruct two images. The image reconstruction through the non-peak spectrum presents the non-periodic structure including pills, and that from the peak spectrum shows the fabric weaving. In the non-periodic image, pills appear to be solid circular regions; a template matching technique is suitable for the further detection of pills in the periodic image. A template is a pictorial representation of a known feature. For pill detection, the template is designed to be a small square that contains a centred white circle surrounded by black pixels. The size of the template should be equivalent to the size of the repeating units in the fabric. Template matching is the process of moving the template over the entire image and calculating the similarity between the template and the covered window on the image. The normalized correlation is one commonly used measure of similarity to determine match.

If the image and the template are denoted as $f(x, y)$ and $t(x, y)$, the correlation coefficient at point (m, n) is given by

$$r(m, n) = \frac{\sum_x \sum_y [f(x, y) - \bar{f}_{xy}][t(x-m, y-n) - \bar{t}]}{\sqrt{\sum_x \sum_y [f(x, y) - \bar{f}_{xy}]^2 [t(x-m, y-n) - \bar{t}]^2}} \quad (3)$$

where, \bar{f}_{xy} is the intensity of image pixels within the window that is translated across the entire image, and \bar{t} is the intensity of the template. The double summation is

carried out over the moving template and the covered window. This equation can be further simplified to reduce redundant calculations in the program as follows:

$$r(m, n) = \frac{M \sum_x \sum_y [f(x, y) t(x-m, y-n) - \bar{f}_x \bar{t}] }{\sqrt{[M \sum_x \sum_y [f^2(x, y) - \bar{f}_x^2]] [M \sum_x \sum_y t^2(x-m, y-n) - \bar{t}^2]}} \quad (4)$$

where, M is the number of pixels in the template and r(m, n) is the position of the pill in the matching map.

Wrinkle analysis

Wrinkles are defined as undesirable three-dimensional creases or short and irregular deformations on the fabric surface. These deformations depend on the viscoelastic properties of the fabric. They are three-dimensional versions of creases and formed when legs and sleeves are bent along the opposite direction and kept in a place for either a long period of time or intermittently. This property of a fabric is reflected in the criteria of a consumer's choice through the appearance of fabrics during ordinary wear.

A computer vision system is developed to measure the surface characteristics of a fabric, based on the method of image processing. The underlying assumption in this study is that the digitized intensities are proportionally related to the height and wrinkle of the surface features. A horizontal direction pixel is referred to as the X-axis and a vertical direction pixel as the Y-axis. The wrinkle properties can be judged by analyzing the grey level of images and are depicted using the distribution of grey level Gsd. The standard deviation of grey level (Gsd) is defined as:

$$Gsd = \sqrt{\frac{\sum \sum (Z(i, j) - \bar{Z})^2}{m \times n}} \quad (5)$$

where, Z(i, j) is the grey level of point A(i, j), Z is the mean of data points and (m × n) are the pixels in the X direction and Y direction separately. A smooth fabric is expected to exhibit a uniform appearance, resulting in a narrow grey level histogram and a low standard deviation. When there are more wrinkles in the fabric, there are variations in the amount of light reflected at each point on the fabric surface resulting in a wide histogram and high standard deviation of the grey level.

Texture analysis

Texture refers to the surface characteristics, i.e. smoothness or roughness and the spacing of warp and weft yarn in a fabric. Texture analysis is one of the most important techniques used in the image analysis and classification of the images where repetition of a fundamental image element occurs. Studies revealed that wavelet transform is capable of providing features that may be used to discriminate between different cloth textures. The effectiveness of using wavelet transform

features depends on classifying texture from spatial grey level dependency matrices called co-occurrence matrices.

For texture measurement a statistical approach is chosen for image analysis called the spatial grey level co-occurrence measurement method. The size of the image is 257 by 257 pixels. Each pixel has values of 256 grey scales, with the zero value representing black and 256 representing white. The spatial grey level co-occurrence probability function $f(i, j, d, a)$ is a second-order probability density function; it is the relative frequency with which two pixels separated by a distance d in the a direction occur on the image, one with i grey level and the other with j grey level. From this definition, one can calculate co-occurrence matrices in the directions 0° , 45° , 90° and 135° , and from these matrices the following parameters are calculated.

Fractional contribution

To develop the subjective total appearance value TAV, a survey of persons who were the experts in the apparel fabric sector was carried out. In this survey, 20 fabric samples covering a wide range of areal density (fabric weight in gram per square meter), mostly polyester-viscose, blended suiting fabrics were collected from well-known industries and the relative importance of each of the above four attributes was determined by assigning suitable rank given by the experts to all the fabric samples. The survey results are given in Fig. 9, which shows the percentage opinion in favor of each of the attributes in order of their priority towards fabric appearance.

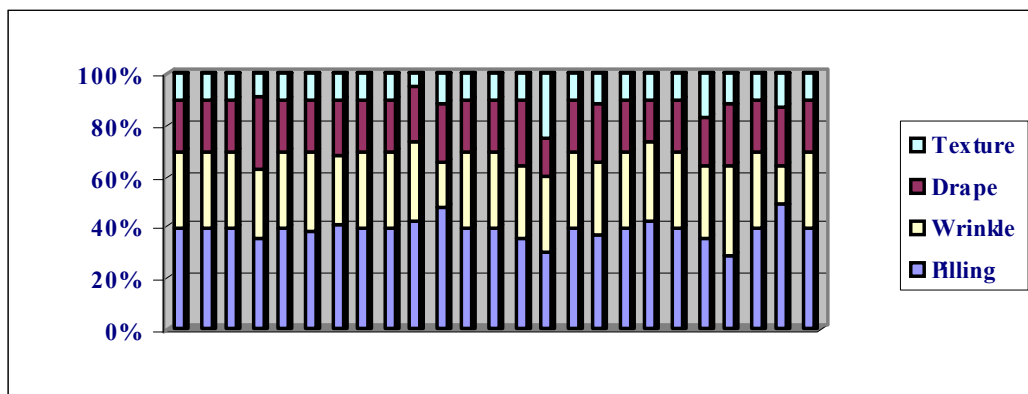


Fig. 9: Relative importance of appearance attributes.

From the above survey it was found that the pilling property has the maximum contribution towards appearance followed by wrinkle, and then drape and texture in the descending order. The final average rating and weightage of the four fabric properties in evaluation of the TAV are shown in Table 1.

Samples of fabrics were evaluated by using the calculated DS as well as TAV evaluated by fabric experts subjectively. Each of these four parameters is quantified based on scientific principles using digital image processing and integrated together to estimate a parameter called degree of satisfaction (DS) as follows (Meloun, & Militký, 2011):

$$DS = \exp\left(\sum_{i=1}^n W_i \log(u_i)\right) \quad (2)$$

where, n is the total number of properties, u_i is nonlinear transformation of the grade A_i of the i^{th} property obtained by digital image processing and W_i is the fractional contribution of the i^{th} property (Černý, Gluckhaufová, & Toms, 1980).

Table 1: Fractional contribution of appearance attributes

Property	Importance	Actual Contribution (%)	Approximate Contribution (%)
Pilling	1	39.7	40
Wrinkle	2	31.7	30
Drape	3	19.9	20
Texture	4	8.7	10

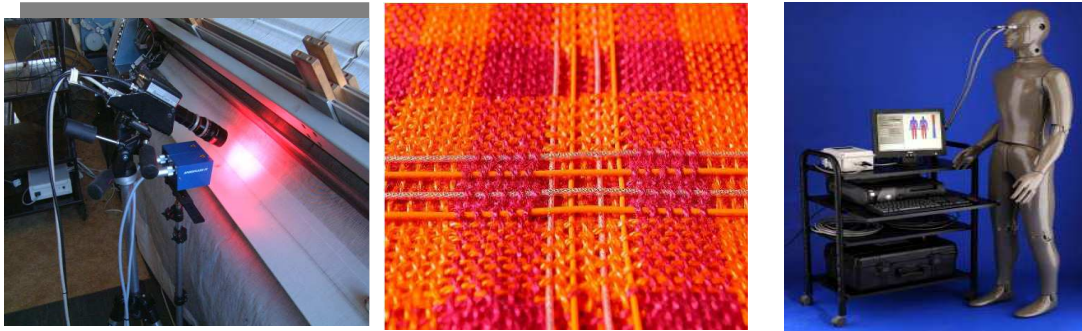


Fig. 10: Psychological attributes

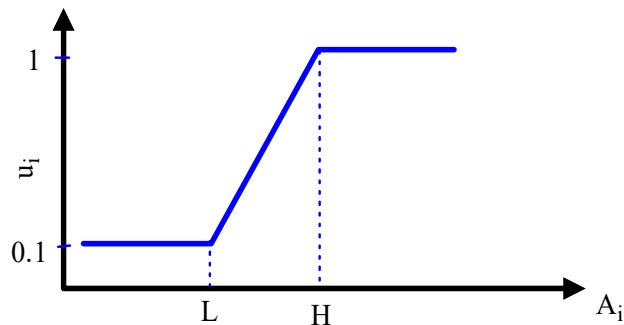


Fig. 11: One side bounded characteristic of Degree of satisfaction.

The lowest level $L = 1$ and the highest level $H = 4$ were here selected. The DS varies from 0 to 1. Higher the value of DS , better is the appearance. In order to determine the fractional contribution of each attribute, an expert panel was constituted and a survey was conducted to decide the contribution of each element to fabric appearance. Samples of fabrics were evaluated by using the calculated DS as well as TAV evaluated by fabric experts subjectively. The Bootstrap type technique described in book [5] has been applied for computation of the statistical characteristics of DS. This technique is based on the assumption that for attribute A_j the mean value x_j and

variance s_j^2 are determined by standard treatment of the measured data. The procedure of the statistical characteristics of DS estimation is divided to the following parts:

- I. Generation of $x(k)_j$ ($j=1, \dots, m$) values having normal distribution with mean values x_{Mj} and variances s_j^2 . The pseudorandom number generator built in MATLAB is used.
- II. Calculation of the degree of satisfaction $DS(k)$ using the relation (1).
- III. The steps I and II are repeated for $k=1, \dots, n$ (usually $n = 3600$ is chosen).
- IV. Construction of a histogram from the values $DS(k)$ ($k=1, \dots, n$) and computation of the estimators of $E(DS)$, $D(DS)$.

The core of Bootstrap is generations of artificial samples from proper distribution. The generation based on the normal distribution is used. It is generally useful if the only mean values x_{Mj} of all attributes are given. The variability is expressed as coefficient of variation CV (the value $CV = 10\%$ is used). For generation of simulated samples the random numbers $N(0,1)$ generated by random number generator are used. These values are transformed to the individual attributes mean x_j by relation $x_j = x_{Mj} (1 + CV/100)$ where CV_j are variation coefficients. As robust characteristics of total mean from all simulated samples $E(U)$, the median value is used and as robust alternative of standard deviation, the difference between 97.5 % and 2.5 % of all bootstrap sample quantiles divided by 1.394 are calculated. A very good correlation between DS and subjective grades given by experts can be seen from Fig. 12.

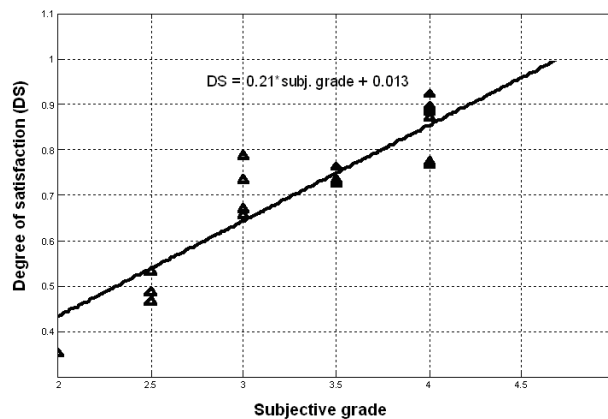


Fig. 12: The DS vs subjective grades TAV

Histogram of DS for fabric No. 20 estimated from Bootstrap samples is shown in the Fig. 13.

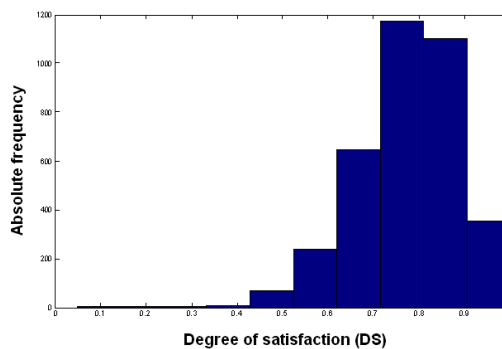


Fig. 13: Histogram of Bootstrap samples

The corresponding interval covering 95% of Bootstrap sample medians is shown in the Fig. 6.

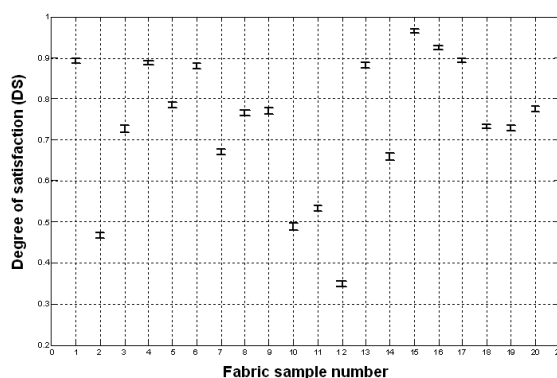


Fig. 14: The 95% confidence interval of DS for all fabrics

It is visible that the confidence intervals are relatively narrow.

Conclusion

Evidently expressing the quality based on complex variant evaluation is of a universal character (fibers, yarns etc.) is successfully implemented. There are, of course, many other techniques; some of them (e.g. polar property diagram) do not even carry out any aggregation. The advantage of the complex quality criterion U manifests itself especially in the case when quality of a whole series of clothing textiles is being compared. It can be expected that procedures for objective evaluation of textiles quality will keep on developing and they will thus simplify a complex optimization of clothing textiles manufacturing process in respect of their required utility. The application in the computer aided textile design will be more precisely oriented to the better quality of products.

REFERENCES

1. Barker, R.L. (2002). From fabric hand to thermal comfort: the evolving role of objective measurements in explaining human comfort response to textiles. *International Journal of Clothing Science and Technology*, 14: 3/4, 181–200.
2. Behera, B. K., Chowdhry, S., & Sobti, M. (1998). Studies on handle of microdenier polyester filament dress materials. *International Journal of Clothing Science and Technology*, 10, 2, 104-113.
3. Behera, B. K. (2004). Image processing in textiles. *Textile Progress*, 35, 1-193.
4. Behera, B. K. (2007). Comfort and handle behaviour of lnen-blended fabrics. *AUTEX Research Journal*, 7, 1, 104-113.
5. Behery, H. M. (2005). *Effect of mechanical and physical properties on fabric hand*. Woodhead Publishing Limited in Association with the Textile Institute, Published in North America by CRC Press LLC.
6. Černý, M. Gluckhaufová, D., & Toms M. (1980). Methods for complex evaluation of variants. *Academia*, Praha.
7. Dobrov, G. M. (1977). *Expert Estimates in Scientific Prognoses*, Kiev.

8. Hes, L., & Dolezal, I. (1989). New method and equipment for measuring thermal properties of textiles. *Journal of the Textile Machinery Society of Japan*, 42, T124-128
9. Hes, L., Geraldès, M. J., & Araujo, M. (2002). How to improve the thermal comfort with high performance pp fibers. *Proceedings of 2nd AUTEX Conference*, Bruges, Belgium.
10. Kawabata, S. (1973). Fabric hand evaluation by objective methods. *Journal of the Textile Machinery Society of Japan*, 26, 10, P721.
11. Kawabata, S. (1980). *The standardization and analysis of hand evaluation, 2nd edition, Hand Evaluation and Standardization Committee*. Textile Machinery Society of Japan, Osaka.
12. Kawabata, S. (1986). Objective evaluation method of clothing fabrics and its application. *Journal of the Textile Machinery Society of Japan*, 39, 1-4.
13. Kawabata, S. (1988). *Basic course of fibrous materials in Kyoto*. (1st) mechanical characteristics and fabric hand of clothing fabrics, Fibrous Materials Research Group.
14. Kawabata, S., & Niwa, M. (1989). Tailoring process control. *Journal of the Textile Institute*, 80, 19-20.
15. Meloun, M., Militký, J., & Forina, M. (1993). *Chemometrics in instrumental analysis*. Ellis Horwood, London.
16. Meloun, M., & Militký, J. (2011). *Statistical data analysis*. Woodhead Publishing. New Delhi.
17. Militký, J. (1980). Statistical properties of complex quality indices. *Proceedings of Conference STAQUAREL 80*, Praha.
18. Militký, J., & Bajžík, V. (1997). Influence of washing/ironing cycles on selected properties of cotton type weaves. *International Journal of Clothing Science and Technology*, 9, 3, 193-199.
19. Militký, J. (2001). MATLAB program for complex quality evaluation. *National Textile Centre Report*, Liberec.
20. Militký, J. (2010). Complex quality evaluation of textile fabrics, *Proceedings of Conference CLOTECH*, Radom.
21. Moran, M., & Shapiro, H. (1988). *Fundamentals of engineering thermodynamics*, 7, 1-489.

Aliphatic polyamide fibres

Mohanapriya Venkataraman, Jiri Militký, Rajesh Mishra
*Department of Material Engineering, Faculty of Textile Engineering,
 Technical University of Liberec, Czech Republic*

Introduction

Polyamides are tough, strong, durable fibres useful in a wide range of textile applications. Off the synthetic nonwoven bonded fabrics, polyamide fibres are the first ones to be used since they increase serviceability of the end product prone to frequent folding and thus requiring high resistance to abrasion [1]. The polyamide fibres include nylons and aramid fibres formed from polymers of long-chain polyamides. Nylon is defined as a generic term for any long chain synthetic polymeric amide which has recurring amide groups as an integral part of the main polymer chain and which is capable of being formed into a filament in which the structural elements are oriented in the direction of the axis. It is the generic word used to refer a family of polyamides. Nylon was the first of the “miracle” yarns made entirely from chemical ingredients through the process of polymerization [2]. The number of carbon atoms in each monomer or comonomer unit is commonly designated for the nylons. The two main types of fibre are polyamide 6, usually known as Perlon, and polyamide 6.6, which is generally called Nylon to distinguish it from Perlon. The number or numbers after the word ‘polyamide’ indicate how many carbon atoms there are in each molecule making up the polyamide. The fact that there is only one number in one instance and two in the other shows that polyamide 6 contains only one basic module and polyamide 6.6 contains two, with six carbon atoms in each molecule [1]. Types of polyamide fibres are shown in Figure 1.

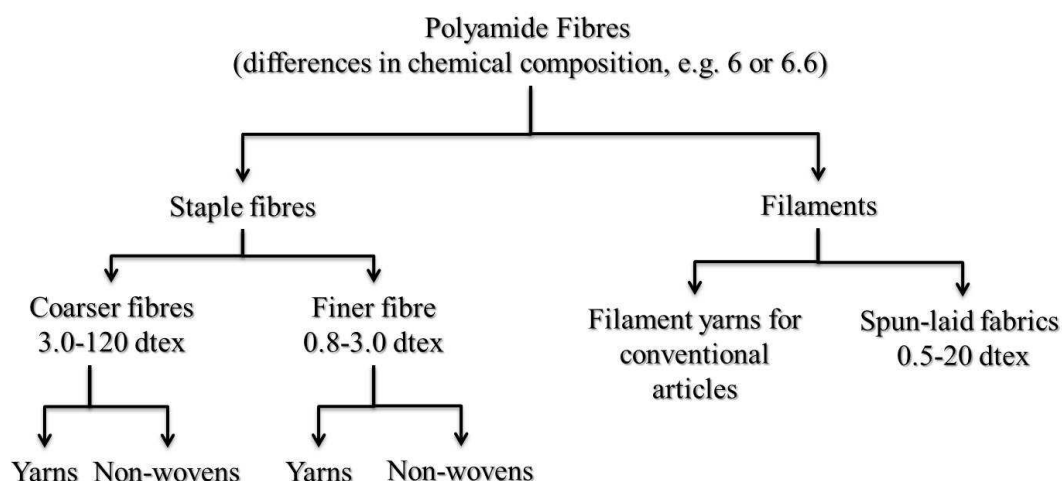


Fig. 1: Types of polyamide fibres [1].

The nylons generally are tough, strong, durable fibres useful in a wide range of textile applications. The distinguishing characteristics are being highly elastic, tear and abrasion free, low humidity absorption capability, fast drying, no loss of solidity in a wet condition, crease-free, rot and seawater proof. Some of the applications of

polyamides include fine stockings (for example nylon), outer sporting and motorcycle garments (for example Tactel, Cordura), female underclothes (for example Perlon) and parachutes.

History of polyamide fiber and its design advantage

The development of nylon started in 1927 by many researchers, notable among them was W.H. Carothers and P. Schlack. In the middle of the 1930's, American chemical company DuPont brought to market a polyamide called nylon. It was the first material fully obtained from basic chemical elements and had major implications in the textile and clothing domain. Polyamide 6.6 was first produced in the laboratory in 1935 by W H Carothers at DuPont, USA which started commercial production in 1938. The same year, I Farbenindustrie developed polyamide 6 in Germany. In 1939, the introduction of nylon into sheer stockings revolutionized the women's hosiery market. Silk and cotton were quickly replaced by this more durable and easy-care product. Nylon soon found its way into other end uses. In parachutes and fishing line, nylon provided a moisture- and mildew-resistant replacement for silk. In flak vests, nylon offered a strength and durability previously unattainable for protection against shell fragments and, when used as aircraft tire reinforcement, nylon enabled heavy bombers to land safely on improvised air strips. Today, as the global leader in nylon polymer, DuPont offers a wide range of nylon-66 polymer types for use in industrial, textile, and furnishing/floor covering applications [2]. Later, research activities on all types of polyamides like aliphatic, aliphatic-aromatic and fully aromatic polyamides were focused on (a) fundamental research that would provide the foundation for all future developments; development of different types of polyamides, their synthesis, manufacture and their suitability for use as a new fibre (c) Commercial production of the fibres and (d) Development of the properties and serviceability of the fibres.

Uses of polyamides

Initially, the textile industry focused primarily on space research and equipment for soldiers, and later extended to consumer applications. To this end, a series of new synthetic textiles and techniques for processing textiles were developed. A major milestone is the invention of active breathing membranes (such as Gore-Tex) [1]. Polyamides 6 and 6, 6 are the most widely used polyamides for fibres and for engineering materials. The properties of the polyamides (nylons), which include high strength, abrasion resistance, and resilience, make them very important in the manufacture of clothing and carpets. Polyamides account for about 5% of the total fibres used to make clothing which is more than either the acrylics or wool. However, it is substantially less than either cotton or polyesters. Other commercial polyamides like polyamides 11 and 12, and 6.10, are mostly used as engineering plastics, for example, in cars, and for making films for food packaging. They are used in films for their good balance between mechanical strength and barrier properties against oxygen, smells and oils [3]. For use as an engineering plastic, polyamides are often compounded with fillers, pigments, glass fibre and toughening agents to give specific properties to the polymer. However, for either continuous filament or staple fibres,

which are melt spun at very high speeds of about *ca* 6 km every minute, emphasis is on controlling the polymer chemistry and the way the yarn is produced. This is to ensure the production of the high quality material needed for specialized purposes. For example, the thread for use in stockings needs to be strong, as well as very fine, so the molecular mass and hence tensile properties of the polymer must be carefully controlled. The versatility of polyamides can be seen in Figure 2.

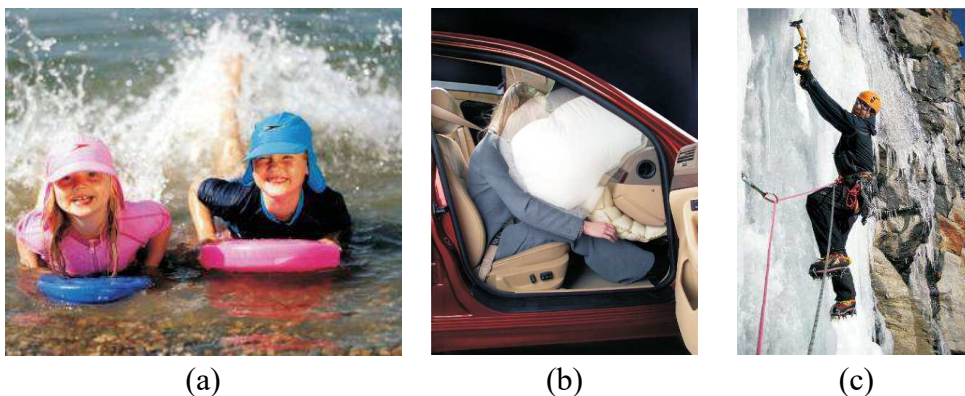


Fig. 2: (a) Children clothing (Pic courtesy: BASF); (b) Airbags for cars (Pic courtesy: Delphi Automotive) and (c) Climbing ropes (Pic courtesy: Tony Moody) [3]

Children clothing made of polyamide 6, impregnated with nanoparticles of titanium dioxide provides protection against UV radiation. Ropes made from polyamides are used by rock and ice climbers. They are not only very strong but they are also stretchy and thus reduce forces in the event of a fall, by spreading the duration of loading transmitted to anchors and to the body via the harness. Another important development is the use of polyamides to make safety airbags [3].

Global market for polyamides

Northeast Asia continues to be the centre of the world's nylon fibre manufacturing industry. In 2015, Asia accounted for nearly two-thirds of the world's nylon fibre output. In the past five years, production of nylon fibre in China has increased at about 7.6% per year. The only other region to exhibit positive growth over the same time frame was Southeast Asia. Most other Asian countries, such as Japan, South Korea, Taiwan, and India, experienced no growth or even declining production [4]. As nylon-producing regions, North America and Western Europe are expected to remain, at best, stable. Both are important nylon fibre consumers, but both regions are growing at below-average rates. Carpets and rugs account for 16% of the resin consumed and are expected to grow at only 0.7% per year. North America and Western and Central Europe continue to be the major producers of carpets and rugs, accounting for about 78% of the nylon fibre consumed. Regions with above-average annual growth rates for fibre consumption include the Indian subcontinent (about 3%), Northeast Asia (3%), and Southeast Asia (2.5%). Major regions with below-average annual growth rates include North America (0.6%) and Western Europe (0.6%) [4].

Textile and industrial filaments account for 80% of the nylon resin consumed in 2015 and expected to grow at about 2.5% per year for the next five years. Northeast Asia consumes 78% of the world's nylon fibre for textile filaments and 51% of the world's nylon fibre for industrial filaments. In both cases, China is the largest producer in the region. China's textile filament market is expected to be the fastest growing in the next five years, at about 4% per year [4]. Figure 3 shows the world consumption of nylon fibres. In the next five years, China will account for about 40% of the world's nylon production and 51% of the nylon fibre consumed globally.

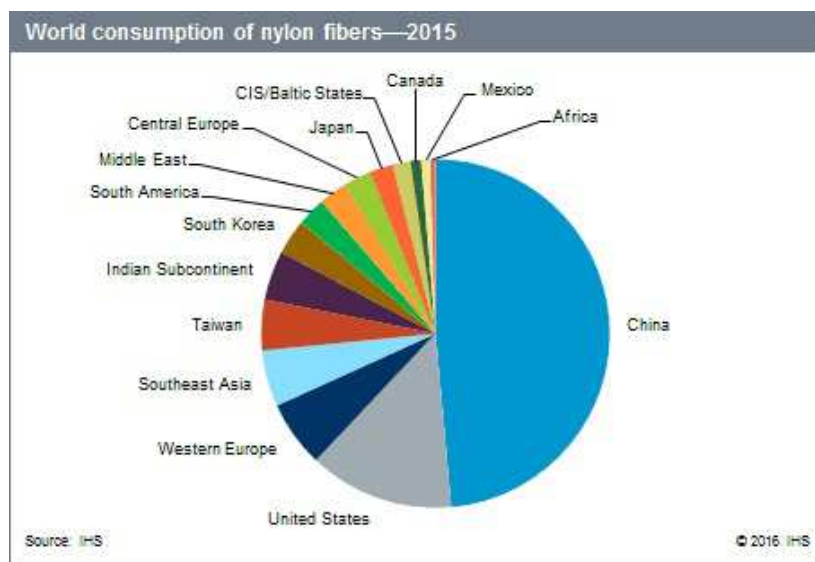


Fig. 3: World consumption of Nylon fibres (Source: IHS) [4].

China is expected to increase its production capacity for nylon by almost 7% per year, while consumption of nylon fibre is expected to grow at about 3.5% per year for the next five years. This growth will impact other regions or countries, particularly with declining imports of nylon 6 resin. Annual production of polyamides is shown in Table 1.

Table 1: Annual production of polyamides (in million tonnes) [3].

	<i>World</i>			<i>Europe</i>	
Polyamide 6.6	3.4			0.7	
Polyamide 6	4.3			1.2	
Caprolactam (monomer of polyamide 6)	<i>Europe</i>	<i>US</i>	<i>FSU</i>	<i>China</i>	<i>Rest of Asia</i>
	1.1	800	500	460	1.2

Chemistry and production of polyamide fibres

Polyamides are polymers which contain repeating amide, -CO-NH-, linkages. Proteins are examples of naturally occurring polyamides. The most popular aliphatic polyamides are often called nylons and these are linear, aliphatic polyamides. The nomenclature for the nylons is based on the number of carbon atoms in the repeating unit [3]. However, other manufactured polyamides are also important and these include an aromatic polyamide (e.g., Kevlar[®]) and plastics produced from carbamide

(urea). Polyamides are characterized according to the number of carbon atoms present in the structural unit of the molecule. Nylon made from condensation of a diamine and a dicarboxylic acid is classified according to the number of carbon atoms present in the amine and acid respectively. Thus, nylon formed by hexamethylene diamine ($\text{NH}_2(\text{CH}_2)_6\text{-NH}_2$) having 6 carbon atoms and sebacic acid ($\text{COOH}(\text{CH}_2)_8\text{-COOH}$) having 10 carbon atoms is generally referred to as nylon 6.10. Nylon, made from amino acid, is classified according to the number of carbon atoms present in the acid. It will have only one number. For example, Nylon 6 can be made from amino acid having 6 carbon atoms i.e., amino capronic acid or its condense product caprolactam. So, the numbers indicate the number of carbon atoms in the monomer taking part in the polymerization [2]. In general, the chemical structure of nylon is shown in Figure 4.

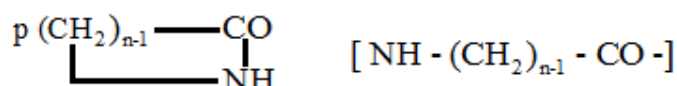
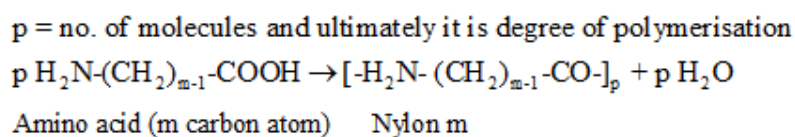
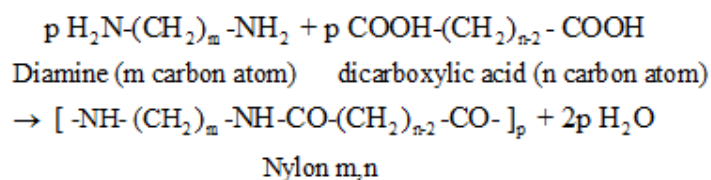


Fig. 4: Chemical structure of Nylons.

Types of polyamide fibres and their raw materials are shown in Table 2.

Table 2: Some polyamides and their raw materials [2].

Nylon	Raw materials
Nylon 4.6	1,4 diamino butane, Adipic acid
Nylon 6.6	Hexamethylene diamine, Adipic acid
Nylon 6.10	Hexamethylene diamine, Sebacic acid
Nylon 6.12	Hexamethylenediamine, Dodecanedioic acid
Nylon 3	Acrylamide
Nylon 4	2-pyrrolidane
Nylon 6	Caprolactam
Nylon 7	Lactum of heptonoic acid
Nylon 11	W-amino-cendecanoic acid
Nylon 12	Dodelactum

Molecular aspects of nylon fibers

Due to highly complexity in structure and orientation of Nylon fibres, it is challenging to prescribe a model that describes their fracture mechanics protocol or constitutive model to describe their behaviour. The primary and secondary bonds provide the intensity to bind the atoms. In polymeric materials, the covalent bonds are the responsible primary bonds, dissimilar to metallic and ionic bonds in other materials. The chemical structure is composed of hydrogen, nitrogen, carbon, and oxygen atoms which form a repeating unit. A schematic of this is shown below in Figure 5 [5].

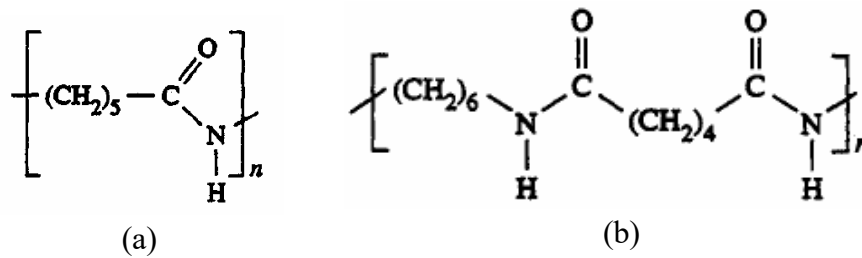


Fig. 5: (a) chemical structure of Nylon 6; (b) chemical structure of Nylon 6.6 [6].

Crystallinity in nylon fibres affects the fatigue and fracture performance significantly. Polyamides contain chain disentanglements among the atoms due to semicrystallinity. They remain semicrystalline because the long chains are entangled when melt and, upon cooling, cannot disentangle sufficiently rapidly to crystallize. In Figure 5, only two of the four chains are displayed. The difference between the polyamides nylon 6,6 and nylon 6 are given in Figure 6 and Figure 7 [5].

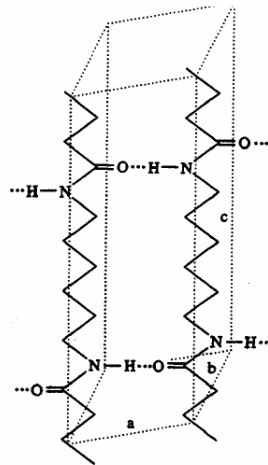


Fig. 6: Unit cell of Nylon 6.6 [7].

A molecule of nylon 6.6 penetrates each corner of the unit cell, and hydrogen bonding needs are satisfied [5]. The structure of nylon 6 is very similar to that of nylon 6.6. Additionally, the behaviour and morphological features of nylon 6 form a close resemblance to that of nylon 6.6. The structure of nylon 6.6 consists of two phases, in which there are crystalline and amorphous regions of the chemical structure. This semicrystalline nature is considered adverse in most circumstances, as it causes brittleness and premature fracture of the nylon fibres leads to reduced fatigue and fracture performance, which lowers the amount of useful energy that is available during the deformation process. It can be noticed from Figure 7 the discontinuities

produced by the amorphous regions and the ordered phases of the crystalline regions [5].

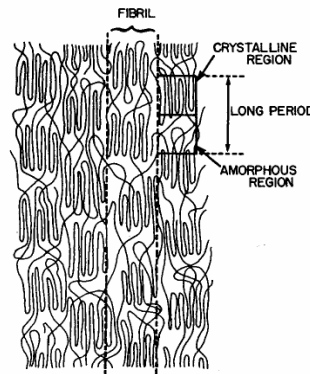


Fig. 7: Molecular arrangement of a drawn Nylon 6 fibre [8].

Production of polyamide fibers

The polyamide is melt spun and drawn after cooling to give the desired properties for each intended use. Production of nylon industrial and carpet fibres begins with an aqueous solution of monomers and proceeds continuously through polymerization, spinning, drawing, or draw-texturing shown in Figure 8 [9].

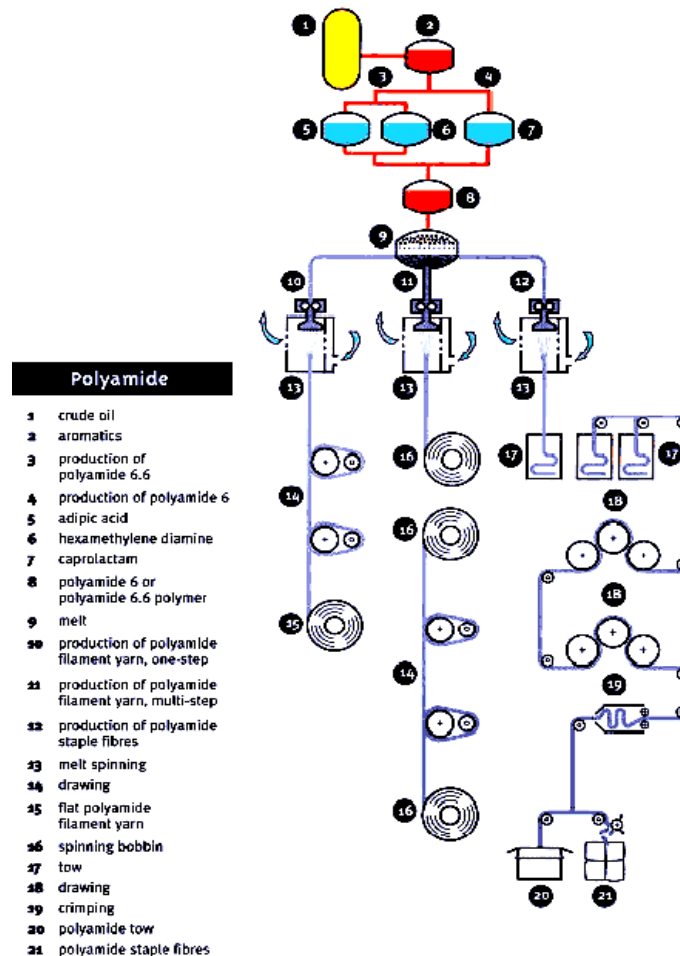


Fig. 8: Production process of polyamide (Source: IVC, Frankfurt) [9].

In melt spinning, the fibre-forming substance is melted for extrusion through the spinneret and then directly solidified by cooling. Nylon, olefin and polyesters are produced in this manner. The molten mass is forced through the holes in the spinneret by pressure pumps and metering pumps, after which it is pulled off in the form of filaments. They cool rapidly in the (air) blasting chamber and are then either baled or wound onto bobbins at a constant speed. The macromolecules are still randomly distributed in the filaments, which is why they are stretched so that molecules are more longitudinally oriented. Once they have this orientation, the filaments take on their characteristic physical properties and can be cut to the lengths needed to make the fibres. Then the filaments of staples are prepared to ensure that they retain their processing properties [1]. Melt spun fibres can be extruded from the spinneret in different cross-sectional shapes (round, trilobal, pentagonal, octagonal, and others). Trilobal-shaped fibres reflect more light and give an attractive sparkle to textiles. Pentagonal-shaped and hollow fibres, when used in carpet, show less soil and dirt. Octagonal-shaped fibres offer glitter-free effects. Hollow fibres trap air, creating superior insulation and loft characteristics [9].

Research on improvements of production of polyamide fibers

Orientation factor and birefringence of polyamide fibres

In the fracture behaviour of nylon 6.6 fibres, the orientation and birefringence provide an assessment to the degree of molecular axial orientation [10]. Hermans et al. [11] have provided a thorough analysis of the orientation factor, f , and its effects on axial alignment. Ziabicki and Kedzierska [10, 12, 13] proved that the birefringence of the as-spun fibres increases at a monotonic rate with the reciprocal of fibre diameter. Also, Ishibashi [10, 14] has provided an equation that describes how birefringence decreases with spinning temperature. This equation is described as:

$$\frac{d\Delta n}{dt} = A(\theta) \left(\frac{dV}{dx} \right) - \frac{\Delta n}{\tau(\theta)} \quad (2)$$

Here, $A(\theta)$ is an optical constant, $\tau(\theta)$ is the associated relaxation time, $d\Delta n/dt$ is the resultant speed of molecular orientation, and dV/dx is the velocity gradient along the spin line. A pictorial representation of the melt spinning apparatus used to develop this correlation is shown in Figure 9.

A theoretical framework developed by Shigemitsu et al.[15] is used for analysing polarized fluorescence intensity in an anisotropic polymer and verified its direct application to molecular orientation measurements in nylon 6 fibres. They proved that the fluorescence technique can be used to measure the effects and structural changes to nylon 6 under the drawing process. Figure 7 depicts a fibre that has undergone the drawing process. An extensive investigation by Lim et al. [10] on nylon 6 determined that molecules orient themselves preferentially either parallel or approximately parallel to the fibre axis because of the drawing process. Figure 7 also illustrates the randomness and unpredictability of the molecular arrangement in polyamides due to

the drawing process. Also, in reference to the effects of drawing on molecular orientation and birefringence, Ito et al. [16] have shown that molecular weight affects these factors significantly. From a comparison of tensile modulus vs. draw ratio, the researchers revealed that the draw efficiency of nylon 6 was greatly affected by the draw technique, pre drawn morphology, and molecular weight. They concluded that the draw efficiency increased with increasing molecular weight, with a tendency more prominent in the noncrystalline networks than crystalline networks. The effects of annealing on the structural characteristics of nylon 6 fibres were investigated by Murthy et al. [17]. This was done in conjunction with the drawing experiments in an effort to increase the crystallinity and crystalline volume. From experimental results, they deduced that annealing increases the crystallinity and crystalline perfection, and in addition increases the density of the fibre to a large extent. Figure 10 clearly demonstrates this effect. These consequences of the annealing process are due to the crystallization of the amorphous phase in the fibre, in contrast to the drawing process. This is one of a plethora of studies that have been conducted on single nylon filaments with the aim of increasing the structural and mechanical properties. It was an early research effort and relatively unsophisticated method with the aim of increasing microstructural attributes in high-performance nylon fibres. Some sophisticated methods to enhance the microstructure and physical properties of nylon fibres include high-temperature zone drawing (HTZD), in which the drawing process was performed in different temperature Phases [18].

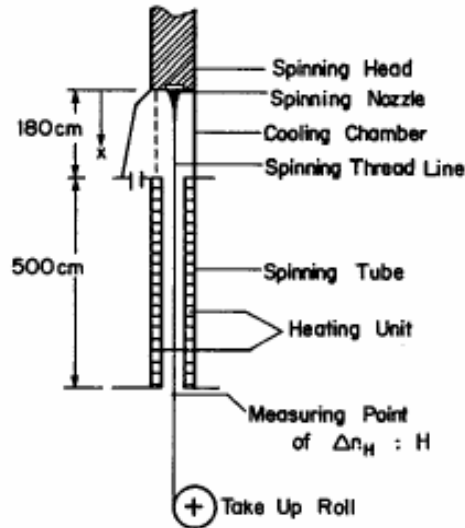


Fig. 9: Melt-spinning apparatus with heater hood installed 180 cm below the spinneret [14].

This method led to increased elastic modulus and fracture strength for the fibres. A later study applied high tension annealing (HTA) along with HTZD to obtain further increased crystallinity and mechanical properties [19]. Further augments in the elastic modulus and tensile strength were obtained, due to increases in the crystallinity and orientation factors. A summary of the improvements in tensile properties from HTZD

and HTA treatments for nylon fibres are shown in Table 3. Suzuki et al. [20] also developed a continuous zone-drawing (CZD) technique for enhancement of microstructural and mechanical properties of nylon 6,6 fibres. For this method, the crystallinity increased from 25% to 37% and the orientation factor increased dramatically for the fibres tested. As with the other methods, increases in the elastic modulus and fracture strength were obtained as well.

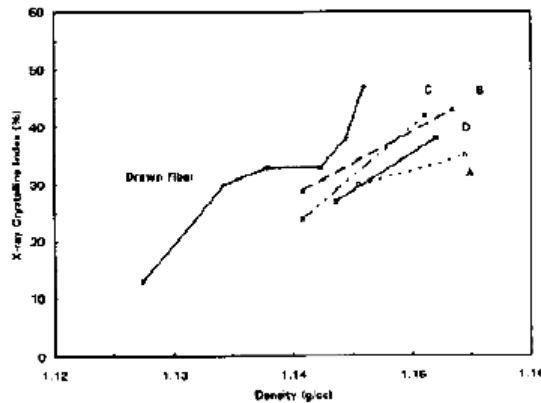


Fig. 10: Crystallinity vs. fibre density for Nylon 6 [17].

Penning et al. applied a network model to describe the deformation mechanisms in nylon 6 fibres under numerous spinning and drawing conditions [21]. They found that the network draw ratio can be discovered by superposition of the true stress-strain curves, and can be associated with fibre orientation using relationships for network deformation. These enrichment techniques can be used in conjunction with the fracture mechanics protocol to fabricate a robust, high-performance nylon fibre.

Table 3: Increase in tensile properties from HTZD and HTA treatments [19].

Fibre	Initial modulus [GPa]	Tensile Strength [GPa]	Elongation at break [%]
Original	1.1	0.18	385.9
HT-ZD1	4.7	0.54	34.5
HT-ZD2	6.4	0.75	12.9
HTA1	8.2	1.1	13.4
HTA2	9.5	1.18	12.6
HTA3	12.3	1.42	13.1

Anisotropy in nylon fibres

Ward and Hadley [22] have summarized that the mechanical anisotropy of solid polymers is determined by the factors like the structure of the molecular chain and the crystal structure, the molecular orientation and morphology and thermally activated relaxation processes in crystalline and non-crystalline regions. Lim et al. [10] confirmed that the existence of an anisotropic phase in a polymer is critical to the formation of fibrils. They also discussed how an anisotropic material possesses the intrinsic low entropy characteristic, which is reminiscent of fibrillar structures. These

fibrillar structures have been examined by many researchers and have been proven to materialize from amorphous fluids. Cook and Gordon [23, 24] determined the stress components at the crack tip in an anisotropic solid and confirmed that the crack propagates in the direction that displays the least material strength. Cherry and Harrison [23, 25] proved that in quasi-static deformation the two crack paths have equal probabilities of occurring when:

$$\frac{1}{R_{\parallel}} \left(\frac{d(u/X)}{dA} \right)_{\parallel} = \frac{1}{R_{\perp}} \left(\frac{d(u/X)}{dA} \right)_{\perp} \quad (3)$$

Here, R is the resistance of the material to crack propagation, u is the energy released during the deformation process, and A is the crack surface area. This study was actually performed on composite materials, in which they considered alternative cases of cracking perpendicular to fibres or cracking parallel to fibres. This is analogous to the case of single fibre deformation, where anisotropy in the longitudinal or transverse direction governs the crack path. A typical crack propagation path of an oriented polymer, provided by Kausch [26], is provided in Figure 11.

Nylon 6,6 is characterized as a transversely isotropic polymer. The compliance equation for transverse isotropy is given as:

$$s_{\theta} = s_{11} \sin^4 \theta + s_{33} \cos^4 \theta + (2s_{13} + s_{44}) \sin^2 \theta \cos^2 \theta \quad (4)$$

In essence, as molecular orientation in the fibre direction increases, Young's modulus in the axial direction increases dramatically. The converse to this statement also holds true, in that Young's modulus measured in the transverse direction decreases as the molecular orientation increases along the fibre axis [6]. The tensile modulus, when measured perpendicular to the chain direction, is considerably lower because of the weak secondary van der Waals' bonds between the chains.

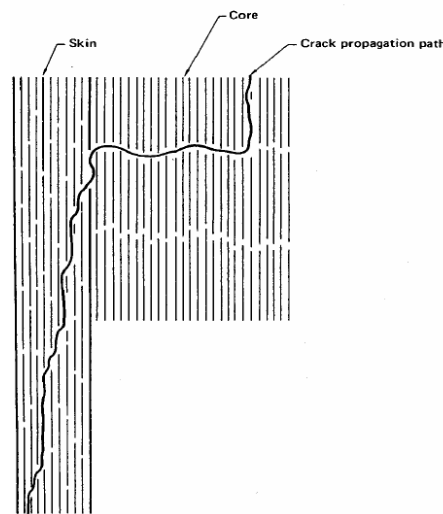


Fig. 11: Crack propagation path in typical polymeric fibre skin [26].

Hadley et al. [22, 27] determined the five elastic constants for oriented filaments of nylon 6.6, where the orientation was determined in terms of draw ratio and optical birefringence. Further studies showed that X-ray diffraction measurements were also pertinent to the determination of mechanical anisotropy. Figure 12 shows extensional (E_3), transverse (E_1), and torsional moduli (G) vs. draw ratio for nylon 6.6 single filaments. The figure also depicts theoretical estimates of these moduli based on simple aggregate theory for comparison to the experimental data. Murthy et al. [17] examined the effects of drawing and annealing on anisotropy in nylon 6 fibres using X-ray diffraction and other methods. Concomitant with the results from Ward and Hadley [22], they confirmed that the distinct ramifications of the drawing process are increases in crystallinity, crystalline perfection, and molecular orientation.

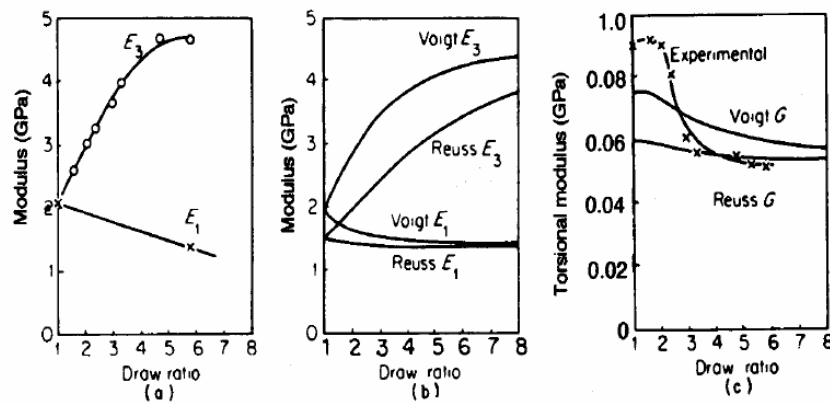


Fig. 12: Nylon filaments: extensional (E_3), transverse (E_1), and torsional moduli (G);

Figure 12 shows the comparison between experimental results and simple aggregate theory for E_3 and E_1 ((a) and (b)) and for G (c) [22]. In addition, they determined that the anisotropy in the amorphous region increases with increasing draw ratio of the sample. Both of these observations are shown in Figure 12 which displays the effect of draw ratio on orientation in the sample and amorphous anisotropy [5].

Preparation of polyamide fibres with antistatic properties

Synthetic fibres have the ability to build up static electricity charges create serious difficulties for manufacturers and users. Therefore, efforts of researchers have been directed towards the preparation of fibres with stable antistatic properties. Research has found polyether compounds are the most appropriate compounds for the antistatic treatment of polyamide fibres. Studies have been conducted with the objective of reducing the static charge of polycapronamide (Nylon 6 = PCA) by introducing an ethoxylated phenol with various numbers of ethoxyl groups compounds F4, F5, F20, and F30, containing 4, 15, 20, and 30 moles of ethylene oxide, respectively. The indicated compounds have not been investigated as internal antistatic agents. For comparison ethoxylated nonylphenol (NP) containing 4 moles of ethylene oxide were studied. Garvanska et. al. investigated the antistatic action of the ethoxylated phenol used as an internal antistatic in PCA as a function of its concentration, content of ethoxyl groups, and relative air humidity. The effect of alkyl radical content in the

aromatic ring on the antistatic properties of ethoxylated phenols was also examined. The additives were introduced during the ϵ -caprolactam preparation process, in the amount of 2-10% of the monomer weight. The synthesis was conducted in a thermostat block in an inert medium for 8 h: 2 h at 453°K and 6 h at 533°K. The modified PCA resin was analysed using thermographic studies and UV and IR spectra. Antistatic properties were determined by measuring the surface ρ_s and the bulk ρ_v electrical resistances at various atmospheric relative humidity on an electrometric instrument of the "Teralin III" type [28]. In Figure 13 the results of determinations of ρ_v and ρ_s for PCA modified with F4, F15, F20, and F30, at concentrations of 2, 4, 7, and 10%-by weight, respectively, at a relative atmospheric humidity $\phi = 25\%$. From the data in this figure, it is evident that the ethoxylated phenol has an antistatic action. This is supported by the decrease in ρ_v and ρ_s of PCA which has been modified by the introduction of 4% by wt. of compounds F4 and F15; ρ_v and ρ_s were reduced by 2.5 orders of magnitude. In increase in modifier content, the ρ_v and ρ_s values decrease; this is explained by an increase in the number of ions- which are carriers of static charges.

Some researchers [29-31] consider the limiting values of O_w and $0\sim$ as criteria of antistatic protection. It is considered that $\rho_v \leq 10^{10} \Omega \text{ m}$ and $\rho_s \leq 10^{13} \Omega$ guarantee distinctive antistatic properties. Considering these requirements and the values of ρ_v and ρ_s which have been obtained, even at a very low atmospheric relative humidity ($\phi = 25\%$), when compound F4 or F15 is used, one may consider that the PCA obtained will have distinctive antistatic properties. It was found that, with increase in degree of ethoxylation at a content of 4 to 30 ethoxy groups (Figure 13), the ρ_v and ρ_s values of the modified PCA rise significantly, that is, the static-proofing effect is diminished.

Based on the assumption that the transfer of static charges in polymeric materials is effected by ions [32, 33], and the mechanism proposed by Grady [34] according to which hydrogen ions perform this role in polyethers, the dependences of ρ_v and ρ_s on ethoxyl groups shown in Figure 13 may be explained by an intensification of the possibility of forming free hydrogen ions the carriers of static charges in the presence of an aromatic ring in polyether compounds. At the same weight concentration of ethoxylated phenol, with increase in the number of ethoxy groups from 4 to 30 (Figure 13), the number of acting macromolecules is reduced; there upon the relative content of aromatic rings is also reduced, which, in turn, leads to a decrease in content of mobile ions charge carriers and, consequently, to a decrease in the antistatic effect.

According to the foregoing, when there is an alkyl radical on the aromatic ring of the polyether compounds, one should expect a decrease in antistatic effect due to the negative inductive effect of these radicals, which will lead to a definite decrease in the degree of mobility of the hydrogen in the α -position relative to the phenoxide oxygen atom. This is supported by a comparison of the antistatic action of an ethoxylated phenol and an ethoxylated nonylphenol with an identical content of ethoxyl groups (Figure 13). The presence of the alkyl radical (in the present case, nonyl) on the benzene ring reduces the antistatic action of the ethoxylated alkylphenols. The ethoxylated phenols used have an antistatic action even at a low relative atmospheric humidity (Figure 14), the decrease in the ρ_v and ρ_s values of the modified PCA on

increase in relative humidity of the air depending on the absorption of moisture by the PCA matrix. The results of the present studies contradict the statements of [35, 36] according to which polyether compounds have antistatic properties at a high relative humidity, but agree with the opinion [34-36] that antistatic properties are displayed even at a low relative humidity.

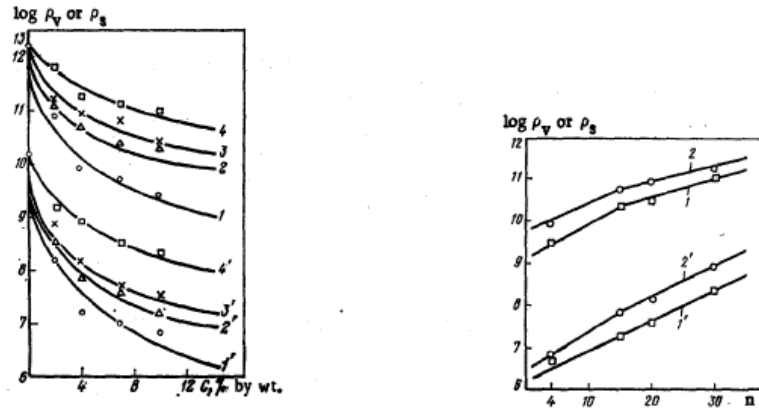


Fig. 13: (a) Dependence of surface electrical resistance, ρ_s , (1-4) and of bulk electrical resistance ρ_v (1'-4') of modified PCA on modifier content, C: 1, 1') F4; 2, 2') F15; 3, 3') F20; 4, 4') F30. (b) Dependence of ρ_s (1, 2) and ρ_v (1', 2') of PCA modified by ethoxylated compounds on content of ethoxy groups (n) at an atmospheric relative humidity of 25%: 1, 1') 10% by wt.; 2, 2') 4% by wt.

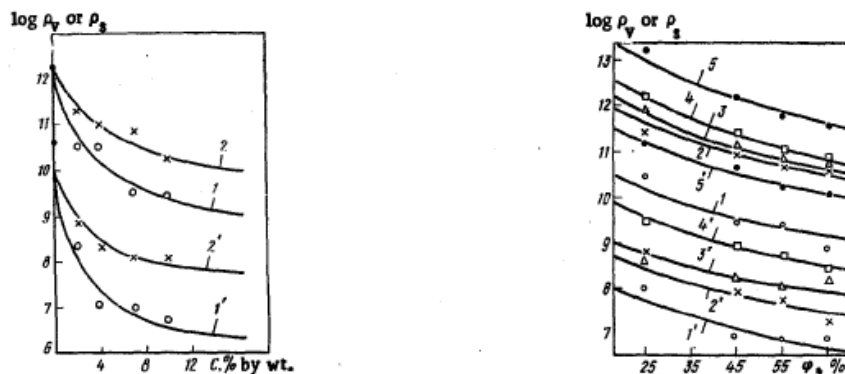


Fig. 14: (a) Dependence of ρ_s (1, 2) and of ρ_v (1', 2') of modified PCA on content, C, of additives F4 (1, 1') and NF~ (2, 2') at an atmospheric relative humidity of 45%. (b) Dependence of ρ_s (1-4) and of ρ_v (1'-4') of modified PCA at a modifier content of 7% by wt. and of ρ_s (5) and of ρ_v (5') of unmodified PCA on relative atmospheric humidity ϕ : 1, 1') F4; 2, 2') F15; 3, 3') F20; 4, 4') F30.

With increase in ethoxy group content, the resistance of the antistatic effect of the PCA fibres to water treatments is reduced. Probably [37], the oxyethylene groups interact with water by electron exchange wherein, with increase in ethoxy group content, the possibility of forming such bonds is increased. It is well known that polyether compounds have an antistatic action only in the case where they are not bonded with the polymer to form chemical bonds [13, 14]. Absence of chemical bonds was determined by use of UV and IR spectra. To do this, the modifier - the ethoxylated phenol--was removed from the specimen of modified PCA fibre by the

use of a selective solvent. It was found that the UV spectra of the modifier coincide with the spectra of the modified polymer, but the UV spectra of the unmodified PCA coincide with the spectra of PCA from which the modifier has been removed. The results of studies of the IR spectra proved to be similar. The presence of the modifier (an aromatic ring) is followed from the absorption bands at 830 cm^{-1} . At 1500 and 1600 cm^{-1} , the aromatic ring is also recorded, but the signals are weaker in this case. In modified PCA from which the modifier had been removed, no aromatic ring was recorded; its spectrum completely coincides with the spectrum of unmodified PCA. No changes in the form or position of the endothermic peaks in modified or unmodified PCA were observed when differential thermal analysis (DTA) was carried out; nor was the presence of a chemical bond between the ethoxylated phenols and the PCA matrix detected. The resistance of the antistatic effect to a fivefold water treatment was determined after laundering in a solution of a nonionogenic surface-active compound at a concentration of 1 g/liter at 40°C for 150 min (single cycle). It was found that ethoxylated phenols with low ethoxy group content (F4) have an antistatic effect which is resistant to water treatments is show in Table 4.

Table 4: Antistatic properties

Modifier	ρ_v [$\Omega\text{ m}$]	ρ_{sI} [Ω]
-	$3.0 \cdot 10^{12}$	$2.7 \cdot 10^{14}$
F4	$5.8 \cdot 10^9$	$6.5 \cdot 10^{11}$
F15	$2.8 \cdot 10^{10}$	$3.2 \cdot 10^{12}$
F20	$5.8 \cdot 10^{11}$	$4.5 \cdot 10^{13}$
F30	$7.8 \cdot 10^{11}$	$6.2 \cdot 10^{13}$

Processing and structure evolution in polyamide 6,6 fibres

Nylon-6.6 (polyhexamethylene diamine adipamide) is a polyamide made from adipic acid and hexamethylenediamine by polycondensation. The resulting polymer is extruded into a wide range of fibre types. The fibres are drawn, or stretched, in a process that increases their length and reorients the material's molecules parallel to one another to produce a strong, elastic filament. The thermo-plasticity of nylon permits permanent crimping or texturing of the fibres and provides bulk and stretch properties. The nylon developed by Carothers at DuPont was nylon 6,6. Because of the importance of starting out with equal amounts of the two reactants, salts of the diamine and of the diacid are made and then used in the commercial synthesis of nylon 6,6 [2].

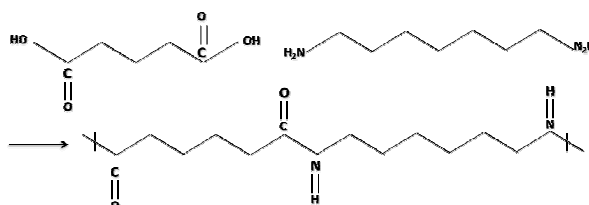


Fig. 15: Chemical structure of Nylon 6.6.

Polyamide 6 is made from caprolactam, and polyamide 6.6 from hexamethyldiamine and adipic acid. Chemical structure of nylon 6.6 is shown in Fig. 15. For fibre production, the resulting polyamide has to have the capacity to be spun into filaments, i.e. it must have the capacity to be melted without decomposing and to be forced through a jet the molten mass must be such that the filaments that are still ductile when formed do not break during cooling. Certain conditions must be met, one of them being a minimum prescribed length for the macromolecule. These nylon polymers form strong, tough, and durable fibres useful in a wide variety of textile applications. The major differences in the fibres are that nylon 6.6 dyes lighter, has a higher melting point, and a slightly harsher hand than nylon 6 [1].

Advantages of Nylon-6.6

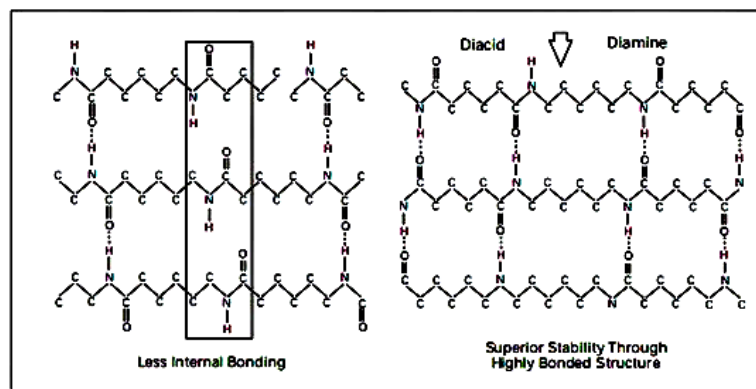


Fig. 16: The molecular structure of nylon 6 versus nylon 6.6 yields enhanced properties.

Nylon 6.6 is superior in many applications to Nylon 6—the other large volume nylon—due to its outstanding dimensional stability, higher melting point, and more compact molecular structure (see Fig. 16). Nylon 6.6 exhibits only about half the shrinkage of Nylon 6 in steam, for instance. And, with a less open structure, the Nylon 6.6 fibre has good dye wash fastness and UV light-fastness, and excellent performance in high-speed spinning processes. Typical advantages of Nylon 6.6 over Nylon 6 are its high tensile strength, excellent abrasion resistance, and higher melting point. Nylon 6.6 provides high tensile strength for tough fibres at fine deniers, excellent performance for tyre applications, and high-speed mill processing. Excellent abrasion resistance makes it ideal for use in carpets, upholstery, and conveyor belts. The rubber industry takes advantage of the higher melting point of Nylon 6.6 in high-temperature tire curing. A high melting point also results in a fibre with high stretch and recovery in false-twist textured yarns (e.g., hosiery and socks) and thermal stability in high-temperature coating operations.

Nylon 6.6 fiber production

The processing of nylon usually begins by conditioning the Nylon 6,6 chip, with or without an increase in the as received molecular weight. The chip is then melted, usually in a screw-type extruder, and spun into filament form. The filaments are then

packaged in a process that may include drawing, bulking, or cutting into lengths of staple [2].

Preparing nylon 6.6 chip

Chip is normally conditioned in an inert atmosphere at temperatures in the 120–180°C (248–356°F) range. Processors may employ higher temperatures to increase molecular weight, especially for industrial uses. Both batch- and continuous-type conditioners may be used. It is important to avoid excessive exposure of the chip to oxygen, which may lead to degradation and yellowing of the product.

Remelting nylon 6,6 chip

Remelting is normally performed in a single or twin screw-type extruder, although the melting can be done in a heated grid-type melter. Single screws are preferred for smaller spinning plants because of their simplicity. Twin screws are preferred for larger installations or when more extensive mixing during remelt is required. Equipment must have the capability of heating the polymer to 280–290°C (536–554°F). Handling of the Molten Polymer Nylon 66 may produce undesirable cross-linked material (gel) if processing temperatures and holdup times are not properly maintained. Care must be taken to eliminate areas of stagnation in the screw and in the polymer piping. Good engineering practices require the application of optimum shear rates and frequent mixing of the melt. Conversion of molten polymer to final product form depends on the wide variety of nylon 66 products and the range of processing equipment available. In general, most modern filament-producing equipment will process nylon 66 polymer adequately [2].

Preparation of the monomer

Adipic acid (ADA) and hexamethylene diamine (HMD) are used as raw materials for Nylon 6.6 polymer. The schemes of preparation of adipic acid and hexamethylene diamine.

Manufacture of adipic acid

Mostly cyclohexane (CH), cyclohexanol (CHL) and cyclohexanone (CNH) are used to obtain adipic acid (ADA). For oxidation, only nitric acid and oxygen can be used economically. The most important process is the oxidation of cyclohexanol with 50% nitric acid at 60-70°C. In a stainless steel kettle the cyclohexanol is added to the acid under cooling and stirring, the acid is crystallized from water. The yield exceeds 85%. The oxidation of cyclohexanone with nitric acid requires higher temperatures. Also cyclohexanone is oxidized in the presence of acetic acid as diluent and with 0.1% manganese acetate or nitrate at 80-100°C. The yield is about 70% [2]. The simplest method for the production of adipic acid is direct oxidation of cyclohexane. Most useful is the catalytic oxidation with air by soluble Mn or Co catalysts at 120-150°C. The reaction is interrupted at a conversion of 10-15% and leads away to a mixture of cyclohexanol and cyclohexanone in equal amounts with adipic acid, cyclohexanol adipate, and lower aliphatic acids. The unchanged product is recycled

and the crude oxidation product fractionated. Since cyclohexane is an important petrochemical product, production of cyclohexanol and cyclohexanone is based on this process.

Manufacture of adiponitrile

Adiponitrile is the intermediate for the production of hexamethylene diamine. It can be produced by different methods:

Vapour phase from adipic acid and ammonia

This method involves condensation from ammonia and adipic acid in the vapor phase. Adipic acid is vaporized with an excess of ammonia gas (mol. ratio 20:1) at 350°C over a catalyst of boron phosphate. The reaction is endothermic at 57 cal/mole. The yield is 88%.

Liquid phase process

In a liquid phase process, ammonia is introduced in molten adipic acid at 200-250 in the presence of such alkyl or alkyl phosphates catalysts like 0.1 -0.5% phosphonic acid or boron phosphate. The yield is around 88%.

1, 4 dichlorobutane and sodium cyanide

1, 4 Dichlorobutane can be obtained by addition of chlorine to butadiene. This can be converted to 1, 4 dicyanobutane by NaCN. Dry NaCN is mixed with adiponitrile as diluent and the calculated amount of 1, 4 dichlorobutane is added at 185-190°C. By addition of water, the oily layer is distilled. The yield is about 95%.

Electrohydro dimerisation of acrylonitrile

By electrohydro dimerisation, yield will be 82%. The pH will be 9 and the current density will be 2 to 30 MA/dm². The cathode potential was found to be independent of pH above 2.5. The overall reaction will be



Manufacture of hexamethylene diamine

Hexamethylene Diamine (HMD) is manufactured exclusively by the hydrogenation of the dinitriles. Palladium is used as catalyst. Another effective catalyst is cobalt oxide mixed with calcium oxide. In all cases, the reaction must be carried out in the presence of excess ammonia. Pure HMD is a colourless crystal, melting at 40°C, B.P. 100°C, soluble in water, and alcohol.

Polymerisation

Nylon-66 production from adipic acid and hexamethylene diamine comprises four steps: (1) Salt preparation (2) Polycondensation (3) Melting. (4) Extrusion. High molecular weight Nylon 6.6 is only obtained if equimolecular amounts of the components are used. An excess of the components would terminate the chain by

formation of an acid or amino end group. So stoichiometric portions of hexamethylene diamine and adipic acid must be used (amine to acid of 1:1). For this reason, the salt of 1 mole adipic acid and hexamethylene diamine (AH salt) is used as intermediate. The hexamethylene diamine is used as a 60-70% solution and the adipic acid as a 20% solution. The monomers are fed and mixed in the mixer and transferred to the pre polymeriser. Methanol is added and the reaction takes place. Methanol can be refluxed. The separated salt is centrifuged and washed with methanol. It is stored as a 60% solution in distilled water. It is a snow white crystal (melting point is 190°C). Owing to all these constraints, batch processing is used [2]. The concentrated salt solution is then fed to the polymerisation reactor, where the second-stage of the reaction begins. 60% Aq. Solution of the salt in distilled water, 0.5% acetic acid (stabilizer) is pumped into an autoclave. Increased temperature and pressure are used to initiate the polymerisation reaction. So the autoclave is heated to 275°C. The pressure is generally kept constant (1.8 MPa). Before the reaction, the autoclave is purged with very pure nitrogen (less than 0.005% oxygen) to avoid degradation and discoloration of the polymer. When the temperature of the batch reaches 275°C, the pressure is allowed to fall to atmospheric pressure. The batch is held at 270°C and atmospheric pressure for half an hour to allow removal of the water vapour. The heating is continued until all water has been distilled off. Towards the end of the distillation, the autoclave is evacuated. The polymer is obtained as a clear, low-viscous melt which is removed from the autoclave by pressure with pure nitrogen. The melt is extruded through the bottom of the reactor to form a ribbon. It is solidified and cooled in cold water cut into chips and dried. The dried chips are stored in a storage hopper in a similar manner like that of Nylon 6 [2].

Spinning

Nylon has sufficient stability of the melt and adequate viscosity. So, it can be spun in the molten state with usual velocity (up to 2000 m/min). The polymer chips are fed to the hopper and then it is melted and homogenized in an extruder. The molten polymer after filtration is passed to the spinnerets. The melt is pumped through this system and solidifies immediately on contact with air. Cross air flow is used for solidification. The melting temperature for spinning is around 300°C. After spinning like nylon 6, the flows are stretched to get the desired elongation. The different parameters which can be varied to influence fibre properties like Mass output, Winding speed, Spin draw ratio, Draw ratio and Draw temperature. The properties to be considered are tensile strength, elongation, modulus, crystallinity and orientation [2].

Production Process

Nylon 6.6 fibres for use in textiles, carpet, and tire cord are produced by extruding molten polymer through spinnerets and stretching to their final thickness and weight. The polymer melt must be homogeneous, gel free, and without oversize additive agglomerates to achieve high quality fibre and yields. Filtration of the process feed streams, additive slurries, and polymer melt itself are essential to help eliminate fibre

breaks and enhance fibre strength and uniformity. Not only is fibre quality improved, but production rates can be higher with less process downtime.

- 1) Hexamethylene diamine and adipic acid - Ultipor GF Plus® grade U2-20Z is recommended for this feed stream for promoting an efficient nylon salt reaction.
- 2) Water feed to the nylon salt reactor should be filtered with Ultipor GF Plus grade U2-20Z cartridges to remove harmful minerals that will contaminate the nylon salt intermediate.
- 3) For the nylon salt solution a Pall Rigimesh® grade K backwash filter is recommended if contaminant concentration levels are high, followed by an Ultipor GF Plus grade U2-20Z polishing filter. These filters remove extrinsic particulate contamination such as iron oxides and other debris which will reduce polymerization efficiency and fiber quality.
- 4) For the TiO₂ slurry in water, Profile® II cartridge grades RF100 to RF200 (rated 10-20 µm absolute) are recommended for Nylon 6.6 manufacture. The makeup water should also be filtered with Ultipor GF Plus grade U010Z before mixing with TiO₂. Filtration of TiO₂/water slurry stops passage of large particles which could reduce the tensile strength and quality of the finished fiber.
- 5) The final Nylon 6.6 polymer “transfer line” filter typically consists of high pressure pleated PMF™ elements 10-40 µm depending on the denier fiber being produced. For the finest denier nylon fiber grade FH100 10 µm absolute is recommended. *PMF* elements ensure superior quality nylon fiber, and the ability to spin at high draw off rates with near "zero breaks."
- 6) Screen packs at the spinneret are commonly used to remove oversized particles and gel which might plug the spinneret die. Where the flow versus pressure drop will allow, FS or FH Series PMF media in the 10-40 µm range with Rigimesh support is recommended.
- 7) Deionized Water used in preparing additive slurries, nylon salt solution, and spin finishes should be filtered both upstream and downstream of the mixed bed deionizers and at point of use in the nylon process to ensure consistently clean DI water free of iron and other foreign matter. Profile II 10 µm cartridges are recommended in the utilities area and 2 µm at point of use [38].

Processing and structure evolution in polyamide 6 fibres

In the last few years, production of polyamide fibres have undergone structural changes caused by the market situation and competition between polyamide 6 (PA 6) and polyester fibre manufacturers. Increasing profitability, reduction of expense and improvement in product quality are the drivers for production. High, in comparison to other polymers, prices are only real for special types of fibres (micro, multifilament, non-round section) or fibres with special additives that modify the matrix to improve the existing properties of the fibres (dyeability, flame-resistant properties, light fastness, thermal stability, etc.). Fibre spinning efficiency also increases. The other important factor in increasing the competitiveness of polyamides is reduction of the cost of raw materials [39].

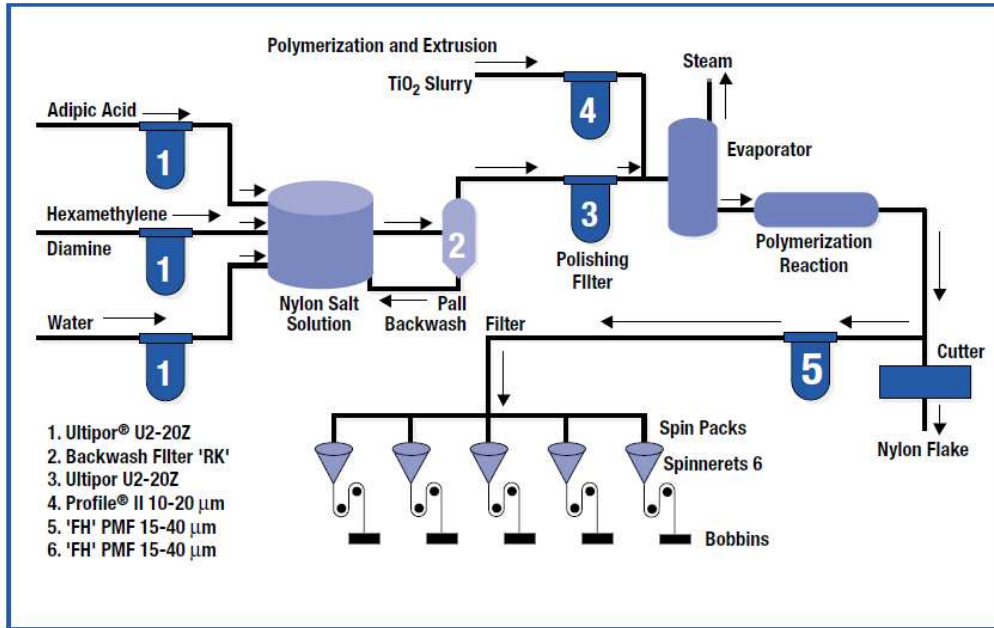


Fig. 17: Schematic of production process of Nylon 6.6 [38].

Manufacturing of Nylon 6

The raw material for manufacturing Nylon 6 is coal. Cyclohexanone oxime is produced by a series of chemical reactions on coal. Cyclohexanone oxime is then treated with sulphuric acid to form caprolactam. The caprolactam is a monomer with 6 carbon atoms that are polymerized to form chains of caprolactam. Polymerization is done by gently heating it in a steam – jacked stainless steel vessel. The solution is stabilised as a super polymer under constant steam and pressure. Nylon may be delustered by adding the delustering agents like titanium di oxide, barium sulphate, zinc oxide, and zinc sulphate. The molten nylon 6 polymer is allowed to flow onto a slowly revolving casting wheel. These are sprayed with cold water, which hardens it into milky white ribbons. The ribbons are transformed into flakes that are sent for spinning and are then drawn into the fibre form [2].

Spinning

Spinning of the nylon fibres is carried out with melt spinning. There are two methods of melt spinning are grid spinning and extruder spinning. Grid spinning is employed for the production of finer filaments. The nylon flakes are made to fall on a hot grid that melts the nylon flakes. The molten nylon is pumped through a sand filter to the spinneret. The type of filament produced depends upon the number of holes on the spinneret, the size and the shape of the holes. The molten nylon as extruded from the spinneret solidifies and forms filaments as exposed to the air. Extruder spinning is generally used for heavier yarns. The nylon chips flow by gravity into a device that forces them by screw action through the heated zones. The combined action of the heat and screw pressure melts the chips. The molten polymer is then extruded through the spinneret, which solidifies when the polymer comes in contact with the air.

Drawing

The filaments obtained from spinning are stretched by drawing process. The drawing process is accomplished in two stages: unwinding the yarn from one godet, or wheel, winding it onto another godet that is rotating much faster. The speed of the second wheel determines the amount of cold-drawing or stretching. The yarn from the second godet is wrapped on a cylindrical tube called a pirn. The filaments can be stretched from 2 to 7 times their original length. The molecules in the filament structure straighten out, become parallelized, and are brought very close together [2].

New production technologies

Advanced technologies that are reliable in continuous use are required for manufacturing a high-quality polymer. Production of PA 6 includes stages of polymerization, extraction, and drying. Economical production implies the possibility of using extractants. For the new process, it is necessary to use special additives. The basic stages of the actual process and possible alternatives are examined below.

Polymerization

The concept of a two-stage reactor (Figure 18) which replaces the single-stage process (with a U-shaped tube reactor) used previously for production of a polymer with medium viscosity was used for polymerization of caprolactam. The two-stage process has the following advantages:

- preliminary and final polymerization allows manufacturing PA-6 in a wide viscosity range in the first reactor; the viscosity is regulated by changing the pressure in the second reactor; this concept increases the flexibility of the line;
- the product processing time can be significantly reduced due to the higher degree of conversion, especially in the first polymerizers;
- the decrease in the product residence time in the reactor allows designing reactors of smaller volume: for a given production capacity, the reactor diameter can be decreased, ensuring flow close to ideal “cork-like flow;”
- the stable polymer requires sufficient processing time in the final polymerizers to attain thermodynamic equilibrium; due to the “cork-like” flow, homogeneous molecular-weight distribution is attained;
- the coefficient of variation of the viscosity of the polymer is much lower than in the tube-reactor process due to the kinetics of the reaction and optimization of heat and mass transfer; the water content in the system can be regulated during the ring-opening cycle in the first polymerizers and in polycondensation in the final polymerizers; this parameter probably significantly affects the stability of the spinning process [39].

The advantages of this technology are short product residence time in reactor, wide range of viscosity values, improved design guaranteeing cork-like movement of polymer and homogeneous molecular-weight distribution [39]. The two-stage polymerization technology is used on the largest production line in the world with a

unit capacity of 200 tons/day, constructed by Zimmer AG. The company's design for a unit capacity of 300 tons/day has been developed and prepared for implementation.

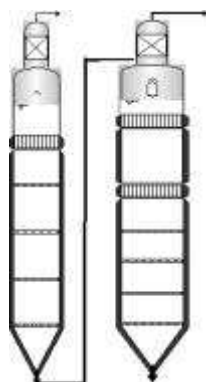


Fig. 18: Diagram of two-stage polymerization reactor.

Extraction

During polymerization, only approximately 90% of the caprolactam is converted into PA 6. The remainder consists of extracted substances which must be removed from the polymer. Extraction is realized in a counter current of water in an extraction column through which the granulate moves by gravity. A low content of extracted substances in the granules improves spinning by reducing the so-called “smoking” effect. Economical production must ensure a high content of extractable substances in the extracted water to reduce the expense of evaporating the water in reusing them. This is achieved by using specially developed inserts that separate the extractor into sections. Equilibrium distribution of extracted substances in water and granules is attained in each section. In addition, back flow of extraction water into the lower part of the column is prevented. For output of more than 100 tons/day, multistage extraction is expedient, since it ensures a higher rate of movement of the granules relative to the flow rate of the water, and this increases the efficiency of the process.

Drying

Granules ready for spinning must be dried to a water content below the thermodynamically equilibrium content. This takes place in the drying column using nitrogen as the drying agent. Surface moisture is removed from the granules in the upper section of the column, while bound moisture is distilled off in the lower section, and two intakes are provided for this reason. In drying at high temperatures, polycondensation in the solid phase (SSP) is possible, for which the same drying column design is appropriate. Nitrogen circulates in a closed cycle with an oxygen content of less than 1 ppm. Nitrogen inserts (inputs) guarantee uniform distribution of the gas over the diameter of the tube, ensuring the same moisture content in the granules. The combination of very stable viscosity with a low water content is a necessary condition for quality and high-efficiency spinning. The design of the distribution inserts also ensures uniform movement of the granules, which allows reducing the working temperature slightly and excluding thermal degradation of the granules. A drying process with output of up to 100 tons/day is used. Lines with individual output of up to 130 tons/day are proposed to further decrease investments.

Regeneration

Polyamide plant requires an efficient regeneration system. In selecting an economic and ecological regeneration design, it is necessary to consider the area of application of PA 6, taking into account the required quality indexes and the type of material that must be regenerated: extracted substances, wastes in spinning, etc. [39].

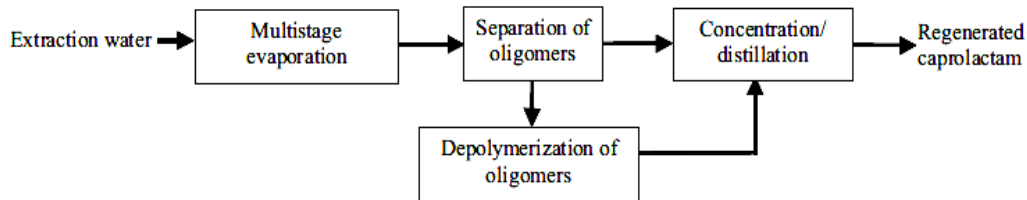


Fig. 19: Diagram of extraction water processing and oligomer depolymerisation [39].

Extraction water is used as raw material and the end product is regenerated caprolactam. This is a continuous process. The major advantage of this method are its economical production that produces highest quality of caprolactam [39]. The simplest and most economical design provides for multistage evaporation of extracted water. A concentrated solution is fed back into the preliminary polymerizers. The unfavourable effect of this technology is that it results in low-quality PA 6 due to the high content of extracted substances. This technology is appropriate for production of carpet twist and engineering plastics. However, this technology has not yet been approved for manufacture of high-quality fine textile fibres (basically mat fibres). When the plant has different polymerization lines, the concentrated solution can go into any of the lines. With the elevated requirements for the quality of PA 6, for example, for production of fibres of low linear density, use of continuous multistage extraction is recommended. In addition to extraction of water, this technology includes an additional treatment (Figure 19) in the oligomer separator, caprolactam vapours are separated from the concentrated solution of oligomers; the oligomers undergo hydrolysis to obtain monomeric caprolactam; subsequent chemical treatment is used to improve its quality.

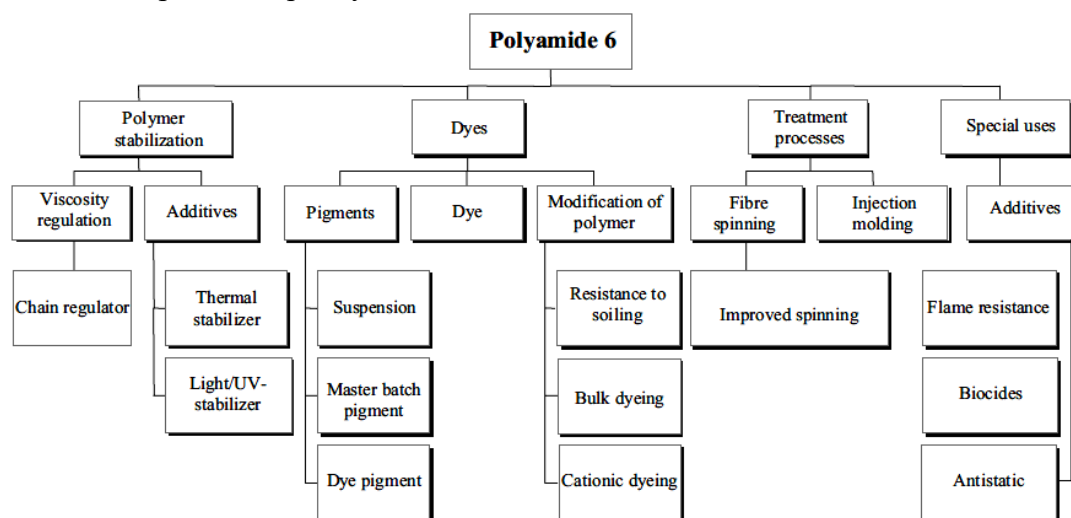


Fig. 20: Modification of PA 6 used by Zimmer AG [39].

Multistage distillation results in caprolactam of the highest quality. Caprolactam regenerated with the described technology can be used for production of polyamide for any area of application. This regeneration technology is a constituent part of the polymerization plant built by Zimmer AG which is successfully operating in Taiwan. All of the mentioned regeneration systems are operating continuously, a key factor for attaining a polymer of the highest quality. The reliability and ease of controlling the continuous regeneration process should be emphasized. The negative experience in operating old regeneration units, the “dirty back alleys” of polymerization units, is receding into the past. The existing designs can be supplemented by solid waste treatment using depolymerisation devices.

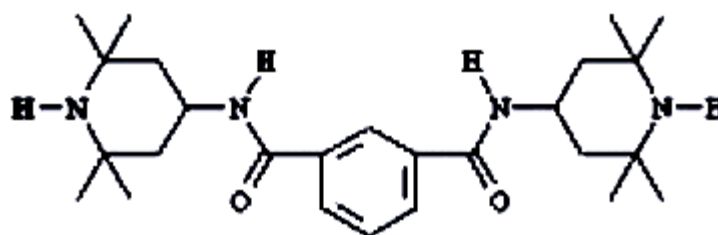


Fig. 21: Chemical structure of Nylostab S-EED additive [39].

Additives

As noted previously, modification of polyamides guarantees significant market advantages for them. Manufacturers and suppliers of the technologies are concentrating their efforts on developments in this area. Zimmer AG uses a large variety of special additives. The modifications made by the company are shown in Figure 20. Special attention is focused on modifications that improve the spinning process. ASP-PA6 technology improves product properties and increases production efficiency. The overall strategy for development of plants in accordance with market requirements can be broken down into several directions like (a) ensuring high melt stability and decreasing its viscosity in spinning; (b) improving the properties of the fibres, for example, increasing the strength, thermal stability, and light resistance and (c) improving spin ability, increasing the number of full-weight packs, and increasing the spinning speed. All of these goals are attained with the combination of monomeric additives called ASP-PA6. It is necessary to distinguish one of these components — Nylostab S-EED, since it appeared on the market comparatively recently. The chemical structure of this component is shown in Figure 21. It belongs to the group of new amine light stabilizers (hindered amine light stabilizers, or HALS). Nylostab S-EED not only improves the light resistance of the polymer but also softens the extrusion process by acting as a lubricant, enhances the dye affinity of the polymer matrix (due to the presence of amino groups), and improves the thermal stability of the polymer. This is a real multifunctional additive. Nylostab S-EED, manufactured by Clariant, can be added both in the polymerization and in the processing stage. However, addition in the polymerization stage has advantages: finer dispersion and more homogeneous distribution in the fibres increases its effectiveness [39].

New methods for Nylon 6 production process

Table 5 indicates the main methods [41-51] for Nylon 6 with the chief researchers and the maximum values of modulus (E) and tensile strength (σ) in the order of the publications. There are many interesting methods in the list, for example, the spinning of mixture of nylon 6 and lithium halide by Ciferri et al. [42] and Ward et al., [44] the plasticization with ammonia or iodine by Porter et al., [43, 48] and the dry spinning of nylon 6 solution in formic acid/ chloroform by Pennings et al. [47]. However, the attained moduli are still low; even the maximum value in Table I is only 12.7% of the crystal modulus along molecular chains of 165 GPa [52]. To overcome this situation, Kunugi et al. [40] had applied the vibrating hot-drawing and zone-annealing method to the Nylon 6 fibre, which succeeded in a further improvement of the mechanical properties.

Processing and structure evolution of other polyamides

In addition to the popular polyamides like Nylon 6 and Nylon 6.6, there are several other polyamides which have been introduced for use as fibres in specialty applications where certain combinations of properties are desired. The major specialty nylons include nylon 3, nylon 4, nylon 5, nylon 6.10, nylon 7, nylon 8, nylon 11 and nylon 12 [1].

Nylon 3

Nylon 3 polymers are highly crystalline, with melting points in the region of 300°C. It is made by self-condensation of the lactams of ϵ -amino acids. Nylon 3 has high molecular weight and may be obtained using polymerization techniques. Decomposition tends to occur at the high temperatures needed in melt spinning. Nylon 3 polymers are difficult to dissolve, but solutions have been prepared using mixtures of methanol and calcium thiocyanate, and fibres have been wet-spun from these solutions [53].

Nylon 4

Nylon 4 fibres are spun from polypyrrolidone. Fibres spun from Nylon 4 polymer with characteristics as speciality polyamide fibres [53]. It has reduced tendency for build-up of static electricity and has improved fabric comfort. Nylon 4 is susceptible to oxidation and is sensitive to hypochlorite bleaches. Fabrics are easy to launder and dry easily. Its chemical structure is:



Nylon 4 may be obtained by polymerization of 2-pyrrolidone in the presence of alkali catalyst. It has a higher melting point and it tends to decompose readily at temperatures above 265 °C. Melt spinning may be carried out with difficulty. The process describes the changes in superstructure and mechanical properties with the processing.

Table 5: Various spinning, drawing, and annealing methods for Nylon 6 fibres and films [40].

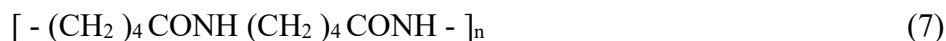
Year	Method	Chief Researchers	E (GPa)	σ (GPa)	Ref.
1979	Zone drawing/zone annealing	Kunugi	8.3	1.0	1
1979	Spinning of mixture of nylon with LiCl/LiBr/drawing/annealing	Ciferris	14	—	2
1979	Plasticization with NH_3 /coextrusion	Porter	13	0.6	3
1981	Spinning of mixture of nylon with LiCl/drawing/annealing	Ward	8	—	4
1981	Solution crystallization in 1,4-butandiol/solid-state coextrusion	Porter	6.7	—	5
1982	Zone drawing (one time)/Zone annealing (six times)	Kunugi	10.8	1.0	6
1983	Zone drawing (four times)/zone annealing (six times)/Heat setting	Kunugi	16.9	1.17	7
1985	Dissolution in formic acid/chloroform/dry spinning/hot drawing	Pennings	19	1.0	8
1986	Plasticization with iodine/drawing at 55°C/removal of iodine	Porter	6	—	9
1986	Gellation with benzyl alcohol/partially dried film/coextrusion	Porter	5.6	—	10
1993	Repeated heating and cooling cycles under sinusoidal deformation	Kunugi	21	—	11
1993	High-temperature zone drawing/heat treatment under high tension	Kunugi	21.1*	1.11	12

Table 6: Properties of Nylon 4 [53].

Melting point [°C]	273
Tenacity [cN/dtex]	4.0
Water absorption	High
Regain [%]	8

Nylon 5

Nylon 5 fibres are spun from polyvalerolactam. These fibres of high quality have properties similar to nylon 6.6. Commercial scale production of Nylon 5 will depend on the economics of monomer production [53]. Its chemical structure is:



Valerolactam may be made from cyclopentadiene shown in Figure 22. Cyclopentadiene is hydrogenated to cyclopentane (1), which is then oxidized to cyclopentanone (2). Conversion to the oxime (3) is followed by the Beckmann transformation which produces valerolactam (4). Valerolactam may be polymerized in a manner similar to caprolactam at a temperature of about 280-290°C. The polymer produced in this way (molecular weight about 15,000-16,000) is in equilibrium with some 15 per cent of low molecular weight cyclic oligomers. Poly valerolactam may also be melt spun. The properties of nylon 5 are given in Table 7.

Table 7: Properties of Nylon 5 [53].

Tenacity [cN/dtex]	4.2 – 4.4. Wet is about 90 per cent of dry. Fibres of up to 8.4 may be produced.
Elongation [%]	20-28
Initial modulus	Higher than nylon 6.6.
Creep characteristics	Nylon 5 fibres have low creep at elevated temperatures, and are an improvement on nylon 6.6 in this respect.

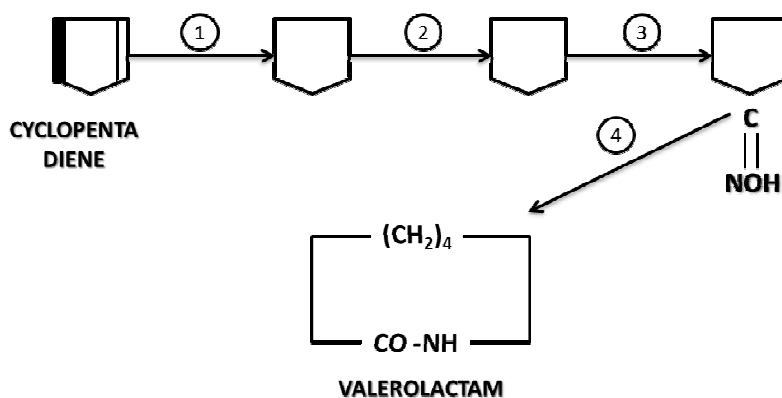


Fig. 22: Production of Valerolactam [53].

Nylon 6.10

Nylon 6.10 fibre is spun from polyhexamethylene sebacate, made by the condensation of hexamethylene diamine and sebacic acid as shown in Figure 23.

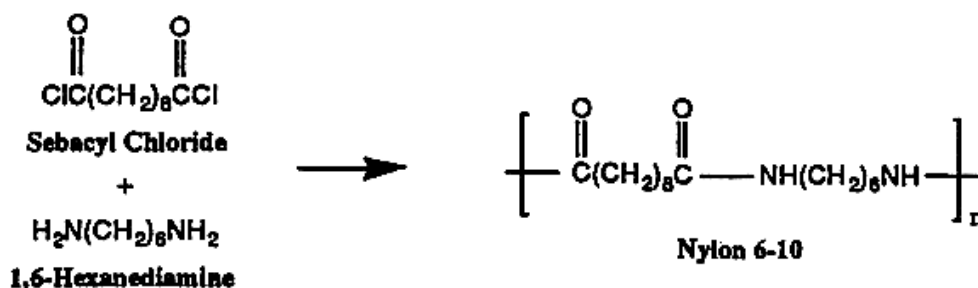


Fig. 23: Chemical structure of Nylon 6,10 [53].

Fibres spun from Polyhexamethylene sebacate have a number of interesting characteristics. Sebacic acid is produced from castor oil. It is condensed with hexamethylene diamine, the process being similar to that used in the production of nylon 6.6. The product, polyhexamethylene sebacate, may be melt spun without difficulty. The moisture absorption of nylon 6.10 is lower than that of either nylon 6 or 6.6, and nylon 6.10 fibres are unusually resilient. Costly Sebacic acid makes major scale production a distant possibility.

Nylon 7

Nylon 7 fibres are spun from polyheptanoamide (polyoentanamide or polyenanthamide). While the physical properties of these fibres are generally similar to those of nylon 6 and 6.6, there are differences in certain characteristics which could be of commercial significance [53]. The higher melting point (by comparison with nylon 6) and the low moisture absorption could be important advantages for Nylon 7 in certain applications. Nylon 7 has superior wash-and-wear characteristics due to the increased initial modulus and low moisture absorption. Its chemical structure is:



Polyheptanoamide is made by self-condensation of either 7-amino*heptanoic acid or its lactam. The monomer may be made by the following methods:

(a) Telomerization

Telomerization of ethylene in the presence of carbon tetrachloride is carried out. One of the products is 1-chloro-7-trichloro-heptane (1). Hydrolysis of this material by aqueous sulphuric acid (2) yields 7-chloro-heptanoic acid. Treatment of this with aqueous ammonia (3) forms 7-amino-heptanoic acid. 7-chloro-heptanoic acid may also be reacted with anhydrous ammonia (4) to form heptano-lactam shown in Figure 24. Telomerization produces a mixture of tetrachloro-alkanes, and the successful commercial development depends upon the economic use of tetrachloro-alkanes other than 1-chloro-7-trichloro-heptane. Self-condensation of the monomer is carried out in a manner similar to that used in making Nylon 6, to yield a Nylon 7 polymer. In the absence of oxygen, Nylon 7 is thermally stable up to about 300°C. Melt spinning may be carried out without difficulty. Under equilibrium conditions, nylon 7 contains only a very small proportion (about 1.5 per cent) of monomer and other low molecular weight materials. There is no necessity for extraction of either the polymer or the fibre.

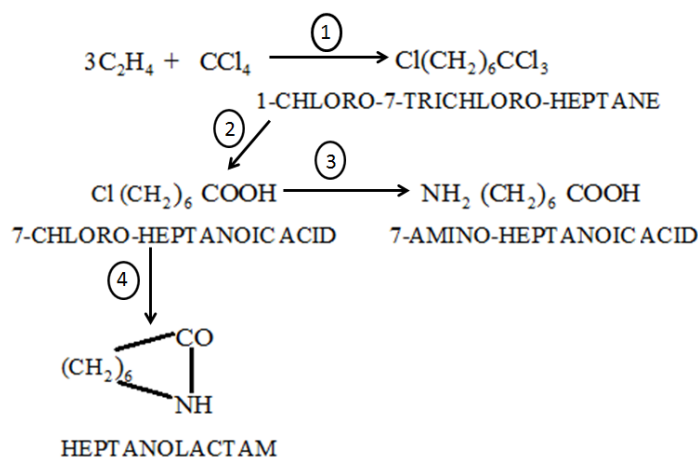


Fig. 24: Production of Heptanolactam. Telomerization Route [53].

The physical properties of nylon 7 are (Table 8).

Table 8: Physical properties of Nylon 7 [53].

Molecular weight	As high as 30,000
Tenacity [cN/dtex]	3.7 dry; 3.5 wet.
Elongation [%]	35 per cent.
Initial modulus [cN/dtex]	Higher than that of either nylon 6 or nylon 6.6 at 40-60°C.
Specific gravity [kg/m ³]	1100
Melting point [°C]	220-230

Nylon 8

Nylon 8 fibres are spun from polycaprylamide and can be synthesized by using Butadiene or Acetylene. Its chemical structure is:



Dimerization of butadiene provides cyclooctadiene (1), which is hydrogenated to cyclooctane (2). This may be converted to capryl lactam by routes similar to those used in converting cyclohexane to caprolactam shown in Figure 25.

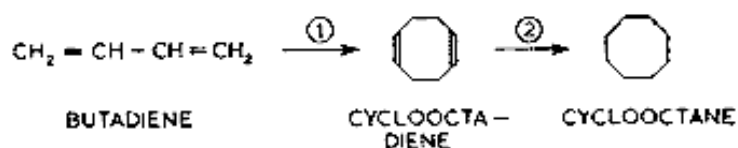


Fig. 25: Capryl Lactam Production using Butadiene [53].

Polymerization of acetylene produces cyclooctatetrene (1), which is partly hydrogenated to cyclooctene (2). This is oxidized to cyclooctene epoxide (3) and transformed to cyclooctanone (4). This is converted to the oxime (5), which undergoes the Beckmann transformation to capryl lactam (6) shown in Fig. 26.

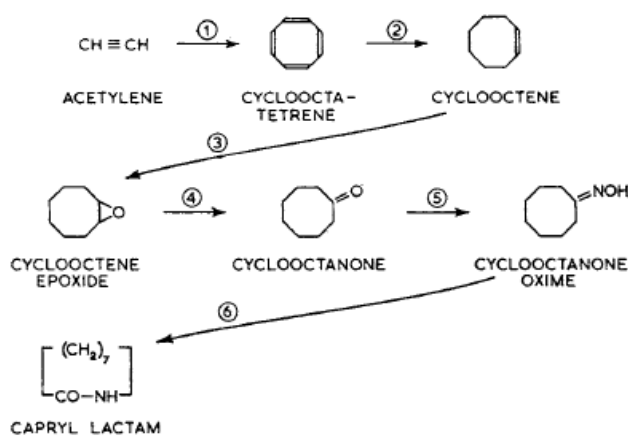


Fig. 26: Capryl Lactam Production. Acetylene Route [53].

Capryl lactam polymerizes readily to nylon 8 polymer, in a manner similar to the polymerization of caprolactam. The polymer contains only a very small proportion of low molecular weight material (e.g. 0.5-2.5 extractable with water). It may be melt spun without difficulty.

Table 9: Properties of Nylon 8 [53].

Molecular weight	16 000 to 23 000
Tenacity [cN/dtex]	3.7 dry; 3 .6 wet.
Elongation [%]	38.
Specific gravity [kg/m ³]	1090
Melting point [°C]	200-20

Nylon 9

Nylon 9 fibres are spun from polynonanoamide. These fibres have been produced commercially and known as Telargon. Its chemical structure is:



9-amino-nonanoic acid is one of the products of the telomerization reaction. In any large scale production of other amino acids, 9-amino-nonanoic acid would be available as by-product. Self-condensation of 9-amino-nonanoic acid takes place readily. The polymer contains only a very small proportion of low molecular weight material at equilibrium (about 0.5-1.5 per cent extractable with water). It may be melt spun as readily as Nylon 6. The molten polymer is thermally stable so long as it is protected from atmospheric oxygen. The water absorption is lower than that of Nylon 6, Nylon 6.6 or Nylon 7. The following properties are typical of a polymer of molecular weight in the region.

Table 10: Properties of Nylon 9 [53].

Molecular weight	20 000-25 000
Tenacity [cN/dtex]	3.7 dry; 3.6 wet
Elongation [%]	40
Specific gravity [kg/m ³]	1090
Melting point [°C]	210-215

Nylon 11

Nylon 11 possesses certain features opening up interesting applications. The melting point of nylon 11 (189°C.) is on the low side for general textile use, and great care must be taken in ironing and other elevated-temperature treatments. The initial modulus of nylon 11 is higher than those of the other nylons, resulting in increased stiffness and rigidity. This is advantageous in applications such as brush bristles, and it also makes for easier processing. Nylon 11 yarns do not stretch so easily when subjected to physical processing such as winding. The high initial modulus of nylon 11 suggests that this is a useful nylon for the huge tyre cord market. Tyres reinforced with nylon 11 would not be subject to flat-spotting to the extent that nylon 6 and nylon 6.6 reinforced tyres are. The low moisture absorption of nylon 11 enables it to retain its excellent insulation properties at high humidity. This is a useful characteristic in electrical applications. Nylon 11, with a specific gravity of only 1.04, is a very light fibre, with much greater covering power than the other polyamides.

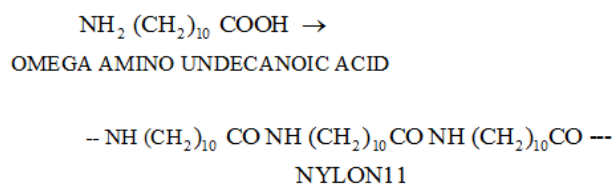


Fig. 27: Chemical structure of Nylon 11 [53].

Nylon 11 is composed of polymerized 11-amino-undecanoic acid. The chemical structure of nylon 11 is shown in Figure 27. Nylon 11 was originally made from castor bean oil and marketed under the trademark of Rilsan®. Nylon 11 fibres have similar properties to nylon 6 and 6,6. Nylon 11, however is less dense, melts at a lower temperature and has better dimensional stability. It is often used for brush bristles, lingerie, bulked yarns, and injection moulded plastics [54]. Nylon 11 may be melt spun into fibres. Nylon 11 has been made as multifilament yarns, monofilaments, staple and tow, in a range of deniers and staple lengths. It was produced under the trade name 'Rilsan', for example, in the following sizes:

Table 11: Sizes of Rilsan [53].

Filament	12/1, 12/2, 18/3, 29/10, 45/16, 57/20, 90/32, 145/50, 290/100.
Staple	1.4/32, 37, 62 mm.; 2.9/37, 62, 95, 112 mm.; 6/40, 70, 100, 120 mm.
Tow	110 000 dtex (100 000 den).

The 11-amino-undecanoic acid used in production of nylon 11 may be made by obtained from three commercially-important routes; (a) from castor oil, (b) from ethylene and carbon tetrachloride, and (c) from dodecane. Nylon 11 has been produced from 11-aminoundecanoic acid made from castor oil which is shown in Figure 28. The oil is obtained from castor beans; it is extracted by the combined action of pressure and organic solvents. The oil contains 85 per cent of triglyceryl ricinoleate. Triglyceryl ricinoleate is converted to methyl ricinoleate by treatment with methyl alcohol. Methyl ricinoleate is pyrolyzed at high temperature, yielding heptaldehyde, methyl undecylenate and a small amount of fatty acids (1). Pure heptaldehyde and methyl undecylenate are isolated by fractional distillation. Methyl undecylenate is hydrolyzed to undecylenic acid (2). Undecylenic acid is aminated by reaction with ammonia, to form 11-amino-undecanoic acid (3).

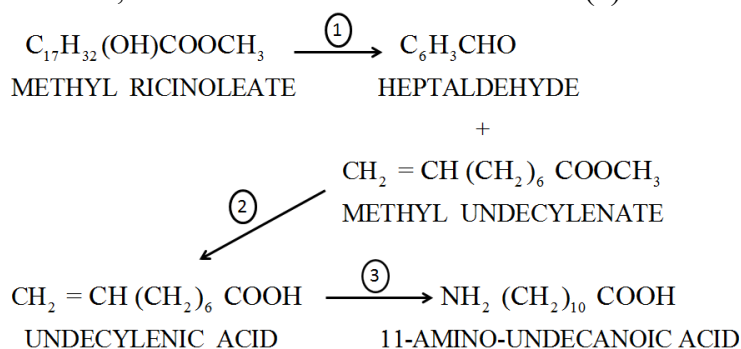


Fig. 28: Production of 11-Amino-undecanoic Acid from Castor Oil [53].

When ethylene and carbon tetrachloride are heated together at high temperature in the presence of a catalyst (e.g. benzoyl peroxide), the ethylene undergoes polymerization until such time as the ends of the polymer chain are blocked by CCl_2 and CCl_3 radicals formed from the carbon tetrachloride. Conditions may be adjusted so that this occurs after only 1, 2, 3, 4 or 5 ethylene molecules, for example, have linked together (1).

The product obtained by telomerizing ethylene and carbon tetrachloride is a mixture of compounds of general structure $\text{Cl}(\text{C}_2\text{H}_4)_n\text{CCl}_3$, where n is a small number, e.g. 1 to 5. One of the products, which may be separated by distillation, is 1-chloro-11-trichloroundecane i.e. $\text{Cl}(\text{CH}_2)_{10}\text{CCl}_3$. Hydrolysis of this by aqueous sulphuric acid yields 11-chloroundecanoic acid (2), which is reacted with ammonia to produce 11-amino-undecanoic acid (3).

A process for the production of undecanolactam from dodecane has been developed. Polymerization of 11-undecanoic acid is carried out in three stages, the monomer being fed as an aqueous suspension into the reaction vessel. In stage 1, water is removed, and the 11-undecanoic acid is melted. The temperature is raised to 215°C , and polycondensation begins. Moving to stage 2, Polycondensation is allowed to proceed until the desired degree of polymerization has been reached. In the final stage 3, the molten polymer is held for a time at 215°C . to allow the molecular weight distribution to attain a satisfactory state. Then, the molten polymer is passed to a storage tank, from which it may be fed directly to the spinnerets.

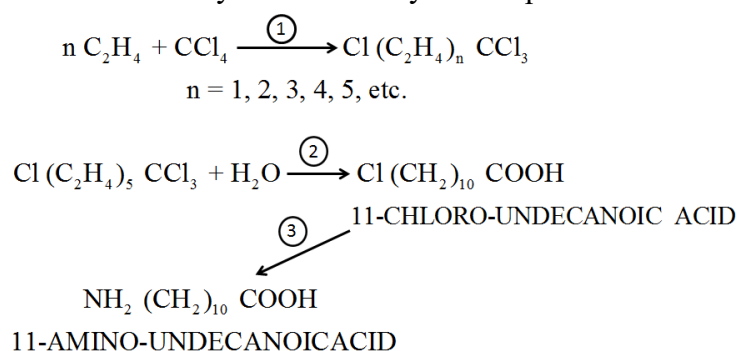


Fig. 29: Production of 11-Amino-undecanoic acid from Ethylene and Carbon Tetrachloride (Telomerization) [53].

The basic reaction which occurs during nylon 11 production is shown in Figure 30. Molten nylon 11 polymer is very stable at the temperature used during melt spinning (about 215°C), and it may be stored for long periods without deterioration. The polymer is commonly spun direct after production, without any intermediate chip-production stage. Spinning is carried out in a manner similar to that used in nylon 6 production, and the filaments are drawn to a degree depending on the type of fibre required. The differences between nylon 11 and nylons 6.6 and 6 are those that would be anticipated from the lengthening of the chain of carbon atoms separating the amide groups. The moisture absorption has decreased, and the specific gravity is lower, making nylon 11 the lightest textile fibre other than the polyolefines. The melting point of nylon 11 is lower than that of nylon 6, in accordance with the tendency for melting point to fall with increase in the number of methylene groups between the amide groups. But as the methylene groups are an even number, nylon 11 falls into the higher of the two series of polyamides. For this reason, the melting point is not very much lower than that of nylon 6, which has 5 methylene groups between amide groups, and therefore comes in the 'odd-number*' series.

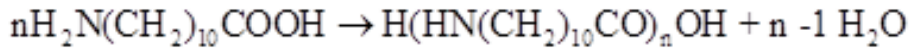


Fig. 30: Basic reaction of nylon 11 [53].

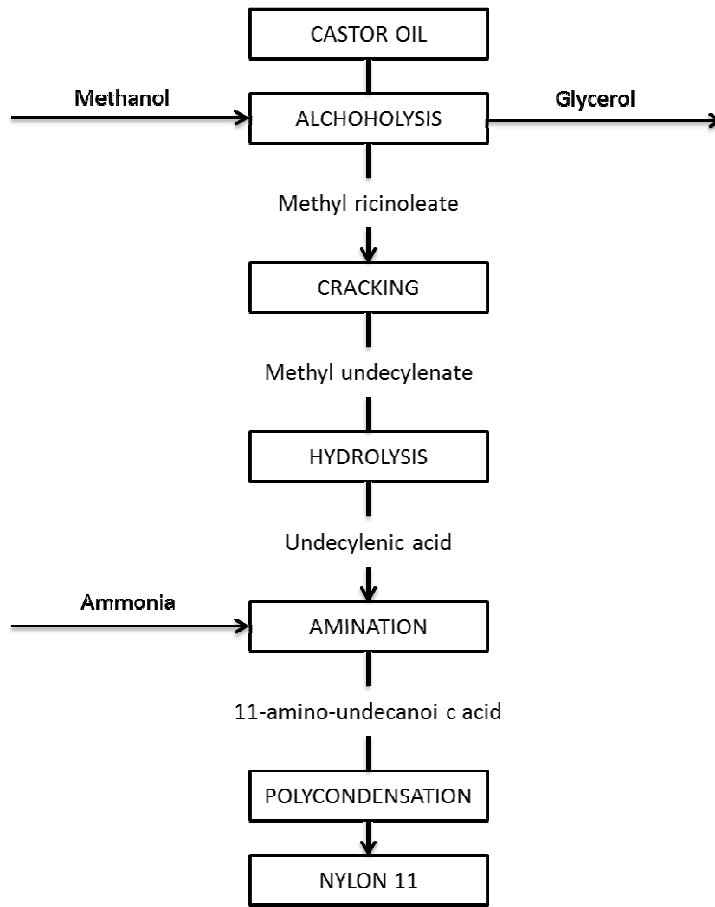


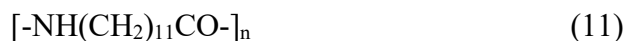
Fig. 31: Nylon 11 flow chart [53].

Table 12: Properties of Nylon 11 [53].

Structure and Appearance	Smooth surfaced, and commonly of circular cross-section.
Tenacity [cN/dtex]	4.4-6.6 The tenacity is virtually unaffected by moisture.
Elongation Regular filament [%]	25 wet or dry.
Elastic Recovery [%]	100 at 6 % elongation.
Initial Modulus [cN/dtex]	Nylon 11 has a higher initial modulus than either nylon 6 or nylon 6.6. It is typically about 44. The higher rigidity of nylon 11 gives it a better dimensional stability to repeated strains and a better resistance to creep than other polyamides.
Flex Resistance	Excellent.
Specific gravity [kg/m ³]	1040

Nylon 12

Nylon 12 fibres are spun from polylaurylamide. Nylon 12 is inherently expensive, however, and it is unlikely that it could become of importance as a general purpose polyamide fibre. Its chemical structure is:



Stages in the synthesis of lauryl lactam from butadiene are shown in Figure 32. Butadiene is trimerized to 1, 5, 9-cyclododecatriene (1), which is converted to cyclododecanone (2). This is converted to the oxime (3), which undergoes the Beckmann transformation to 12-amino-dodecanorc acid (4). The lactam of this is lauryl lactam (5). Polycondensation of the monomer is carried out in the usual way and polymers may be obtained without difficulty. Nylon 12 polymer contains only a very small proportion of low molecular weight material (0.75 per cent extractable with water). Nylon 12 polymer melts at 180-190°C, and is readily melt-spun into fibres. The moisture absorption is low, and dielectric properties are excellent. The melting point (180-190°C.) is rather low for general textile applications.

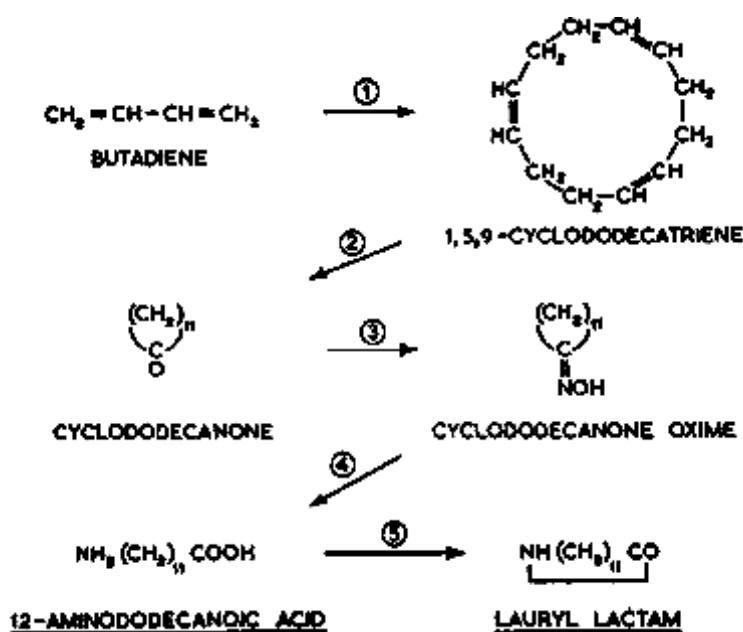


Fig. 32: Production of Lauryl Lactam from Butadiene [53].

Table 13: Properties of Nylon 12 [53].

Molecular weight	22 000
Tenacity [cN/dtex]	3.36 dry or wet.
Elongation [%]	40
Specific gravity [kg/m^3]	1080
Moisture regain [%]	2.2
Melting point [$^{\circ}\text{C}$]	180-190

Polycondensation of the monomer is carried out in the usual way and polymers may be obtained without difficulty. Nylon 12 polymer contains only a very small proportion of low molecular weight material (0.75 per cent extractable with water). Nylon 12 polymer melts at 180-190°C, and is readily melt-spun into fibres. The moisture absorption is low, and dielectric properties are excellent. The melting point (180-190°C.) is rather low for general textile applications. The following properties are typical of a nylon 12 fibre.

Strength of polyamide fibres

High modulus/high tenacity fibres are either produced by solution spinning of liquid crystalline polymers or by gel spinning. The current method of fabrication for these technologies produces fibres that are uneconomical, and in some instances the manufacturing processes are environmentally unfriendly. For the majority of industrial applications, a 50% increase in the modulus and tenacity of the conventional fibres would be adequate, if they retain some of their high toughness and can be produced at a price lower than the current high performance fibres. The modulus of fibres is controlled by the orientation distribution of the chain segments and the degree of crystallinity [55]. Since the fibre tenacity is determined by flaws, not morphology, an extensive investigation has been conducted on the failure analysis of polyamide fibres. The investigation assumes that these imperfections lead to cracks and ultimately catastrophic failure. Because the cross-section of the fibres is microscopic (35µm diameter), only modestly successful research exists on the mode and analysis of failure in single nylon fibres. Most research dedicated to the determination of tensile failure in single nylon filaments has been based on Weibull statistics. In this theory, the fibre is viewed as a continuous array of interwoven links, and the flaws represent the “weakest links” of the domain [56].

The Weibull distribution function is given as:

$$F_i = 1 - \exp\left(-\left(\frac{\sigma}{\sigma_0}\right)^m\right) \quad (12)$$

Here, F_i represents the probability of failure for a particular link in the fibre at a stress level σ . The scale factor is represented by σ_0 and m represents the flaw distribution shape factor. Additionally, Kausch et al. [26] expressed the strength distribution of the fibre in a similar manner, evincing that increases in specimen length generates a decrease in the ultimate mechanical strength of the sample. The relationship is given as:

$$g(L, x) = Ln_0 f(x) \left[1 - \int_{\infty}^x f(y) dy \right]^{Ln_0 - 1} \quad (13)$$

Here, n_0 represents the number of defects per unit length and $f(x)$ is the cumulative strength distribution function. For nylon 6 fibres, the effect of specimen length on the strength is depicted in Figure Figure 33. These results are intuitive, nevertheless, given that an increase in specimen length increases the defect density of the sample and thus reduces the fracture strength. These techniques for analysing failure in nylon

fibres are adequate for statistical failure studies, but have obvious inadequacies in the field of fracture mechanics. The main component omitted in the Weibull distribution function is the size, shape, and geometry of the flaws present in the sample. Furthermore, the Weibull parameter does not reveal how the flaws led to critical propagation, or at what value it actually occurred. The field of fracture mechanics encompasses maximum stress level, flaw size and geometry, and many other factors that Weibull statistics fail to quantify in materials.

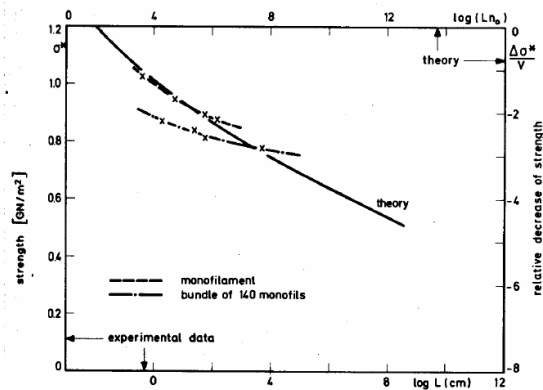


Fig. 33: Theoretical and experimental data displaying effect of specimen length on ultimate tensile strength in nylon 6 fibres [26].

Understanding yield and plasticity effects in polymers can also help to illuminate the fracture process in nylon 6,6, since these phenomena precede fracture and are responsible for much of the damage accumulation that is experienced by the material. One should first be conversant with elasticity theory, since it is a basic constituent of plasticity, and Timoshenko and Goodier [57] have developed a rigorous elasticity framework that is applicable to most engineering materials. Specifically, the classical theory of plasticity was developed to study the stress-strain relationship of plastically deformed metals. However, these laws are applicable to a wide range of materials, and can be utilized to quantify plasticity effects in Nylon 6.6 and Nylon 6 fibres. The initial experimental stress-strain response of the Nylon 6.6 filaments considered for this study are linear-elastic, strain hardening with varying elastic moduli for different draw ratios. One can employ empirical relationships such as Ramberg-Osgood, linear-elastic strain hardening, or inverse hyperbolic tangent to reproduce experimental data. These empirical relationships are exponential in nature, however, and one should devise constitutive equations to determine the relationships of stress to strain/strain rate. Before discussing such rigorous mathematical models, rudimentary thermodynamic principles will be presented to establish the basis of plasticity theory. These two concepts, based on considerations by Khan and Huang [58], are presented as:

- 1) Plastic deformation involves dissipation effects in materials, which affirms that it is an irreversible process.
- 2) Because of the nature of irreversibility, plastic deformation is a path dependent process.

Krempl and Bordonaro [59] have validated path dependence for biaxial-torsional loading of Nylon 6.6, in which they performed displacement-controlled experiments on 50% crystalline tubular specimens. They also determined that the time-dependent effects interact with plasticity effects for biaxial-torsional loading of Nylon 6.6. For the classical theory of plasticity, plastic deformation is considered to be rate insensitive. However, the viscous component in the constitutive model for polyamide fibres precludes this assumption, and rate sensitivity should be considered for this analysis. The constitutive laws for polyamides in general will include time dependent parameters, which serve as an auxiliary in quantifying the effects of creep, strain rate, and viscosity.

New developments of polyamide fibres

New types of polyamide fiber

During the past decades, intensive efforts have been spent on identifying potential fibre forming materials. Different types of dibasic acid, diamine, amino acid and lactam have been polymerized, and the polymer spun into fibre. The development of polyamide fibres with properties different from the 'standard' nylon fibres has followed three directions of (1) Physical modification of existing nylon types, (2) Chemical modification of existing nylon types and (3) Production of new types of polyamide. The development approach for new polyamide fibres was to evaluate the effect of using diamines, diacids, amino acids and lactams containing more or less than the 6 carbon atoms present in the monomers of nylon 6 and 6.6. While the basic properties would remain the same, the changes in the spacing between the amide groups in the polymer chain might affect certain other properties melting point, moisture absorption, temperature resistance, high dielectric strength etc. Similarly, it might be possible to modify other properties of the polyamide in significant ways. These new initiatives have resulted in production of polyamides which are now being used in specialized fields for which the normal nylon fibres are unsuitable. Some examples of such fibres are Nomex - High-temperature resisting polyamides and polyamides of high dielectric strength (e.g. nylon 11).

The relatively low moisture absorption of nylon, for example, contributes to its ease-of-care characteristics. But it also encourages the accumulation of static electricity, which may be undesirable or even dangerous in certain circumstances. There are applications in which it would be advantageous to have a nylon with higher water absorption. Other properties too have proved inadequate in specific applications. Polyamide fibres generally have a sunlight resistance which is adequate for normal textile uses, but they are affected by ultra-violet light and hence requires modifications to make them the preferred choice in applications that must withstand continuous sunlight. Degradation by light is commonly less serious in the lustrous types of nylon fibre than in fibre which has been dulled by addition of titanium dioxide. Much can be done to improve light resistance by the use of chemical additives, but nylon's tendency to undergo degradation in sunlight has told against it in curtains and similar applications. When nylon is washed in water containing iron

salts, it tends to absorb the dissolved materials, and acquires a yellow colour which is difficult to remove. The initial modulus of nylon is low, and the fibre thus extends readily at low loadings. This makes for difficulty in processing, and in certain applications. It is a factor in the flat-spotting which occurs when nylon is used for reinforcing tyres. Nylon is sensitive to bleaching agents and to acids, and it tends to lose strength when heated for prolonged periods, e.g. at temperatures above 150°C. These characteristics of nylon fibres are of little significance over a vast range of nylon's textile applications. But in certain applications, they are sufficient to make nylon less competitive than it might be. And in specific applications, they may render nylon altogether inadequate. For most purposes, for example, nylon has an adequate resistance to heat, and the melting point - especially of nylon 6.6 - is high enough for normal textile applications. In recent years, however, developments in space travel, supersonic flight and other fields have created a demand for fibres which can withstand temperatures higher than those encountered in everyday applications. The normal nylons offer a range of properties which is attractive for these specialized applications, but in many cases their melting points are too low to permit of their use. In many electrical fields, similarly, the characteristics of polyamide fibres are generally attractive, but there are specific applications in which they would be more satisfactory if the moisture absorption was lower. It is apparent that nylon would be able to play an important role in many specialized fields of application if certain characteristics were changed to suit specific needs. Some of these fields, though specialized in the sense that they may require particular properties in the fibre, are of great importance and absorb great quantities of fibre. Tyre cord, for example, is a 'specialized' application which is a major outlet for nylon and other fibres [53].

Modification of existing nylon types

Physical Modification

Polymer modification

Using the knowledge of detailed study of the polyamides from which nylon 6 and nylon 6.6 fibres are spun, the physical properties of nylon 6 and nylon 6.6 may be modified within limits by influencing the average molecular weight, molecular weight distribution, degree of crystallinity and degree of orientation of the polymers. Such techniques allow the manufacturer to control tenacity, flexibility and other mechanical properties. The melting point of polyhexamethylene adipamide (nylon 6.6 polymer) may be increased, for example, by increasing the molecular weight. However, an optimal point is reached beyond which the possibility of effecting dramatic changes in properties by adjustment of the physical state of the polymer is remote.

Fibre modification

- The cross-sectional shape of a fibre has an important influence on many important characteristics, and nylon is being produced in a variety of noncircular cross-sections. Multilobal cross-section nylons have advantages like increased cover; crisp, silk-like, firm handle; reduced pilling in spun yarn fabrics; increased bulk;

sparkle or highlight effect and resistance to soiling. The increase in surface area of a multilobal filament requires more dyestuff and reduces wash-fastness [53].

- Nylon may be textured and bulked by the various processes in common use.
- Bicomponent polyamide fibres are made by two filaments of different constitution have been brought together during spinning to form a single bicomponent filament. The two components of the twin filament display different shrinkage properties on application of wet or dry heat, and the application of heat to the bicomponent fibre causes differential shrinkage which produces a crimp.
- Heterofil fibres and filaments are bicomponent fibres with a core/sheath structure. Nylon heterofil fibres may be used for making non-woven fabrics by a technique called melding (a combination of melting and welding). The heterofil fibres may have a core of relatively high melting point polymer and a sheath of relatively low melting point polymer which is designed to flow on heating. Fibre webs are melded by the application of controlled heat and pressure, the fibres being bonded at cross-over points.

Chemical modification

- The structure of the chemically active polymers may be modified by carrying out certain chemical reactions. Such modification of the characteristics of existing nylon fibre types opens up many interesting possibilities. During the production of nylon fibres, the polymer molecules come together in places to form regions of crystallinity. Elsewhere, the long molecules remain in a more or less random arrangement, forming regions of amorphous polymer. The crystalline regions are much less readily penetrated by chemical reagents than the amorphous regions, and it is much easier, therefore, to bring about chemical modification of the polyamide in the amorphous regions. Chemical modification thus tends to have a more significant effect on dyeability and moisture absorption. Through chemical modifications, it is difficult to influence tenacity and flexibility are less readily influenced [53].
- Cross linking has been used successfully in attempts to modify nylon fibres. The long chain molecules of nylon may be linked together by reacting them with chemicals carrying an active group at each end of the molecule. The isocyanate group, for example, will react readily with amine or carboxylic groups, such as may be present at the ends of polyamide molecules. Reaction of polyamides with a di-isocyanate, therefore, would be expected to link up adjacent polyamide molecules. Exposure of nylon 6 brought about increased initial modulus and lower extensibility, with a significant improvement in flat-spotting characteristics [53].
- Another technique is grafting of polymers and other substances on to the sides of polyamide molecules. Acrylic acid grafts on nylon 6.6 provide sodium salts which have an attraction for moisture. Fibre treated in this way has high wet-crease recovery properties. Calcium salts of acrylic acid grafts tend to raise the melting point of the nylon, e.g. to 360°C. or higher depending upon the degree of grafting. Moisture absorption of nylon fibres may be increased by the graft polymerization of ethylene oxide on to the fibre. This also improves flexibility [53].

Conclusion

The polyamides generally are tough, strong, durable fibres useful in a wide range of textile applications. They are the most preferred material off all the synthetic nonwovens. This is attributed to the relatively simpler production process, cheaper raw materials and versatile applications. The distinguishing characteristics are being highly elastic, tear and abrasion free, low humidity absorption capability, fast drying, no loss of solidity in a wet condition, crease-free, rot and seawater proof. The application areas range from underclothes to outer sporting garments. Nylon is the generic word used to refer a family of polyamides. It was the first of the “miracle” yarns made entirely from chemical ingredients through the process of polymerization. In this chapter, the properties and production process of various polyamide fibres have been discussed. While nylon 6 and 6,6 have been discussed in detail. Other types of polyamides have also been discussed with their structure, process and properties. Various production processes have been illustrated elaborately. The new approaches to develop specialized polyamides which can be used for specific purposes have been endeavoured to explore. Tensile strength and failure mechanisms have been discussed. Polyamides have distinct advantages favourable to the manufacturers and users. Their application can be extended to present as well as future applications. With further research, the complete potential of this “miracle” yarn can be realized.

References

1. <http://www.textileschool.com/articles/85/polyamide-fibres-manmade-artificial-fibres>. [cited 2016 25 Sep].
2. <http://textilelearner.blogspot.com/2013/09/preparation-properties-and-applications.html#ixzz4OAreqhSE>.
3. <http://www.essentialchemicalindustry.org/polymers/polyamides.html>. [cited 2016 25 Sep].
4. <https://www.ihs.com/products/nylon-fibers-chemical-economics-handbook.html>. August 2016 [cited 2016 25 Sep].
5. Averett, R.D., *Fracture Mechanics of High Performance Nylon Fibers*, in *The Academic Faculty*. 2004, Georgia Institute of Technology: Georgia. p. 134.
6. Steven, W.B., *Fiber Science*. 1995, Upper Saddle River, NJ 07458.: Prentice Hall.
7. Bunn, C.W., & Garner, E.V. in *Proceedings of the Royal Society of London*. 1947.
8. Huevel, H.M., Huisman, R., & Lind, K. C. J. B., *Journal of Polymer Science, Polymer Physics Edition*, 1976. **14**.
9. <http://www.fibersource.com/f-tutor/nylon.htm>. [cited 2016 25 Sep].
10. Lim, J.G., et al., *Progress in Polymer Science*, 1989. **14**(6): p. 763-809.
11. Hermans, J.J., et al., *Recueil des Travaux Chimiques des Pays-Bas*, 1946. **65**(427).
12. Ziabicki, A., & Kedzierska, K., *Journal of Applied Polymer Science*, 1959. **2**(14).
13. Ziabicki, A.K., K., *Journal of Applied Polymer Science*, 1962. **6**(111).
14. Ishibashi, T., Aoki, K., & Ishii, T., *Journal of Applied Polymer Science*, 1970. **1597**(14).

15. Shigemitsu, M., et al., *Polymer*, 1998. **38**(18): p. 4577-4585.
16. Ito, M., et al., *Polymer*, 2001. **42**(1): p. 241-248.
17. Murthy, N.S., et al., *Polymer*, 1995. **36**(20): p. 3863-3873.
18. Suzuki, A.E., A., *Polymer*, 1997. **38**(12): p. 3085-3089.
19. Suzuki, A., Murata, H. & Kunugi, T., *Polymer*, 1999. **39**(6-7): p. 1351-1355.
20. Suzuki, A., Y. Chen, and T. Kunugi., *Polymer*, 1998. **39**(22): p. 5335-5341.
21. Penning, J.P., et al. , *Polymer*, 2003. **44**(19): p. 5869-5876.
22. Ward, I.M., & Hadley, D.W., *Mechanical Properties of Solid Polymers*. 1993, Chichester, New York: J. Wiley & Sons.
23. Atkins, A.G., & Mai, Y.W., *Elastic and Plastic Fracture: Metals, Polymers, Ceramics, Composites, Biological Materials*. 1985, Chichester, West Sussex, England: Ellis Horwood Limited.
24. Cook, J., & Gordon, J. E. in *Proceedings of the Royal Society of London*. 1964.
25. Cherry, B.W., & Hang, P.T. in *Proceedings of the Australian Fracture Group*. 1974. Melbourne: Monash University.
26. Kausch, H.H., *Polymer Fracture*. 2nd ed. 1985, New York: Springer-Verlag.
27. Hadley, D.W., et al. , *Journal of Material Science*, 1969. **4**: p. 152.
28. Koritskii, Y.V., *Energiya*, Moscow, 1976.
29. Dietrich, K., *Faserf. u. Textiltechn.*, 1976. **287**(27).
30. Lobel, W., *Textiltechnik*, 1976. **778**(26).
31. Teger, E., *Chem. Wlagna.*, 1978. **8**.
32. Budin, J., *Textil 9*, 1977. **203**(32).
33. Coen, A., *Mater. Plast. Elast.*, 1964. **30**(12).
34. Grady, P.L., *Institute of Physics Conference Series*, 1975. **141**(27).
35. Hennicker, J., *Nature*, 1962. **474**(196).
36. Lemnicke, D.J., *Am. Dyest, Rep.*, 1949. **38**: p. 853-862.
37. *Static Electricity in the Processing of Man-Made Fibres [in Russian]*. Legkaya Industriya. 1966, Moscow.
38. <https://www.pall.com/pdfs/Fuels-and-Chemicals/PPG3a.pdf>. [cited 2016 23 Sep].
39. Raimer, D., *Fibre Chemistry*, 2005. **37**(4).
40. Kunugi, T., Chida, K., & Suzuki, A., *Journal of Applied Polymer Science*, 1998. **67**.
41. Kunugi, T., Suzuki, A., Akiyama, I., & Hashimoto, M. , *Division of Polymer Chemistry - American Chemical Society*, 1979. **778**(20).
42. Acierno, D., La Mantia, F.P., Polizzotti, G. & Ciferri, A., *Journal of Polymer Science Part B: Polymer Physics*, 1979. **1903**(17).
43. Zachariades, A.E., & Porter, R. S., *Journal of Applied Polymer Science*, 1979. **1371**(24).
44. Richardson, A.W., I.M. , *Journal of Polymer Science Part C*, 1981. **1549**(19).
45. Shimada, T., & Porter, R.S., *Polymer*, 1981. **1124**(22).
46. Kunugi, T., Akiyama, I., & Hashimoto, M., *Polymer*, 1982. **1193**(23): p. 23,1199(1982).
47. Gogolewski, S., & Pennings, A.J., *Polymer*, 1985. **1394**(26).
48. Chuah, H.H., & Porter, R. S., *Polymer*, 1986. **241**(27).
49. Chuah, H.H.P., R. S., *Polymer*, 1986. **1022**(27).
50. Kunugi, T., Suzuki, A. & Chida, K. , *Journal of Polymer Science Part B: Polymer Physics*, 1993. **803**(31).

51. Suzuki, A., Kunugi, T., & Kondo, M., *Kobunshi Ronbunshu*, 1993. **93**(50).
52. Sakurada, I., & Kaji, K. , *Journal of Polymer Science Part C*, 1970. **57**(31).
53. Cook, J.G., *Handbook of Textile Fibres: Man-Made Fibres*. Vol. 2. 2001, Cambridge, England: Woodhead Publishing Limited.
54. http://cameo.mfa.org/wiki/Nylon_11.
55. Michielsen, S., *Fundamentals of High Modulus/High Tenacity Melt Spun Fibers*. 2003.
56. Newell, J.A., & Edie, D.D. , *Carbon*, 1996. **34**(5): p. 551-560.
57. Timoshenko, S., & Goodier, J. N., *Theory of Elasticity*. 3rd ed. 1970, New York: McGraw-Hill.
58. Khan, A.S., & Huang, S., *Continuum Theory of Plasticity*. 1995, New York: John Wiley & Sons, Inc.
59. Krempl, E., & Bordonaro, C.M., *International Journal of Plasticity*, 1998. **14**(1-3): p. 245-258.
60. Valanis, K.C., *Archives of Mechanics*, 1980. **32**: p. 171.
61. Valanis, K.E., *Archives of Mechanics*, 1971. **23**: p. 517.
62. Ahzi, S., Lee, B. J., & Asaro, R. J. , *Materials Science and Engineering*, 1994. **A189**: p. 35-44.
63. Northolt, M.G., Baltussen, J.J.M., & Schaffers-Kor, B., *Polymer*, 1995. **36**(18): p. 3485-3492.
64. Northolt, M.G., & Sikkema, D.J., *Advanced Polymer Science*, 1990. **115**(98).
65. Northolt, M.G., & van der Hout, R., *Polymer*, 1985. **230**(26).
66. Northolt, M.G., Roos, A., & Kampschreur, J.H., *Journal of Polymer Science, Physical Edition*, 1989. **1107**(27).
67. Cottrell, A.H., *Dislocations and Plastic Flow in Crystals*, in *Clarendon Press*. 1953: Oxford.
68. Ward, I.M., *Mechanical Properties of Solid Polymers*. 1971, New York: Wiley-Interscience.
69. Coulomb, C.A., *Memoirs on Differential equations and Mathematical Physics*, 1773. **343**(7).
70. Kausch, H.H., Hassell, J. A., & Jaffee, R. I. , *Deformation and Fracture of High Polymers*. 1973, Plenum Press. New York: New York.
71. Drucker, D.C., & Prager, W. , *Quarterly of Applied Mathematics*, 1952. **157**(10).
72. Termonia, Y., & Smith, P. in *Materials Research Society Symposium Proceedings*. 1987.
73. Anderson, T.L., *Fracture Mechanics: Fundamentals and Applications*. 2nd ed. 1995, Boca Raton, FL: CRC Press.
74. Tobolsky, A.V., & Mark, H., *Polymer Science and Materials*. 1971, New York: Wiley-Interscience.
75. Inglis, C.E.T., *Royal Institution of Naval Architects*, 1913. **55**: p. 219-233.
76. Griffith, A.A. 1920, *M. Eng. (of the Royal Aircraft Establishment)*. p. 163-198.
77. Becht, J., DeVries, K. L. & Kausch, H.H., *European Polymer Journal*, 1971. **71**: p. 105-114.
78. Kausch, H.H. *Polymer Fracture*. in *Springer-Verlag*. 1978. Berlin.
79. Andrews, E.H., *Fracture in Polymers*. 1968, New York: American Elsevier.
80. Bershtein, V.A., et al., *Polymer Science U.S.S.R.*, 1977. **20**: p. 654-660.

81. Hearle, J.W.S., et al. , *Fibre Failure and Wear of Materials: An Atlas of Fracture, Fatigue and Durability*. 1989, Chichester, West Sussex, England: Ellis Horwood Limited.
82. NTC Proposal, G.T.; Available from:
<http://www.ptfe.gatech.edu/faculty/michielsen/michelsenhighmod.htm>.
83. Rice, J.R., *Journal of Applied Mechanics*, 1968: p. 379-386.
84. Benham, P.P., Crawford, R.J., & Armstrong, C.G. , *Mechanics of Engineering Materials*. 2nd ed. 1996, London: Longman Group Limited.
85. Hutchinson, J.W., *Journal of the Mechanics and Physics of Solids*, 1968. **16**: p. 13-31.
86. Dowling, N.E., *Mechanical Behavior of Materials: Engineering Methods for Deformation, Fracture, and Fatigue*,. 2nd ed. 1999, New Jersey: Prentice Hall. Upper Saddle River.
87. Dowling, N.E., & Begley, J.A. , *ASTM STP 590* 1976, American Society for Testing and Materials: Philadelphia. p. 82-103.
88. Hertzberg, R.W., & Manson, J.A. , *Fatigue of Engineering Plastics*. 1980, Academic Press, Inc.: New York, NY.
89. Adams, G.C., et al. , *Polymer Engineering Science*, 1990. **30**: p. 241.
90. Bernal, C.R., Cassanelli, A. N., & Frontini, P. M., *Polymer Testing*, 1995. **14**(1): p. 85-96.
91. *Standard Test Method for Measurement of Fracture Toughness*., in *ASTM E 1820-01*. 2001, ASTM International: West Conshohocken, PA.
92. 6068-96., A.D., *Standard Test Method for Determining J-R Curves of Plastic Materials*. 1996, ASTM International: West Conshohocken, PA.

The mechanical, comfort & UV resistance properties on interlock derivatives

Hafsa Jamshaid, Habib Awais, Rajesh Mishra

Department of Material Engineering, Technical university of Liberec, Czech Republic

Department of Knitting, National Textile University, Faisalabad, Pakistan

Abstract:

The aim of present research is to study interlock structures and its derivative on mechanical properties i.e tensile & bursting, air permeability and Ultraviolet protection factor (UPF). Five type of interlock structures are studied which are formed from spun polyester. The testing performed shows among the different type of interlock structures studied, the interlock half cardigan structure and interlock plain structure have good air permeability. Half Milano structures shows good bursting strength and the highest UPF values. Co- relation analysis is also done for air resistance and bursting strength with UPF.

1. Introduction:

Knitted fabrics have a versatile using area because of their fast and easy production, low cost, softness, elasticity and comfort properties Knitting is the second most used technique of fabric formation. It is fastest method of fabric production as compared to woven fabric. The idea of fabric formation by using interloping process (i.e. knitting) came about 3000 years ago. The first type of knitting done by using hand held pins was weft knitting. Cap knitting was started by Britain in 1424, men first started knitting as profession in 15th century and parliament controlled the prices of knitting caps in 1488[1]. William lee was the one who invented the stocking hand frame in 1589 first. William started his efforts in 1561 and worked to made fast needle movement. The frame was commercialized in 1589. This concept was so effective that brought an evolutionary process in this field and this was the foundation of today's weft and warp knitting machine industries[1-2].

With the passage of time, the innovations and inventions are introduced and the new devices and technologies results in the formation of modern flat and circular knitting machines. Latch needle was introduced in market in 1847 and then the compound needle was invented which was a great revolution to the high speed production of knitting as the loop formation cycle is reduced by this needle. The electronic needle selection, Relanit technology, further loop transfer and stitch transfer technologies all these contributed toward the development of high speed and seamless knitting machines. Knitting has basically two types used for fabric formation which are Warp knitting & Weft knitting. Weft knitted fabrics are vastly used for daily uses. For the production perspectives, knitted fabrics are easier to produce than woven fabrics. As it is known that yarn used for knit fabric needs no preparations like warping and sizing,

yarn can directly feed on machine after receiving from spinning mills. Knitted fabrics are made from different types of yarn, of different yarn fineness, composition of the raw material and different structures.

The major eras of improvement and advancements in knitting are[1]:

Period/Year

Machine development

1000 BC	Hand knitting technique using fingers only is invented
11 th Century	Knitted gloves in rituals of church services
12 th Century	knitted caps, gloves and socks from wool and silk
15 th Century	Men started knitting and appears as a profession
1580 AD	Knitting education and teaching started
1589 AD	Knitted frame with boarded needles was invented
1750 AD	Knitting industry started in Europe and UK
1758 AD	Double knits production in derby rib frame by j. Strutt.
1769 AD	Rotary drives were introduced in knitting machines
1847 AD	Invention of latch needles by Matthew Townsend
1850 AD	Power-driven circular knitting frame with vertical bed
1863 AD	V-Bed Flat knitting machine
1892 AD	Hosiery industry started in India at Kolkata
1900 AD	Automatic foot-wear (socks) machine
1915 AD	Tricot warp knitting machine development in Germany
1947 AD	Tricot warp knitting machine is commercialized
1953 AD	Rachel warp knitting machine development
1963 AD	Electronic needle selection mechanism is introduced
1970 AD	Seamless technology using double needle bar developed
1987 AD	Relanit Technology
1999 AD	Double needle bar warp knitting machine with electronic jacquard

Due to the exceptionally good property of knits like excellent elasticity, light weight and due to highly developed and economical production of knitted fabrics a major segment of market is captured by knitted products. The high flexibility and comfort of knitted garments have significantly increased their application in many other areas of human needs i.e. sports, medicine, geo applications and safety. Weft knitted fabrics which have been very popular in recent years are among the preferred fabrics in casual wear, sportswear and underwear. Basic weft knitting structures is single jersey, Rib, Interlock and Purl. Weft knitted fabrics is made from connecting of yarn loops in horizontal direction, courses. Each loop is consisted of one head loop, two vertical stems and two horizontal half circles as lower stems. While vertical force is applied along courses to the fabric, the loop elongated in vertical position and jamming phenomena is occurred in vertical position. This matter is occurred in horizontal position while the force is applied along walls. Therefore, the knitted fabrics have remarkable work up to rapture resistance against both vertical and horizontal forces

specially, forces along courses. Weft knitted fabrics which are knitted in one needle series have hierarchical courses in one surface. The other rib fabrics which are knitted in two needle series (cylinder/dial in circular and two beds in flat knitting machines) have two series of courses in two surfaces.

Interlock has the technical face of plain fabric on both sides, but its smooth surface cannot be stretched out to reveal the reverse meshed loop wales because the wales on each side are exactly opposite to each other and are locked together. Each interlock pattern row requires two feeder courses, each with a separate yarn that knits on separate alternate needles, producing two half gauge 1 x 1 rib courses whose sinker loops cross over each other. Thus odd feeders will produce alternate wales of loops on each side and even feeders will produce the other wales. Interlock fabric is double knit fabric produced by formation and interlinking of loops by the action of two knitting needles namely cylinder needle and dial needle. Interlock fabric is manufactured on interlock knitting machines of various diameter and gauges depending upon the requirement of final products to be made from the fabric. Interlock fabric and plain knitted fabric can be distinguished by way it looks on the reverse side. Fabric structure of interlock will be same from front and back side and we cannot define the technical face and technical back of the fabric. A major difference between rib and interlock fabric is that the loops of interlock are in front of each other while loops of rib fabric are on alternate position. An interlock fabric is relatively thicker than rib fabric because loops are in front of each other and enhance the thickness of fabric. Interlock structure has Moderate extensibility in length, width and area wise extensibility [1-3]. The interlock fabric has good dimension stability and do not curl at the edges. The fabric can be unraveled from the knitted last. Two yarns must be removed to unravel a complete repeat of knitted courses. The interlock fabric is heavier and thicker, twice than that of single jersey fabric Interlock fabric are widely used in t-shirting, socks formation and other summer wears so there must be good comfort along with better performance.

A loop is the basic element of knitted fabric and by changing the shape of loop different types of structures are produced. There are three basic types of stitches produced in all weft knitted fabrics. These are knit, tuck and miss or float stitches. Plain, rib, interlock and purl are the four basic structures of weft knitted fabrics. These structures consists of all knit stitches. All derivatives of basic knitting structures are produced by the combination of knit, tuck and miss stitches. In a knitted structure apart from the basic loop other types of stitch may be produced by varying the timing of the intermeshing sequence of the old and new loops. These stitches may be deliberately selected as part of the design of a knitted structure. A knit stitch is produced when needle clears its old loop and receives a new loop. A tuck stitch is composed of a held loop, one or more tuck loops, and knitted loops. It is produced when a needle holding its loop also receives yarn to form a new loop which becomes a tuck loop. Thus the tuck loop forms an inverted U-shaped configuration as the yarn passes from the sinker loops to the head, which is intermeshed with the new loop of a course above it in the normal manner so that the head of the tuck is on the reverse of the stitch. A float or miss stitch is also composed of a held loop, one or more miss

loops and knitted loops. It is produced when a needle holding its old loop fails to receive the new yarn as shown in which passes, as a float loop, to the back of the needle and to reverse side. The float stitch shows the missed yarn floating freely on the reverse side of the held loop [4].

To obtain a good quality, product focus is not only on aesthetics but also its behavior in certain physical and mechanical demands. Tensile strength and bursting strength are important mechanical properties. Tensile strength is the measurement of the force required to pull a fabric structure to the point where it breaks. Tensile properties of weft knitted fabrics are influenced by factors such yarns interactions, structure and knitting parameters. The longer inlaid yarns on different directions increased the fabric extensibility, the thickness of the fabric and the cover factor, but reduced tensile recover [5]. The use of structures which contain float and knit loops has benefits on tensile behavior and fabrics stiffness (elastic modulus) [6]. Brad and Dinu [7] study the technical and home textiles consist in mechanical properties evaluation. They concluded that hat the double layer knit presents the best mechanical behavior, followed by Birdseye backing Jacquard and then back stripes Jacquard. For tensile stress in bias direction, the twill backing Jacquard has a good breakage resistance value due to the higher number of rib sinker loops in structure that are positioned on the same direction with the tensile force. As a conclusion of their paper, the twill backing Jacquard structure could be considered as an alternative for the quilted double-layer structure for the base material for mattress covers or other applications where a good resistance and elasticity are required [7-8]. Treigienø and Laureckienø [9] investigate plated jersey knits of different composition and stabilized under hydrothermal conditions of 85°C for 10, 20 or 30 min in steam ambience. The influence of stabilization duration on knit structure was estimated as well as change of mechanical properties of the yarns. Other researchers have tried to improve the knitted fabrics suitability for composite materials by the pre-stretch of knitted perform uni-axially and/or bi-axially before consolidation [10-13].Z. Jinyun et al. [14] describe a method for testing the elastic knitted fabric Poisson ratio and modulus was proposed based on orthotropic theory and strip biaxial tensile test.

Bursting strength is a measurement that shows how much force an object can take before it ruptures. It is one of the most important mechanical properties of knitted fabrics. Knitted fabrics are exposed to multi-axial forces not only during their dry and wet processing in the industry but also during their end-use. Therefore, bursting strength test of knitted fabrics is conducted to assess the fabric's ability to withstand multiaxial stresses without breaking off. In the bursting strength property of the fabric, the elongation and strength of the yarn as well as the structure of the fabric are the effective parameter. The bursting strength of the fabrics are measured by the pneumatic or hydraulic method. In both methods vertical pressure is put on the sample under a vacuum and the pressure is determined at the first bursting detect. Kaya [15] investigated performances such as the dimensional stability, skewness, pilling resistance and bursting strength of plain knit and lacoste fabric. She observed that the bursting strength of lacoste was less than plain knit, and there was not an important difference in the bursting strength of unwashed and washed fabrics. Shahbaz et al.[16]

revealed that fabric strength largely depends upon that of the yarn. Ertugrul and Ucar [17] reported that the fabric weight, yarn strength and yarn elongation are the major parameters. In another research bursting strength of various derivatives of single jersey knit fabric in both grey and finished state [18]. Higher presence of tuck and miss loops in wales direction affect the bursting strength. The mechanical properties of Rib structures are also predicted or tested in many papers. In [19], the mechanical performance of the composites which are reinforced with glass knitted fabrics composed of tuck stitches have been investigated. Tensile, compression, impact and compression after-impact tests were performed and the results of the composites reinforced with full cardigan derivative knitted fabrics and 1×1 rib knitted fabrics of glass fibers have been compared. The paper in [20] shows that the weft knitted fabrics with Rib structure have a superior tenacity. Also, double jersey fabrics of Full Cardigan and Full Milano represent better mechanical properties in comparison with single jersey fabrics. In [21], the Milano rib knit fabric structure has been approximated by several simpler plain stitches and its stiffness and strength of each unidirectional composite is predicted.

Clothing comfort properties have significant effect on human body. Clothing comfort is an extremely complex phenomenon resulting from the interaction of various physical and nonphysical stimuli on a person wearing given clothing under given environmental conditions. There are three types of comfort i.e thermo physiological comfort, sensorial comfort and tactile comfort.

Thermo physiological comfort has two distinct phases. During normal wear, insensible perspiration is continuously generated by the body. Steady state heat and moisture vapor fluxes are thus created and must be gradually dissipated to maintain thermoregulation and a feeling of thermal comfort. The clothing becomes a part of the steady state thermoregulatory system. In transient wear conditions, characterized by intermittent pulses of moderate or heavy sweating caused by strenuous activity or climatic conditions, sensible perspiration and liquid sweat occur and must be rapidly managed by the clothing in order to maintain thermal regulation. The behavior of clothing in these two different domains may be predicted by certain measurable fabric properties, including thermal insulation, water vapor permeation resistance, and moisture transport. When a person runs their fingers across the surface of a fabric, a complex multi-sensory emotional and cognitive experience takes place. A memory is stirred, an emotion feeling and association is evoked and a decision is made. An impression becomes embossed in mind. By touching something we get signals by our sensory organs. Sensorial comfort is determined, to some extent, by moisture transport and moisture vapor buffering capacity.

When someone wears clothing, friction between skin and fabric can arise in many areas. This friction is the tangential force to the surface of the skin when the fabric slides over the skin. This is called tactile comfort. One of the basic variables that has a great influence on comfort is fabric construction. Air permeability is one of the important factors on which thermal properties depend. Generally, air permeability depends on the material of constitutive yarns and structural parameters (type of knit structure, type of yarn (spun or filament), yarn size (linear density), twist factor in the

yarn, loop density (wales and courses) and thickness) of the fabric. Air permeability which is mainly a fabric transport property is more sensitive to fabric structure. Generally, the air permeability of a fabric can influence its comfort behaviors in several ways. In the first case, a material that is permeable to air is, in general, likely to be permeable to water in either the vapor or the liquid phase. Thus, the moisture-vapor permeability and the liquid-moisture transmission are normally related to air permeability. In the second case, the thermal resistance of a fabric is strongly dependent on the enclosed still air, and this factor is in turn influenced by the fabric structure. Kane et al.[22] indicated that the combination order of knit-tuck stitches played an important role in all the fabric properties. The result of their study showed that the addition of tuck stitches to knit stitches improved fabric properties like abrasion resistance, air permeability, water absorbency, thermal insulation, compression, bending, shear, tensile properties and handle values Emirhanova and Kavusturan [23] revealed that the effect of knit structure on the bursting strength, air permeability and bending rigidity is highly significant, and tuck stitch fabrics have the lowest resistance to abrasion. Some researchers made a research on the various comfort properties i.e air permeability & water permeability of cotton interlock knitted fabrics, which is one of the most preferred fabric textures in casual wear and sportswear. Nida Oglakcioglu [24] suggested that Interlock and 1*1 rib have a remarkable high thermal conductivity and thermal resistance value as compare to single jersey. On the other hand single jersey have high relative water vapor permeability values than rib and interlock fabric, give warmer feeling at first touch due to lower thermal absorptivity values. Melten Vanilmaz et.al. [25] studied that investigation of wicking, wetting and drying properties of wetting, wicking and drying properties of single jersey 1*1 rib and interlock fabric acrylic fabrics. Ultraviolet radiation is a form of energy traveling through space. Ultraviolet radiation is that part of the electromagnetic spectrum between visible light and x-rays. It was discovered by Johann Wilhelm Ritter, a German physicist which was also credited with the invention of dry cell and dry storage batteries in 1801. The distinguishing factor among the different types of electromagnetic radiation is their energy content. Ultraviolet radiation is more energetic than visible radiation and therefore has a shorter wavelength. To be more specific, Ultraviolet rays have a wavelength between approximately 10 nm 400nm whereas visible radiation includes wavelengths between 400 to 780 nm. An interesting characteristic of UV radiation occurs when it falls upon certain substances known as phosphors, where it causes the phosphors to emit specific visible radiation which is known as fluorescence. A similar effect is phosphorescence in which the emission lasts longer after the UV source is removed. Many practical applications have been developed that take advantage of these unique properties triggered by UV light. Ultraviolet light is divided into three regions, based on wavelength. They are categorize as:

1. UVA
2. UVB
3. UVC

UVA: It is also known as long wave or backlight. It is a radiation with wavelengths between 315nm and 400nm. UV-A is least energetic and least harmful.

UVB: It is a midrange spans wavelengths from 280 to 315nm. UV-B rays have a lower energy level and a longer wavelength than UV-C. As their energy is often not sufficient to split an ozone molecule, some of them extend down to the earth's surface.

UVC: It is termed as shock wave and it covers 280nm down to about 30nm. UV-C is most energetic and most harmful. UV-C rays do not reach the earth's surface because of the ozone layer. When UV-C rays meet the ozone molecules at high layers of the atmosphere, the energy inherent in them is enough to break apart the bond of the molecule and absorb the energy. Therefore, no UV-C rays from the sun ever come into contact with life on earth, though man-produced UV-C rays can be a hazard in certain professions, such as welders.

UVA, UVB, and UVC rays are emitted from the sun and into the Earth's atmosphere and are not visible to the human eye. Though they serve some good purposes when controlled, they're also a potential danger to us. The sun is a major source of ultraviolet rays. Though the sun emits all of the different kinds of electromagnetic radiation, 99% of its rays are in the form of visible light, ultraviolet rays, and infrared rays (also known as heat). Man-made lamps can also emit UV radiation, and are often used for experimental purposes.

The sun is the source of emission of UV rays to the atmosphere. Most UVB and UVC rays emitted by sun are absorbed by the ozone layer in the atmosphere. 97% of all UV radiations that ever reaches the surface of the earth is the UVA type of ultraviolet radiations, depending on cloud coverage and atmospheric condition.

UV levels are not constant over the course of a day, or even over the course of a year. An obvious factor is the position of the sun in the sky. At noon, for example, the electromagnetic waves emitted from the sun travel a much shorter path through the earth's atmosphere than they would at, say, 5 pm, and thus noon-time intensity is stronger. A second important parameter determining UV at the ground is the amount of ozone present in the stratosphere. Low ozone correlates with much UV. However, there are many other features of the environment that contribute to UV radiation variability. Most important are clouds. On cloudy days, UV levels are usually lower than during clear skies as clouds can deflect rays up into space. Clouds can, however, also lead to increased UV levels. This happens, for example, when the sun is not obscured by clouds but clouds in the vicinity of the sun reflect additional radiation to the ground. So a general rule is not to feel safe from UV radiation just because it's cloudy. The amounts of UV one is exposed to also vary with altitude. As a rule of thumb, UV levels increase about 4% for every 1,000 foot gain in altitude. This increase has nothing to do with being closer to the sun - any elevation you might gain would be miniscule in comparison to the distance from the earth to the sun, and so would have an insignificant outcome on UV levels. Instead, the increase is the result of a thinner atmosphere with a smaller number of molecules being present to absorb or scatter UV. Examples of such molecules are tropospheric ozone (commonly associated with smog) and aerosols, molecules that remain suspended in the air. Aerosols can be a multitude of substances - dust, soot, sulfates, etc.

These aerosols absorb and scatter UV rays, and so cut down on the ultimate UV irradiance.

Other factors that have an influence on UV levels are the physical features of the land - sand, snow, and water all tend to reflect UV rays. This phenomenon is called albedo. Some of the ultraviolet rays reflected off the ground encounter scattering by air molecules, aerosols or clouds back down to the earth, thus increasing the total irradiance. When there is snow on the ground the amount of time it takes for sunburn to occur is therefore significantly reduced. Also, the closer one is to the equator, the more ultraviolet rays one is exposed to. This can be explained by the fact that the sun is usually higher at the sky at low latitudes. In addition, the ozone layer is thinner at the equator as it is over, for example the United States or Europe, and this also contributes to more UV.

Since the 1980s, Polar Regions are affected by the ozone hole. Under the ozone hole, biologically relevant UV levels are 2-3 times as high as they were before. Learn, based on real data, how UV levels are affected by the ozone hole by going here you can compare UV radiation measured by the NSF network in Antarctica with satellite ozone data.

Ultraviolet protection factor (UPF) is the scientific term used to indicate the amount of ultraviolet (UV) protection provided to skin by fabric. UPF values are analogous to SPF (Sun Protection Factor) values the only distinction being that SPF values for sunscreens are determined through human testing whereas UPF values are based on instrumental measurements. UPF is defined as the ratio of the average effective UV irradiance calculated for unprotected skin to the average UV irradiance calculated for skin protected by the test fabric. The general approaches to testing fabrics for the ability to prevent sun burning are laboratory testing in vivo and instrumental evaluation in vitro. The quantitative measure of an in vivo determination is the sun protection factor (SPF), and that used to indicate the result obtained instrumentally is the ultraviolet protection factor (UPF). The quantification of protection that a fabric offers against ultraviolet radiation is obtained by the determination of the in vitro ultraviolet protection factor (UPF). The amount of UV light reaching the ground in any given place depends on a number of factors, including the time of day, time of year, elevation, and cloud cover. For better understanding the strength of UV light in their area on a given day, The National Weather Service and the Environmental protection Agency (EPA) have developed the UV Index. It gives people an idea of how strong the UV light is in their area, on a scale from 1 to 11+, A higher number means greater risk of exposure to UV rays and a higher chance of sunburn and skin damage that could ultimately lead to skin cancer.

UV Absorbers:

UV absorbers are organic or inorganic colorless compounds with strong absorption in the UV range of 290 – 360 nm. UV absorbers incorporated into the fibers convert electronic excitation energy into thermal energy, function as radical scavengers and singlet oxygen quenchers. The high-energy, short-wave UVR excites the UV absorber to a higher energy state; the energy absorbed may then be dissipated as longer-wave

radiation. Alternately, isomerization can occur and the UV absorber may then fragment into non-absorbing isomers. Sunscreen lotions contain UV absorbers that physically block UVR. The most widely used UVB screens, 2-ethyl hexyl-4-methoxy cinnamate with high RI, make a substantial contribution to the RI matching of skin, i.e. 'refractive index matching'. An effective UV absorber must be able to absorb throughout the spectrum, to remain stable against UVR, and to dissipate the absorbed energy to avoid degradation or loss in color.

Organic UV absorbers are mainly derivatives of o-hydroxyl benzophenones, o-hydroxy phenyl triazines, o-hydroxy phenyl hydrazines. The orthohydroxyl group is considered essential for absorption and to make the compound soluble in alkaline solution. Some of the substituted benzophenones penetrate into synthetic fibers much like disperse dyes. Commonly-used UV absorbers are 2-hydroxy benzophenones, 2-hydroxy phenyl benzotriazoles, 2-hydroxy phenyl-Triazines and chemicals such as benzoic acid esters, and hindered amines. The strong absorption in the near UV of 2, 4 dihydroxy benzophenone is attributed to conjugating chelation between the orthohydroxyl and carbonyl groups. Organic products like benzotriazole, hydro benzophenone and phenyl triazine are primarily used for coating and padding processes in order to achieve broad protection against UV rays. Suitable combinations of UV absorbers and antioxidants can yield synergistic effects. Benzophenone derivatives have low energy levels, easy diffusibility and a low sublimation fastness. Orthohydroxy phenyl and diphenyl triazine derivatives have an excellent sublimation fastness, and a self-dispersing formulation can be used in high temperature dyeing in pad baths and also in print pastes.

UV absorbers incorporated into the spinning dope prior to the fiber extrusion and dye bath in bath dyeing improve the light fastness of certain pastel shades and the weather ability of spun-dyed fibers. UV absorbers to the extent of 0.6 – 2.5% are sufficient enough to provide UVR protection fabrics. The presence of UV absorbers in PET, nylon, silk and wool protects the fibers against sunlight-induced photo degradation. On wool, UV absorbers can retard the photo-yellowing that occurs upon exposure to sunlight. Triazine class-hindered amine light stabilizers are used in PP to improve the UV stability. The addition of HALS to 0.15% weight is sufficient to improve stability substantially. Even pigmented PP requires UV stabilizers if the fibres are exposed to UV during their services. High-energy UV absorbers suitable for PET include derivatives of o-hydroxyphenyl diphenyl triazine, suitable for dye baths, pad liquor or print paste.

UV absorbers have refractive indices of about > 2.55 , by means of which maximum covering capacity and opacity is achieved. The presence of inorganic pigments in the fibers results in more diffuse reflection of light from the substrate, and provides better protection. TiO_2 added in the spinning dope for matt effects in the fibers also acts as a UV absorber. Titanium dioxide and ceramic materials have an absorption capacity in the UV region between 280 and 400 nm, and reflects visible and IR rays; these absorbers are also added as dope additives. For maximum effect, the particles have to be monomolecularly distributed, and are often applied in one bath.

Nano scale titanium gel particles strongly bound to the cotton fabrics can give a UPF ≥ 50 without impairing the tensile properties. Brighter viscose yarns provide the highest UV transmittance compared to the dull pigmented viscose yarns, modal yarns. Zinc oxide nanoparticles, which have a very narrow size distribution (20-40 nm) and minimal aggregation, can result in higher levels of UV blocking. Use of TiO₂, ZnO alone produces less absorption of UVR than a mixture of (67/33) titanium dioxide and zinc oxide on cotton and nylon fabrics. Microfine nylon fabrics with a porosity of 0.1% are capable of giving UPF > 50 with 1.5% TiO₂. Incorporating UV absorber in dyeing decreases the dye uptake slightly, except in post-treatment application.

Many commercial products and processes have been developed to produce fabrics with a high level of UPF using various dope additions and topical applications for almost all types of fabrics produced from cellulosic fibres, wool, silk and synthetic fibres. Most of the commercial products are compatible with the dyes and other finishing agents applied to the textile materials, and these agents can be applied using simple padding, the exhaust method, the pad thermo fix and the pad-dry-cure methods.

Benefits of UV

- i. UVB exposure increases the production of vitamin D in the skin.
- ii. Vitamin D deficiency leads to some kinds of cancer and thousands of premature deaths annually.
- iii. Use - UV rays (wavelengths shorter than 300 nm) helpful for killing bacteria and viruses (germicidal lamps, sterilize surgical instruments, water, and air in operating rooms).
- iv. Detection – many different satellites (used to study ultraviolet astronomy).
- v. UV is used in diagnosis of many diseases and many curing techniques sometime.

Harmful Effects of UV

Following are the different harmful effects on the human body by the ultraviolet radiations. All the types of UV are harmful to human skin in most of the cases as it:

- i. Degrades the components of paper, photographs, inks, paints, and adhesives.
- ii. Ultraviolet rays with wavelengths below 320 nm are harmful to living things. There Over exposure can cause painful eye irritation or eye inflammation it can also cause bad sunburns, as well skin cancer. May be prevented with Sunscreens.
- iii. Ultraviolet B causes sunburn and a number of damaging photochemical changes within cells, including damage to DNA, leading to premature aging of the skin, premalignant and malignant changes, and a variety of photosensitivity reactions.
- iv. In general, UVB produces much greater short-term effects on the skin, such as tanning, sunburn, and damage to DNA, than UVA. UVB is also known to reduce the functioning of the immune system but this is less clear for UVA.

- v. UVB is likely to be the main cause of premature skin ageing and of one type of skin cancer. However, for the most lethal type of skin cancer, the roles of UVA and UVB are not yet known. UVA can also destroy vitamin A in the skin.

UVA light has been shown to cause DNA damage, but not directly like UVB. Due to its longer wavelength, the UVA light is absorbed less and reaches deeper into skin layers, where it produces reactive chemical intermediates, which in turn can damage single-strand breaks of DNA. UVA is capable of causing damage to collagen fibers, so it has the potential to accelerate skin aging and cause wrinkles.

Effect of UV on Textile Materials

UV radiation is one of the major causes of degradation of textile materials, which is due to excitations in some parts of the polymer molecule and a gradual loss of integrity, and depends on the nature of the fibers. Because of the very large surface volume ratio, textile materials are susceptible to influences from light and other environmental factors. The penetration of UVR in nylon causes photo oxidation and results in decrease in elasticity, tensile strength and a slight increase in the degree of crystallinity. In the absence of UV filters, the loss in tensile strength appears to be higher in the case of nylon (100% loss), followed by wool, cotton and polyester, with approximately 23%, 34% and 44% respectively after 30 days of exposure. Elevated temperature and UVB radiation on cotton plants result in severe loss of bolls. Naturally-colored cottons contain pigment ranges from light green to tan, brown and inherent long-term UV protection properties with a UPF of 64 and 47, whereas normal cotton shows a UPF of 8. Researches prove that ultraviolet radiation (UVR) from the sun could be a primary cause of skin cancer [26-27]. The number of skin cancer cases found has been increasing around the world in the recent years, including both non-melanoma and melanoma skin cancers. As a result, the adverse impact caused by overexposure to UVR has increased the public awareness of the need to adopt personal UV protective strategies such as the use of sunscreens on the parts of body that are exposed to the sun. Ultraviolet rays constitute a very low fraction in the solar spectrum but influence all living organisms and their metabolisms. These radiations can cause a range of effects from simple tanning to highly malignant skin cancers, if unprotected. Apart from sunscreen and shading, wearing textile garments could be a practical solution to avoid the contact of skin and UVR. Alterations in the construction parameters of fabrics with appropriate light absorbers and suitable finishing methods can be employed as UV protection fabrics. The paper deals with the deleterious effects of UV rays and protection against them through textile materials. UVR exposure can be reduced by implementing behavioral changes such as avoiding sunlight at its maximum, using protection such as hats, sunscreens, sun glasses and clothing. Ultra violet-blocking treatment for cellulosic fiber (cotton) is developed using the sol-gel method. Treatment create a thin layer of titania on the cotton fiber surface and the treated cotton fabrics shows very improved protection against ultra violet radiations including UPF factor of 50+ or excellent protection

according to the Australia/Newzeland standards. There is a high adhesion between the Titania layer and cotton fabric even and can be maintained even after 55 home laundering. UV absorption of the Titania layer substantial and gives excellent UV protection to the treated fabrics. This treatment has no adverse effect on mechanical strength of the treated fabric as indicated by the bursting strength fast .

UV protected fabric formation utilizing the sol-gel method. In this the zinc oxide nanosol 5% solution is used and fabric is dipped in this solution for 10 minutes and then dried at 90°C for 10 minutes and for post heat treatments are made at different temperatures for 2-3 minutes. After post treatment at different conditions of samples the comparison of coatings were made. Tests for UV protection properties were determined according to the standards, and excellent results were obtained for UV protection by using nanosol solution. The UPF achieved in this treatment were 50+ which is considered as excellent. The samples even after 50 washings show good UV protection [28]. Different parameters of UV protection were studied by researchers, most of their research was on woven fabrics and chemical approaches that can increase the ultraviolet protection factor. Fabric protection from ultraviolet knitted fabric constructions by studying the weight, thickness and stitch density of knitted fabrics. Knitted structures like plain, locaste, combinations of knit miss and tuck stitches along with half Milano, full Milano, cardigan structures , 1x1 rib, interlock were prepared and testing observed that weight was most important factor while thickness and density were also effects but not primarily factors in determining UV protection. Many researchers have studied various fabric parameters that influence UVR transmission including fiber composition, fabric construction, yarn twist, thickness weight wetness or moisture content, stretch or extensibility, chemical treatment or additives, and coloration [28-29] .However, most of the studies have concentrated on the fabric parameters with woven fabrics only, whereas there have been few studies concerning knitted fabrics. The knitted fabric is of great importance in this case as the knitting production is increasing day by day. The work on knitted fabrics was done mostly on single jersey fabric by changing stitch density, count variation, use of different type of yarn and by variation in GSM. In knitting there is little work on interlock fabric. Interlock fabric has greater stability due to moderate extensibility in all directions and greater UPF factor. The aim of present investigation is to study the effect of interlock structures and its derivatives i.e pique and half cardigan (tuck stich), cross miss and half Milano (miss stich) .Effect of tuck and miss stiches on mechanical, comfort and Ultraviolet protection factor(UPF).Correlation analysis is also used to study the relationship between UPF & Air permeability and Bursting strength. The research will contribute towards the development of knitted fabric with a high ultraviolet protection value.

2. Material & Methods:

Materials used for the production interlock knitted fabrics and its derivatives are spun Polyester. The interlock structures made were Plain interlock, pique, half cardigan, half Milano and cross miss. Yarn counts used is 30^s.Interlock circular knitting machine of Fukuhara, Japan is used for the production of structures. The machines

have gauge E = 20 needles/inch and machine diameter is 26 inch. Total of 10 samples were produced.

2.1 Testing:

Samples were washed in room temperature to achieve relaxed state. After that samples were tumble dried. Following testing were performed according to standards.

2.11 Tensile strength

Tensile testing of samples were done according to standard ASTM-D5034. The machine works on the principle of constant rate of extension (CRE). The testing machine runs with a speed of 100 mm/min. A 6×4 inch sample is mounted in clamps of tensile tester machine. A force applied until the specimen breaks. For each sample, 3 measurements were done and the mean (\bar{m}) and standard deviation (\bar{r}) were calculated. All the measurements were made under standard atmospheric conditions.

2.12 Bursting strength

It is the force, applied at specific region that cause the rupture of the textile fabric. Testing of samples were done according to ASTM-D3786. This test method is used for textile industry for the evaluation of a wide variety of end use. Apparatus required are Hydraulic bursting strength tester machine. The machine works with hydraulic pressure and uses a mixture of air and oil to create pressure. Fabric was placed above the rubber and tightens with the help of lever to avoid slippage. After placing the fabric, starting lever is pulled towards right side to start the machine. Pressure generated by air and oil mixture filled in the rubber and it started to swell. At the certain point the stitches broke and reading on the meter was noted. For each sample, 3 measurements were done and the mean (\bar{m}) and standard deviation (\bar{r}) were calculated. All the measurements were made under standard atmospheric conditions.



Fig. 1: Hydraulic bursting strength tester

2.13 Air Permeability

Air permeability of all the samples were done according to standard ISO -9237. This test method is used to measure the rate of air flow perpendicular through the fabric under prescribed air pressure. It is applicable to the woven fabrics, air bag fabrics, blankets, napped fabrics, knitted fabrics, layered fabrics and pile fabrics. Air

permeability is an important feature for the breathability of the fabric. The fabric' air permeability helps crucially in the transport of water vapors from the Skin-Fabric atmosphere to outer atmosphere. Air permeability is measured in mm/sec. Equipment used are SDL Atlas Air Permeability Tester



Fig. 2: SDL ATLAS Air Permeability Tester

The fabric whose air permeability is to be measured is placed in the circular Test area (20 cm²) where the air of Pressure 100 Pa is sucked through the fabric. To measure the air permeability of each side of the interlock fabric, the both sides of the interlock fabrics were passed through this test. For each sample, 10 measurements were done and the mean (m) and standard deviation (r) were calculated. All the measurements were made under standard atmospheric conditions.

2.14 Ultraviolet protection factor

In this study, in vitro approach was used to measure the protection ability of knitted fabrics instead of in vivo one since it was able to provide a simple method of rating the UV protective abilities of fabrics by using relatively low-cost procedures. The in vitro measurement of fabric protective ability was conducted with a spectrophotometer Double Beam UV/Visible Spectrophotometer M-550 in accordance with the AATCC-183 standard. Ultraviolet protective factor (UPF) was used in this study as a quantitative indicator to represent the UV protective capabilities of knitted fabrics from sunburn



Fig. 3: Double beam UV/Visible light Spectrophotometer

The 2/2 inch sample of fabric is placed between the two plates of the machine and the radiation is allowed to pass through the sample so the ultraviolet protection is measured. The sensors are used to measure the passage of UV from the fabric.

3. Results & Discussions:

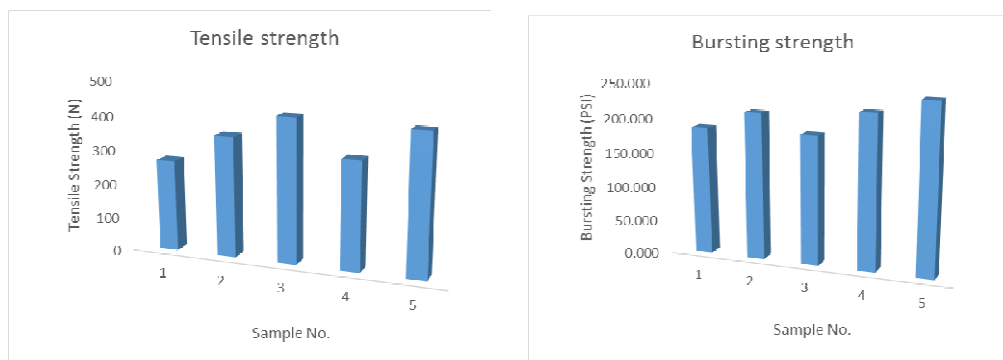
Results of all testing are mentioned in Table 1.

3.1 Tensile strength:

Tensile strength in wale direction shows that half cardigan has highest strength. Plain interlock structure has less tensile strength which is due to fact that tensile strength depends upon the number of yarn accumulation. If there is high yarn accumulation then the tensile strength will increases and vice versa. Since tuck loop on application of applied load tuck loop provides more resistance than knit loop. The results are given in Figure 4(a). It is also observed from above results that pique, cross miss and half Milano interlock structures have the greater tensile strength value than for the plain interlock structure.

Table 1: Results of all knitted samples

Sample #	Tensile strength (N)	Bursting strength (PSI)	Air permeability(mm/s)	UPF
1	267.56	185.667	1328	124.25
2	352.69	211.667	1658	116.475
3	418.98	186.333	1474.5	115.325
4	314.76	221.667	1221.5	134.325
5	407.39	242.667	983	159.475



(a) Tensile strength

(b)Bursting strength

Fig. 4: Mechanical Properties of Knitted samples

3.2 Bursting Strength:

In this study it is observed that as shown in Figure 4 (b) ,bursting strength is due to the fabric structure, as there are more no of combination of miss and knit stitches in the fabric, bursting strength will be higher .Interlock half Milano and cross miss have higher bursting strength . Due to miss stitches, greater slippage also occurs, fabric need more pressure to burst and ultimately the bursting strength of the fabric increases. Miss stitch is able to produce a tighter structure and hence, the elongation increases, resulting in a higher bursting strength. Fabric width is increased because tuck loops pull the held loops downwards, causing them to spread outwards and make

extra yarn available for width-wise extensibility. So structures with tuck stitches have higher bursting strength increase than plain interlock structure.

3.3 Air permeability:

Structure with miss stitches showed i.e half Milano and cross miss has low airflow permeability. Pique and half cardigan structures showed highest airflow permeability and in between these Plain fabrics. Air permeability depends upon no. of pores and also on pore size. With all knit stitches, the fabric become compact and the space between loops reduces and fabric become air resistant. It is clear that with the addition of tuck loop in interlock knitted fabric air permeability increase. As tuck loop create more open space on the fabric .By introducing the combination of knit and tuck stitch the, air permeability increases as described by other researcher[30]. When using tuck stitches the fabric is wider, thicker and slightly less extensible. Tuck stitch structure is more open and porous than the knit stitched fabrics. Hence, the fabrics from plain stitches showed high air permeability resistance than those fabrics from knit-tuck combination stitches.

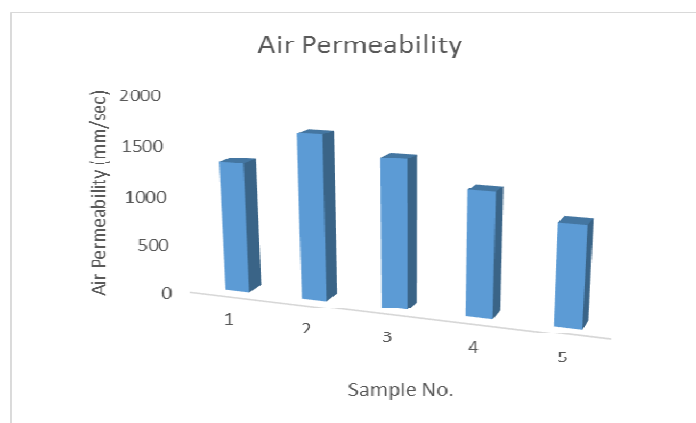


Fig. 5: Air permeability of all samples

3.4 Ultraviolet Protection Factor (UPF)

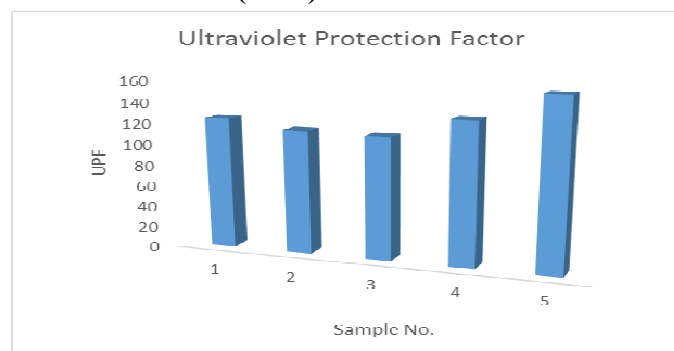
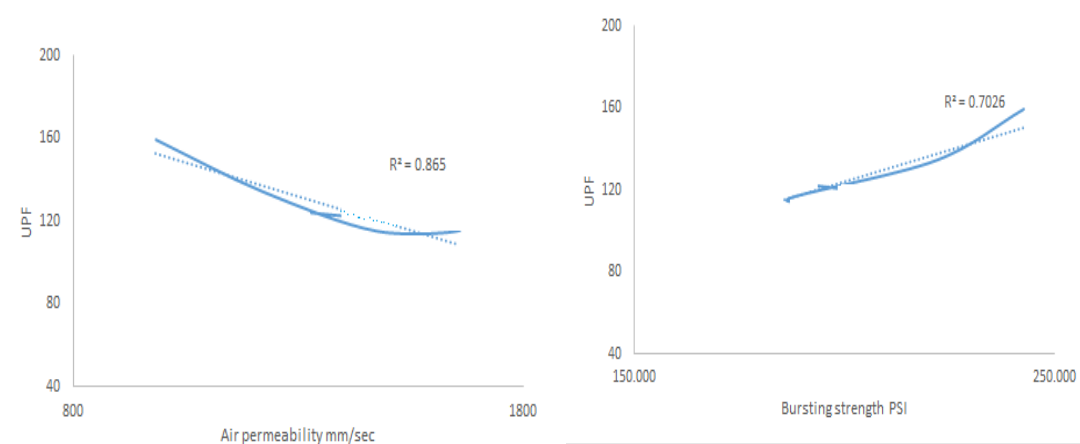


Fig. 6: Ultraviolet Protection Factor of all samples

From the Figure 6, it is clear that, a structures with miss stitches i.e half Milano and cross miss has a higher UPF. It is due to the effect of miss stitches which would narrow and tighten the fabrics and hence results in higher UPF. The miss loops would pull the knit loops closer to each other and give the fabric higher stitch density. Therefore UV radiation is scattered and becomes more difficult to penetrate through the fabric and contact the skin. Meanwhile, the miss loop floats at the back of the fabric and therefore less UV radiation can pass through the fabric, resulting in higher UPF value as found by other researchers [31-32]. Plain interlock structure have intermediate UPF values. Tuck stiches made the fabric open so UPF values are lower for them.

3.5 Co-relation between air permeability and UPF:

The way for UVR to pass through fabric can be divided into two paths. The first path passes partially or totally through fibers and the second path passes through fabric pores. Therefore, air permeability can be one of the indications for the accessibility of UVR approaching the skin. Air permeability is measured by the rate of air flow passing perpendicularly through the fabric test area over a given period of time. Higher the air resistance means the fabric is less permeable because it required higher air pressure to pass through the fabric layer. In other words, fabric with lower air permeability have better UV protection as it allows less UVR to transmit through the pores of fabric. In our study dependence of UPF and air permeability is shown in Figure 7(a). UPF is increasing with decreasing air permeability. Corresponding coefficient of determination $R^2 = 0.863$ indicates a good quality of fit.



(a)UPF vs Air permeability

(b)UPF vs Bursting strength

Fig. 7: Co-relation of UPF with Air permeability and Bursting strength

3.6 Co-relation between Bursting strength and UPF:

In order to analyses the correlation between bursting strength and UPF of all knitting structures, Figure 7 (b) is drawn, which shows that bursting strength is strongly positively correlated with UPF. In this research, the R_2 value of all knit structures is

0.70. This indicates that the correlation between bursting strength and UPF of all knit structures is strong.

Conclusions:

The purpose of this research was to study the effect of interlock and its derivative on properties. Interlock half cardigan has highest tensile strength than all other structures due to accumulation of yarn. Generally speaking, the knit and miss single-knitted fabrics have greater bursting strength than the others due to the effect of miss stitches. Half Milano has highest bursting strength among all structures due to miss stitches. Half Milano has highest air resistant due to compact structure. Half Milano has highest UPF value among all structures.

Structure and type of stitches play a more important role in determination of the UPF in interlock knitted structure. It can generally be summarized that, for knitted fabric structures with knit and miss, higher UPF values would be obtained than with knit and tuck structure. Due to miss stitches, decrease in width occur leads to high covering, showing reduction in UV transmission.

Relationship between UV radiation and air permeability was found significant in this study. The addition of tuck stitches to the knit stitches improved air permeability. Relationship between UPF and bursting strength of Interlock fabrics with different derivatives were also studied. It is found that the change of bursting strength with UPF was significant. Combination of stitches played an important role in the mechanical, comfort, and Ultraviolet protection properties. Interlock half Milano fabric showed better performance for the summer wear.

References:

1. D. J. Spencer, *Knitting Technology A comprehensive handbook and practical guide*. 2001, p. 413.
2. Sadhan Chandra Ray, [2011] *Fundamentals and advances in knitting technology*. 2011, p. 393.
3. S. R. Chan, *Fundamentals and advances in knitting technology*, First. New Dehli: Woodhead Publishing India Pvt Ltd, 2011.
4. J. J. F. Knapton and D. L. Munden, "A study of the mechanism of loop formation on weft-knitting machinery: Part I: The effect of input tension and cam setting on loop formation," *Text. Res. J.*, vol. 36, no. 12, pp. 1072–1080, Dec. 1966.
5. M. De Araújo, R. Figueiro, H. Hong, "Modelling and Simulation of the Mechanical Behaviour of weft-Knitted Fabrics for Technical Applications, Part II", *Autex Research Journal*, vol. 3, iss. 3, pp. 117-123, 2003.
6. M. De Araújo, R. Figueiro, H. Hong, "Modelling and Simulation of the Mechanical Behaviour of weft-Knitted Fabrics for Technical Applications, Part III", *Autex Research Journal*, vol. 4, iss. 1, pp. 107-112, 2004

7. Brad R, Dinu M. Experimental investigation on tensile strength of jacquard knitted fabrics, 2015: 21-26.
8. Sudipta PS, Mahish S, Patra AK, Thakur R. Functional properties of bamboo/polyester blended knitted apparel fabrics, *Indian Journal of fiber and Textile Research* 2012;37:231-237
9. Treigienė R, Laureckienė G. The Influence of Stabilization on the Structure of Knits and Tensile Properties of Their Yarns, *ISSN 1392–1320 Materials Science (Medžiagotyra)* 2012; 18(4).
10. Yexiong Q, Jialu L, Liangsen L. Tensile properties of multilayer-connected biaxial weft knitted fabric reinforced composites for carbon fibers, *Composites Research Institute of Tianjin Polytechnic University & Tianjin and Education Ministry Key Laboratory of Advanced Textile Composite Materials, Tianjin 300160, China, 2013,*
11. F. Zaixia, G. Y. Zhangyu, L. Hairu, “Effects of Pre-stretching on the Tensile Properties of Knitted Glass Fiber Fabric Reinforced Polypropylene Composite, *Journal of Thermoplastic Composite Materials*”, SAGE Publications, vol. 19, iss. 4, pp. 399-411, 2006.
12. T.B Bini, S. Ramakrishna, Z. M. Huang, C.T. Lim, “Structure–tensile property relationship of knitted fabric composites”, *Polymer Composites*, vol. 22, iss. 1, pp. 11 – 21, 2001.
13. S. Ramakrishna, Z. Maekawab & N.K. Cuongc, “Analytical methods for prediction oftensile properties of plain knitted fabric reinforced composites”, *Advanced Composite Materials*, volume 6, issue 2, pp. 123-151, 1997.
14. Z. Jinyun, L. Yi, J. Lam and C. Xuyong, “The Poisson Ratio and Modulus of Elastic Knitted Fabrics”, *Textile Research Journal*, vol. 80, iss. 18, pp. 1965–1969, 2010.
15. Kaya T. An Investigation about the Performance of Circular Knitted Fabrics Manufactured with Polypropylene Continuous Filament Yarns. M.Sc. Thesis *Textile Engineering University of Gaziantep*, 2006.
16. Shahbaz B, Jamil AN, Farooq A, Saleem F. Comparative Study of Quality Parameters of Knitted Fabric from Air-jet and Ring Spun Yarn *J. Applied Sci* 2005; 5 (2): 277-280
17. Ertugrul S, Ucar N. Predicting Bursting Strength of Cotton Plain Knitted Fabrics using Intelligent Techniques. *Textile Res. J.* 2000; 70: 845-851.
18. Azharul Islam, “Effect Of Wale Wise Increasing Of Tuck And Miss Loops On Bursting Strength Of Single Jersey Fabric At Grey And Finish State”, *JRET: International Journal of Research in Engineering and Technology*, volume 03, issue 02, Feb 2014.
19. T. Alpyildiz, B. Murat Icten, R. Karakuzu, A. Kurbak, “The effect of tuck stitches on the

- mechanical performance of knitted fabric reinforced composites”, *Composite Structures*; vol. 89, iss. 3, pp. 391-398, 07/2009.
20. D. Semnani, “Mechanical Properties of Weft Knitted Fabrics in Fully Stretched Status long Courses Direction: Geometrical Model Aspect”, *Universal Journal of Mechanical Engineering*, vol. 1, iss. 2, pp. 62-67, 2013.
 21. Zheng-Ming Huang, S. Ramakrishna, K. H. Leong, “Modeling the Tensile Behavior of Milano Rib Knit Fabric Composites”, *Journal of Reinforced Plastics and Composites*, vol. 21, pp.1123-1146, August 2002.
 22. Kane CD, Patil UJ, Sudhakar P. Studies on the Influence of Knit Structure and Stitch length on Ring and Compact Yarn Single Jersey Fabric Properties. *Textile Res. J.* 2007; 77: 572-582.
 23. Emirhanova N, Kavusturan Y. Effects on Knit Structure on the Dimensional and Physical Properties of Winter Outerwear Knitted Fabrics. *Fibres & Textiles in Eastern Europe* 2008; 16: 69-74
 24. N. Oğlakcioğlu and A. Marmarali, “Thermal Comfort Properties of Some Knitted Structures,” *Fibres Text. East. Eur.*, vol. 15, no. 5, pp. 94–96, 2007.
 25. M. Yanilmaz and F. Kalaoglu, “Investigation of wicking, wetting and drying properties of acrylic knitted fabrics,” *Text. Res. J.*, vol. 82, no. 8, pp. 820–831, 2012.
 26. R. N. Saladi and A. N. Persaud, “The causes of skin cancer: a comprehensive review,” *Drugs of Today*, vol. 41, no. 1, pp. 37–53,2005.
 27. D. L. Narayanan, R. N. Saladi, and J. L. Fox, “Ultraviolet radiation and skin cancer,” *International Journal of Dermatology*, vol. 49, no. 9, pp. 978–986, 2010.
 28. Vihodceva, S.; Kukle, S. ,Improvement of UV Protection Properties of the Textile from Natural Fibres by the Sol-gel Method, *IOP Conference Series: Materials Science and Engineering*, Volume 49, Issue 1, article id. 012022 (2013).
 29. A. Riva and I. Algaba, “Ultraviolet protection provided by woven fabrics made with cellulose fbres: study of the influence of fibre type and structural characteristics of the fabric,” *Journalof the Textile Institute*, vol. 97, no. 4, pp. 349–358, 2006.
 30. P. D. Dubrovski and D. Golob, “Effects of woven fabric construction and color on ultraviolet protection,” *Textile Research Journal*, vol. 79, no. 4, pp. 351–359, 2009.
 31. H. K. S. Chong, C. W. Kan, J. K. C. Lam, S. P. Ng, H. Hu, and C. W. M. Yuen, “Study on the relationship between UV protection and knitted fabric structure,” *Journal of Textile Engineering*, vol. 59, no. 4, pp. 71–74, 2013
 32. Wai-yin Wong, Jimmy Kwok-Cheong Lam, Chi-wai Kan, Ron Postle “Influence of knitted fabric construction on the ultraviolet protection factor of greige and bleached cotton fabrics”*Textile Research Journal* Vol 83, Issue 7, pp. 683 - 686.

Textile sector in Turkey

Hamdi Ayyildiz ¹, Hana Křížová ²

¹ *Turkoglu Vocational School, Dept. of Management and Organization,
Kahramanmaras Sutcu Imam University, Turkey*

² *Faculty of Textile Engineering, Dept. of Material Engineering,
Technical University of Liberec, Czech Republic*

1. INTRODUCTION

The word "Textile", which means woven fabric with word meaning, has a different meaning in Turkey. The text in Turkish language is expressed in phonetic structure in English, "mensucat" in Ottoman, "textiles" in French, and "textil" in German. Textile word while expressing "weaving" in international literature, has a wider meaning in Turkish economic literature and includes not only weaving but also knitting, apparel and even leather. The textile industry is one of the oldest production activities in the world, consisting of the steps of making various fiber types into yarn first, followed by the combination of fabric and colors in certain patterns and then obtaining the final product. The textiles and ready-to-wear sectors are often confronted as two interrelated terms because of their close interaction with each other and the production and distribution chain of the garment industry. Textile does not only mean yarn and fabric production, it also uses technical textiles and extensively exploits many different areas such as carpet, automotive, fire extinguishing hoses. In the recent period, after the development of ecological textiles, intelligent textiles, which now contain more technology, multifunctional fibers, military clothes, protective hospital clothes, high-performance sports clothes, etc. are used in many areas.

According to the Standard International Trade Classification, Rev.3, which is made by United Nations Statistics Division, the textile industry data in section 65 of the Manufactured goods classified chiefly by material in the class number 6 and Miscellaneous manufactured we observe the apparel sector data in section 84 of articles.

2. HISTORY OF TEXTILE INDUSTRY IN TURKEY

2.1 From Ottoman Empire to 2nd World War

The development of the textiles and ready-to-wear sector dates to the time of the Ottoman Empire. Turkey started industrialization in the 19th century with the period called the Tanzimat period. In this period, the state was established in 1835 as a tarboosh factory, the state was established broadcloth/baize factory in 1845 in Izmit and Islimiye factory, in 1855 Cotton and Silk fabrics in Hereke, Silk weaving factory in Bursa, aba factory in Balikesir and special factory beside Samako factory weaving factories have been established by individuals. Significant development efforts were also observed in the weaving field as well as in all industrial branches with the second Constitutional Monarchy in 1908 and the establishment of enterprises for the purpose

of industrialization was encouraged. Although the Encouragement in Industrial Law was accepted for the first time in 1913, the development of the textile industry remained after the Turkish War of Independence took place at the beginning and the beginning of the First World War. Between 17 February and 4 March 1923, industrial reforms were planned in the İzmir Economy Congress in İzmir. The planned industrialization was tried to be realized with the understanding of statism which was adopted after the Izmir Economy Congress. The state began the construction of Five-Year Industrial Plans in response to a private enterprise that could not be developed until 1933 [1]. With the First Five-Year Industrial Plan, efforts to develop the Turkish textile industry were intensified and the establishment of Sumerbank in 1933 accelerated the process of dissemination of technological information [2]. Established in 1933 Sümerbank started to business taking over the Bakirkoy cotton fabric, Feshane wool fabric, Hereke silk-woven fabric and Beykoz leather-shoe factory. The main aim of Sumerbank is to help domestic entrepreneurs in every aspect. With the start of the planned industrialist, 56 million Turkish Liras were invested in different industrial branches and 27 million Turkish Lira (48.2%) of this money was allocated to textile industry only. Thus, weaving / textile sector plan is more accurate in the first development plan [3]. In the I. Development Plan, 21 million Turkish Liras (80 %) of the 27 million Turkish Lira allocated to the textile industry are divided into cotton yarn and weave. The Bakırköy factory was first adapted to the technological conditions of the day, followed by the establishment of Kayseri, Eregli, Nazilli and Malatya cotton weaving factories and more recently the establishment of a yarn factory in Erzurum. As it can be understood from this, in the first industrialization plan started to be implemented in 1934, the greatest weight was given to the textile industry.

2.2 From 2nd World War to 1980

In the ongoing period, beginning with the development of textile sector with the impact of World War II, the textile sector entered a period of stagnation. In the textile sector, which is positioned as the priority industry, II. In the post-World War era, in particular the 1950s and 1960s, the emphasis was on incentives of private enterprise instead of statism. Thanks to the incentives given in these years, since the 1950's, significant improvements have been made in the textile industry and a very small number of private enterprises have been established. For the first time in 1952, the share of the private sector in cotton weaving production reached 38%, and in 1953 the share of production in the private sector surpassed Sumerbank, the state's economic enterprise. Between the 1960s and 1980s, the textile sector, which undertook the primary order in the outsourcing of the Turkish economy, employed about 1/5 of the workers. With the development plans, the transformation of the enterprises into big enterprises in the weaving sector has accelerated, II, III. and IV. During the planning periods, cotton woven, cotton yarn, and then wool yarn and woolen weaving stepped in and the outcomes achieved improved the garment industry. On January 24, 1980, the government issued a new economic program and decided to liberalize the market by restricting state intervention and increasing trade liberalization, exports. Most of

quotations and export declarations in textile and apparel are abolished and protective measures are reserved for raw materials. Export incentives have been passed on. Exporters have benefited greatly from exporters' exemption from paying production tax on final export products and removal of customs duty payment obligations on imports of intermediate products for textile and ready-to-wear production [4].

2.3 From 1980 to the 90s

After 24 January 1980, export-oriented development policies, textile and apparel development, investment and machine support have been misunderstood. As a result of this process, the competitiveness of the Turkish textile and garment industry has increased and exports have increased [5]. Added value has come to the forefront and export incentives have been taken into consideration since the import substitute industrialist in Turkey has left its place to growth model based on export and export from the 1980s onwards, so importance has been attached to the rapid development of weaving and ready-to-wear industries. In the 1990s, Turkey became the second largest supplier of Europe after Italy [6]. The Customs Union agreement with the EU entered into force in 1996, facilitating trade between the EU and Turkey in intermediate goods. With the agreement, Turkey's average customs tariff has decreased by 3.6%. The EU's quantitative restrictions have also come to an end with the Customs Union. Many new arrangements have been enacted, such as the Customs Union and the competition law, the consumer protection law, the protection of industrial designs and the protection of brands. With the liberal trade decisions taken in 1980, textile and apparel sectors played a vital role in the economy of the country in the last thirty years, both in terms of industrialization and market formation. For this reason, with its share in economic indicators, the sector is regarded as one of the basic industries of the country. Table 1 gives an overview of key historical points in the development of the textile industry in Turkey.

Table 1: Historical Development of the Turkish Textile and Ready-to-Wear Sector

Year	Key Points
1923	İzmir Economy Congress and the introduction of State Economic Enterprise system (Statism of state)
1933	Establishment of Sumerbank
1952	Private Sector leaving behind Sumerbank in production
1960s	Ready-to-wear sector begins to develop
1974	Multi-Party Agreement (MFA)
1980	24 January 1980 Decisions and Growth model based on exports
1994	Turkish Economic Crisis
1995	Customization of Sumerbank
1995	Textile and Clothing Agreement (ATC) (With the acceptance of the WTO, the abolition of trade quotas was put into effect in 2005.)
1996	Customs Union Agreement
2000	Turkish Economic Crisis
2005	Turkey has become the world's 4th largest apparel supplier and 11th textile supplier

The Turkish textile and apparel sectors have grown rapidly and have shifted from high-value-added products to high-value-added manufacturing. Because of these

developments, Turkey's share in world markets has increased. Turkey's exports of textiles and garment sectors, which were calculated as \$ 474 million in 1980, have approached 26 billion dollars (25,960) [7]. The development of the Industrial production index, which includes the number of textile enterprises is reported in Table 2.

Table 2: Manufacture of Textiles, Industrial production index (2005-2017)

Year	Annual Average
2005	115.6
2006	117.6
2007	116.8
2008	102.8
2009	90.4
2010	100.0
2011	102.1
2012	106.5
2013	110.2
2014	111.4
2015	107.2
2016	108.3

*Gross Indices: 2010=100, Economic Activity [8]

3. TODAY'S TURKISH TEXTILE SECTOR

3.1 Structure

Below are number of employees, production value, added value and total investment amounts of textile and apparel sectors of Turkey in 2016 (Table 3). When the structure of the employees is examined, the fact that the total number of women working in the sector as a whole is above the manufacturing industry average indicates that the textile and apparel sectors play an important social role in the spread of the economy to the idle sectors.

Table 3: Textile and Ready-to-Wear Industries Export Amount 2016 Year

Year	STIC (Division)	Export (Dollar)
2016	65*	11.095.184.270***
2016	84**	15.047.490.299***

* Division: 65 - Textile yarn, fabrics, made-up articles, n.e.s., and related products

** Division: 84 - Articles of apparel and clothing accessories

*** Datas are based on TURKSTAT database. Source: Turkstat

- 651 - Textile yarn
- 652 - Cotton fabrics, woven (not including narrow or special fabrics)
- 653 - Fabrics, woven, of man-made textile materials (not including narrow or special fabrics)

- 654 - Other textile fabrics, woven
- 655 - Knitted or crocheted fabrics (including tubular knit fabrics, n.e.s., pile fabrics and openwork fabrics), n.e.s.
- 656 - Tullies, lace, embroidery, ribbons, trimmings and other smallwares
- 657 - Special yarns, special textile fabrics and related products
- 658 - Made-up articles, wholly or chiefly of textile materials, n.e.s.
- 659 - Floor coverings, etc.
- 841 - Men's or boys' coats, capes, jackets, suits, blazers, trousers, shorts, shirts, underwear, nightwear and similar articles of textile fabrics, not knitted or crocheted (other than those of subgroup 845.2)
- 842 - Women's or girls' coats, capes, jackets, suits, trousers, shorts, shirts, dresses and skirts, underwear, nightwear and similar articles of textile fabrics, not knitted or crocheted (other than those of subgroup 842.2)
- 843 - Men's or boys' coats, capes, jackets, suits, blazers, trousers, shorts, shirts, underwear, nightwear and similar articles of textile fabrics, knitted or crocheted (other than those of subgroup 845.2)
- 844 - Women's or girls' coats, capes, jackets, suits, trousers, shorts, shirts, dresses and skirts, underwear, nightwear and similar articles of textile fabrics, knitted or crocheted (other than those of subgroup 845.2)
- 845 - Articles of apparel, of textile fabrics, whether or not knitted or crocheted, n.e.s.
- 846 - Clothing accessories, of textile fabrics, whether or not knitted or crocheted (other than those for babies)
- 848 - Articles of apparel and clothing accessories of other than textile fabrics; headgear of all materials

There are more than 50,000 companies in the Turkish textile and ready-to-wear industry, 95% of which are family companies and 25% are exporting. The vast majority of companies in ready-to-wear companies are small and medium-sized enterprises (about 85%), but technology intensive production is carried out by large firms. Only 1,000 of 50,000 companies are dominant in the whole market and industry. There are two types of companies in Turkey's textile and ready-to-wear industry: (1) yarn producers and weavers with high quality raw materials, which designate market strands with their unique designs and high qualities; and (2) ready-to-wear manufacturers that produce untradeed final products from Turkish and foreign fabrics. These manufacturers sell their brand-free products to third-party chains on the percanee. Unbranded products constitute a large part of industrial production and exports. In addition, there are wholesalers and retailers who are fully dependent on the textile and ready-to-wear industry but are not manufacturers. [9]

3.2 Development stages of Turkish textiles companies

The development stages of companies in the Turkish textile sector are as follows: Fason-OEM-ODM-OBM.

Fason: Companies that can do one or more of cutting, sewing, ironing and packaging stages.

OEM (Original equipment manufacturing): Companies that can perform all production related activities, such as procurement of fabric and accessories, financing, in addition to freewheeling. These companies mainly manufacture according to the design of the ordering company.

ODM (Original design manufacturing - full package): It is a firm that can design and provide logistic support beside the production, and the organizer is advanced.

OBM (Original brand manufacturing): In addition to the complete production and service components for the product, the company can sell the product under its own brand, have a marketing network, and can distribute and advertise.

The Turkish ready-to-wear industry has a great deal of ODM competencies. Our various firms improve OBM competencies. Regional branding, including local and primarily neighboring countries, is of great importance for the transition to OBM. It manufactures almost all types of yarns, from industrial ready-to-wear to home textiles. Especially the use of technology in cotton based production is very high and there is a very well-structured structure. Most of the fabric production in Turkey is made with cotton. The cotton industry has two segments; large-scale companies and small-scale companies that have integrated facilities and are located in all stages of vertical integration. While large companies are ready-made and produce in home textiles, small enterprises are generally involved in the product completion phase which is a subset of Turkish textile industry.

3.3 Textile marketing

The marketing activities of foreign products in Turkey are carried out by foreign procurement agencies or distributors. Distributors install sales and marketing networks depending on the consumer location or product request. As a global supply center for Asia and Europe, many foreign firms have international procurement offices, trade contact points and retail stores in Istanbul. Istanbul is on its way to become a fashion center and become a regional shopping point by branding in design. At this stage, it seems that the production of textile and ready-to-wear has been shifted from the city to the surrounding areas. These trends show themselves in cities like Istanbul, Izmir, Bursa, Ankara, Denizli, Gaziantep, Kayseri, Tekirdağ and Adana (Figure 1) which are the leaders in textile and garment production [10]. Table 4 clearly shows the positive and negative aspects associated with Turkish textile marketing.

Table 4: SWOT Analysis of Turkish Textile and Ready-to-Wear Sector [11, 12]

Strengths	Weaknesses
<ul style="list-style-type: none"> • Fast and flexible mobility • Responding to small orders • Proximity to major markets (such as the EU and Russia) • Quality and experienced workforce • Organization experience, active management and managerial presence • Presence of a strong textile production 	<ul style="list-style-type: none"> • High production costs • Need for qualified intermediate staff • The requirement of the production of basic raw materials can not be met • The need for strengthening of R & D capacity • No university-industry collaboration required • Recurring problems due to small and medium sized company structure

Strengths	Weaknesses
<p>infrastructure and horizontal integration in textile and apparel industries</p> <ul style="list-style-type: none"> • Production of all segments from raw materials (integrated production) • Strong infrastructure in subsidiary industry and finishing sector • Presence of modern technological infrastructure • Significant distance in recent design and branding activities • Concentration in R & D operations • Fast development of overseas retail stores increase • Prevalence in environmentally and human health-friendly production, 	
Opportunities	Threats
<ul style="list-style-type: none"> • The crisis in EU economies creates an opportunity for Turkey to produce fast and small order based production • Proximity to the dynamic Eurasian and Middle Eastern markets • A stable and growing economy (Proximity to the EU market and most of the developing markets - the development of trade with neighboring countries - accessibility to China, the US and Japan after 2005) 	<ul style="list-style-type: none"> • The global crisis is widespread and the continuing tendency is a shrinking market • The deepening instability in the Middle East in the face of living developments • We are losing geographical preference for this market due to the change of trade policies of the EU • We are geographically distant from emerging markets like China and Brazil. • Development and services in other sectors of our country to limit the employment opportunities of the development of the sector (Unfair competition environment created by China due to the rise of quotas in the world - Cost advantage of export similar countries (Asian countries) - Increasing international competition - Increasing value added of China in production)

3.4 Textile exports

Turkey's Textiles and Clothing sector remains one of the strongest segments of the economy and is amongst the largest contributors to Turkey's total exports. Exports statistics are the most important indicators for foreign trade success. Table 5 and Table 6 state that from 2005 to 2008 exports grew significantly but 2008 World Trade Crisis effect dominantly. But exports were growing in 2009 to 2016. When we compare the textile and clothing industries together, Turkey is the one of the main exporters of textile products.



Figure 1: Textile and Ready-to-Wear Sector Production Map of Turkey [14]

4. NATURAL DYES SOURCES IN TURKEY

4.1 Plants and mordants

Usage of plants for making dye is an art known since the ancient times of history. It is known that the use of natural dyeing in textile fibers began in 4000 BC in India and Mesopotamia. It is known to have stained silk weaves with special dyes called Chinese indigo and chinese green in 2000 years. It is understood that herbal and mineral paintings are known in the mummy excavations made in Egypt. Vegetable dyes, which have also been used in natural dyeing, have gradually decreased along with the synthesis of synthetic dyes at the end of the 19th century and have even come to the fore. Nowadays, synthetic fuels are toxic, carcinogens and their wastes are known to cause environmental pollution [15]. Natural dye plants are not toxic and carcinogenic, which have not any environmental pollution. The dye industry in Anatolia is formed by the products available in Anatolia with the information provided from the eastern countries as a result of various cultural exchanges. In France Turkish red dyeing reached the most developed stage in 1750s. Madder (*Rubia tinctorum L.*), a plant, was cultivated in Anatolia for many years. The Ottoman Empire alone received this plant for a two-thirds portion of world trade. Even more importantly, the cultivation of this plant has begun to be abandoned by the synthesis of Alizarin, the main ingredient of this plant.

Turkey; Contrary to 11,000 plants in Europe, there are 9,000 plants and about 3,000 of them are endemic. As a feature of this rich flora, the number of plants used in natural

dyeing is about 150. Some of them are shown in the Table 8. Vegetable dye is the dye obtained from parts of the plant such as leaf, flower, cone, body crusts and roots without chemical treatment or at least as a result of chemical treatment. With the parts of the paint plants used in the paint, the material to be painted is painted either directly or with the addition of an additive. This is called mordanting. Mordants can be chemical or natural. The most important chemical mordant substances:

screed [$\text{KAl}(\text{SO}_4)_3 \cdot 12\text{H}_2\text{O}$], iron screed ($\text{FeSO}_4 \cdot 7\text{H}_2\text{O}$), copper screed ($\text{CuSO}_4 \cdot 5\text{H}_2\text{O}$), $\text{SnCl}_2 \cdot 2\text{H}_2\text{O}$ and wine stone. Mordant is an auxiliary material that allows the dye to bond with the fibers, and it is possible to obtain hundreds of color nuances by using different mordants at the same end. For example; Mordant used to make the tile color from the root dye plant (25 % water for 1 kg of wool), prepared by copper screed up to 4 % (40 g for 1 kg of wool) mordant is added to the bathtub. When the ingredients are dissolved in the bathing water, wool is added and the mordanting process is completed for 60 minutes at 100 °C. The mordanted wools are removed from the mordanting bath and left to dry out in the air for 3-4 days) (25 liters of water for 1 kg of wool) made of alum, up to 20 % of the amount of wool to be dyed before mordanting (200 g for 1 kg of wool), prepared for obtaining the same color of pomegranate red color, Add the wool after mixing in the bath water and add the wool and complete the mordanting process for 60 minutes at 100 °C. The blended wool is removed from the mordant bath 3-4 days in the open air in the air is left to leave. There are different recipes and conditions affecting the result of dyeing (Table 7). [15] As an example of dyeing with vegetable natural dye which is quite simple to obtain synthetic dye; to use the root paint plant to obtain the tile color;

For dyeing, the roots of shoots pulverized to 30 % of the amount of wool (300 g for 1 kg of wool) are added to the prepared 1/30 (30 liters for 1 kg wool) dye box. Mordant wool is added by M6 mordant method after dissolving in mixing bath water. The dyeing operation is completed for 30 minutes at 100 °C. The dyed wools are removed from the dyeing bath and washed and rinsed. The wools are left to dry out in the shadows prescription will be applied.

Table 7: Factors that can affect color tone in natural dyeing

Numbers	Factors
1	Set and content of water used in mordanting and painting.
2	Amount of mordant materials used.
3	Different mordant and mordant mixtures used.
4	Waiting for your yarn after Mordanting.
5	Mordanting and painting bath rates.
6	Temperature and time during mordanting and painting.
7	The content of the used yarn, the yarn number, the bending frequency, the bending shape and the bending direction.
8	Amount of plant used, collection area, part used and grain size.

Despite that; the processes that take place during dyeing of fiber and yarn in the textile sector are quite diverse and unlike dyeing processes with natural stains, these processes can not be used in significant quantities in terms of environment. Water polluting substances may be derived from the basic chemicals and auxiliary substances used in the dyeing process (eg alkali, salts, water, etc.) from the dyes themselves (e.g. aqueous media toxicity, metals, color), auxiliary substances (eg dispersants, defoamers, reducing and oxidizing substances, etc.), and foreign matter residues in the fibers (for example, pesticide residues on the ground, preparations in synthetic fibers and avivage materials). Consumption and emission levels are closely related to the type of fiber, discovery form, dyeing method used and machine. Table 9, for example, shows the difference in dyeing process with the use of a metal complex dye and a natural dye. At the same time, the use of hypochlorite is quite disadvantageous, and a two-step bleaching process is now possible using hydrogen peroxide instead. However, it is stated that this option is two to six times more expensive.

Table 8: Some Plants Used in Isparta Ponds and Wool Painting [16]

Plant name (Turkish-Latin)	English name	Family	Color	Part of plant	Usage of mordanting	Dominant ingredients
Ada çayı (<i>Salvia triloba</i>)	Three-leaved sage	<i>Labiataeae</i>	Brown	Body, Leaf	Schappe	Luteolin
Asma (<i>Vitis vinifera</i>)	Wine	<i>Vitaceae</i>	Green, yellow	Leaf	Schappe, potassium dichromate	Quercetin, quercitrin, carotene
Aspir (<i>Carthamus tinctorius L.</i>)	Safflower	<i>Asteraceae</i>	Yellow, Hardal yellow, Hell Green, Olive drab	Leaf	Schappe, potassium dichromate bluestone, saçıkıbrıs	Carthamin, corocetin
Cehri (<i>Rhamnus petiolaris Boiss, Rhamnus tinctoria</i>)	Anatolian Buckthorne, Persian Berries	<i>Rhamnaceae</i>	Yellow, Mustard yellow, Olive drab	Leaf	Schappe, potassium dichromate saçıkıbrıs	Rhamnetin, rhamnezin, quercetin, kempferol.
Çivit otu (<i>Isatis tinctoria</i>)	Woad, Dyer's Woad	<i>Brassica-ceae</i>	Blue	flower		Indikan, isatin B.
Hayıt (<i>Vitex agnus-castus</i>):	Chaste Tree, Monk's Pepper Tree	<i>Verbenae-ceae</i>	Green	Flower, leaf	Schappe, göztaş	Luteolin
Kekik (<i>Thymus sp.</i>)	Thyme	<i>Lamiaceae</i>	Yellow, green	Leaf, bough	Schappe, (saçıkıbrıs)	Luteolin

Plant name (Turkish-Latin)	English name	Family	Color	Part of plant	Usage of mordanting	Dominant ingredients
Kök boya (<i>Rubia tinctorum</i>)	Madder	<i>Rubiaceae</i>	Red, brown	Root	Oxalic acid, schappe, tartar, saçıkıbrıs	Alizarin, pseudo-purpu rin, purpurin, munjistin, rubiadin, xantho-purpu rin purpuro-xant hin lucidin, chinizarin, christofin, anthragallol
Kantaron (<i>Hypericum empetrifolium</i>)	St. John's Wort	<i>Hyperica-ceae</i>	Yellow, brown	Flowe r, leaf, stem	Schappe, potassium di chromate	Quercetin
Sütleğen euphorbia sp.)	Pear routet spurge	<i>Euphorbia-ceae</i>	Orange, yellow, brown	Root, Flowe r, leaf, stem	Şap, stannic, II chloride	Quercetin

Table 9: The difference between the dyeing of yin with 1: 1 metal complex dye and the dyeing with natural dye [17, 18]

	Painting of yin with 1: 1 metal complex dye	Painting of wool with natural dyes
Painting Prescription	1:20 Bath ratio 5 g Goods weight % 1 Luminescent material 0,5 g / l Fiber protection 0,5 g / Kö Foam cutter 5-10 % Sodium sulphate (by color percentage) 1.5 % Equalize The pH is adjusted with 2 H ₂ SO ₄ (sulfuric acid). 1 g/ Y Washing soap (when standing)	50 % of the amount of wool (500 g for 1 kg of wool) 1/30 (30 kg for 1 kg of wool) dye box Mordant wool is added by mordant method after dissolving in suspension bath water by mixing. The yellow dyeing process is completed at 100 °C for 30 minutes

5. TURKISH CARPETS

5.1 Old hand-made art of carpets-weaving

Carpet-making is a traditional craft that has been practised in Turkey since ancient times, and is still found in almost all regions today. Especially in rural areas, a number of families are engaged in hand-woven carpets. For them, this production is the main or at least important additional financial source. This traditional craft contributes significantly to the reduction of unemployment and, at the same time, this tradition represents a connection with the past, strengthens the feeling of the Turkish nation's cultural belonging and is an important export item wanted worldwide. Hand weaving

carpets has many positives for rural and tourism development. Initial costs for this production are not high. The equipment consists of a loom, a pair of scissors, and a loom reed and a knife. Hand-woven rugs are traditionally trained at home, and the loom itself does not occupy much space. This craft is transferred to the younger generation from the elderly, most often from mother to daughter because in Turkey, carpets are usually woven by women. Young girls learn this craft by watching her mothers or grannies. So, they can learn the whole carpet manufacturing process, from spinning threads from fleece, through their dyeing and preparation of warp up to knotting. But today there are also specialized courses where young people can learn it. Some public institutions (such as the Ministry of Agriculture, the Ministry of Industry and Trade, Special Provincial Administrations and Universities) also provide training for the craft of carpet making. [19]

5.2 Regional carpet weaving centers in Turkey

The carpet making is commonly run from the West to the Middle and Southeast Anatolia. Towards the east, the quality of agricultural land is declining, and therefore, the more to the east, the more important is the carpet production as complementary activity and source of livelihood.


Some important carpet-making centers are Konya, Sivas, Kayseri, Karapınar, Taşpınar, Ladik, Bünyan, Sarayönü, Yahyalı, Mucur, Şarkışla, Eskişehir, Sivrihisar and Niğde in Middle Anatolia; Isparta, Bergama, Balıkesir, Çanakkale, Ezine, Yağcıbedir, Demirci, Uşak, Kula, Gördes, Milas, Muğla, Fethiye, Bodrum and Döşemealtı; and Malatya, Kars, Erzurum, Van and their environments in East and Southeast Anatolia [19]. Color, pattern and motif are the main factors determining the quality of hand-woven carpets. An overview of the most commonly used colors and motifs on some typical Turkish rugs is summarized in Table 10.


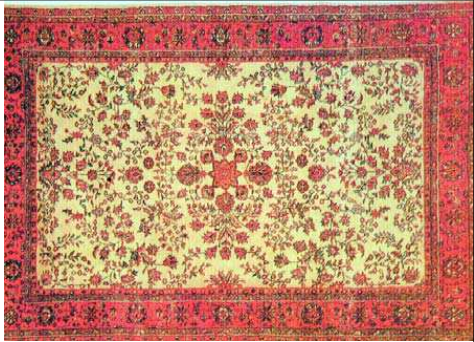
5.3 Isparta carpets

With the investments made in carpet in recent years, Turkey has acquired the world's newest machine park, and in 2013 it became the world's second largest exporter of carpets and floor coverings (STIC 659). In this context, when it comes to the use of natural dyeing in Turkey, Isparta households come to mind. When the Turkmen settlements in Western Anatolia in 12th and 13th centuries especially in Isparta and its surroundings and the records of these Turkmens related to carpet trade are examined, traditional weaving cultures have developed considerably in this region.

With the initiative of various pioneers who developed the pre-Republican Isparta carpets (Figure 2, Figure 3) and settled in the region, Eastern Carpet Company which reached as far as the villages in Isparta was established and gave a number of names according to the pattern composition of the carpet designs produced by wool rope, paint and pattern. These; Kandahar, grape, hour, wood, five, elvan, tapestry, goncalı, wreath are the names. It is possible to see all the features of the decoration in the best way in the motif, color and surface arrangement used in the rooms. The Turkish Standards Institute has developed specific standards for the local carpets, taking into account local characteristics.

Table 10: Typical carpet's colors and motifs of selected Turkish regions (based on [19])

City or region	Colors	Motifs	
Kayseri	red blue yellow	influenced by Iranian carpet patterns	
Niğde	dark and light blue, navy blue, burgundy, red, green, brown and white	floral motifs, kilim designs, geometrical motifs, animal figures, Latin letter figures, Turkmen medallion motifs, figures symbolising the infinity	
Muğla	warp yarn: white weft yarn: reddish, brown	large angular motifs, medallions and corner motifs, single motif or double motifs, pattern with carnations (Milas carpets)	
Uşak	dark blue, dark red, green, yellow, white or light brown	carpets with stars (octagon-shaped star or small diamond-shaped medallions, the idea of infinity	

City or region	Colors	Motifs	
Hereke	navy blue and red backgrounds	traditional patterns of the Ottoman sultan Abdülmecid I, traditional Anatolian and contemporary figurative patterns	
Isparta	navy blue, brick red, turquoise, blue, dark yellowish green, off white and cream	floral motifs from flowers and leaves, mainly of roses, human figures, animal motifs, butterflies, oil-lamp, candlestick	

For example; The criteria set for the properties of the Isparta II carpets middle class are given below. Technical characteristics of Isparta residents (Isparta II middle class):

- Carpet type: Isparta II
- Thread yarn fiber type: Wool
- Standard number of nodes in the loop Ad / dm: 26
- Standard number of nodes in length Ad / dm: 33
- Total number of standard nodes in dm²: 858
- Number of total nodes in dm² at least: 830
- Node style: Single link
- Thread yarn number and coat name: Wool according to TS 626 2.5 / 2 Nm
- Weft thread weft yarn number and genus: 6/9 Ne cotton
- Number of warp threads: 130
- Lower weft yarn number and genus: 6/8 Ne cotton
- Bottom weft thread bend number L / m: 40
- Upper weft thread number and genus: 6/8 Ne cotton
- Upper weft thread twist count: 40
- Pile height: 10-14 [20]

In the early days, 25-30 colors were used in different tones, but today 8-10 colors do not pass. In Isparta there are generally dark blue, tile red, cyan blue, dirty yellow, yellow-green, greens tinted, beige tinted shades and broken white. Indigo blue, meanwhile, is often found in dark brown coats, which often strengthen the edges of motives. The floor colors are mostly white and navy blue. There are also flat colored carpets woven as floor and runners. It is also seen that motifs and beauties in the same character are used in white or navy blue. [20]



Figure 2: Isparta's carpet (Kandahar) [21]



Figure 3: Isparta's carpet (Beşir) [21]

5.4 Current problems of Turkish hand-woven carpet-making

Handmade carpets are faced with a number of problems that need to be addressed to avoid quality degradation and reduced sales. The tradition of weaving hand-woven carpets in the original area is getting worse. One of the most important features of hand-woven carpets is that they are woven in the original area with high quality and uniqueness. The hand-woven carpet reflects the culture of the area that was created there to be woven. The rug reflects the weaving style as well as locally available warp, weft and pile yarns, weaving fabrics, natural dyes, weaving techniques, motifs and colors. When carpets are not woven in their own area, they lack the features associated with this tradition of weaving. For example Milas carpets are woven in Isparta and Bergama, Kars and Yağcıbedi, or even in other Asian countries (China, India, Pakistan) because of cheap labour. This is perceived as the main problem of hand weaving carpets [22]. Another important problem is the imitation of the motifs and patterns of Turkish carpets by weavers in other countries. Carpets made in Central Asia, China or India with labels that claim they are Turkish rugs are sold around the world. That is unethical and unfair. Today, there are many carpets woven on the basis of patterns organized in an attempt to create "modern" designs prepared by non-professionals. This shift towards changing the pattern is particularly noticeable in hand-woven carpets aimed at the domestic market where it has to compete with machine weaving carpets. Changes in the pattern in the Turkish carpets can be found in a number of private companies. Some experts are pushing standards based on old Turkish handmade carpets at the Turkish Institute of Standards. It is important that carpets conform to standards. Turkey has a list of standards, namely the TS 43 "Handmade Turkish Carpets" [23], which were first promoted in 1962 by the "Turkish Institute for Standardization", updated at certain intervals and still ongoing. 1992 is the latest date of published revisions to standards. These standards were determined to

characterize the standard number of knots in the width and length of Turkish hand-woven carpets, the number of knots per square decimeter, node style, warp figures, weft and hair yarn, fiber type, twin count, and number of layers. Trademark is another problem of Turkish hand weaving of carpets in connection with marketing. Trademark can usually be identified by people's perception if they are familiar with the company, provided that the trademark has been effectively used in marketing. The control and inspection mechanism are important for compliance, protect craftsmen and manufacturers against the unfair competition and maintain the effectiveness of Turkish carpet manufacturing.

6. TURKISH FASHION

6.1 History of Turkish clothing

Historical sources show that the main textile materials that have been used in Turkey for more than 100 years BC were the wool and cotton woven in handlooms, and felt materials. Other common clothing materials were fur and leather, as well as silk, but the silk originally came from China. Female and male clothes were very similar to each other, which was the result of everyday life, such as regular horse riding as well as climate causes. Turks wore leather boots, shirts, a short caftan with a belt, and some trousers loose at the top of a narrow, downhill ride suitable for riding. Bashlyks, head coverings and at the same time the status symbols, were made of fur or sheepskin with the purpose of protection from the cold. Turkish clothing and motifs reflect the influence of many cultures migrating from Asia to Anatolia, such as Tatar, Uygur or Azerbaijan. The diverse climatic conditions in Anatolia required clothing that could be used in all conditions. Clothing tradition is stabilized at the time of the Ottoman Empire (Figure 6). Istanbul, Bursa, Bilecik, Denizli, Ankara, Konya, Trabzon, Rize Kastamonu, Gürün were districts specialized on weaving. Socio-economic differences between administrators and ordinary people also influenced the styles of clothing. Unlike the palace and nobility, who were dressed in a beautiful exhibition robes, ordinary people used especially generally available textile materials for clothing [24]. Fashion and decoration are deeply rooted in Turkish culture since the time of the Ottoman Empire. The top-class wardrobe and the palace were characterized by sophistication, plush adornments, woven patterns with gold and silver threads, filigree embroidery and the finest materials. The best silk, brocade, velvet and taffeta, fur collars, plush fabrics with rare lining were used to make garments. Ottoman "palace fabrics" (Figure 4, Figure 5) were handmade especially for members of the Sultan's family and palace. The use of make-up among harem women was also common.



Figure 4: Turkish female caftan
(from Seyranl Kaftan Dessins)



Figure 5: Turkish male caftan

After the demise of the Ottoman Empire and the founding of the Republic of Turkey in 1923, fashion changed completely. Ataturk, the founding father of Turkey, has launched a series of reforms to modernize the country: it has been forbidden to wear a veil for women and fez for men, the Arabic alphabet has been replaced by Latin, families have had family names, and women have been granted civil rights, including the right to vote and to hold public office. Europe, especially Paris, was a fashionable inspiration for young Turkey republic. In large cities like Istanbul or Izmir, Western-style of clothing has begun to be promoted in everyday life. Women had short hair, flapper dresses, coats with fur collars, fancy clutches and glamorous cigarette holders. (Figure 7) Men wore well-tailored double row suits worn with hats, and tuxedos.

6.2 Turkish fashion today

Turkey has just begun to make its mark in the fashion world. Today Turkey is one of world's largest textile and garment producers. Today's modern Turkish women combine their love for gentle decorations - the heritage of Ottoman times- with the ability to follow the latest international trends developed by the early women of the Republic. Turkish women and their sense of fashion are similar to French or Italian women. They spend a lot of money on clothing, care and cosmetics. Public appearance has great value here. The love for care and dressing of Turkish women is deeply rooted in society. A typical woman here sees it as a sign of respect for oneself, peers and society to be as well dressed and well dressed as possible.



Figure 6: Anatolia Turkish traditional clothes:1- mercenary soldier of Ankara, 2-Muslim shepherd from Ankara, 3-Muslim peasant woman from Ankara. 1873.

[25]

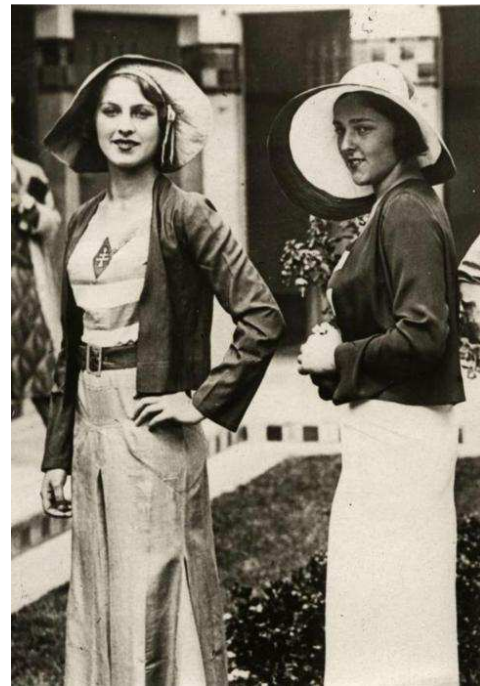


Figure 7: Miss Turkey and Miss Italy, 1930

[26]

Turkey becomes a crossroads of fashion - it brings the best of international fashion to its streets and exports its home fashion to the world. Turkish brands are increasingly found in shopping streets around the world because they use the combination of international trends and Turkey's own multicultural style. High-quality brand designers such as Erd Moralioglu, Bora Aksu and Hussein Chalayan are the world's notion. However, they are mostly dressed by demanding rich clients. And the brands such as Koton, Sarar, Roman, Que, Mach and Tween represent an affordable Turkish version. [27]

6.3 Turkish fashion brands

Turkey has many brands that offer the best types of clothing. Turkey is already well known as one of the world's leading manufacturers of high-street fashion and denim. The Turkish government supports Turkish clothing industry not only financially and politically, but also medially. For example, Turquality is a campaign declared 10 years ago by the Ministry of Economy. It supports key brands designs, including Sarar, Colin, Damat Tween, İpekyol, Koton, Mach and Mavi - all over the world. Top Turkish fashion brands can be seen in the best stores around the world, from Las Vegas to Moscow. "Everyone deserves to dress well" [27] is the motto of the most famous and biggest Turkish brand LC Waikiki.



Figure 8: Born in France and raised in Turkey, LC Waikiki is a multi-cultural fashion brand with global appeal. [29]

LC Waikiki participates in the market with more than 16 %. In 2013, it had more than 400 stores in Turkey and more than 100 worldwide [28]. Another brand, Sarar, opened almost two dozen of stores in Washington DC and plans to have 100 stores throughout the United States in the next 10 years. The brand Sarar also recently opened its first store in Pakistan, while brands such as Mudo and İpekyol are successfully penetrating the Middle East clothing shops. İpekyol has become a favourite with Istanbul fashion bloggers for its combination of clean, modern lines with bold prints and glamorous embellishments. Sarar is winning fans for its chic urban style. Twist is gaining attention for its colourful, youthful edge. The cosmopolitan and really-Turkish style is created primarily thanks to the young urban population in Turkey. Women are a huge driving force behind this fashion development. The number of working women is growing, and they want quality, fashionable and affordable clothing. Young urban working women live an active busy life and create and manage their own fashion and style. A growing number of fashion bloggers across the country suggest future trends in the development of Turkish fashion. (Figure 8) Again, here is well manifested the Turkish ability to associate European and Asian elements. Fashion bloggers show their fans how to mix different styles of combining local brands such as İpekyol, Hotiç or Twist with international brands such as Primark, Chanel, Mango and Zara. And it's this mix of global trends and individual style, as well as high fashion at high-street prices, that is making Turkey a thoroughly 21st-century trendsetter.

CONCLUSION

Manufacturing is considered the main engine of the economy for most developing countries. On January 24, 1980, the public authority approached the planning of

production sectors with the Stabilization Program adopted in Turkey foreseeing structural changes. These economic stabilization decisions which set the stage of liberalization, deeply affected the development of the textile sector. Textile and ready-to-wear sectors, especially since the 1980s, have grown out of export-oriented economic growth model with an export-oriented approach, becoming an important producer and supplier in world trade. The textile and ready-to-wear sectors are one of the most important sectors in Turkey with registered employment which is worth 65 billion dollars, 29 billion dollars exports and 1 million people. However, the high level of labor intensive activity in the sector is faced with a constant competitive pressure as a result of increasing market share of low priced and low-quality products especially from the Far East. For this reason, increasing competition and sustainability in this sector is of great importance. As one of the Strategic Targets set out in the Development Plans of Turkey, while the export target of the sector in the year 2023, which corresponds to the 100th anniversary of the Republic of Turkey, is 80 billion dollars, the exports realized by 2016 are 29 billion dollars. It is important to support small measured entrepreneur ships to give them an opportunity of competition and help them take advantage of trademarking process as a way of identifying true Turkish carpets, and protecting them against the unfair competition of foreign-made copies. Hand-woven carpets and rugs, which are among the most important cultural products in Turkey, have emerged from centuries-old experience in choosing the raw materials to be used, spinning and dyeing yarn, using different weaving techniques and integrating color, patterns and motifs in harmony. Carpets designed for the market and mostly weaving carpets with traditional features should continue as this production is not only an important economic resource for Turkey but also a strong connection with its national tradition.

REFERENCES

- [1] TOBB: Cotton Yarn and Cotton Textile Industry in Turkey, Ankara 1958, p. 9.
- [2] SPO, Textile Industry in the World and Turkey, pp. 143-146, Ankara 1985.
- [3] Casper, K.; Turkish Mensucat Sanayii (Translation: Orhan Tuna), Business, Philosophy, Ethics and Internal Medicine, pp. 27-29.
- [4] RIDDLE, L.; REHMAN, S.: Turkish apparel exporters' attitude, expectations, and strategic preparations for a quota-free world The George Washington Center for the Study of Globalization Occasional Paper Series. Washington DC, 2005.
- [5] SPO (DPT), Annual Reports, 2004: 22.
- [6] DEİK (Foreign Economic Relations Board), Annual Report, 2002.
- [7] WTO, 2017, www.stat.wto.org
- [8] EUROSTAT, N. A. C. E. Rev. 2—statistical classification of economic activities in the european community. Office for Official Publications of the European Communities, Luxemburg, 2008.
- [9] SPO (DPT), Annual Reports, 2004: 24.
- [10] TGSD (Turkish Clothing Manufacturers Association), Annual Reports, 2008.
- [11] Ulaş, Dilber, Özer, Alper, ve Koçak, Akın (2008). Hazır Giyim Sektörü.
- [12] Turkish Republic Ministry of Development's Tenth Development Plan Textile-Leather- Ready Wear Working Group Report (2014).
- [13] <http://stat.wto.org/StatisticalProgram/WSDBViewData.aspx?Language=E>

- [14] <http://www.nationsonline.org/oneworld/map/turkey-map.htm>
- [15] DOĞAN, Yunus, et al. Plants used as natural dye sources in Turkey. *Economic Botany*, 2003, 57.4: 442-453.
- [16] EYÜBOĞLU, Üner; OKAYGÜN, İtir; YARAŞ, Füsün. Doğal boyalarla yün boyama: uygulamalı ve geleneksel yöntemler. Uygulamalı Eğitim Vakfı, 1983.
- [17] Ministry of Culture and Tourism, Traditional Handicrafts and Department Store Operations Publications No: 4, ISBN: 978-975-17-3318-4, page:55, December, 2008, Ankara
- [18] Ministry of Educ., Textile Technology, Protein Dyeing 1, p.10, 2011, Ankara
- [19] SÖYLEMEZOĞLU, Feryal; TAĞI, Sema. Sustainability of Handwoven Carpets in Turkey: The Importance of Technical Distinctions Between Regional Carpet Styles. 2006.
- [20] Ministry of Educ. Handicrafts Technology, Isparta's Rug Patterns, p. 7-12, 2011, Ankara
- [21] Ministry of Educ., Handicrafts Technology, Isparta's Rug Patterns, p.50, 2011, Ankara
- [22] ERDOĞAN, Zeynep; ÖZGEN, Özlen. Sustainability of Handwoven Carpets in Turkey: Problems and Solution Proposals in Relation to Standards and Market Issues. 2006.
- [23] Textile floor coverings- handmade carpets- Turkish carpets TS 43. (Turkish Standards Institution, 1992
- [24] <http://www.turkishculture.org/fabrics-and-patterns/clothing-593.htm>
- [25] <http://photographium.com>
- [26] <http://holdthisphoto.tumblr.com/>
- [27] <http://www.globalblue.com/destinations/turkey/best-turkish-fashion-brands#>
- [28] <https://www.cctinvestments.com/6-famous-brands-in-turkey/>
- [29] <http://www.fawazalhokairfashion.com/portfolio/lc-waikiki/>